WYDZIAŁ CHEMICZNY
KATEDRA TECHNOLOGII CHEMICZNEJ ORGANICZNEJ
I PETROCHEMII

mgr inż. Anna Wolny

Inżynieria Chemiczna

ROZPRAWA DOKTORSKA

Projektowalne układy katalityczne dla sektora lekkiej syntezy organicznej

Projectable catalytic systems for the fine chemicals synthesis sector

Promotor pracy: prof. dr hab. inż. Anna Chrobok

Praca realizowana w ramach konsorcjum Uniwersytet Europejski EURECA-PRO

GLIWICE 2024

Pragnę z głębi serca podziękować mojej Promotor, **prof. dr hab. inż. Annie Chrobok**,
za wieloletnią inspirację, wsparcie merytoryczne, cierpliwość oraz bezcenną wiedzę, której przekazanie umożliwiło mi ukończenie niniejszej pracy. Jestem również wdzięczna za wiarę w moje umiejętności i otwarcie przede mną wielu ścieżek rozwoju w przyjaznym otoczeniu.

Składam serdeczne podziękowania: **dr inż. Piotrowi Latosowi, dr hab. inż. Jakubie Zdarcie, prof. PP, prof. dr hab. inż. Teofilowi Jesionowskiemu, dr hab. inż. Katarzynie Szymańskiej prof. PŚ, dr inż. Agnieszce Siewniak, dr hab. inż. Agacie Jakóbik-Kolon, prof. PŚ, dr Sebastianowi Jurczykowi oraz mgr inż. Dagmarze Więcławik**
za owocną współpracę naukową.

Dziękuję również naukowcom z Monash University w Melbourne, w szczególności
prof. Douglas Macfarlane oraz dr inż. Karolinie Matuszek
za współpracę naukową i umożliwienie odbycia stażu.

Bardzo dziękuję wszystkim **Pracownikom Katedry Technologii Chemicznej Organicznej i Petrochemii**,
z którymi miałam okazję współpracować w trakcie studiów doktoranckich, a w szczególności, dr hab. inż. Alinie Brzęczek-Szafran, dr inż. Karolowi Erfurtowi, dr inż. Annie Szelwickiej, mgr inż. Natalii Barteczko, mgr inż. Bartłomiejowi Gaidzie, mgr inż. Justynie Więcławik mgr inż. Magdalenie Gwóźdź oraz mgr Angelice Mieszczanin
za ogromną życzliwość i okazaną pomoc, a także za to,
że każdy dzień w pracy dawał mi wiele radości.

Chciałabym w szczególności podziękować **Narzeczonemu**, **Rodzicom**, **Babci** *oraz* **Przyjaciołom**
za nieustającą wiarę w moje możliwości, motywowanie do pokonywania słabości oraz wieloletnie wsparcie, które pozwoliły mi się znaleźć w tym miejscu, w którym obecnie się znajduję.
To właśnie im chciałabym dedykować niniejszą pracę.

Spis treści

WYKAZ PUBLIKACJI MONOTEMATYCZNYCH

Publikacja P1. A. Wolny, A. Chrobok, Silica-Based Supported Ionic Liquid-like Phases as Heterogeneous Catalysts, *Molecules* **2022**, 27, 5900. IF_{2022} = 4,600; $MNiSW_{2022}$ = 140.

Publikacja P2. A. Wolny, A. Chrobok, Ionic Liquids for Development of Heterogeneous Catalysts Based on Nanomaterials for Biocatalysis, *Nanomaterials* **2021**, 11, 2030. IF_{2021} = 5,719; $MNiSW_{2021}$ = 100.

Publikacja P3. A. Wolny, A. Chrobok, Supported Ionic Liquid Phase for Biocatalysis: The Current Applications, Synthesis and Prospects, *Curr. Org. Chem.* **2023**, 27, 1119–1122. IF_{2023} = 1,700; $MNiSW_{2023}$ = 70.

Publikacja P4. A. Wolny, P. Latos, K. Szymańska, S. Jurczyk, A. Jakóbik-Kolon, A. Chrobok, Construction of trifloaluminate ionic liquid catalyst on the silica surface dedicated for continuous flow Diels-Alder synthesis, *Appl. Catal. A Gen.* **2024**, 676, 119676. IF_{2023} = 4,700; $MNiSW_{2024}$ = 100.

Publikacja P5. A. Wolny, A. Siewniak, J. Zdarta, F. Ciesielczyk, P. Latos, S. Jurczyk, L.D. Nghiem, T. Jesionowski, A. Chrobok, Supported ionic liquid phase facilitated catalysis with lipase from Aspergillus oryzae for enhance enantiomeric resolution of racemic ibuprofen *Environ. Technol. Innov.* **2022**, 28, 102936. IF_{2022} = 7,100; $MNiSW_{2022}$ = 70.

Publikacja P6. A. Wolny, D. Więcławik, J. Zdarta, S. Jurczyk, T. Jesionowski, A. Chrobok, Robust biocatalyst for the green continuous flow synthesis of esters from biomass-derived furfuryl alcohol and C8-C18 carboxylic acids *Green Chem.* **2024**, Advance article. doi.org/10.1039/D4GC03821E. IF_{2023} = 9,300; $MNiSW_{2024}$ = 200.

OSIĄGNIĘCIA NAUKOWE ZWIĄZANE Z PRACĄ DOKTORSKĄ

A. Zgłoszenia patentowe:

1. A. Wolny, A. Chrobok, A. Siewniak, P. Latos, Sposób otrzymywania (S)-(+)-ibuprofenu (P.441467; WIPO ST 10/C PL441467) 2022.
2. A. Wolny, A. Chrobok, Sposób otrzymywania estrów furfurylowych (WIPO ST 10/C PL447899) 2024.

B. Projekty:

1. Projekt NCN PRELUDIUM22 UMO-2023/49/N/ST8/01633 pt. Projektowanie biokatalizatorów na bazie cieczy jonowych i projektowalnych nośników w modelowych procesach chemicznych (01.2024-01.2026). Pełniona funkcja: kierownik.
2. Projekt NCN OPUS20 2020/39/B/ST8/00693 pt. Projektowalne ciekłe związki kompleksowe metali jako katalizatory modelowych procesów chemicznych i elektrochemicznych (07.2023-07.2024). Pełniona funkcja: wykonawca stypendysta.
3. Realizacja doktoratu w ramach Uniwersytetu Europejskiego projektu EURECA-PRO „Odpowiedzialna konsumpcja i produkcja” (13.01.2023-30.09.2024).

C. Staże naukowe i szkoły letnie:

1. 01.08.2021 – 01.12.2021: uczestnictwo w „International Summer School 2021 Responsible consumption and production for digitized higher education” finansowane w ramach Uniwersytetu Europejskiego EURECA-PRO, TU Bergakademia Freiberg, Niemcy.
2. 7.11.2022 – 26.11.2022: uczestnictwo w „International PhD Journey 2022 Clean energy"” finansowane w ramach Uniwersytetu Europejskiego EURECA-PRO, Montanuniversität Leoben, Austria.
3. 12.02.2024 – 12.03.2024: staż zagraniczny w Monash University w Melbourne, Australia finansowany w ramach projektu Narodowej Agencji Wymiany Akademickiej (PPI/ APM/2018/1/00004).
4. 24.06.2024 – 26.08.2024: staż krajowy w Instytucie Katalizy i Fizykochemii Powierzchni PAN w Krakowie finansowany w ramach Stypendium Rektora dla najlepszych doktorantów 2023/2024 (Uczelnia Doskonałości – Uczelnia Badawcza).

D. Prezentacje na konferencjach krajowych i międzynarodowych

1. VI International Interdisciplinary Conference of PhD students of Technical Universities – InterTechDoc'2021 21-23.07.2021, Ustroń, Polska; New method for pure ibuprofen synthesis (wystąpienie ustne).
2. VIII Łódzkie Symposium of Chemistry PhD Students 24.09.2021, Łódź, Polska; Supported ionic liquid phase as innovative biocatalysts for fine chemicals synthesis (poster).
3. 6th International Conference on Ionic Liquid-Based Materials 22-26.11.2021, Strasbourg, Francja; High enantioselective resolution of ibuprofen racemate via enzymatic esterification (poster).
4. VII International Interdisciplinary Conference of PhD students of Technical Universities – InterTechDoc'2022 5-7.04.2022, Ustroń, Polska; Synteza czystego (S)-ibuprofenu (Synthesis of (S)-ibuprofen) (wystąpienie ustne).
5. X Kongres Technologii Chemicznej 11-14.05.2022, Wrocław, Polska; Heterogeniczny rozdział kinetyczny racematu ibuprofenu poprzez enzymatyczną estryfikację do estru (S)-ibuprofenu (wystąpienie ustne).
6. 5th Symposium on Biotransformations for Pharmaceutical and Cosmetic Industry 13-15.06.2022, Kraków-Częstochowa, Polska; Heterogeneous kinetic resolution of the ibuprofen racemate by enzymatic esterification to (S)-ibuprofen ester (poster).
7. The 3rd International Congress on Advanced Materials Sciences and Engineering 21-25.07.2022, Opatija, Chorwacja; Title: Supported ionic liquid phase as catalyst for fine chemicals synthesis (poster).
8. IV National Symposium Bioorganic and Organic Chemistry, and Biomaterials 3.12.2022, Poznań, Polska; Biotransformacja α-angelika laktonu w obecności rozpuszczalników głęboko eutektycznych (poster).
9. 9th Congress on Ionic Liquids 24-28.04.2023, Lyon, Francja; Water-tolerant silica-based trifloaluminate ionic liquids dedicated for Diels-Alder reaction (wystąpienie ustne).
10. Ogólnopolska Konferencja Naukowa – Zrównoważony Rozwój w Obszarze Kosmetyków i Detergentów, ICSO 12.04.2024, Kędzierzyn Koźle, Polska; Wysoce aktywny heterogeniczny biokatalizator dedykowany dla syntezy estrów furfurylowych kwasów C8 – C18 w systemie ciągłym (poster).

11. XXII Konferencja Ochrona Środowiska – Nauka i Przemysł dla ochrony Ziemi, 24-26.04.2024, Ustroń, Polska; Biodegradowalny biokatalizator dedykowany dla zielonej syntezy estrów furfurylowych kwasów C8 – C18 w systemie ciągłym (poster).
12. 6th Symposium on Biotransformations for Pharmaceutical and Cosmetic Industry, 17-19.06.2024, Kraków, Polska; Active and stable biocatalyst for the continuous flow synthesis of C8-C18 carboxylic acids esters of biomass-derived furfuryl alcohol (wystąpienie ustne).
13. XI Kongres Technologii Chemicznej 16-19.09.2024, Poznań, Polska; Biokatalizator do syntezy estrów kwasów karboksylowych C8-C18 i alkoholu furfurylowego w systemie przepływowym (wystąpienie ustne).
14. Green Technology for Sustainable Environment 2024 22.09-26.09.2024, Poznań, Polska; An effective biocatalyst for the continuous flow production of C8-C18 carboxylic acid esters derived from biomass based furfuryl alcohol (wystąpienie ustne).

E. Nagrody oraz wyróżnienia

1. Nagroda II stopnia za prezentację posterową na 5th Symposium on Biotransformations for Pharmaceutical and Cosmetic Industry, Kraków, 13-15.06.2022.
2. Nagroda II stopnia w konkursie BASF Polska „Drive Innovation – Rozwiązania dla Zrównoważonego Rozwoju", Warszawa, 14.03.2024.
3. Nagroda I stopnia za prezentację posterową na Ogólnopolskiej Konferencji Naukowej – Zrównoważony Rozwój w Obszarze Kosmetyków i Detergentów, ICSO Kędzierzyn Koźle, 12.04.2024.
4. Nagroda I i III stopnia za prezentacje posterowe na XXII Konferencji Ochrony Środowiska – Nauka i Przemysł dla ochrony Ziemi, Ustroń, 24-26.04.2024.
5. Stypendium Rektora Politechniki Śląskiej dla najlepszych doktorantów w latach 2021/2022, 2022/2023, 2023/2024.
6. Nagroda II stopnia Rektora Politechniki Śląskiej w 2023 roku za wysoko punktowane publikacje, udzielone patenty, pozyskane projekty badawcze, prace naukowo-badawcze.

ALFABETYCZNY SPIS SKRÓTÓW I AKRONIMÓW

^{29}Si MAS NMR	Spektroskopia magnetycznego rezonansu jądrowego ciała stałego krzemu
AILs	Kwasowe ciecze jonowe (z ang. *Acidic Ionic Liquids*)
BET	Analiza powierzchni właściwej metodą Brunauer-Emmett-Tellera
BJH	Analiza powierzchni właściwej metodą Barrett-Joyner-Halenda
CALB	Lipaza B z *Candida antarctica*
COX	Cyklooksygenazy
EDX	Rentgenowska spektroskopia dyspersji energii
ee	Nadmiar enancjomeryczny (z ang. *enantiomeric excess*)
FT-IR	Spektroskopia w podczerwieni z transformacją Fouriera
GC	Chromatografia gazowa
HPLC	Wysokosprawna chromatografia cieczowa
ILs	Ciecze jonowe (z ang. *Ionic Liquids*)
LAO	Lipaza z *Aspergillus oryzae*
MA	Bezwodnik maleinowy
RME	Efektywność masowa reakcji (z ang. *Reaction Mass Efficiency*)
SCIL	(z ang. *Solid Catalyst with Ionic Liquid Layer*)
SEM	Skaningowa mikroskopia elektronowa
SILC	(z ang. *Supported Ionic Liquid Catalyst*)
SILLP	(z ang. *Supported Ionic Liquid-Like Phase*)
SILP	(z ang. *Supported Ionic Liquid Phase*)
TGA	Analiza termograwimetryczna
TOF	Częstotliwość cykli katalitycznych (z ang. *Turnover Frequency*)

I WPROWADZENIE I CEL PRACY

Celem badań realizowanych w ramach pracy doktorskiej było opracowanie wysoce aktywnych i stabilnych katalizatorów opartych o enzymy lub kwasowe ciecze jonowe dedykowanych dla czystych technologii chemicznych z sektora lekkiej syntezy organicznej.

Projektowanie zrównoważonych procesów chemicznych wpisuje się w światowy trend dążenia do wdrażania neutralnych dla środowiska technologii produkcyjnych. Idea ta jest ściśle powiązana z Agendą 2030 na rzecz zrównoważonego rozwoju przyjętą przez kraje członkowskie ONZ. Szczególny nacisk nakłada się na modernizację procesów produkcji związków z sektora lekkiej syntezy organicznej, które charakteryzuje często wieloetapowość i generowanie dużych ilości odpadów. Do głównych wyzwań związanych z ekologiczną transformacją metod syntezy tych związków zalicza się poszukiwanie alternatywnych, wysoce selektywnych, aktywnych i stabilnych katalizatorów w miejsce dotychczas stosowanych konwencjonalnych kwasowych katalizatorów, eliminację lotnych związków organicznych oraz toksycznych reagentów i środków pomocniczych.[1,2]

Zgodnie z ideą gospodarki w obiegu zamkniętym, katalizator powinien nie tylko charakteryzować się wysoką aktywnością i selektywnością w procesie, ale również wysoką stabilnością umożliwiającą jego ponowne wykorzystanie. Choć katalizatory homogeniczne charakteryzują się wysoką aktywnością, głównie dzięki łatwej dostępności miejsc aktywnych, to ich trudności w oddzielaniu od mieszaniny poreakcyjnej sprawiają, że w przemyśle częściej stosuje się katalizatory heterogeniczne. Zwiększona dystrybucja miejsc aktywnych w katalizatorach heterogenicznych, a tym samym aktywność, może być modelowana za pomocą materiałów o rozbudowanej powierzchni właściwej, na których unieruchamiana jest faza katalityczna. Dodatkową przewagą katalizatorów heterogenicznych nad katalizatorami homogenicznymi jest możliwość ich zastosowania w reaktorach przepływowych.[3]

Poszukiwania alternatywnych katalizatorów dla przemysłowych procesów chemicznych, o niskiej toksyczności, bezpiecznych dla środowiska są istotnym elementem transformacji technologii chemicznych na świecie. Dlatego też w pracy doktorskiej skupiłam się nad badaniami dotyczącymi wykorzystania jako faz aktywnych katalizatorów kwasowych cieczy jonowych lub enzymów.

Ciecze jonowe (z ang. *Ionic Liquids*, ILs) to związki składające się z organicznego kationu oraz organicznego lub nieorganicznego anionu. Ich główną zaletą jest możliwość projektowania struktury poprzez odpowiedni dobór kationu i anionu, co pozwala na uzyskanie specyficznych właściwości, dzięki czemu znajdują one szerokie zastosowanie w przemyśle chemicznym. Dodatkowymi atutami wykorzystania ILs w technologiach chemicznych jest niska prężność par, wysoka stabilność termiczna oraz szeroki zakres temperaturowy, w którym pozostają w stanie ciekłym.[4-6] Istotną grupę cieczy jonowych stosowanych jako katalizatory stanowią kwasowe ciecze jonowe (z ang. *Acidic Ionic Liquids*, AILs).[7] AILs można sklasyfikować na podstawie rodzaju kwasowego centrum na typy kwasów Brønsteda i Lewisa. Możliwe jest wprowadzenie więcej niż jednej grupy kwasowej do struktury AILs oraz projektowanie cieczy jonowych poprzez połączenie kwasowych typów Brønsteda i Lewisa. Kwasowe centrum Brønsteda można wprowadzić do cieczy jonowych jako: kwasowy wodór w kationie (A), anionie (B) lub obu jonach (C), kwasowy wodór znajdujący się w grupie funkcyjnej (D) lub kwasowy wodór znajdujący się zarówno w grupie funkcyjnej, jak i w kationie/anionie (E). Kwasowe ciecze jonowe typu kwasu Lewisa są głównie oparte na anionach halometalicznych (F) oraz atomie boru w kationie (G) (Rysunek 1). Powstawanie mieszanych cieczy jonowych Brønsteda–Lewisa zostało również przedstawione na Rysunku 1 (H).[8-10]

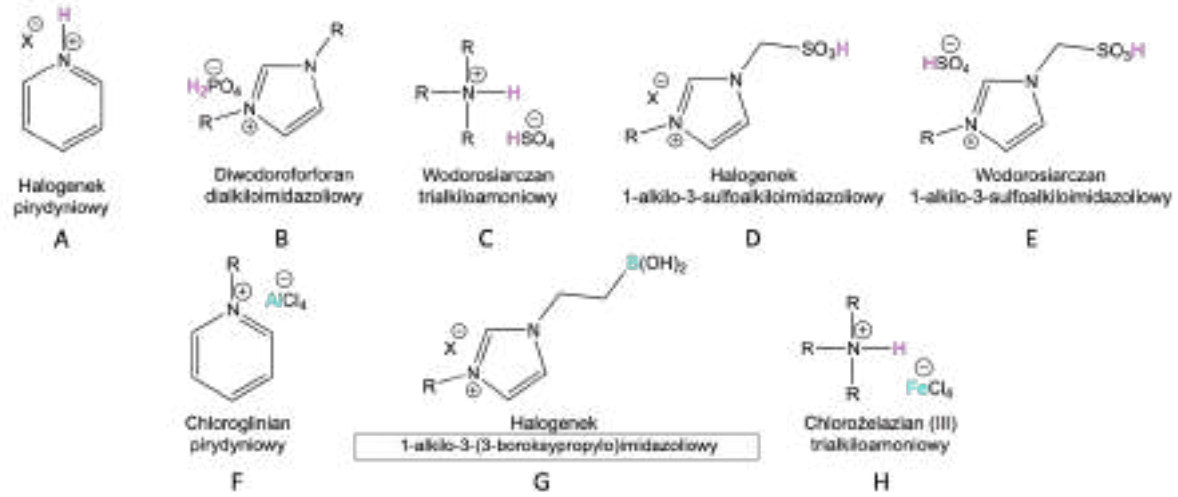

Rysunek 1. Przykładowe struktury kwasowych cieczy jonowych typu Brønsteda i Lewisa.

Głównym wyzwaniem związanym z zastosowaniem kwasowych cieczy jonowych w przemyśle jest ich stabilność w procesie i możliwość stosowania w wielu cyklach reakcyjnych. Możliwość immobilizacji AILs na stałej matrycy w sposób fizyczny (z ang. *Supported Ionic Liquid Phase,* SILP) lub poprzez wiązania chemiczne (z ang. *Supported Ionic Liquid-Like Phase*, SILLP),

pozwala na łatwe oddzielenie katalizatora od mieszaniny reakcyjnej. Graficzną wizualizację obu opisanych technik immobilizacji AILs przedstawiono na Rysunku 2. Podczas unieruchomienia, AIL tworzy cienką warstwę na nośniku, co redukuje jej ilość w procesie. Dodatkowo immobilizacja AIL poprawia transfer masy do centrów katalitycznych na granicy faz ciecz-ciecz. Co więcej, heterogeniczny katalizator SILP lub SILLP może być z powodzeniem stosowany zarówno w procesach okresowych, jak i ciągłych, w tym w reaktorach ze złożem stałym lub fluidalnym.[10-13]

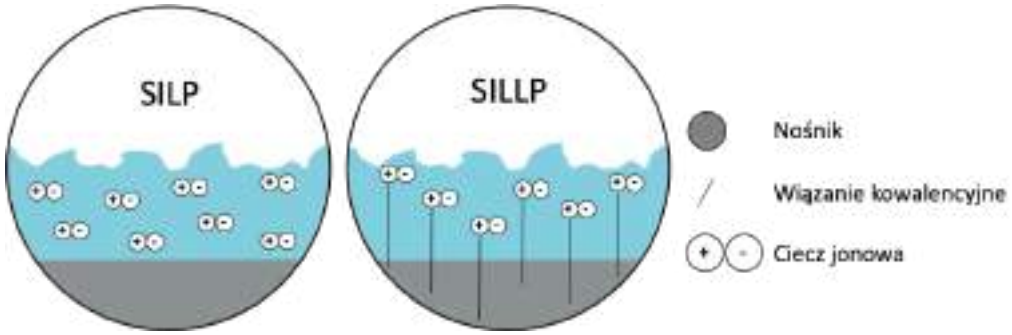

Rysunek 2. Graficzne przedstawienie technik SILP i SILLP.

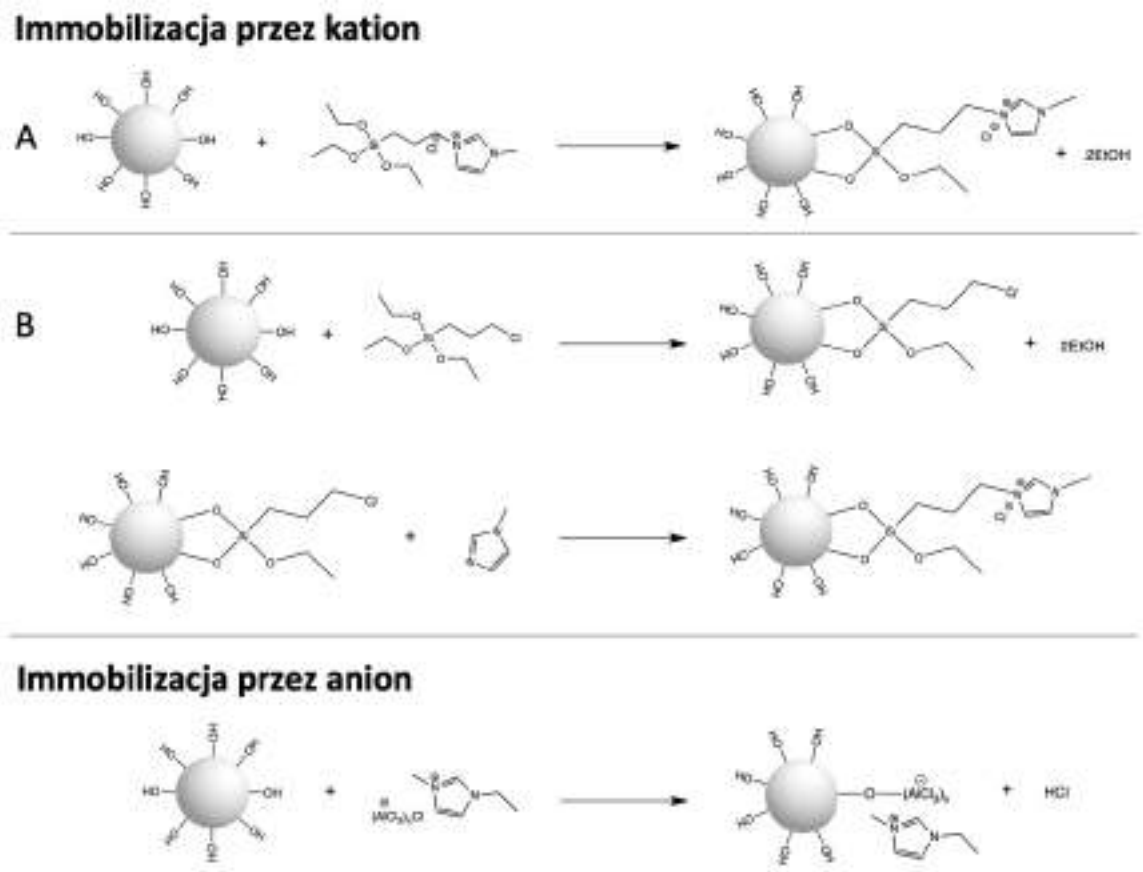

Rysunek 3. Immobilizacja chemiczna cieczy jonowej na powierzchni krzemionki poprzez kation lub anion. Przywiązanie IL do nośnika można uzyskać poprzez bezpośrednią immobilizację IL (A) lub poprzez budowanie struktury IL na nośniku (B).

Chemiczne wiązanie cieczy jonowej z powierzchnią nośnika zapobiega jej wymywaniu. Dzięki obecności licznych grup hydroksylowych, dobrze rozwiniętej powierzchni właściwej oraz kontrolowanej porowatości, materiały krzemionkowe stały się powszechnie stosowanymi nośnikami do chemicznej immobilizacji IL. Metody przygotowania materiałów SILLP na bazie krzemionki obejmują reakcję między IL lub prekursorem IL a grupami hydroksylowymi obecnymi na powierzchni krzemionki lub technikę zol-żel. IL może być przyłączona do grupy Si-OH poprzez kation lub anion (Rysunek 3). Przywiązanie IL do nośnika można uzyskać poprzez bezpośrednie unieruchomienie IL (Rysunek 3A) lub przez budowanie struktury IL na nośniku (Rysunek 3B).[10]

Katalizatory SILLP typu Lewisa na bazie materiałów krzemionkowych są zazwyczaj syntezowane poprzez przywiązanie kationu IL z wykorzystaniem prekursorów, takich jak: 3-(chloropropylo)trietoksysilan, 3-(chloropropylo)trimetoksysilan lub 3-(merkaptopropylo)trimetoksysilan, uzyskując struktury przedstawione na Rysunku 4. Materiał SILLP może charakteryzować się centrum kwasowym Lewisa zlokalizowanym w łańcuchu alkilowym zmodyfikowanym grupami $-SO_2Cl$ lub $-SO_2OH$ (Rysunek 4A), bądź w anionie na bazie halogenku metalu, który powstaje w reakcji kompleksowania z odpowiednim halogenkiem metalu (Rysunek 4B, C).[8,10-12]

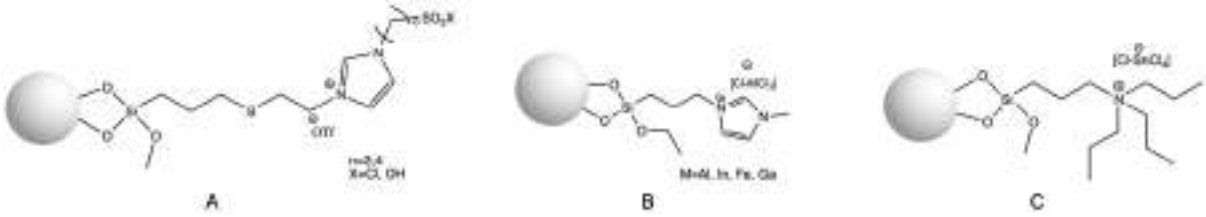

Rysunek 4. Struktury katalizatorów SILLP typu Lewisa.

Katalizatory SILLP typu Brønsteda na bazie materiałów krzemionkowych są syntezowane poprzez przywiązanie kationu IL. Ciecze jonowe typu Brønsteda są przyłączane do powierzchni krzemionki za pomocą takich samych prekursorów jak wymienione powyżej, tworząc struktury przedstawione na Rysunku 5. Centrum kwasowości Brønsteda, które znajduje się w anionie, to najczęściej $[HSO_4]^-$, natomiast w kationie zazwyczaj jest zlokalizowane w łańcuchu alkilowym zmodyfikowanym grupą $-SO_3H$.[10,11]

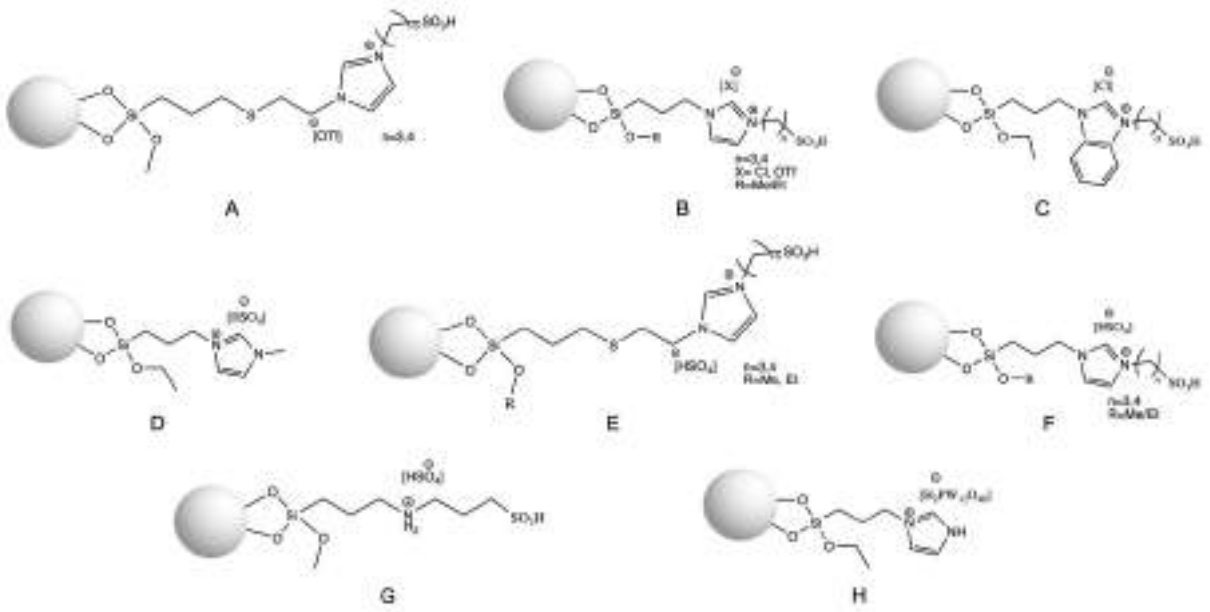

Rysunek 5. Struktury katalizatorów SILLP typu Brønsteda.

Większość katalizatorów typu SILLP zawiera w swojej strukturze aniony halogenkowe, co stanowi istotny problem w ich potencjalnym przemysłowym zastosowaniu. W celu zapobiegania hydrolizie i powstawaniu niebezpiecznych kwasów, takich jak HCl, zastępowanie anionów halogenkowych jest kluczowym elementem badań w tej dziedzinie. Ich eliminacja pozwala na obniżenie kosztów związanych z potrzebą stosowania specjalistycznego sprzętu, korozją aparatury oraz toksycznymi mi odpadami. Dodatkowo budowa anionu cieczy jonowej ma kluczowy wpływ na właściwości katalityczne SILLP, które mogą być może być bardziej lub mniej kwasowe, w zależności od specyficznych wymagań.

W pracy przeglądowej pt.: „*Silica-Based Supported Ionic Liquid-like Phases as Heterogeneous Catalysts*" zaprezentowałam przegląd literatury dotyczącej zastosowania chemicznie immobilizowanych kwasowych cieczy jonowych na materiałach krzemionkowych jako katalizatorów w syntezie organicznej. Opisałam metody immobilizacji AILs na materiałach krzemionkowych, przedstawiłam również metody ich charakterystyki oraz przykłady zastosowania jako katalizatorów z podziałem na SILLP typu Lewisa i Brønsteda w reakcjach syntezy organicznej (np. alkilowanie Friedla-Craftsa, cykloaddycja Dielsa-Aldera, estryfikacja Fischera, utlenianie Bayera-Villigera, transestryfikacja, hydroliza, kondensacja).[14]

Enzymy stanowią kolejny typ alternatywnych biokatalizatorów, które znajdują coraz szersze zastosowanie w przemyśle chemicznym.[15] Enzymy to biodegradowalne wielkocząsteczkowe związki zbudowane z uporządkowanej sekwencji od kilkudziesięciu do nawet tysięcy aminokwasów, gdzie centrum aktywne zazwyczaj tworzy jedynie kilka z nich.

W związku z tym enzymy posiadają unikalną zdolność katalizowania reakcji z wyjątkową selektywnością oraz specyficznością. Dużą zaletą enzymów jest wysoka aktywność, co umożliwia prowadzanie procesów w łagodnych warunkach. Podwyższenie stabilności enzymów w zmiennych warunkach reakcyjnych jest przedmiotem wielu badań.[16]

Lipazy są najpowszechniej stosowanymi enzymami w syntezie organicznej ze względu na ich szeroką specyficzność substratową i wysoką enancjoselektywność. Lipazy należą do grupy hydrolaz i są naturalnie odpowiedzialne za hydrolizę trójglicerydów w organizmach żywych. W porównaniu z innymi enzymami wykazują one stosunkowo wysoką stabilność w środowisku organicznym pozwalając na przeprowadzanie procesów w wysokich temperaturach (nawet do 120 °C) i w szerokim zakresie pH. Dzięki temu lipazy zyskały znaczące znaczenie w wielu gałęziach przemysłu chemicznego, takich jak: produkcja farmaceutyków, tekstyliów, biopaliw, polimerów, surfaktantów czy w przemyśle spożywczym oraz piekarniczym.[17,18] Białka te wykazują zdolność katalizowania reakcji na granicy faz olej-woda dzięki zjawisku zwanemu „aktywacją międzyfazową". W przypadku większości lipaz centrum aktywne jest osłonięte zewnętrznie hydrofilowym, a wewnętrznie hydrofobowym wieczkiem. W środowisku hydrofobowym wieczko to częściowo się otwiera, odsłaniając centrum aktywne, które staje się bardziej dostępne dla substratów, co zwiększa efektywność katalizy.[19-20]

Na aktywność i stabilność lipaz w procesach organicznych wpływa wiele czynników, z których najważniejszym jest obecność niezbędnej ilości wody umożliwiającej lipazom utrzymanie katalitycznej konformacji w środowisku hydrofobowym. Przekroczenie optymalnej ilości wody powoduje natomiast szybszą dezaktywację białka.[21]

Jedną z metod zwiększenia stabilności lipaz w zmiennych warunkach procesu jest ich immobilizacja na stałej matrycy poprzez oddziaływania fizyczne (adsorpcja, pułapkowanie) lub wiązania chemiczne (związanie kowalencyjne z nośnikiem, sieciowanie). Często immobilizacja enzymów nie tylko zwiększa ich stabilność podczas procesu, ale także powoduje wzrost ich aktywności, selektywności, odporności na uszkodzenia mechaniczne i termiczne oraz umożliwia łatwy zawrót do kolejnego cyklu reakcyjnego. Najpopularniejszą z metod immobilizacji enzymów jest adsorpcja fizyczna na nośniku ze względu na niski koszt i prostotę procedury. Istotnym aspektem podczas immobilizacji danego białka jest dobór właściwego nośnika, który powinien charakteryzować się odpornością mechaniczną i termiczną, dobrze rozwiniętą powierzchnią właściwą i porowatością oraz możliwością modyfikacji powierzchni.[22-24]

Jedną z najskuteczniejszych metod stabilizacji lipaz jest fizyczna immobilizacja na hydrofobowej matrycy, która jednocześnie zwiększa ich aktywność dzięki mechanizmowi aktywacji międzyfazowej.[25-27] W związku z tym najczęściej wybieranymi matrycami do immobilizacji lipaz są materiały węglowe (np. węgiel aktywny, nanorurki węglowe) lub materiały polimerowe (np. poli(metakrylan metylu-co-diwinylobenzen)).[22-24] W niektórych przypadkach, ze względu na korzystniejszą cenę oraz korzystniejsze właściwości strukturalne, do immobilizacji lipaz wybiera się materiały hydrofilowe, takie jak krzemionka. Obecność grup hydroksylowych na powierzchni krzemionki umożliwia jej funkcjonalizację cząsteczkami hydrofobowymi, takimi jak n-alkilotrietoksysilany lub ciecze jonowe, co zapewnia efektywną immobilizację lipaz (Rysunek 6).[28,29]

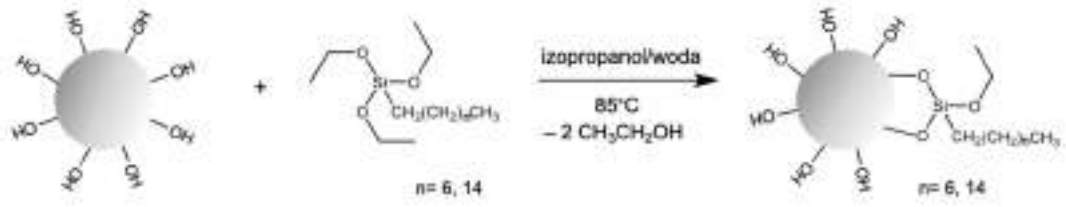

Rysunek 6. Chemiczna funkcjonalizacja materiałów krzemionkowych grupami alkilowymi.

Ciecze jonowe odgrywają istotną rolę w procesie stabilizacji enzymów. Struktura ILs przypomina sieć, w której kationy i aniony są połączone za pomocą wiązań wodorowych, tworząc zarówno regiony polarne, jak i niepolarne. Białka zajmują hydrofilowy obszar supramolekularnej sieci ILs, który jest stabilizowany przez silne interakcje jonowe. Interakcja między enzymami a ILs odgrywa kluczową rolę w stabilizacji złożonej, trójwymiarowej struktury białek. Kluczowe właściwości ILs, które wpływają na aktywność enzymatyczną, to: polarność, hydrofobowość, nukleofilowość anionu, długość łańcucha alkilowego w kationie, zdolność do tworzenia wiązań wodorowych oraz lepkość. Najpopularniejszymi ILs stosowanymi w stabilizacji lipaz są związki oparte o kation imidazoliowy i aniony, takie jak: chlorkowy Cl^-, bis(trifluorometanosulfonowy)imidkowy $[NTf_2]^-$, dietylosiarczanowy (VI) $[Et_2SO_4^-]$, heksafluorofosforanowy $[PF_6]^-$ i tetrafluoroboranowy $[BF_4]^-$ (Rysunek 7).[30,31]

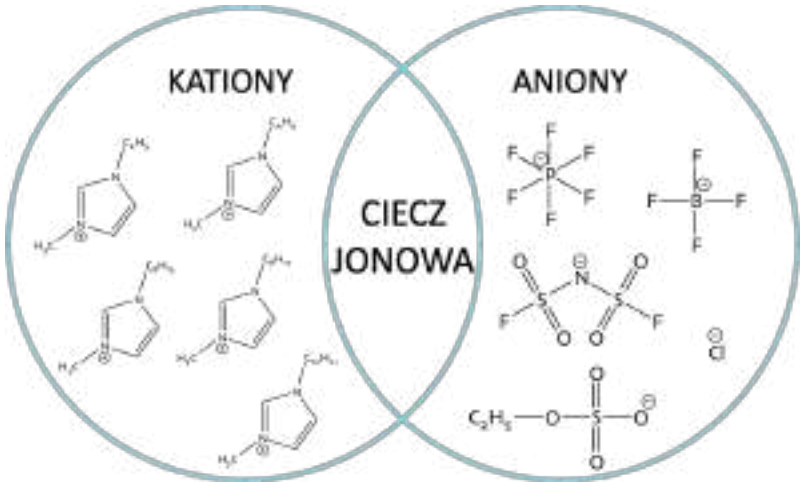

Rysunek 7. Struktury cieczy jonowych stosowanych w stabilizacji enzymów.

Interesującym podejściem jest połączenie techniki immobilizacji białek z ich stabilizacją w środowisku IL. W tej metodzie można wyróżnić cztery różne techniki (Rysunek 8). Pierwsza z nich polega na fizycznym unieruchomieniu enzymu na nośniku, na którym wcześniej została zaadsorbowana ciecz jonowa (SILP), natomiast gdy białko zostanie fizycznie unieruchomione na nośniku chemicznie zmodyfikowanym cieczą jonową, proces ten określa się jako SILLP. Różnica w syntezie opisanych nośników polega na odmiennym podejściu do unieruchomienia cieczy jonowej na matrycy: dla SILP jest to sposób fizyczny, a dla SILLP poprzez wiązanie kowalencyjne. Inne rozwiązanie zakłada unieruchomienie enzymu na stałej matrycy, która następnie jest pokrywana warstwą cieczy jonowej (z ang. *Solid Catalyst with Ionic Liquid Layer*, SCIL), a ostatnia technika polega na przyłączeniu enzymu, poprzez wiązanie kowalencyjne, do grup cieczy jonowej, które są chemicznie osadzone na stałej matrycy (z ang. *Supported Ionic Liquid Catalyst*, SILC). Wykorzystanie nośników modyfikowanych cieczami jonowymi do immobilizacji lipaz minimalizuje ryzyko wymywania enzymów z matrycy, a dzięki zdolności cieczy jonowej do utrzymania aktywnej konformacji lipazy, można znacząco poprawić aktywność, stabilność i możliwość wielokrotnego użycia immobilizowanych enzymów.[29,32]

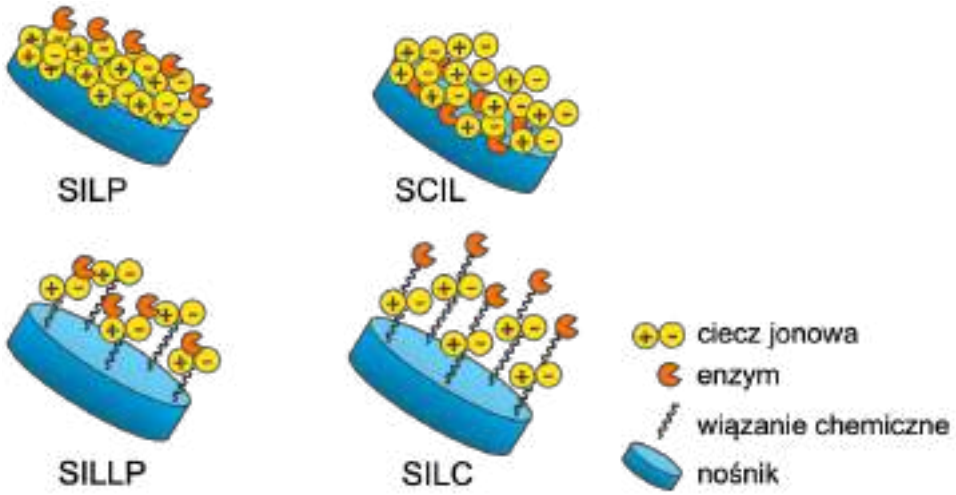

Rysunek 8. Techniki stabilizacji enzymów na nośnikach modyfikowanych cieczami jonowymi.

W pracy przeglądowej pt.: „*Ionic Liquids for Development of Heterogeneous Catalysts Based on Nanomaterials for Biocatalysis*" zaprezentowałam przegląd literatury dotyczącej zastosowania fizycznie immobilizowanych enzymów na nośnikach typu SILP i SILLP jako biokatalizatorów w syntezie organicznej. Przedstawiłam metody immobilizacji enzymów na materiałach modyfikowanych ILS, opisałam czynniki wpływające na stabilizację enzymów w ILs oraz przykłady zastosowania biokatalizatorów typu SILP i SILLP w reakcjach syntezy organicznej ze szczególnym wyróżnieniem nośników opartych o nanomateriały.[33] Dodatkowo przedstawiłam krytyczne spojrzenie na zastosowanie biokatalizatorów typu SILP i SILLP w syntezie organicznej wraz z perspektywami rozwoju tej ścieżki badawczej w komentarzu naukowym pt.: „*Supported Ionic Liquid Phase for Biocatalysis: The Current Applications, Synthesis and Prospects*". Kluczowym aspektem dotyczącym układów biokatalitycznych typu SILP i SILLP jest ocena cyklu życia, analiza egzergii oraz analiza energetyczna. To cenne narzędzia do oceny wpływu na środowisko opracowanej technologii oraz zrównoważonego rozwoju powinny zostać używane do oceny każdego biokatalizatora typu SILP i SILLP.[34]

Podsumowując, wpisując się w nurt transformacji przemysłu chemicznego w kierunku zrównoważonych technologii i poszukiwania nowych, wysoce selektywnych, aktywnych i stabilnych układów katalitycznych dla procesów z sektora lekkiej syntezy organicznej, w ramach pracy doktorskiej zaprezentowałam nowe układy katalityczne (Tabela 1), które zostały wykorzystane w modelowych procesach syntezy związków z grupy *fine chemicals.*

Tabela 1. Nowe układy katalityczne opracowane w ramach pracy doktorskiej zastosowane w wybranych procesach chemicznych.

Lp.	Katalizator (skrót)	Reakcja modelowa	System
1	Katalizator typu SILLP oparty o trifloglinianową ciecz jonową oraz krzemionkę (SILLP(1)/[tespmim][OTf-Al(OTf)$_3$])[35]	Cykloaddycja Dielsa-Aldera	Okresowy oraz ciągły
2	Biokatalizator typu SILLP oparty o lipazę z *Aspergillus oryzae* oraz materiały krzemionkowe (SiO_2/Mg(1:1)/[tespmim][NTf_2]/LAO)[36]	Rozdział kinetyczny racematu ibuprofenu	Okresowy
3	Biokatalizator oparty o lipazę z *Aspergillus oryzae* oraz hybrydowy materiał krzemionkowy modyfikowany grupami alkilowymi (MgO-SiO_2-C8-LAO)[37]	Estryfikacja alkoholu furfurylowego i wyższych kwasów tłuszczowych	Okresowy oraz ciągły

Zaprojektowane przeze mnie katalizatory heterogeniczne oparte są o fazy aktywne składające się z kwasowych cieczy jonowych typu Lewisa lub lipaz oraz ich nośniki w postaci materiałów krzemionkowych. Ich potencjał katalityczny został zaprezentowany zarówno w układach reakcyjnych ciągłych jak i okresowych.

W szczególności w ramach niniejszej pracy doktorskiej opracowałam następujące układy katalityczne (Tabela 1):

- katalizator typu SILLP oparty o imidazoliową trifloglinianową ciecz jonową oraz mezoporowatą krzemionkę o hierarchicznej strukturze porów zastosowany w cykloaddycji Dielsa-Aldera bezwodnika maleinowego i innych dienów w układzie okresowym oraz ciągłym,[35]
- biokatalizator typu SILLP oparty o lipazę z *Aspergillus oryzae* oraz hybrydowe materiały krzemionkowe zastosowany w rozdziale kinetycznym racematu ibuprofenu poprzez enancjoselektywną estryfikację w układzie okresowym,[36]
- biokatalizator oparty o lipazę z *Aspergillus oryzae* oraz hybrydowy materiał krzemionkowy modyfikowany grupami oktylowymi zastosowany w estryfikacji alkoholu furfurylowego i wyższych kwasów tłuszczowych w układzie okresowym oraz ciągłym.[37]

W wyniku realizacji pracy doktorskiej powstały dwie prace przeglądowe,[14,33] komentarz naukowy[34] (opisane powyżej) oraz 3 publikacje opisujące wyniki badań.[35-37] Poniżej zostaną przedstawione najważniejsze osiągnięcia uzyskane w ramach publikacji wyników badań. Szczegółowe informacje znajdują się w załączonych do przewodnika publikacjach.

II OMÓWIENIE WYNIKÓW

1. Synteza, charakterystyka oraz zastosowanie katalizatora typu SILLP opartego o trifloglinianową ciecz jonową i krzemionkę o multimodalnej porowatości w reakcji Dielsa-Aldera w systemie okresowym oraz ciągłym.

Wprowadzenie metalu (np. Al, Fe, Sn, In) do struktury cieczy jonowej zapobiega jego wymywaniu się podczas procesu, dzięki czemu otrzymywane są produkty o wysokiej czystości, co jest istotnym aspektem w szczególności w syntezie farmaceutyków. Dotychczas stosowane i szeroko opisane w literaturze chlorometaliczne ciecze jonowe wykazywały niską stabilność hydrolityczną.[14,38,39] Poszukiwania stabilniejszych ILs na bazie metali doprowadziły do opracowania trifloglinianowych odpowiedników chlorometalicznych ILs.[37,38]

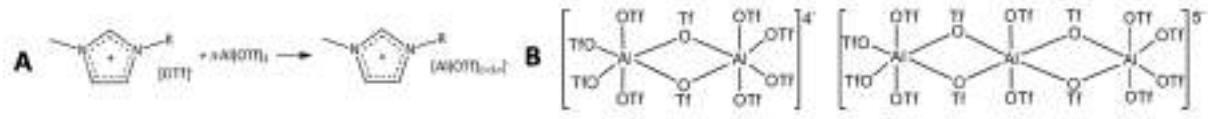

Rysunek 9. Schemat syntezy imidazoliowej trifloglinianowej cieczy jonowej (A). Prawdopodobne struktury anionów występujące w trifloglinianowej cieczy jonowej, blisko maksymalnego stężenia of $Al(OTf)_3$: $[Al_2(OTf)_{10}]^{4-}$ and $[Al_3(OTf)_{14}]^{5-}$ (B).

Trifloglinianowe ILs otrzymuje się w reakcji kompleksowania triflanu glinu i triflanowej imidazoliowej cieczy jonowej, np. triflanu1-etylo-3-metyloimidazoliowyego w 85 °C, przy ułamku molowym triflanu glinu w cieczy jonowej $\chi Al(OTf)_3$ wynoszącym 0,15 lub 0,25 (Rysunek 9A). Wcześniejsze badania prowadzone w naszej grupie wykazały, że trifloglinianowe ILs składają się z sześciokrotnie skoordynowanego atomu glinu w wielokrotnie naładowanych, oligonuklearnych kompleksach anionowych, wykazujących różne sposoby mostkowania anionu triflanowego (Rysunek 9B). Kwasowość Lewisa trifloglinianowych IL została zmierzona za pomocą wyznaczenia liczby akceptorowej Gutmanna (AN), która klasyfikuje je jako kwasy Lewisa o średniej mocy (AN = ok. 65).[40]

Trifloglinianowe ILs zostały już wykorzystane w katalizie, w szczególności ich fizycznie immobilizowane na wielościennych nanorurkach węglowych formy zostały użyte w syntezie chromanów otrzymując wysokie wartości konwersji 2,4-dimetylofenolu (99%) oraz selektywności do 2,2-dimetylo-2,4-dimetylochromanu (84%).[40] Ten sam układ katalityczny wykorzystano do produkcji lewulinianu butylu z laktonu α-angelika obserwując pełne

przereagowanie surowca oraz 100% selektywności otrzymywania estru.[41] W poprzednich badaniach prowadzonych z moim udziałem, triflogliniановa IL została unieruchomiona za pomocą wiązań kowalencyjnych na powierzchni krzemionki oraz hybrydowych materiałów krzemionkowych ($CaO\text{-}SiO_2$, $MgO\text{-}SiO_2$) i zastosowana w aminolizie epoksydów w systemie okresowym oraz ciągłym. W obecności katalizatora SILLP opartego na $MgO\text{-}SiO_2$ osiągnięto 81,1% przereagowania tlenku styrenu z selektywnością do 2-anilino-1-fenyloetanolu wynoszącą 95,9% w ciągu 72 h w układzie przepływowym.[42]

Celem niniejszych badań było opracowanie optymalnej metody chemicznej immobilizacji imidazoliowych triflogliniановych ILs na powierzchni krzemionki dla uzyskania stabilnego układu katalitycznego o dużym potencjale aplikacyjnym.

1.1. Synteza i charakterystyka katalizatora typu SILLP opartego o imidazoliową triflogliniановą ciecz jonową i krzemionkę o multimodalnej porowatości.

We wcześniejszych doniesieniach literaturowych zauważono, że podczas unieruchamiania chlorogliniановych ILs za pomocą grup trietoksysililowych zlokalizowanych w kationie i następczego kompleksowania anionu już na powierzchni nośnika poprzez dodawanie chlorku glinu, jako ubocznie mogą tworzyć się wiązania między glinem a tlenem znajdującym się na powierzchni krzemionki i wewnątrz jej porów. Prowadzi to do bezpośredniego przywiązania $AlCl_3$ do powierzchni krzemionki, co obniża aktywność powstałego katalizatora.[11,14]

W związku z powyższym głównym celem tej części badań w ramach pracy doktorskiej było ustalenie optymalnej kolejności etapów stosowanych w syntezie układów typu SILLP z wykorzystaniem triflogliniановych cieczy jonowych (Schemat 1).

Do badań wybrałam krzemionkę o multimodalnej hierarchicznej strukturze porów z makroporami, małymi mezoporami o średnicy 4 nm i większymi o rozmiarze 36 nm oraz powierzchni właściwej równej 284,2 m^2g^{-1}. Wybór tego typu materiału był uzasadniony jego dobrze rozwiniętą powierzchnią właściwą zapewniającą efektywną immobilizację triflogliniановych ILs. Dodatkowo wysoce rozbudowana porowatość multimodalnej krzemionki usprawnia transport masy podczas katalizy oraz intensyfikuje mieszanie i przepływ reagentów przez materiał poprawiając właściwości katalityczne w systemie przepływowym. Krzemionka do prowadzonych przeze mnie badań została zsyntezowana przez Panią dr hab. inż. Katarzynę Szymańską, prof. Politechniki Śląskiej.

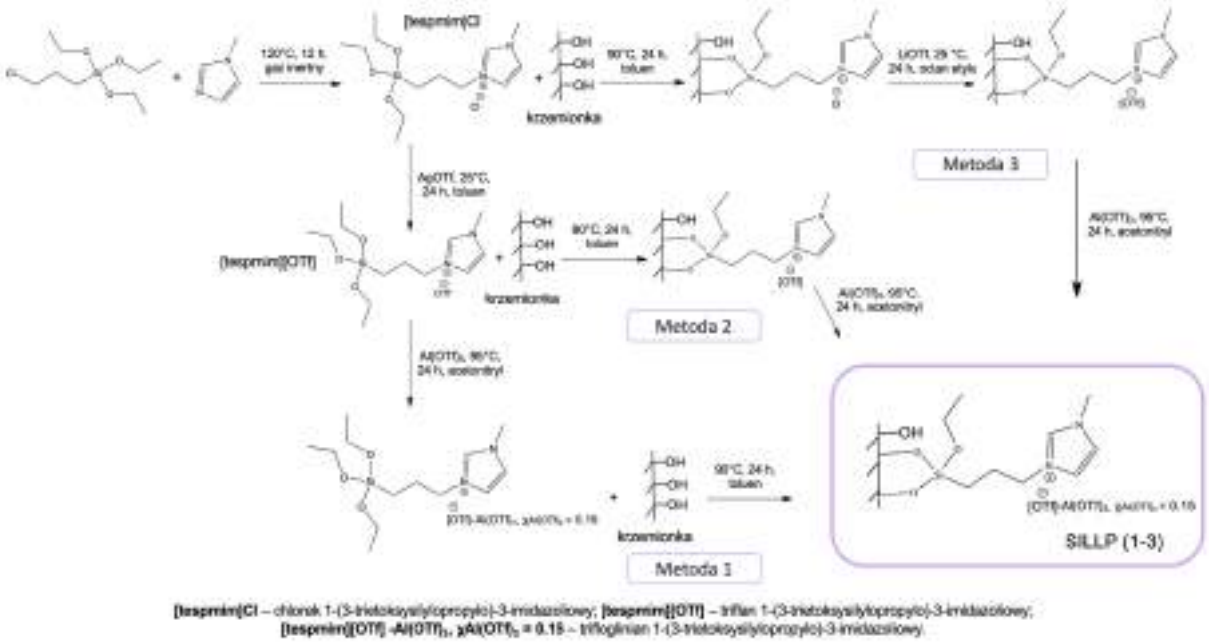

Schemat 1. Synteza katalizatorów typu SILLP (1–3) za pomocą trzech różnych ścieżek.

W każdej wybranej przeze mnie ścieżce (Metoda 1-3) otrzymywania katalizatora (SILP 1-3) wykorzystałam jako pierwszy etap syntezę [tespmim]Cl w celu wprowadzenia grupy trietoksysililowej do struktury cieczy jonowej pełniącej funkcję łącznika z grupami hydroksylowymi na powierzchni krzemionki. Dla wszystkich metod zastosowałam ciecz jonową zawierającą odpowiednią ilość triflanu glinu, $\chi Al(OTf)_3 = 0{,}15$ (ułamek molowy $Al(OTf)_3$ użyty do kompleksowania anionu $[OTf]^-$), aby zaprojektować katalizator o średniej sile kwasowości Lewisa. Zawartość przywiązanej IL oraz $Al(OTf)_3$ do materiału krzemionkowego została oznaczona za pomocą analizy termograwimetrycznej (TGA).

Pierwsza metoda (Metoda 1) syntezy SILLP (1) polega na tym, że w pierwszym kroku sytezuje się trifloglinianową ciecz jonową ([tespmim][OTf-$Al(OTf)_3$], $\chi Al(OTf)_3 = 0{,}15$), poprzez wymianę anionu [tespmim]Cl z triflanem srebra (1:1, n/n), reakcję kompleksowania z triflanem glinu ($\chi Al(OTf)_3 = 0{,}15$) w temperaturze 95 °C. W następnym kropku- następuje chemiczna immobilizacja IL na powierzchni krzemionki w toluenie w temperaturze 90 °C (zawartość IL 25,3 wt%). Następne podejście (**Metoda 2** do syntezy SILLP (2)) zakłada najpierw syntezę [tespmim][OTf], następnie chemiczną immobilizację cieczy jonowej na powierzchni krzemionki (zawartość IL 19,2 wt%) i kolejno kompleksowanie anionu poprzez dodanie triflanu glinu ($\chi Al(OTf)_3 = 0{,}15$) w acetonitrylu w temperaturze 95 °C (zawartość IL 19,2 wt%). **Metoda 3** syntezy SILLP (3) polega na bezpośrednim przywiązaniu [tespmim]Cl do powierzchni krzemionki

(zawartość IL 19,7 wt%), następnie wymianie anionu chlorkowego na triflanowy poprzez działanie LiOTf w octanie etylu (zawartość IL 19,7 wt%), kończąc na kompleksowaniu z triflanem glinu ($\chi Al(OTf)_3$ = 0,15) w acetonitrylu w temperaturze 95 °C (zawartość IL 19,7 wt%). Wszystkie trzy metody prowadziły do otrzymania materiałów SILLP o właściwościach katalitycznych. Dla dalszych celów porównawczych zsyntezowałam również triflan glinu przewiązany do krzemionki (SiO_2-$Al(OTf)_3$) poprzez rozpuszczenie w acetonitrylu i mieszanie w temperaturze 90 °C (zawartość $Al(OTf)_3$ 36,5 wt%) z następczym sączeniem. W Tabeli 1 przedstawiono charakterystykę zsyntezowanych materiałów.

Tabela 2. Charakterystyka zsyntezowanych materiałów typu SILLP i krzemionki o multimodalnej porowatości.

Materiał	S_{BET}, (m^2g^{-1})	V_p, (cm^3g^{-1})	d_p, (nm)	IL zawartość, (wt% ±0.3)[a]	Al stężenie (zmierzone) (mgL^{-1} ±2%) [b]	Al stężenie (teoretyczne) (mgL^{-1})
SiO_2	284,2	1,12	36	-	-	-
SILLP (1)	92,9	0,55	28	25,3	1,14	1,18
SILLP (2)	113,7	0,59	28	19,2	1,70	1,79
SILLP (3)	109,7	0,61	28	19,7	1,74	1,83

[a]analizowane za pomocą TGA, odchylenie standardowe z 3 prób; [b]analizowane za pomocą ICP, odchylenie standardowe z 3 prób.

W celu dokonania pełnej charakterystyki otrzymanych materiałów typu SILLP zostały przeprowadzone następujące analizy: analiza termograwimetryczna, analiza atomowej spektrometrii emisyjnej (ICP), analiza adsorpcji – desorpcji metodami Barrett-Joyner-Halenda (BJH) i Brunauer-Emmett-Tellera (BET), analiza skaningowej mikroskopii elektronowej (SEM) sprzężonej z spektrometrią dyspersji energii promieniowania rentgenowskiego (EDX) oraz analiza spektroskopii magnetycznego rezonansu jądrowego ciała stałego krzemu (^{29}Si MAS NMR). Zawartość [tespmim][OTf-$Al(OTf)_3$], $\chi Al(OTf)_3$ = 0,15 unieruchomionej na krzemionce o multimodalnej porowatości została zmierzona za pomocą TGA (Tabela 2). Najwyższą zawartość IL uzyskano dla SILLP (1) wynoszącą 25,3 wt%, podczas gdy dla SILLP (2) i SILLP (3) wartości wynosiły odpowiednio 19,7 wt% i 19,2 wt%. Analiza ICP również potwierdziła wysoką efektywność kompleksowania triflanu glinu z anionem IL niezależnie od stosowanej metody syntezy SILLP (Tabela 2). Mniejsze zawartości IL w przypadku SILLP (2–3) mogą sugerować mniejsze powinowactwo konkretnych cieczy jonowych (w zależności od budowy anionu, Cl^- lub $[OTf]^-$) do powierzchni krzemionki, co utrudniło ich immobilizację.

Po unieruchomieniu IL na powierzchni krzemionki zaobserwowałam obniżenie powierzchni właściwej BET we wszystkich materiałach SILLP, co potwierdza obecność IL na powierzchni nośnika (Tabela 2). Modyfikacja krzemionki o multimodalnej porowatości cieczą jonową doprowadziła do zmniejszenia rozmiaru i objętości porów, co potwierdziłam za pomocą analizy BJH. Krzemionka wykazuje małe mezopory (4 nm), większe mezopory (36 nm) zgodnie z diagramem rozkładu wielkości porów oraz makropory widoczne na obrazach SEM. W przypadku materiałów SILLP (1–3) widoczne są większe mezopory wraz z makroporami. Izotermy adsorpcji-desorpcji dla krzemionki i SILLP (1–3) wykazują podobny charakter typu IV, typowy dla materiałów mezoporowatych, co stanowi dowód na zachowanie charakterystyki materiału pomimo modyfikacji. Dobrze rozwinięta porowatość SILLP (1–3) jest wyraźnie widoczna na obrazach SEM, uzupełnionych analizami EDX, które pokazują obecność nowych pierwiastków, takich jak Al, C, N, S, na powierzchni materiału.

Chemiczne przywiązanie [tespmim][OTf-Al(OTf)$_3$], χAl(OTf)$_3$ = 0,15 do powierzchni krzemionki zostało potwierdzone za pomocą ^{29}Si MAS NMR. Widma MAS NMR wskazują na zanik sygnałów pochodzących od grup (SiO)$_2$Si-(OH)$_2$ i (SiO)$_3$Si-OH oraz pojawienie się nowego sygnału przy –66 ppm.

1.2. Badanie wpływu wybranych parametrów na przebieg reakcji Dielsa-Aldera w obecności katalizatora typu SILLP w układzie okresowym.

Aktywność katalityczna heterogenicznych materiałów typu SILLP (1–3) została przeze mnie przetestowana w modelowej reakcji Dielsa-Aldera pomiędzy bezwodnikiem maleinowym (MA) a izoprenem (Schemat 2). Cykloaddukty powstające podczas reakcji Dielsa-Aldera są głównie wykorzystywane jako półprodukty w produkcji farmaceutyków, agrochemikaliów, aromatów, zapachów, surfaktantów lub polimerów pochodzenia biologicznego.[43,44] Reakcja Dielsa-Aldera jest zazwyczaj przeprowadzana przy użyciu szkodliwych rozpuszczalników organicznych i często wymaga długich czasów reakcji oraz podwyższonego ciśnienia.[45-47]

Stosując wszystkie typy katalizatorów SILLP 1–3 uzyskałam bardzo wysokie wartości konwersji MA wynoszące 97,5% po 180 min ze 100% selektywnością do cykloadduktu (Tabela 3). Aktywność katalityczna tych związków nie różniła się od aktywności wolnej immobilizowanej cieczy jonowej. Dodatkowo w porównaniu do triflanu glinu oraz immobilizowanego triflanu glinu, opracowane katalizatory wykazywały wyższą aktywność w badanym procesie. Wyższa zawartość fazy aktywnej na krzemionce o multimodalnej porowatości (36,5 wt%) spowodowała

pogorszenie przepływu wolnych reagentów przez materiał, a w konsekwencji do spadku wydajności katalitycznej SiO_2-$Al(OTf)_3$.

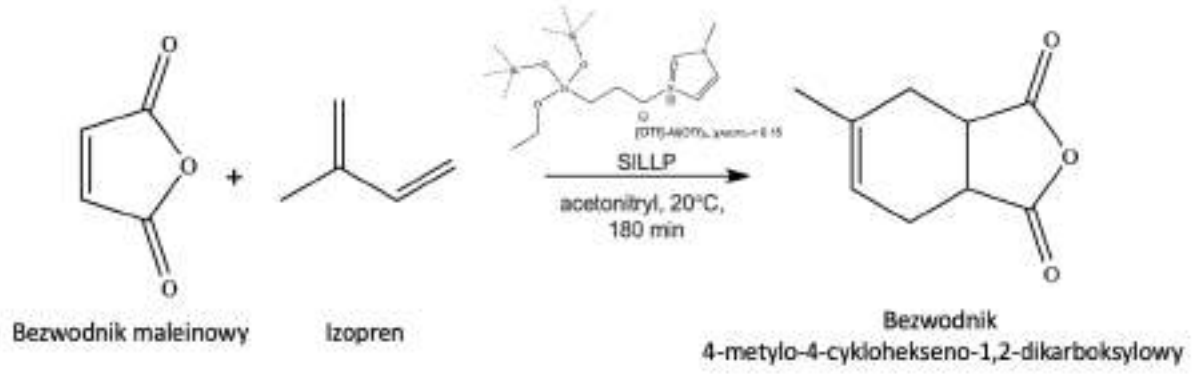

Schemat 2. Schemat reakcji modelowej Dielsa-Aldera zachodzącej w obecności opracowanego katalizatora typu SILLP.

Tabela 3. Wpływ struktury katalizatorów opartych na $Al(OTf)_3$ na aktywność katalityczną w reakcji modelowej Dielsa-Aldera.

Katalizator	Czas (min)	Konwersja MA (%)
SILLP (1)	180	97,45
SILLP (2)	180	97,31
SILLP (3)	180	97,45
SiO_2-$Al(OTf)_3$	240	91,17
[tespmim][OTf-$Al(OTf)_3$)]	180	95,57
$Al(OTf)_3$	240	84,01

Warunki reakcji: izopren 3 mmol, MA 2 mmol, acetonitryl 0,5 mL, katalizator SILLP (1–3), SiO_2-$Al(OTf)_3$, $Al(OTf)_3$ lub [tespmim][OTf-$Al(OTf)_3$)] 0,1 mol% $Al(OTf)_3$ względem MA, 20 °C. Konwersję MA analizowałam za pomocą chromatografii gazowej GC.

Biorąc pod uwagę brak różnic w aktywności katalitycznej pomiędzy otrzymanymi materiałami SILLP (1–3) na tym etapie badań, wybrałam SILLP (1) do dalszej optymalizacji warunków reakcji. Zastosowanie wyższej temperatury (40 °C) doprowadziło do niemal pełnej konwersji (97,8%) MA po 120 min, natomiast zaobserwowałam pojawienie się ciemnej barwy w mieszaninie reakcyjnej, prawdopodobnie wynikającej z częściowej polimeryzacji nadmiarowego izoprenu. Badania doboru rozpuszczalnika koniecznego do rozpuszczenia stałego bezwodnika maleinowego obejmowały zastosowanie: acetonitrylu, dichlorometanu i octanu etylu, gdyż MA nie rozpuszcza się w toluenie, heksanie, cykloheksanie, izopropanolu i eterze dietylowym. Podobne stopnie przereagowania MA uzyskano przy użyciu acetonitrylu i dichlorometanu (97,5% po 180 min), a dla octanu etylu konwersja MA wyniosła 89,4% po

180 min. Ze względu na konieczność eliminacji chlorowanych rozpuszczalników w trakcie projektowania zielonych technologii do dalszych badań używałam acetonitrylu. Badania nad wpływem ilości rozpuszczalnika na konwersję MA wykazały, że 0,5 ml acetonitrylu jest optymalną ilością stosowaną na 2 mmol bezwodnika maleinowego (4 $mmolmL^{-3}$). Mniejsze ilości utrudniały efektywne mieszanie reagentów ze względu na dużą objętość katalizatora. Następnie określiłam wpływ stosunku molowego MA do izoprenu na jego konwersję. Najkorzystniejszy wynik uzyskałam przy stosunku molowym 1:1,5 MA: izopren. Dalsze zwiększenie ilości izoprenu nie wpływało na zwiększenie stopnia konwersji MA. Finalnie zbadałam wpływ ilości katalizatora na przebieg reakcji modelowej. Otrzymane wyniki wskazały, że zastosowanie 0,1 mol% $Al(OTf)_3$ na 2 mmol MA wystarcza do osiągnięcia 97,5% przereagowania MA w 180 min. Mniejsze ilości nie były wystarczające, aby uzyskać prawie pełną konwersję substratu.

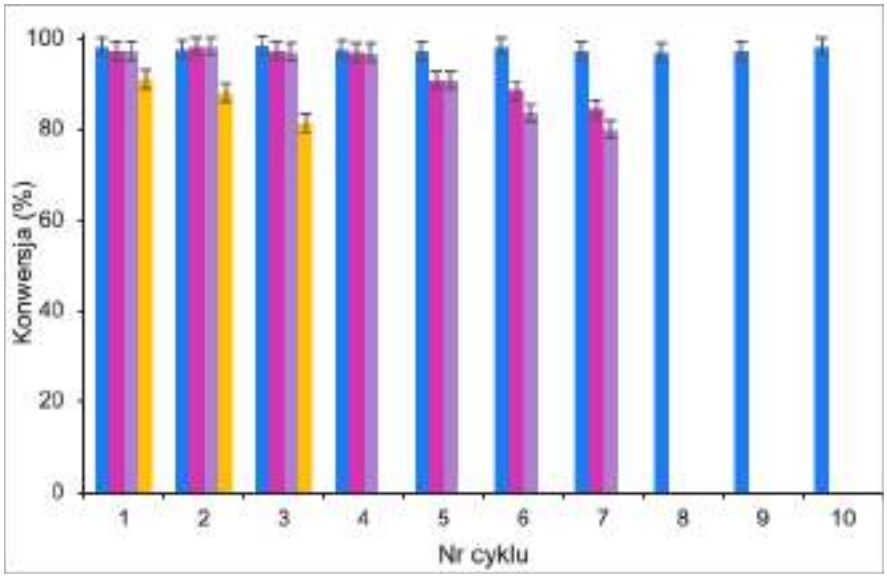

Wykres 1. Badanie zawrotu katalizatorów SILLP (1–3) oraz SiO_2-$Al(OTf)_3$ w reakcji modelowej Dielsa-Aldera (SILLP (1) – niebieski; SILLP (2) – różowy; SILLP (3) – fioletowy; SiO_2-$Al(OTf)_3$ – żółty). Warunki reakcji: izopren 3 mmol, MA 2 mmol, acetonitryl 0,5 mL, katalizator SILLP (1–3) lub SiO_2-$Al(OTf)_3$ 0,1 mol% $Al(OTf)_3$ względem MA, 20 °C, czas procesu 180 min. Konwersję MA analizowałam za pomocą GC.

Kolejnym krokiem było wykazanie stabilności otrzymanych katalizatorów SILLP w 10 kolejnych cyklach reakcji Dielsa-Aldera w opracowanych warunkach. Po każdym zakończonym cyklu katalizator był odfiltrowywany, przemywany acetonitrylem, suszony na linii Schlenka i wykorzystywany ponownie. Tym razem różnice w aktywności katalitycznej były wyraźne, co pokazało znaczenie kolejności etapów modyfikacji powierzchni krzemionki trifloglinianową

cieczą jonową (Wykres 1). Najwyższą stabilność wykazał materiał SILLP (1), który utrzymywał aktywność we wszystkich badanych cyklach. SILLP (2) i SILLP (3) zaczęły tracić aktywność w piątym cyklu reakcji, a konwersja MA po 180 min spadła odpowiednio do 91,1% i 90,9%. Warto podkreślić, że oba materiały zostały zsyntezowane z kompleksowaniem triflanu glinu po immobilizacji IL ([tespmim][OTf] dla SILLP (2) lub [tespmim]Cl dla SILLP (3)) na powierzchni krzemionki. Może to wskazywać, że niektóre cząsteczki triflanu glinu zostały unieruchomione bezpośrednio na powierzchni krzemionki i częściowo reakcja kompleksowania nie miała miejsca, bądź niektóre fragmenty [tespmim][OTf]-$Al(OTf)_3$, $\chi Al(OTf)_3$ = 0.15 zostały wymyte z matrycy nośnika (zawartość IL wyniosła 10,8 wt% dla SILLP (2) i 9,2 wt% dla SILLP (3) po czwartym cyklu). Katalizator SILLP (1) zachował prawie taką samą ilość IL (25,1 wt%) jak przed recyklem (25,3 wt%). Przeprowadzone przez mnie badania zawrotu katalizatorów wykazały także, że wprowadzenie triflanu glinu do struktury cieczy jonowej zwiększa jego stabilność i zapobiega wymywaniu z materiału. Potwierdziły to próby zawrotu SiO_2-$Al(OTf)_3$, gdzie triflan glinu jest bezpośrednio związany z powierzchnią. Dla tego katalizatora konwersja MA wyniosła jedynie 82% po 180 min w trzecim cyklu reakcyjnym.

Podsumowując, najbardziej stabilnym układem katalitycznym był SILLP (1) otrzymany w następującej sekwencji reakcji: synteza trifloglinianowej cieczy jonowej, a następnie jej chemiczne związanie z powierzchnią krzemionki.

Ważnym aspektem w trakcie opracowywania technologii jest również uniwersalność badanego układu katalitycznego. Przeprowadziłam szereg reakcji cykloaddycji z zastosowaniem różnych dienów (np. izopren, cyklopentadien, β-myrcen, ocimen) i dienofili (np. bezwodnik maleinowy, akrylan metylu, akrylan etylu) w obecności katalizatora SILLP (1). Uzyskano całkowite konwersje w czasie 1–300 min w temperaturze 20 °C, gdzie konwersja badanych substratów mieściła się w zakresie 80,2–98,7 %.

1.3. Transformacja procesu Dielsa-Aldera przebiegającego w obecności katalizatora typu SILLP z systemu okresowego na ciągły.

Na podstawie obiecujących wyników uzyskanych w układzie okresowym opracowany katalizator trifloglinianowy SILLP (1) został przetestowany w trybie ciągłym. Eksperymenty przeprowadzałam w pełni zautomatyzowanym kolumnowym reaktorze przepływowym Syrris Asia, wyposażonym w dwie pompy. Pompa A pompowała roztwór bezwodnika maleinowego w acetonitrylu, podczas gdy pompa B – izopren. Strumienie reagentów były łączone w standardowym mikserze typu T, a następnie były kierowane do reaktora kolumnowego wypełnionego 0,3 g materiału SILLP (1) (Wykres 2).

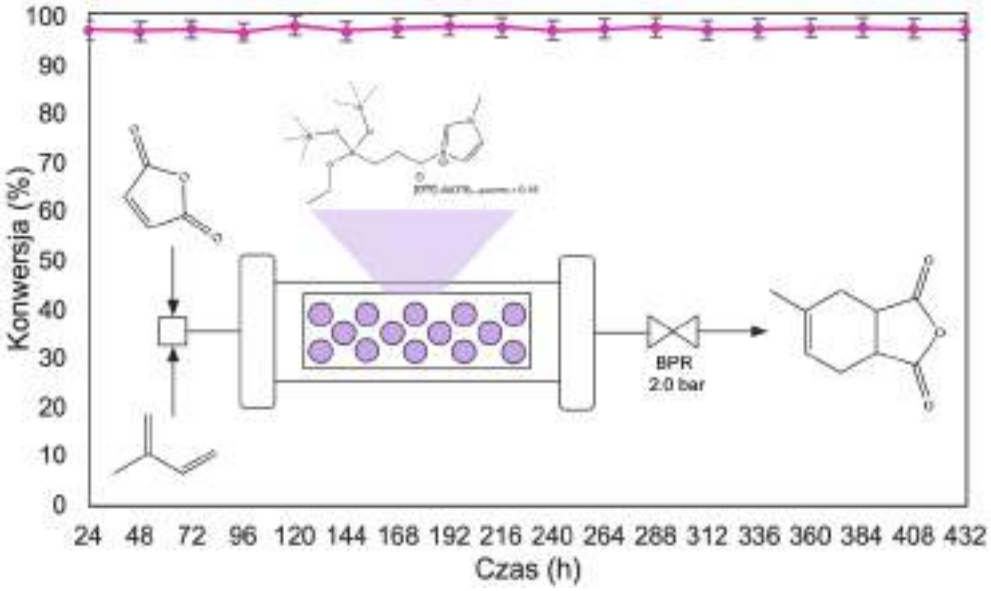

Wykres 2. Stabilność katalityczna SILLP (1) w cykloaddycji Dielsa-Aldera między MA a izoprenem w systemie przepływowym. Warunki reakcji: izopren 0,007 $mLmin^{-1}$, MA 0,023 $mLmin^{-1}$ (2 M w acetonitrylu), katalizator SILLP (1) 0,3 g, 20 °C. Konwersję MA analizowałam za pomocą GC.

Wpływ molowego stosunku substratów na konwersję MA badałam w zakresie od 1:1 do 1:2,5 (MA : izopren) dla całkowitego przepływu reagentów wynoszącego 0,06 $mLmin^{-1}$. Konwersja bezwodnika maleinowego rosła wraz z nadmiarem izoprenu aż do osiągnięcia optymalnego stosunku molowego 1:1,5 MA do izoprenu. Dalsze zwiększanie stosunku molowego substratów nie prowadziło do wyższej konwersji MA. Wszystkie badania optymalizacyjne prowadziłam przez 48 h, a ustalenie stanu stacjonarnego następowało w bardzo krótkim czasie).

Wpływ czasu przebywania na konwersję MA określiłam dla stosunku molowego 1:1,5 MA do izoprenu przy całkowitym przepływie od 0,03 do 0,06 $mLmin^{-1}$. Wydłużenie czasu przebywania z 18,3 do 36,7 min skutkowało wyższą wydajnością katalizatora, a konwersja substratu wzrosła z około 78% do 97%. Bezpośrednie porównanie czasów przebywania dla systemów okresowego i przepływowego wykazało lepszą efektywność syntezy w przepływie. We wszystkich przeprowadzonych eksperymentach w systemie ciągłym zaobserwowałam stabilną aktywność katalityczną co najmniej przez 48 h trwania procesu.

Wyjątkowa stabilność trifloglinaniowego materiału SILLP (1) w testach okresowych i przepływowych skłoniła do badań nad długoterminową stabilnością katalizatora. Eksperyment przeprowadziłam w wyznaczonych korzystnych warunkach, przy stosunku molowym 1:1,5 MA do izoprenu, przy całkowitym przepływie 0,06 $mLmin^{-1}$ w temperaturze 20 °C (Rysunek 7). Opracowany katalizator SILLP (1) wykazał niezwykle stabilną aktywność, osiągając 97% konwersji MA przez 432 h z TOF (z ang. *Turnover Frequency*) wynoszącym 104,3 h^{-1}. Wyjątkowa aktywność katalizatora SILLP (1) w warunkach przepływowych może być wyjaśniona zastosowaniem krzemionki o multimodalnej porowatości jako nośnika dla IL. Wysoka porowatość krzemionki intensyfikowała mieszanie reagentów i przepływ przez materiał, poprawiając właściwości katalityczne.

Podsumowując, w przedstawionych badaniach wykazałam, że kolejność wprowadzania fazy aktywnej na powierzchnię nośnika ma kluczowe znaczenie. W ramach badań przeprowadziłam optymalizację syntezy katalizatora typu SILLP opartego o imidazoliową trifloglinianową IL oraz krzemionkę o multimodalnej porowatości, co umożliwiło otrzymanie wysoce aktywnego i stabilnego katalizatora. Metoda zakładająca początkową syntezę trifloglinianowej cieczy jonowej, a następnie jej związanie z powierzchnią krzemionki (zawartość IL 25,3 wt%) pozwoliła na otrzymanie katalizatora, dla którego zaobserwowałam konwersję MA wynoszącą 97% w dziesięciu cyklach reakcyjnych. Transformacja modelowej reakcji Dielsa-Aldera na tryb ciągły doprowadziła do 97% konwersji MA przez 432 h (TOF 104,3 h^{-1}). W tej pracy, dzięki dokładnemu przeanalizowaniu syntezy trifloglinianowych materiałów SILLP osiągnięto wysoce wydajny i stabilny katalizator, który umożliwił opracowanie technologii syntezy cykloadduktów Dielsa-Aldera w systemie okresowym oraz ciągłym.

2. Synteza, charakterystyka oraz zastosowanie biokatalizatora typu SILLP opartego o lipazę z *Aspergillus oryzae* oraz hybrydowy materiał krzemionkowy modyfikowany imidazoliową ciecz jonową w rozdziale kinetycznym racematu ibuprofenu w systemie okresowym.

Projektowanie nośników do immobilizacji lipaz, które zwiększają ich stabilność i aktywność w procesie, stanowi obecnie kluczowy obszar badań. Unieruchomienie białka na stałej matrycy nie tylko poprawia jego właściwości, ale także umożliwia łatwą separację z mieszaniny reakcyjnej oraz ponowne wykorzystanie w kolejnych cyklach reakcji, co jest istotnym aspektem podczas syntezy farmaceutyków, których wysoka czystość jest szczególnie pożądana.[1] Wiele z nich należy do związków chiralnych, a ich przemysłowa produkcja początkowo prowadzi często do powstania racematów, czyli mieszaniny równych ilości molowych obu enancjomerów. W większości przypadków dwa enancjomery tego samego związku różnią się od siebie pod względem efektów terapeutycznych i toksykologii. Z tego względu enancjoselektywna konwersja chiralnych farmaceutyków jest przedmiotem istotnego zainteresowania środowiska naukowego.

Ibuprofen, lek przeciwbólowy i przeciwgorączkowy, jest jednym z najbardziej powszechnie stosowanych chiralnych farmaceutyków. Dwa enancjomery ibuprofenu, *(R)-(-)*-ibuprofen i *(S)-(+)*-ibuprofen, wykazują znacznie różniące się właściwości farmakologiczne i profile metaboliczne. Enancjomer *(S)-(+)*-ibuprofenu ma pożądane działanie farmakologiczne i jest zdolny do inhibicji cyklooksygenazy (COX), podczas gdy *(R)-(-)*-ibuprofen nie jest inhibitorem COX i odpowiada za intensyfikację procesu zapalnego. Enancjomer *(S)-(+)*-ibuprofenu jest 160 razy bardziej aktywny terapeutycznie niż *(R)-(-)*-ibuprofen, a dodatkowo *(R)-(-)*-ibuprofen może powodować potencjalne skutki uboczne.[48,49]

Rozdział mieszaniny racemicznej ibuprofenu może być osiągnięty w rozdziale kinetycznym poprzez enzymatyczną estryfikację, wysokosprawną chromatografię cieczową lub krystalizację diastereoizomeryczną. Rozdział kinetyczny racematu ibuprofenu poprzez estryfikację polega na wykorzystaniu różnic w szybkości reakcji enancjomerów z alkoholem w obecności enancjoselektywnego biokatalizatora. W zależności od rodzaju lipazy może ona konwertować *(R)-(-)*-ibuprofen do *(R)-(-)*-estru ibuprofenu lub *(S)-(+)*-ibuprofen do *(S)-(+)*-estru ibuprofenu. Najważniejszymi parametrami procesu jest wysoki nadmiar enancjomeryczny

(z ang. *enantiomeric excess*, *ee*) oraz konwersja wynosząca maksymalnie 50% (przy ee = 100%).[50]

W wielu doniesieniach literaturowych *ee* czystego estru ibuprofenu osiągany był na poziomie znacznie poniżej 50% przy uzyskaniu wysokich wartościach konwersji, podczas gdy pozostałe badania przedstawiały jedynie średnie wartości *ee*, do 90% przy niskiej konwersji enancjomeru ibuprofenu.[51,52] Tylko trzy prace opisują zarówno wysoką konwersję jak i nadmiar enancjomeryczny. W jednaj z nich uzyskano niemal całkowitą konwersję *(S)-(+)*-ibuprofenu (49,8%) z wysokim nadmiarem enancjomerycznym do *(S)-(+)*-enancjomeru estru ibuprofenu (97,3%) przy użyciu lipazy z *Candida rugosa* w postaci mikrokryształów jako katalizatora. Podane wyniki otrzymano po 8 h trwania procesu prowadzonego w izooktanie z użyciem 1-izooktanolu.[53] W innym doniesieniu literaturowym immobilizowana na krzemionce lipaza z *Candida rugosa* umożliwiła uzyskanie 45% konwersji *(S)-(+)*-ibuprofenu do estru 1-propylowego (*ee* = 96%) w 37 °C po 50 min.[54] Interesujące wyniki otrzymano również w obecności esterazy (EST10) z *Thermotoga maritima* stabilizowanej w cieczy jonowej o anionie $[BF_4]^-$. Ester etylowy *(S)-(+)*-ibuprofenu został otrzymany z konwersją wynoszącą 47,4% i ee równym 96,6% w 75 °C po 10 h trwania procesu.[55]

Aktywacja lipaz podczas procesu zachodzi na granicy faz-olej woda, dlatego kluczowe jest zaprojektowanie nośnika o charakterze hydrofobowym w celu utrzymania aktywnej konformacji biokatalizatora. Zastosowanie nośnika typu SILLP opartego o hydrofobową ciecz jonową zapewnia efektywną immobilizację białka, stabilne i wysoce aktywne działanie enzymu podczas reakcji oraz umożliwia łatwe wydzielenie białka z mieszaniny poreakcyjnej. Dodatkowo wprowadzenie jonów metali (np. Mg^{2+}, Ca^{2+}, K^+) do układu reakcyjnego często zwiększa aktywność lipaz.[56,57]

Celem niniejszych badań było opracowanie aktywnego układu biokatalitycznego opartego o lipazę z *Aspergillus oryzae* (LAO) i krzemionkowych materiałów SILLP do efektywnego rozdziału kinetycznego racematu ibuprofenu w systemie okresowym.

2.1. Opracowanie i badanie wpływu wybranych parametrów na rozdział kinetyczny racematu ibuprofenu w obecności natywnej lipazy z *Aspergillus oryzae*.

W badaniach wstępnych przeprowadziłam optymalizację warunków prowadzenia reakcji estryfikacji racematu ibuprofenu z dwukrotnym nadmiarem molowym 1-propanolu jako modelowego alkoholu, używając izooktanu jako rozpuszczalnika w obecności komercyjnie dostępnego roztworu LAO (Schemat 3). Konwersja racematu ibuprofenu oraz nadmiar enancjomeryczny enancjomeru *(S)-(+)* lub *(R)-(-)* zostały określone za pomocą chiralnej wysokosprawnej chromatografii cieczowej (HPLC).

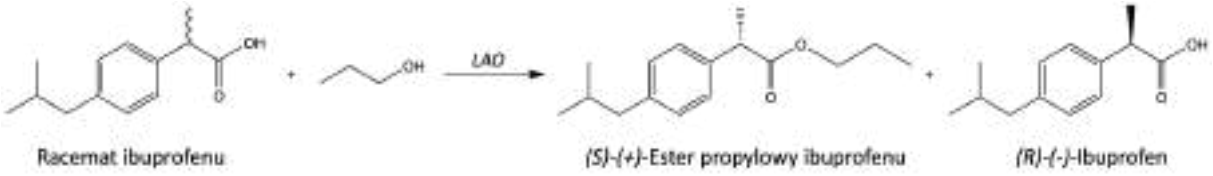

Schemat 3. Enancjoselektywna estryfikacja racematu ibuprofenu z 1-propanolem w izooktanie.

Badania rozpoczęłam od zbadania ilości LAO niezbędnej do konwersji racematu ibuprofenu do estru z wysoką konwersją i selektywnością. Zwiększenie ilości LAO z 0,50 do 1,0 mL spowodowało wzrost szybkości reakcji, natomiast konwersja *(S)-(+)*-ibuprofenu nie była pełna. Użycie 1,5 mL LAO umożliwiło przekształcenie racematu ibuprofenu z konwersją równą 34,8% (*ee* = 99,9%) po 24 h oraz przereagowaniem wynoszącym 45,2% (*ee* = 99,9%) po 48 h. Dalsze zwiększenie ilości LAO do 2,0 mL nie miało wpływu na wydajność i selektywność procesu. Dla porównania reakcję przeprowadziłam w tych samych warunkach przy użyciu lipazy B z *Candida antarctica* przy użyciu 1,5 mL enzymu, w wyniku czego uzyskano jedynie 11% konwersji substratu po 48 h (z 26,1% *ee* do estru *(R)-(-)*-ibuprofenu).

Następnie zbadałam wpływ temperatury w zakresie od 15 °C do 40 °C. Zaobserwowałam jedynie niewielki wzrost szybkości reakcji, a konwersja osiągnęła prawie 50% przy 40 °C, natomiast *ee* gwałtownie spadło do 82% z powodu postępującej dezaktywacji enzymu w wyższej temperaturze. Najbardziej korzystną temperaturą procesu jest 20 °C. Dalej sprawdziłam wpływ rozpuszczalnika na szybkość reakcji. Zadowalającą konwersję i *ee* (ok. 90%) uzyskano w takich rozpuszczalnikach jak heksan, cykloheksan i heptan. Dichloroetan, acetonitryl i węglan propylu miały negatywny wpływ na przebieg reakcji. Przetestowałam również dodatek hydrofobowej IL [bmim][NTf_2] (bis(trifluorometanosulfonylo)imidek 1-butylo-3-metyloimidazoliowy) do izooktanu, co doprowadziło do otrzymania obiecujących wyników

(konwersja 46,9% i 90,4% *ee* po 48 h). Podsumowując, najlepsze wyniki uzyskano w izooktanie (konwersja 45,2% i 99,9% *ee* po 48 h), gdzie system reakcyjny był dwufazowy. Górna faza składała się z rozpuszczalnika i reagentów, a LAO tworzyło drugą fazę. Dodatkowo, testy dotyczące ilości izooktanu użytego do reakcji wykazały, że im bardziej stężona mieszanina reakcyjna, tym niższa uzyskiwana enancjoselektywność.

Odpowiedni dobór alkoholu (C1–C4) ma znaczący wpływ na konwersję i enancjoselektywność reakcji estryfikacji. Zastosowanie 1-butanolu i 1-propanolu prowadziło do otrzymania konwersji oraz *ee* równych odpowiednio 45,4% (*ee* = 99,9%) i 45,2% (*ee* = 99,9%) po 48 h. Użycie metanolu lub etanolu do estryfikacji powoduje drastyczne obniżenie czystości produktu (*ee* poniżej 88% dla metanolu). Dłuższy łańcuch alkoholu, a co za tym idzie, zwiększona hydrofobowość substratu poprawia stabilność lipazy.

Na koniec zbadałam wpływ stosunku molowego ibuprofenu do 1-propanolu. Rozcieńczenie mieszaniny reakcyjnej alkoholem (1:4, *n:n*) spowodowało spowolnienie reakcji, z kolei zwiększenie stężenia ibuprofenu (1:0,5, *n:n*) spowodowało obniżenie *ee*.

Podsumowując tę część badań, wykazałam wysoką wydajność dwufazowego układu reakcyjnego w rozdziale kinetycznym racematu ibuprofenu w obecności roztworu LAO z wysoką konwersją *(S)-(+)*-ibuprofenu wynoszącą 45,2% oraz *ee* równym 99,9% w optymalnych warunkach. Kolejnym krokiem było podjęcie próby immobilizacji enzymu na nośniku typu SILLP w celu umożliwienia łatwej separacji białka z mieszaniny poreakcyjnej oraz zwiększenie jego aktywności katalitycznej w badanym procesie.

2.2. Synteza i charakterystyka biokatalizatora typu SILLP opartego o lipazę z *Aspergillus oryzae* oraz materiały krzemionkowe modyfikowane imidazoliową cieczą jonową.

W celu zaprojektowania odpowiedniego nośnika typu SILLP dla enzymu LAO wybrałam różne materiały krzemionkowe o zróżnicowanych właściwościach strukturalnych. W celu poprawy właściwości strukturalnych krzemionek są one często łączone z tlenkami metali, w tym m.in. tlenkiem magnezu, tlenkiem wapnia lub tlenkiem cyrkonu. Przygotowanie takich materiałów hybrydowych pozwala na tworzenie nośników o bardziej rozwiniętej powierzchni właściwej lub porowatości, co poprawia ich właściwości sorpcyjne. Funkcjonalność przygotowanych lub komercyjnie dostępnych materiałów na bazie krzemionki wynika w większości przypadków z charakteru powierzchniowych grup silanolowych (≡Si-OH) lub innych (-Mg-OH, -Ca-OH, ≡Zr-OH), które wykazują względnie wysokie powinowactwo, np. do

enzymów, a jednocześnie poprawiają ich aktywność i enancjoselektywność poprzez oddziaływania elektrostatyczne i zmiany konformacji białka.[56,57] Krzemionkowe materiały hybrydowe oparte o tlenek krzemu (SiO_2) oraz tlenek magnezu ($MgO\text{-}SiO_2$), tlenek cyrkonu ($ZrO_2\text{-}SiO_2$), lub tlenek wapnia ($CaO\text{-}SiO_2$), zostały dostarczone przez Pana dr hab. inż. Jakuba Zdartę, prof. Politechniki Poznańskiej z grupy badawczej Pana prof. dr hab. inż. Teofila Jesionowskiego.

W kolejnym etapie ciecz jonowa została unieruchomiona na wcześniej przygotowanych materiałach krzemionkowych poprzez grupy trietoksysililowe zlokalizowane w łańcuchu alkilowym kationu IL (Schemat 4). W pierwszym kroku otrzymałam IL chlorek 1-metylo-3-(trietoksysililopropylo)imidazoliowy ([tespmim]Cl) w reakcji 3-(chloropropylo)trietoksysilanu z 1-metyloimidazolem. Następnie ciecz jonowa została kowalencyjnie przyłączona do materiałów krzemionkowych i przeprowadziłam wymianę anionu Cl^- na $[NTf_2]^-$, co doprowadziło do otrzymania końcowych nośników typu SILLP, np. $SiO_2/Mg(1:1)/[tespmim][NTf_2]$ (Schemat 4). Wymianę anionu na $[NTf_2]^-$ przeprowadziłam ze względu na doniesienia literaturowe, które wskazują wyższą aktywność lipaz w środowisku IL z anionem bis(trifluorometanosulfonylo)imidkowym.[33] W Tabeli 3 przedstawiłam charakterystykę zsyntezowanych materiałów.

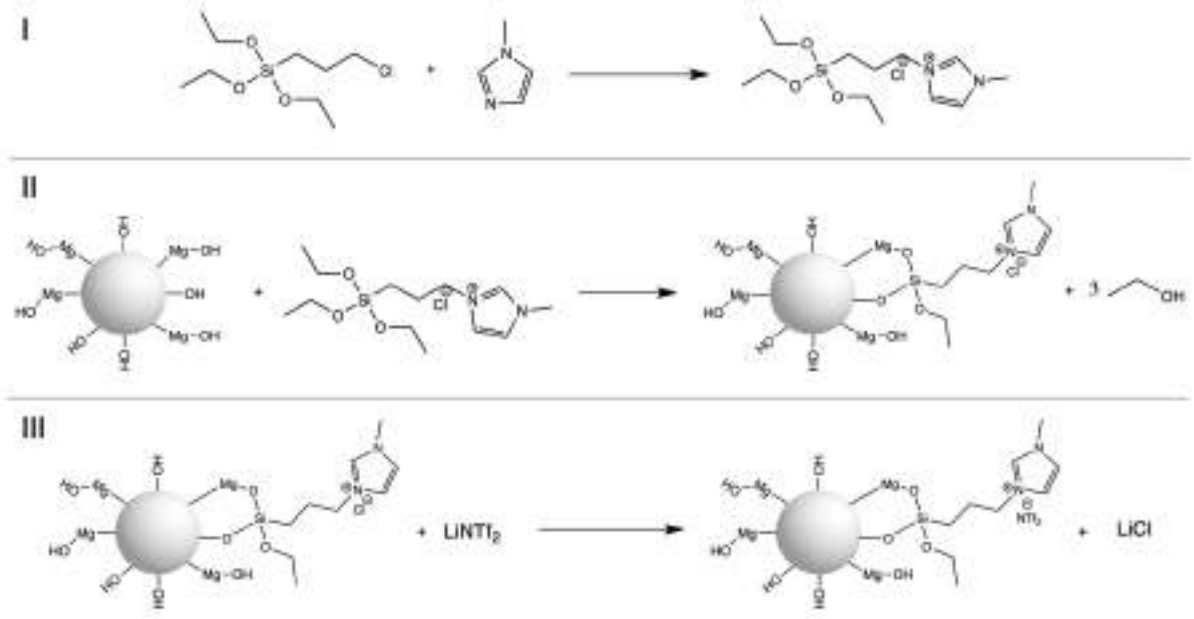

Schemat 4. Chemiczna immobilizacja $[tespmim][NTf_2]$ na powierzchni materiałów krzemionkowych.

W celu dokonania pełnej charakterystyki otrzymanych materiałów typu SILLP zostały przeprowadzone analizy: TGA, analizy powierzchni właściwej BET, SEM, EDX oraz ^{29}Si MAS NMR. Zawartość IL została oznaczona za pomocą TGA. Maksymalną ilość cieczy jonowej przywiązanej do nośnika uzyskano w reakcji 0,3 mmol IL na 0,3 g materiału krzemionkowego, np. dla MgO-SiO2 (1:1) 6,79 wt%. Zwiększenie ilości cieczy jonowej w procesie jej immobilizacji (z 0,3 mmol do 0,5 mmol) nie spowodowało zwiększenia ilości IL na matrycy, natomiast zmniejszenie ilości IL (z 0,3 mmol do 0,2 mmol) skutkowało obniżeniem jej ilości (zawartość IL 4,09 wt%).

Tabela 3. Charakterystyka materiałów krzemionkowych i biokatalizatorów.

Materiał	S_{BET}, (m^2g^{-1})	V_p, (cm^3g^{-1})	d_p, (nm)	IL zawartość, (wt% ±0.3)[a]	LAO zawartość (wt% ±0.3)[a]
MgO-SiO_2 (1:1)	469	0,07	2,1	6,79	3,96
MgO-SiO_2 (1:5)	289	0,12	2,8	5,05	5,12
MgO-SiO_2 (5:1)	72	0,05	1,3	7,53	2,64
CaO-SiO_2 (1:1)	24.9	0,01	1,2	4,29	4,98
ZrO_2-SiO_2 (1:1)	394	0,10	2,3	-	-
SiO_2[b]	118	0,33	11,1	-	-
SiO_2[c]	200	0,59	11,8	9,4	19,38

[a]analizowane za pomocą TGA, odchylenie standardowe 3 z prób; [b]krzemionka przygotowana metodą zol-żel; [c]krzemionka komercyjnie dostępna.

Przyłączenie cieczy jonowej do materiałów krzemionkowych zostało potwierdzone za pomocą analizy ^{29}Si MAS NMR. Spektra MAS NMR obrazują zanik sygnałów przypisanych grupom $(SiO)_2Si-(OH)_2$ i $(SiO)_3Si-OH$, a także pojawienie się nowego sygnału przy −66 ppm, co jednoznacznie wskazuje na przywiązanie IL do powierzchni matrycy. Dodatkowo, obrazy SEM materiałów przed i po immobilizacji IL pokazały obecność cząsteczek o nieregularnym kształcie, z większą tendencją do tworzenia aglomeratów w przypadku próbek z cieczą jonową.

Materiał MgO-SiO_2 (1:1) charakteryzuje się najwyższą wartością powierzchni właściwej BET wynoszącą 469 m^2g^{-1} spośród badanych materiałów, z objętością porów 0,07 cm^3g^{-1} i rozmiarem porów 2,1 nm. Zmiany w początkowym stosunku prekursorów (z MgO-SiO_2 (1:1), na MgO-SiO_2 (1:5) oraz MgO-SiO_2 (5:1)) podczas syntezy materiału hybrydowego spowodowały znaczący spadek powierzchni właściwej materiałów, natomiast ilość cieczy jonowej wahała się od 5,05 wt% dla MgO-SiO_2 (1:5) do 7,53 wt% dla MgO-SiO_2 (5:1), sugerując, że właściwości strukturalne nośnika, jak i również rodzaj grup funkcyjnych na powierzchni, wpływają na ilość

immobilizowanej cieczy jonowej. W przypadku nośnika MgO-SiO_2 im więcej MgO w strukturze materiału tym większa ilość IL została unieruchomiona. Połączenie krzemionki z CaO skutkowało obniżeniem ilości immobilizowanej IL wynoszącą 4,29 wt%. Największa ilość cieczy jonowej została unieruchomiona na komercyjnie dostępnej krzemionce (9,4 wt%), głównie ze względu na dobrze zdefiniowaną strukturę porowatą, obecność licznych grup hydroksylowych na powierzchni i ich równomierne rozmieszczenie, co zmniejsza przeszkody steryczne i sprzyja efektywnemu związaniu znacznych ilości cząsteczek cieczy jonowej.

Ostatni etap przygotowania biokatalizatora obejmował unieruchomienie LAO na powierzchni nośnika za pomocą metody adsorpcji fizycznej. Natywna lipaza z *Aspergillus oryzae* jest komercyjnie dostępnym produktem (Sigma-Aldrich) w formie wodno-glicerynowego roztworu (aktywność 100 000 Ug^{-1}). W celu określenia ilości białka w roztworze lipazy przeprowadziłam test Lowry'ego, (43,7 $mgmL^{-1}$). Ilość osadzonego enzymu na nośniku oznaczono za pomocą TGA. Fizyczne unieruchomienie LAO przeprowadziłam w wodzie, przy 7-krotnym nadmiarze masy roztworu LAO w stosunku do nośnika SILLP, uzyskując np. 3,96 wt% zawartości enzymu dla SiO_2/Mg(1:1)/[tespmim][NTf_2]/LAO, którego graficzną wizualizację przedstawiono na Rysunku 10. Zwiększenie ilości LAO podczas etapu unieruchamiania (z 7-krotnej do 10-krotnej) nie zwiększyło ilości zaadsorbowanej lipazy, natomiast zmniejszenie ilości do 3-krotnej spowodowało jej obniżenie (2,09 wt%).

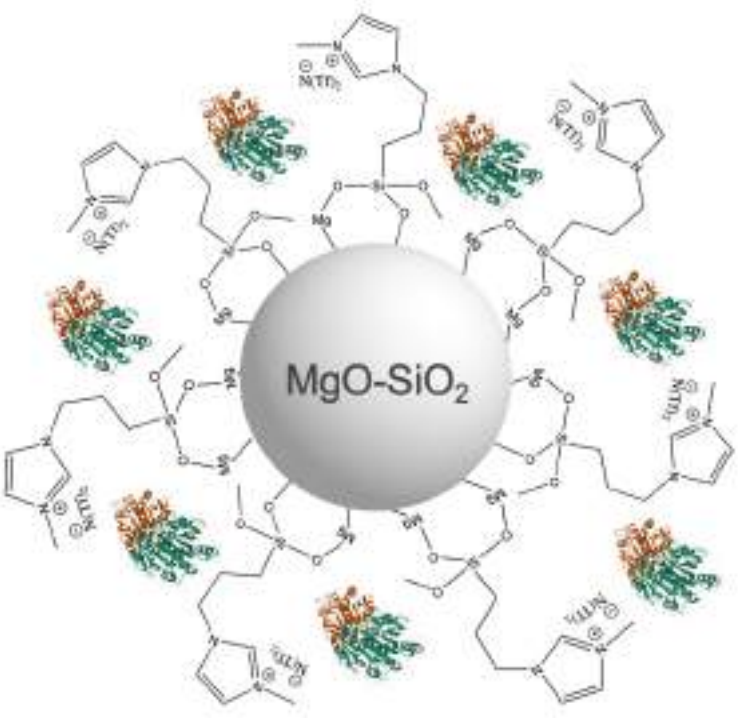

Rysunek 10. Graficzna wizualizacja biokatalizatora SiO_2/Mg(1:1)/[tespmim][NTf_2]/LAO.

Zsyntezowane biokatalizatory typu SILLP, np. SiO_2/Mg(1:1)/[tespmim][NTf_2]/LAO, zostały poddane analizie TGA oraz SEM-EDX, których wyniki potwierdzają skuteczne osadzenie się enzymu. Największa ilość LAO (19,38 wt%) została zaadsorbowana na powierzchni komercyjnie dostępnej krzemionki. Zwiększona funkcjonalizacja cieczą jonową niż w przypadku pozostałych materiałów wpłynęła pozytywnie na efektywność osadzenia się enzymu. Inne materiały zawierały od 2,64 wt% do 5,12 wt% LAO. Zaobserwowałam, że najmniejsza ilość IL (5,05 wt%) została przyłączona do materiału MgO-SiO_2 (1:5), na którym jednocześnie oznaczono największą ilość immobilizowanego enzymu (5,12 wt%). To potwierdza, że nawet mała ilość IL jest w stanie dostarczyć wystarczającą ilość grup funkcyjnych zdolnych do efektywnego unieruchomienia lipazy.

Dla najlepszego układu biokatalitycznego SiO_2/Mg(1:1)/[tespmim][NTf_2]/LAO oraz samego nośnika SiO_2/Mg(1:1)/[tespmim][NTf_2] przeprowadzono analizę powierzchni właściwej BET oraz określono rozmiar i objętość porów (Tabela 4). Zmniejszanie się powierzchni właściwej po immobilizacji IL oraz enzymu świadczy o efektywnym przeprowadzeniu obu procesów.

Tabela 4. Charakterystyka materiałów krzemionkowych i biokatalizatorów.

Materiał	S_{BET}, (m^2g^{-1})	V_p, (cm^3g^{-1})	d_p, (nm)
MgO-SiO_2 (1:1)	469	0,07	2,1
SiO_2/Mg(1:1)/[tespmim][NTf_2]	117	0,07	2,2
SiO_2/Mg(1:1)/[tespmim][NTf_2]/LAO	82,2	0,04	2,2

Podsumowując, zsyntezowałam i scharakteryzowałam 7 układów biokatalitycznych opartych o LAO oraz różne materiały krzemionkowe chemiczne modyfikowane [tespmim][NTf_2]. Wprowadzenie do krzemionki również innych tlenków metali ma istotny wpływ na rozwinięcie powierzchni właściwej oraz zmianę porowatości materiału, a dodatkowo skutkuje obecnością nowych grup funkcyjnych związanych, np. z magnezem, które powodują wzrost efektywności immobilizacji cząstek cieczy jonowych oraz enzymów na powierzchni matrycy.

2.3. Testy aktywności katalitycznej opracowanych biokatalizatorów typu SILLP opartych o lipazę z *Aspergillus oryzae* oraz materiały krzemionkowe modyfikowane imidazoliową cieczą jonową w rozdział kinetycznym racematu ibuprofenu.

Aktywność katalityczna heterogenicznych biokatalizatorów typu SILLP przetestowałam w rozdziale kinetycznym racematu ibuprofenu w opracowanych wcześniej warunkach reakcji w układzie homogenicznym (Wykres 2). Masę każdego biokatalizatora przeliczyłam, tak aby uzyskać biokatalizator o tej samej zawartości LAO (3,56 mg/1 mmol racematu ibuprofenu). W tym celu użyłam 0,082 mL natywnego LAO, który zawiera 3,56 mg białka. Najbardziej aktywnym biokatalizatorem był SiO_2/Mg(1:1)/[tespmim][NTf_2]/LAO, który pozwolił na uzyskanie 35% konwersji racematu ibuprofenu po 7 dniach z 95% *ee (S)-(+)*-estru butylowego.

Zaskakującym faktem była całkowita dezaktywacja LAO na nośnikach MgO-SiO_2 (5:1) oraz MgO-SiO_2 (1:5), a więc ze zwiększoną lub zmniejszoną zawartością MgO w strukturze. Prawdopodobnie ilość MgO w nośniku MgO-SiO_2 (1:1) zgodnie z zaproponowanym mechanizmem unieruchamiania cieczy jonowej poprzez wiązanie chemiczne była na odpowiednim poziomie, co powodowało efektywną immobilizację IL i aktywację LAO.

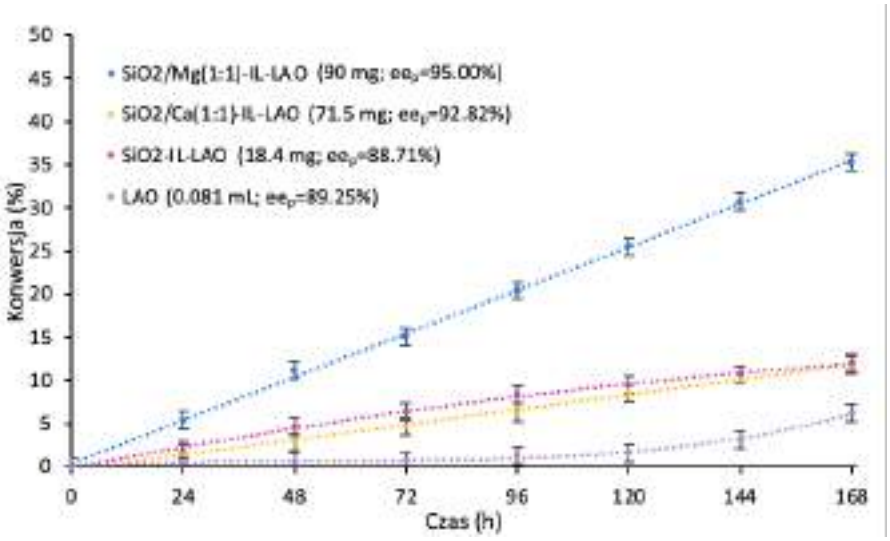

Wykres 2. Wpływ nośnika SILLP na aktywność LAO w estryfikacji racematu ibuprofenu. Warunki reakcji: racemat ibuprofenu 0.1 mmol, 1-butanol 0.2 mmol, izooktan 0.4 mL, 3.56 mg LAO w formie natywnej lub immobilizowanej, 20 °C, 250 rpm. Konwersję racematu ibuprofenu analizowałam za pomocą chiralnej HPLC.

Wydłużenie czasu trwania procesu nie poprawiło wydajności procesu ani uzyskania wyższego *ee*, natomiast należy podkreślić, że mniejsza ilość enzymu osadzonego na powierzchni generuje wyższą aktywność heterogenicznego biokatalizatora, a dodatkowo

immobilizacja białka poprawia jego stabilizację i ułatwia jego potencjalny zawrót do kolejnego cyklu reakcyjnego. Biokatalizator SiO_2/Ca(1:1)/[tespmim][NTf_2]/LAO nie wykazał wystarczającej aktywności, co skutkowało niską konwersją racematu ibuprofenu. To samo zjawisko zaobserwowałam w przypadku biokatalizatora o bardzo wysokiej zawartości lipazy osadzonej na powierzchni komercyjnej krzemionki SiO_2/[tespmim][NTf_2]/LAO. Zastosowanie tego biokatalizatora nie wpłynęło znacząco na konwersję racematu ibuprofenu, prawdopodobnie z powodu przeładowania powierzchni krzemionki lipazą (aglomeracja), co doprowadziło do blokowania miejsc aktywnych enzymu i powstawania ograniczeń dyfuzyjnych reagentów.

Eksperyment aktywności natywnej LAO użytej w takiej samej ilości (3,56 mg), jakiej użyto w przypadku heterogenicznych biokatalizatorów, wykazał niską aktywność homogenicznego białka. Jest to dowód na aktywację LAO na powierzchni krzemionki domieszkowanej magnezem modyfikowanej [tespmim][NTf_2]. Immobilizacja lipazy na niemodyfikowanej matrycy MgO-SiO_2 (1:1) nie powiodła się (metodą TGA nie wykryto białka). Dopiero po modyfikacji powierzchni cieczą jonową, lipaza była w stanie osadzić się na nośniku i katalizować proces rozdziału kinetycznego ibuprofenu. Nośnik SILLP, bez enzymu na powierzchni, nie był katalitycznie aktywny w reakcji.

Następnie zbadałam wpływ ilości SiO_2/Mg(1:1)/[tespmim][NTf_2]/LAO w zakresie 40–90 mg biokatalizatora w celu przyspieszenia procesu estryfikacji racematu ibuprofenu. Większa ilość biokatalizatora (150 mg) wymagała zwiększenia ilości rozpuszczalnika, co było spowodowane utrudnionym mieszaniem mieszaniny reakcyjnej, która była wyjątkowo gęsta. Dodanie dodatkowej ilości rozpuszczalnika spowodowało rozcieńczenie mieszaniny reakcyjnej, spowolnienie tempa reakcji i obniżenie konwersji do 19%. Optymalna ilość SiO_2/Mg(1:1)/[tespmim][NTf_2]/LAO w reakcji wynosiła 90% umożliwiając osiągnięcie konwersji racematu ibuprofenu równej 35% z *ee (S)-(+)*-estru butylowego równym 95% po 7 dniach.

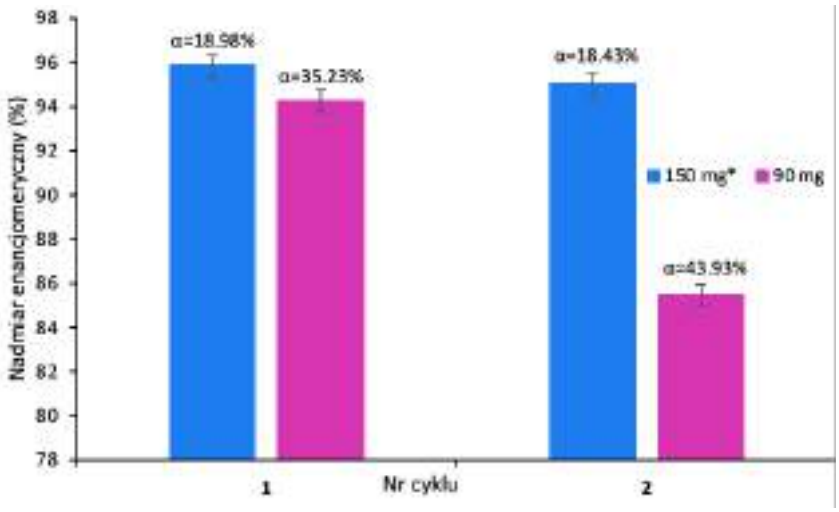

Wykres 3. Badanie zawrotu biokatalizatorów SiO_2/Mg(1:1)/[tespmim][NTf_2]/LAO w estryfikacji racematu ibuprofenu. Warunki reakcji: racemat ibuprofenu 0.1 mmol, 1-butanol 0.2 mmol, izooktan 0,4 mL, 3.56 mg LAO w formie natywnej lub immobilizowanej, 20 °C, 250 rpm. Konwersję racematu ibuprofenu analizowałam za pomocą chiralnej HPLC. *izooktan 1 mL.

Kolejnym krokiem było zbadanie możliwości zawrotu SiO_2/Mg(1:1)/[tespmim][NTf_2]/LAO do kolejnego cyklu reakcyjnego. Uzyskane wyniki przedstawiłam na Wykresie 3. W przypadku zastosowania 90 mg biokatalizatora zaobserwowałam spadek nadmiaru enancjomerycznego w drugim cyklu reakcji z *ee* 96,7% do 88% po 5 dniach reakcji oraz z *ee* 95,5% do 85,5% po 7 dniach. Pomimo, że rozcieńczenie układu reakcyjnego do 1 mL spowodowało spadek szybkości reakcji, pozwoliło to na utrzymanie tak samo wysokiego nadmiaru enancjomerycznego (1. cykl *ee* 96,3%, 2. cykl *ee* 95,4% po 5 dniach oraz 1. cykl *ee* 95,8%, 2. cykl *ee* 94,2% po 7 dniach). Długotrwała stabilność biokatalizatora wynika z efektu stabilizacji SILLP, który charakteryzuje się zdolnością do utrzymania aktywnych konformacji enzymów. Dodatkowo, użyta ciecz jonowa zapewnia odpowiednie mikrośrodowisko dla immobilizowanej lipazy, co ułatwia ponowne użycie biokatalizatorów typu SILLP. Analiza TGA biokatalizatora po drugim cyklu (eksperyment z użyciem 90 mg biokatalizatora) wykazała, że ilość enzymu na zmodyfikowanej powierzchni krzemionki (SiO_2/Mg(1:1)/[tespmim][NTf_2]/LAO) pozostała niezmieniona (4,04 wt%). Dodatkowo, eksperyment polegający na szybkiej filtracji biokatalizatora z mieszaniny reakcyjnej wykazały brak dalszej konwersji ibuprofenu w przesączu po usunięciu SiO_2/Mg(1:1)/[tespmim][NTf_2]/LAO. Uzasadnia to, że przyczyną niższej aktywności lipazy jest jej inhibicja w długotrwałym procesie (186 h), która była widoczna nawet przy zastosowaniu nadmiaru biokatalizatora (150 mg).

Podsumowując, w niniejszych badaniach zastosowałam dwa nowatorskie podejścia do kinetycznego rozdzielania racematu ibuprofenu poprzez enancjomeryczną estryfikację w obecności lipazy z *Aspergillus oryzae.* Nośnik typu SILLP został wykorzystany do zaprojektowania heterogenicznego biokatalizatora opartego na hybrydowych nośnikach krzemionkowych poprawiając aktywność i stabilność białka oraz umożliwiając jego recykl. Zastosowanie natywnej LAO umożliwiło osiągnięcie *ee* 99,9% *(S)-(+)*-estru ibuprofenu przy konwersji równej 34,8% po 24 h oraz odpowiednio *ee* 99,9% przy konwersji 45,2% po 48 h, co jest konkurencyjne wobec innych doniesień literaturowych. Przy użyciu heterogenicznego biokatalizatora SiO_2/Mg(1:1)/[tespmim][NTf_2]/LAO (zawartość IL 6,79 wt%, zawartość LAO 3,96 wt%) konwersja racematu ibuprofenu osiągnęła 35% po 7 dniach z 95% *ee* estru. Pomimo, że rozcieńczenie układu reakcyjnego spowodowało spadek szybkości reakcji, pozwoliło utrzymać wysoki nadmiar enancjomeryczny *(S)-(+)*-enancjomeru ibuprofenu w drugim cyklu.

3. Synteza, charakterystyka oraz zastosowanie biokatalizatora opartego o lipazę z *Aspergillus oryzae* oraz materiał krzemionkowy domieszkowany tlenkiem magnezu i modyfikowany grupami oktylowymi w reakcji estryfikacji alkoholu furfurylowego i kwasów tłuszczowych C8-C18 w systemie okresowym oraz ciągłym.

Korzystanie z surowców odnawialnych, do których należy biomasa lignocelulozowa, kieruje przemysł chemiczny w stronę zrównoważonego rozwoju i gospodarki o obiegu zamkniętym. Biomasa lignocelulozowa jest dobrym surowcem do produkcji wartościowych chemikaliów pochodzenia biologicznego. Hemiceluloza, składnik lignocelulozy, ulega hydrolizie, w wyniku której powstaje D-ksyloza, a następnie podlega dehydratacji, przekształcając się w furfural.[58] Furfural następnie konwertowany jest do alkoholu furfurylowego.[59] Większość alkoholu furfurylowego jest wykorzystywana do produkcji żywic furanowych, alkoholu tetrahydrofurfurylowego, kwasów karboksylowych oraz estrów.[60] Estry alkoholufurfurylowego i kwasów tłuszczowych są głównie stosowane jako biolubrykanty, surfaktanty, rozpuszczalniki, plastyfikatory, dodatki do biopaliw, emulgatory, dodatki do żywności oraz aromaty.[61,62]

Osiągnięcie wysokiej selektywności estryfikacji alkoholu furfurylowego stanowi istotny problem, ponieważ łatwo ulega on polimeryzacji w obecności kwasów mineralnych lub silnych kwasów organicznych, co prowadzi do powstawania termostabilnych polimerów lub eterów difurfurylowych.[63-65]

Alternatywnym podejściem jest wdrożenie biokatalizy z wykorzystaniem lipaz, które charakteryzują się wysoką aktywnością w procesach estryfikacji. W dostępnych doniesieniach literaturowych można znaleźć prace, w których komercyjnie dostępny Novozyme 435 został użyty w estryfikacji alkoholu furfurylowego z kwasem oleinowym, kwasem oktanowym lub olejem rycynowym w temperaturach od 55 do 60 °C, co skutkowało niemal pełną konwersją kwasu oleinowego (99%) i oleju rycynowego (89%) oraz tylko 77% przereagowaniem kwasu oktanowego po 24 h.[66-68] Novozyme 435 to lipaza z *Candida antarctica* B (CALB) unieruchomiona na makroporowatej żywicy akrylowej. Ponowne wykorzystanie Novozyme 435 jest ograniczone z powodu tendencji żywicy do pęcznienia w rozpuszczalnikach organicznych, co utrudnia izolację i ponowne użyciet.[69-70]

Prowadzenie badań w kierunku projektowania trwałych, stabilnych i aktywnych biokatalizatorów jest kluczowe, aby sprostać wyzwaniom wdrożenia ich do technologii

przepływowych. Immobilizacja cząsteczek enzymu na odpowiednio zaprojektowanej matrycy poprawia wszystkie wyżej wymienione cechy, które są niezbędne do opracowania efektywnej metody produkcji. Jak wykazano w poprzedniej pracy dotyczącej enzymatycznej estryfikacji racematu ibuprofenu odpowiednie zaprojektowanie nośnika poprzez nadanie mu właściwości hydrofobowych oraz wprowadzenie tlenków metali może znacznie poprawić aktywne działanie lipaz oraz ich immobilizację.[36]

Nadanie właściwości hydrofobowych materiałom krzemionkowym może być osiągnięte przez chemiczną modyfikację grupami alkilowymi. Modyfikacja krzemionki grupami alkilowymi (np. metylowymi, oktylowymi, heksadecylowymi) i jej zastosowanie jako nośnika dla CALB zostało już wcześniej przetestowane w reakcji utleniania Bayera-Villigera cyklicznych ketonów do laktonów z użyciem 60% roztworu nadtlenku wodoru. Wysoka aktywność biokatalizatora (98% wydajności syntezy γ-butyrolaktonu) została osiągnięta pomimo trudnych warunków reakcji.[28]

Głównym celem tej pracy było opracowanie zrównoważonej metody estryfikacji alkoholu furfurylowego pochodzącego z biomasy z kwasami karboksylowymi C8-C18 w obecności immobilizowanej lipazy z *Aspergillus oryzae* na materiale krzemionkowym domieszkowanym tlenkiem magnezu i modyfikowanym grupami oktylowymi w systemie okresowym oraz ciągłym. Opracowana technologia została przeanalizowana pod kątem zgodności z zasadami zielonej chemii.

3.1. Synteza i charakterystyka biokatalizatora opartego o lipazę z *Aspergillus oryzae* oraz materiał krzemionkowy domieszkowany tlenkiem magnezu i modyfikowany grupami oktylowymi.

Wybór lipazy z *Aspergillus oryzae* wynikał z jej wysokiej aktywności katalitycznej w reakcjach estryfikacji. Dodatkowo, LAO jest stosunkowo stabilna w rozpuszczalnikach organicznych oraz przy wysokich stężeniach substratów. Co ważne, LAO została uznana przez Agencję Żywności i Leków jako enzym powszechnie uznany za bezpieczny.[71] W celu uproszczenia protokołu immobilizacji enzymu zastosowałam prostą adsorpcję LAO. Jako nośnik enzymu LAO wybrałam hybrydowy materiał składający się z MgO i krzemionki ($MgO\text{-}SiO_2$ (1:1)). Jak wspomniałam wcześniej w Rozdziale 2, MgO wprowadza zmiany w strukturalnych właściwościach materiału poprzez wprowadzenie, oprócz grup silanolowych (≡Si–OH), także grup magnezylowych (–Mg–OH), co dodatkowo zwiększa aktywność lipaz. Wzmocnienie

powinowactwa enzymu do powierzchni uzyskałam poprzez zwiększenie hydrofobowości nośnika.[56,57] Hydrofobowość powierzchni krzemionki można wprowadzić poprzez prostą modyfikację za pomocą fizycznego unieruchomienia lub chemicznego wiązania np. alkilowych organosilanów, hydrofobowych cieczy jonowych lub poprzez prowadzenie reakcji w hydrofobowych rozpuszczalnikach, takich jak ciecze jonowe.[28,29] W tej pracy przeprowadziłam modyfikację chemiczną przy użyciu oktylotrietoksysilanu lub heksadecylotrietoksysilanu (Schemat 5).

W pierwszym etapie syntezy biokatalizatora, nośnik MgO-SiO_2 (1:1), *n:n*) został otrzymany metodą zol-żel zgodnie z metodą opisaną w literaturze.[72] Zsyntetyzowany materiał hybrydowy został chemicznie zmodyfikowany alkilowymi organosilanami, takimi jak oktylotrietoksysilan (C8) lub heksadecylotrietoksysilan (C16), poprzez mieszanie reagentów w mieszaninie izopropanolu z wodą w temperaturze 85 °C przez 24 h. Do celów porównawczych nośnik MgO-SiO_2 został poddany procesowi kalcynacji w temperaturze 800 °C, aby sprawdzić, jak zmiany w porowatości materiału wpłyną na jego właściwości w kontekście modyfikacji grupami alkilowymi oraz immobilizacji LAO.

W celu uzyskania pełnej charakterystyki otrzymanych materiałów i biokatalizatorów przeprowadzono analizy: TGA, SEM, EDX, adsorpcji – desorpcji (BJH i BET) oraz spektroskopii w podczerwieni z transformacją Fouriera (FT-IR).

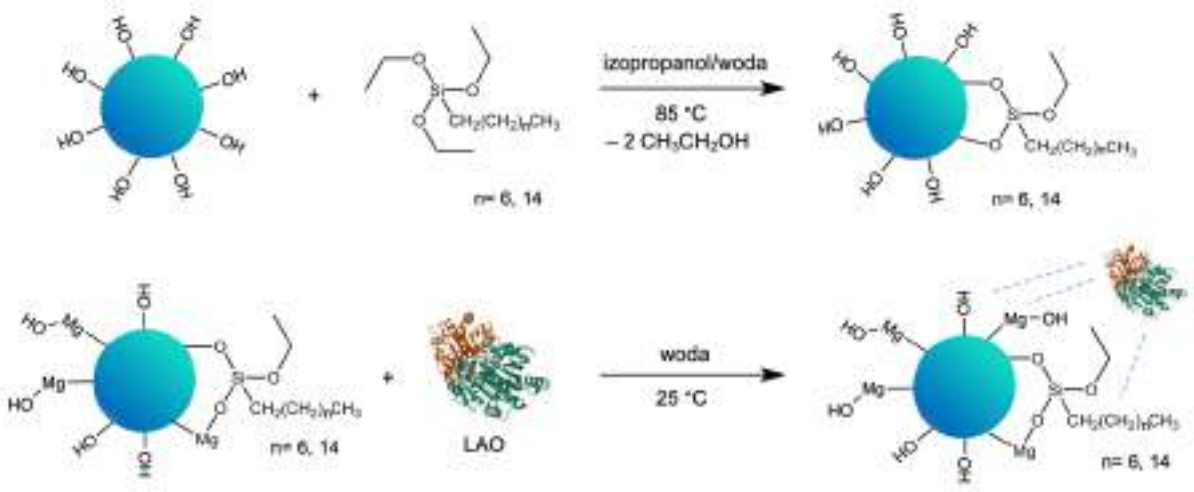

Schemat 5. Przygotowanie MgO-SiO_2-C8-LAO, gdzie niebieskie linie przerywane oznaczają oddziaływania fizyczne.

Chemiczne przywiązanie grup alkilowych do materiałów krzemionkowych ($MgO\text{-}SiO_2$-C8, $MgO\text{-}SiO_2$-C16, $MgO\text{-}SiO_2\text{-}C8_{(kalc.)}$, SiO_2-C8) zostało potwierdzone za pomocą FT-IR. Dzięki obecności charakterystycznych pasm grup metylowych i metylenowych pochodzących od cząsteczek modyfikatora w zakresie 2850–3000 cm^{-1}, można jednoznacznie stwierdzić, że zarówno grupy C8 i C16 zostały skutecznie przyłączone.

Tabela 5. Zawartość grup alkilowych oraz LAO na materiałach krzemionkowych.

Materiał	Grupy alkilowe zawartość, (wt% ±0,3)[a]	LAO zawartość (wt% ±0,3)[a]
$MgO\text{-}SiO_2$-C8-LAO	8,03	4,24
$MgO\text{-}SiO_2\text{-}C8_{(kalc.)}$-LAO	1,21	2,16
$MgO\text{-}SiO_2$-C16-LAO	5,86	1,54
SiO_2-C8-LAO	5,87	9,25
$MgO\text{-}SiO_2$-LAO	-	*nie wykryto*

[a]analizowane za pomocą TGA, odchylenie standardowe z 3 prób.

Obecność oraz ilość przyłączonych grup alkilowych do powierzchni $MgO\text{-}SiO_2$ została określona za pomocą TGA i przedstawiona w Tabeli 5. Z otrzymanych analiz wynika, że im dłuższy łańcuch węglowy modyfikatora, tym mniejsza ilość grup alkilowych została przyłączona do materiału, odpowiednio 8,03 wt% C8 i 5,86 wt% C16. Dodatkowo, kalcynacja nośnika $MgO\text{-}SiO_2$ doprowadziła do zmniejszenia ilości immobilizacji grup C8 (1,21 wt%), co prawdopodobnie jest związane z mniejszą liczbą dostępnych powierzchniowych grup hydroksylowych zdolnych do wiązania modyfikatora. Ten sam efekt zaobserwowałam przy modyfikacji krzemionki, co skutkowało wprowadzeniem jedynie 5,87 wt% grup C8. Sugeruje to, że obecność tlenku magnezu dostarczyła dodatkowe grupy hydroksylowe na powierzchni materiału hybrydowego, co umożliwiło bardziej efektywne przyłączenie grup oktylowych.

Dodatkowo, obrazy SEM przed i po modyfikacji grupami alkilowymi pokazały tendencję cząsteczek materiałów krzemionkowych do aglomeracji i tworzenia nieregularnych struktur po wprowadzeniu grup alkilowych. Jednocześnie skład pierwiastkowy powierzchni materiałów SiO_2, $MgO\text{-}SiO_2$, $MgO\text{-}SiO_{2(kalc.)}$ przed i po modyfikacji został przeanalizowany przy użyciu detektora EDX. Analizy potwierdziły obecność atomów węgla równomiernie rozmieszczonych na powierzchni, pochodzących od przyłączonych grup alkilowych, co potwierdza skuteczne wprowadzenie grup hydrofobowych na powierzchnię materiałów krzemionkowych.

W celu przygotowania biokatalizatorów i przeprowadzenia fizycznej immobilizacji LAO, wodny roztwór lipazy został zmieszany z materiałami krzemionkowymi MgO-SiO_2-C8, MgO-SiO_2-C16, MgO-SiO_2-C8$_{(kalc.)}$, SiO_2-C8 oraz MgO-SiO_2 w temperaturze pokojowej przez 3 h. Na podstawie analiz TGA (Tabela 5) zaobserwowałam, że dłuższy łańcuch alkilowy prowadził do zmniejszenia ilości immobilizowanej lipazy z 4,24 wt% dla MgO-SiO_2-C8-LAO do 1,54 wt% dla MgO-SiO_2-C16-LAO. Prawdopodobnie było to spowodowane większą zawadą steryczną w przypadku dłuższego łańcucha alkilowego. Mniejsza ilość grup funkcyjnych wprowadzonych podczas etapu modyfikacji (1,21 wt%) skutkowała zmniejszoną adsorpcją LAO (2,16 wt%) na kalcynowanym materiale. W porównaniu z SiO_2-C8 (9,25 wt% LAO), MgO-SiO_2-C8 wykazywał mniejszą zdolność sorpcyjną z powodu większej ilości wprowadzonych grup C8 na powierzchni MgO-SiO_2, co powodowało większą zawadę steryczną w adsorpcji cząsteczek LAO. Brak LAO na powierzchni niemodyfikowanego MgO-SiO_2, co zostało stwierdzone na podstawie TGA, potwierdził, że obecność grup alkilowych jest kluczowa do immobilizacji lipazy. Powierzchnia pierwotnego MgO-SiO_2 ma zbyt niską zdolność do adsorpcji lipazy, aby umożliwić efektywną immobilizację jej cząsteczek. Modyfikacja powierzchni krzemionki MgO zwiększyła zarówno powinowactwo enzymu do matrycy, jak i zdolność adsorpcyjną nośnika. Zwiększona porowatość powierzchni, przypisywana dodatkowym grupom –Mg–OH, została również zaobserwowana w poprzednich badaniach (Rozdział 2).

Po immobilizacji lipazy, obrazy SEM zobrazowały jeszcze większą aglomerację cząstek materiału, która nasilała się od pierwotnych matryc SiO_2 i MgO-SiO_2 poprzez materiały zmodyfikowane alkilami aż do końcowych biokatalizatorów. Największa aglomeracja cząstek była obserwowana dla biokatalizatora SiO_2-C8-LAO, gdzie zaadsorbowała się największą ilość lipazy (9,25 wt%), co wyraźnie pokazywało, że immobilizacja zwiększyła skłonność cząstek nośnika do tworzenia agregatów. Analizy EDX potwierdziły obecność atomów azotu pochodzących ze struktury białka we wszystkich biokatalizatorach.

Tabela 6. Charakterystyka strukturalna biokatalizatora MgO-SiO_2-C8-LAO.

Materiał	S_{BET}, (m^2g^{-1})	S_{BET}, mikropory (m^2g^{-1})	V_p, (cm^3g^{-1})	d_p, (nm)	Grupy C8 zawartość, (wt% ±0,3)[a]	LAO zawartość (wt% ±0,3)[a]
MgO-SiO_2	421	314	0,06	2,1	-	-
MgO-SiO_2-C8	325	243	0,05	2,1	8,03	-
MgO-SiO_2-C8-LAO	236	169	0,02	2,1	8,03	4,24

[a]analizowane za pomocą TGA, odchylenie standardowe z 3 prób.

Biokatalizator, MgO-SiO_2-C8-LAO, który wykazał najwyższą aktywność katalityczną w procesie estryfikacji alkoholu furfurylowego i kwasu oktanowego został poddany analizie adsorpcji – desorpcji (BJH, BET) (Tabela 6). Izotermy adsorpcji-desorpcji, diagram rozkładu rozmiaru porów, powierzchnia właściwa S_{BET} i analiza mikroporów wykazały wysoką mikroporowatość nośników oraz biokatalizatora. Dane zamieszczone w Tabeli 6 wyraźnie pokazują, że wprowadzenie grup alkilowych, a także adsorpcja lipazy spowodowały zmniejszenie powierzchni właściwej i częściowe zablokowanie mikroporów, co wynika z sukcesywnego zmniejszania się powierzchni właściwej mikroporów. Spadek powierzchni i objętości porów są typowe dla materiałów po immobilizacji enzymów.

Podsumowując, w tej części badań zsyntezowałam i scharakteryzowałam biokatalizatory oparte o lipazę z *Aspergillus oryzae* oraz nośniki krzemionkowe modyfikowane grupami alkilowymi, których aktywność katalityczną porównałam w następnym dziale.

3.2. Badanie wpływu wybranych parametrów na przebieg reakcji estryfikacji alkoholu furfurylowego i kwasów tłuszczowych C8-C18 w obecności opracowanych biokatalizatorów w systemie okresowym.

Aktywność katalityczną MgO-SiO_2-C8-LAO zbadałam w przemysłowo istotnym procesie estryfikacji alkoholu furfurylowego z kwasami tłuszczowymi (C8-C18). W badaniach wstępnych przetestowałam aktywność opracowanych biokatalizatorów w modelowej estryfikacji alkoholu furfurylowego i kwasu oktanowego w układzie okresowym (Schemat 6). Reakcję przeprowadziłam w temperaturze pokojowej z użyciem cykloheksanu jako rozpuszczalnika oraz trzykrotnego nadmiaru molowego kwasu oktanowego względem alkoholu furfurylowego. W każdym przypadku zaobserwowałam 100% selektywność, co oznacza, że konwersja równała się wydajności. Ilość użytego biokatalizatora w reakcjach porównawczych, przedstawiona w Tabeli 7, została przeliczona w taki sposób, aby każdy układ reakcyjny zawierał taką samą ilość enzymu (6,36 mg LAO).

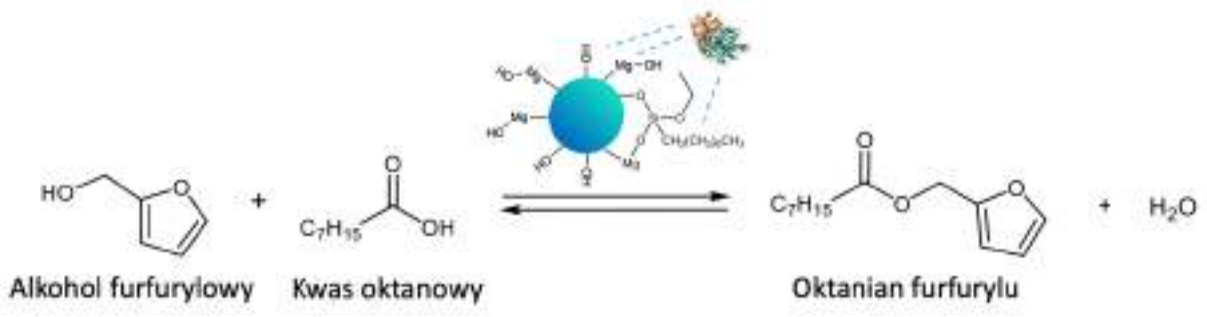

Schemat 6. Estryfikacja alkoholu furfurylowego i kwasu oktanowego w obecności opracowanych katalizatorów.

Tabela 7. Wpływ modyfikacji nośnika krzemionkowego na aktywność katalityczną biokatalizatora w estryfikacji alkoholu furfurylowego.

Biokatalizator	Czas (min)	Konwersja alkoholu furfurylowego (%)[a]	Aktywność ($\mu molmin^{-1}$)	Aktywność właściwa ($\mu molmg^{-1}min^{-1}$)	Aktywność zachowana (%)
LAO	120	83,5	7,3	1,1	-
CALB	120	74,7	6,1	1,0	-
Novozyme 435	30	92,4	30,1	4,7	493
$MgO\text{-}SiO_2$-LAO[c]	120	6,1	-	-	-
SiO_2-C8-LAO	90	87,1	10,0	1,6	137
$MgO\text{-}SiO_2$-C8-LAO	45	90,2	20,2	3,2	277
$MgO\text{-}SiO_{2(kalc)}$-C8-LAO	45	89,4	20,3	3,2	277
$MgO\text{-}SiO_2$-C16-LAO	45	87,3	20,4	3,2	277

Warunki reakcji: alkohol furfurylowy 1,0 mmol, kwas oktanowy 3,0 mmol, cykloheksan 0.5 mL, biokatalizator zawierający 6,36 mg LAO, (146 µL roztworu natywnej LAO (43.7 mgmL-1); 530 µL roztworu natywnej CALB (12 mgmL-1); 118 mg Novozyme 435; 300 mg $MgO\text{-}SiO_2$-LAO; 69 mg SiO_2-C8-LAO; 150 mg $MgO\text{-}SiO_2$-C8-LAO; 294 mg $MgO\text{-}SiO_{2(kalc)}$-C8-LAO; 413 mg $MgO\text{-}SiO_2$-C16-LAO), 25°C, 250 rpm; [a]oznaczono za pomocą GC; [b]Aktywność zachowana=(aktywność immobilizowanego enzymu/aktywność natywnego enzymu) ·100%; [c]300 mg biokatalizatora (maksymalna możliwa ilość w mieszaninie reakcyjnej).

Heterogenizacja LAO doprowadziła do znacznie wzrostu aktywności katalitycznej lipazy w porównaniu do jej formy natywnej (konwersja alkoholu wynosząca 87,1–90,2% w porównaniu do 83,5%), wykazując 277% aktywności (względem formy natywnej lipazy) i 90,2% konwersji alkoholu furfurylowego w obecności $MgO\text{-}SiO_2$-C8-LAO po 45 min reakcji. Jest to istotny aspekt w kontekście izolacji i zawrocie enzymu. Dostępna komercyjnie natywna forma CALB, użyta w takiej samej ilości jak LAO, była nieco mniej aktywna (74,7%).

Zgodnie z oczekiwaniami, najwyższą aktywność zaobserwowałam dla wzorcowego Novozyme 435 (92,4% konwersji alkoholu furfurylowego po 30 min), natomiast test zawrotu Novozyme 435 wykazał problemy z odfiltrowaniem biokatalizatora po reakcji z powodu

pęcznienia żywicy. Jak wspomniałam wcześniej, celem tego badania było znalezienie alternatywy dla Novozyme 435 z powodu problemów technicznych związanych z jego użyciem, takich jak filtracja, pełnienie funkcji złoża stacjonarnego w reaktorze przepływowym oraz trudności z regeneracją.

Kluczowym parametrem opracowanych heterogenicznych biokatalizatorów jest struktura i hydrofilowość powierzchni nośnika. Dodatkowa kalcynacja matrycy MgO-SiO_2 nie wpłynęła na stabilizację aktywnej konformacji LAO (89,4% konwersji po 45 min). Zmiany w strukturze krystalicznej miały wpływ na ilości przyłączonych grup C8 (dla MgO-SiO_2-C8 8,03 wt% C8, dla MgO-$SiO_{2(kalc)}$-C8 1,21 wt% C8) oraz adsorbowanego LAO na powierzchni (dla MgO-SiO_2-C8-LAO 4,24 wt% LAO, dla MgO-$SiO_{2(kalc)}$-C8-LAO 2,16 wt% LAO), które są mniejsze w przypadku niekalcynowanych materiałów. Warto podkreślić, że niższe obciążenie nośnika enzymem skutkowało zwiększeniem jego aktywności (względem natywnej formy enzymu) i konwersją substratu, prawdopodobnie dzięki równomiernemu osadzeniu enzymu oraz uniknięcia blokowania się centrów aktywnych białka. Z tego względu, aby uniknąć dodatkowego energochłonnego etapu w przygotowaniu katalizatora, który nie poprawia aktywności lipazy, kalcynacja matrycy nie jest zalecana.

Wprowadzenie dłuższej grupy alkilowej C16 zamiast C8 do materiałów tlenkowych miało wpływ na etap immobilizacji lipazy (dla MgO-SiO_2-C16 1,54 wt% w porównaniu do MgO-SiO_2-C8-LAO 4,24 wt%) i nieznacznie zmniejszyło aktywność enzymu (87,3% konwersji po 45 min). Dłuższe łańcuchy alkilowe powodowały większą zawadę steryczną, zmniejszając zdolność białka do adsorpcji na powierzchni i efektywną dyfuzję substratów do centrów aktywnych.

Obecność hydrofobowych grup alkilowych na powierzchni MgO-SiO_2 jest kluczowa dla efektywnej immobilizacji LAO i utrzymania jej wysokiej aktywności, co zostało udowodnione przez analizy TGA. W reakcji z udziałem MgO-SiO_2-LAO zaobserwowałam tylko 6,1% konwersji alkoholu furfurylowego po 120 min, nawet przy maksymalnej możliwej ilości biokatalizatora w mieszaninie reakcyjnej (300 mg). Większa ilość biokatalizatora utrudniała efektywne mieszanie.

Ważnym aspektem poprawy aktywności LAO było wprowadzenie jonów magnezu do krzemionki i otrzymanie tlenkowego materiału MgO-SiO_2. Obecność magnezu w materiale krzemionkowym poprawiła aktywację i stabilizację aktywnej konformacji enzymu prawdopodobnie poprzez oddziaływania elektrostatyczne między jonami Mg^{2+}

a aminokwasami LAO, co prowadziło do dodatkowych zmian w ułożeniu α-helis i β-harmonijek. Ten efekt skutkował wyższą aktywnością katalityczną unieruchomionych białek.

W dalszej części badań przeprowadziłam optymalizację parametrów modelowej reakcji w obecności biokatalizatora MgO-SiO_2-C8-LAO. Na początku przetestowałam wpływ rodzaju rozpuszczalnika (cykloheksan, toluen, heksan, izooktan) użytego w reakcji. Wybór odpowiedniego rozpuszczalnika w biokatalizie jest niezbędny, aby uniknąć szybkiej dezaktywacji enzymu. Biokatalizator wykazał najwyższą aktywność katalityczną w cykloheksanie (konwersja alkoholu 86,2% w 60 min), a następnie w toluenie (konwersja 85,7% w 90 min), osiągając 100% selektywności w obu przypadkach. Przy użyciu heksanu i izooktanu, konwersje alkoholu furfurylowego wyniosły odpowiednio 52,6% i 37,4% w czasie 180 min. Przetestowałam również acetonitryl, będący bardziej hydrofilowym rozpuszczalnikiem, w którym nie zaobserwowałam przereagowania alkoholu furfurylowego. Można to przypisać silnemu powinowactwu acetonitrylu do wody, która jest niezbędna do utrzymania aktywnej konformacji lipazy. Rozpuszczalniki takie jak metanol, etanol czy alkilowe węglany jako bardziej ekologiczne alternatywy nie były odpowiednie z powodu ich reaktywności w stosunku do kwasu oktanowego. Zastosowanie mniej niż 0,50 mL cykloheksanu na 1 mmol alkoholu furfurylowego skutkowało niższą aktywnością biokatalizatora z powodu problemów z mieszaniem reagentów w obecności heterogenicznego MgO-SiO_2-C8-LAO. Większe ilości cykloheksanu, takie jak 0,75 mL i 1,0 mL, prowadziły do obniżenia szybkości reakcji ze względu na zmniejszenie się stężeń reagentów.

Następnie zbadałam wpływ ilości biokatalizatora MgO-SiO_2-C8-LAO. Użycie 150 mg biokatalizatora na 1 mmol alkoholu furfurylowego skutkowało wysoką konwersją alkoholu furfurylowego (90,2%) w 45 min. Zwiększenie ilości biokatalizatora do 175 mg nie doprowadziło do uzyskania większego przereagowania alkoholu furfurylowego ani zwiększenia szybkości reakcji (90,4% w 45 min). Zaobserwowałam, że użycie tylko 25 mg biokatalizatora nadal umożliwiło uzyskanie wysokiej konwersji alkoholu furfurylowego (84,8%), ale w dłuższym czasie 180 min. Obserwacja ta potwierdza wyjątkowo wysoką aktywność opracowanego biokatalizatora MgO-SiO_2-C8-LAO. Zbadałam również wpływ stosunku molowego alkoholu furfurylowego do kwasu oktanowego na aktywność katalityczną biokatalizatora w reakcji estryfikacji alkoholu furfurylowego. Najlepszy wynik uzyskano przy trzykrotnym nadmiarze molowym kwasu oktanowego, osiągając 90,2% konwersji alkoholu furfurylowego w 45 min. Zwiększenie nadmiaru molowego kwasu nie wpłynęło na przereagowanie alkoholu

furfurylowego. Badania dotyczące wpływu temperatury wykazały podobną aktywność katalityczną MgO-SiO_2-C8-LAO w temperaturach 25 °C, 30 °C i 35 °C. Zgodnie z oczekiwaniami, niższa temperatura (20 °C) spowodowała niewielkie zmniejszenie szybkości reakcji, co wskazuje 25 °C jako optymalną temperaturę procesu. Wyższa temperatura (40 °C) spowodowała spowolnienie reakcji, prawdopodobnie z powodu częściowej dezaktywacji biokatalizatora opartego o lipazę. Zgodnie z literaturą, LAO utrzymuje optymalną aktywność w temperaturze około 30 °C i pH 7, przy czym znaczny spadek aktywności obserwuje się przy 40 °C, co jest zgodne z uzyskanymi wynikami.[73]

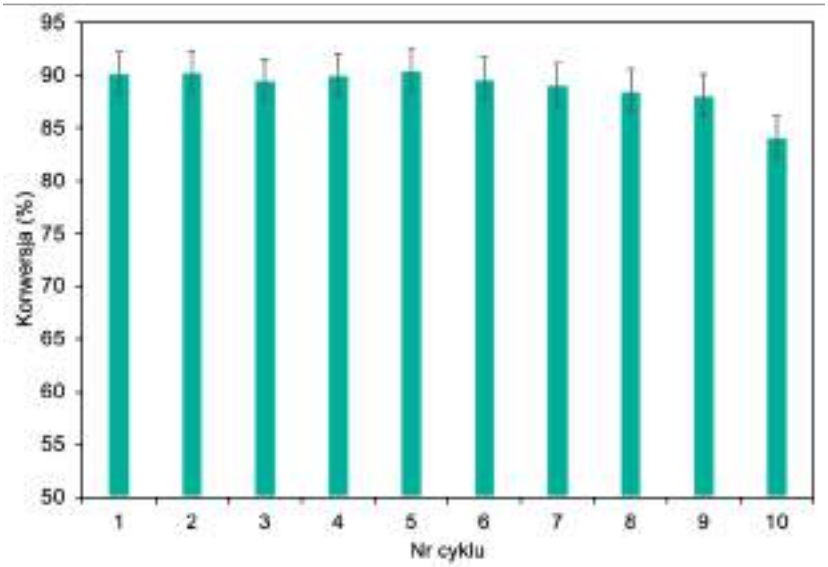

Wykres 4. Badanie zawrotu MgO-SiO_2-C8-LAO w estryfikacji alkoholu furfurylowego. Warunki reakcji: alkohol furfurylowy 1,0 mmol, kwas oktanowy 3,0 mmol, cykloheksan 0.5 mL, MgO-SiO_2-C8-LAO 150 mg, 25 °C, 250 rpm, 45 min. Konwersję alkoholu furfurylowego oznaczono za pomocą GC.

Kolejnym krokiem było wykazanie możliwości łatwego i bezpiecznego ponownego użycia biokatalizatora, co jest kluczowe dla rozwoju przyjaznych środowisku i efektywnych systemów katalitycznych. Zdolność do ponownego wykorzystania MgO-SiO_2-C8-LAO zbadałam w reakcji estryfikacji alkoholu furfurylowego, przy dwukrotnym zwiększeniu skali procesu do 2 mmol alkoholu furfurylowego, co wymagało użycia 300 mg biokatalizatora w układzie okresowym. Opracowany MgO-SiO_2-C8-LAO zachował swoją aktywność katalityczną przez 9 kolejnych cykli estryfikacji alkoholu furfurylowego (Wykres 4), po którym dopiero zaobserwowałam stopniowy spadek. W 10 cyklu reakcji zaobserwowałam zmniejszenie konwersji alkoholu furfurylowego do 84,6%. Analizy TGA biokatalizatora po kolejnych cyklach nie wykazały zmian w ilości LAO, co wskazuje na powolną dezaktywację LAO w procesie.

Dodatkowo, eksperyment „reakcja stop", który polegał na szybkim usunięciu biokatalizatora z mieszaniny reakcyjnej, wykazał brak dalszej konwersji alkoholu furfurylowego w filtracie, co potwierdza, że nie wystąpiło wymywanie LAO do układu reakcyjnego. Zatem zaobserwowany spadek właściwości biokatalitycznych jest głównie związany z inhibicją enzymu przez substrat lub produkty lub z dezaktywacją białka wskutek denaturacji.

Ważnym aspektem w trakcie opracowywania technologii jest również uniwersalność badanego układu katalitycznego. Przeprowadziłam szereg reakcji estryfikacji z zastosowaniem różnych kwasów tłuszczowych (kwas oktanowy, kwas nonanowy, kwas dekanowy, kwas laurynowy, kwas oleinowy) w obecności biokatalizatora MgO-SiO_2-C8-LAO. Uzyskałam wysokie wartości konwersji alkoholu furfurylowego (88,7%–60,2%) w temperaturze 25 °C w czasie 45–90 min, gdzie wydajności wyizolowanych produktów mieściła się w zakresie 85–88%. Selektywność estryfikacji osiągnęła 100% dla każdego estru.

3.3. Transformacja procesu estryfikacji alkoholu furfurylowego i kwasów tłuszczowych C8-C18 w obecności opracowanych biokatalizatorów z systemu okresowego na ciągły.

Na podstawie obiecujących wyników uzyskanych w układzie okresowym opracowany biokatalizator MgO-SiO_2-C8-LAO przetestowałam w trybie ciągłym. Eksperymenty przeprowadziłam w pełni zautomatyzowanym kolumnowym mikroreaktorze przepływowym Syrris Asia, wypełnionym 300 mg MgO-SiO_2-C8-LAO. Przed każdym eksperymentem przygotowywałam świeżą mieszaninę alkoholu furfurylowego (6,2 g), kwasu oktanowego (27,4 g) i cykloheksanu (31,7 mL), która następnie była pompowana do reaktora wypełnionego biokatalizatorem. W celu utrzymania stabilnego przepływu reagentów przez złoże, układ został wyposażony w regulator ciśnienia wstecznego, ustawiony na 2 bary (Wykres 5). Eksperymenty przeprowadzałam w warunkach zoptymalizowanych dla systemu okresowego.

Wpływ czasu przebywania na konwersję alkoholu furfurylowego określiłam przy całkowitym natężeniu przepływu reagentów od 0,04 do 0,20 $mLmin^{-1}$. Czasy przebywania reagentów w strefie katalitycznej w zakresie od 10,5 do 18,4 min, związane z przepływem reagentów na poziomie 0,04 $mLmin^{-1}$, 0,06 $mLmin^{-1}$, 0,07 $mLmin^{-1}$ (τ = 18,4 min, 12,3 min, 10,5 min), skutkowały wysoką konwersją alkoholu furfurylowego, sięgającą 96,8% i utrzymującą się stabilnie przez co najmniej 3 h. Skrócenie czasu przebywania poniżej 10,5 min prowadziło do obniżenia konwersji alkoholu furfurylowego. Dla przepływów reagentów

0,08 mLmin^{-1}, 0,1 mLmin^{-1} i 0,2 mLmin^{-1} zauważyłam znaczące pogorszenie się wartości konwersji alkoholu furfurylowego do odpowiednio 92,3%, 85,2% i 79,1%.

Biorąc pod uwagę najwyższą konwersję alkoholu furfurylowego (96,8%) przy przepływie 0,07 mLmin^{-1} (τ = 10,5 min) i wydajności objętościowej syntezy 6651 (gh^{-1}L^{-1}), uznałam te warunki jako optymalne i wykorzystałam do długotrwałych testów stabilności biokatalizatora MgO-SiO_2-C8-LAO. Biokatalizator wykazał doskonałą stabilność przez 30 h, z konwersją alkoholu furfurylowego wynoszącą 96,8%. Niewielki spadek do 85,7% zaobserwowałam po 48 h prowadzenia procesu (Wykres 5).

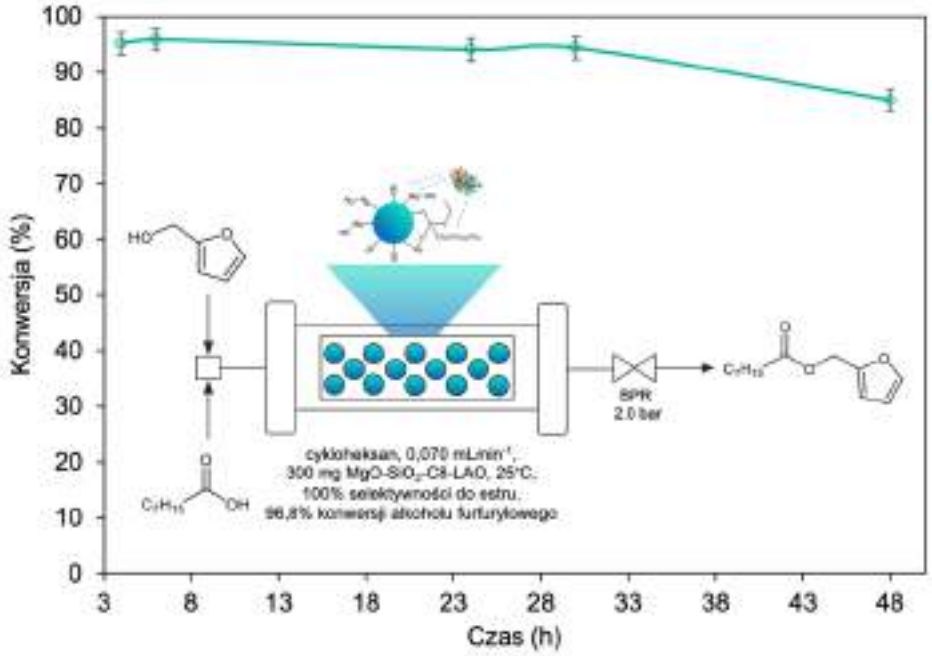

Wykres 5. Stabilność katalityczna MgO-SiO_2-C8-LAO w estryfikacji alkoholu furfurylowego i kwasu oktanowego w systemie przepływowym. Warunki reakcji: alkohol furfurylowy w cykloheksanie (2 M), kwas oktanowy (1:3, *n:n*, alkohol furfurylowy : kwas oktanowy), 0,07 mLmin^{-1}, MgO-SiO_2-C8-LAO 300 mg, 25 °C. Konwersję alkoholu furfurylowego analizowałam za pomocą GC.

Produktywność przeprowadzonego procesu wynosząca 0,376 g/h (1,67 mmol/h) jest dość efektywna, zwłaszcza biorąc pod uwagę rozmiar reaktora (objętość złoża 0,735 mL) i wydajność równą 6651 gh^{-1}L^{-1}. Dodatkowo, stabilność biokatalizatora przez 30 h pozwala na wytworzenie 11,28 g estru. Warto podkreślić, że osiągnęłam 21 razy wyższą produktywność w systemie ciągłym w porównaniu do procesu w układzie okresowym (6651 gh^{-1}L^{-1} system ciągły i 320 gh^{-1}L^{-1} system okresowy).

Podsumowując, w warunkach przepływowych uzyskałam wyższą konwersję alkoholu furfurylowego wynoszącą 96,8% w porównaniu do 90,2% w systemie okresowym, przy

jednoczesnym skróceniu czasu przebywania reagentów do 10,5 min w porównaniu do 45 min w procesie okresowym. Te doskonałe wyniki dla procesu przepływowego mogą być wyjaśnione skuteczną adsorpcją enzymu oraz zapewnieniem odpowiedniego dla lipazy hydrofobowego mikrośrodowiska, co skutkowało wysoką aktywnością enzymu przez dłuższy okres czasu.

3.4. Analiza opracowanych technologii reakcji estryfikacji alkoholu furfurylowego i kwasów tłuszczowych C8-C18 w obecności zaprojektowanego biokatalizatora w systemie okresowym oraz ciągłym pod kątem zielonej chemii.

W celu podkreślenia zrównoważonego charakteru opracowanej metody otrzymywania estrów furfurylowych, przeprowadziłam analizę *Green Metrics* wszystkich dostępnych danych literaturowych dotyczących syntezy estrów furfurylowych zgodnie z zasadami Zielonej Chemii, korzystając z zestawu narzędzi Green Chemistry Metrics J. Clark (Tabela 8).[74]

Biokatalizator MgO-SiO_2-C8-LAO użyty w syntezie oktanianu furfurylu w systemie okresowym i ciągłym porównałam z katalizatorami metalicznymi (Y_2O_3-ZrO_2, Fe-DTP-ZIF-8), komercyjnym biokatalizatorem (Novozyme 435) oraz odczynnikiem sprzęgającym (*N*-(3-dimetyloaminopropylo)-*N*'-etylokarbodiimid, EDC), które zostały opisane w literaturze w syntezie: octanu furfurylu, oleinianu furfurylu, oktanianu furfurylu, rycynolanu furfurylu i 2-furanianu furfurylu.

W prawie wszystkich przypadkach nie zaobserwowałam produktów ubocznych, osiągając 100% selektywności procesu, z wyjątkiem niższej selektywności estryfikacji wynoszącej 86,3%, uzyskanej w obecności katalizatora Fe-DTP-ZIF-8 (heteropolikwas zamknięty w zeolicie typu ZIF-8 domieszkowany żelazem). Wydajność estru wyższa niż 90% została otrzymana tylko w dwóch przypadkach: z biokatalizatorami opisanymi w tej pracy i z Novozyme 435 (Nr 3, 7, 8), co podkreśla znaczenie przeprowadzonych badań. W tym miejscu warto podkreślić, że brak lub trudności z recyklingiem Novozyme 435 mogą stanowić istotną przeszkodę w jego zastosowaniu w systemie ciągłym.

Tabela 8. Analiza syntezy estrów furfurylowych pod kątem zielonej chemii.

Katalizator/Reagent	Y_2O_3-ZrO_2[a]	Fe-DTP-ZIF-8[b]	Novozyme 435[c]	Novozyme 435[d]	Novozyme 435[e]	EDC[f]	MgO-SiO_2-C8-LAO System okresowy[g]	MgO-SiO_2-C8-LAO System ciągły[h]
Nr	1	2	3	4	5	6	7	8
Kwas	Kwas octowy	Kwas octowy	Kwas oleinowy	Kwas oktanowy	Kwas rycynolowy	Kwas furanowy	Kwas oktanowy	Kwas oktanowy
Wydajność produktu (%)	88	75,7	99,9	73	88,6	70,8	90,2	96,8
Selektywność reakcji (%)	100	86,3	100	100	100	100	100	100
Ekonomia atomu (%)	88,6	88,6	95,3	92,6	95,5	91,4	92,6	92,6
RME (%)	31	47,9	95,1	68,7	56,1	31,3	38,1	40,9
Rozpuszczalnik	🚩	_ [i]	_ [i]	_ [i]	_ [i]	🚩	🚩	🚩
Katalizator czy reagent	🚩	🚩	🚩	🚩	🚩	🚩	🚩	🚩
Recykl	🚩	🚩	Brak danych	Brak danych	Brak danych	🚩	🚩	🚩
Pierwiastki krytyczne	🚩	🚩	🚩	🚩	🚩	🚩	🚩	🚩
Energia	🚩	🚩	🚩	🚩	🚩	🚩	🚩	🚩
Reakcja prowadzona poniżej punktu wrzenia	🚩	🚩	🚩	🚩	🚩	🚩	🚩	🚩
System okresowy/ciągły	🚩	🚩	🚩	🚩	🚩	🚩	🚩	🚩
Metoda wydzielenia produktu	🚩	_ [i]	_ [i]	_ [i]	_ [i]	🚩	🚩	🚩
Zdrowie I bezpieczeństwo	🚩	🚩	🚩	🚩	🚩	🚩	🚩	🚩
Literatura	76	75	66	67	68	77	Ta praca	Ta praca

[a]Warunki reakcji: alkohol furfurylowy 10 mmol, kwas octowy 50 mmol, Y_2O_3-ZrO_2 0,2 g, 110 °C, 7 h. [b]Warunki reakcji: alkohol furfurylowy 46 mmol, kwas octowy 28 mmol, Fe-DTP-ZIF-8 0,006 g, 100 °C, 6 h. [c]Warunki reakcji: alkohol furfurylowy 71 mmol, kwas oleinowy 71 mmol, Novozyme 435 1 g, 60°C, 533,29 Pa, 6 h. [d]Warunki reakcji: alkohol furfurylowy 1 mmol, kwas oktanowy 1 mmol, Novozyme 435 (0,01 g), 55 °C, 24 h. [e]Warunki reakcji: alkohol furfurylowy 3 mmol, kwas oktanowy 1 mmol, Novozyme 435 0,06 g, 60 °C, 28 mmHg próżnia, 5 h. [f]Warunki reakcji: alkohol furfurylowy 2 mmol, kwas 2-furanowy 6 mmol, EDC 0,06 g, dichlorometan 3 mL, 90 °C, mikrofale 200 W, 30 min. [g]Warunki reakcji: alkohol furfurylowy 1 mmol, kwas oktanowy 3 mmol, cykloheksan 0,50 mL, MgO-SiO_2-C8-LAO 0,15 g, 25 °C, 45 min. [h]Warunki reakcji: alkohol furfurylowy 19 mmol, kwas oktanowy 57 mmol, cykloheksan 95 mL, MgO-SiO_2-C8-LAO 0,30 g, 0,070 $mLmin^{-1}$, 25 °C, 10,5 min (czas przebywania), 48 h (pełna konwersja). [i]bez rozpuszczalnika, brak danych dotyczących wydzielania; System flagowania: zielona – preferowany, żółta – akceptowalny, czerwona – niepożądany.

Biokatalizatory są uważane za biodegradowalne i przyjazne dla środowiska alternatywy dla katalizatorów metalicznych i tradycyjnych kwasów, co zwiększa ekologiczny charakter opracowanych metod (Nr 3, 4, 5, 7, 8). Możliwość zawrotu katalizatora i jego stabilność w procesie to jedne z najważniejszych aspektów przy rozważaniu wpływu na środowisko i zastosowalności opracowanej metody. Możliwość ponownego wykorzystania opisanych w literaturze układów katalitycznych wykazano tylko dla Fe-DTP-ZIF-8 przez co najmniej 5 cykli (Nr 2) w porównaniu do co najmniej 10 cykli uzyskanych dla MgO-SiO_2-C8-LAO w systemie okresowym oraz wysokiej wydajności produkcji równej 6651 $gh^{-1}L^{-1}$ w systemie ciągłym (odpowiednio Nr 7 i 8). Możliwość zawrotu Y_2O_3-ZrO_2 (Nr 1) i Novozyme 435 (Nr 4) była tylko postulowana.

Ekonomia atomowa dla reakcji estryfikacji jest niższa niż 100% z powodu tworzenia się cząsteczki wody podczas syntezy. Jak wspomniałam wcześniej, obecność wody może być korzystna podczas procesów katalizowanych przez lipazy. Efektywność masowa reakcji (z ang. *Reaction Mass Efficiency*, RME) dla syntezy estrów furfurylowych zazwyczaj wynosi od 31% do 69%, z wyjątkiem Nr 3 (95,1%). Zależy ona w dużej mierze od wydajności i nadmiaru reagentów używanych w każdej metodzie.

Synteza estrów furfurylowych może być przeprowadzana w warunkach bezrozpuszczalnikowych, ale w wysokiej temperaturze, pod ciśnieniem i z długim czasem reakcji (110°C, 7 h, Nr 1; 100 °C, 6 h, Nr 2; 60 °C, 533,29 Pa, 6 h, Nr 3; 55°C, 24 h, Nr 4; 60. °C, 28 mmHg próżni, Nr 5) lub z rozpuszczalnikiem, takim jak dichlorometan (90 °C, mikrofale 200 W, 30 min, Nr 6) i cykloheksan (25 °C, 45 min, Nr 7; 25 °C, 10,5 min czasu przebywania, Nr 8).

Warto zauważyć, że większość opisanych przykładów otrzymywania estrów furfurylowych były prowadzone w systemach okresowych (Nr 1–7). Synteza w systemie ciągłym zaprezentowana w tej pracy nie tylko zwiększa efektywność produkcji, ale także poprawia aspekty dotyczące oddziaływania technologii na środowisko.

Procedura oczyszczania została opisana tylko dla Nr 1, 6 oraz 7, 8. Estry furfurylowe można izolować poprzez destylację w warunkach obniżonego ciśnienia lub wysokiej temperatury, lub ekstrakcję rozpuszczalnikami organicznymi, takimi jak heptan (co opisano w tej pracy), dichlorometan[76,77] oraz chromatografia kolumnowa[76,77]. Czerwone flagi w wierszu Zdrowie i bezpieczeństwo dla naszych badań wynikały z konieczności użycia hydrofobowego rozpuszczalnika organicznego do ekstrakcji estru furfurylowego z mieszaniny poreakcyjnej.

Dodatkowo w ramach niniejszej pracy rozważyłam inne podejście oceny ekologiczności opracowanej metody, analizując nie tylko metodę syntezy estrów, ale także wcześniejsze etapy cyklu życia. W celu analizy opracowanej metody w kontekście cyklu życia, przygotowałam drzewo syntetyczne (Schemat 7).[78]

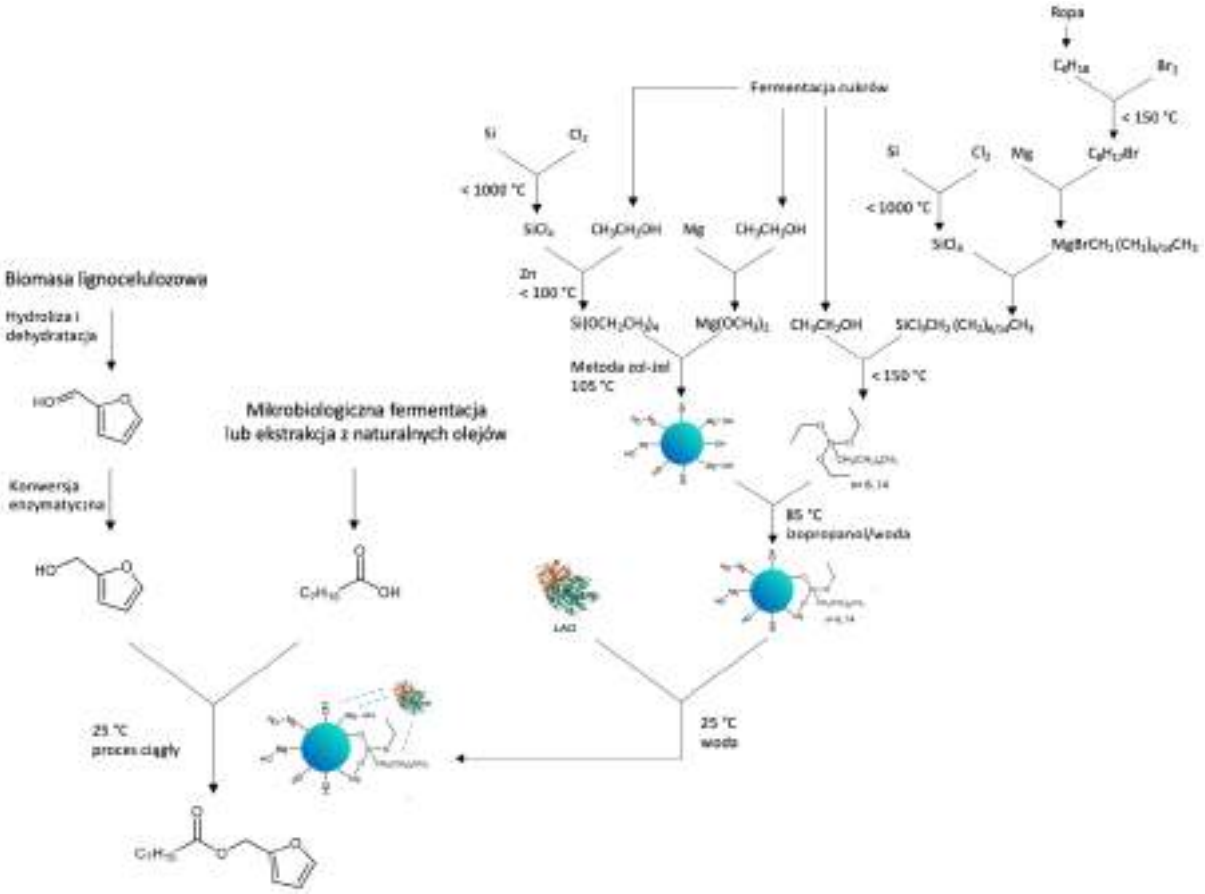

Schemat 7. Drzewo syntetyczne dla syntezy oktanianu furfurylu w systemie ciągłym katalizowanym przez MgO-SiO_2-C8-LAO.

Wszystkie niezbędne substraty do produkcji estru, alkoholu furfurylowego i kwasu oktanowego można pozyskać ze źródeł naturalnych, takich jak biomasa lignocelulozowa,[79-81] olej kokosowy i palmowy[82] lub poprzez produkcja mikrobiologiczną z odnawialnych źródeł węgla.[83] W kontekście zarządzania odpadami i zasad gospodarki w obiegu zamkniętym, szczególnie ważne jest wykorzystanie odpadów jako surowca do produkcji innych substancji. Metody produkcji dotyczące alkoholu furfurylowego i kwasu oktanowego obejmują różne strategie, w tym produkcję w systemie ciągłym, wykorzystanie rozpuszczalników głęboko eutektycznych, cieczy jonowych oraz enzymów. Wszystkie opisane podejścia mają na celu osiągnięcie najbardziej ekologicznych metod syntezy.[79-83] Produkcja biokatalizatora MgO-SiO_2-C8-LAO obejmuje wykorzystanie LAO, która jest uznawana za enzym bezpieczny, natomiast

w procesie syntezy nośnika MgO-SiO_2-C8 można zaobserwować kilka krytycznych elementów. Głównym problemem jest włączenie lotnych fluorowodorów w syntezę związków krzemoorganicznych, co stwarza ryzyko dla środowiska, takie jak kwaśne deszcze, niszczenie warstwy ozonowej i globalne ocieplenie. Niemniej jednak, trwają prace nad poszukiwaniem alternatywnych metod syntezy cennych cząsteczek krzemoorganicznych przy użyciu enzymów.[84]

Podsumowując, opracowana w tej pracy metoda ciągłej syntezy estrów furfurylowych w obecności biokatalizatora MgO-SiO_2-C8-LAO, analizowana pod kątem zielonej chemii, znajduje równowagę między wysoko aktywnym, stabilnym, nadającym się do wielokrotnego zastosowania i biodegradowalnym katalizatorem, a także podejściem przyjaznym dla środowiska i zrównoważonym w produkcji chemicznej.

III PODSUMOWANIE

Głównym celem badań realizowanych w ramach niniejszej pracy było opracowanie aktywnych i stabilnych układów katalitycznych opartych o enzymy lub kwasowe ciecze jonowe dedykowanych dla sektora lekkiej syntezy organicznej. Zaprezentowałam trzy nowe układy katalityczne, które zostały wykorzystane w trzech modelowych procesach: cykloaddycji Dielsa-Aldera, rozdziale kinetycznym racematu ibuprofenu oraz estryfikacji alkoholu furfurylowego i wyższych kwasów tłuszczowych. Nowe heterogeniczne katalizatory były oparte o kwasowe ciecze jonowe typu Lewisa lub lipazę z *Aspergillus oryzae* oraz materiały krzemionkowe. Graficzne przedstawienie opracowanych katalizatorów oraz schematy reakcji modelowych zaprezentowałam na Rysunku 10. Wszystkie nowo otrzymane katalizatory poddawałam w pierwszej kolejności szczegółowej charakterystyce metodami TGA, SEM-EDX, ^{29}Si MAS NMR, FT-IR, ICP oraz analizie adsorpcji-desorpcji (BET/BJH), a następnie przeprowadzałam ich testy aktywności katalitycznej w wybranych reakcjach modelowych z sektora lekkiej syntezy organicznej w systemie okresowym.

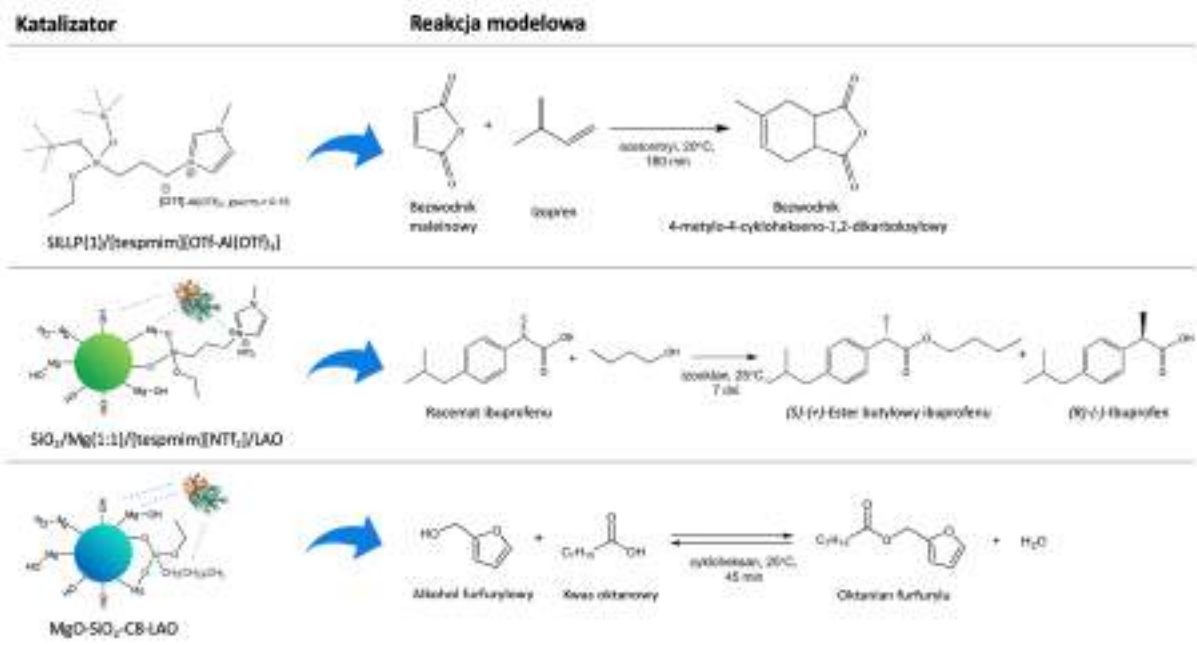

Rysunek 10. Struktury katalizatorów oraz schematy reakcji modelowych stosowanych w badaniach.

W badaniach nad opracowaniem heterogenicznego katalizatora opartego o kwasową ciecz jonową typu Lewisa [tespmim][OTf-Al(OTf)$_3$] i krzemionkę o multimodalnej porowatości wykazałam, że kolejność wprowadzania fazy aktywnej na powierzchnię nośnika ma kluczowe znaczenie. Metoda zakładająca początkową syntezę trifloglinianowej cieczy jonowej, a następnie jej związanie z powierzchnią krzemionki (zawartość IL 25,3 wt%) pozwoliła na otrzymanie katalizatora, dla którego zaobserwowałam wysoką konwersję MA z izoprenem w reakcji Dielsa-Aldera (97%) w dziesięciu cyklach reakcyjnych.

W dalszych badaniach opracowałam dwa systemy biokatalityczne do kinetycznego rozdzielania racematu ibuprofenu poprzez enancjomeryczną estryfikację w obecności lipazy z *Aspergillus oryzae*. Zaprojektowałam heterogeniczny biokatalizator oparty na nośniku SILLP oraz hybrydowych materiałach krzemionkowych, co przyczyniło się do zwiększenia aktywności i stabilności białka oraz umożliwiło jego ponowne wykorzystanie. Użycie natywnej LAO pozwoliło uzyskać enancjoselektywność 99,9% *(S)-(+)*-estru ibuprofenu przy konwersji racematu wynoszącej 34,8% po 24 h, oraz 99,9% *ee* przy 45,2% konwersji po 48 h, co jest konkurencyjne w stosunku do obecnych danych literaturowych. Heterogeniczny biokatalizator SiO_2/Mg(1:1)/[tespmim][NTf_2]/LAO (z 6,79 wt% IL i 3,96 wt% LAO) osiągnął 35% konwersji racematu ibuprofenu po 7 dniach, z 95% *ee* estru. Chociaż rozcieńczenie układu reakcyjnego spowodowało spadek szybkości reakcji, wysoki nadmiar enancjomeryczny *(S)-(+)*-estru ibuprofenu został zachowany w kolejnym cyklu reakcji.

Kolejne badania, które prowadziłam w ramach pracy doktorskiej doprowadziły do opracowania wysoce aktywnego i stabilnego biokatalizatora opartego o lipazę z *Aspergillus oryzae* oraz materiał krzemionkowy domieszkowany tlenkiem magnezu i modyfikowany grupami oktylowymi MgO-SiO_2-C8-LAO. Aktywność układu biokatalitycznego testowałam w estryfikacji alkoholu furfurylowego i kwasu oktanowego. Udowodniłam, że odpowiednie przygotowanie matrycy pod immobilizację lipazy umożliwia jej efektywną immobilizację na nośniku oraz aktywne działanie w procesie. Domieszkowanie krzemionki tlenkiem magnezu dodatkowo spowodowało wzrost aktywności katalitycznej białka. Opracowany przeze mnie biokatalizator wykazał swoją aktywność katalityczną przez 9 kolejnych cykli estryfikacji alkoholu furfurylowego, po którym dopiero zaobserwowałam stopniowy spadek konwersji substratu z 90,2% do 84,6%. MgO-SiO_2-C8-LAO umożliwił syntezę estrów furfurylowych kwasu oktanowego, nonanowego, dekanowego, laurynowego oraz oleinowego ze 100% selektywnością.

W przypadku, gdy stabilność katalizatora w układzie reakcyjnym była wystarczająca, proces dostosowywałam do warunków przepływowych (Rysunek 11). Technologie przepływowe umożliwiają maksymalizację procesu produkcji poprzez efektywniejszą wymianę masy, dzięki korzystnemu stosunkowi powierzchni kontaktu do objętości wprowadzanych reagentów. Dodatkowo, syntezy ciągłe są łatwiejsze do skalowania, bardziej ekologiczne oraz łatwiej je integrować z zaawansowanymi systemami monitoringu i automatyzacji. Wszystkie wymienione zalety procesów prowadzonych w systemie przepływowym prowadzą do zwiększenia bezpieczeństwa i efektywności produkcji.

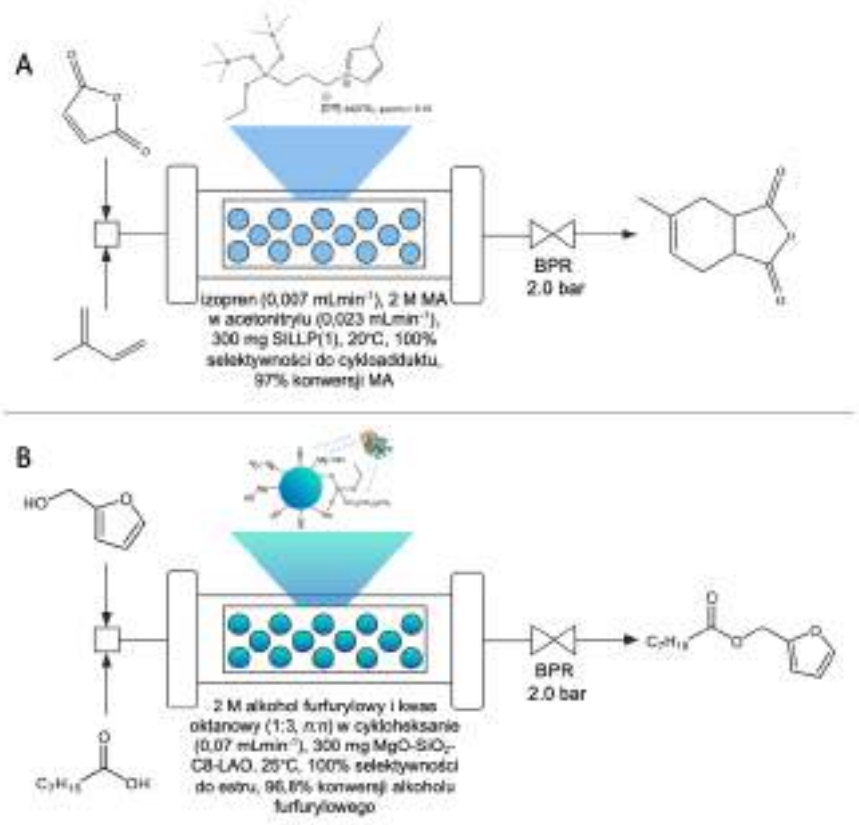

Rysunek 11. Graficzne przedstawienie opracowanych procesów w systemach przepływowych.

Transformacja modelowej reakcji Dielsa-Aldera bezwodnika maleinowego z izoprenem na tryb ciągły w obecności katalizatora SILLP(1)/[tespmim][OTf-Al(OTf)$_3$], po optymalizacji warunków w systemie przepływowym, doprowadziła do 97% konwersji MA przez 432 h (TOF 104,3 h^{-1}) (Rysunek 11A). W tej części pracy, dokładna optymalizacja ścieżki syntezy trifloglinianowych materiałów SILLP pozwoliła na otrzymanie wysoce wydajnego i stabilnego katalizatora, który umożliwił opracowanie technologii syntezy cykloadduktów Dielsa-Aldera w systemie okresowym oraz ciągłym.

Transformacja syntezy oktanianu furfurylu w obecności biokatalizatora MgO-SiO_2-C8-LAO umożliwiła intensyfikację procesu do 96,8% konwersji alkoholu furfurylowego przy przepływie 0,07 $mLmin^{-1}$ (τ = 10,5 min) i wydajności syntezy 6651 ($gh^{-1}L^{-1}$) (Rysunek 11B). W tych warunkach biokatalizator wykazał doskonałą stabilność przez 30 h, z konwersją alkoholu furfurylowego wynoszącą 96,8%, a niewielki spadek do 85,7% zaobserwowałam po 48 h prowadzenia procesu. Osiągnięta przeze mnie produktywność w układzie ciągłym jest 21 razy wyższa w porównaniu do procesu w układzie okresowym (6651 $gh^{-1}L^{-1}$ system ciągły i 320 $gh^{-1}L^{-1}$ system okresowy).

Podsumowując, zaprojektowane przeze mnie układy katalityczne wykazują się wysoką aktywnością oraz stabilnością. Pozwoliło to na opracowanie technologii z sektora lekkiej syntezy organicznej, które wpisują się w ideę zielonej chemii oraz cele zrównoważonego rozwoju przemysłu chemicznego. Część prowadzonych przeze mnie badań została wyróżniona grantem naukowym Narodowego Centrum Nauki w ramach programu Preludium-22. Dodatkowo, procesy oraz metody syntezy katalizatorów były przedmiotem dwóch zgłoszeń patentowych.

IV LITERATURA

[1] R.A. Scheldon, *Green. Chem*. 2017, 19, 18–43.

[2] R. Ratti, *SN Appl. Sci.* 2020, 2, 263.

[3] C.M. Friend, B. Xu, *Acc. Chem. Res.* 2017, 50, 517–521.

[4] N.V. Plechkova, K.R. Seddon, *Chem. Soc. Rev.* 2008, 37, 123–150.

[5] J.P. Hallett, T. Welton, *Chem. Rev.* 2011, 111, 3508–3576.

[6] T. Welton, *Chem. Rev.* 1999, 99, 2071–2084.

[7] Chiappe, C.; Rajamani, S.; D'Andrea, F. *Green Chem.* 2013, *15*, 137–143.

[8] L.C. Brown, J.M. Hogg, M. Swadźba-Kwaśny, *Top Curr. Chem.* 2017, 375, 78.

[9] T.L. Greaves, C.J. Drummond, *Chem. Rev*. 2008, 108, 206–237.

[10] A.S. Amarasekara, *Chem. Rev.* 2016, 116, 6133–6183.

[11] R. Skoda-Földes, *Molecules* 2014, 19, 8840–8884.

[12] M.H. Valkenberg, C. deCastro, W.F. Hölderich, *Top. Catal.* 2000, 14, 139–144.

[13] F. Giacalone, M. Gruttadauria, *ChemCatChem* 2016, 8, 664–684.

[14] A. Wolny, A. Chrobok, *Molecules* 2022, 27, 5900. [Publikacja 1]

[15] R.A. Scheldon, J.M. Woodley, *Chem. Rev.* 2018, 118, 801–838.

[16] M.T. Reetz, *J. Am. Chem. Soc.* 2013, 135, 12480.

[17] E.M. Anderson, K.M. Larsson, O. Kirk, *Biocatal. Biotransform.* 1998, 16, 181.

[18] F. Hasan, A. A. Shah, A. Hamed, *Enzyme Microb. Technol.* 2006, 39, 235.

[19] R. Verger, *Trends Biotechnol.* 1997, 15, 32–38.

[20] A. Brzozowski, U. Derewenda, Z.S. Derewenda, G.G. Dodson, D.M. Lawson, J.P. Turkenburg, F. Bjorkling, B. Huge-Jensen, S.A. Patkar, L. Thim, *Nature* 1991, 351, 491–494.

[21] A. Kumar, K. Dhar, S.S. Kanwar, *Biol. Proced. Online* 2016, 18, 1–11.

[22] C. Mateo, J.M. Palomo, G. Fernandez-Lorente, J.M. Guisan, R. Fernandez-Lafuente, *Enzyme Microb. Technol.* 2017, 40, 1451–1463.

[23] C. Garcia-Galan, Á. Berenguer-Murcia, R. Fernandez-Lafuente, R.C. Rodrigues, *Adv. Synth. Catal.* 2011, 353, 2885–2904.

[24] E.P. Cipolatti, A. Valério, R.O. Henriques, D.E. Moritz, J.L. Ninow, D.M.G. Freire, E.A. Manoel, R. Fernandez-Lafuente, D. De Oliveira, *RSC Adv.* 2016, 6, 104675–104692.

[25] R. Fernandez-Lafuente, P. Armisén, P. Sabuquillo, G. Fernández-Lorente, J.M. Guisán, *Chem. Phys. Lipids*, 1998, 93, 185–197.

[26] G. Fernandez-Lorente, J. Rocha-Martín, J.M. Guisan, *Methods Mol. Biol.* 2020, 2100, 143–158.

[27] S. Arana-Peña, N.S. Rios, D. Carballares, L.R.B. Gonçalves, R. Fernandez-Lafuente, *Catal. Today* 2021, 362, 130–140.

[28] A. Drozdz, A. Chrobok, S. Baj, K. Szymańska, J. Mrowiec-Białoń, A.B. Jarzębski, *Appl. Catal. A Gen*. 2013, 467, 163–170.

[29] E. Garcia-Verdugo, P. Lozano, S.V. Luis, Biocatalytic Processes Based on Supported Ionic Liquids. W R. Fehrmann, A. Riisager, M. Haumann, *Supported Ionic Liquids: Fundamental and Applications*, Wiley-VCH Verlag GmbH: Berlin, Germany, 2014, str. 351–368.

[30] F. Van Rantwijk, *Angew. Chem. Int. Ed.* 2013*,* 52, 3065–3066.

[31] M. Potdar, G. Kelso, L. Schwarz, C. Zhang, M. Hearn, *Molecules* 2015, 20, 16788–16816.

[32] A. Riisager, R. Fehrmann, M. Haumann, P. Wasserscheid, *Eur. J. Inorg. Chem*. 2006, 4, 695–706.

[33] A. Wolny, A. Chrobok, *Nanomaterials* 2021, 11, 2030. [Publikacja 2]

[34] A. Wolny, A. Chrobok, *Curr. Org. Chem.* 2023, 27, 1119–1122. [Publikacja 3]

[35] A. Wolny, P. Latos, K. Szymańska, S. Jurczyk, A. Jakóbik-Kolon, A. Chrobok, *Appl. Catal. A Gen.* 2024, 676, 119676. [Publikacja 4]

[36] A. Wolny, A. Siewniak, J. Zdarta, F. Ciesielczyk, P. Latos, S. Jurczyk, L.D. Nghiem, T. Jesionowski, A. Chrobok, *Environ. Technol. Innov.* 2022, 28, 102936. [Publikacja 5]

[37] A. Wolny, D. Więcławik, J. Zdarta, S. Jurczyk, T. Jesionowski, A. Chrobok, *Green Chem.* 2024, [Publikacja 6]

[38] A.P. Abbott, G. Capper, D.L. Davies, H.L. Munro, R.K. Rasheed, V. Tambyrajah, *Chem. Commun*. 2001, 2010–2011.

[39] B.A. Silveira Neto, G. Ebeling, R.S. Gonçalves, F.C. Gozzo, M.N. Eberlin, J. Dupont, *Synthesis* 2004, 8, 1155–1158.

[40] P. Latos, A. Culkin, N. Barteczko, S. Boncel, S. Jurczyk, L.C. Brown, P. Nockemann, A. Chrobok, M. Swadźba-Kwaśny, *Front. Chem.* 2018, 6, 535.

[41] P. Latos, A. Szelwicka, S. Boncel, S. Jurczyk, M. Swadźba-Kwaśny, A. Chrobok, *ACS Sustainable Chem. Eng.* 2019, 7, 5184–5191.

[42] P. Latos, A. Wolny, J. Zdarta, F. Ciesielczyk, S. Jurczyk, T. Jesionowski, A. Chrobok, *Environ. Technol. Innov.* 2023, 31, 103164.

[43] J.A. Funel, S. Abele, *Angew. Chem.* 2013, 52, 3822–3863.

[44] B. Briou, B. Am´eduri, B. Boutevin*, Chem. Soc. Rev.* 2021, 50, 11055–11097.

[45] X.-C. Lv, Z.-C. Tan, Q. Shi, H.-T. Zhang, L.-X. Sun, T. Zhang, *J. Chem. Eng. Data* 2005, 36, 932–935.

[46] N. Tomotaka, I. Yusuke, S. Masaki, I. Yoshio, A. Yasuhiko, *AIChE J.* 1998, 44, 1706–1708.

[47] Y. Ikushima, N. Saito, M. Arat*, Bull. Chem. Soc. Jpn.* 1990, 64, 282–284.

[48] A.M. Evans, *Clin. Rheumatol.* 2001, 20, 9–14.

[49] S.S. Adams, P. Bresloff, C.G. Mason, *J. Pharm. Pharmacol.* 1976, 28, 256–257.

[50] C. Jose, M.V. Toledo, L.E. Briand, *Crit. Rev. Biotechnol.* 2015, 36, 891–903.

[51] T. Siódmiak, J.K. Rumiński, M.P. Marszałł, *Curr. Org. Chem.* 2012, 16, 972–977.

[52] M. Mohammadi, S. Gandomkar, Z. Habibi, M. Yousefi, *RSC Adv.* 2016, 6, 52838–52849.

[53] S. Huang, X. Li, L. Xu, C. Ke, R. Zhang, Y. Yan, *Appl. Biochem. Biotechnol.* 2015, 177, 36–47.

[54] S. Ghofrani, A. Allameh, P. Yaghmaei, D. Norouzian, *J. Pharm. Sci.* 2021, 29, 117–123.

[55] T. Wei, K. Yang, B. Bai, J. Zang, X. Yu, D. Mao, *Molecules* 2016, 21, 905.

[56] S. Salgin, S. Takac, *Chem. Eng. Technol.* 2007, 30, 1739–1743.

[57] A. Kołodziejczak-Radzimska, J. Zdarta, F. Ciesielczyk, T. Jesionowski, *Korean J. Chem. Eng.* 2018, 35, 2220–2231.

[58] A. Racha, C. Samanta, S. Sreekantan, B. Marimuthu, *Energy and Fuels* 2023, 37, 11475–11496.

[59] N. Li, M. H. Zong, *ACS Catal.* 2022, 12, 10080–10114.

[60] Q. Li, C. Ma, J. Di, J. Ni, Y.C. He, *Bioresour. Technol.* 2022, 34.

[61] V. Ant.n, J. Mu.oz-Embid, I. Gasc.n, M. Artal, C. Lafuente, *Energy and Fuels* 2017, 31, 4143–4154.

[62] M.E. Fortunato, F. Taddeo, R. Vitiello, R. Turco, R. Tesser, V.Russo, M. Di Serio, *ACS Sustain. Chem. Eng.* 2023, 11, 12406–12413.

[63] E.M. Wewerka, *J. Appl. Polym. Sci.* 1968, 12, 1671–1681.

[64] R. González, R. Martínez, P. Ortiz, *Die Makromol. Chemie* 1992, 193, 1–9.

[65] H.E. Hoydonckx, D.E. De Vos, S.A. Chavan, P.A. Jacobs, *Top. Catal.* 2004, 27, 83–96.

[66] A. Sengupta, T. Dey, M. Ghosh, J. Ghosh, S. Ghosh, *J. Inst. Eng. Ser. E.* 2012, 93, 31–36.

[67] Y. Satyawali, V. Akemeier, W. Dejonghe, H. De Wever, W. Van Hecke, *Waste Biomass Valor*. 2019, 10, 311–317.

[68] S. Mukherjee, M. Ghosh, *Carbohydr. Polym.* 2017, 157, 1076–1084.

[69] M. Markiton, S. Boncel, D. Janas, A. Chrobok, *ACS Sustain. Chem. Eng.* 2017, 5, 1685–1691.

[70] A. Szelwicka, S. Boncel, S. Jurczyk, A. Chrobok*, Appl. Catal. A Gen.* 2019, 574, 41–47.

[71] J.J. Shangguan, Y.Q. Liu, F.J. Wang, J. Zhao, L.Q. Fan, S.X. Li, J.H. Xu, *Appl. Biochem. Biotechnol.* 2011, 165, 949–962.

[72] F. Ciesielczyk, M. Przybysz, J. Zdarta, A. Piasecki, D. Paukszta, T. Jesionowski, *J. Sol-Gel Sci. Technol.* 2014, 71, 501–513.

[73] J. Toida, K. Kondoh, M. Fukuzawa, K. Ohnishi, J. Sekiguchi, *Biosci. Biotechnol. Biochem.* 1995, 59, 1199–1203.

[74] C.R. McElroy, A. Constantinou, L.C. Jones, L. Summerton, J.H. Clark, *Green Chem.* 2015, 17, 3111-3121.

[75] R.S. Malkar, H. Daly, C. Hardacre, G.D. Yadav, *React. Chem. Eng.* 2019, 4, 1790–1802.

[76] P. Kumar, R.K. Pandey, M.S. Bodas, S.P. Dagade, M.K. Dongare, A. V. Ramaswamy, *J. Mol. Catal. A Chem.* 2002, 181, 207–213.

[77] Ł. Janczewski, D. Zieliński, B. Kolesińska, *Open Chem*. 2021, 19, 265–280.

[78] P. Jessop, *Green Chem.* 2020, 22, 13–15.

[79] V. K. Vaidyanathan, K. Saikia, P. S. Kumar, A. K. Rathankumar,G. Rangasamy, G. D. Saratale, *Bioresour. Technol.* 2023, 378, 128975.

[80] Y. Bao, Z. Du, X. Liu, H. Liu, J. Tang, C. Qin, C. Liang, C. Huang, S. Yao, *Green Chem.* 2024, 26, 6318-6338.

[81] K. J. Yong, T. Y. Wu, C. B. T. Loong Lee, Z. J. Lee, Q. Liu, J. Md Jahim, Q. Zhou, L. Zhang, *Biomass Bioenergy*, 2022, 161, 106458.

[82] Y. Chen, Y. She, J. Lei, D. Wang, S. Wu, K. Men, *Conf. Ser.: Earth Environ. Sci.* 2021, 705, 012013.

[83] J. H. Ahn, K. H. Jung, E. S. Lim, S. M. Kim, S. O. Han, Y. Um, *Bioresour. Technol.* 2023, 381, 129147.

[84] N. S. Sarai, B. J. Levin, J. M. Roberts, D. E. Katsoulis, F. H. Arnold, *ACS Cent. Sci.* 2021, 7, 944–953.

V INNE OSIĄGNIĘCIA NAUKOWE

A. Publikacje naukowe

1. P. Latos, A. Wolny, J. Zdarta, F. Ciesielczyk, S.Jurczyk, T. Jesionowski, A. Chrobok, Highly stable Lewis acidic trifloaluminate ionic liquid supported on silica and metallosilicates as an efficient catalyst for continuous flow aminolysis of epoxides, *Environ. Technol. Innov.* 2023, 31, 103164.
2. A. Szelwicka, A. Wolny, M. Grymel, S. Jurczyk, S. Boncel, A. Chrobok, Chemo-enzymatic Baeyer-Villiger oxidation facilitated with lipases immobilized in the supported ionic liquid phase, *Materials*, 2021, 14, 3443.
3. M. Heba, A. Wolny, A. Kastelik-Hryniewiecka, D. Stradomska, S. Jurczyk, A. Chrobok, N. Kuźnik, Green Dynamic Kinetic Resolution—Stereoselective Acylation of Secondary Alcohols by Enzyme-Assisted Ruthenium Complexes. *Catalysts* 2022, 12, 1395.
4. P. Latos, A. Wolny, A. Chrobok, Supported ionic liquid phase catalysts dedicated for continuous flow synthesis, *Materials*, 2023, 16, 1-18.
5. S. Bajkacz, K. Rusin, A. Wolny, J. Adamek, K. Erfurt, A. Chrobok, Highly efficient extraction procedures based on natural deep eutectic solvents or ionic liquids for determination of 20-hydroxyecdysone in spinach, *Molecules*, 2020, 25, 4736.
6. N. Barteczko, A. Brzęczek-Szafran, A. Wolny, S. Jurczyk, A. Jakóbik-Kolon, A. Chrobok, Supported ionic liquids for effective ruthenium olefin metathesis, *Appl. Catal. A. Gen.* 2023, 661, 119226.
7. A. Tabaszewska, A. Wolny, Zastosowanie enzymów w produkcji przemysłowej, *Chemik*, 2024, 1, 42-47.
8. W. Chromy, A. Wolny, Metody stabilizacji biokatalizatorów w syntezie organicznej, *Chemik*, 2024, 1, 36-40.

B. Patenty:

1. P. Latos, A. Chrobok, A. Wolny, Sposób immobilizacji enzymów na stałym nośniku, PL442134A1, 2024.

C. Projekty:

1. Projekt o symbolu NB-87/RCh-5/2020 pt. Badanie aktywności innowacyjnych enzymów w wybranych reakcjach chemicznych (5.06.2020-4.12.2020). Pełniona funkcja: wykonawca.
2. Projekt o symbolu 04/050/NB_22/0160 pt. Testy aktywności roztworów lipaz pochodzenia mikrobiologicznego w wybranych reakcjach modelowych (9.06.2022-5.09. 2022). Pełniona funkcja: wykonawca.
3. Projekt o symbolu NB-187/RCH-5/2022 – Losentech sp. z o.o. pt. Przeskalowanie skali procesu przemysłowego. Optymalizacja parametrów procesu utleniania Bayera-Villigera (24.08.2022-25.01.2023). Pełniona funkcja: wykonawca.
4. Projekt NCN OPUS23 UMO-2022/45/B/ST8/02288 pt. Projektowanie kompozytów cementowych z wykorzystaniem zrównoważonych związków jonowych: Ocena właściwości strukturalnych i użytkowych (03.02.2022-do teraz). Pełniona funkcja: wykonawca.
5. Projekt o symbolu NB-262/RCH-5/2023 – Orlen Południe S.A. Opracowanie metod otrzymywania zielonych rozpuszczalników organicznych: estrowych i jonowych, wraz z optymalizacją procesu ich produkcji w skali laboratoryjnej (5.10.2023 – 04.10.2024). Pełniona funkcja: wykonawca.
6. Projekt o symbolu NB-296/RCH-5/2023 – Losentech sp. z o.o. Prowadzenie reakcji utleniania kwasu dekanowego z rozdziałem faz (9.11.2023 – 10.04.2024). Pełniona funkcja: wykonawca.

D. Prezentacje na konferencjach krajowych i międzynarodowych:

1. II Pomeranian Students Chemical Symposium 20-21.03.2021, Gdańsk, Polska; Innovative supported ionic liquid phase biocatalysts in Bayer-Villiger oxidation (poster).
2. 7th International Conference on Ionic Liquid-Based Materials, 21-24.11.2023, Porto, Portugalia; Poly(ionic liquid) compounds as multifunctional cement additives (poster).

E. Inne aktywności naukowe i dydaktyczne

1. Członek Uczelnianej Rady Samorządu Doktorantów Politechniki Śląskiej w kadencji 2023/2024.
2. Członek Students Council EURECA-PRO w kadencji 2023/2024.
3. Opiekun naukowy w Studenckim Kole Naukowym Chemików przy Politechnice Śląskiej.

4. Opiekun pomocniczy w 3 projektach badawczych ze szkołami średnimi w ramach „Projekt Politechnika": Rozdział racematu metoprololu – produkcja leku na nadciśnienie (31/010/SDU/2-26-39), Bio-produkcja dodatków do biopaliw z biomasy lignocelulozowej (31/010/SDU/2-26-10), Zielona synteza czystego *(S)*-ibuprofenu (31/010/SDU/2-26-145).
5. Opiekun pomocniczy w projekcie „Opracowanie aktywnego układu biokatalitycznego w syntezie dodatków do biopaliw z biomasy lignocelulozowej" finansowanym w ramach VI konkursu finansowania projektów studenckich kół naukowych (IDUB).
6. Liczne prowadzenie zajęć laboratoryjnych dla uczniów szkół ponadpodstawowych.
7. Nagroda II stopnia za pracę pt. „Badania nad metodami modyfikacji nanorurek węglowych przeznaczonych do immobilizacji lipaz" w 31. edycji konkursu na najlepszą pracę dyplomową z zakresu chemii, posiadającą praktyczne znaczenie dla przemysłu 2019/2020, SITPChem, Gliwice, 27.07.2021.

VI WKŁAD AUTORSKI

Publikacja P1 (80%):

- konceptualizacja badań,
- przeprowadzenie przeglądu literatury,
- przygotowanie roboczego manuskryptu,
- przygotowanie wszystkich grafik i tabel,
- wkład w edycje manuskryptu i przygotowanie odpowiedzi dla recenzentów.

Publikacja P2 (80%):

- konceptualizacja badań,
- przeprowadzenie przeglądu literatury,
- przygotowanie roboczego manuskryptu,
- przygotowanie wszystkich grafik i tabel,
- wkład w edycje manuskryptu i przygotowanie odpowiedzi dla recenzentów.

Publikacja P3 (90%):

- konceptualizacja badań,
- przeprowadzenie przeglądu literatury,
- przygotowanie roboczego manuskryptu,
- przygotowanie wszystkich grafik i tabel,
- wkład w edycje manuskryptu i przygotowanie odpowiedzi dla recenzentów.

Publikacja P4 (55%):

- konceptualizacja badań,
- przeprowadzenie przeglądu literatury,
- opracowanie warunków analizy GC oraz analiza otrzymanych danych,
- przeprowadzenie syntezy materiałów typu SILLP oraz eksperymentów dotyczących testów aktywności katalitycznej materiałów SILLP w reakcji modelowej Dielsa-Aldera, optymalizacji warunków procesu, przeprowadzenie testów stabilności katalitycznej oraz uniwersalności katalizatora wobec innych dienów i dienofili w systemie okresowym,

- analiza materiałów krzemionkowych typu SILLP za pomocą SEM-EDX,
- wydzielenie wszystkich otrzymanych cykloadduktów,
- przeprowadzenie eksperymentów aktywności i stabilności katalitycznej wybranego materiału SILLP w reakcji modelowej Dielsa-Aldera w systemie ciągłym oraz optymalizacja warunków procesu,
- analiza i interpretacja wszystkich otrzymanych wyników badań,
- przygotowanie wszystkich wykresów, grafik i tabel,
- przygotowanie roboczego manuskryptu,
- wkład w edycje manuskryptu i przygotowanie odpowiedzi dla recenzentów.

Publikacja P5 (40%):

- konceptualizacja badań,
- przeprowadzenie przeglądu literatury,
- opracowanie warunków analizy HPLC oraz analiza otrzymanych wyników,
- przeprowadzenie eksperymentów dotyczących rozdziału racematu ibuprofenu poprzez estryfikację w obecności natywnych lipaz, optymalizacja warunków procesu,
- analiza nośników krzemionkowych oraz biokatalizatorów za pomocą SEM-EDX,
- przeprowadzenie syntezy nośników krzemionkowych typu SILLP i biokatalizatorów oraz eksperymentów dotyczących aktywności biokatalizatorów SILLP w reakcji modelowej rozdziału racematu ibuprofenu poprzez estryfikację, optymalizacja warunków procesu i testy stabilności katalitycznej biokatalizatora,
- wydzielenie otrzymanego estru ibuprofenu,
- analiza i interpretacja wszystkich otrzymanych wyników badań,
- przygotowanie wszystkich wykresów, grafik i tabel,
- przygotowanie roboczego manuskryptu,
- wkład w edycje manuskryptu i przygotowanie odpowiedzi dla recenzentów.

Publikacja P6 (50%):

- konceptualizacja badań,
- przeprowadzenie przeglądu literatury,
- opracowanie warunków analizy GC oraz analiza otrzymanych wyników,
- przeprowadzenie eksperymentów dotyczących estryfikacji alkoholu furfurylowego i kwasu oktanowego w obecności natywnych lipaz,
- przeprowadzenie modyfikacji nośników krzemionkowych grupami alkilotrietoksysilanowymi i syntezy biokatalizatorów oraz eksperymentów dotyczących aktywności biokatalizatorów w reakcji modelowej estryfikacji alkoholu furfurylowego i kwasu oktanowego, optymalizacja warunków procesu, przeprowadzenie testów stabilności katalitycznej oraz uniwersalności biokatalizatora wobec innych kwasów tłuszczowych w systemie okresowym,
- analiza nośników krzemionkowych oraz biokatalizatorów za pomocą SEM-EDX,
- przeprowadzenie eksperymentów aktywności i stabilności katalitycznej biokatalizatora w reakcji modelowej estryfikacji alkoholu furfurylowego i kwasu oktanowego w systemie ciągłym oraz optymalizacja warunków procesu,
- opracowanie metody wydzielenia wszystkich otrzymanych estrów furfurylowych,
- analiza i interpretacja wszystkich otrzymanych wyników badań,
- przeprowadzenie analizy opracowanego procesu estryfikacji alkoholu furfurylowego i kwasu oktanowego pod kątem zieloności metody za pomocą analizy *Green Metrics*, porównanie z innymi metodami opisanymi w literaturze oraz przygotowanie drzewa syntetycznego produkcji obejmującego wszystkie wykorzystane reagenty,
- przygotowanie wszystkich wykresów, grafik i tabel,
- przygotowanie roboczego manuskryptu,
- wkład w edycje manuskryptu i przygotowanie odpowiedzi dla recenzentów.

VII WKŁAD POZOSTAŁYCH WSPÓŁAUTORÓW

Deklaracje i wkład wszystkich pozostałych współautorów publikacji wchodzących w cykl publikacji monotematycznych niniejszej pracy doktorskiej zostały zamieszczone poniżej. W Tabeli 9 przedstawiono wszystkich współautorów oraz ich procentowy wkład w poszczególne publikacje wchodzący w skład pracy doktorskiej.

Tabela. 9. Lista współautorów i ich procentowy wkład w publikacje wchodzące w skład pracy doktorskiej.

Autor	P1, %	P2, %	P3, %	P4, %	P5, %	P6, %
Anna Wolny	80	80	90	55	40	50
Anna Chrobok	20	20	10	20	15	20
Agnieszka Siewniak					5	
Agata Jakóbik-Kolon				5		
Dagmara Więcławik						10
Filip Ciesielczyk					5	
Jakub Zdarta					10	10
Katarzyna Szymańska				10		
Long D. Nghiem					10	
Piotr Latos				5	5	
Sebastian Jurczyk				5	5	5
Teofil Jesionowski					5	5

Politechnika Śląska
UCZELNIA BADAWCZA

Wydział Chemiczny
Katedra Technologii Chemicznej Organicznej i Petrochemii
Prof. dr hab. inż.
Anna Chrobok
Profesor

Gliwice, 23.09.2024 r.

Deklaracja

o indywidualnym wkładzie procentowym i merytorycznym współautora

Jako współautor wymienionych publikacji:

P1: A. Wolny, A. Chrobok, Silica-Based Supported Ionic Liquid-like Phases as Heterogeneous Catalysts, *Molecules* **2022**, 27, 5900.

Oświadczam, że mój wkład procentowy w tą pracę wynosił 20% i obejmował:

- konceptualizacja badań,
- pomoc w interpretacji i opisie danych literaturowych,
- edycja i przygotowanie ostatecznej wersji manuskryptu,
- korespondencja z wydawnictwem i przygotowanie odpowiedzi dla recenzentów.

P2: A. Wolny, A. Chrobok, Ionic Liquids for Development of Heterogeneous Catalysts Based on Nanomaterials for Biocatalysis, *Nanomaterials* **2021**, 11, 2030.

Oświadczam, że mój wkład procentowy w tą pracę wynosił 20% i obejmował:

- konceptualizacja badań,
- pomoc w interpretacji i opisie danych literaturowych,
- edycja i przygotowanie ostatecznej wersji manuskryptu,
- korespondencja z wydawnictwem i przygotowanie odpowiedzi dla recenzentów.

Politechnika Śląska
Wydział Chemiczny
Katedra Technologii Chemicznej Organicznej i Petrochemii
ul. Krzywoustego 4, 44-100 Gliwice
+48 32 237 20 17/+48 32 237 10 52 (fax)
anna.chrobok@polsl.pl
NIP 631 020 87 36
ING Bank Śląski S.A. w Gliwicach 60 1050 1220

Politechnika Śląska
UCZELNIA BADAWCZA

Wydział Chemiczny
Katedra Technologii Chemicznej Organicznej i Petrochemii

Prof. dr hab. inż.
Anna Chrobok
Profesor

P3: A. Wolny, A. Chrobok, Supported Ionic Liquid Phase for Biocatalysis: The Current Applications, Synthesis and Prospects, *Curr. Org. Chem.* **2023**, 27, 1119–1122.

Oświadczam, że mój wkład procentowy w tą pracę wynosił 10% i obejmował:

- konceptualizacja badań,
- pomoc w interpretacji i opisie danych literaturowych,
- edycja i przygotowanie ostatecznej wersji manuskryptu,
- korespondencja z wydawnictwem i przygotowanie odpowiedzi dla recenzentów.

P4: A. Wolny, P. Latos, K. Szymańska, S. Jurczyk, A. Jakóbik-Kolon, A. Chrobok, Construction of trifloaluminate ionic liquid catalyst on the silica surface dedicated for continuous flow Diels-Alder synthesis, *Appl. Catal. A Gen.* **2024**, 676, 119676.

Oświadczam, że mój wkład procentowy w tą pracę wynosił 20% i obejmował:

- konceptualizacja badań,
- pomoc w interpretacji i opisie wszystkich otrzymanych wyników badań,
- edycja i przygotowanie ostatecznej wersji manuskryptu,
- zapewnienie finansowania badań,
- korespondencja z wydawnictwem i przygotowanie odpowiedzi dla recenzentów.

P5: A. Wolny, A. Siewniak, J. Zdarta, F. Ciesielczyk, P. Latos, S. Jurczyk, D.L. Nghiem, T. Jesionowski, A. Chrobok, Supported ionic liquid phase facilitated catalysis with lipase from Aspergillus oryzae for enhance enantiomeric resolution of racemic ibuprofen, *Environ. Technol. Innov.* **2022**, 28, 102936–102947.

Oświadczam, że mój wkład procentowy w tą pracę wynosił 20% i obejmował:

- konceptualizacja badań,
- pomoc w interpretacji i opisie wszystkich otrzymanych wyników badań,
- edycja i przygotowanie ostatecznej wersji manuskryptu,

Politechnika Śląska
Wydział Chemiczny
Katedra Technologii Chemicznej Organicznej i Petrochemii
ul. Marcina Strzody 9, 44-100 Gliwice
tel. +48 32 237 20 17/+48 32 237 28 32 (fax)
www.chemorgpetrol.pl
NIP 631 020 07 36
ING Bank Śląski S.A. Oddział w Gliwicach 65 1050 1230
0000 0000 0000 0000

Politechnika Śląska
UCZELNIA BADAWCZA

Wydział Chemiczny
Katedra Technologii Chemicznej Organicznej i Petrochemii

Prof. dr hab. inż.
Anna Chrobok
Profesor

- zapewnienie finansowania badań,
- korespondencja z wydawnictwem i przygotowanie odpowiedzi dla recenzentów.

P6: A. Wolny, D. Więcławik, J. Zdarta, S. Jurczyk, T. Jesionowski, A. Chrobok, Robust biocatalyst for the green continuous flow synthesis of esters from biomass-derived furfuryl alcohol and C8-C18 carboxylic acids, *Green Chem.* **2024**, Advance article, doi.org/10.1039/D4GC03821E.

Oświadczam, że mój wkład procentowy w tą pracę wynosił 20% i obejmował:

- konceptualizacja badań,
- pomoc w interpretacji i opisie wszystkich otrzymanych wyników badań,
- edycja i przygotowanie ostatecznej wersji manuskryptu,
- zapewnienie finansowania badań,
- korespondencja z wydawnictwem i przygotowanie odpowiedzi dla recenzentów.

.....

podpis

Politechnika Śląska
Wydział Chemiczny
Katedra Technologii Chemicznej Organicznej i Petrochemii
ul. Krzywoustego 4, 44-100 Gliwice
+48 32 237 29 17/+48 32 237 10 32 (fax)
anna.chrobok@polsl.pl
NIP 631 020 27 96
PKO Bank Polski S.A. 2/Oddział 60 1050 1230 1000 0005 0101 9864

Politechnika Śląska
UCZELNIA BADAWCZA

Wydział Chemiczny
Katedra Technologii Chemicznej Organicznej i Petrochemii
dr inż.
Agnieszka Siewniak
adiunkt

Gliwice, 20.09.2024

Deklaracja

o indywidualnym wkładzie procentowym i merytorycznym współautora

Jako współautor wymienionej publikacji:

P5: A. Wolny, A. Siewniak, J. Zdarta, F. Ciesielczyk, P. Latos, S. Jurczyk, D.L. Nghiem, T. Jesionowski, A. Chrobok, *Supported ionic liquid phase facilitated catalysis with lipase from Aspergillus oryzae for enhance enantiomeric resolution of racemic ibuprofen*, Environ. Technol. Innov. 2022, 28, 102936–102947.

Oświadczam, że mój wkład procentowy w tą pracę wynosił 5% i obejmował:

- asystę w opracowaniu metody analitycznej (HPLC) i analizie danych

Siewniak

podpis

Politechnika Śląska
Wydział Chemiczny
Katedra Technologii Chemicznej Organicznej i Petrochemii
ul. Krzywoustego 4, 44-100 Gliwice
+48 32 237 2633
agnieszka.siewniak@polsl.pl
NIP 631-020-07-38
ING Bank Śląski S.A. w Gliwicach 50 1050 1230 1000 0002 0215 3058

Wydział Chemiczny
Katedra Chemii Nieorganicznej, Analitycznej i Elektrochemii

dr hab. inż.
Agata Jakóbik-Kolon
Prof. PŚ.

Gliwice, dn. 23.09.2024 r.

Deklaracja o indywidualnym wkładzie procentowym i merytorycznym współautora

Jako współautor wymienionej publikacji:

P4: A. Wolny, P. Latos, K. Szymańska, S. Jurczyk, A. Jakóbik-Kolon, A. Chrobok, Construction of trifloaluminate ionic liquid catalyst on the silica surface dedicated for continuous flow Diels-Alder synthesis, Appl. Catal. A Gen. 2024, 676, 119676.

Oświadczam, że mój wkład procentowy w tą pracę wynosił 5% i obejmował:

- przeprowadzenie analiz ICP katalizatorów SILLP.

Politechnika Śląska
Wydział Chemiczny
Katedra Chemii Nieorganicznej Analitycznej i Elektrochemii
ul. B. Krzywoustego 6, pok. 231A, 44-100 Gliwice
+48 32 237 19 90
agata.jakobik@polsl.pl
NIP 631 020 07 36
ING Bank Śląski S.A. o/Gliwice 60 1050 1230 1000 0002 0211 3056

Politechnika Śląska
UCZELNIA BADAWCZA

Wydział Chemiczny
Katedra Technologii Chemicznej Organicznej i Petrochemii
mgr inż.
Dagmara Więcławik

Gliwice, 23.09.2024 r.

Deklaracja

o indywidualnym wkładzie procentowym i merytorycznym współautora

Jako współautor wymienionej publikacji:

P6: A. Wolny, D. Więcławik, J. Zdarta, S. Jurczyk, T. Jesionowski, A. Chrobok, Robust biocatalyst for the green continuous flow synthesis of esters from biomass-derived furfuryl alcohol and C8-C18 carboxylic acids, *Green Chem.* **2024**, Advance article, doi.org/10.1039/D4GC03821E.

Oświadczam, że mój wkład procentowy w tą pracę wynosił 10% i obejmował:

- asystę w przeprowadzaniu eksperymentów dotyczących syntezy biokatalizatorów oraz testów ich aktywności katalitycznej, optymalizacji warunków reakcji modelowej alkoholu furfurylowego i kwasu oktanowego oraz testów stabilności wybranego biokatalizatora w systemie okresowym,

- asystę we wstępnych eksperymentach aktywności katalitycznej biokatalizatora w reakcji modelowej alkoholu furfurylowego i kwasu oktanowego w systemie ciągłym.

Dagmara Więcławik
.....

podpis

Politechnika Śląska
Wydział Chemiczny
Katedra Technologii Chemicznej Organicznej Petrochemii

POLITECHNIKA POZNAŃSKA

WYDZIAŁ TECHNOLOGII CHEMICZNEJ
dr hab. inż. Filip Ciesielczyk, prof. PP
Prodziekan ds. nauki
ul. Berdychowo 4, 60-965 Poznań, tel. +48 61 665 2351, fax +48 61 665 2852
e-mail: office_dd@put.poznan.pl, filip.ciesielczyk@put.poznan.pl, www.fd.put.poznan.pl

Poznań, 23.09.2024 r.

Deklaracja

o indywidualnym wkładzie procentowym i merytorycznym współautora

Jako współautor wymienionej publikacji:

P5: A. Wolny, A. Siewniak, J. Zdarta, F. Ciesielczyk, P. Latos, S. Jurczyk, D.L. Nghiem, T. Jesionowski, A. Chrobok, Supported ionic liquid phase facilitated catalysis with lipase from Aspergillus oryzae for enhance enantiomeric resolution of racemic ibuprofen, *Environ. Technol. Innov.* **2022**, 28, 102936–102947.

Oświadczam, że mój wkład procentowy w tą pracę wynosił 5% i obejmował:

- syntezę hybrydowych materiałów krzemionkowych,

- wkład w edycję manuskryptu.

F. Ciesielczyk

podpis

POLITECHNIKA POZNAŃSKA

dr hab. inż. Jakub Zdarta, prof. PP
WYDZIAŁ TECHNOLOGII CHEMICZNEJ
Instytut Technologii i Inżynierii Chemicznej
ul. Berdychowo 4, 60-965 Poznań,
tel. +48 616653747, fax +48 61 665 3648
e-mail: jakub.zdarta@put.poznan.pl

Poznań, 23.09.2024

Deklaracja
o indywidualnym wkładzie procentowym i merytorycznym współautora

Jako współautor wymienionej publikacji:

P5: A. Wolny, A. Siewniak, J. Zdarta, F. Ciesielczyk, P. Latos, S. Jurczyk, D.L. Nghiem, T. Jesionowski, A. Chrobok, Supported ionic liquid phase facilitated catalysis with lipase from Aspergillus oryzae for enhance enantiomeric resolution of racemic ibuprofen, *Environ. Technol. Innov.* 2022, 28, 102936–102947.

Oświadczam, że mój wkład procentowy w tą pracę wynosił 10% i obejmował:

- syntezę hybrydowych materiałów krzemionkowych oraz charakterystykę ich powierzchni właściwej,
- wkład w interpretację i opis wyników badań,
- wkład w edycje manuskryptu i przygotowanie odpowiedzi dla recenzentów.

P6: A. Wolny, D. Więcławik, J. Zdarta, S. Jurczyk, T. Jesionowski, A. Chrobok, Robust biocatalyst for the green continuous flow synthesis of esters from biomass-derived furfuryl alcohol and C8-C18 carboxylic acids, *Green Chem.* 2024, Advance article, doi.org/10.1039/D4GC03821E.

Oświadczam, że mój wkład procentowy w tą pracę wynosił 10% i obejmował:

- syntezę hybrydowych materiałów krzemionkowych,
- wkład w interpretację i opis wyników badań,
- wkład w edycje manuskryptu i przygotowanie odpowiedzi dla recenzentów.

podpis

Dr hab. inż. Katarzyna Szymańska, prof. PŚ
Katedra Inżynierii Chemicznej
Projektowania Procesowego
Politechnika Śląska

Gliwice, 23.09.2024

Deklaracja
o indywidualnym wkładzie procentowym i merytorycznym współautora

Jako współautor wymienionej publikacji:

P4. A. Wolny, P. Lasek, K. Szymańska, S. Turczyk, A. Jakóbik-Kolon, A. Cherbański, Construction of Intensification Heterogeneous Liquid Catalyst on the Silica Surface Gasketed for Continuous Flow Diosmectite, *Appl. Catal. A Gen.* 2024, 670, 119570.

Oświadczam, że mój wkład procentowy w tą publikację wynosił 20% i obejmował:

- syntezę materiału krzemionkowego o modyfikowanej powierzchni oraz przeprowadzenie analizy adsorpcji – desorpcji (BET, BJH) oraz katalizatora SILF,
- pomoc merytoryczną w przygotowaniu i eksperymentów oraz udział w opracowaniu wyników,
- wkład w przygotowanie ostatecznej wersji manuskryptu.

Katarzyna Szymańska
podpis

Politechnika Śląska
UCZELNIA BADAWCZA

Wydział Chemiczny
Katedra Technologii Chemicznej Organicznej i Petrochemii
Prof. dr hab. inż.
Anna Chrobok
Profesor

Gliwice, 23.09.2024 r.

Deklaracja

o indywidualnym wkładzie procentowym i merytorycznym współautora

prof. Long D. Nghiem

Jako autor korespondencyjny publikacji:

P5: A. Wolny, A. Siewniak, J. Zdarta, F. Ciesielczyk, P. Latos, S. Jurczyk, D.L. Nghiem, T. Jesionowski, A. Chrobok, Supported ionic liquid phase facilitated catalysis with lipase from Aspergillus oryzae for enhance enantiomeric resolution of racemic ibuprofen, *Environ. Technol. Innov.* **2022**, 28, 102936–102947.

Oświadczam, że wkład procentowy prof. Long D. Nghiem w tą pracę wynosił 10% i obejmował:

- konsultację merytoryczną otrzymanych wyników badań,
- korektę językową ostatecznej wersji manuskryptu,
- przygotowanie odpowiedzi dla recenzentów.

.....

podpis

Politechnika Śląska
Wydział Chemiczny
Katedra Technologii Chemicznej Organicznej i Petrochemii
al. Krzywoustego 4, 44-100 Gliwice
+48 32 237 20 17/+48 32 237 10 33 (fax)
anna.chrobok@polsl.pl
NIP 631 333 07 36
Bank Śląski S.A. o/Gliwice 83 1050 1230 1000 0000 0001 4444

Politechnika Śląska
UCZELNIA BADAWCZA

Wydział Chemiczny
Katedra Technologii Chemicznej Organicznej i Petrochemii
Prof. dr hab. inż.
Anna Chrobok
Profesor

Gliwice, 23.09.2024 r.

Deklaracja

o indywidualnym wkładzie procentowym i merytorycznym współautora

dr inż. Piotra Latosa

Jako autor korespondencyjny wymienionych publikacji:

P4: A. Wolny, P. Latos, K. Szymańska, S. Jurczyk, A. Jakóbik-Kolon, A. Chrobok, Construction of trifloaluminate ionic liquid catalyst on the silica surface dedicated for continuous flow Diels-Alder synthesis, *Appl. Catal. A Gen.* **2024**, 676, 119676.

Oświadczam, że wkład procentowy dr inż. Piotra Latosa w tą pracę wynosił 5% i obejmował:

- analizę NMR wydzielonych cykloadduktów,
- pomoc merytoryczną w zakresie syntezy i immobilizacji trifloglinianowych cieczy jonowych.

P5: A. Wolny, A. Siewniak, J. Zdarta, F. Ciesielczyk, P. Latos, S. Jurczyk, D.L. Nghiem, T. Jesionowski, A. Chrobok, Supported ionic liquid phase facilitated catalysis with lipase from Aspergillus oryzae for enhance enantiomeric resolution of racemic ibuprofen, *Environ. Technol. Innov.* **2022**, 28, 102936–102947.

Oświadczam, że wkład procentowy dr inż. Piotra Latosa w tą pracę wynosił 5% i obejmował:

- analizę NMR wydzielonego estru ibuprofenu,
- pomoc merytoryczną w zakresie immobilizacji cieczy jonowych.

.....

podpis

Politechnika Śląska
Wydział Chemiczny
Katedra Technologii Chemicznej Organicznej i Petrochemii
ul. Krzywoustego 4, 44-100 Gliwice
+48 32 237 20 17/+48 32 237 10 32 (fax)
anna.chrobok@polsl.pl
NIP 631 020 07 46
[illegible]

Gliwice, 24.09.2024

Dr Sebastian Jurczyk
Instytut Inżynierii Materiałów Polimerowych i Barwników
Oddział Farb i Tworzyw w Gliwicach
Sieć Badawcza Łukasiewicz

Deklaracja
o indywidualnym wkładzie procentowym i merytorycznym współautora

Jako współautor wymienionej publikacji:

P4: A. Wolny, P. Latos, K. Szymańska, S. Jurczyk, A. Jakóbik-Kolon, A. Chrobok, Construction of trifloaluminate ionic liquid catalyst on the silica surface dedicated for continuous flow Diels-Alder synthesis, *Appl. Catal. A Gen.* **2024**, 676, 119676.

Oświadczam, że mój wkład procentowy w tą pracę wynosił 5% i obejmował:

- przeprowadzenie analiz TGA wszystkich materiałów i katalizatorów SILLP.

P5: A. Wolny, A. Siewniak, J. Zdarta, F. Ciesielczyk, P. Latos, S. Jurczyk, D.L. Nghiem, T. Jesionowski, A. Chrobok, Supported ionic liquid phase facilitated catalysis with lipase from Aspergillus oryzae for enhance enantiomeric resolution of racemic ibuprofen*, Environ. Technol. Innov.* **2022**, 28, 102936–102947.

Oświadczam, że mój wkład procentowy w tą pracę wynosił 5% i obejmował:

- przeprowadzenie analiz TGA wszystkich nośników i biokatalizatorów.

P6: A. Wolny, D. Więcławik, J. Zdarta, S. Jurczyk, T. Jesionowski, A. Chrobok, Robust biocatalyst for the green continuous flow synthesis of esters from biomass-derived furfuryl alcohol and C8-C18 carboxylic acids, *Green Chem*. **2024**, Advance article, doi.org/10.1039/D4GC03821E.

Oświadczam, że mój wkład procentowy w tą pracę wynosił 5% i obejmował:

- przeprowadzenie analiz TGA wszystkich materiałów i biokatalizatorów.

Sebastian Jurczyk

.....
podpis

POLITECHNIKA POZNAŃSKA

Prof. dr hab. inż. Teofil Jesionowski
WYDZIAŁ TECHNOLOGII CHEMICZNEJ
Instytut Technologii i Inżynierii Chemicznej
ul. Berdychowo 4, 60-965 Poznań,
tel. +48 616853747, fax +48 61 665 3649
e-mail: teofil.jesionowski@put.poznan.pl

Poznań, 23.09.2024

Deklaracja

o indywidualnym wkładzie procentowym i merytorycznym współautora

Jako współautor wymienionej publikacji:

P5: A. Wolny, A. Siewniak, J. Zdarta, F. Ciesielczyk, P. Latos, S. Jurczyk, D.L. Nghiem, T. Jesionowski, A. Chrobok, *Supported ionic liquid phase facilitated catalysis with lipase from Aspergillus oryzae for enhance enantiomeric resolution of racemic ibuprofen*, Environ. Technol. Innov. 2022, 28, 102936–102947.

Oświadczam, że mój wkład procentowy w tą pracę wynosił 5% i obejmował:

- wkład w edycję oraz weryfikację ostatecznej wersji manuskryptu.

P6: A. Wolny, D. Więcławik, J. Zdarta, S. Jurczyk, T. Jesionowski, A. Chrobok, Robust biocatalyst for the green continuous flow synthesis of esters from biomass-derived furfuryl alcohol and C8-C18 carboxylic acids, *Green Chem.* 2024, Advance article, doi.org/10.1039/D4GC03821E.

Oświadczam, że mój wkład procentowy w tą pracę wynosił 5% i obejmował:

- wkład w edycję oraz weryfikację ostatecznej wersji manuskryptu.

podpis

VIII PUBLIKACJE

W dalszej części pracy zamieszczono artykuły naukowe wraz z materiałami uzupełniającymi, które stanowią cykl publikacji monotematycznych niniejszej rozprawy doktorskiej, w podanej kolejności:

Publikacja P1. A. Wolny, A. Chrobok, Silica-Based Supported Ionic Liquid-like Phases as Heterogeneous Catalysts, *Molecules* **2022**, 27, 5900. IF_{2022} = 4,600; $MNiSW_{2022}$ = 140.

Publikacja P2. A. Wolny, A. Chrobok, Ionic Liquids for Development of Heterogeneous Catalysts Based on Nanomaterials for Biocatalysis, *Nanomaterials* **2021**, 11, 2030. IF_{2021} = 5,719; $MNiSW_{2021}$ = 100.

Publikacja P3. A. Wolny, A. Chrobok, Supported Ionic Liquid Phase for Biocatalysis: The Current Applications, Synthesis and Prospects, *Curr. Org. Chem.* **2023**, 27, 1119–1122. IF_{2023} = 1,700; $MNiSW_{2023}$ = 70.

Publikacja P4. A. Wolny, P. Latos, K. Szymańska, S. Jurczyk, A. Jakóbik-Kolon, A. Chrobok, Construction of trifloaluminate ionic liquid catalyst on the silica surface dedicated for continuous flow Diels-Alder synthesis, *Appl. Catal. A Gen.* **2024**, 676, 119676. IF_{2023} = 4,700; $MNiSW_{2024}$ = 100.

Publikacja P5. A. Wolny, A. Siewniak, J. Zdarta, F. Ciesielczyk, P. Latos, S. Jurczyk, L.D. Nghiem, T. Jesionowski, A. Chrobok, Supported ionic liquid phase facilitated catalysis with lipase from Aspergillus oryzae for enhance enantiomeric resolution of racemic ibuprofen *Environ. Technol. Innov.* **2022**, 28, 102936. IF_{2022} = 7,100; $MNiSW_{2022}$ = 70.

Publikacja P6. A. Wolny, D. Więcławik, J. Zdarta, S. Jurczyk, T. Jesionowski, A. Chrobok, Robust biocatalyst for the green continuous flow synthesis of esters from biomass-derived furfuryl alcohol and C8-C18 carboxylic acids *Green Chem.* **2024**, Advance article. doi.org/10.1039/D4GC03821E. IF_{2023} = 9,300; $MNiSW_{2024}$ = 200.

molecules

MDPI

Review

Silica-Based Supported Ionic Liquid-like Phases as Heterogeneous Catalysts

Anna Wolny and Anna Chrobok *

Department of Chemical Organic Technology and Petrochemistry, Faculty of Chemistry, Silesian University of Technology, Krzywoustego 4, 44-100 Gliwice, Poland
* Correspondence: anna.chrobok@polsl.pl; Tel.: +48-32-237-2917

Abstract: Supported ionic liquid phases offer several advantages related with catalysis. Immobilization of ionic liquid on the solid support provides catalytic activity or efficient matrix for active phases, as enzymes or metal compounds. Ionic liquid can be physically adsorbed on the carrier (supported ionic liquid phase) or chemically grafted to the material surface (supported ionic liquid-like phase). The use of supported ionic liquid phases improves mass transport, reduces ionic amount in the process and, most importantly, enables effortless catalyst separation and recycling. Moreover, chemical modification of the surface material with ionic liquid prevents its leaching, enhancing length of catalyst life. Silica-based materials have become an effective and powerful matrix for supported ionic liquid-like phase due to its cost-efficiency, presence of hydroxyl groups on the surface enabling its functionalization, and specific material properties, such as the size and shapes of the pores. For these reasons, supported ionic liquid-like phase silica-based materials are successfully used in the organic catalysis.

Keywords: ionic liquids; acidic ionic liquids; supported ionic liquid phase; heterogeneous catalysis; silica; immobilization

Citation: Wolny, A.; Chrobok, A. Silica-Based Supported Ionic Liquid-like Phases as Heterogeneous Catalysts. *Molecules* **2022**, *27*, 5900. https://doi.org/10.3390/molecules27185900

Academic Editor: Lu Liu

Received: 29 August 2022
Accepted: 8 September 2022
Published: 11 September 2022

1. Introduction

In recent years, responsible production and consumption has been one of the main topics of interest in both academia and industry. The chemical industry generates large amounts of hazardous waste, along with high energy consumption, use of volatile organic solvents, expensive equipment, and often harsh work conditions [1,2]. Subsequent restrictive regulations concerning health, climate, and environmental protection have forced the chemical industry to improve its existing technologies. The 2030 Agenda for Sustainable Development, adopted by all United Nations Member States in 2015, provides 17 Sustainable Development Goals. New rules for green chemistry can be a useful tool to increase the use of green technologies and achieve sustainable development in the chemical industry [3]. Green catalysis is focused on the minimization or preferably the elimination of waste, relying on the atom economy concept and the search for new effective catalysts while avoiding toxic substances. The newly developed catalysts should be characterized by high activity, selectivity, and stability under the specific process conditions [4]. Meaningful alternatives for conventional hazardous and usually expensive catalysts are enzymes and ionic liquids [5,6].

Ionic liquids (ILs), also known as low-temperature molten salts, are compounds consisting of an organic cation and an organic or inorganic anion. A major advantage of ILs is the possibility of designing their structure by selecting the proper cation and anion while projecting specific properties, meaning they have many applications in the chemical industry [7,8]. Firstly, ILs are significant alternatives for the conventional volatile organic solvents [8]. For example, in the Bayer–Villiger oxidation of ketones in the presence of ILs, lactones and esters are obtained in short reaction times (2–20 h) and

in high yields (up to 95%) [9]. ILs can also stabilize enzymes in an active conformation and enhance biocatalytic processes [10]. For example, 1-butyl-3-methylimidazolium bis(trifluoromethylsulfonyl)imide ([bmim][NTf_2]) was used as solvent in the chemo-enzymatic oxidation of cyclobutanones and cyclohexanones to lactones with high yields (79–95%) in the presence of 30% hydrogen peroxide. In this case, the IL improved the stability of the enzyme under harsh reaction conditions [11]. The ionic nature of ILs also makes them useful as electrolytes for lithium-ion batteries and supercapacitors [12]. Furthermore, ILs are known as extractive solvents for the isolation of high-added value compounds from biomass [13], extractive solvents for analytical chemistry [14], and absorbents for gas capture, e.g., carbon dioxide [15]. ILs can also be employed as catalysts or solvent and catalyst at the same time in many reactions, e.g., Diels–Alder cycloaddition, alkylation, and acylation, as well as various types of condensations, oxidation, esterification, and transesterification reactions [16,17].

One significant group of ILs that are used as catalysts are acidic ionic liquids (AILs). AILs can be classified according to the nature of the acidic site on the Brønsted and Lewis acid types. It is possible to introduce more than one acidic function to the structure of AILs and design ILs by the combination of Brønsted and Lewis acidic types. Brønsted acidity can be introduced to ionic liquids (BAILs) as either: an acidic hydrogen in the cation (A), an anion (B) or both (C), an acidic hydrogen located in the functional group (D) or an acidic hydrogen located in the functional group and in cation/anion (E). Lewis acidic ionic liquids (LAILs) are mainly based on halometallate anions (F) and boric atom in the cation (G) (Figure 1). The formation of dual Brønsted–Lewis AILs is also presented in Figure 1 (H) [18–20].

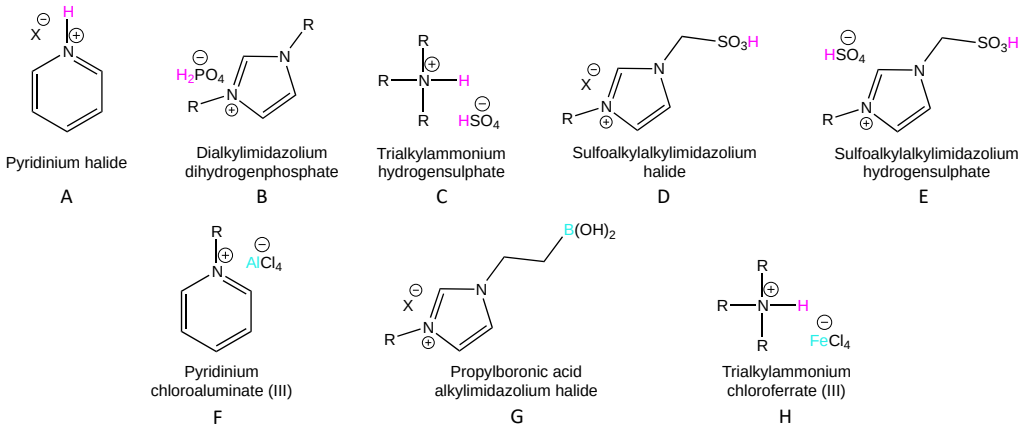

Figure 1. Examples of the structures of some acidic ionic liquids.

The most common group of BAILs are ILs with an acidic hydrogen located at the cation (A), which are also called protic acidic ionic liquids. Cations widely used for the synthesis of this type of BAIL are: 1-alkylimidazolium, 1-alkyl-2-alkylimidazolium, primary/secondary/tertiary ammonium, pyridinium, pyrolidonium, and 1,1,3,3-tetramethylguanidininium [19]. A functional group with an acidic hydrogen (e.g., -SO_3H, -CO_2H) can also be attached to the cation to obtain a BAIL [20]. An acidic site in the BAIL's anion is formed using polybasic acids such as H_2SO_4, h_3PO_4, maleic, and fumaric acids creating dialkylimidazolium, hydrogensulfate, or dihydrogenphosphate ILs [20–22]. A growing interest in green chemistry has also led to the discovery of bio-BAILs based on amino acids introduced into the structure of the cation or anion, e.g., alanine, glycine, serine, proline, and valine [23]. BAILs have been implemented in many organic reactions. For example, imidazolium-based ionic liquids functionalized with a sulfonic group were successfully employed for the hydration of alkynes under mild conditions to give ketones in high yields [24]. Some dicationic ionic liquids based on a diammonium cation and hydrogensulfate anion as environmentally benign BAILs were used for biodiesel synthesis,

which was obtained with high yields and reused without significant loss of activity [25]. Imidazolium based hydrogensulfate ILs were also determined to be very efficient catalysts in the synthesis of cyclic carbonates from carbon dioxide and epoxides. high yields of cyclic carbonates (69–99%) were achieved using these ILs, which can be recycled without any loss of activity [21]. In another example for the dehydration of glycerol to acrolein using the BAIL 1-butyl-3-metylimidazolium dihydrogen phosphate, which was conducted in the liquid phase, full conversion of glycerol was achieved [22].

For the Lewis AILs, metals such as Al, Ga, Zn, Fe, In, and Sn in the form of chloride or triflate salts are used to create LAILs via complexation of the neutral IL and the metal salt in various molar ratios [18,26]. Lewis acidic cations can be formed in two ways: via a tricoordinate borenium center as a cation, or via solvation of metal cation, e.g., Li^+ as [Li(glyme)][NTf_2]/[OTf] [18]. LAILs, as well as BAILs, are readily used in organic synthesis. Water tolerant trifloaluminate ILs, synthesized from 1-alkyl-3-methylimidazolium triflates, were employed as catalysts in the cycloaddition of 2,4-dimethylphenol and isoprene to obtain a chromane. Use of the catalysts provided full conversion and high selectivity (80%) under mild reaction conditions [26]. In another example, chlorogallate(III) ILs were applied in a Bayer–Villiger oxidation of cyclic ketones to lactones. high yields (99%) in short reaction times under mild reaction conditions were also achieved [27]. Borenium LAILs used in a Diels–Alder reaction ensured good yields (90–94%) and selectivities of various dienes and dienophiles [28]. All such AILs have many applications as homogeneous catalysts [18,19], however, reducing costs and waste led to the use of heterogeneous catalysis.

Immobilization of ILs on a solid insoluble support can be performed via physical adsorption, known as supported ionic liquid phase (SILP), or via chemical bonding into the matrix, known as supported ionic liquid-like phase (SILLP) [29]. A visual representation of each can be seen in Figure 2. The IL creates a thin layer of liquid on the carrier, which decreases the amount of IL compared to the reaction in the bulk. This improves mass transfer to the catalytic centers on the fluid-fluid phase boundary and facilitates separation of the catalyst from the reaction mixture. Moreover, a heterogeneous SILP or SILLP catalyst can be successfully employed in both batch and flow processes, including fixed-bed or fluidized-bed reactors. Such applications are described later in this paper.

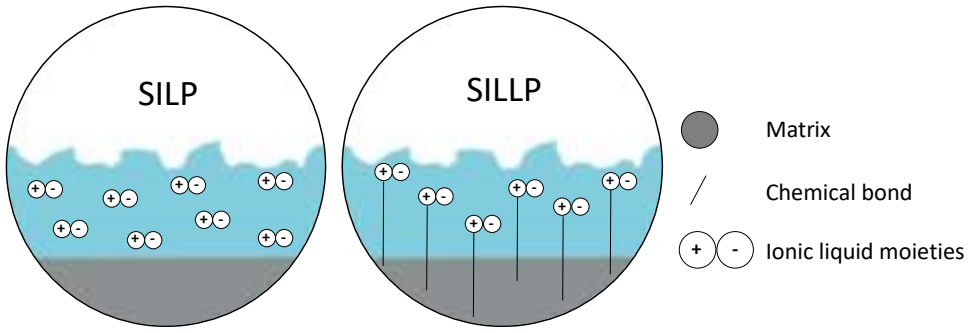

Figure 2. Supported ionic liquid phase (SILP) and supported ionic liquid-like phase (SILLP).

In this paper, achievements on the SILLP silica-based materials and their use in the organic synthesis are described. Previously, Mehnert [30] outlined the first contribution of SILPs in catalysis. Then, Sokolova et al. [31] reviewed flow processes based on catalysts immobilized on monolithic SILLPs. Next, Skoda-Földes [32] summarized the use of supported AILs in the organic synthesis, and hartmann et al. [33] characterized inorganic materials for SILLP synthesis and briefly described their input to catalysis. After that, Amarasekara [20] characterized AILs and described applications of acidic ionic liquids as SILP/SILLP, and Gruttadauria et al. described covalently-supported ionic liquid phases (SILLP) as matrices and catalysts [34], while Alinezhad et al. pointed out BAILs as SILLP in organic catalysis [35]. Then, Swadźba-Kwaśny et al. [18] briefly mentioned the applications of Lewis ILs

immobilized into a solid matrix, and Leitner et al. [36] described SILP and SILLP based on nanoparticles and their applications in organic catalysis. Additionally, Vekariya [16] mentioned SILPs in the review of ILs in organic transformations. Haumann et al. [37] then presented 15 years of using SILP/SILLP catalysts in hydroformylation reactions, both in the liquid and gas phase, and Freire et al. [38] described the immobilization of ionic liquids, types of materials, and their applications. Maciejewski et al. described participation of ILs in heterogeneous catalysis, including supported IL phase catalysts (SILPC), solid catalysts with ILs (SCILL), and supported ionic liquid catalysis (SILC) techniques, as well as porous ionic liquids [39]. Moreover, Lozano et al. [40] presented applications of SILP and SILLP as supports for enzyme immobilization in organic synthesis, and Chrobok et al. [41] described SILP/SILLP biocatalysts based on nanoparticles and their applications for biocatalysis. The aim of this work is to complete the time gap and collect silica-based SILLP applications in catalysis to improve selection of the best systems for organic synthesis.

2. Immobilization of Ionic Liquids on Silica-Based Materials

The immobilization of ILs on the solid supports enables the issues related with the bulk IL systems to be overcome, such as high viscosity, mass transfer problems, IL high-cost separation, purification, regeneration, and recycling. A reduced amount of immobilized IL creates a thin layer on the matrix which, in turn, reduces costs. The possibility of creating numerous structures of ILs caused various SILPs to be designed, generating wide application potentials. Different types of materials such as silica, alumina, zeolites, polymers (e.g., polystyrene-based materials), and carbon materials (e.g., single-walled carbon nanotubes (SWCNTs), multi-walled carbon nanotubes (MWCNTs), and activated carbon) were used for such SILPs [37,41]. The most commonly used matrices are silica-based materials (e.g., silica gel, SBA-15, MCM-41 types), which are characterized by their low cost, large surface area, ordered porosity, well-defined pore geometry, and mechanical and thermal stability (except for MCM-41 type). Moreover, magnetic properties can be incorporated by coating Fe_3O_4 nanoparticles with silica, obtaining a hybrid that is even easier to separate from the reaction mixture using a magnetic field. The most important feature of silica-based materials is the presence of silanol groups (-Si-OH) on the surface, which determines the method of IL immobilization, particularly via covalent bonding (SILLP).

Physisorption is a simple method for IL immobilization that can be performed through the impregnation and adsorption from IL solution and the sol-gel procedure. The impregnation method relies on mixing the IL solution and support together before removing the solvent under vacuum conditions. The adsorption from the IL solution is accomplished by filtration, washing (to remove any excess IL), and drying under vacuum conditions. The sol-gel procedure consists of hydrolysis and polycondensation reactions of tetraethoxyorthosilicate (TEOS) in the presence of the IL, which can be described by the entrapment of the IL in the silica pores (Figure 3). The main strength of the sol-gel technique is that there is control of the molecule's growth [42]. The interactions between the IL and the silanol groups on the silica surface are based on hydrogen bonding. however, van der Waals and electrostatic interactions, as well as π-π-stacking (in the case of aromatic cation) between the IL moieties also occurs, increasing the stabilization of the SILP structure [43]. The h-bonds between -Si-OH and the IL can be confirmed via FTIR analysis, where the intensity of the characteristic peak at 952 cm^{-1} (assigned to -Si-OH) decreases if IL is present on the silica surface [44].

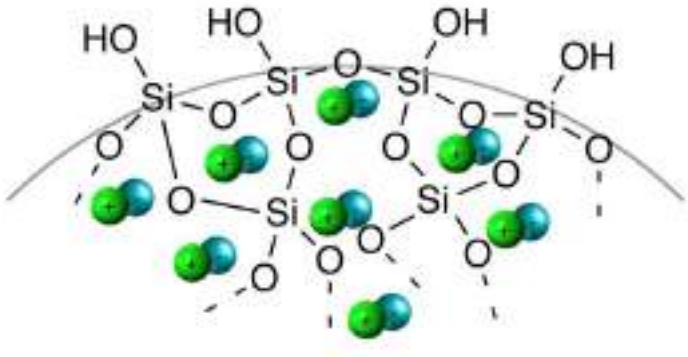

Figure 3. Ionic liquids moieties entrapped in the silica pores.

SILPs are commonly used for both chemical and biochemical processes. Entrapped triethylammonium propanesulfonate bis(trifluoromethanesulfonyl)imide [TEAPS][NTf_2] in the silica structure has been used for dehydration of *rac*-1-phenyl ethanol with high selectivity to styrene and recyclability (for at least 6 runs) [45]. Another BAILs, 1-methyl imidazolium hydrogen sulphate ([HMIM]HSO_4) and 1-methyl benzimidazolium hydrogen sulphate ([HMBIM]HSO_4), immobilized on silica, was applied in the isomerization of *n*-heptane and *n*-octane. The acidic SILPs showed good thermal stability high isomerization yields, were easy recyclable and environmentally friendly [46]. Then, 1-butyl-3-methylimidazolium acidic ILs with Rh-complex were immobilized on partly dehydroxylated silica surface, which created a highly active Rh/SILP catalyst dedicated for continuous hydroformylation of propene. high thermal stability, selectivity to *n*-butanal (over 95%), and TOF (turnover frequency) were observed using syn-gas and syn-gas with CO_2 addition [47]. For the hydrosilylation reaction, rhodium complexes immobilized in four various phosphonium based ILs anchored on silica support were applied. The amount of catalyst was reduced compared to biphasic reactions by a factor of 1000, the reaction times were shortened, and easy recycling of the Rh complexes were demonstrated [48]. The advantage of SILP catalysts in biocatalysis has also been shown. Lipase B from *Candida antarctica* (CALB) was immobilized on a SILP based on an imidazolium cation and a bis(trifluoromethanesulfonyl)imide anion used for a continuous kinetic resolution of 1-phenylethanol under supercritical CO_2 conditions. high enzyme activity, enantioselectivity (>99.9%), and stability (16 cycles) was achieved [49]. SILP catalysts have many advantages, such as easy and cost-efficient synthesis, where an IL multilayer on the support maintains the IL bulk properties, as well as the possibility to tailor the structure of the ILs that can be immobilized. It is worth noting that the main disadvantage is the detachment or leaching of the IL from the matrix, which is related to weak interactions between the IL and the carrier.

Covalent bonding of the IL on the surface of the support prevents its leaching and detachment. ILs immobilized as SILLPs usually create a monolayer, thus the bulk properties are lost. Methods for the preparation of SILLP silica-based materials include chemical reactions between an IL or IL precursor and hydroxyl groups present on the silica surface, or the sol-gel technique. ILs can be attached to -Si-OH group via the cation or the anion (Figure 4). Anchoring the IL into support can be obtained by direct immobilization of IL (Figure 4A) or by building the IL structure on the support (Figure 4B).

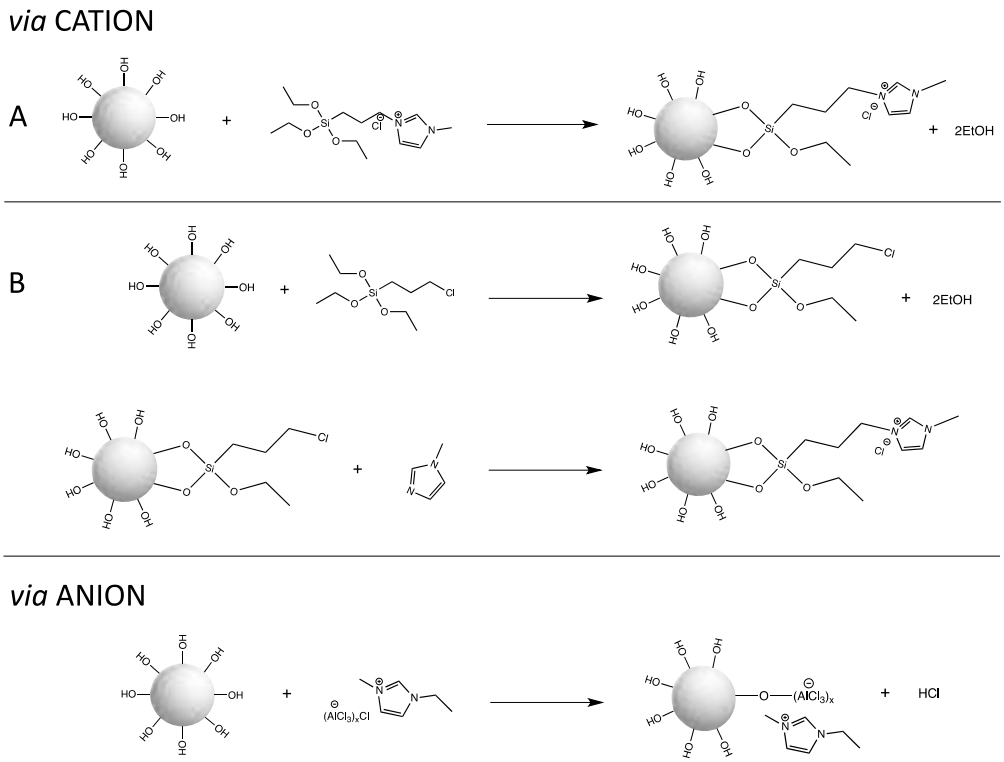

Figure 4. Covalent immobilization of ionic liquid on the silica surface via cation and via anion. Anchoring the IL into support can be obtained by direct immobilization of IL (**A**) or by building the IL structure on the support (**B**).

Typical immobilization of the IL via the cation is performed using the siliceous precursor 3-(chloropropyl)triethoxysilane, however, other precursors can also be used, e.g., 3-mercaptopropyl-trimethoxysilane [32]. As mentioned before, prepared in advance, an IL modified with ethoxysilane groups can be directly grafted to hydroxyl groups or precursors, and can be firstly anchored and be the subject of subsequent quaternization. Immobilization of IL via the cation to the siliceous surface can be confirmed by ^{29}Si MAS NMR. Peaks at −91 ppm and −101 ppm assigned to $(SiO)_2Si(OH)_2$ and $(SiO)_3Si$-OH groups, respectively, disappear, thus exposing the $(SiO)_4Si$ signal. Signals at −54 ppm and −66 ppm assigned to -Si-O-SiR-$(OEt)_2$ and $(Si-O)_2$-SiR-OEt, respectively, are in turn revealed [29]. If necessary, an anion exchange can be performed after the IL immobilization. Immobilization of the IL via the anion is usually observed mainly for chlorometallate ILs during the wet impregnation method where -Si-O-M bonds are obtained. For example, ^{27}Al MAS NMR spectra shows signals at 102 ppm attributed to $[Al_2Cl_7]^-$ and allows the control of the presence of $AlCl_3$ on the silica surface (1.2 ppm), which can be removed though the Soxhlet extraction [29,32]. The sol-gel method is also often used for SILLP preparation. This technique consists of polycondensation of alkoxysilane-functionalized ILs with tetralkoxysilanes, e.g., TEOS (Figure 5), and allows the control of material mesoporous character from the proper silica source/IL ratio. Besides MAS NMR spectroscopy, chemical immobilization of IL to the silica surface can be proved using FT-IR, XRD, and TEM methods.

Figure 5. Covalently immobilized ionic liquid via the sol-gel method.

3. Silica-Based Supported Ionic Liquid-like Phases in Organic Catalysis

3.1. Lewis Type SILLPs

Lewis type SILLPs based on silica materials are normally synthesized via the cation method using 3-(chloropropyl)triethoxysilane, 3-(chloropropyl)trimethoxysilane, or 3-mercaptopropyltrimethoxysilane precursors, where the structures shown in Figure 6 are obtained. As can be seen in Figure 6, the material can be characterised by Lewis acidity with the Lewis center located on the alkyl chain modified with $-SO_2Cl$ or $-SO_2OH$ groups, or the Lewis acidity can be found in the metal halide based anion created in the complexation reaction. Table 1 presents applications of Lewis type silica based SILLP materials as catalysts in organic synthesis.

The first report on Lewis type SILLPs appeared in 2000. The presented investigations included two different immobilization methods of chloroaluminate imidazolium ILs on amorphous silica and MCM-41 supports. One of the possible SILLP synthesis routes was immobilization via the anion (Figure 4), with the second one being via the cation (**1**, Figure 6), where aluminium chloride was introduced to the IL structure in the complexation reaction. If the molar ratio of the metal halide component in the IL is more than 0.5, oligonuclear ($[Al_2Cl_7]^-$) anions are formed. The obtained heterogeneous catalysts were tested on the Friedel–Crafts alkylation, which resulted in high conversion (>90%) and selectivity (>90%) of the main product using catalyst **1** in Figure 6. In comparison, the reaction catalysed by immobilised $AlCl_3$ on the silica surface yielded only 15.7% of the main product. The better activity shown by the MCM-41 based SILLP is due to higher surface area and IL loading. Furthermore, leaching of the active phase occurred for the SILLP catalyst prepared by anion immobilization, partly due to unbonded IL moieties on the silica surface [29]. In the next report, chloroaluminate SILLP catalysts prepared via anion, cation, and sol-gel methods were used in the Friedel–Crafts alkylation of benzene with different olefins, as well as in acylation reaction. Again, leaching of the IL occurred in the SILLP prepared via anion complexation. The best activity was shown by the SILLP catalyst, where IL was grafted via the cation—almost full conversion and very high selectivity of the monoalkylated product were achieved, even at 20 °C. The lower activity of other SILLPs was most likely the result of only partly bonded acidic anions on the silica surface, which was confirmed via ^{29}Si MAS NMR analysis [50]. A tetrapropylammonium based chlorostannate (IV) IL was grafted to the silica surface via the cation (**2**, Figure 6), and used in the condensation of isobutene and formaldehyde to 3-methylbut-3-en-1-ol. Comparison of silica and MCM-41 materials resulted in better activity of the MCM-41 based SILLP catalyst in the tested reaction (α = 76%, S = 94%, Y = 71.4%, TON = $2.63 \cdot 10^{-3}$ s^{-1}). Well-ordered and regular hexagonal pores in the MCM-41 material created micro-reactors that enhanced the SILLP catalyst activity. It is worth mentioning that the obtained heterogeneous catalyst was recyclable, and that the active phase can be used as a catalyst in the homogeneous phase as well [51]. The next report described applications of triflate Lewis type SILLP materials (**3**, Figure 6) in the synthesis of bis(indolyl)methanes [52] (Scheme 1, Figure 7), esterification of acetic or decanoic acid with various alcohols [53], nitration of aromatic compounds [53], and the addition of indole to vinyl ketones [54] (Scheme 2, Figure 7). Covalent bonding between the IL and hydroxyl groups on the silica surface was created in a radical chain transfer reaction of a 1-allylimidazolium based IL on silica gel modified with 3- mercaptopropyltrimethoxysilane. The obtained materials exhibited excellent yields, conversions, and reusability in all presented reactions. It should be pointed out that the replacement of chloroaluminate anion to triflate, and creation of Lewis centre in the cation, makes SILLP materials more resistant to water.

Table 1. Lewis type silica-based SILLP in organic catalysis.

Catalyst	Reaction Type	Reaction Conditions	Reaction Parameters	Lit.
SiO_2 [tespmim][Cl-$AlCl_3$] [a]	Friedel–Crafts alkylation of benzene with dodecene	6% wt. cat., benzene:dodecene (10:1; n/n), 80 °C, 1 h	A [b] > 90%, S [c] > 90%	[29]
SiO_2 [pmim][Cl-$AlCl_3$] [d]	Friedel–Crafts alkylation of benzene with olefins	1% wt. cat., benzene:olefin (10:1; n/n), 20 °C, 2 h	C_6: α = 45.3%, S = 73.8% C_8: α = 44.9%, S = 96.5% C_{10}: α = 34.1%, S = 89.6% C_{12}: α = 35.2%, S = 80.3% (for 6% wt. cat., 80 °C, 1 h; α = 99.4%, S = 99.7%)	[50]
SiO_2 [tms(p)$_4$N][Cl-$SnCl_4$] [e]	Condensation of isobutene and formaldehyde	4% mol of $SnCl_4$, isobutene:formaldehyde (1:0.1; n/n), chloroform 26 mL, 60 °C, 2 h	α = 76%, S = 94%, Y [f] = 71.4%, TON [g] = $2.63 \cdot 10^{-3}$ s^{-1}	[51]
SiO_2 [p(p-SO_2Cl)im][OTf] [h]	Synthesis of bis(indolyl)methanes	143 mg cat., aldehyde 0.3 mmol, indole 0.5 mmol, MeCN 3 mL, rt, 1.5–9 h	Yields for: bezaldehyde 97%, p-nitrobenzaldehyde 97%, p-chlorobenzaldehyde 90%, p-acetoxybenzaldehyde 64%, p-methoxybenzaldehyde 97%, hydrocinnamaldehyde 98%	[52]
SiO_2 [p(p-SO_2Cl)im][OTf]	Esterification of acetic or decanoic acid with alcohols	Mole ratio of carboxylic acid to ionic liquid: 350, alcohol 20 mmol, carboxylic acid, 10 mmol, 100 °C, 8 h	Yields for various alcohols: (a) acetic acid: C_8H_{17} 94.6%, $C_{10}H_{21}$ 95.1% (b) decanoic acid: C_2H_5 86.3%, $C_{10}H_{21}$ 90.4%	[53]
SiO_2 [p(p-SO_2OH)im][OTf] [i]	Nitration of aromatic compounds	Mole ratio of aromatic compound:ionic liquid: 20, mole ratio of aromatic compound:nitric acid: 1:3, 80 °C, 4 h	Conversions for R-groups in aromatic ring: H 61.6%, Me 85.8%, Cl 10.4%, Br 22.2%	[53]
SiO_2 [p(p-SO_2Cl)im][OTf]	Addition of indole to vinyl ketones	171 mg cat., vinyl ketone 0.6 mmol, indole 0.3 mmol, Et_2O 0.2 mL, rt, 1.5–9 h	Yields for various ketones: 1-penten-3-one 92%, 2 2-cyclopentenone 88%, 3-penten-2-one 90%, benzalacetone 72%, dibenzylideneacetone 93%	[54]
SiO_2 [tespmim][Cl-$AlCl_3$]	Production of alkylated gasoline	0.5 g cat., iC4/C4 = 20, 80 °C, 90 min	α = 97%, S_{C8} = 59.7%	[55]
SiO_2 [tespmim][Cl-$AlCl_3$]	Trimerization of isobutene	30% wt. cat., isobutane:isobutene molar ratio 10:1, 25 °C, 600 h^{-1}	α = 91.4%, S_{C12} = 79.4%	[56]
SiO_2 [tespmim][Cl-$FeCl_3$] [j]	Friedel–Crafts reaction between benzene and benzyl chloride	0.05 g cat., benzene:benzyl chloride molar ratio 10:1, benzyl chloride 0.32 g, 80 °C, 45 min	α = 100%, S = 100%, 10 cycles	[57]
SiO_2 [(tesp)$_2$im][Cl-$InCl_3$] [k]	Friedel–Crafts reaction between benzene and benzyl chloride	0.05 g cat., benzene:benzyl chloride molar ratio 10:1, benzyl chloride 0.32 g, 80 °C, 15 min	α = 100%, S = 100%, 6 cycles	[58]
SiO_2 [tespmim][Cl-$GaCl_3$] [l]	Diels–Alder cycloaddition of cyclopentadiene to various dienophiles	5% mol of $GaCl_3$, cyclopentadiene:dienophile (12:8; n/n), 25 °C, 5–30 min	Methyl acrylate: α = 99%, endo:exo ratio: 95:5, 4 cycle; ethyl acrylate: α = 99%, endo:exo ratio: 93:7; diethyl maleate: α = 99%, endo:exo ratio: 93:7; methacrolein: α = 100%, endo:exo ratio: 80:20; benzoquinone: α = 83%; maleic anhydride: α = 89%	[59]
SiO_2 [tespmim][Cl] [m]	Cycloaddition of CO_2 to styrene oxide	0.5% mol cat., 0.1% mol $ZnBr_2$, styrene oxide 0.13 mol, 100 °C, P_{CO2} = 1 MPa, 6 h, 700 rpm	α = 83%, Y = 72%	[60]
SiO_2-Zn [tespmim][Cl]	Cycloaddition of CO_2 to propylene oxide	S/C = 200 (PO mol per cat. mol), V_{PO} = 8 mL, P_{CO2} = 1.25 MPa, 100 °C, 8 h	MCM-41: α = 33%, S = 98% MSN: α = 76%, S = 97% BMMs: α = 77%, S = 98%	[61]

[a] 1-methyl-3-(triethoxysilylpropyl)imidazolium chloride—chloroaluminate (III), [b] conversion, [c] selectivity, [d] 1-propyl-3-methylimidazolium chloroaluminate (III) immobilized via anion, [e] 3-trimethoxypropyltripropylammonium chloride—chlorostannate (IV), [f] yield, [g] turnover number, [h] 1-(3-chlorosulfonylpropyl)-3-(3-trimethoxysilylmerkaptopropyl)imidazolium trifluoromethanesulfonate (triflate), [i] 1-(3-hydroxysulfonylpropyl)-3-(3-trimethoxysilylmerkaptopropyl)imidazolium triflate, [j] 1-methyl-3-(triethoxysilylpropyl)imidazolium chloride—chloroferrate (III), [k] 1-(triethoxysilylpropyl)-3-(triethoxysilylpropyl)imidazolium chloride—chloroindate (III), [l] 1-methyl-3-(triethoxysilylpropyl)imidazolium chloride—chlorogallate (III), [m] 1-methyl-3-(triethoxysilylpropyl)imidazolium chloride.

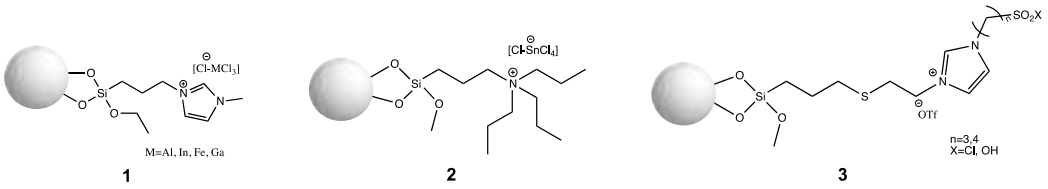

Figure 6. Structures of Lewis type silica-based SILLP materials.

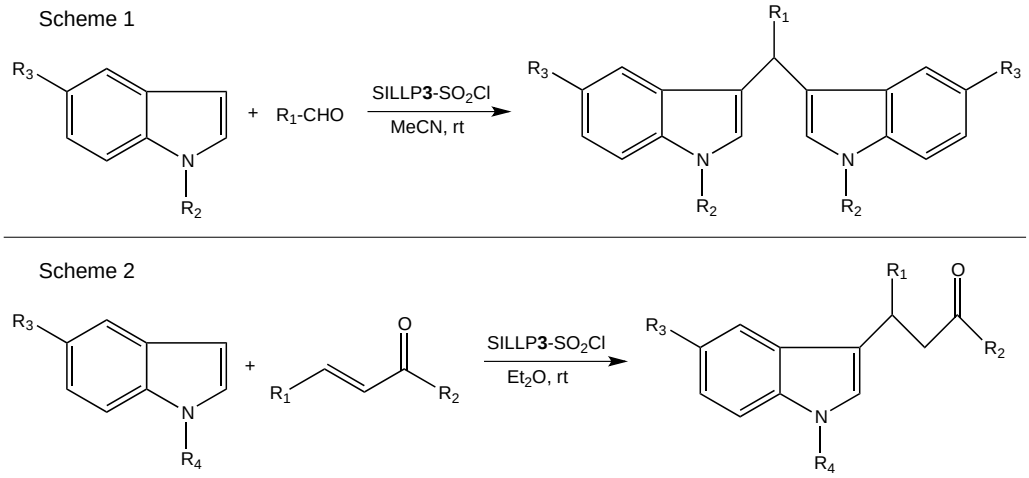

Figure 7. Applications of Lewis type SILLP material **3** in the synthesis of bis(indolyl)methanes (Scheme 1) and addition of indole to vinyl ketones (Scheme 2).

Further reports have presented a chloroaluminate imidazolium-based IL grafted to MCM-41 (**1**, Figure 6). High conversion (97%) and selectivity to isooctane (59.7%) in gasoline production were obtained, and the SILLP catalyst showed better activity than the IL immobilized via the anion, zeolite H-Beta, and Nafion/Silica Composite SAC 13 [55]. The same IL was immobilized on silica, MCM-41, SBA-15, active carbon, and glass materials, and the activity of the prepared SILLP was examined in the continuous gas phase trimerization of isobutene using a fixed-bed reactor under atmospheric pressure. Only silica-based SILLP catalysts enabled the trimerization reaction to occur due to synergic interactions between the IL anion and the silanol groups. In other cases, the alkylation reaction was observed. For the trimerization reaction, the MCM-41 based SILLP (α = 91.4%, S_{C12} = 79.4%) turned out to be the most active, owing to its regular hexagonal array channels that behave similar to micro-reactors, increasing the catalytic activity [56]. Apart from Al (III) and Sn (IV), other metals such as Fe, In, and Ga were used for silica-based SILLP synthesis. Chloroferrate (III) imidazolium-based IL moieties were grafted for the siliceous support of MCM-41 after complexation with $FeCl_3$ (**1**, Figure 6). The SILLP catalyst showed high efficiency and long reusability (10 cycles) in the Friedel–Crafts reaction between benzene and benzyl chloride [57]. The chloroindate (III) imidazolium-based IL was anchored to SBA-15 silica material (**1**, Figure 6), which exhibits ordered hexagonal structure, however less so than MCM-41 material. The obtained SILLP catalyst was used in the Friedel–Crafts reaction between benzene and benzyl chloride, gaining 100% conversion and 100% selectivity over 6 reaction cycles. Introducing the IL to the catalyst structure prevents $InCl_3$ from leaching [58]. A chlorogallate (III) imidazolium-based IL was covalently tethered to a multimodal silica porous silica support (**1**, Figure 6) and applied to Diels–Alder cycloaddition reactions for the synthesis of intermediates for pharmacologically active ingredients, agrochemicals, flavors, and fragrances (Scheme 1, Figure 8). The synthesized materials demonstrated a hierarchical pore structure and contained micro-, meso-, and macropores, which results in easy mass transport to and from active sites. The SILLP chlorogallate (III) catalyst showed great conversions and endo/exo selectivities in short reaction times,

which is superior to other results presented in the literature. Moreover, the catalyst could be recycled five times without significant loss of activity [59].

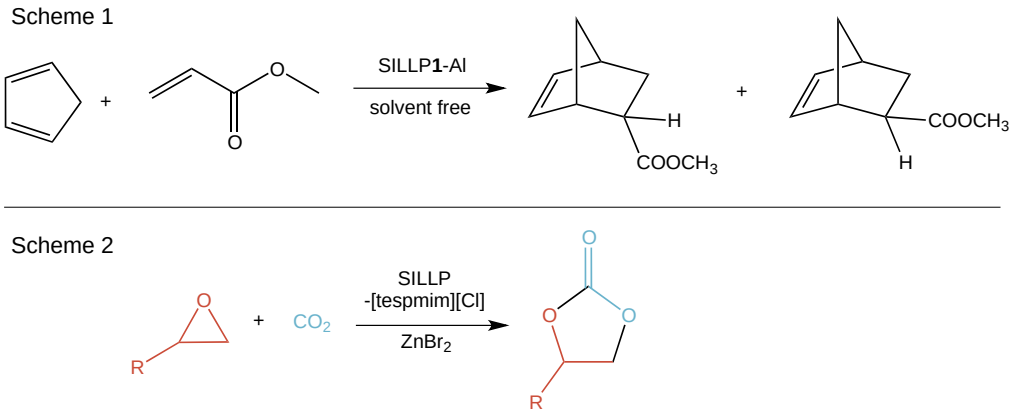

Figure 8. Diels–Alder cycloaddition (Scheme 1) and CO_2 cycloaddition for cyclic carbonates synthesis (Scheme 2) with SILP catalysts.

Other reports concern the application of ILs as co-catalysts for CO_2 cycloaddition for cyclic carbonates synthesis in the presence of a Zn Lewis centre (Scheme 2, Figure 8). It is postulated that the Zn Lewis site coordinates with the oxygen atom of epoxides, and a nucleophilic attack of the halide anion on the less sterically anion carbon atom of epoxide occurs. The first approach includes [tespmim][Cl] anchored to various silica materials such as macro/mesoporous silica, MCM-41, MSU-F (cellular foam), and MSU-H (large pore 2D hexagonal). The better results in the reaction of CO_2 with styrene oxide in the presence of $ZnBr_2$ were achieved for the silica SILLP, and the worst occurred for the MCM-41 SILLP. In this case, catalytical activity depends on pore size and not on surface area. The synthesised catalyst could be recycled four times without any loss of activity [60]. In other reports, Zn atoms and [tespmim][Cl] were grafted to the silica surface. Various materials such as MCM-41 (regular, long, hexagonal channels), MSN (nanosphere morphology, order mesopores, mainly inside pores), and BMMs (mesoporous structure, a large number accumulated inside and outside of the pores) were applied. The catalytic activity of the SILLP catalyst was examined in reaction of CO_2 with propylene oxide, where the best performance was exhibited by SILLPs with shorter and regular pore channels [61].

3.2. Brønsted-Type SILLPs

Brønsted-type SILLPS based on silica materials are synthesized via the cation method. Brønsted IL moieties are grafted to the silica surface through precursors such as 3-(chloropropyl)triethoxysilane, 3-(chloropropyl)trimethoxysilane, 3-mercaptopropyltrimethoxysilane, or (3-aminopropyl)-trimethoxysilane, creating the structures presented in Figure 9. The Brønsted acidic center located in the anion that is most often used is $[HSO_4]$, whereas the cation Brønsted site can be found in the alkyl chain modified with an $-SO_3H$ group through the reaction between, for example, 1,3-propanesultone and vinylimidazole. Some applications of Brønsted-type silica-based SILLP materials as catalysts in organic synthesis are presented in Table 2.

Table 2. Brønsted-type silica-based SILLP in organic catalysis.

Catalyst	Reaction Type	Reaction Conditions	Reaction Parameters	Lit.
SiO_2 [p(b-SO_3H)im][OTf] [a]	Estrification of oleic acid and methanol	0.2 mmol IL in cat., oleic acid 17.7 mmol, methanol 531.05 mmol, 100 °C, 4 h	α = 84%, 3 cycles	[62]
SiO_2 [p(b-SO_3H)im][OTf]	Transestrification of glicerol trioleate and methanol	0.2 mmol IL in cat., glicerol trioleate 17.7 mmol, methanol 531.05 mmol, 100 °C, 4 h	α = 30%, $S_{methyl\ oleate}$ = 36%	[62]
SiO_2 [tesp(b-SO_3H)im][Cl] [b]	hydrolysis of cellulose	0.02 mmol h^+ in cat., cellulose 0.185 mmol, 2 mL H_2O, 190 °C 3 h	Y_{TRS} = 48.1%, $Y_{glucose}$ = 21.9%, 4 cycles	[63]
SiO_2 [p(p-SO_3H)im][OTf] [c]	Dehydration of fructose	0.175 mmol IL in cat., fructose 0.35 mmol, DMSO 2.0 g, MW: 200 W, 4 min	α = 100%, Y = 70.1% (5-hydroxymethylfurfural)	[64]
SiO_2 [tmsp(p-SO_3H)im][I] [d]	Biginelli reaction	0.8% mol cat., aldehyde 1 mmol, ethyl/methyl-acetoacetate 1 mmol, urea 1.5 mmol, 75 °C, 50–90 min	Yields for aldehydes with Ar groups: (a) ethylacetoacetate: Ph 96%, 4-$OMeC_6H_4$ 97%, 2-$OMeC_6H_4$ 86%, 4-MeC_6H_4 96%, 4-ClC_6H_4 90%, 3-BrC_6H_4 96% (b) methylacetoacetate: Ph 96%, 4-$OMeC_6H_4$ 96%, 2-$OMeC_6H_4$ 89%, 4-MeC_6H_4 95%, 4-ClC_6H_4 92%, 3-BrC_6H_4 95%	[65]
SiO_2 [tmsp(p-SO_3H)im][I]	Esterification of acetic acid with various alcohols	5% mol cat., alcohol 2 mmol, acetic acid 4 mmol, 60–70 °C, 12–24 h	Yields for alcohols: $PhCH_2OH$ 95%, $PhCH(OH)CH_3$ 86%, $PhCH(OH)CH_2CH_3$ 85%, $PhCH_2CH_2OH$ 88%, CH_3CH_2OH 93%, $C_8H_{17}OH$ 93%, $C_9H_{19}OH$ 92%, $C_{10}H_{21}OH$ 92%	[66]
SiO_2 [tesp(p-SO_3H)im][OTf] [e]	Self-condensation of pentanal	10% wt. cat, 120 °C, 6 h	α = 77.4%, Y = 69.4%, S = 89.6%, TON = 230.5	[67]
SiO_2 [tesp(p-SO_3H)bim][Cl] [f]	Synthesis of fatty acid methyl esters	3% wt. cat., castor/jatropha/neem oil:methanol 1:12 molar ratio, 70 °C, 6–7 h	Castor oil Y = 94.9% Jatropha oil Y = 95.7% Neem oil Y = 94.4%	[68]
SiO_2 [tesp(p-SO_3H)bim][Cl]	Synthesis of 1-amidoalkyl naphthols	80 mg cat., aldehyde 20 mmol, 2-naphthol 20 mmol, acetamide 24 mmol, 100 °C, 7–10 h	Yields for benzaldehydes with R group: H 90%, 3-NO_2 95%, 4-OH 87%, 4-OMe 89%, 2-Cl 92%, 4-Cl 93%, 4-NO_2 89%	[69]
SiO_2 [tespmim][HSO_4] [g]	Bayer–Villiger oxidation of cyclic ketones	0.4 g cat., ketone 1 mmol, 68% $H_2O_{2(aq.)}$ 3 mmol, dichloromethane 4 mL, 50 °C, 5–15 h	cyclobutanone: α = 100%, Y = 96%; cyclopentanone: α = 98%, Y = 75%; cyclohexanone: α = 86%, Y = 64%; 2-adamantanone: α = 95%, Y = 89%; 1-indanone: α = 81%, Y = 78%; 1-tetralone: α = 78%, Y = 77%	[70]
SiO_2 [tespmim][HSO_4]	Esterification of acetic acid and butanol	4% wt. cat., 96°C, butanol 0.12 mol, acetic acid 0.10 mol, cyclohexane 6 mL, 3 h	α = 99.4%, 6 cycles	[71]
SiO_2 [tespmim][HSO_4]	Synthesis of 1-(benzothiazolylamino) phenylmethyl-2-naphthols	150 mg cat., aldehyde 1 mmol, 2-aminobenzothiazole 1 mmol, 2-naphthol 1 mmol, 110 °C, 3–5 h	Yields for various aryl aldehydes with R-groups: H 93%, 2-Cl 89%, 4-Cl 92%, 3-Br 93%, 4-Br 91%, 3-Me 93%, 2-OMe 90%, 3-OMe 92%, 4-OMe 93%, 2-NO_2 90%, 3-NO_2, 92%, 4-NO_2 91%	[72]
SiO_2 [tespmim][HSO_4]	Formylation of amines	0.8% mol cat., amine 1 mmol, formic acid 2 mmol, 60 °C, 1–15 h	Yields and TOF for amines: aniline 94%, 1428 h^{-1}; 4-methoxy aniline 97%, 7275 h^{-1}; benzyl amine 93%, 465 h^{-1}	[73]
SiO_2 [tespmim][HSO_4]	Knoevenagel–Michael cyclization for polyhydroquinolines synthesis	2% mol cat., aldehyde 1 mmol, dimedone 1 mmol, enaminone 1.2 mmol, NH_4OAc 1.5 mmol, H_2O 3 mL, 45 °C, 2–3 h	Yields for enaminone-COOMe with aldehydes with Ar-group: C_6H_5 90%, 4-C_6H_5 93%, 2-C_6H_5 92%, 4-$OMeC_6H_5$ 88%, 2-MeC_6H_5 90%	[74]
SiO_2 [tespmim][HSO_4]	Synthesis of 3,4-dihydropyrano[c] chromenes	0.15 g cat., 4-hydroxycoumarin 1 mmol, malononitrile 1 mmol, Ar-aldehyde 1 mmol, 100 ○ C, 30 min	Yields for aldehydes with Ar-groups: C_6H_5 94%, 4-ClC_6H_4 95%, 3-ClC_6H_4 93%, 4-BrC_6H_4 94%, 2,4-$(Cl)_2C_6H_3$ 90%, 3-$O_2NC_6H_4$ 93%, 4-$O_2NC_6H_4$ 90%, 2-$O_2NC_6H_4$ 89%, 4-MeC_6H_4 94%, 3,4,5-$(CH_3O)_3C_6H_2$ 89%, 4-HO-C_6H_4 93%	[75]

Table 2. *Cont.*

Catalyst	Reaction Type	Reaction Conditions	Reaction Parameters	Lit.
SiO_2 [tespmim][HSO_4]	Synthesis of pyrano[3,2-b]indole derivatives	10% mol cat., 3-hydroxypyrrole 1 mol, benzaldehyde, 1 mol, malononitrile 1 mol, acetonitrile 8 mL, 80 °C, 6–8 h	Yields for aldehydes with Ar groups: 4-$CH_3OC_6H_4$ 84%, C_6H_5 90%, 4-$CH_3C_6H_4$ 85%, 4-BrC_6H_4 90%, 2-BrC_6H_4 86%, 4-ClC_6H_4 90%, 2-ClC_6H_4 86%, 4-CNC_6H_4 90%, 4-$NO_2C_6H_4$ 85%, 2-$NO_2C_6H_4$ 88%	[76]
SiO_2 [tespmim][HSO_4]	Synthesis of pyrano[2,3-b]pyrrole derivatives	10% mol cat., 2-hydroxypyrrole 1 mol, benzaldehyde 1 mol, malonoitrile 1 mol, acetonitrile 4 mL, 60 °C, 2–8 h	Yields for aldehydes with Ar groups: 4-$CH_3OC_6H_4$ 76%, C_6H_5 90%, 4-$CH_3C_6H_4$ 82%, 4-BrC_6H_4 90%, 2-BrC_6H_4 88%, 4-ClC_6H_4 90%, 2-ClC_6H_4 86%, 4-CNC_6H_4 73%, 2-CNC_6H_4 70%, 4-$NO_2C_6H_4$ 64%, 2-$NO_2C_6H_4$ 62%	[77]
SiO_2 [tespmim][HSO_4]	Synthesis of benzo[f]chromene compounds	15% mol cat., 2-naphthol 1 mol, benzaldehyde 1 mol, triethyl orthobenzoate 1 mol, acetonitrile 4 mL, 65 °C, 4–8 h	Yields for benzaldehydes with 4-group: H 85%,Br 85%, Cl 88%, NO_2 80%, Me 88%, OMe 90%, OH 84%	[78]
SiO_2 [tespmim][HSO_4]	Synthesis of 2,9-dihydro-9-methyl-2-oxo-4-aryl-1H-pyrido[2, 3-b]indole-3-carbonitrile compounds	15% mol cat., 1-methyl-1H-indol-2-ol 1 mol, (triethoxymethyl)arene 1 mol, cyanoacetamide 1 mol, DMF 6 mL, 100 °C, 2–7 h	Yields for (triethoxymethyl)arene with groups: 4-OMe 73%, h 65%, 4-Me 65%, 4-Br 61%, 2-Br 56%, 4-Cl 61%, 2-Cl 55%, 4-F 53%	[79]
SiO_2 [tespmim][HSO_4]	Synthesis of acenaphtho[1,2b]pyrroles.	10% mol cat., silyl enol of acenaphthylen-1(2H)-one 1 mol, 2,4-dimethoxybenzaldehyde 1 mol, isocyanocyclohexane 1 mol, DMF 50 mL, reflux, 10 h	Y = 97%	[80]
SiO_2 [tespmim][HSO_4]	Synthesis of 5-Amino-7-aryl-6-cyano-4H-pyrano[3,2-b]pyrroles	10% mol cat., 3-hydroxypyrrole 1 mol, aldehyde 1 mol, malononitrile 1 mol, acetonitrile 4 mL, 50 °C, 1–8 h	Yields for aldehydes with Ar groups: 4-$CH_3OC_6H_4$ 62%, C_6H_5 89%, 4-$CH_3C_6H_4$ 80%, 4-BrC_6H_4 91%, 2-BrC_6H_4 89%, 4-ClC_6H_4 88%, 2-ClC_6H_4 88%, 4-CNC_6H_4 70%, 2-CNC_6H_4 67%, 4-$NO_2C_6H_4$ 61%, 2-$NO_2C_6H_4$ 69%	[81]
SiO_2 [tespmim][$H_2PW_{12}O_{40}$] [h]	Oxidation of dibenzothiophene	0.01 g cat., O/S molar ratio: 3:1 (H_2O_2 0.8 mmol), 60 °C, 40 min	α = 100%, 4 cycles	[82]
SiO_2 [p(p-SO_3H)im][HSO_4] [i]	Esterification of acetate acid and n-butanol	6% wt. cat., n-butanol:acetic acid (2:1, n/n), 94 °C, 3 h	Y = 99.5%	[83]
SiO_2 [tesp(b-SO_3H)im][HSO_4] [j]	Synthesis of amidoalkyl naphtols	80 mg cat., aldehyde:2-naphtol:acetamide (2:2:2.4; n/n/n), 85 °C, 5–15 min	Yields and TOF for different aldehydes with R-groups: Ph 90%, 6.43 min^{-1}; 4-Cl–C_6H_4 89%, 3.18 min^{-1}; 2,4-Cl_2–C_6H_3 86%, 3.84 min^{-1}; 4-Br–C_6H_4 88%, 3.15 min^{-1}; 3-NO_2–C_6H_4 92%, 6.59 min^{-1}; 4-NO_2–C_6H_4 93%, 6.65 min^{-1}; 3-MeO–C_6H_4 86%, 3.07 min^{-1}; 4-MeO–C_6H_4 80%, 1.91 min^{-1}; 4-Me–C_6H_4 87%, 3.11 min^{-1}	[84]
SiO_2 [tesp(b-SO_3H)im][HSO_4]	Thioacetalization of carbonyl compounds	5% mol cat., 4–methoxybenzaldehyde with thiophenol, rt, 5 h	Y = 96%, 6 cycles	[85]
SiO_2 [tesp(b-SO_3H)im][HSO_4]	Acetalization of benzaldehyde or furfural with diols	4% wt. cat., benzaldehyde 70 mmol, ethanediol 126 mmol, cyclohexane 8 mL, reflux, 1.5–3 h	Yields: (a) benzaldehyde: ethanediol 95.2%, 1,2-propanediol 93%, 1,4-Butanediol 87.1% (b) furfural: ethanediol 85%, 1,2-propanediol 95.9%	[86]
SiO_2 [tesp(p-SO_3H)im][HSO_4]	Synthesis of 2H-indazolo[1,2-b]phthalazine-triones	30 mg cat., benzaldehyde 1 mmol, dimedone 1 mmol, phthalhydrazide 1 mmol, 80 °C, 10 min	Y = 94%, 8 cycles	[87]
SiO_2 [tesp(b-SO_3H)im][HSO_4]	Synthesis of polyoxymethylene dimethyl ethers	4% wt. cat., molar ratio of methylal to trioxane 3, 105 °C, 1 h	α = 92%, S = 52%, 6 cycles	[88]
SiO_2 [tesp(p-SO_3H)im][HSO_4] [k]	Lignin depolymerization	0.5 g cat., dealkaline lignin 2% wt., 30 mL H_2O:C_2H_5OH (1:5, *v*/*v*), 200 °C, 1 h	Yields for THF soluble products 90%,	[89]
SiO_2 [p(p-SO_3H)im][HSO_4]	Esterification of acetic acid and n-butanol	8% wt. cat., acetic acid 4.8 g, n-butanol 7.12 g, cyclohexane 8 mL, 89 °C, 3 h	Y = 99.2%, S = 100%, 7 cycles; yields for other alcohols: C_6H_{13} 99.4%, C_2H_5 84.1%, $C_6H_5CH_2$ 98.5%	[90]

Table 2. *Cont.*

Catalyst	Reaction Type	Reaction Conditions	Reaction Parameters	Lit.
SiO_2 [tesp(p-SO_3H)a][HSO_4] [l]	Biodiesel synthesis	0.05 g cat., rapeseed oil 5 g, methanol 2.33 g, 70 °C, 9 h	Y = 99%, 6 cycles	[91]
SiO_2 [tesp(p-SO_3H)a][HSO_4]	Acetalization of benzaldehyde and 1,2-ethanediol	0.05 g cat., benzaldehyde 0.1 mol, 1,2-ethanediol 0.15 mol, 25 °C, 12 h	Y = 98%	[91]
SiO_2 [tespim][$H_2PW_{12}O_{40}$] [m]	Oxidations of alkenes	0.05 g cat., alkene 5 mmol, hydrogen peroxide (30%) 5 mmol, acetonitrile 4.5 mL, 60 °C, 4 h	Conversion, selectivity and TOF for alkenes: cyclooctene 90%, 99%, 162 h^{-1}; 1-octene 34%, 99%, 61 h^{-1}; norbornene 85%, 99%, 153 h^{-1}; limonene 76%, 29%, 137 h^{-1}	[92]
SiO_2 [p(p-SO_3H)im] [$H_2PW_{12}O_{40}$] [n]	Esterification of palmitic acid	15% wt. cat., methanol:palmitic acid molar ratio 9, 65 °C, 8 h	Y = 88.1%, 5 cycles	[93]

[a] 3-(4-sulfobutyl)-1-(3-trimethoxysilylmerkaptopropyl)imidazolium triflate, [b] 3-(4-sulfobutyl)-1-(3-propyltriethoxysilane)imidazolium chloride, [c] 3-(3-sulfopropyl)-1-(3-propyltriethoxysilane)imidazolium triflate, [d] 3-(3-sulfopropyl)-1-(3-propyltrimethoxysilane)imidazolium iodide, [e] 3-(3-sulfopropyl)-1-(3-propyltrimethoxysilane)imidazolium triflate, [f] 3-(3-sulfopropyl)-1-(3-propyltriethoxysilane)benzimidazolium chloride, [g] 1-methyl-3-(3-propyltriethoxysilane)imidazolium hydrogensulfate, [h] 1-methyl-3-(3-propyltriethoxysilane)imidazolium dihydrogenphosphotungstate, [i] 3-(3-sulfopropyl)-1-(3-trimethoxysilylmerkaptopropyl)imidazolium hydrogensulfate, [j] 3-(4-sulfobutyl)-1-(3-propyltriethoxysilane)imidazolium hydrogensulfate, [k] 3-(3-sulfopropyl)-1-(3-propyltriethoxysilane)imidazolium hydrogensulfate, [l] N-(3-sulfopropyl)-N-(3-propyltriethoxysilane)ammonium hydrogensulfate, [m] 1-(3-propyltriethoxysilane)imidazolium dihydrogenphosphotungstate, [n] 3-(3-sulfopropyl)-1-(3-trimethoxysilylmerkaptopropyl)imidazolium dihydrogenphosphotungstate.

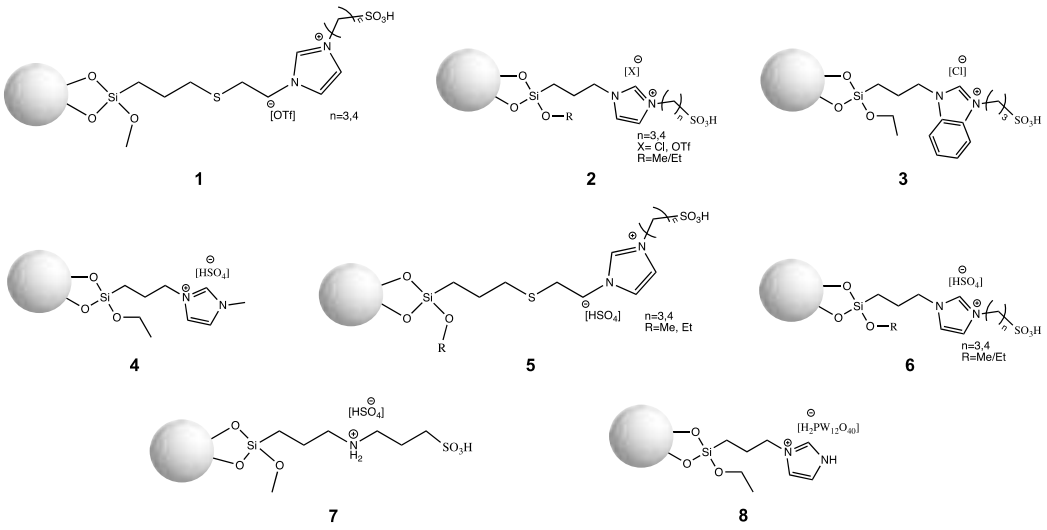

Figure 9. Structures of Brønsted-type silica-based SILLP materials.

Brønsted acidic vinylimidazolium-based IL moieties modified with -SO_3H groups were grafted to a sulfhydryl group-modified silica surface through free radical addition obtaining SILLP catalyst **1** (Figure 9). The prepared material was used in the esterification of oleic acid with methanol and the transesterification of glycerol trioleate with methanol. It was reported that the loading density of the IL influenced both reactions. Increasing the loading of the IL on the support induced the conversion of oleic acid.However, for the conversion of glycerol trioleate, the opposite effect is observed. This is due to the size of glycerol trioleate molecules and the decreasing pore size of the SILLP. The SILLP catalyst could be used in the esterification for three cycles, after which the catalytic activity dropped and the hydrolysis or alcoholysis of the -Si-O-Si- bonds occurred [62]. In the following report, the structure of a Brønsted imidazolium IL modified with -SO_3H groups was produced in three stages: first, 3-(chloropropyl)trimethoxysilane was anchored to the silica surface. Next, imidazole moieties were introduced to the structure before 1,4-

butanesultone was used to modify the imidazole ring with a -$C_4H_9SO_3H$ group (**2**, Figure 9). The catalytic activity of the obtained SILLP material was tested in a cellulose hydrolysis and yielded a 48.1% reduction of sugar and 21.9% of glucose. In this case, the catalyst maintained activity for three cycles. Due to the use of the SILLP catalyst, the total yields in the reduction of sugar and glucose were higher than using $SO_3HC_3H_7$-SiO_2 or SO_3H-SiO_2, keeping the same -SO_3H group loading. This effect results from the interaction between the imidazolium IL and the hydroxyl groups in cellulose [63]. The SILLP catalyst **1** (Figure 9) was also used in the dehydration of fructose to 5-hydroxymethylfurfural (HMF) with 100% conversion and 70.1% yield of the main product (Scheme 1, Figure 10). In this reaction, the catalyst was reused without significant loss of activity for 7 cycles. Simultaneously, the same SILLP material with a Lewis -SO_2Cl center was tested for this reaction. However, the catalyst exhibited inferior efficiency compared with the Brønsted-type SILLP [64]. The next report described the functionalization of bifunctional periodic mesoporous organosilica with IL and -SO_3H groups, as well as its application in a Biginelli condensation reaction for the synthesis of pharmacological and biological activities compounds. The novel material assured high yields of various products (Table 2) and could be recycled over 10 times without any decrease in efficiency [65]. The same catalyst was also used in the esterification of acetic acid with various alcohols and, again, high yields of the main products were reached and the SILLP material could be reused several times [66]. Another report mentioned a triflate imidazolium-based IL with a -SO_3H group anchored to the silica, MCM-41, and SBA-15 materials (**2**, Figure 9). Activity tests were performed for the self-condensation of pentanal to 2-propyl-2-heptenal, where the best results were achieved for the silica based SILLP (69.4% yield, 89.6% selectivity), which was due to the highest IL loading on the surface [67]. A benzimidazolium IL with a -SO_3H group in alkyl chain was grafted to silica surface (**3**, Figure 9) in stages (which were described above). The SILLP catalyst was employed in the transesterification of non-edible oils with high free fatty acids, as well as for the synthesis of 1-amidoalkyl naphthols from 2-naphthol, amides, and aldehydes (Scheme 2, Figure 10). This eco-friendly and efficient catalyst for transesterification provided 95% yield of fatty acid methyl esters and catalytic stability over 5 runs [68]. Moreover, the SILLP material in the synthesis of 1-amidoalkyl naphthols exhibited high yield of the obtained products (Table 2), high product quality, short reaction times, and reusability for five reaction cycles, which makes the catalyst very useful for industrial practices [69].

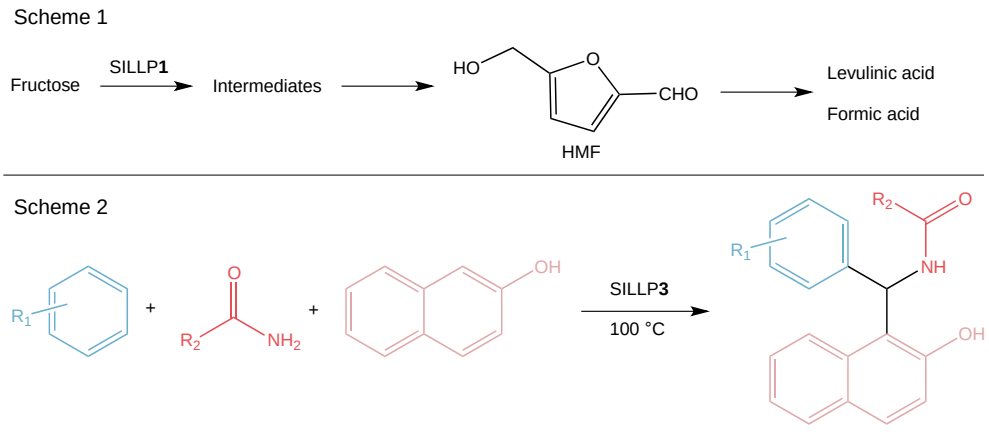

Figure 10. Brønsted-type SILLP based on silica material in the dehydration of fructose (Scheme 1) and synthesis of 1-amidoalkyl naphthols (Scheme 2).

Further reports concern the application of covalently immobilized imidazolium-based ILs with a hydrogensulfate anion on silica materials (**4**, Figure 9). The Bayer–Villiger oxidation of cyclic ketones to lactones (Figure 11) is one example of numerous reactions catalyzed by SILLP **4** (Figure 9). For that purpose, a silica material with the extensive

system of meso- and macropores was used. Here, the catalyst showed great activity, which resulted in high conversions of ketones and yields of lactones (60–91%), short reaction times, and good reusability (three cycles) [70]. The same SILLP catalyst was used in the esterification of acetic acid with butanol with a 99.4% conversion, and a reusability of six catalytic cycles with a slight decrease of conversion were observed [71]. The synthesis of 1-(benzothiazolylamino)phenylmethyl-2-naphthols catalyzed by SILLP **4** (Figure 9) was also reported. In this case, IL was anchored to rice husk ash, which is a natural source of amorphous silica. High yields for various aldehydes (90–93%) and high TOF (92 h^{-1}) were achieved (Table 2) in very short reaction times. Furthermore, the catalyst could be reused six times without activity loss [72]. The same catalytic system was examined for the formylation of amines. Again, the catalyst proved to be simple, stable, and efficient, since high yields (93–97%), TOF (465–7275 h^{-1}) and reusability over 10 cycles were reached [73]. In another report, an IL containing a hydrogensulfate anion was immobilized on nanoporous silica SBA-15 and used in the synthesis of hexahydroquinolines via the Knoevenagel–Michael cyclization as an alternative to conventional catalysts. Excellent yields (90–93%), short reaction times, aqueous conditions, and reusability (seven runs) made the process more environmentally friendly [74]. The synthesis of 3,4-dihydropyrano[c]chromenes (Scheme 1, Figure 12) and pyrano[2,3-c]pyrazoles were also proceeded in the presence of SILLP **4** (Figure 9). Various ILs with anions, such as $[HSO_4]^-$, $[H_2PO_4]^-$, $[Br]^-$, and $[OTf]^-$ were tested, with the best results gained for the hydrogensulfate anion. The catalyst exhibited very good yields (89–95%) and reusability (five cycles) [75]. The use of SILLP **4** (Figure 9) was also successful for the synthesis of pyrano[3,2-b]indoles (Scheme 2, Figure 12) [76], pyrano[2,3-b]pyrroles (Scheme 3, Figure 12) [77], benzo[f]chromenes [78], 2,9-dihydro-9-methyl-2-oxo-4-aryl-1H-pyrido[2, 3-b]indole-3-carbonitriles [79], acenaphtho[1,2b]pyrroles [80], and 5-amino-7-aryl-6-cyano-4H-pyrano[3,2-b]pyrroles [81]. As shown in Table 2, satisfying yields for different aldehydes, arenes, and components were achieved, which indicates the versatility of SILLP 4 (Figure 9) catalyst, as well as the developed methods. Moreover, the catalyst could be reused several times [76–81]. The dihydrogenphosphotungstate anion ($[H_2PW_{12}O_{40}]^-$) was reported in an SBA-15 based SILLP, exhibiting well-ordered, mesoporous specific high surface area. This novel catalyst found application in the oxidation of dibenzothiophene, 4,6-dimethylbenzothiophene, and benzothiophene for fuel desulfurization. This SILLP showed excellent efficiency, with 100% conversion of dibenzothiophene and 4,6-dimethylbenzothiophene, which means the total ability of removal of toxic compounds from the fuel. Furthermore, the catalyst could be successfully reused four times [82].

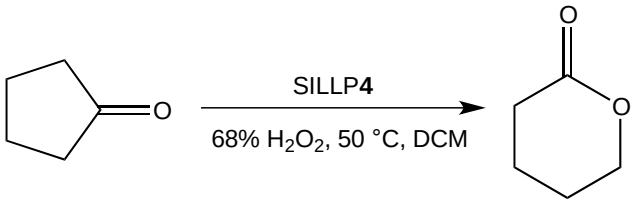

Figure 11. Brønsted-type SILLP based on silica material in Bayer–Villiger oxidation.

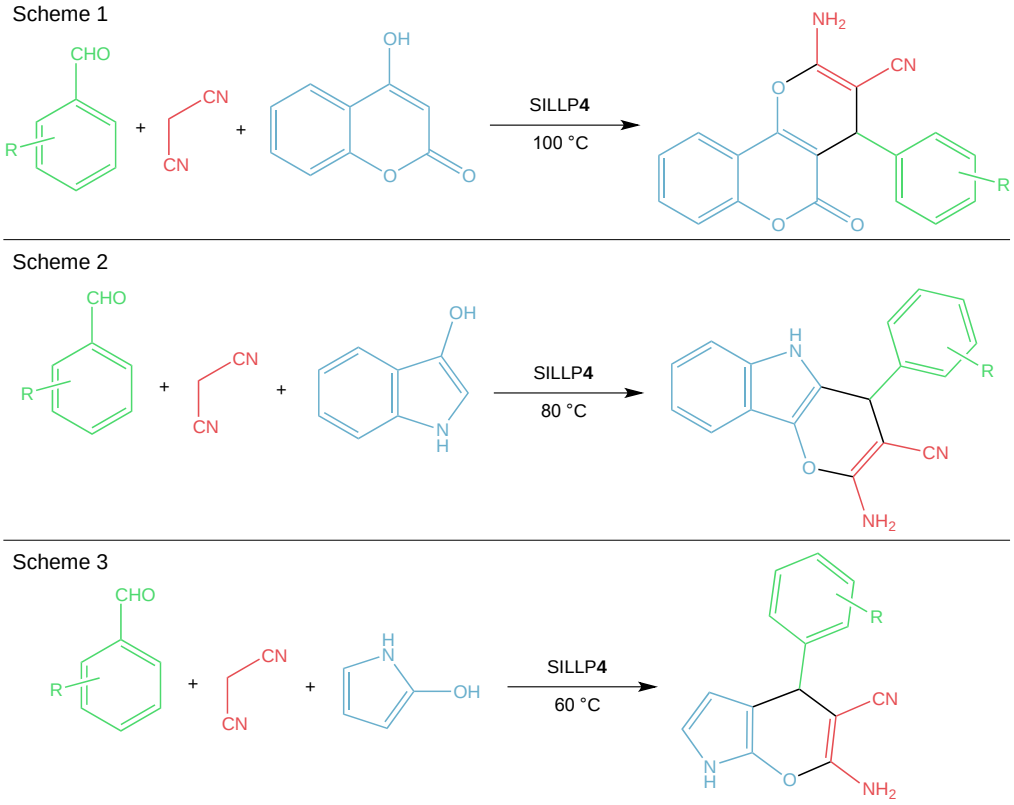

Figure 12. Brønsted-type SILLP based on silica material in the synthesis of 3,4 -dihydropyrano[c]chromenes (Scheme 1), pyrano[3,2-b]indoles (Scheme 2), and pyrano[2,3-b]pyrroles (Scheme 3).

Dual Brønsted acidic ILs immobilized on silica materials are another group of Brønsted-type SILLPs. In this case, the Brønsted centers are located both in the cation and anion, like the -SO_3H groups grafted to the alkyl chain in the cation and like the $[HSO_4]^-$ in the anion (**5**, **6**, Figure 9). This kind of catalyst is quite often used according to the literature. One use is the esterification of acetic acid and n-butanol. SILLP **5** (Figure 9) material caused 99.5% yield of n-butyl acetate, where it could be recycled eight times with only a slight decrease in conversion to 90.1% [83]. The next report presents 3-sulfopropyl-1-(3-propyltrimethoxysilane)imidazolium hydrogensulfate IL anchored to silica gel forming SILLP **6** (Figure 9) in the synthesis of amidoalkyl naphthols by the multicomponent condensation. high yields and TOFs (Table 2) were obtained, and the catalyst kept activity for seven cycles without significant loss [84]. SILLP **6** (Figure 9) was also used as a catalyst in the thioacetalization of carbonyl compounds, providing high yields (85–96%). The reaction between 4-methoxybenzaldehyde with thiophenol (Scheme 1, Figure 13) was characterized by 96% yield, mild reaction conditions, and short reaction times, with the catalyst efficiently being recycled six times [85]. Furthermore, the same catalyst was employed in acetalization of benzaldehyde or furfural with various diols. High catalytic activity (yields 85–96%) for 10 reaction runs was reached for the synthesis of benzaldehyde ethanediol acetal [86]. Again, SILLP **6** (Figure 9) was used as a catalyst in the synthesis of 2H-indazolo[1,2-b]phthalazine-triones (Scheme 2, Figure 13) [87] and polyoxymethylene dimethyl ethers [88]. In the first case, nano-silica formed a matrix for IL immobilization. The synthesized material showed high catalytic activity, gaining 81–96% yield of indazolophthalazine-triones and bisindazolophthalazine-triones, while maintaining activity over seven reaction cycles [87]. Various types of such silica gels used in SILLP synthesis are described widely throughout the literature. In order to reduce the ratio of the catalyst in the reactants, the SILLP with the highest surface area and IL loading was selected as the catalyst. This resulted in a 52% trioxane conversion and 92% polyoxymethylene dimethyl ethers selectivity [88]. Next,

SILLP **6** (Figure 9) was also employed in a lignin depolymerization. This highly thermally stable catalyst allowed a 90% yield of tetrahydrofuran soluble products to be obtained in 1 h at 200 °C [89]. It was also found that SILLP **5** (Figure 9) catalyzed the esterification of acetic acid and n-butanol. The catalyst provided a 99.2% yield and 100% selectivity and was active for seven cycles. Moreover, high yields for reactions with various alcohols were achieved (Table 2) [90]. The novel silica-based SILLP **7** (Figure 9) material was also synthesized from the (3-aminopropyl)-trimethoxysilane precursor. The prepared catalyst was used in the acetalization of benzaldehyde with 1,2-ethanedioland and biodiesel synthesis. In both cases, the SILLP exhibited high catalytic activity, assuring 99% yields of the main product and reusability over six cycles. In comparison with conventional biodiesel synthesis, SILLP catalysts are a very promising alternative [91]. SILLP **8** (Figure 9) with Brønsted acidic sites introduced with an imidazolium cation and dihydrogenphosphotungstate anion was tested in the oxidation of alkenes. The catalyst proved to be efficient in this reaction, providing high selectivities, conversions, and TOF (Table 2) [92]. The dihydrogenphosphotungstate anion was involved in the synthesis of SILLP **5** (Figure 9) instead of the hydrogensulfate anion. The SBA-15 SILLP catalyst was applied in the biodiesel synthesis from palmitic acid. In comparison to other anions such as hydrogensulfate and triflate, the dihydrogenphosphotungstate anion performed the highest IL loading and catalytic activity, giving an 88.1% yield and reusability of over five times [93].

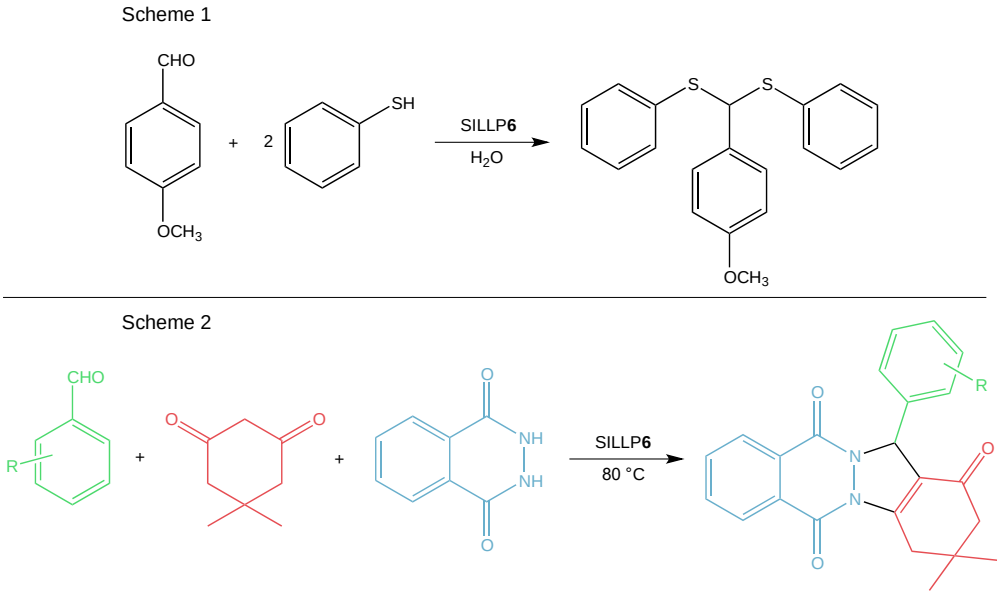

Figure 13. Brønsted-type SILLP based on silica material in the synthesis of thioacetalization of (Scheme 1)), 2H-indazolo[1,2-b]phthalazine-triones (Scheme 2).

3.3. Fe_3O_4-Silica hybrid Based SILLPs

Immobilization of an ionic liquid on a solid matrix provides easy catalyst separation from the reaction mixture, as well as its recycling. Doping silica materials with Fe_3O_4 offers new features, such as magnetic properties, for example. A silica-Fe_3O_4 hybrid could be even faster and more easily separated from the reaction mixture using an external magnetic field, making it an attractive support. Table 3 shows applications of silica-Fe_3O_4-based SILLP in organic catalysis, and Figure 14 presents chosen structures of silica-Fe_3O_4-based SILLPs.

Table 3. Silica-Fe_3O_4-based SILLPs in organic catalysis.

Catalyst	Reaction Type	Reaction Conditions	Technological Parameters	Lit.
SiO_2·Fe_3O_4 [tmspmim][Cl-$AlCl_3$] [a]	Synthesis of β-keto enol ethers	0.27 g cat., 5,5-dimethylcyclohexane-1,3-dione 1 mmol, alcohol 3 mL, rt, 50–95 min	Yields for alcohols: methanol 94%, ethanol 93%, n-butanol 89%, n-pentanol 87%, 2-propanol 88%, cyclohexanol 86%	[94]
SiO_2·Fe_3O_4 [tmspmim][Cl-$ZnCl_2$] [b]	Synthesis of benzoxanthenes	15 mg cat., benzaldehyde 1 mmol, 2-naphthol 1 mmol, dimedone 1 mmol, sonication, 80 °C, 30 min	Yields for benzaldehydes with R-groups: H 96%, 4-Me 84%, 2-OH 81%, 4-F 81%, 4-Cl 72%, 4-Br 76%, 2-F 70%, 2-Cl 75%, 2-Br 79%, 2-NO_2 90%	[95]
SiO_2·Fe_3O_4 [tmspmim][Cl-$ZnCl_2$]	Synthesis of pyrroles	15 mg cat., aniline 1 mmol, acetonylacetone 1.2 mmol, sonication, 30–90 min	Yields for anilines with R-groups: H 91%, 4-I 98%, 4-OH 95%, 2-OH, 5-Me 78%, 3,5-Cl 77%	[95]
SiO_2·Fe_3O_4 [tmspmim][HSO_4] [c]	Synthesis of 1,8-dioxodecahydro-acridines	cyclic diketones: amines:aldehydes: catalyst (2:1:1:0.01), 80 °C, 10–30 min	Yields 87–97%	[96]
SiO_2·Fe_3O_4 [tmspim][HSO_4] [d]	Synthesis of 3-thiocyanato-1H-indole	5 mg cat., indole:H_2O_2:KSCN (1:3:3; n/n), water:ethanol (1:4; *v*/*v*), rt	Y = 95%; for various substrates 88–98%	[97]
SiO_2·Fe_3O_4 [tmsptetrazole-SO_3H][Cl] [e]	Synthesis of	0.2 g cat., arylcyanamide 1 mmol, NaOCN 1 mmol, H_2O 10 mL, reflux	Yields for arylcyanamide with R-groups: 3-Br 90%, 4-Cl 89%, 4-Me 92%, 4-OMe 93%	[98]
SiO_2·Fe_3O_4 [tmspim][HSO_4]	1-carbamoyl-1-phenylureas	50 mg cat., benzaldehyde 1 mmol, acetic anhydride 5 mmol, rt, 10–120 min	Yields for benzaldehydes with R-groups: H 91%, 4-Cl 95%, 4-Me 93%, 4-OH 91%, 2-OH 97%, 4-MeO 90%, 2-MeO 87%, 4-COOH 90%, 4-CN 88%, 4-NO_2 98%	[99]
SiO_2·Fe_3O_4 [tmspdabco(SO_3H)] $[OTf]_2$ [f]	Acetylation of aldehydes with acetic anhydride	50 mg cat., isatin 0.5 mmol, indole 1 mmol, H_2O 2 mL, 90 °C, 2 h	Y = 85–96%, 8 cycles	[100]
SiO_2·Fe_3O_4 [tespmim][$H_2PW_{12}O_{40}$] [g]	Synthesis of 3,3-di(indolyl)indolin-2-ones	0.1 mg cat., hydrazine hydrate 2 mmol, ethyl acetoacetate 2 mmol, aryl aldehydes 1 mmol, ammonium acetate 3 mmol, water 15 mL, rt, 30 min.	Yields for different Ar-aldehydes: H 96%, Cl 95%, F 97%, NO_2 98%, OMe 92%, Me 93%, OH 90%, CN 95%	[101]
SiO_2·Fe_3O_4 [tesp(b-SO_3H)im][HSO_4] [h]	Synthesis of tetrahydrodipyrazolo-pyridines	55 mg cat., aldehyde 2 mmol, 2-naphthol 2 mmol, dimedone 2.4 mmol, 90 °C, 35–65 min	Yields for aldehydes with Ar groups: C_5H_6 89%, 4-MeC_6H_4 86%, 4-$OMeC_6H_4$ 84%, 4-ClC_6H_4 91%, 3-ClC_6H_4 84%, 4-BrC_6H_4 90%, 3-BrC_6H_4 88%, 4-$NO_2C_6H_4$ 93%, 3-$NO_2C_6H_4$ 90%, 2-$NO_2C_6H_4$ 85%	[102]
SiO_2·Fe_3O_4 [tesp(b-SO_3H)im][HSO_4]	Synthesis of benzoxanthenes	50 mg cat., isatin 1 mmol, 1,3-dimethyl-2-amino uracil 1 mmol, barbituric acid 1 mmol, H_2O, 1 mL, rt, 4–8 h	Y = 81–90%, 5 cycles	[103]
SiO_2·Fe_3O_4 [tmsp(p-SO_3H)im][HSO_4] [i]	Synthesis of spirooxindoles	0.2 g cat., oleic acid 10 mmol, alcohol 60 mmol, 373K, 4 h	Methanol: Y = 89.6% Ethanol: Y = 93.5% n-propanol: Y = 92% n-butanol: Y = 91.5%	[104]
SiO_2·Fe_3O_4 [tesp(p-SO_3H)im][HSO_4]	Biodiesel production from oleic acid	10.8% wt. cat., methanol:oleic acid molar ratio 6, 110 °C, 4 h	α = 92.9%, 8 cycles	[105]
SiO_2·Fe_3O_4 [tesp(Ph-SO_3H)$_3$P][Cl] [j]	Biodiesel production from oleic acid	0.06 g cat., benzaldehyde 30 mmol, ethylene glycol 90 mmol, cyclohexane 185 mmol, reflux, 2 h	Yields for: benzaldehyde 97% (5 cycles), propionaldehyde 96%, butanone 95%, cyclohexanone 94%	[106]

Table 3. *Cont.*

Catalyst	Reaction Type	Reaction Conditions	Technological Parameters	Lit.
SiO_2·Fe_3O_4 [Cl][diammonium] $[HSO_4]$ [k]	Acetalization of aldehyde or ketone with ethylene glycol	0.048 cat., dimedone 1 mmol, benzaldehyde 1 mmol, 6-amino-1,3-dimethyluracil 1 mmol, 120 °C, 15–30 min	Yields for various benzaldehydes with R-group: H 94%, 3-Br 92%, 4-Br 90%, 2-Cl 88%, 4-Cl 96%, 4-Me 93%, 4-OMe 94%, 4-OH 81%	[107]
SiO_2·Fe_3O_4 [tesp2pyr][HSO_4] [l]	Synthesis of pyrimido[4,5-b]quinolines.	200 mg cat., aromatic amine 1 mmol, $NaNO_2$ 2.5 mmol, NaI 2.5 mmol, rt, 12–15 min	Yields for aromatic amines: $C_6H_5NH_2$ 73%, 4-$H_2NC_6H_4COOH$ 95%, 4-$NO_2C_6H_4NH_2$ 83%, 4-$BrC_6H_4NH_2$ 78%, 4-$ClC_6H_4NH_2$ 82%, 4-$MeC_6H_4NH_2$ 62%	[108]
SiO_2·$CoFe_2O_4$ [p(b-SO_3H)im] [OTf] [m]	Diazotization–iodination of the aromatic amines	1:30 equimolar amount of oleic acid and the catalyst, alcohol 17.02 g, 100 °C, 4 h	CH_3: α = 75%, C_4H_9: α = 40%, C_6H_{13}:α = 20%, C_8H_{17}:α = 16%	[109]
SiO_2·Fe_3O_4 [tmsptetrazole-SO_3H][HSO_4] [n]	Esterification of oleic acid with straight-chain alcohols	20 mg cat., benzaldehyde 1 mmol, 2-thiobarbituric acid 2 mmol, acetate ammonium 1 mmol, H_2O 5 mL, rt, 35–60 min	Yields for benzaldehydes with R-groups: H 89%, 4-Cl 91%, 4-NO_2 95%, 4-Me 87%, 4-OMe 84%, 2-NO_2 93%, 2-OH 82%, 2-OMe 85%, 2–80%, 3-OMe 90%	[110]
SiO_2·Fe_3O_4 [OH-etNH_3][b-SO_3] [o]	Synthesis of pyrimidine derivatives	Aldehyde:malononitrile: thiophenol:catalyst (1/2/1/0.012; n/n/n/n), 50 °C, 5–20 min	Y = 81–91%; 5 cycles (benzaldehyde, malononitrile and thiophenol)	[111]
SiO_2·Fe_3O_4 [tmspdabco][Cl] [p]	Synthesis of 2-amino-3,5-dicarbonitrile-6-thio-pyridines	Aldehyde, ethyl cyanoacetate, H_2O-polyethylene glycol	8 cycles, high yields	[112]
SiO_2·Fe_3O_4 [tespmim][Cl] [r]	Knoevenagel condensation	0.0007 g cat., aromatic aldehyde 1 mmol, anilines 1 mmol, thioglycolic acid 1 mmol, 70 °C, 55–70 min	(a) aniline + aromatic aldehydes Yields for R-groups in aldehydes: H 94% (10 cycles), 4-Me 88%, 4-Cl 95%, 4-NO_2 92%, 3-NO_2 89% (b) p-methylaniline + aromatic aldehydes Yields for R-groups in aldehydes: H 90%, Me 93%, 90%	[113]
SiO_2·Fe_3O_4 [tespmim][Cl]	Synthesis of 1,3-thiazolidin-4-ones	20% mol cat., 6-amino-N,N-dimethyuracil 1 mmol, 3-(2-methyl-1H-indol-3-yl)-3-oxopropanenitrile 1 mmol, arylaldehydes 1 mmol, DMF 10 mL, 120 °C, 55–120 min	Yields for aldehydes with Ar-groups: 4-FC_6H_4 90% (3 cycles), 4-ClC_6H_4 90%, 4-BrC_6H_4 85%, 4-CNC_6H_4 90%, 4-$CF_3C_6H_4$ 90%, C_6H_5 80%, 3-ClC_6H_4 90%, 3-$OMeC_6H_4$ 75%	[114]
SiO_2·Fe_3O_4 [tespmim][Cl]	Synthesis of indole-substituted pyrido[2,3-d]pyrimidines	1% mol cat., epoxide 10 mmol, P_{CO2} = 1 Mpa, 140 °C, 4–12 h	Styrene oxide Y = 93% (11 cycles), propylene oxide Y = 99%, epichlorohydrin Y= 99%	[115]
SiO_2·Fe_3O_4 [tespmim][Cl]	Cycloaddition of CO_2 to epoxides	0.05 g cat., aromatic aldehyde 2 mmol, ethyl acetoacetate 2 mmol, urea/thiourea 3 mmol, 100 °C, 25–40min	Yields for aldehydes: (a) urea: Ph 95%, 3-ClC_6H_4 97%, 3-$NO_2C_6H_4$ 97%, 2-tiophen 98%, 3-FC_6H_4 92% (b) thiourea: Ph 96%, 4-$OMeC_6H_4$ 90%, 2-tiophen 95%	[116]

Table 3. *Cont.*

Catalyst	Reaction Type	Reaction Conditions	Technological Parameters	Lit.
SiO_2·Fe_3O_4 [tespmim][Cl]	Synthesis of 3,4-dihydropyrimidin-2(1H)-ones/thiones	7 mg cat., aniline 1 mmol), formic acid 3 mmol, rt, 5–10 min	Yields for anilines with R-groups: H 99% (5 cycles), 4-Me 98%, 4-OMe 98%, 4-Cl-90%, 4-NO_2 98%	[117]
SiO_2·Fe_3O_4 [tesptriazinium][Cl] [s]	N-formylation	0.02 g cat., aromatic aldehyde 1 mmol, malononitrile 1 mmol, 5-hydroxy-2-hydroxymethyl-4H-pyran-4-one (kojic acid) 1 mmol H_2O 5 mL, reflux, 30–45 min	Yields for benzaldehydes with R-groups: H 94%, 2,3-Cl_2 94%, 2,6-Cl_2 97%, 4-NO_2 98%, 3-NO_2 97%, 4-OH 85%	[118]
SiO_2·Fe_3O_4 [tesampmim][Cl] [t]	of amines	10 mg cat., benzylalcohol 1 mmol, anhydride 2 mmol, rt, 20–60 min	Yields for various benzylalcoholes with R-groups: 4-Br 96% (9 cycles), 4-OMe 94%, 4-F 94%, i-C_3H_7 93%	[119]
SiO_2·Fe_3O_4 [tmsp(alanine)im][Cl] [u]	Synthesis of 4H-dihydropyrano	0.001 g cat., arylaldehyde 2.5 mol, arylamine 2.5 mol cyclohexanon 3 mol, EtOH 20 mL, sonication (70 W)	Yields and selectivity (anti:syn) for anilinę+ benzaldehydes with R-groups: H 92%, 99:1; 2-Cl 91%, 97:3; 4-Me 88%, 99:1; 4-Cl 92%, 99:1; 4-Br 92%, 99:1; 4-OMe 89%, 99:1; 2-OMe 86%, 99:1	[120]
SiO_2·Fe_3O_4 [tespdeaim][PF_6] [w]	[3,2-b]pyran-3-carbonitrile	25 mg cat., aldehyde or ketone 2 mmol, malonitrile 2 mmol, water 10 mL, 30 °C, 1 h	α for aldehydes/ketones: cyclohexanone >99%, furfural >99%, benzaldehyde >99%, 4-nitrobenzaldehyde 91.6%, 4-hydroxybenzaldehyde 89.4%, 2-hydroxybenzaldehyde 80.3%, 2-methylpropanal 92%	[121]
$Fe_{3-x}Ti_xO_4$-SiO_2 [$TrpEt_3$][I] [x]	Derivatives	0.12 g cat., anilines 1 mmol, dialkyl acetylenedicarboxylates 1 mmol, terminal alkynes or acetophenones 1.2 mmol, 100 °C, 15–18 h	Methyl 4-propylquinoline2-carboxylate: Y = 75% ethyl 6-hydroxy4-propylquinoline-2-carboxylate: Y = 92%	[122]
$Fe_{3-x}Ti_xO_4$-SiO_2 [$TrpEt_3$][I]	Acetylation of alcohols	0.12 g cat., anilines 1 mmol, dialkyl acetylenedicarboxylates 2.2 mmol, 100 °C, 10–22 h	Ethyl 4-(4-bromophenyl)benzo quinoline-2-carboxylate: Y = 77% dimethyl 8-nitroquinoline2,4-dicarboxylate: Y = 82%	[122]

[a] 1-methyl-3-(trimethoxysilylpropyl)imidazolium chloride—chloroaluminate (III), [b] *N*-(trimethoxysilylpropyl)imidazolium chloride—chlorozincate (II), [c] 1-methyl-3-(trimethoxysilylpropyl)imidazolium hydrogensulfate, [d] 1-methyl-3-(trimethoxysilylpropyl)imidazolium hydrogensulfate, [5]*N*-(trimethoxysilylpropyl)-5-phenyl-1H-tetrazolium-SO_3H chloride, [e] *N*-(3-sulfopropyl)-*N*-(3-propyltrimethoxysilane)triethylenediammonium ditriflate, [f] 1-methyl-3-(trimethoxysilylpropyl)imidazolium dihydrogenphosphotungstate, [g] 3-(4-sulfobutyl)-1-(3-propyltriethoxysilane)imidazolium hydrogensulfate, [h] 3-(3-sulfopropyl)-1-(3-propyltriethoxysilane)imidazolium hydrogensulfate, [i] *P*-(trimethoxysilylpropyl)-*P*,*P*,*P*-tri(4-sulfophenyl)phosphonium chloride, [j] *N*-(trimethoxysilylpropyl)-*N*,*N*-dimethyl-*N*-(dimethylammonium)ammonium chloride hydrosulfate, [k] *N*-(propyl-triethoxysilane)-2-pyrrolidinium hydrogensulfate, [l] 3-(4-sulfobutyl)-1-(3-trimethoxysilylmerkaptopropyl)imidazolium triflate, [m] *N*-(trimethoxysilylpropyl)-5-phenyl-1H-tetrazolium-sulfobutyl hydrogensulfate, [n] 2-hydroxyethylammonium butylsulphonate, [o] *N*-(3-propyltrimethoxysilane)triethylenediammonium chloride, [p] 1-methyl-3-(triethoxysilylpropyl)imidazolium chloride, [r] N-(triethoxysilylpropyl)triazinium chloride, [s] 3-((3-(trisilyloxy)propyl)propionamide)-1-methylimidazolium chloride, [t] 3-(trimethoxysilylpropyl)-1-(2-aminopropanoate)imidazolium trimethylethanolammonium chloride, [u] imidazolium alanine based IL, [w] 3-(trimethoxysilylpropyl)-1-(triethylamine)imidazolium hexafluorophosphate, [x] triethyltryptophanium iodide.

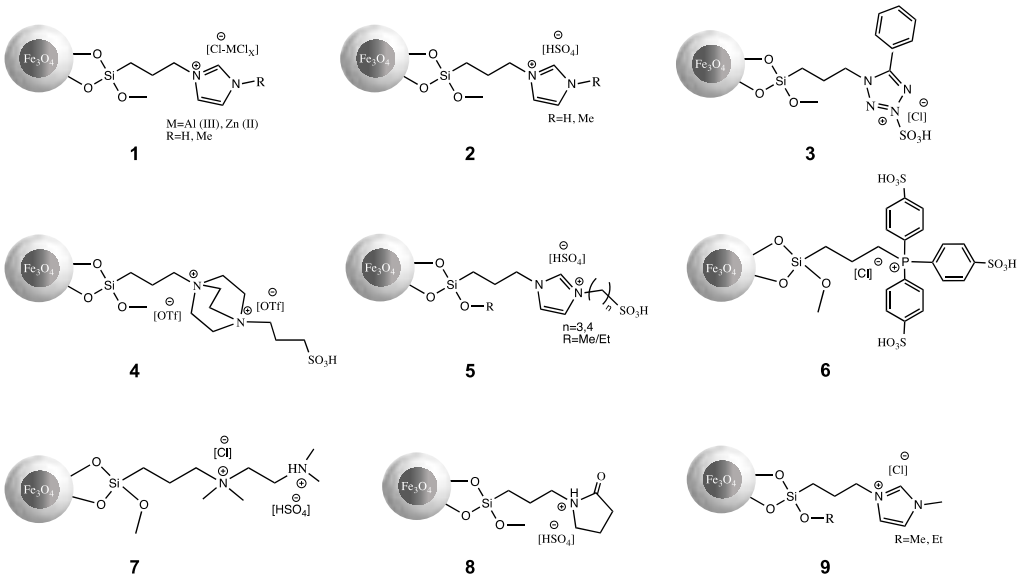

Figure 14. Structures of silica-Fe_3O_4-based SILLPs.

A Lewis chloroaluminate IL was grafted to a $SiO_2 \cdot Fe_3O_4$ nanomaterial, and the catalytic activity of obtained SILLP **1** (Figure 14) was tested in the synthesis of β-keto enol ethers. The magnetic catalyst showed proper efficiency and provided high yields under mild reaction conditions. Moreover, the SILLP maintained activity for six reaction cycles, and its recovery through external magnetic field was very effective [94]. The next report examined Lewis magnetic SILLP **1** (Figure 14) based on the chlorozincate (II) anion in the synthesis of benzoxanthenes (Scheme 1, Figure 15) and pyrroles (Scheme 2, Figure 15). In both reactions, the SILLP presented excellent activity, reusability for 5 runs, and achieved 76–96% yields of benzoxanthenes and pyrroles. In comparison with the described catalysts, the magnetic SILLP is a promising alternative due to its versatility [95]. Brønsted hydrogensulfate IL was anchored to magnetic silica-based material, where SILLP **2** (Figure 14) exhibited excellent activity and achieved 87–97% yields in the condensation reaction of cyclic diketones with aromatic aldehydes and ammonium acetate or primary amines. The catalyst could be reused nine times, which additionally proves the wide applicability of this nanomaterial [96]. In another report, SILLP **2** (Figure 14) found application as a catalyst for the thiocyanation of aromatic and heteroaromatic compounds. High yields of 88–98%, regioselectivity, short reaction times, and reusability (seven runs) were achieved [97]. The next report described the magnetic SILLP **3** (Figure 14) based on the phenyltetrazole cation. The SILLP nanocatalyst examined its efficiency in the synthesis of antibacterially active 1-carbamoyl-1-phenylureas in water. The magnetic nanomaterial gave 89–93% yields of the main products and kept good catalytic activity during five reaction cycles [98]. Hydrogensulfate poly(ionic liquid) was grafted to silica magnetic nanoparticles via the polymerization of vinylimidazolium moieties. The catalytic activity of the prepared heterogeneous catalyst was checked in the acetylation of aldehydes with acetic anhydride, which resulted in 90–98% yields and 10 reaction cycles without activity loss. Moreover, the SILLP also showed good efficiency in the deprotection reaction of acyl [99]. The Brønsted triethylenediammonium ditriflate based magnetic SILLP **4** (Figure 14) was found to be a great catalyst in the synthesis of 3,3-di(indolyl)indolin-2-ones. A yield of 85–96% of various indolines compounds with medical properties and eight efficient catalytic cycles were achieved with SILLP **4** [100]. In other work, Fe_3O_4 nanoparticles coated with silica SILLP **2** (Figure 14) based on the dihydrogenphosphotungstate anion catalyzed the synthesis of tetrahydrodipyrazolo-pyridines. This catalytic system could be reused several times using magnetic external forces and high loadings of the IL, providing excellent yields (90–98%) under mild conditions [101]. Further reports present Dual Brønsted acidic ILs immobilized on

silica coated magnetic nanoparticles. SILLP **5** (Figure 14) found applications as a catalyst in the synthesis of benzoxanthenes [102], spirooxindoles [103], and biodiesel production from oleic acid [104,105]. This novel catalyst demonstrated great versatility and activity in all mentioned processes, achieving high yields for benzoxanthenes (84–91%), spirooxindoles (81–90%), biodiesel (90–94%) synthesis, as well as short reaction times, high products quality, easy catalyst recovery via magnetic field, and great reusability, which makes SILLP **5** very attractive for industrial use [102–105]. In other work, a phosphonium-SO_3H based IL was anchored to the magnetic silica nanomaterial, creating the Brønsted-type SILLP **6** (Figure 14) catalyst. Its activity was tested in the acetalization of aldehyde or ketone with ethylene glycol, which resulted in high product yields of 94–97% with various substrates, and the possibility of SILLP catalyst recycling five times without significant loss of activity [106]. Interestingly, the dicationic IL grafted to magnetic nanoparticles (**7**, Figure 14) found application in the synthesis of pyrimido[4,5-b]quinolines (Scheme 3, Figure 15). The novel SILLP **7** hydrogensulfate anion provides one acidic hydrogen and one weakly basic (negative oxygen) site, and was successfully used in the synthesis that requires an acidic and a basic catalyst. This magnetic catalytic system performed well, with yields of 81–96%, short reaction times, and recovery for four reaction cycles, with only a slight decrease in activity [107].

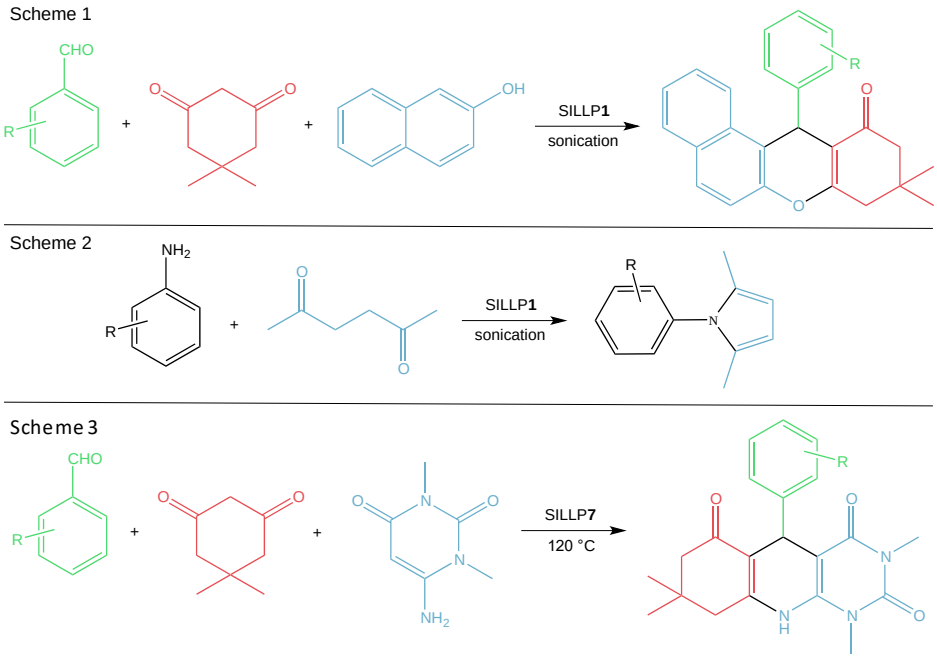

Figure 15. Silica-ferrite hybrid-based SILLP as the catalyst in synthesis of benzoxanthenes (Scheme 1), pyrroles (Scheme 2), pyrimido[4,5-b]quinolines (Scheme 3).

A follow-up report described *N*-(propyl-triethoxysilane)-2-pyrrolidinium hydrogensulfate immobilized on Fe_3O_4 silica nanoparticles (**8**, Figure 14) as an efficient catalyst for the one-pot diazotization–halogenation of the aromatic amines. Utilization of SILLP **8** as a green catalyst turned out to provide satisfying yields and short reaction times [108]. Silica coated cobalt ferrite nanoparticles were modified with a 3-(4-sulfobutyl)-1-(3-trimethoxysilylmerkaptopropyl)imidazolium triflate IL, and were used in the esterification of oleic acid with straight-chain alcohols. higher SH-group loading on the silica surface resulted in a decreasing pore diameter and surface area. On the other hand, however, less IL moieties could be immobilized on the surface of the nanomaterial. Increasing the alkyl chain in the alcohol caused mass transfer resistance, which resulted in a decreased conversion. This kind of SILLP could find application in shape-selective catalysis [109]. Other work described a sulfo-tetrazolium hydrogen-

sulfate based IL anchored to magnetic nanoparticles. Its activity was tested in the one-pot synthesis of pyrimidine derivatives under mild conditions. The catalyst provided 80–95% yields, an easy separation method using magnetic forces, and could be recycled for six reaction cycles without any activity loss. Moreover, in comparison with another catalyst described in literature, this SILLP is an outstanding green alternative [110]. 2-hydroxyethylammonium sulphonate IL was immobilized via the anion on a magnetic silica-based material. The catalyst possesses basic sites such as hydroxyl groups and acidic sites such as ammonium moieties, and was therefore successfully used in the one-pot three-component synthesis of 2-amino-3,5-dicarbonitrile-6-thio-pyridines. Satisfying yields of 81–91% of various pyridines were achieved, as well as a reusability of five reaction cycles in the reaction between benzaldehyde, malononitrile, and thiophenol characterized this catalyst as very efficient [111]. More recent work was also carried out on a 1,4-diazabicyclo[2.2.2]octane-based basic IL immobilized on silica coated ferrite nanomolecules for a Knoevenagel condensation. The SILLP showed excellent catalytic performance, high yields, short reaction times, and could be reused for eight times. Specific activity could be explained with synergistic action of the tertiary amine, IL, and nanoparticles [112]. Further reports concern the applications of Fe_3O_4-silica nanoparticles modified with 1-methyl-3-(triethoxysilylpropyl)imidazolium chloride. SILLP **9** (Figure 14) catalytic activity was investigated in the synthesis of 1,3-thiazolidin-4-ones [113], indole-substituted pyrido[2,3-d]pyrimidines [114], 3,4-dihydropyrimidin-2(1H)-ones/thiones [116], cycloaddition of CO_2 to epoxides [115], and N-formylation of amines [117]. As shown in Table 3, high reaction yields, easy catalyst recovery, and the possibility of recycling make SILLP **9** not only versatile, but also very efficient. The same catalyst type, but with a triazinium cation, was tested for the synthesis of 4H-dihydropyrano[3,2-b]pyran-3-carbonitrile derivatives. High yields of 85–98% were achieved for various benzaldehydes (Table 3), and newly synthesized compounds indicate potential antioxidant and antifungal properties. Furthermore, this catalyst could be reused four times without any loss of activity [118]. Next, a 3-((3-(trisilyloxy)propyl)propionamide)-1-methylimidazolium chloride IL anchored to silica magnetic nanoparticles was used in the acetylation of alcohols with acetic anhydride under mild conditions. Good yields (93–96%), simple separation by magnetic decantation, and reusability for nine cycles without activity loss were reported for this SILLP [119]. The SILLP magnetic nanoparticles formed from imidazolium-aniline based IL were applied in the Mannich reaction between arylaldehydes, anilines, and cyclohexanone under ultrasound irradiation. The catalyst provided high yields of the main product, high diastereoselectivity (anti:syn), short reaction times, and could be easy reused six times without activity loss, which makes it competitive to previous achievements in this field [120]. In another report, a basic 1-triethylamineimidazolium based IL immobilized on silica coated magnetic nanoparticles was tested for Knoevenagel condensation between various aldehydes and malonitrile. As shown in Table 3, high yields and five reaction cycles with this magnetic SILLP were achieved. In comparison, the IL was immobilized on polystyrene-divinylbenzene resin, but the magnetic silica-based SILLP showed better activity than the polymeric one, presumably due to a more basic character of the silica-ferrite matrix [121]. Studies on immobilized triethyltryptophanium iodide IL on titanomagnetite silica matrix as the catalyst in the synthesis of 6-substituted quinolinedialkyl-2,4-dicarboxylates showed that the library of compounds achieved good yields, the possibility of convenient catalyst recovery, and reusability for three reaction runs were reached in the presence of the SILLP [122].

3.4. SILLP as Matrix for Metals, Organocatalysts, and Enzymes

The catalytic features of the developed SILLPs applications as a matrix or co-catalyst are known, and there are many reports of the use of an SILLP as a matrix/co-catalyst for metal particles, organocatalysts, or enzymes. In Table 4, only examples of silica-based SILLP applications as a matrix are shown due to existing accurate reviews on this topic [34,39–41,123].

Table 4. Examples of silica-based SILLP as a matrix or co-catalyst in organic catalysis.

Catalyst	Reaction Type	Reaction Conditions	Reaction Parameters	Lit.
SiO_2/Rh [tespbim][BF_4] [a]/(tppti) [b]	Hydroformylation of 1-hexene	CO/H_2(1:1; *v*/*v*), Rh/P (1:10, n/n), 100 °C, 5 h	α = 33%, S = 2.4 (n/i-heptanal ratio), TOF = 65 min^{-1}	[124–126]
SiO_2/Ni [tesp(p-SO_3H)im][OTf] [c]	Hydrogenation of n-valeraldehyde	4.5 g cat., n-valeraldehyde 30 mL, P_{H2} = 3 MPa, 200 °C 8 h	α = 100%, S = 98.6%	[127]
SiO_2/PbS [tespmim][Cl] [d]	Dehydrogenation of formic acid	0.0007 g cat., HCOOH/HCOONa 9.00 mmol, 8:1; n/n, H_2O 2.5 mL, 40 °C, 750 rpm	Y = 97% (formic acid decomposition), S_{H2} = 78%, TOF = 604 h^{-1}	[128]
SiO_2/Pd [bvim][Br] [e]	Suzuki coupling	1% mol. cat. phenylboronic acid:aryl halide (1.1:1; n/n), H_2O/EtOH (1.2 mL; 1:1; *v*/*v*), K_2CO_3 (0.6 mol), 50 °C, 19 h	Yields for aryl bromides with R-groups: 4-CHO 81%, 4-OMe 89%, 3-OMe 85%, 4-NO_2 80%, 2-CHO 95%, 4-$COCH_3$ 88%, 3-$COCH_3$ 70%, 4-COOH 88%, 2-CH_3 86%, 2-CN 88%, 3,5-$(CF_3)_2$ 89%, H 78%, 1-naphthyl 85%)	[129]
SiO_2/POSS [f]/Pd [tesppim][Cl] [g]/[tespmim][Cl]	Suzuki coupling	0.07% mol. cat. phenylboronic acid:aryl halide (1.1:1; n/n), H_2O/EtOH (1.2 mL; 1:1; *v*/*v*), K_2CO_3 (0.6 mol), 50 °C, 19 h	Yields and TOF for aryl bromides with R-groups: 4-CHO 99%, 1429 h^{-1};4-OMe 95%, 1327 h^{-1}; 3-OMe 75%, 1071 h^{-1}; 4-NO_2 99%, 1429 h^{-1}; 4-$COCH_3$ 99%, 1429 h^{-1}; 3-$COCH_3$ 99%,1429 h^{-1}; 3-CH_3 99%, 1414 h^{-1}; 4-CH_3 93%, 1329 h^{-1}; 4-CN 99%, 1429 h^{-1}	[130]
SiO_2/POSS/Pd [tesppim][Cl]/[tespmim][Cl]	Heck reaction	0.07% mol. cat. aryl halide, 0.5 mmol, methyl acrylate 0.75 mmol, triethylamine 1 mmol, DMF 1 mL, 120 °C, 3 h	Yields and TOF for aryl iodides with R-groups: H >99%, 476 h^{-1}; 4-CH_3 >99%, 476 h^{-1}; 4-$COCH_3$ 99%, 471 h^{-1}; 4-OCH_3 99%, 471 h^{-1}; 3-OCH_3 99%, 471 h^{-1}; 4-NO_2 >99%, 476 h^{-1}; 2-C_4H_3S 91%, 433 h^{-1}; 4-CHO >99%, 286 h^{-1}	[130]
SiO_2/Pd [bvim][Br]	Suzuki coupling	0.1% mol. cat. phenylboronic acid:aryl halide (45.2:40; n/n mmol), 0.33 M EtOH (121.2 mL), K_2CO_3 (48 mmol), 50 °C, 1.5 mLmin^{-1}, 36 h	Yields for different aryl bromides (H 96%, CH_3 96%, CHO 98%) TON = 3800	[131]
SiO_2/Proline [bvim][NTf_2] [h]	Asymmetric aldol reaction	5% mol cat., aldehyde 1 mmol, cyclohexanone 5 mmol, 1.2 mmol H_2O, rt, 2.5 h	Yields and enantiomeric excess (ee) for aldehydes: 4-NO_2Ph Y = 99%, ee = 98%; 4-ClPh Y = 92%, ee = 99%; 4-BrPh Y = 95%, ee = 97%, 4-CNPh Y = 99%, ee = 92%	[132]
SiO_2/CALB [i] [tespmim][BF_4] [j]	Diacylglycerol production	5% wt. cat., corn oil 4.4 g, glycerol 0.23 g, tert-pentanol 17 mL, 50 °C, 12 h	α = 70.94%, 5 cycles	[133]
SiO_2/PPL [k] [tmspmim][BF_4] [l]	Triacetin hydrolysis	6.83 g of glyceryl triacetate, pH = 7, 45 °C, 10 min	5 cycles	[134]
SiO_2·Fe_3O_4/CRL [m] [tespmim][Cl]	Production of trans-free plastic fats	Palm stearin or liquid rice bran oil, 45 °C, 48 h	4 cycles	[135]

[a] 1-butyl-3-(triethoxysilylpropyl)imidazolium tetrafluoroborate, [b] tri(m-sulfonyl)triphenyl phosphine tris(1-butyl-3-methyl-imidazolium) salt as a ligand, [c] 3-(3-sulfopropyl)-1-(3-propyltriethoxysilane)imidazolium triflate, [d] 1-methyl-3-(triethoxysilylpropyl)imidazolium chloride, [e] 1,4-bis(3-vinylimidazolium-1-yl) bromide, [f] polyhedral oligomeric silsesquioxanes, [g] 1propyl-3-(triethoxysilylpropyl)imidazolium chloride, [h] 1,4-bis(3-vinylimidazolium-1-yl) bis(trifluoromethane)sulfonimide, [i] *Candida antarctica* lipase B, [j] 1-methyl-3-(triethoxysilylpropyl)imidazolium tetrafluoroborate, [k] *Porcine pancreas* lipase, [l] 1-methyl-3-(trimethoxysilylpropyl)imidazolium tetrafluoroborate, [m] *Candida rugosa* lipase.

The hydroformylation reaction is one of the firsts reports on the application of silica based-SILLP as a matrix for metal-based catalysts. Rh particles were introduced to the SILLP with a ligand (to prevent any leaching of Rh) and used for *n*,*i*-heptanal production with TOF = 65 min^{-1}, which, compared to the typical biphasic IL approach (TOF = 23 min^{-1}), was a major accomplishment. The catalyst owes its higher activity to a higher concentration of Rh particles on the surface, as well as a larger surface area. Further studies on this topic included physical adsorption of ILs on solid supports (SILP) as Rh particles matrix and continuous-flow processes, which is more accurately described by haumann in the review [37,124–126]. Next, research shows a novel bifunctional Ni-IL/SiO_2 in 2-propylheptanol synthesis through a one-pot, self-condensation and hydrogenation from *n*-valeraldehyde. Ils possess a Brønsted -SO_3H group and act like both a matrix and a co-catalyst. With the Ni-SILLP catalytic system, 100% conversion, 75.4% selectivity of the main product, and 98.6% production of 2-propylheptanol and pentanol were achieved [127]. Other reports present SILLP as effective matrices for PbS nanoparticles. A high surface area and IL presence enabled high loading of PdS molecules without aggregation. Additionally, synergistic effects between metal-based particles and Ils provided great catalytic activity in the dehydrogenation of formic acid, with 100% degradation of the acid, 78% selectivity to hydrogen, and TOF = 604 h^{-1} [128]. Further studies present immobilization and stabilization of Pd particles via SBA-15-based SILLP. New versatile and efficient catalytic systems were tested in the Suzuki coupling and heck reactions. As shown in Table 4, the library of compounds was synthesized with high yields, and a catalyst could be recycled several times. Applications of SBA-15 with hexagonal pores as a matrix, which behaved as nanoreactors, assured excellent catalytic activity [129–131]. Moreover, transition from a batch to a continuous process provided conversion of 27 g of substrate to the main product using only 42 mg of the Pd-SILLP catalyst as well as reducing waste, which significantly reduced the E-factor [131]. The next report shows a silica-based SILLP as a carrier for the *cis*-ion-tagged proline. Proline moieties dissolved in covalently immobilized multilayered IL film performed with excellent activity in an asymmetric aldol reaction. The catalyst provided high yields and enantioselectivity of the main products (Table 4) and could also be recycled up to 15 times [132]. SILLPs can also be used for enzyme immobilization. Moreover, many reports confirmed an IL stabilizing effect on three-dimensional structures of enzymes, increasing protein activity. For example, the catalytic activity of lipase from *Candida antarctica* (CALB) adsorbed on an imidazolium silica-based SILLP was examined in corn oil glycerolysis to diacylglycerol production. The presence of the IL resulted in increasing the catalytic activity from 1855 to 5044 U/g and selectivity from 3.72 to 11.99 (ratio of diacylglycerols/monoacylglycerols). Additionally, the biocatalyst could be recycled for five reaction cycles, and even retained its activity at 50 °C [133]. Another lipase from *Porcine pancreas* immobilized on the same SILLP matrix was used in triacetin hydrolysis. Immobilized enzyme exhibited extremely high thermal stability, where even at 65 °C activity loss did not occur [134]. Lipase from *Candida rugosa* (CRL) was adsorbed on magnetic silica nanoparticles and used in the production of trans-free plastic fats. CRL-SILLP bionanomaterial catalyzed interesterifications of solid palm stearin and liquid rice bran oil for product possesses desirable physicochemical properties. In this case, convenient separation of the biocatalyst enabled its recycling up to four times [135].

4. Conclusions

In summary, achievements in the use of silica-based supported ionic liquid-like phases in heterogeneous organic catalysis were presented. Many Lewis and Brønsted acidic ionic liquids were found to be extremely active as heterogeneous catalysts. For the synthesis of Lewis type silica-based SILLP, chloroaluminate (III), chlorogallate (III), chloroferrate (III), chloroindate (III), chlorostannate (II), chlorozincate (II) anions or hydroxysulfonyl/chlorosulfonyl groups in the cation alkyl chain were used. In case of the forming of Brønsted-type silica-based SILLP, hydrogensulfate, dihydrogenphosphate, dihydrogenphosphotungstate anions, and/or sulfoalkyl group on the cation were found.

Replacement of the halogen anions should be further investigated to prevent hydrolysis and the formation of hazardous acids as hCl. This would result in the reduction of costs, toxic waste, specific equipment, and apparatus corrosion. The anion of the ionic liquid has a crucial influence on the SILLP properties—the synthesized catalyst could be more or less acidic depending on the specific requirements, therefore application of SILLP as a catalyst is very convenient. For the SILLP synthesis, various cations such as imidazolium, alkylammonium, phosphonium, pyrrolidinium, tetrazolium, diammonium, triazinium, and tryptophanium were used, though their selection depended mainly on the substrate or nature of the reaction. It was mainly acidic ILs that were anchored to the silica surface that exhibited great catalytic activity and reusability, and from this the heterogeneous catalyst recovery was very easy. By cross-referencing the presence of the homogeneous and heterogeneous catalysis in the ionic liquids, it can be concluded that IL immobilization increases its catalytic activity due to enhanced mass transfer and availability of active sites. The selection of the silica material also brings many options in terms of size, shape, and density of pores, and hydroxyl groups on the surface. Silica materials such as SBA-15 and MCM-41, with their well-ordered, regular, and hexagonal array of pores, form microreactors that enhance the process efficiency. Obviously, the most important feature is the simplicity of the chemical modification of the surface via trimethoxysilyl/triethoxysilyl groups present as IL precursors, e.g., (3-(chloropropyl)triethoxysilane, 3-(chloropropyl)trimethoxysilane, 3-mercaptopropyltrimethoxysilane, or (3-aminopropyl)-trimethoxysilane). Moreover, the silica can be doped with ferrate nanoparticles, giving the surface magnetic properties. These magnetic-silica nano-catalysts can be removed and recycled by applying external magnetic forces, which is a very convenient approach. Additionally, the magnetic separation also increases the product purity and quality. It should be noted, however, that few examples of the continuous processes with silica-based SILLP have been developed. Flow catalysis offers many advantages compared to batch processes, for example: waste reduction, optimization of pure product synthesis and isolation, reduction of the amount of solvent required, and optimization of the catalyst recovery and recycling. Continuous catalysis simply means an efficient process, as well as green and environmentally friendly production, which is very attractive to the chemical industry. Silica-based SILLPs are versatile, stable catalysts, easy to synthesize, and reusable, with big potential for continuous-flow processes. SILLPs are also potential candidates for the development of sustainable and green chemical processes.

Author Contributions: Conceptualization, A.C. and A.W.; literature survey A.W.; writing—original draft preparation, A.W.; writing—review and editing, A.C. and A.W.; visualization, A.W.; supervision, A.C. All authors have read and agreed to the published version of the manuscript.

Funding: This work was financed by the National Science Centre, Poland (grant no. UMO-2020/39/B/ST8/00693) and Silesian University of Technology (Poland), grant No. 04/050/BKM22/0151.

Institutional Review Board Statement: Not applicable.

Informed Consent Statement: Not applicable.

Data Availability Statement: Data sharing is not applicable for this article.

Conflicts of Interest: The authors declare no conflict of interest. The funders had no role in the design of the study; in the writing of the manuscript, or in the decision to publish.

References

1. Thore, S.; Tarverdyan, R. *Measuring Sustainable Development Goals Performance*; Elsevier: Amsterdam, The Netherlands, 2021.
2. Scheldon, R.A. The E factor 25 years on: The rise of green chemistry and sustainability. *Green Chem.* **2017**, *19*, 18–43. [CrossRef]
3. Ratti, R. Industrial applications of green chemistry: Status, Challenges and Prospects. *SN Appl. Sci.* **2020**, *2*, 263. [CrossRef]
4. Sheldon, R.A.; Arends, I.; Hanefeld, U. *Green Chemistry and Catalysis*; Wiley-VCH Verlag GmbH: Berlin, Germany, 2020.
5. Scheldon, R.A.; Woodley, J.M. Role of biocatalysis in sustainable chemistry. *Chem. Rev.* **2018**, *118*, 801–838. [CrossRef]
6. De los Ríos, A.P.; Irabien, A.; Hollmann, F.; Fernández, F.J.H. Ionic Liquids: Green Solvents for Chemical Processing. *J. Chem.* **2013**, *2013*, 402172. [CrossRef]

7. Greer, A.J.; Jacquemin, J.; Hardacre, C. Industrial applications of ionic liquids. *Molecules* **2020**, *25*, 5207. [CrossRef]
8. Padvi, S.A.; Dalal, D.S. Task-Specific Ionic Liquids as a Green Catalysts and Solvents for Organic Synthesis. *Curr. Green Chem.* **2020**, *7*, 105–119. [CrossRef]
9. Chrobok, A. The Baeyer–Villiger oxidation of ketones with Oxone® in the presence of ionic liquids as solvents. *Tetrahedron* **2010**, *66*, 6212–6216. [CrossRef]
10. Domínguez de María, P. *Ionic Liquids in Biotransformations and Organocatalysis: Solvents and Beyond*; John Wiley & Sons, Inc.: Hoboken, NJ, USA, 2012; pp. 1–435.
11. Drożdż, A.; Erfurt, K.; Bielas, R.; Chrobok, A. Chemo-enzymatic Baeyer–Villiger oxidation in the presence of Candida antarctica lipase B and ionic liquids. *New J. Chem.* **2015**, *39*, 1315–1321. [CrossRef]
12. Karuppasamy, K.; Theerthagiri, J.; Vikraman, D.; Yim, C.-J.; Hussain, S.; Sharma, R.; Kim, H.S. Ionic Liquid-Based Electrolytes for Energy Storage Devices: A Brief Review on Their Limits and Applications. *Polymers* **2020**, *12*, 918. [CrossRef]
13. Passos, H.; Freire, M.G.; Coutinho, J.A.P. Ionic liquid solutions as extractive solvents for value-added compounds from biomass. *Green Chem.* **2014**, *16*, 4786–4815. [CrossRef]
14. Bajkacz, S.; Rusin, K.; Wolny, A.; Adamek, J.; Erfurt, K.; Chrobok, A. Highly efficient extraction procedures based on natural deep eutectic solvents or ionic liquids for determination of 20-Hydroxyecdysone in Spinach. *Molecules* **2020**, *25*, 4736. [CrossRef] [PubMed]
15. Shukla, S.K.; Khokarale, S.G.; Bui, T.Q.; Mikkola, J.-P.T. Ionic Liquids: Potential Materials for Carbon Dioxide Capture and Utilization. *Front. Mater.* **2019**, *6*, 42. [CrossRef]
16. Vekariya, R.L. A review of ionic liquids: Applications towards catalytic organic transformations. *J. Mol. Liq.* **2017**, *227*, 44–60. [CrossRef]
17. Welton, T. Ionic liquids in catalysis. *Coord. Chem. Rev.* **2004**, *248*, 2459–2477. [CrossRef]
18. Brown, L.C.; Hogg, J.M.; Swadźba-Kwaśny, M. Lewis Acidic Ionic Liquids. *Top Curr. Chem.* **2017**, *375*, 78. [CrossRef]
19. Greaves, T.L.; Drummond, C.J. Protic Ionic Liquids: Properties and Applications. *Chem. Rev.* **2008**, *108*, 206–237. [CrossRef] [PubMed]
20. Amarasekara, A.S. Acidic Ionic Liquids. *Chem. Rev.* **2016**, *116*, 6133–6183. [CrossRef]
21. Jasiak, K.; Siewniak, A.; Kopczyńska, K.; Chrobok, A.; Baj, S. Hydrogensulphate ionic liquids as an efficient catalyst for the synthesis of cyclic carbonates from carbon dioxide and epoxides. *J. Chem. Technol. Biotechnol.* **2016**, *91*, 2827–2833. [CrossRef]
22. Shen, L.; Yin, H.; Wang, A.; Lu, X.; Zhang, C.; Chen, F.; Chen, H. Liquid phase catalytic dehydration of glycerol to acrolein over Brønsted acidic ionic liquid catalysts. *J. Ind. Eng. Chem.* **2014**, *20*, 759–766. [CrossRef]
23. Zhang, L.; He, L.; Hong, C.-B.; Qin, S.; Tao, G.-H. Brønsted acidity of bio-protic ionic liquids: The acidic scale of [AA]X amino acid ionic liquids. *Green Chem.* **2015**, *17*, 5154–5163. [CrossRef]
24. Kore, R.; Kumar, T.J.D.; Srivastava, R. Hydration of alkynes using Brönsted acidic ionic liquids in the absence of Nobel metal catalyst/H_2SO_4. *J. Mol. Cat. A Chem.* **2012**, *360*, 61–70. [CrossRef]
25. Fang, D.; Yang, J.; Jiao, C. Dicationic Ionic Liquids as Environmentally Benign Catalysts for Biodiesel Synthesis. *ACS Catal.* **2010**, *1*, 42–47. [CrossRef]
26. Latos, P.; Culkin, A.; Barteczko, N.; Boncel, S.; Jurczyk, S.; Brown, L.C.; Nockemann, P.; Chrobok, A.; Swadźba-Kwaśny, M. Water-Tolerant Trifloaluminate Ionic Liquids: New and Unique Lewis Acidic Catalysts for the Synthesis of Chromane. *Front. Chem.* **2018**, *6*, 535. [CrossRef]
27. Markiton, M.; Chrobok, A.; Matuszek, K.; Seddon, K.R.; Swadźba-Kwaśny, M. Exceptional activity of gallium(iii) chloride and chlorogallate(iii) ionic liquids for Baeyer–Villiger oxidation. *RSC Adv.* **2016**, *6*, 30460–30467. [CrossRef]
28. Matuszek, K.; Coffie, S.; Chrobok, A.; Swadźba-Kwaśny, M. Borenium ionic liquids as catalysts for Diels–Alder reaction: Tuneable Lewis superacids for catalytic applications. *Catal. Sci. Technol.* **2017**, *7*, 1045–1049. [CrossRef]
29. Valkenberg, M.H.; deCastro, C.; Hölderich, W.F. Immobilisation of chloroaluminate ionic liquids on silica materials. *Top. Catal.* **2000**, *14*, 139–144. [CrossRef]
30. Mehnert, C.P. Supported Ionic Liquid Catalysis. *Eur. J. Chem.* **2005**, *11*, 50–56. [CrossRef]
31. Burguete, M.I.; García-Verdugo, E.; Karbass, N.; Luis, S.V.; Sans, V.; Sokolova, M. Development of efficient processes under flow conditions based on catalysts immobilized onto monolithic supported ionic liquid-like phases. *Pure Appl. Chem.* **2009**, *81*, 1991–2000. [CrossRef]
32. Skoda-Földes, R. The Use of Supported Acidic Ionic Liquids in Organic Synthesis. *Molecules* **2014**, *19*, 8840–8884. [CrossRef]
33. Schwieger, W.; Selvam, T.; Klumpp, M.; Hartmann, M. Porous Inorganic Materials as Potential Supports for Ionic Liquids. In *Supported Ionic Liquids: Fundamental and Applications*, 1st ed.; Fehrmann, R., Riisager, A., Haumann, M., Eds.; Wiley-VCH Verlag GmbH: Berlin, Germany, 2014; pp. 37–74.
34. Giacalone, F.; Gruttadauria, M. Covalently Supported Ionic Liquid Phases: An Advanced Class of Recyclable Catalytic Systems. *ChemCatChem* **2016**, *8*, 664–684. [CrossRef]
35. Vafaeezadeh, M.; Alinezhad, H. Brønsted acidic ionic liquids: Green catalysts for essential organic reactions. *J. Mol. Liq.* **2016**, *218*, 95–105. [CrossRef]
36. Migowski, P.; Luska, K.L.; Leitner, W. Nanoparticles on Supported Ionic Liquid Phases - Opportunities for Application in Catalysis. Nanocatalysis in Ionic Liquids. In *Nanocatalysis in Ionic Liquids*, 1st ed.; Martin, H., Prechtl, G., Eds.; Wiley-VCH Verlag GmbH: Berlin, Germany, 2017; pp. 249–273.

37. Marinkovic, J.M.; Riisager, A.; Franke, R.; Wasserscheid, P.; Haumann, M. Fifteen Years of Supported Ionic Liquid Phase-Catalyzed Hydroformylation: Material and Process Developments. *Ind. Eng. Chem. Res.* **2019**, *58*, 2409–2420. [CrossRef]
38. Pedro, A.Q.; Coutinho, J.A.P.; Freire, M.G. Immobilization of Ionic Liquids, Types of Materials, and Applications. In *Encyclopedia of Ionic Liquids*; Zhang, S., Ed.; Springer Nature: Singapore, 2019; pp. 1–12.
39. Bartlewicz, O.; Dąbek, I.; Szymańska, A.; Maciejewski, H. Heterogeneous Catalysis with the Participation of Ionic Liquids. *Catalysts* **2020**, *10*, 1227. [CrossRef]
40. Garcia-Verdugo, E.; Lozano, P.; Luis, S.V. Biocatalytic Processes Based on Supported Ionic Liquids. In *Supported Ionic Liquids: Fundamental and Applications*, 1st ed.; Fehrmann, R., Riisager, A., Haumann, M., Eds.; Wiley-VCH Verlag GmbH: Berlin, Germany, 2014; pp. 351–368.
41. Wolny, A.; Chrobok, A. Ionic Liquids for Development of Heterogeneous Catalysts Based on Nanomaterials for Biocatalysis. *Nanomaterials* **2021**, *11*, 2030. [CrossRef] [PubMed]
42. Stöber, W.; Fink, A.; Bohn, E. Controlled growth of monodisperse silica spheres in the micron size range. *J. Colloid Interface Sci.* **1968**, *26*, 62–69. [CrossRef]
43. Donato, K.Z.; Matějka, L.; Mauler, R.S.; Donato, R.K. Recent Applications of Ionic Liquids in the Sol-Gel Process for Polymer–Silica Nanocomposites with Ionic Interfaces. *Colloids Interfaces* **2017**, *1*, 5. [CrossRef]
44. Du, A.; Wang, Z.; Shang, Y.; Sun, X. Interactions Between an Ionic Liquid and Silica, Silica and Silica, and Rubber and Silica and Their Effects on the Properties of Styrene-Butadiene Rubber Composites. *J. Macromol. Sci. Phys.* **2019**, *58*, 99–112. [CrossRef]
45. Wang, Y.-M.; Ulrich, V.; Donnelly, G.F.; Lorenzini, F.; Marr, A.C.; Marr, P.C. A Recyclable Acidic Ionic Liquid Gel Catalyst for Dehydration: Comparison with an Analogous SILP Catalyst. *ACS Sustain. Chem. Eng.* **2015**, *3*, 792–796. [CrossRef]
46. Dhar, A.; Siva Kumar, N.; Khimani, M.; Al-Fatesh, A.S.; Ibrahim, A.A.; Fakeeha, A.H.; Patel, H.; Vekariya, R.L. Silica-immobilized ionic liquid Brønsted acids as Highly effective Heterogeneous catalysts for the isomerization of n-heptane and n-octane. *RSC Adv* **2020**, *10*, 15282. [CrossRef]
47. Riisager, A.; Fehrmann, R.; Haumann, M.; Wasserscheid, P. Supported Ionic Liquid Phase (SILP) Catalysis: An Innovative Concept for Homogeneous Catalysis in Continuous Fixed-Bed Reactors. *Eur. J. Inorg. Chem.* **2006**, *4*, 695–706. [CrossRef]
48. Kukawka, R.; Pawlowska-Zygarowicz, A.; Dzialkowska, J.; Pietrowski, M.; Maciejewski, H.; Bica, K.; Smiglak, M. A highly effective supported ionic liquid phase (SILP) catalysts—Characterization and application to the hydrosilylation reaction. *ACS Sustain. Chem. Eng.* **2019**, *7*, 4699–4706. [CrossRef]
49. Lozano, P.; Diego, T.; de Carrié, D.; Vaultier, M.; Iborra, J.L. Continuous green biocatalytic processes using ionic liquids and supercritical carbon dioxide. *Chem. Commun.* **2002**, *7*, 692–693. [CrossRef] [PubMed]
50. Valkenberg, M.H.; deCastro, C.; Hölderich, W.F. Immobilisation of ionic liquids on solid supports. *Green Chem.* **2001**, *4*, 88–93. [CrossRef]
51. Jyothi, T.M.; Kaliya, M.L.; Herskowitz, M.; Landau, M.V. A comparative study of an MCM-41 anchored quaternary ammonium chloride/SnCl4 catalyst and its silica gel analogue. *Chem. Commun.* **2001**, *11*, 992–993. [CrossRef]
52. Hagiwara, H.; Sekifuji, M.; Hoshi, T.; Qiao, K.; Yokoyama, C. Synthesis of Bis(indolyl)methanes Catalyzed by Acidic Ionic Liquid Immobilized on Silica (ILIS). *Synlett* **2007**, *8*, 1320–1322. [CrossRef]
53. Qiao, K.; Hagiwara, H.; Yokoyama, C. Acidic ionic liquid modified silica gel as novel solid catalysts for esterification and nitration reactions. *J. Mol. Catal. A Chem.* **2006**, *246*, 65–69. [CrossRef]
54. Hagiwara, H.; Sekifuji, M.; Hoshi, T.; Suzuki, T.; Quanxi, B.; Qiao, K.; Yokoyama, C. Sustainable Conjugate Addition of Indoles Catalyzed by Acidic Ionic Liquid Immobilized on Silica. *Synlett* **2008**, *4*, 608–610. [CrossRef]
55. Kumar, P.; Vermeiren, W.; Dath, J.-P.; Hoelderich, W.F. Production of alkylated gasoline using ionic liquids and immobilized ionic liquids. *Appl. Catal. A Gen.* **2006**, *304*, 131–141. [CrossRef]
56. Liu, S.; Shang, J.; Zhang, S.; Yang, B.; Deng, Y. Highly Efficient Trimerization of Isobutene Over Silica Supported Chloroaluminate Ionic Liquid Using C4 Feed. *Catal. Today* **2013**, *200*, 41–48. [CrossRef]
57. Wang, G.; Yu, N.; Peng, L.; Tan, R.; Zhao, H.; Yin, D.; Yin, D. Immobilized Chloroferrate Ionic Liquid: An Efficient and Reusable Catalyst for Synthesis of Diphenylmethane and its Derivatives. *Catal. Lett.* **2008**, *123*, 252–258. [CrossRef]
58. Zhao, H.; Yu, N.; Wang, J.; Zhuang, D.; Ding, Y.; Tan, R.; Yin, D. Preparation and catalytic activity of periodic mesoporous organosilica incorporating Lewis acidic chloroindate(III) ionic liquid moieties. *Microporous Mesoporous Mater.* **2009**, *122*, 240–246. [CrossRef]
59. Matuszek, K.; Chrobok, A.; Latos, P.; Markiton, M.; Szymańska, K.; Jarzębski, A.; Swadźba-Kwaśny, M. Silica-supported chlorometallate(iii) ionic liquids as recyclable catalysts for Diels–Alder reaction under solventless conditions. *Catal. Sci. Technol.* **2016**, *6*, 8129–8137. [CrossRef]
60. Siewniak, A.; Forajter, A.; Szymańska, K. Mesoporous Silica-Supported Ionic Liquids as Catalysts for Styrene Carbonate Synthesis from CO_2. *Catalysts* **2020**, *10*, 1363. [CrossRef]
61. Yao, J.; Sheng, M.; Bai, S.; Su, H.; Shang, H.; Deng, H.; Sun, J. Ionic Liquids Grafted Mesoporous Silica for Chemical Fixation of CO_2 to Cyclic Carbonate: Morphology Effect. *Catal. Lett.* **2021**, *152*, 781–790. [CrossRef]
62. Zhen, B.; Jiao, Q.; Wu, Q.; Li, H. Catalytic performance of acidic ionic liquid-functionalized silica in biodiesel production. *J. Energy Chem.* **2014**, *23*, 97–104. [CrossRef]
63. Wiredu, B.; Amarasekara, A.S. Synthesis of a silica-immobilized Brönsted acidic ionic liquid catalyst and Hydrolysis of cellulose in water under mild conditions. *Catal. Commun.* **2014**, *48*, 41–44. [CrossRef]

64. Bao, Q.; Qiao, K.; Tomida, D.; Yokoyama, C. Preparation of 5-hydroymethylfurfural by dehydration of fructose in the presence of acidic ionic liquid. *Catal. Commun.* **2008**, *9*, 1383–1388. [CrossRef]
65. Elhamifar, D.; Nasr-Esfahani, M.; Karimi, B.; Moshkelgosha, R.; Shábani, A. Ionic Liquid and Sulfonic Acid Based Bifunctional Periodic Mesoporous Organosilica (BPMO-IL-SO_3H) as a Highly Efficient and Reusable Nanocatalyst for the Biginelli Reaction. *ChemCatChem* **2014**, *6*, 2593–2599. [CrossRef]
66. Elhamifar, D.; Karimi, B.; Moradi, A.; Rastegar, J. Synthesis of Sulfonic Acid Containing Ionic-Liquid-Based Periodic Mesoporous Organosilica and Study of Its Catalytic Performance in the Esterification of Carboxylic Acids. *ChemPlusChem* **2014**, *79*, 1147–1152. [CrossRef]
67. Wang, W.; Wang, D.; Yang, Q.; An, H.; Zhao, X.; Wang, Y. Silica-immobilized acid ionic liquid: An efficient catalyst for pentanal self-condensation. *J. Chem. Technol. Biotechnol.* **2020**, *95*, 2964–2972. [CrossRef]
68. Kotadia, D.A.; Soni, S.S. Sulfonic acid functionalized solid acid: An alternative eco-friendly approach for transesterification of non-edible oils with high free fatty acids. *Monatsh. Chem.* **2013**, *144*, 1735–1741. [CrossRef]
69. Kotadia, D.A.; Soni, S.S. Silica gel supported –SO_3H functionalised benzimidazolium based ionic liquid as a mild and effective catalyst for rapid synthesis of 1-amidoalkyl naphthols. *J. Mol. Catal. A Chem.* **2012**, *353–354*, 44–49. [CrossRef]
70. Chrobok, A.; Baj, S.; Pudło, W.; Jarzębski, A. Supported hydrogensulfate ionic liquid catalysis in Baeyer–Villiger reaction. *Appl. Catal. A Gen.* **2009**, *366*, 22–28. [CrossRef]
71. Zhang, J.; Wan, H.; Guan, G. Preparation and Catalytic Performance of Silica Gel Immobilized Acidic Ionic Liquid Catalyst. *Reaction. Eng. Technol.* **2008**, *24*, 503–508.
72. Seddighi, M.; Shirini, F.; Mamaghani, M. Brønsted acidic ionic liquid supported on rice husk ash (RHA-[pmim]HSO_4): A highly efficient and reusable catalyst for the synthesis of 1-(benzothiazolylamino)phenylmethyl-2-naphthols. *Comptes Rendus Chim.* **2015**, *18*, 573–580. [CrossRef]
73. Shirini, F.; Seddighi, M.; Mamaghani, M. Brönsted acidic ionic liquid supported on rice husk ash (RHA–[pmim]HSO_4): A highly efficient and reusable catalyst for the formylation of amines and alcohols. *RSC Adv.* **2014**, *4*, 50631–50638. [CrossRef]
74. Rostamnia, S.; Hassankhani, A.; Hossieni, H.G.; Gholipour, B.; Xin, H. Brønsted acidic Hydrogensulfate ionic liquid immobilized SBA-15: [MPIm][HSO_4]@SBA-15 as an environmentally friendly, metal- and halogen-free recyclable catalyst for Knoevenagel–Michael-cyclization processes. *J. Mol. Catal. A Chem.* **2014**, *395*, 463–469. [CrossRef]
75. Niknam, K.; Piran, A. Silica-Grafted Ionic Liquids as Recyclable Catalysts for the Synthesis of 3,4-Dihydropyrano[c]chromenes and Pyra-no [2,3-c]pyrazoles. *Green Sustain. Chem.* **2013**, *3*, 31420. [CrossRef]
76. Damavandi, S. Immobilized Ionic Liquid-Catalyzed Synthesis of Pyrano[3,2-b]indole Derivatives. *E-J. Chem.* **2012**, *9*, 1490–1493. [CrossRef]
77. Damavandi, S.; Sandaroos, R. Novel Synthetic Route to Pyrano[2,3-b]pyrrole Derivatives. *Syn. React. Inorg. Metal Org. Nano Metal Chem.* **2012**, *42*, 621–627. [CrossRef]
78. Eshghi, H.; Zohuri, G.H.; Sandaroos, R.; Damavandi, S. Synthesis of novel benzo[f]chromene compounds catalyzed by ionic liquid. *Heterocycl. Commun.* **2012**, *18*, 67–70. [CrossRef]
79. Damavandi, S.; Sandaroos, R. Novel Multicomponent Synthesis of 2,9-Dihydro-9-methyl-2-oxo-4-aryl-1H-pyrido [2, 3-b] indole-3-carbonitrile Compounds. *J. Chem. Sci.* **2013**, *125*, 95–100. [CrossRef]
80. Goldani, M.T.; Sandaroos, R.; Damavandi, S. Efficient Polymeric Catalyst for One-pot Synthesis of Acenaphtho [1, 2-b] Pyrroles. *Res. Chem. Intermed.* **2014**, *40*, 139–147. [CrossRef]
81. Sandaroos, R.; Damavandi, S.; Salimi, M. Facile one-pot synthesis of 5-amino-7-aryl-6-cyano-4H-pyrano[3,2-b]pyrroles using supported hydrogen sulfate ionic liquid. *Monatsh. Chem.* **2012**, *143*, 1655–1661. [CrossRef]
82. Xiong, J.; Zhu, W.; Ding, W.; Yang, L.; Chao, Y.; Li, H. Phosphotungstic Acid Immobilized on Ionic Liquid-Modified SBA-15: Efficient hydrophobic heterogeneous Catalyst for Oxidative Desulfurization in Fuel. *Ind. Eng. Chem. Res.* **2014**, *53*, 19895–19904. [CrossRef]
83. Wan, H.; Zhang, J.; Guan, G. Preparation of Supported Acidic Ionic Liquid by Covalent Bond Grafting and its Catalysis in Synthesis of n-Butyl Acetate. *Shiyou Huagong/Petrochem. Technol.* **2009**, *38*, 134–138.
84. Zhang, Q.; Luo, J.; Wei, Y. A silica gel supported dual acidic ionic liquid: An efficient and recyclable Heterogeneous catalyst for the one-pot synthesis of amidoalkyl naphthols. *Green Chem.* **2010**, *12*, 2246–2254. [CrossRef]
85. Vafaeezadeh, M.; Dizicheh, Z.B.; Hashemi, M.M. Mesoporous silica-functionalized dual Brønsted acidic ionic liquid as an efficient catalyst for thioacetalization of carbonyl compounds in water. *Catal. Commun.* **2013**, *41*, 96–100. [CrossRef]
86. Miao, J.; Wan, H.; Shao, Y.; Guan, G.; Xu, B. Acetalization of carbonyl compounds catalyzed by acidic ionic liquid immobilized on silica gel. *J. Mol. Catal. A Chem.* **2011**, *348*, 77–82. [CrossRef]
87. Safaei, S.; Mohammadpoor-Baltork, I.; Khosropour, A.R.; Moghadam, M.; Tangestaninejad, S.; Mirkhani, V. Nano-silica supported acidic ionic liquid as an efficient catalyst for the multi-component synthesis of indazolophthalazine-triones and bis-indazolophthalazine-triones. *Catal. Sci. Technol.* **2013**, *3*, 2717. [CrossRef]
88. Wu, Y.; Li, Z.; Xia, C. Silica-Gel-Supported Dual Acidic Ionic Liquids as Efficient Catalysts for the Synthesis of Polyoxymethylene Dimethyl Ethers. *Ind. Eng. Chem. Res.* **2016**, *55*, 1859–1865. [CrossRef]
89. Singh, S.K.; Dhepe, P.L. Novel Synthesis of Immobilized Brønsted- Acidic Ionic Liquid: Application in Lignin Depolymerization. *ChemistrySelect* **2018**, *3*, 5461–5470. [CrossRef]

90. Miao, J.; Wan, H.; Guan, G. Synthesis of immobilized Brønsted acidic ionic liquid on silica gel as heterogeneous catalyst for esterification. *Catal. Commun.* **2011**, *12*, 353–356. [CrossRef]
91. Ma, W.; Wang, W.; Liang, Z.; Hu, S.; Shen, R.; Wu, C. Synthesis of novel acidic ionic liquid immobilized on silica. *Kinet. Catal.* **2014**, *55*, 665–670. [CrossRef]
92. Sofia, L.T.A.; Krishnan, A.; Sankar, M.; Kala Raj, N.K.; Manikandan, P.; Rajamohanan, P.R.; Ajithkumar, T.G. Immobilization of Phosphotungstic Acid (PTA) on Imidazole Functionalized Silica: Evidence for the Nature of PTA Binding by Solid State NMR and Reaction Studies. *J. Phys. Chem. C.* **2009**, *113*, 21114–21122. [CrossRef]
93. Wang, Y.; Zhao, D.; Wang, L.; Wang, X.; Li, L.; Xing, Z.; Ding, H. Immobilized phosphotungstic acid based ionic liquid: Application for heterogeneous esterification of palmitic acid. *Fuel* **2018**, *216*, 364–370. [CrossRef]
94. Li, P.-H.; Li, B.-L.; Hu, H.-C.; Zhao, X.-N.; Zhang, Z.-H. Ionic liquid supported on magnetic nanoparticles as highly efficient and recyclable catalyst for the synthesis of β-keto enol ethers. *Catal. Commun.* **2014**, *46*, 118–122. [CrossRef]
95. Nguyen, H.T.; Thi Le, N.-P.; Nguyen Chau, D.-K.; Tran, P.H. New nano-Fe_3O_4-supported Lewis acidic ionic liquid as a highly effective and recyclable catalyst for the preparation of benzoxanthenes and pyrroles under solvent-free sonication. *RSC Adv.* **2018**, *8*, 35681–35688. [CrossRef]
96. Alinezhad, H.; Tajbakhsh, M.; Ghobadi, N. Ionic liquid immobilized on Fe_3O_4 nanoparticles: A magnetically recyclable heterogeneous catalyst for one-pot three-component synthesis of 1,8-dioxodecahydroacridines. *Res. Chem. Intermed.* **2015**, *41*, 9979–9992. [CrossRef]
97. Nezhad, E.R.; Karimian, S.; Sajjadifar, S. Imidazole functionalized magnetic Fe_3O_4 nanoparticles a highly efficient and reusable Brønsted acid catalyst for the regioselective thiocyanation of aromatic and heteroaromatic compounds at room temperature in water:ethanol. *J. Sci.* **2015**, *26*, 233–240.
98. Nasrollahzadeh, M.; Issaabadi, Z.; Sajadi, S.M. Fe_3O_4@SiO_2 nanoparticle supported ionic liquid for green synthesis of antibacterially active 1-carbamoyl-1-phenylureas in water. *RSC Adv.* **2018**, *8*, 27631–27644. [CrossRef] [PubMed]
99. Pourjavadi, A.; Hosseini, S.H.; Doulabi, M.; Fakoorpoor, S.M.; Seidi, F. Multi-Layer Functionalized Poly(Ionic Liquid) Coated Magnetic Nanoparticles: Highly Recoverable and Magnetically Separable Brønsted Acid Catalyst. *ACS Catal.* **2012**, *2*, 1259–1266. [CrossRef]
100. Gupta, R.; Yadav, M.; Gaur, R.; Arora, G.; Rana, P.; Yadav, P.; Sharma, R.K. Silica-Coated Magnetic-Nanoparticle-Supported DABCO-Derived Acidic Ionic Liquid for the Efficient Synthesis of Bioactive 3,3-Di(indolyl)indolin-2-ones. *ACS Omega.* **2019**, *4*, 21529–21539. [CrossRef] [PubMed]
101. Sadeghzadeh, S.M. A heteropolyacid-based ionic liquid immobilized onto magnetic fibrous nano-silica as robust and recyclable heterogeneous catalysts for the synthesis of tetrahydrodipyrazolopyridines in water. *RSC Adv.* **2016**, *6*, 75973–75980. [CrossRef]
102. Zhang, Q.; Su, H.; Luo, J.; Wei, Y. A Magnetic Nanoparticle Supported Dual Acidic Ionic Liquid: A "Quasi-Homogeneous" Catalyst for the One-pot Synthesis of Benzoxanthenes. *Green Chem.* **2012**, *14*, 201–208. [CrossRef]
103. Khalafi-Nezhad, A.; Mohammadi, S. Magnetic, Acidic, Ionic Liquid-catalyzed One-pot Synthesis of Spirooxindoles. *ACS Comb. Sci.* **2013**, *15*, 512–518. [CrossRef] [PubMed]
104. Wan, H.; Wu, Z.; Chen, W.; Guan, G.; Cai, Y.; Chen, C.; Liu, X. Heterogenization of ionic liquid based on mesoporous material as magnetically recyclable catalyst for biodiesel production. *J. Mol. Catal. A Chem.* **2015**, *398*, 127–132. [CrossRef]
105. Wu, Z.; Li, Z.; Wu, G.; Wang, L.; Lu, S.; Wang, L.; Guan, G. Brønsted Acidic Ionic Liquid Modified Magnetic Nanoparticle: An Efficient and Green Catalyst for Biodiesel Production. *Ind. Eng. Chem. Res.* **2014**, *53*, 3040–3046. [CrossRef]
106. Wang, P.; Kong, A.; Wang, W.; Zhu, H.; Shan, Y. Facile Preparation of Ionic liquid Functionalized Magnetic Nano-solid Acid Catalysts for Acetalization Reaction. *Catal. Lett.* **2010**, *135*, 159–164. [CrossRef]
107. Zare, A.; Barzegar, M. Dicationic ionic liquid grafted with silica-coated nano-Fe_3O_4 as a novel and efficient catalyst for the preparation of uracil-containing Heterocycles. *Res. Chem. Intermed.* **2020**, *46*, 3727–3740. [CrossRef]
108. Isaad, J. Acidic ionic liquid supported on silica-coated magnetite nanoparticles as a green catalyst for one-pot diazotization–halogenation of the aromatic amines. *RSC Adv.* **2014**, *4*, 49333–49341. [CrossRef]
109. Zhen, B.; Jiao, Q.; Zhang, Y.; Wu, Q.; Li, H. Acidic ionic liquid immobilized on magnetic mesoporous silica: Preparation and catalytic performance in esterification. *Appl. Catal. A Gen.* **2012**, *445–446*, 239–245. [CrossRef]
110. Naeimi, H.; Nejadshafiee, V.; Islami, M.R. Iron (III)-doped, ionic liquid matrix-immobilized, mesoporous silica nanoparticles: Application as recyclable catalyst for synthesis of pyrimidines in water. *Microporous Mesoporous Mater* **2016**, *227*, 23–30. [CrossRef]
111. Sobhani, S.; Honarmand, M. Ionic liquid immobilized on γ-Fe2O3 nanoparticles: A new magnetically recyclable heterogeneous catalyst for one-pot three-component synthesis of 2-amino-3,5-dicarbonitrile-6-thio-pyridines. *Appl. Catal. A Gen.* **2013**, *467*, 456–462. [CrossRef]
112. Jia, X.; Zhang, X.; Wang, Z.; Zhao, S. Tertiary amine ionic liquid incorporated Fe_3O_4 nanoparticles as a versatile catalyst for the Knoevenagel reaction. *Synth. Commun.* **2022**, *52*, 774–786. [CrossRef]
113. Azgomi, N.; Mokhtary, M. Nano-Fe_3O_4@SiO_2 supported ionic liquid as an efficient catalyst for the synthesis of 1,3-thiazolidin-4-ones under solvent-free conditions. *J. Mol. Catal. A Chem.* **2015**, *398*, 58–64. [CrossRef]
114. Mamaghani, M.; Sheykhan, M.; Sadeghpour, M.; Tavakoli, F. An expeditious one-pot synthesis of novel bioactive indole-substituted pyrido[2,3-d]pyrimidines using Fe_3O_4@SiO_2-supported ionic liquid nanocatalyst. *Monatsh. Fur Chem.* **2018**, *149*, 1437–1446. [CrossRef]

115. Zheng, X.; Luo, S.; Zhang, L.; Cheng, J.-P. Magnetic nanoparticle supported ionic liquid catalysts for CO_2 cycloaddition reactions. *Green Chem.* **2009**, *11*, 455. [CrossRef]
116. Safari, J.; Zarnegar, Z. Brønsted Acidic Ionic Liquid based Magnetic Nanoparticles: A New Promoter for the Biginelli Synthesis of 3, 4-Dihydropyrimidin-2 (1 h)-ones/thiones. *New J. Chem.* **2014**, *38*, 358–365. [CrossRef]
117. Garkoti, C.; Shabir, J.; Mozumdar, S. An imidazolium based ionic liquid supported on Fe_3O_4@SiO_2 nanoparticles as an efficient heterogeneous catalyst for N-formylation of amines. *New J. Chem.* **2017**, *41*, 9291–9298. [CrossRef]
118. Azarifar, D.; Ebrahimiasl, H.; Karamian, R.; Ahmadi-Khoei, M. s-Triazinium-based ionic liquid immobilized on silica-coated Fe_3O_4 magnetic nanoparticles: An efficient and magnetically separable heterogeneous catalyst for synthesis of 2-amino-4,8-dihydropyrano[3,2-b]pyran-3-carbonitrile derivatives for antioxidant and antifungal evaluation studies. *J. Iran. Chem. Soc.* **2018**, *16*, 341–354.
119. Ghorbani-Choghamarani, A.; Norouzi, M. Synthesis and characterization of ionic liquid immobilized on magnetic nanoparticles: A recyclable heterogeneous organocatalyst for the acetylation of alcohols. *J. Magn. Magn. Mater.* **2016**, *401*, 832–840. [CrossRef]
120. Safaei Ghomi, J.; Zahedi, S. Novel ionic liquid supported on Fe_3O_4 nanoparticles and its application as a catalyst in Mannich reaction under ultrasonic irradiation. *Sonochemistry* **2017**, *34*, 916–923. [CrossRef] [PubMed]
121. Zhang, Y.; Xia, C. Magnetic hydroxyapatite-encapsulated γ-Fe2O3 nanoparticles functionalized with basic ionic liquids for aqueous Knoevenagel condensation. *Appl. Catal. A Gen.* **2009**, *366*, 141–147. [CrossRef]
122. Nikoofar, K.; molaei Yielzoleh, F. Cascade embedding triethyltryptophanium iodide ionic liquid ($TrpEt_3{}^+I^-$) on silicated titano-magnetite core ($Fe_{3-x}Ti_xO_4$-SiO_2@$TrpEt_3{}^+I^-$): A novel nano organic–inorganic hybrid to prepare a library of 4-substituted quinoline-2-carboxylates and 4,6-disubstituted quinoline-2-carboxylates. *J. Chin. Chem. Soc.* **2021**, *68*, 1549–1562.
123. Gu, Y.; Li, G. Ionic Liquids-Based Catalysis with Solids: State of the Art. *Adv. Synth. Catal.* **2009**, *351*, 817–847. [CrossRef]
124. Mehnert, C.P.; Cook, R.A.; Dispenziere, N.C.; Afeworki, M. Supported Ionic Liquid Catalysis—A New Concept for homogeneous hydroformylation Catalysis. *J. Am. Chem. Soc.* **2002**, *124*, 12932–12933. [CrossRef]
125. Riisager, A. Continuous fixed-bed gas-phase hydroformylation using supported ionic liquid-phase (SILP) Rh catalysts. *J. Catal.* **2003**, *219*, 452–455. [CrossRef]
126. Riisager, A.; Eriksen, K.M.; Wasserscheid, P. Propene and 1-Octene hydroformylation with Silica-Supported, Ionic Liquid-Phase (SILP) Rh-Phosphine Catalysts in Continuous Fixed-Bed Mode. *Catal. Lett.* **2003**, *90*, 149–153. [CrossRef]
127. An, H.; Wang, D.; Miao, S.; Yang, Q.; Zhao, X.; Wang, Y. Preparation of Ni-IL/SiO_2 and its catalytic performance for one-pot sequential synthesis of 2-propylheptanol from n-valeraldehyde. *RSC Adv.* **2020**, *10*, 28100–28105. [CrossRef]
128. Sadeghzadeh, S.M. PbS based ionic liquid immobilized onto fibrous nano-silica as robust and recyclable heterogeneous catalysts for the hydrogen production by dehydrogenation of formic acid. *Microporous Mesoporous Mater.* **2016**, *234*, 310–316. [CrossRef]
129. Gruttadauria, M.; Liotta, L.F.; Salvo, A.M.P.; Giacalone, F.; La Parola, V.; Aprile, C.; Noto, R. Multi-Layered, Covalently Supported Ionic Liquid Phase (mlc-SILP) as highly Cross-Linked Support for Recyclable Palladium Catalysts for the Suzuki Reaction in Aqueous Medium. *Adv. Synth. Catal.* **2011**, *353*, 2119–2130. [CrossRef]
130. Calabrese, C.; Campisciano, V.; Siragusa, F.; Liotta, L.; Aprile, C.; Gruttadauria, M.; Giacalone, F. SBA-15/POSS-Imidazolium hybrids as Catalytic Nanoreactor: The role of the support in the stabilization of Palladium species for C−C Cross Coupling Reactions. *Adv. Synth. Catal.* **2019**, *361*, 3758–3767. [CrossRef]
131. Pavia, C.; Ballerini, E.; Bivona, L.A.; Giacalone, F.; Aprile, C.; Vaccaro, L.; Gruttadauria, M. Palladium Supported on Cross-Linked Imidazolium Network on Silica as highly Sustainable Catalysts for the Suzuki Reaction under Flow Conditions. *Adv. Synth. Catal.* **2013**, *355*, 2007–2018. [CrossRef]
132. Montroni, E.; Lombardo, M.; Quintavalla, A.; Trombini, C.; Gruttadauria, M.; Giacalone, F. A Liquid-Liquid Biphasic homogeneous Organocatalytic Aldol Protocol Based on the Use of a Silica Gel Bound Multilayered Ionic Liquid Phase. *ChemCatChem* **2012**, *4*, 1000–1006. [CrossRef]
133. Zhong, N.; Li, Y.; Cai, C.; Gao, Y.; Liu, N.; Liu, G.; Tan, W.; Zeng, Y. Enhancing the catalytic performance of Candida antarctica lipase B by immobilization onto the ionic liquids modified SBA-15. *Eur. J. Lipid. Sci. Tech.* **2018**, *120*, 1700357. [CrossRef]
134. Zou, B.; Chu, Y.; Xia, J.; Chen, X.; Huo, S. Immobilization of lipase by ionic liquid-modified mesoporous SiO_2 adsorption and calcium alginate-embedding method. *Appl. Biochem. Biotechnol.* **2018**, *185*, 606–618. [CrossRef]
135. Xie, W.; Zang, X. Lipase immobilized on ionic liquid-functionalized magnetic silica composites as a magnetic biocatalyst for production of trans-free plastic fats. *Food Chem.* **2018**, *257*, 15–22. [CrossRef]

nanomaterials

MDPI

Review

Ionic Liquids for Development of Heterogeneous Catalysts Based on Nanomaterials for Biocatalysis

Anna Wolny and Anna Chrobok *

Department of Chemical Organic Technology and Petrochemistry, Faculty of Chemistry, Silesian University of Technology, Krzywoustego 4, 44-100 Gliwice, Poland; Anna.Wolny@polsl.pl
* Correspondence: Anna.Chrobok@polsl.pl; Tel.: +48-32-237-2917

Abstract: The development of effective methods of enzyme stabilization is key for the evolution of biocatalytic processes. An interesting approach combines the stabilization process of proteins in ionic liquids and the immobilization of the active phase on the solid support. As a result, stable, active and heterogeneous biocatalysts are obtained. There are several benefits associated with heterogeneous processes, as easy separation of the biocatalyst from the reaction mixture and the possibility of recycling. Accordingly, this work focused on the supported ionic liquid phases as the efficient enzyme stabilization carriers, and their application in both continuous flow and batch biocatalytic processes.

Keywords: supported ionic liquid phase; supported ionic liquid-like phase; biocatalysis; enzyme; heterogeneous catalysis; immobilization; nanomaterials

Citation: Wolny, A.; Chrobok, A. Ionic Liquids for Development of Heterogeneous Catalysts Based on Nanomaterials for Biocatalysis. *Nanomaterials* **2021**, *11*, 2030. https://doi.org/10.3390/nano11082030

Academic Editor: Haralambos Stamatis

Received: 10 July 2021
Accepted: 5 August 2021
Published: 10 August 2021

1. Introduction

Increasing the ecological awareness of the society and subsequent restrictive regulations concerning environmental protection, push the chemical industry to develop clean technologies. In order to achieve the United Nations sustainable development goals 2030, each material or product should be safe and sustainable. The use of volatile organic solvents, hazardous substances, production of large amounts of hazardous wastes, and the need to provide large amounts of energy, are the main problems for the environment, associated with chemical processes [1]. Additionally, nanotechnology is often mentioned as a technology that could enable a green growth [2]. Therefore, solutions reducing both the harmful effects of chemical processes on the environment and enhancing synthesis effectiveness are desirable. Green chemistry rules deliver the clues for sustainable and ecological development. One of the most important paths of chemical industry development is the search for a new effective catalysts or/and biocatalyst [3,4].

Enzymes represent a great alternative to conventional catalysts generating hazardous wastes [4]. Enzymes are protein particles that enable various chemical processes to be carried out under mild conditions, and provide high effectiveness of synthesis, due to high enantio-, regio- and chemo-selectivity. Unfortunately, there are some limitations associated with protein applications. Enzymes are sensitive to temperature, pressure, pH changes, and organic solvents. A non-aqueous environment can lead to their folded three-dimensional structure being destroyed, and, in consequence, to biocatalyst deactivation [5]. For that reason, lots of enzymes stabilization methods were developed, e.g., via ionic liquids (ILs), which will be described in this work. Among them, the most common method for enzyme stabilization is immobilization in, or on, a solid matrix. Immobilization not only provides enzyme stabilization, but also enables the easy separation of heterogeneous biocatalysts from the reaction system. The following methods of enzyme immobilization have been developed: entrapment, encapsulation, cross-linking, and adsorption or covalent attachment onto the insoluble carriers [6,7]. Enzyme entrapment and encapsulation are methods

that close the protein in a support, without attachment to the matrix. For example, *Candida antarctica* B lipase (CALB) was entrapped in electrospun poly(vinyl alcohol) (PVA) nanofibers. It was reported that entrapped CALB showed higher activity, stability, and reusability, when poly(ethylene glycol) (PEG) was added as additive for lipase immobilization [8]. CALB was encapsulated in the hybrid nanoflowers, consisting of copper (II) or manganese (II) ions, combined with magnetic and carbon nanoparticles. The enzyme performed great catalytic activity, stability, and reusability (eight cycles) in tyrosol ester production [9]. On the other hand, cross-linking is the method for the creation of an intermolecular cross-linkage between the enzyme particles and cross-linking agent, e.g., glutaraldehyde. A special example is the cross-linked enzyme aggregates (CLEAs), which are prepared by using different precipitants (e.g., ammonium sulfate, acetone, PEG) and cross-linkers. Cross-linked CALB aggregates that were obtained with PEG, exhibited the highest activity in the esterification of lauric acid with 1-propanol [10]. CALB was attached onto mesoporous silica nanowires via covalent bonding. Immobilized lipase provided a 94.3% yield (Y) of biodiesel production and a long stability (eight cycles), without a significant loss of activity [11]. The most common among enzyme immobilization methods, is the physical adsorption. This technique is inexpensive, fast, and easy to perform. The activity of the CALB immobilized on various silica supports was studied in the Baeyer–Villiger oxidation of cyclic ketones to lactones. The biocatalysts showed great stability, even in 60% hydrogen peroxide, and enabled high yields of lactones to be achieved [12].

An interesting approach, enhancing the stability and activity of enzymes, proved to be combining ionic liquids and immobilization on solid supports. In this method, the following four different types can be distinguished: supported ionic liquid catalyst (SILC), solid catalyst with ionic liquid layer (SCIL), supported ionic liquid phase (SILP), and supported ionic liquid-like phase (SILLP) (Figure 1).

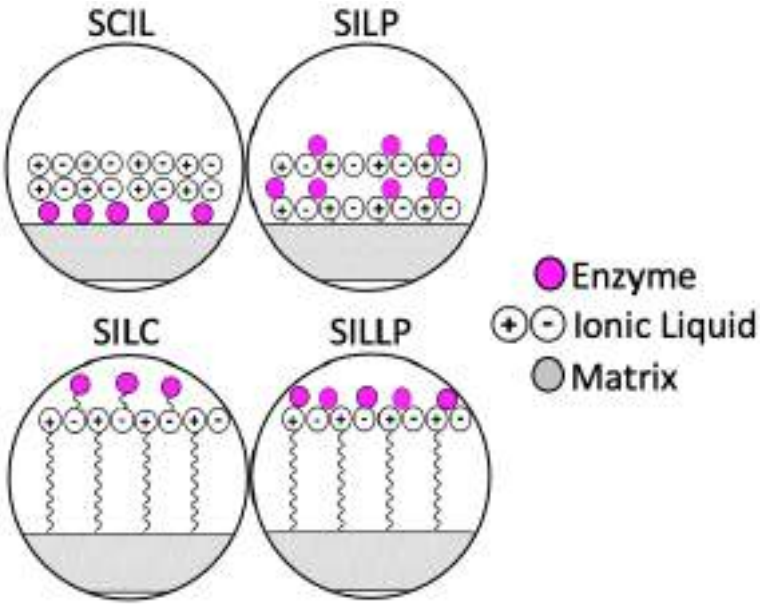

Figure 1. Enzyme immobilized on the supports modified with ionic liquids.

The supported ionic liquid catalyst technique involves the attachment of an enzyme, via covalent bonding, to ionic liquids moieties that are grafted to the solid matrix. Applications of SILC for enzyme immobilization in biocatalysis were reported. *Candida rugosa* lipase (CRL) was covalently anchored to IL particles that were attached to the magnetic nanoparticles (Fe_2O_3). ILs with different chain lengths (C4, C8) and anions (Cl^-, $[BF_4]^-$, $[PF_6]^-$) were tested both as coupling and stabilizing enzyme agents. The activity of the synthesized SILC biocatalysts was examined in the esters hydrolysis. Covalently immobilized CRL exhibited higher activity and stability than its native form [13]. *Porcine pancreas* lipase (PPL), covalently bonded to alginate nanoparticles, modified with imidazolium ILs,

enhanced activity and stability (10 cycles) in triacetin hydrolysis, compared with the free form and immobilized lipase on the magnetic support without IL [14]. IL moieties that were grafted to the magnetic carboxymethyl cellulose nanoparticles, were used in SILC biocatalyst synthesis. The immobilized enzymes PPL and *Penicillin G* acylase activities were tested in triacetin hydrolysis. Both the SILC biocatalysts performed higher activity and stability results than their free forms [15]. *Burkholderia cepacia* lipase (BCL) was covalently anchored to the silica xerogel particles that were treated with protic ionic liquid (PIL), creating an SILC biocatalyst. The synthesized biocatalyst was tested for biodiesel production from different oils (soybean, colza, and sunflower), and provided a conversion between 70–98% [16].

A solid biocatalyst with ionic liquid is the immobilized enzyme on the solid matrix, which is coated with an ionic liquid layer. An example of the SCIL technique in biocatalysis is that CALB immobilized on macroporous acrylic acid beads (Novozyme 435) and coated with 1-butyl-4-methylpyridine hexafluorophosphate [4bmpy][PF_6], presented an 80% yield of methylglucose fatty acid ester synthesis [17]. Other studies presented Novozyme 435 coated with imidazolium-based ionic liquid, with $[PF_6]^-$ anion, in the ring-opening polymerization (ROP) of lactones. The coated and immobilized lipase showed a two times better conversion of δ-valerolactone than uncoated Novozyme 435 [18]. The same immobilized enzyme coated with imidazolium ILs, with $[NTf_2]^-$ anion, was examined in poly(ε-caprolactone) synthesis. The SCIL biocatalyst provided higher enzyme activity, less IL consumption, higher molecular weight of the polymer and the synthesis yield [19].

The supported ionic liquid phase (SILP) technique consists of the physical immobilization of the enzymatic active phase on the matrix, on which the IL was adsorbed, while the supported ionic liquid-like phase (SILLP) is the method for the physical adsorption of an enzyme on the carrier, which is chemically modified with ionic liquid. The difference in the synthesis of the described carriers is in a different approach, to immobilize an IL on the matrix, for SILP in a physical way and for SILLP through covalent bonding. The applications of SILP and SILLP biocatalysts in biosynthesis, are described, in detail, later in the text. Moreover, other applications of enzymes that are immobilized on SILP and SILLP were also reported. The first example concerns the wastewater treatment. Magnetic chitosan nanoparticles, modified with amino-functionalized ionic liquid, containing 2,2-binamine-di-3-ethylbenzothiazolin-6-sulfonic acid based on copper ion chelation, were used as a carrier for laccase immobilization. The SILLP–laccase system allowed the removal of 2,4-dichlorophenol from water (50 mg/L), with 100% efficiency. SILLP provided higher activity and stability for the enzyme, compared with the free form [20]. SILLPs were also employed as great biosensors. Immobilized cytochrome C on SILLP, based on multiwalled carbon nanotubes (MWCNTs) modified glass carbon electrode, was used in the hydrogen peroxide detection. The investigated biosensor system demonstrated high selectivity, stability, and reproducibility [21]. Peroxidase (PER) from *Pisum sativum* was immobilized on SILP, based on chitin containing gold nanoparticles and used as a biosensor in rosmarinic acid determination. The obtained biosensor presented excellent sensitivity, repeatability, reproducibility, and stability [22]. The next interesting approach is called supported ionic liquid membranes (SILMs). It was reported that enzymatic SILM could be effectively used in the separation of CO_2 at high temperatures. *Sulfurihydrogenibium yellowstonense carbonic anhydrase SspCA* isozyme was immobilized on SILM made of polyvinylidene fluoride (PVDF), on which [BMIM][NTf_2] was adsorbed. The thermophilic enzymatic SILM system provided excellent selectivity transport of CO_2 against N_2 in high temperatures [23]. Table 1 shows examples of SILC, SCIL, SILP, SILLP techniques that are used in biocatalysis.

Table 1. Examples of SILC, SCIL, SILP and SILLP applications in biocatalysis.

Type of Technique	Ionic Liquid	Enzyme	Reaction	Ref.
SILC	Imidazolium cation $[Cl]^-$ anion	CRL (16 U/mg) [1]	Esters hydrolysis	[13]
SILC	Imidazolium cation $[PF_6]^-$ anion	PPL (659.4 U/g)	Triacetin hydrolysis	[14]
SILC	Imidazolium cation $[PF_6]^-$ anion	PPL (882.1 U/g)	Triacetin hydrolysis	[15]
SILC	Ammonium cation $[C_4H_9COO]^-$ anion	BCL (3801 U/g)	Hydrolysis and transesterification of different oils α between 70 and 98% [2]	[16]
SCIL	Pyridinium cation $[PF_6]^-$ anion	CALB [3]	Esterification of fatty acids α between 25 and 65%	[17]
SCIL	Imidazolium cation $[PF_6]^-$ anion	CALB [3]	Ring-opening polymerization of lactone α = 60%	[18]
SCIL	Imidazolium cation $[NTf_2]^-$ anion	CALB [3]	Ring-opening polymerization of lactone Y = 62% [4]	[19]
SILP	Imidazolium cation $[NTf_2]^-$ anion	CALB (1.7 U/mg)	Kinetic resolution of 1-phenylethanol via transesterification *ee* > 99.9% [5]	[24]
SILP	Imidazolium cation $[NTf_2]^-$ anion	CALB (71 U/mg)	Transesterification of vinyl butyrate S = 99% [6]	[24]
SILP	Imidazolium cation $[NTf_2]^-$ anion	CALB (9.1 U/mg)	Kinetic resolution of 1-phenylethanol via transesterification *ee* > 99.9%	[25]
SILP	Imidazolium cation $[BF_4]^-$ anion	CALB (58 U/mg)	Transesterification of vinyl butyrate α = 96%	[26]
SILLP	Imidazolium cation $[Cl]^-$ anion	CALB (20 U/mg)	Transesterification of vinyl propionate Y = 93%	[27]
SILLP	Imidazolium cation $[NTf_2]^-$ anion	CALB (1138.3 U/g)	Kinetic resolution of 1-phenylethanol via transesterification Y = 81%, *ee* = 94%	[28]
SILLP	Imidazolium cation $[NTf_2]^-$ anion	CALB (49.8 U/g)	Triolein transesterification Y = 85%	[29]

[1] Specific activity. [2] Conversion. [3] No data available. [4] Yield. [5] Enantioselectivity. [6] Selectivity.

To summarize, four different techniques (SILC, SCIL, SILP, and SILLP) of combining ionic liquids and the solid matrix, for enzyme stabilization, were applied in the biocatalysis. Due to the hydrophobic character, ionic liquids that are composed of an imidazolium cation with a long alkyl chain and $[NTf_2]^-$ anion, are the most suitable for enzyme stabilization. The use of hydrophobic ionic liquids enables high specific activities of the enzymes to be obtained, for all types of techniques. It is associated with "essential" water, which is important to the enzymes action. Protein immobilization, via covalent bonding or physical adsorption on the support, ensures high stabilities and activities. The presented techniques also enable easy separation of the biocatalyst from the reaction mixture, and reusability. All these factors allow high conversions, yields, selectivity, and enantioselectivities to be achieved, and make SILC, SCIL, SILP, and SILLP methods attractive for reactions that are catalyzed by the enzymes.

In this paper, the achievements of SILP and SILLP employed in biocatalysis were described. Previously, Domínguez de María et al. referred to supported ionic liquid biocatalysts briefly in 2012 [30]. Next, Lozano et al. reviewed the influence of ionic liquids on enzyme activity, based on the supported ionic liquids in bath and flow biocatalytic processes in 2014 [31]. Again, Lozano et al., in 2015, discussed the supported ionic liquid phases for enzymatic continuous flow synthesis [32]. Afresh, Potdar et al. mentioned about supported ionic liquid phases in the chosen bioprocesses in 2015 [33]. The aim of this article

is to complement the time gap, and highlight the strengths and weaknesses of each method, so that synthetic chemists can choose the most suitable method for enzyme immobilization.

2. Stabilization of Enzymes via Ionic Liquids

Ionic liquids, known as low-temperature molten salts, are compounds consisting of organic cations and organic or inorganic anions that are classified to green chemistry substances [34]. The lack of volatility, non-flammability, and thermal stability, provide a good alternative as green solvents, which can reduce hazardous organic wastes. The significant characteristic of ionic liquids is the possibility of designing the structure and, as a result, the creation of the unique physicochemical properties [34,35]. Accordingly, ILs have a wide range of industrial applications. Due to their modulated polarity, acidity, and viscosity, ILs are interesting alternatives for conventional organic solvents [36], hazardous catalysts [37], and absorbent and extraction agents [38,39]. Ionic liquids have also been reported as effective enzyme stabilizers [31,40].

In respect to the literature, many methods of enzyme stabilization via ILs were found, which can be classified in two groups.

The first group of methods includes techniques where proteins are modified [30]. Enzyme immobilization is the most common method of enzyme stabilization, it includes sol-gel encapsulation, the cross-linking enzyme aggregates (CLEAs), and the protein attachment to the solid support [31,41]. Sol-gel encapsulation is an irreversible method, where enzymes, via noncovalent interactions, are closed in a support. Encapsulated *Candida rugosa* lipase showed great activities in esterification and hydrolysis reactions. IL was added to the reaction mixture during the immobilization procedure [42]. CLEAs technique is based on the creation of aggregates of enzymes, with the use of glutaraldehyde, which reacts with amino groups in the protein structure. Enzymes are cross-linked in the aqueous solutions with some additives, e.g., ILs. *Burkholderia cepacia* lipase, as CLEA, presented higher catalytic activity than in the native form [43]. The last technique—binding to the solid matrix, via physical adsorption, in the presence of ILs—is known as a supported ionic liquid phases (SILPs) method, and will be described in the next section. Besides the enzyme immobilization technique, there are also methods such as the modification of enzymes with polyethylene glycol (PEG) technique, and propanol-rinsed enzyme preparation (EPRP), but in these cases, ionic liquid is usually used as an additive or solvent [31].

The second category of methods increasing the activity and stability of the enzymes, is environment modification. One of these techniques is the water-in-IL microemulsion (w/IL), which can be described as water droplets, with enzymes dispersed in non-polar ILs. In addition, microemulsion can be stabilized by surfactants, in order to increase the efficiency of emulsifying and protect the protein from denaturation. For example, microemulsion w/IL was tested for *Burkholderia cepacia* lipase in the ester hydrolysis reaction. The catalytic activity of BCL was higher in the w/IL microemulsion than in the w/isooctane microemulsion [44]. Coating proteins with ILs is another method of increasing enzyme stability. Novozyme 435 was coated with ionic liquid and showed higher activity in the synthesis of citronellyl esters than without IL [45].

The modification of the enzyme's environment can also be assigned the designing of ILs structure, for increasing the enzyme's activity and stability [30,46,47]. As mentioned before, the structure of ionic liquid can be designed by selecting a proper cation and anion. Different combinations of ions result in the tailoring of the properties of IL, and interactions between IL and enzymes. Main properties of ionic liquid that are important for enzyme stabilization are polarity, anion nucleophilicity, alkyl chain length in the cation, hydrogen bonds, and viscosity [30,31,46,47]. The folded three-dimensional structure of the enzymes can be easily destroyed in non-aqueous media. The "essential" water is needed by the enzymes to save their active conformations, wherefore a little amount of water is usually added to the organic environment [30,31]. Consequently, the activity of the enzymes should be higher in more hydrophobic solvents, because of the lack of affinity to the enzyme's essential water, which was confirmed by a lot of studies [48–51]. For example, this was

shown by studies on the lipase from *Candida antarctica* activity in butyl butyrate synthesis, via the transesterification reaction of vinyl butyrate and 1-butanol, in the presence of various ionic liquids. CALB exhibited higher activity in more hydrophobic ionic liquids with $[NTf_2]^-$ and $[PF_6]^-$ anions. In this point, the influence of anion nucleophilicity was also explained. The enzyme stability increases with decreasing anion nucleophilicity, due to the more nucleophilic anions that can interact with the positive charges in the enzyme's structure, and, in the result change, the conformation of the protein. The same studies also confirmed that the lipase stability increases with the length of the alkyl chain in the cation [48]. On the other hand, there are also reports where the enzymes demonstrated better activity in hydrophilic ILs [17,52] or in ILs that consisted of more hydrophobic anions and shorter alkyl chains in the cation [53]. The ability of hydrogen bond forming is the next important factor in enzyme stabilization. It was reported that anions that are hydrogen bond acceptors caused changes in the enzyme's conformation and denaturation [54,55].

As has been shown, many factors can affect an enzymes activity and stability. In the designing process of the ionic liquid structure for the biocatalysis process, the nature of the anion, type of cation and the length of alkyl chain, the class of enzyme, and the kind of reaction, should be considered. The most common ionic liquids that are used in biocatalysis, are presented on Figure 2.

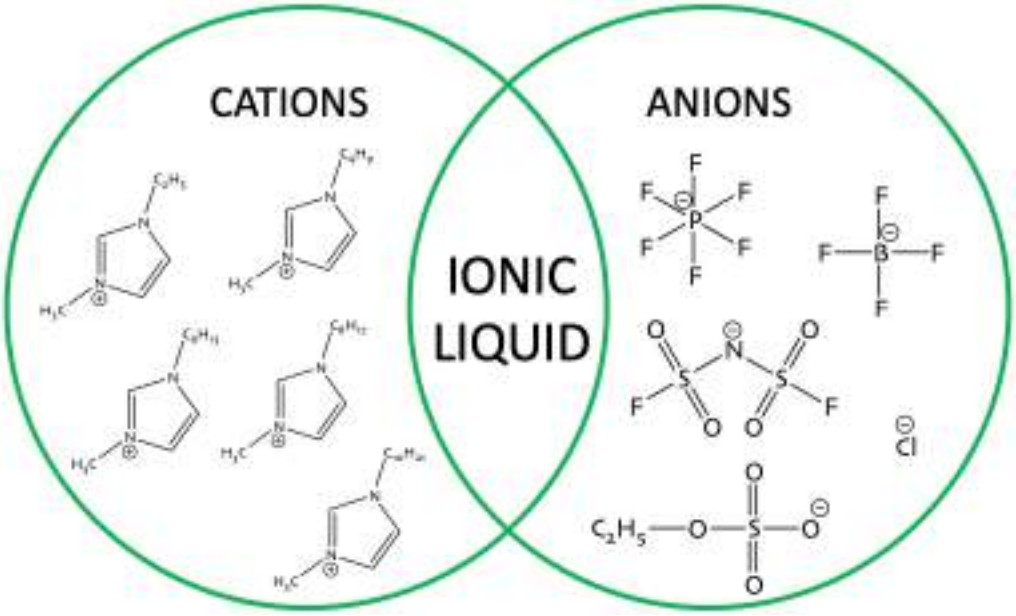

Figure 2. Structures of ionic liquids used for enzyme stabilization.

3. Supported Ionic Liquid Phases in Biocatalysis

The first reports concerning the supported ionic liquid phase (SILP) biocatalysts were reported in 2002. CALB was dissolved in 1-ethyl-3-methylimidazolium triflimide ([EMIM][NTf_2]) or 1-butyl-3-methylimidazolium triflimide ([BMIM][NTf_2]), then immobilized on the solid adsorbent (Celite) and used in a continuous butyl butyrate synthesis and the kinetic resolution of 1-phenylethanol in supercritical carbon dioxide ($scCO_2$). The scheme of the kinetic resolution of 1-phenylethanol racemate is presented in Figure 3. For both the transesterification reactions, the enzyme showed good catalytic activity, selectivity, and, in the case of the kinetic resolution reaction, high enantioselectivity (>99.9%) and stability (16 cycles) in the anhydrous conditions [24]. In the next year, the same SILP system was tested for the kinetic resolution of 1-phenylethanol at a higher temperature (120 °C) and a lower $scCO_2$ pressure (10 MPa). The loss of activity was not observed, even after 10 cycles [25]. In both cases, the use of ionic liquids increased the stability and activity of the enzyme in a high-temperature and $scCO_2$ environment [24,25]. Next, the studies of this group focused on the influence of the alkyl chain in the ionic liquid's cation on the enzyme

stabilization, and pointed out the importance of mass transport phenomena between ionic liquid and $scCO_2$, in the case of the heterogeneous catalyst. The SILP biocatalyst was tested in the continuous kinetic resolution of 1-phenylethanol in $scCO_2$. Immobilized on silica gel, CALB showed a 2000 times longer half-life time in the most hydrophobic IL (hexyl-trimethylammonium bis(trifluoromethylsulfonyl)imide), than in hexane [56]. The SILP-type biocatalyst, in the presence of $scCO_2$, was also studied in glycidyl butyrate synthesis. Firstly, the lipases from *Candida antarctica* A (CALA), *Mucor miehei* (MML), and CALB, were mixed with various ionic liquids and then their activity was tested. The CALB in [EMIM][NTf_2] presented the best R/S ratio. Accordingly, a selected enzyme–IL mixture was immobilized on the solid particles and tested in a continuous process under $scCO_2$ conditions, resulting in high enantioselectivity and a little bit lower activity [57].

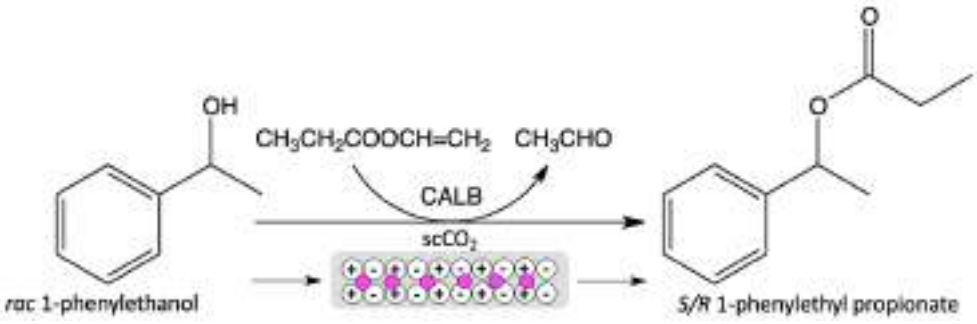

Figure 3. Scheme of kinetic resolution of 1-phenylethanol racemate in SILP biocatalyst and $scCO_2$ presence.

The other approach of performing biocatalysis under $scCO_2$ conditions is supported by the ionic liquid-like phase (SILLP). The enzyme–SILLP biocatalysts were described for the first time in 2007. In most cases, the enzymes were immobilized on polystyrene-divinylbenzene (PS-DVB) monolith, modified with imidazolium-based ionic liquids [27]. PS-DVB monolith is a very attractive support, due to the possibility of preparing proper morphologies, shapes, and properties, by cross-linking method synthesis. Modification of the polymeric surface can decrease the hydrophobicity of the support, when it is too high, which, in turn, can protect an enzyme from deactivation [58]. The first-studied SILLP biocatalyst was CALB immobilized onto PS-DVB, modified with imidazolium ionic liquid that was tested in the continuous flow citronellyl propionate synthesis in $scCO_2$. A high yield (93%) and stable activity (seven cycles) were reported for that catalytic system, at 80 °C [27]. The same SILLP biocatalyst was used in the combination with zeolites, in the continuous kinetic resolution of 1-phenylethanol in supercritical carbon dioxide. Previous reports of this group resulted in the high technological parameters (*ee* = 97.4%, yield = 74%) when immobilized CALB and zeolites were coated with ionic liquid in that process. To avoid the deactivation of the enzyme, the biocatalyst and acidic catalyst were packed under three different layers [59]. Applying the SILLP biocatalyst in the kinetic resolution process, under $scCO_2$ conditions, gave excellent results, such as enantioselectivity >99.9% and a 50% yield (the maximum that is feasible for kinetic resolution). Although, the three-column system, combined with the SILLP biocatalyst–acidic-catalyst–SILLP biocatalyst, resulted in a longer catalyst stability (3 weeks) and higher yield (60%), caused by racemization. Hence, a single column, packed with the mixture of SILLP biocatalyst and zeolite-coated IL, exhibited the best results for the continuous flow kinetic resolution of sec-alcohol (*ee* > 99%, Y = 92%) [60]. The other approach to improve the kinetic resolution of the 1-phenylethanol batch process, involves using the CALB–SILLP biocatalyst under microwave irradiation (MW). The polymeric macroporous PS-DVB support was functionalized in high and low degree. The application of the CALB–SILLP biocatalyst, with a low functionalization degree, containing ionic liquid with $[NTf_2]^-$ anion used in the kinetic resolution process, resulted in high conversion (50%), enantioselectivity (>99%), and stability (12 cycles). The microwave-assisted process showed better performance compared to conventional heating [28]. PS-DVB

polymeric monolith, modified with the following ionic liquids: [BMIM][NTf_2], and 1-octyl-3-methylimidazolium bis(trifluoromethylsulfonyl)imide ([OMIM][NTf_2]), was synthesized for the immobilization of large biomolecules. Azoalbumin was adsorbed on SILLP, with high efficiency. Moreover, CALB, immobilized on that SILLP, did not show deactivation during the kinetic resolution of 1-phenylethanol, and additionally the activity and the enantioselectivity of this biocatalyst stayed unchanged for 12 months [61]. The polymeric SILLP biocatalyst was also used for biodiesel production, via continuous flow synthesis under $scCO_2$ conditions, as presented on Figure 4.

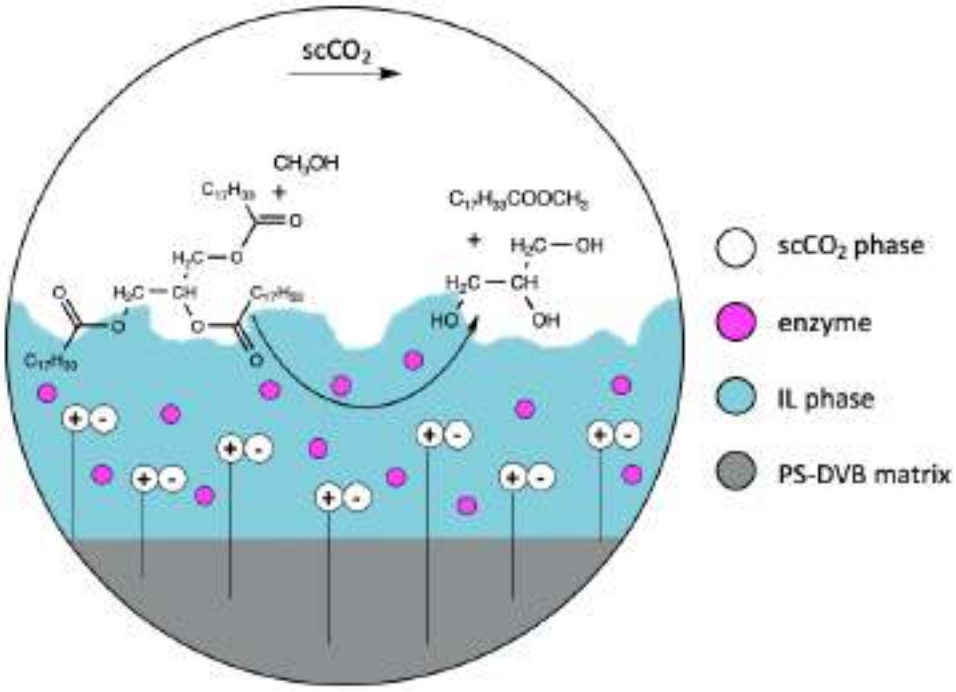

Figure 4. Presentation of enzyme immobilized on SILLP used in methanolysis of triolein under $scCO_2$ conditions.

Alkylimidazolium ionic liquid particles were bonded on a PS-DVB support, in different degrees of functionalization. The CALB–SILLP–[NTf_2]- biocatalyst that was used in the synthesis of methyl oleate, exhibited a yield up to 95% and long stability (45 cycles). Tert-butanol was added in order to prevent the deactivation of the enzyme with the glycerol that was obtained as a by-product [29]. Modified via butylimidazolium, the ionic liquid PS-DVB macroporous support found another one application as a matrix for urease immobilization. SILLP biocatalyst activity was measured for the urea hydrolysis reaction. The activity value was up to 285% higher compared with the native enzyme, and 30 reaction cycles were reported with good activity too [62]. The polymeric PS-DVB matrix was modified in different loading levels of ionic liquids, for dehydrogenase, from *Rhodococcus ruber*, immobilization. Great activity of the biocatalysts was examined in the bioreduction of prochiral ketones to alcohols. Furthermore, enzymatic SILLP material provided high conversion and selectivity values [63].

Besides the PS-DVB matrix, other polymers were also studied as SILP/SILLP supports. A monolithic cellulose-2.5-acetate/polyurethane hybrid, covered with octylmethylimidazolium tetrafluoroborate ([OMIM][BF_4]), was tested as a hybrid matrix for CALB immobilization. SILP biomaterial was used in the continuous flow transesterification reaction of vinyl-butyrate, and 1-butanol achieved a conversion up to 96% over 18 days [26]. The same hybrid material was used for CALB and CRL immobilization. The SILP bioreactor was tested in a batch and flow kinetic resolution of 1-phenylethanol, synthesis of (−)-2-isopropyl-5-methylcyclohexyl propionate, and in the enantioselective amidation of (*R*,*S*)-1-phenylethylamine with ethyl methoxyacetate. CALB–SILP, consisting of

[BMIM][PF_6] for the transesterification of 1-phenylethanol and vinyl butyrate, under flow and batch conditions, achieved enantioselectivity >99%, and the conversion for batch and continuous processes decreased from 90% to 75%, respectively. CRL–SILP, consisting of [OMIM][PF_6] in (−)-2-isopropyl-5-methylcyclohexyl propionate production, expressed 79% enantioselectivity, for both the batch and continuous conditions. Amidation of (*R*,*S*)-1-phenylethylamine with ethyl methoxyacetate, catalyzed by CALB–SILP polymeric hybrid, using [BMIM][BF_4] under flow conditions, resulted in the increase in the enantioselectivity (up to 97%) and activity value compared with the batch process. The SILP hybrid biocatalyst showed great enzyme stability under continuous conditions, at least 7 days for all the described processes, except the esterification reaction, which resulted in the efficient production of enantiomerically pure chemicals technology [64]. The application of cellulose-2.5-acetate beads/hybrid monolith as a CALB–SILP support for the continuous gas-phase transesterification of the vinyl propionate and 2-propanol process, was reported. The best results were obtained with [OMIM][BF_4]. The enzyme showed excellent stability, even at a high temperature, up to 65 °C over 700 h time on stream [65].

It is worth mentioning another polymeric material that is used as an enzymes SILLP carrier—chitin (poly N-acetylglucosamine) and its derivative chitosan. Chitin and chitosan offer lots of sites that can be functionalized, but these matrixes characterized low porosity and surface area, which reduces the efficiency of the enzyme immobilization. It was reported that ionic liquids can change and modify the morphology of polymeric particles, enabling effective enzyme immobilization [66–68]. Studies on the modification of chitin with different ionic liquids were dedicated as SILLP for enzyme stabilization. Various cations, such as (1-methyl-1-propylpyrrolidinium [MPpyrr]$^+$, 1-methyl-1-propylpiperidinium [MPpip]$^+$, 1,4-dimethyl-1-propylpiperazinium [DMPpz]$^+$ and 1-ethyl-3-methylimidazolium [EMIM]$^+$, and lactate or acetate anions, were tested for chitin modification. As a result, an SILLP with a large external surface and proper particle sizes, was obtained [66]. Other approach include combined chitosan with mesoporous silica (SBA-15), covalently modified with ionic liquid ([BF_4]$^-$ anion). SILLP nanoparticles were investigated as an excellent support for *Porcine pancreas* lipase (PPL) immobilization, providing high activity and stability (10 cycles) of the enzymes in the triacetin hydrolysis reaction [67]. Magnetic chitosan nanocomposites (chitosan–Fe_3O_4), covalently modified by imidazolium ionic liquids with various functional groups, were synthesized as SILLP for PPL immobilization. The enzyme presented a 6.7 times higher activity in triacetin hydrolysis compared to the free form, when IL bonded to magnetic nanocomposites was functionalized with a hydroxyl group with eight carbon atoms, in the imidazolium alkyl chain in the cation of IL [68].

Studies on magnetic supported ionic liquid-type biocatalysts, were reported in 2009. Carriers with magnetic properties can be rapidly and easily separated from the reaction mixture, using an external magnetic field. The modification the magnetic nanoparticles surface is crucial for biosynthesis, due to the changing properties of the support and the increasing stability of the enzymes [69–71]. Magnetic nanoparticles (Fe_3O_4), combined with silica, covalently modified with imidazolium based ionic liquids with different alkyl chain lengths and anions ([Cl]$^-$, [BF_4]$^-$, [PF_6]$^-$), increased the surface area. The activity of CRL, immobilized via physical adsorption, was examined in the esterification of oleic acid and butanol. The enzyme exhibited a 118% higher catalytic activity compared to a native protein, and retained its stability, even at 80 °C [69]. The same SILLP magnetic matrix was applied for *Penicillin G* acylase immobilization. The synthesized carrier provided high enzyme loading and catalytic activity [70]. Another example demonstrated the use of SILLP magnetic bionanoparticles in the production of trans-free plastic fats, via enzymatic interesterifications of solid palm stearin and liquid rice bran oil in a shaking water bath. CRL, immobilized on an Fe_3O_4–silica hybrid modified by grafting ionic liquid particles, showed great activity, and provided the synthesis of trans-free plastic fats in the proper composition and desirable physicochemical properties. The lost activity was not reported after the separation of SILLP magnetic nanoparticles, by an external magnetic field [71].

Supported ionic liquid phases based on carbon materials, are another significant group of supports in biocatalysis. Active carbon (AC) is an interesting carbon material, with desirable properties for supports in biocatalysis. AC materials are non-toxic, cheap, commercially available, and have a large internal surface area with different sizes of pores, which enables the effective adsorption of enzymes [72]. Lipase PS from *Burkholderia cepacia* was immobilized on an active carbon, active carbon cloth (ACC), activated carbon paper (STV), and alumina, in the presence of ILs—[EMIM][NTf_2] and [EMIM][BF_4]. The best results for the enzymatic kinetic resolution of 1-phenylethanol were obtained for lipase immobilized on an active carbon cloth, coated with [EMIM][NTf_2] in toluene. After 6 h, the achieved product's enantioselectivity was higher than 99% and the conversion reached 50%, which is the maximum for that reaction type [73]. Another worthwhile carbon material, which can be used as a support, is the carbon nanotube. Carbon nanotubes are an interesting matrix, due to their properties, which include the following: high purity (no possibility of poisoning the enzymatic active phase), mechanical and thermal stability, large surface area, and the possibility of surface functionalization [74]. CALB was immobilized via physical adsorption, on the surface of multiwalled carbon nanotubes (MWCNTs) that were modified with dialkylimidazolium ionic liquids with different lengths of alkyl chains, in combination with $[PF_6]^-$ anion. It was reported that the modification of MWCNTs with ILs did not destroy the support's structure. The immobilization of an enzyme on the SILLP resulted in higher activity, thermal stability, and longer reusability of the biocatalyst in triacetin hydrolysis compared with CALB adsorbed on MWCNTs, without ILs modification. The longer alkyl chain on IL's cation shows that the stabilization of the active enzyme's conformation is more efficient [75]. In the next studies, SILLPs based on MWCNTs were synthesized, as previously described, but the alkyl chain in the imidazolium ring was supplied with different functional groups, such as amino, carboxyl, and hydroxyl. Among them, the CALB–SILLP biocatalyst, functionalized with a hydroxyl group, showed the best results in the triacetin hydrolysis. A selected CALB–SILLP improved activity (18 times compared with CALB–MWCNTs) and thermal stability. Moreover, the biocatalyst retained its stability over four reaction cycles [76]. A further approach considered the selection of an appropriate ionic liquid's anion for enzyme stabilization. The synthesis pathway described above was used for CALB–SILLP production. The activity of CALB–SILLP biocatalysts with various anions ($[Br]^-$, $[BF_4]^-$, $[PF_6]^-$ or $[H_2PO_4]^-$), were examined in the triacetin hydrolysis. Five times higher activity, compared with CALB–MWCNTs, was demonstrated by CALB–SILLP with $[PF_6]^-$ anion [77]. The next approach employs D-glucose-based ionic liquids that are adsorbed on MWCNTs, for CALB immobilization. The CALB–SILP system was used in the esterification reaction of acrylic acid and n-butanol. The biocatalyst provided a high ester yield (99%), selectivity, and long stability. Lipase retained its activity for five cycles and three cycles, with over a 90% yield of n-butyl acrylate [78]. The next studies of this group included two approaches of the chemical modification of MWCNTs, as presented in Figure 5.

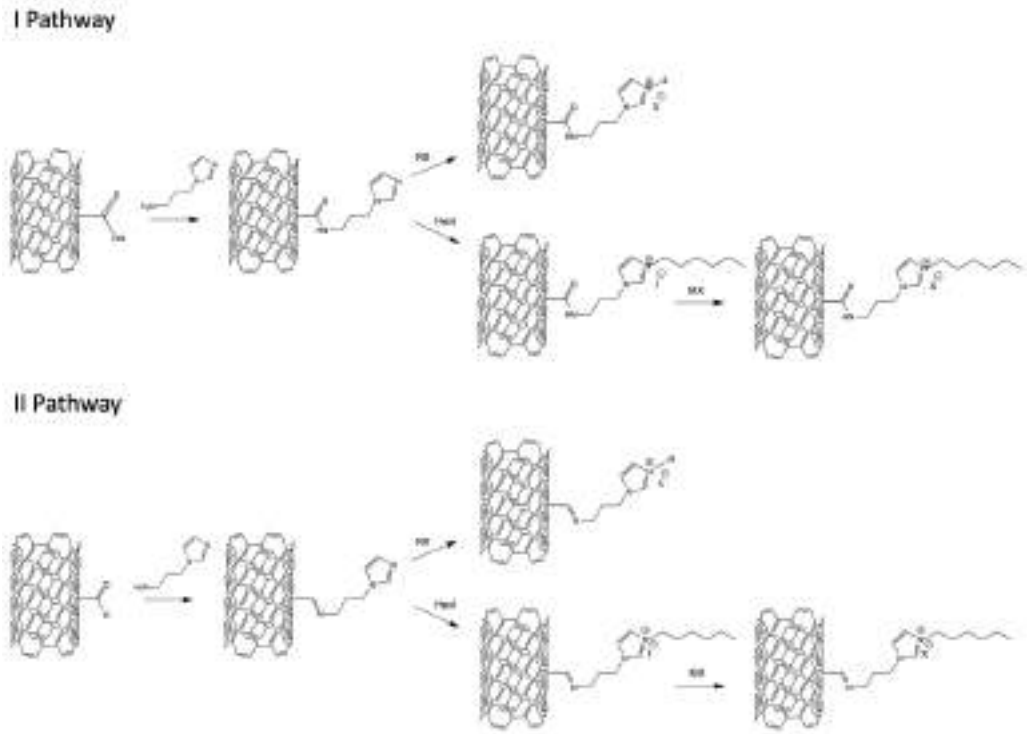

Figure 5. Scheme of MWCNTs chemical modifications with ionic liquids.

Ionic liquids were anchored via amide or imine bonds. Prepared SILLPs were tested as carriers for CALB, CRL, and *Aspergillus oryzae* lipase immobilization. Biocatalysts were used in the Baeyer–Villiger oxidation of 2-adamantanone (Figure 6). All the immobilized lipases demonstrated great activity and stability in the aggressive environment of hydrogen peroxide. Four reaction cycles, without a loss of the enzyme's activity, were performed [79].

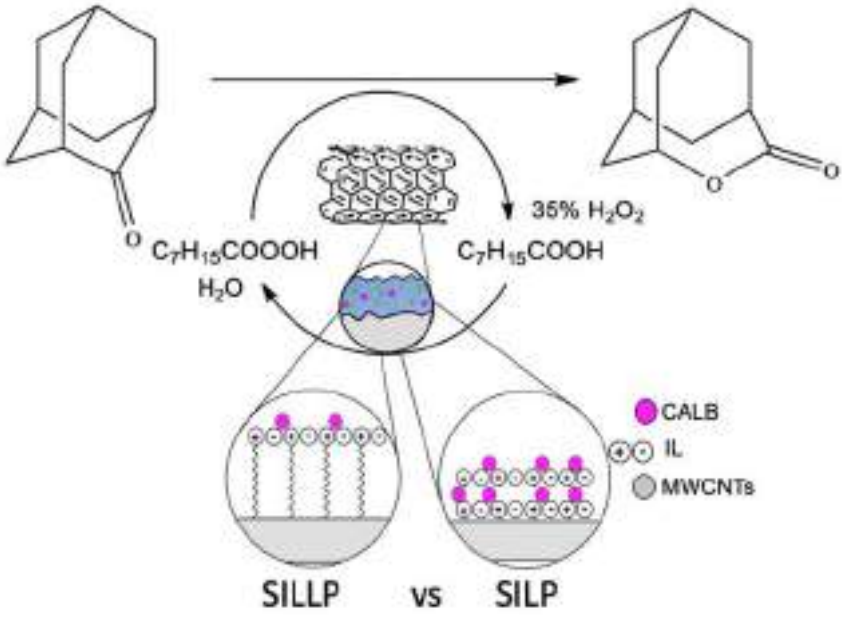

Figure 6. Scheme of Baeyer–Villiger oxidation of 2-adamantanone catalyzed by supported ionic liquid phase biocatalysts.

Silica materials are the most common group of supports used in SILP and SILLP techniques in biocatalysis. Silica mesoporous materials are characterized by ordered porosity, well-defined pore geometry, large surface area, and possibility of surface modification,

which enable high enzyme loading [80]. In the beginning of the section, the first reports about SILP based on silica materials (Celite) were described. The other approach includes supported SILLP for enzyme immobilization. PPL was adsorbed on SILLP, based on mesoporous silica SBA-15. Further, 1-methyl-3-(3-trimethoxysilyl-propyl)imidazolium tetrafluoroborate was attached onto hydroxyl groups on the silica surface via covalent bonding. The enzyme activity in triacetin hydrolysis was improved, from 594 to 975 U/g, after support modification with IL [81]. The next studies of this group focused on the influence of alkyl chain length in the SILLP' s imidazolium ring on PPL stabilization. Once more, the enzyme showed higher stability and reusability if a longer alkyl chain (C8) was presented in the SILLP structure [82]. Further studies included the effect of various functional groups, such as alkyl, amino, and carboxyl, in the IL structure, attached via covalent bonding onto the mesoporous silica, for PPL activity. Lipase was adsorbed on SILLP and examined in triacetin hydrolysis. Each synthesized SILLP improved protein activity. PPL–SILLP, consisting of IL functionalized with an amino group, expressed the highest activity, which was almost 13 times higher compared with PPL–SBA-15 [83]. Another investigation concentrated on the following different techniques for PPL immobilization: via physical adsorption and covalent bonding. For this purpose, SBA-15 was modified with IL functionalized with a carboxyl group. Both of the biocatalysts presented better stability compared with PPL–SBA-15, but lipase that was grafted into SILLP retained 81.25% of its original activity, when the lipase adsorbed on SILLP retained 52.5% after 20 days of incubation and four reaction cycles [84]. The following experiments checked PLL activity, when the lipase was attached onto the IL anion via ionic binding and cross-linking. The activity of the lipase that was immobilized on the support consisting of imidazolium IL with L-lysine anion, did not decrease after five cycles, so leaching of the enzyme was effectively inhibited [85]. The next studies of this group examined the influence of the particle type grafted into mesoporous silica, for enzyme immobilization and activity in triacetin hydrolysis. The following various supports were prepared: C1–SiO_2, C8–SiO_2, C16–SiO_2, SH–SiO_2, Ph–SiO_2, NH_2–SiO_2, CH_3IL–SiO_2 (methyl group in imidazolium ring), and COOHIL–SiO_2 (alkyl chain in imidazolium ring functionalized with carboxyl group). The best PPL immobilization efficiency characterized silicas that were modified with ILs, thiol, amino, and phenyl groups. Moreover, PPL–SILLPs exhibited the best thermal stability, pH resistance, and stability among all of the examined biocatalysts. After five cycles, the activity of PPL–SILLP, functionalized with a carboxyl group, was above 62% [86]. A comparison of PLL adsorbed on SILLP, with PLL immobilized via enzyme aggregates, coating onto SBA-15 modified with IL, was also reported. The lipase immobilized as an enzyme aggregate coating demonstrated, after 25 days of storage, 74.25% of its original activity, when PLL–SILLP was only 48% [87]. Further investigations of enhanced enzyme activity led to the increased stability of immobilized PPL via physical adsorption onto SILLP, by embedding it with microspheres of sodium alginate gel. SILLP was obtained by grafting imidazolium-based IL with $[BF4]^-$ anion into SBA-15. Novel biocatalysts showed extremely higher thermal stability at 65 °C, almost no activity lost was observed [88]. Papain enzyme was immobilized on SILLP, based on SBA-15. Ionic liquid grafted to the support provided higher papain loading (261 mg/g) than for the enzyme on SBA-15 (185 mg/g). What is more, the papain–SILLP biocatalyst presented higher activity in the case of hydrolysis than papain–SBA-15 [89]. Periodic mesoporous organosilica (PMO) combined with IL was used as a carrier for α-amylase from *Bacillus amyloliquefaciens*. PMO is an organic–inorganic material, where organic groups are ordered inside the silica's channel walls. Immobilized amylase on PMO-IL retained 88% of its initial activity after four reaction cycles, and showed two times better thermal stability at 70 °C and 80 °C compared with a native form [90]. The activity of CALB was examined in the glycerolysis of corn oil for diacylglycerol production. For that purpose, SBA-15 was modified by grafting onto a hydroxyl group of the imidazolium ring of IL, with two different anions ($[BF_4]^-$, $[PF_6]^-$) and three different alkyl chain lengths (C1, C4, C8) in the cation. The best results were obtained for the CALB–SILLP consisting of a methyl group in

the imidazolium ring and $[BF_4]^-$ anion. The activity of CALB–SILLP, in comparison with CALB–SBA-15, increased from 1855 to 5044 U/g. Hence, the enzyme exhibited a greater selectivity towards diacylglycerols synthesis, with the diacylglycerols/monoacylglycerols ratio increasing from 3.72 to 11.99, and the content of the diacylglycerols improving from 53.6 to 67.2%. Also, a retained activity of 90%, after five reaction cycles, for the CALB-SILLP biocatalyst was observed [91]. Another approach uses silica aerogels combined with ILs. BCL lipase was immobilized on the mesoporous silica aerogels that were modified with PIL (PIL–N-methylmonoethanolamine pentanoate—C5) via physical adsorption, covalent bonding, and encapsulation. A comparison of the immobilization yield on PIL-modified support for the performed techniques showed the best results for physical adsorption (83%), and the longest stability presented an encapsulated enzyme (23 reuses) in olive oil hydrolysis as the tested reaction [92]. The same SILLP support was used for BCL immobilization, and applied in ethyl ester production from coconut oil. Further, a 70% conversion was achieved for oils after 144 h at 40 °C (coconut oil:ethanol, 1:7, molar ratio), when BCL–SILLP was used [93]. BCL lipase improved the activity of various phosphonium ILs. Selected trihexyltetradecylphosphonium bis(trifluoromethylsulfonyl)amide [P666(14)][NTf_2] allowed a relative activity up to 231% and immobilization yield of 98% to be achieved. The biocatalyst kept more than 50% of its initial activity after 26 cycles. It was reported that using [P666(14)][NTf_2] during the silica support preparation and immobilization procedure significant influences the enzyme activity, stability, and immobilization yield [94].

4. Contribution of Nanomaterials to Effectiveness of Supported Ionic Liquid Phases

Nanomaterials are an attractive group of materials for supported ionic liquid phase techniques. Due to their small particle size, nanomaterials offer a larger specific surface area than conventional materials, which can improve the immobilization of the protein's particles on the support. Moreover, nanomaterials have unique mechanical, thermo-physical properties and surface morphology, which are important in immobilization methods [95,96]. The nanomaterials used in the supported ionic liquid phases, for the biocatalytic reactions described before, are summarized in Table 2.

Table 2. Nanomaterials used for supported ionic liquid phases in the biocatalysis.

Type	Nanomaterial	Ionic Liquid	Enzyme	Reaction	Ref.
SILLP	Chitosan–silica hybrid	Imidazolium $[BF_4]^-$	PLL (2482 U/g [1], 132.1 mg/g [2])	Triacetin hydrolysis 35 °C, 10 cycles	[67]
SILLP	Chitosan–Fe_3O_4 hybrid	Imidazolium $[PF_6]^-$	PPL (2879 U/g, 118 mg/g)	Triacetin hydrolysis 50 °C, 10 cycles	[68]
SILLP	Fe_3O_4	Imidazolium $[PF_6]^-$	CRL (132.3 U/g, 639 mg/g)	Oleic acid esterification 30 °C, 5 cycles	[69]
SILLP	Fe_3O_4	Imidazolium $[Cl]^-$	*Penicillin G* acylase (261 U/g, 209 mg/g)	*Penicillin G* potassium salts hydrolysis 37 °C, 10 cycles	[70]
SILLP	Fe_3O_4–silica hybrid	Imidazolium $[Cl]^-$	CRL	Palm stearin interesterification 45 °C, 4 cycles	[71]
SILLP	MWCNTs	Imidazolium $[PF_6]^-$	CALB (19,354 U/g, 96 mg/g)	Triacetin hydrolysis 60 °C, 4 cycles	[75]
SILLP	MWCNTs	Imidazolium $[PF_6]^-$	CALB (25,350 U/g, 114 mg/g)	Triacetin hydrolysis 60 °C, 4 cycles	[76]

Table 2. *Cont.*

Type	Nanomaterial	Ionic Liquid	Enzyme	Reaction	Ref.
SILLP	MWCNTs	Imidazolium $[PF_6]^-$	CALB (13,636 U/g, 66 mg/g)	Triacetin hydrolysis 60 °C, 4 cycles	[77]
SILP	MWCNTs	D-glucose based $[NTf_2]^-$	CALB (42 mg/g)	Acrylic acid esterification 25 °C, 5 cycles, Y = 99% [3]	[78]
SILLP	MWCNTs	Imidazolium $[Oc_2PO_4]^-$	CALB (64 mg/g)	2-adamantanone oxidation 20 °C, 5 cycles, α = 91% [4]	[79]
SILP	MWCNTs	Imidazolium $[NTf_2]^-$	CALB (22 mg/g)	2-adamantanone oxidation 20 °C, 4 cycles, α = 99%	[79]
SILLP	Silica	Imidazolium $[BF_4]^-$	PPL (975 U/mg)	Triacetin hydrolysis 36 °C, 5 cycles	[81]
SILLP	Silica	Imidazolium $[BF_4]^-$	PPL (975 U/mg)	Triacetin hydrolysis 35 °C, 5 cycles	[82]
SILLP	Silica	Imidazolium $[BF_4]^-$	BCL (10205 U/g, 230 mg/g)	Triacetin hydrolysis 50 °C, 3 cycles	[83]
SILLP	Silica	Imidazolium $[BF_4]^-$	PPL (720 U/g, 227.5 mg/g)	Triacetin hydrolysis 35 °C, 4 cycles	[84]
SILLP	Silica	Imidazolium L-lysine	PPL (244 U/g, 197 mg/g)	Triacetin hydrolysis 50 °C, 5 cycles	[85]
SILLP	Silica	Imidazolium $[BF_4]^-$	PPL (392 U/g, 245 mg/g)	Triacetin hydrolysis 50 °C, 5 cycles	[86]
SILLP	Silica	Imidazolium $[BF_4]^-$	PPL (760 U/g, 117 mg/g)	Triacetin hydrolysis 45 °C, 5 cycles	[87]
SILLP	Silica	Imidazolium $[BF_4]^-$	PPL (468 U/g, 186 mg/g)	Triacetin hydrolysis 45 °C, 5 cycles	[88]
SILLP	Silica	Imidazolium $[Cl]^-$	Papain (0.8 U/mg, 261 mg/g)	L-tyrosine synthesis 50 °C	[89]
SILLP	Organosilica	Imidazolium $[Cl]^-$	Amylase from *Bacillus amyloliquefaciens* (29.35 U/mg, 80 mg/g)	Starch hydrolysis 70 °C, 4 cycles	[90]
SILLP	Silica	Imidazolium $[BF_4]^-$	CALB (5044.44 U/g)	Corn oil glycerolysis 50 °C, 5 cycles, α = 70.94%	[91]
SILP	Silica aerogel	Ammonium $[C_4H_9COO]^-$	BCL (83% [5])	Olive oil hydrolysis 37 °C, 23 cycles	[92]
SILP	Silica aerogel	Ammonium $[C_4H_9COO]^-$	BCL (337 mg/g)	Coconut oil esterification 40 °C, α = 70%	[93]
SILP	Silica	Phosphonium $[NTf_2]^-$	BCL (91.1%)	Olive oil hydrolysis 37 °C, 17 cycles	[94]

[1] Specific activity of enzyme. [2] Enzyme loading on the support. [3] Yield. [4] Conversion. [5] The total activity recovery yield.

As shown in Table 2, several groups of nanomaterials that used in the supported ionic liquid phase techniques can be distinguished. Magnetite Fe_3O_4 nanoparticles are a very interesting group of nanomaterials, solving problems related to the separation of the nanobiocatalyst from the reaction mixture. The magnetite SILLP biocatalyst can be easily removed by a magnetic field. In the literature, Fe_3O_4 nanoparticles were used as a supported ionic liquid biocatalyst, as well as nanocomposites hybrids with chitosan and silica, which prevent the aggregation of magnetite nanoparticles and improve their chemical stability. Additionally, a chemically modified magnetite nanomaterial surface, with hydrophobic ionic liquids, provides high enzyme stability and prevents leaching of the enzyme. Moreover, high ionic liquid loading on magnetite nanomaterials was reported, which can be easily explained by their large surface area [68–71]. The next significant group of nanomaterials that are used as matrices in SILP/SILLP, is carbon nanotube. Immobilized on carbon nanotubes, lipases exhibit high activity, due to the hydrophobicity of the MWCNTs outermost shells. There are reports where the ionic liquid is covalently grafted, or physically adsorbed, on the MWCNTs surface, which causes the increase in hydrophobicity of the SILP or SILLP matrixes. Therefore, lipases that are immobilized on SILP and SILLP, based on carbon nanotubes, showed great activity and enzyme loading. It is worth emphasizing the interesting approach with the D-glucose-based ionic liquid used for SILP synthesis. In consequence, bio-based SILP was obtained and successfully used in esterification reactions [75–79]. The most widely used in supported ionic liquid phases is silica. The surface of the silica nanomaterials can be easily functionalized. Moreover, the porosity of silica nanoparticles increases ionic liquid loading on the surface, and so on the efficiency of enzyme immobilization. The high activity and thermal stability of the enzymes were observed after immobilization on silica-based SILLP or SILLP [67,81–94].

For all the presented examples, nanomaterials improved the ionic liquid and enzyme loading caused by the large surface area:volume ratio. All of the described nanomaterials can be functionalized, which is key for the supported ionic liquid-like phase method. Nanomaterials based on supported ionic liquid phases, enabled the activity and stability of the employed enzymes to be increased. It was due to the imidazolium ionic liquids containing long alkyl chains and proper anions grafted to the nanomaterial, which increased the hydrophobicity of the support. CALB, PPL, and BCL are the most common lipases used in nanomaterial-based SILP and SILLP. Immobilized enzymes on the nanoparticles that are modified with ionic liquids, catalyzed in hydrolysis, esterification, transesterification and oxidation reactions, provide high yields and conversions. Moreover, biocatalysts could be easy separated from the reaction mixture, especially those with magnetic properties, and used in many cycles.

5. Conclusions

In summary, the most important achievements in the use of ionic liquids for the development of heterogeneous catalysts, based on the nanomaterials for biocatalysis, were presented. The environment of the enzyme has a crucial influence on the stabilization of the protein conformation and mass-transport phenomena of products from the support. Ionic liquids play a significant role in the prevention of the enzyme against the destruction of the secondary structure and deactivation under $scCO_2$ conditions, high temperatures, and acidic or polar environments. Due to the structural integrity of ionic liquid, support and active conformation of lipase, the activity, stability, and reusability of immobilized enzymes can be improved substantially. The presence of small amounts of water in the IL increases the activity of the lipases. The authors highlighted the importance of the recycling possibility of SILP/SILLP biomaterials. Over the years, various polymer, silica, magnetic and carbon materials were used as matrixes for the supported ionic liquid phase and supported ionic liquid-like phase technique, for enzyme immobilization. The PS-DVB carrier has many advantages, such as the possibility of the design and control the morphology of the material and surface modification, to obtain desired features. It has been reported that chitin and chitosan with low surface areas can be expand via ionic

liquid modification. Among the inorganic supports, magnetic nanoparticles have a great potential, because they can be easily separated from the reaction systems by applying an external magnetic field, but the long procedure and low yield of the synthesis decreases their applications. Nanomaterials are significant matrices that provide high ionic liquid and enzyme loading on the surface. Chemical modification of the surface, in comparison with physical adsorption, requires high costs and a long term of preparation, but prevents leaching of the ionic liquid and provides longer reusability. However, for both the SILP and SILLP enzymes, leaching can appear. In all the cases, surface modification of the support, with ionic liquids, is key, because it can make significant improvements in the surface properties, as well as activity and stability of the enzymes. The physical, chemical, and morphological modifications of the support, with ionic liquids, minimize the leaching of the active phase and improve the catalytic activity for continuous and discontinuous processes. The presented reports showed that SILP and SILLP for enzyme immobilization, have a great application potential in biocatalysis.

Author Contributions: Conceptualization, A.C. and A.W.; literature survey A.W.; writing—original draft preparation, A.W.; writing—review and editing, A.C. and A.W.; visualization, A.W.; supervision, A.C. All authors have read and agreed to the published version of the manuscript.

Funding: This research was funded by Silesian University of Technology (Poland), grant No. 04/050/BKM21/0133.

Data Availability Statement: Data sharing is not applicable for this article.

Conflicts of Interest: The authors declare no conflict of interest. The funders had no role in the design of the study; in the writing of the manuscript, or in the decision to publish.

References

1. Scheldon, R.A. The E factor 25 years on: The rise of green chemistry and sustainability. *Green Chem.* **2017**, *19*, 18–43. [CrossRef]
2. Gottardo, S.; Mech, A.; Riego, S.; Sintes, J.; Rauscher, H.; Drbohlavova, J.; Malyska, A.; Bowadt, S. Towards safe and sustainable in-novation in nanotechnology: State-of-play for smart nanomaterials. *NanoImpact* **2021**, *21*, 100297. [CrossRef]
3. Sheldon, R.A.; Arends, I.; Hanefeld, U. *Green Chemistry and Catalysis*; Wiley-VCH Verlag GmbH: Berlin, Germany, 2020.
4. Scheldon, R.A.; Woodley, J.M. Role of biocatalysis in sustainable chemistry. *Chem. Rev.* **2018**, *118*, 801–838. [CrossRef]
5. Fernandez-Lafuente, R. Enzyme immobilization and its applications. *Molecules* **2019**, *24*, 4619. [CrossRef]
6. Mohamad, N.R.; Marzuki, N.H.C.; Buang, N.A.; Huyop, F.; Wahab, R.A. An overview of technologies for immobilization of enzymes and surface analysis techniques for immobilized enzymes. *Biotechnol. Biotec. Eq.* **2015**, *29*, 205–220. [CrossRef] [PubMed]
7. Moehlenbrock, M.J.; Minteer, S.D. Introduction to the field of enzyme immobilization and stabilization. *Methods Mol. Biol.* **2016**, 1–7. [CrossRef]
8. Weiser, D.; Sóti, P.L.; Bánóczi, G.; Bódai, V.; Kiss, B.; Gellért, Á.; Nagy, Z.K.; Koczka, B.; Szilagyi, A.; Marosi, G.; et al. Bioimprinted lipases in PVA nanofibers as efficient immobilized biocatalysts. *Tetrahedron* **2016**, *72*, 7335–7342. [CrossRef]
9. Fotiadou, R.; Patila, M.; Hammami, M.A.; Enotiadis, A.; Moschovas, D.; Tsirka, K.; Spyrou, K.; Giannelis, E.P.; Avgeropoulos, A.; Paipetis, A.; et al. Development of effective lipase-hybrid nanoflowers enriched with carbon and magnetic nanomaterials for biocatalytic transformations. *Nanomaterials* **2019**, *9*, 808. [CrossRef] [PubMed]
10. Prabhavathi Devi, B.L.A.; Guo, Z.; Xu, X. Characterization of cross-linked lipase aggregates. *J. Am. Oil Chem. Soc.* **2009**, *86*, 637–642. [CrossRef]
11. Liu, P.; Liu, X.; An, N.; Wang, P. Synthesis of mesoporous silica nanowires and their application in enzyme immobilization. *E3S Web Conf.* **2021**, *245*. [CrossRef]
12. Drożdż, A.; Chrobok, A.; Baj, S.; Szymańska, K.; Mrowiec-Białoń, J.; Jarzębski, A.B. The chemo-enzymatic Baeyer–Villiger oxidation of cyclic ketones with an efficient silica-supported lipase as a biocatalyst. *Appl. Catal. A Gen.* **2013**, *467*, 163–170. [CrossRef]
13. Jiang, Y.; Guo, C.; Gao, H.; Xia, H.; Mahmood, I.; Liu, C.; Liu, H. Lipase immobilization on ionic liquid-modified magnetic nanoparticles: Ionic liquids controlled esters hydrolysis at oil-water interface. *AIChE J.* **2011**, *58*, 1203–1211. [CrossRef]
14. Suo, H.; Xu, L.; Xu, C.; Qiu, X.; Huang, H.; Hu, Y. Enhanced catalytic performance of lipase covalently bonded on ionic liquids modified magnetic alginate composites. *J. Colloid Interf. Sci.* **2019**, *553*, 494–502. [CrossRef]
15. Suo, H.; Xu, L.; Xue, Y.; Qiu, X.; Huang, H.; Hu, Y. Ionic liquids-modified cellulose coated magnetic nanoparticles for enzyme immobilization: Improvement of catalytic performance. *Carbohydr. Polym.* **2020**, *234*, 115914. [CrossRef]
16. Carvalho, N.; Vidal, B.; Barbosa, A.; Pereira, M.; Mattedi, S.; Freitas, L.; Lima, A.S.; Soares, C. Lipase immobilization on silica xerogel treated with protic ionic liquid and its application in biodiesel production from different oils. *Int. J. Mol. Sci.* **2018**, *19*, 1829. [CrossRef] [PubMed]

17. Mutschler, J.; Rausis, T.; Bourgeois, J.-M.; Bastian, C.; Zufferey, D.; Mohrenz, I.V.; Fischer, F. Ionic liquid-coated immobilized lipase for the synthesis of methylglucose fatty acid esters. *Green Chem.* **2009**, *11*, 1793. [CrossRef]
18. He, Y.; Li, J.-J.; Luo, Y.-K.; Song, F.; Wang, X.-L.; Wang, Y.-Z. Coating Novozyme435 with an ionic liquid: More than just a coating for the efficient ring-opening polymerization of δ-valerolactone. *RSC Adv.* **2015**, *5*, 68276–68282. [CrossRef]
19. Wu, C.; Zhang, Z.; Chen, C.; He, F.; Zhuo, R. Synthesis of poly(ε-caprolactone) by an immobilized lipase coated with ionic liquids in a solvent-free condition. *Biotechnol. Lett.* **2013**, *35*, 1623–1630. [CrossRef]
20. Qiu, X.; Wang, S.; Miao, S.; Suo, H.; Xu, H.; Hu, Y. Co-immobilization of Laccase and ABTS onto amino-functionalized ionic liquid-modified magnetic chitosan nanoparticles for pollutants removal. *J. Hazard. Mater.* **2020**, 123353. [CrossRef]
21. Liu, X.; Bu, C.; Nan, Z.; Zheng, L.; Qiu, Y.; Lu, X. Enzymes immobilized on amine-terminated ionic liquid-functionalized carbon nanotube for hydrogen peroxide determination. *Talanta* **2013**, *105*, 63–68. [CrossRef]
22. Brondani, D.; Zapp, E.; Vieira, I.C.; Dupont, J.; Scheeren, C.W. Gold nanoparticles in an ionic liquid phase supported in a biopolymeric matrix applied in the development of a rosmarinic acid biosensor. *Analyst* **2011**, *136*, 2495. [CrossRef]
23. Abdelrahim, M.Y.M.; Martins, C.F.; Neves, L.A.; Capasso, C.; Supuran, C.T.; Coelhoso, I.M.; Crespo, J.G.; Barboiu, M. Supported ionic liquid membranes immobilized with carbonic anhydrases for CO_2 transport at high temperatures. *J. Membr. Sci.* **2017**, *528*, 225–230. [CrossRef]
24. Lozano, P.; Diego, T.; de Carrié, D.; Vaultier, M.; Iborra, J.L. Continuous green biocatalytic processes using ionic liquids and supercritical carbon dioxide. *Chem. Commun.* **2002**, *7*, 692–693. [CrossRef] [PubMed]
25. Lozano, P.; De Diego, T.; Carrie, D.; Vaultier, M.; Iborra, J.L. Lipase catalysis in ionic liquids and supercritical carbon dioxide at 150 °C. *Biotechnol. Prog.* **2003**, *19*, 380–382. [CrossRef]
26. Sandig, B.; Michalek, L.; Vlahovic, S.; Antonovici, M.; Hauer, B.; Buchmeiser, M.R. A Monolithic hybrid cellulose-2.5-Acetate/polymer bioreactor for biocatalysis under continuous liquid-liquid conditions using a supported ionic liquid phase. *Chem. Eur. J.* **2015**, *21*, 15835–15842. [CrossRef] [PubMed]
27. Lozano, P.; García-Verdugo, E.; Piamtongkam, R.; Karbass, N.; De Diego, T.; Burguete, M.I.; Luis, S.V.; Iborra, J.L. Bioreactors based on monolith-supported ionic liquid phase for enzyme catalysis in supercritical carbon dioxide. *Adv. Synth. Catal.* **2007**, *349*, 1077–1084. [CrossRef]
28. Izquierdo, D.F.; Bernal, J.M.; Burguete, M.I.; García-Verdugo, E.; Lozano, P.; Luis, S.V. An efficient microwave-assisted enzymatic resolution of alcohols using a lipase immobilised on supported ionic liquid-like phases (SILLPs). *RSC Adv.* **2013**, *3*, 13123. [CrossRef]
29. Lozano, P.; García-Verdugo, E.; Bernal, J.M.; Izquierdo, D.F.; Burguete, M.I.; Sánchez-Gómez, G.; Luis, S.V. Immobilised lipase on structured supports containing covalently attached ionic liquids for the continuous synthesis of biodiesel in $scCO_2$. *ChemSusChem* **2012**, *5*, 790–798. [CrossRef] [PubMed]
30. Domínguez de María, P. *Ionic Liquids in Biotransformations and Organocatalysis: Solvents and Beyond*; John Wiley & Sons, Inc.: Hoboken, NJ, USA, 2012; pp. 1–435.
31. Garcia-Verdugo, E.; Lozano, P.; Luis, S.V. Biocatalytic Processes Based on Supported Ionic Liquids. In *Supported Ionic Liquids: Fundamental and Applications*, 1st ed.; Fehrmann, R., Riisager, A., Haumann, M., Eds.; Wiley-VCH Verlag GmbH: Berlin, Germany, 2014; pp. 351–368.
32. García-Verdugo, E.; Altava, B.; Burguete, M.I.; Lozano, P.; Luis, S.V. Ionic liquids and continuous flow processes: A good marriage to design sustainable processes. *Green Chem.* **2015**, *17*, 2693–2713. [CrossRef]
33. Potdar, M.; Kelso, G.; Schwarz, L.; Zhang, C.; Hearn, M. Recent developments in chemical synthesis with biocatalysts in ionic liquids. *Molecules* **2015**, *20*, 16788–16816. [CrossRef]
34. Vekariya, R.L. A review of ionic liquids: Applications towards catalytic organic transformations. *J. Mol. Liq.* **2017**, *227*, 44–60. [CrossRef]
35. Amarasekara, A.S. Acidic Ionic Liquids. *Chem. Rev.* **2016**, *116*, 6133–6183. [CrossRef]
36. Greer, A.J.; Jacquemin, J.; Hardacre, C. Industrial applications of ionic liquids. *Molecules* **2020**, *25*, 5207. [CrossRef]
37. Matuszek, K.; Chrobok, A.; Latos, P.; Markiton, M.; Szymańska, K.; Jarzębski, A.; Swadźba-Kwaśny, M. Silica-supported chlorometallate(iii) ionic liquids as recyclable catalysts for Diels–Alder reaction under solventless conditions. *Catal. Sci. Technol.* **2016**, *6*, 8129–8137. [CrossRef]
38. Zhang, W.; Luo, J.; Sun, T.; Yu, F.; Li, C. The absorption performance of ionic liquids–PEG200 complex absorbent for VOCs. *Energies* **2021**, *14*, 3592. [CrossRef]
39. Bajkacz, S.; Rusin, K.; Wolny, A.; Adamek, J.; Erfurt, K.; Chrobok, A. Highly efficient extraction procedures based on natural deep eutectic solvents or ionic liquids for determination of 20-Hydroxyecdysone in Spinach. *Molecules* **2020**, *25*, 4736. [CrossRef]
40. Moniruzzaman, M.; Kamiya, N.; Goto, M. Activation and stabilization of enzymes in ionic liquids. *Org. Biomol. Chem.* **2010**, *8*, 2887. [CrossRef] [PubMed]
41. Szelwicka, A.; Chrobok, A. Methods for increasing activity and stability of enzymes in processes carried out in presence of ionic liquids. *Przem. Chem.* **2018**, *97*, 89–93. [CrossRef]
42. Lee, S.H.; Doan, T.T.N.; Ha, S.H.; Chang, W.-J.; Koo, Y.-M. Influence of ionic liquids as additives on sol–gel immobilized lipase. *J. Mol. Catal. B Enzym.* **2007**, *47*, 129–134. [CrossRef]
43. Shah, S.; Gupta, M.N. Kinetic resolution of (±)-1-phenylethanol in [Bmim][PF6] using high activity preparations of lipases. *Bioorg. Med. Chem. Lett.* **2007**, *17*, 921–924. [CrossRef]

44. Moniruzzaman, M.; Kamiya, N.; Nakashima, K.; Goto, M. Water-in-ionic liquid microemulsions as a new medium for enzymatic reactions. *Green Chem.* **2008**, *10*, 497. [CrossRef]
45. Lozano, P.; Piamtongkam, R.; Kohns, K.; Diego, T.D.; Vaultier, M.; Iborra, J.L. Ionic liquids improve citronellyl ester synthesis catalyzed by immobilized Candida antarctica lipase B in solvent-free media. *Green Chem.* **2007**, *9*, 780. [CrossRef]
46. Itoh, T. Ionic liquids as tool to improve enzymatic organic synthesis. *Chem. Rev.* **2017**, *117*, 10567–10607. [CrossRef]
47. Zhao, H. Methods for stabilizing and activating enzymes in ionic liquids—A review. *J. Chem. Technol. Biotechnol.* **2010**, *85*, 891–907. [CrossRef]
48. De Los Ríos, A.P.; Hernández-Fernández, F.J.; Martínez, F.A.; Rubio, M.; Víllora, G. The effect of ionic liquid media on activity, selectivity and stability of Candida antarcticalipase B in transesterification reactions. *Biocatal. Biotransform.* **2007**, *25*, 151–156. [CrossRef]
49. Nara, S.J.; Harjani, J.R.; Salunkhe, M.M. Lipase-catalysed transesterification in ionic liquids and organic solvents: A comparative study. *Tetrahedron Lett.* **2002**, *43*, 2979–2982. [CrossRef]
50. Nakashima, K.; Okada, J.; Maruyama, T.; Kamiya, N.; Goto, M. Activation of lipase in ionic liquids by modification with comb-shaped poly(ethylene glycol). *Sci. Technol. Adv. Mater.* **2006**, *7*, 692–698. [CrossRef]
51. Zhang, W.-G.; Wei, D.-Z.; Yang, X.-P.; Song, Q.-X. Penicillin acylase catalysis in the presence of ionic liquids. *Bioprocess Biosyst. Eng.* **2006**, *29*, 379–383. [CrossRef] [PubMed]
52. Park, S.; Kazlauskas, R.J. Improved preparation and use of room-temperature ionic liquids in lipase-catalyzed enantio- and regioselective acylations. *J. Org. Chem.* **2001**, *66*, 8395–8401. [CrossRef] [PubMed]
53. De Diego, T.; Lozano, P.; Abad, M.A.; Steffensky, K.; Vaultier, M.; Iborra, J.L. On the nature of ionic liquids and their effects on lipases that catalyze ester synthesis. *J. Biotechnol.* **2009**, *140*, 234–241. [CrossRef]
54. Turner, M.B.; Spear, S.K.; Huddleston, J.G.; Holbrey, J.D.; Rogers, R.D. Ionic liquid salt-induced inactivation and unfolding of cellulase from Trichoderma reesei. *Green Chem.* **2003**, *5*, 443. [CrossRef]
55. Lee, S.H.; Ha, S.H.; Lee, S.B.; Koo, Y.-M. Adverse effect of chloride impurities on lipase-catalyzed transesterifications in ionic liquids. *Biotechnol. Lett.* **2006**, *28*, 1335–1339. [CrossRef] [PubMed]
56. Lozano, P.; deDiego, T.; Gmouh, S.; Vaultier, M.; Iborra, J.L. Criteria to design green enzymatic processes in ionic liquid/supercritical carbon dioxide systems. *Biotechnol. Prog.* **2004**, *20*, 661–669. [CrossRef]
57. Lozano, P. Synthesis of glycidyl esters catalyzed by lipases in ionic liquids and supercritical carbon dioxide. *J. Mol. Catal. A Chem.* **2004**, *214*, 113–119. [CrossRef]
58. Rodrigues, R.C.; Hernandez, K.; Barbosa, O.; Rueda, N.; Garcia-Galan, C.; dosSantos, J.C.S.; Berenguer-Murcia, A.; Fernandez-Lafuente, R. Immobilization of proteins in poly-styrene-divinylbenzene matrices: Functional properties and applications. *Curr. Org. Chem.* **2015**, *19*, 1707–1718. [CrossRef]
59. Lozano, P.; De Diego, T.; Mira, C.; Montague, K.; Vaultier, M.; Iborra, J.L. Long term continuous chemoenzymatic dynamic kinetic resolution of rac-1-phenylethanol using ionic liquids and supercritical carbon dioxide. *Green Chem.* **2009**, *11*, 538. [CrossRef]
60. Lozano, P.; García-Verdugo, E.; Karbass, N.; Montague, K.; De Diego, T.; Burguete, M.I.; Luis, S.V. Supported ionic liquid-like phases (SILLPs) for enzymatic processes: Continuous KR and DKR in SILLP–scCO$_2$ systems. *Green Chem.* **2010**, *12*, 1803. [CrossRef]
61. Izquierdo, D.F.; Yates, M.; Lozano, P.; Burguete, M.I.; García-Verdugo, E.; Luis, S.V. Macroporous polymers tailored as supports for large biomolecules: Ionic liquids as porogenic solvents and as surface modifiers. *React. Funct. Polym.* **2014**, *85*, 20–27. [CrossRef]
62. Kim, H.; Hassouna, F.; Muzika, F.; Arabacı, M.; Kopecký, D.; Sedlářová, I.; Šoóš, M. Urease adsorption immobilization on ionic liquid-like macroporous polymeric support. *J. Mater. Sci.* **2019**, *54*, 14884–14896. [CrossRef]
63. Porcar, R.; Lavandera, I.; Lozano, P.; Altava, B.; Luis, S.V.; Gotor-Fernández, V.; García-Verdugo, E. Supported ionic liquid-like phases as efficient solid ionic solvent for the immobilisation of alcohol dehydrogenases towards the development of stereoselective bioreductions. *Green Chem.* **2021**. [CrossRef]
64. Sandig, B.; Buchmeiser, M.R. Highly productive and enantioselective enzyme catalysis under continuous supported liquid-liquid conditions using a hybrid monolithic bioreactor. *ChemSusChem* **2016**, *9*, 2917–2921. [CrossRef]
65. Lee, C.; Sandig, B.; Buchmeiser, M.R.; Haumann, M. Supported ionic liquid phase (SILP) facilitated gas-phase enzyme catalysis–CALB catalyzed transesterification of vinyl propionate. *Catal. Sci. Technol.* **2018**, *8*, 2460–2466. [CrossRef]
66. Jaworska, M.M.; Stepniak, I.; Galiński, M.; Kasprzak, D.; Biniaś, D.; Górak, A. Modification of chitin structure with tailored ionic liquids. *Carbohydr. Polym.* **2018**, *202*, 397–403. [CrossRef] [PubMed]
67. Xiang, X.; Ding, S.; Suo, H.; Xu, C.; Gao, Z.; Hu, Y. Fabrication of chitosan-mesoporous silica SBA-15 nanocomposites via functional ionic liquid as the bridging agent for PPL immobilization. *Carbohydr. Polym.* **2018**, *182*, 245–253. [CrossRef] [PubMed]
68. Suo, H.; Xu, L.; Xu, C.; Chen, H.; Yu, D.; Gao, Z.; Huang, H.; Hu, Y. Enhancement of catalytic performance of porcine pancreatic lipase immobilized on functional ionic liquid modified Fe_3O_4-chitosan nanocomposites. *Int. J. Biol. Macromol.* **2018**, *119*, 624–632. [CrossRef] [PubMed]
69. Jiang, Y.; Guo, C.; Xia, H.; Mahmood, I.; Liu, C.; Liu, H. Magnetic nanoparticles supported ionic liquids for lipase immobilization: Enzyme activity in catalyzing esterification. *J. Mol. Catal. B Enzym.* **2009**, *58*, 103–109. [CrossRef]
70. Zhou, H.; Li, W.; Shou, Q.; Gao, H.; Xu, P.; Deng, F.; Liu, H. Immobilization of Penicillin G Acylase on magnetic nanoparticles modified by ionic liquids. *Chin. J. Chem. Eng.* **2012**, *20*, 146–151. [CrossRef]

71. Xie, W.; Zang, X. Lipase immobilized on ionic liquid-functionalized magnetic silica composites as a magnetic biocatalyst for production of trans -free plastic fats. *Food Chem.* **2018**, *257*, 15–22. [CrossRef]
72. Iwanow, M.; Gärtner, T.; Sieber, V.; König, B. Activated carbon as catalyst support: Precursors, preparation, modification and characterization. *Beilstein J. Org. Chem.* **2020**, *16*, 1188–1202. [CrossRef]
73. Hara, P.; Mikkola, J.-P.; Murzin, D.Y.; Kanerva, L.T. Supported ionic liquids in Burkholderia cepacia lipase-catalyzed asymmetric acylation. *J. Mol. Catal. B Enzym.* **2010**, *67*, 129–134. [CrossRef]
74. Eatemadi, A.; Daraee, H.; Karimkhanloo, H.; Kouhi, M.; Zarghami, N.; Akbarzadeh, A.; Abasi, M.; Hanifehpour, Y.; Joo, S. Carbon nanotubes: Properties, synthesis, purification, and medical applications. *Nanoscale Res. Lett.* **2014**, *9*, 393. [CrossRef]
75. Wan, X.; Tang, S.; Xiang, X.; Huang, H.; Hu, Y. Immobilization of Candida antarctic Lipase B on functionalized ionic liquid modified MWNTs. *Appl. Biochem. Biotechnol.* **2017**, *183*, 807–819. [CrossRef]
76. Wan, X.; Xiang, X.; Tang, S.; Yu, D.; Huang, H.; Hu, Y. Immobilization of Candida antarctic lipase B on MWNTs modified by ionic liquids with different functional groups. *Colloid Surf. B* **2017**, *160*, 416–422. [CrossRef]
77. Xiang, X.; Wan, X.; Suo, H.; Hu, Y. Study of surface modifications of multiwalled carbon nanotubes by functionalized ionic liquid to immobilize Candida antarctic lipase B. *Acta Phys. Chim. Sin.* **2018**, *34*, 99–107. [CrossRef]
78. Szelwicka, A.; Erfurt, K.; Jurczyk, S.; Boncel, S.; Chrobok, A. Outperformance in Acrylation: Supported D-glucose-based ionic liquid phase on MWCNTs for immobilized lipase B from Candida antarctica as catalytic system. *Materials* **2021**, *14*, 3090. [CrossRef] [PubMed]
79. Szelwicka, A.; Wolny, A.; Grymel, M.; Jurczyk, S.; Boncel, S.; Chrobok, A. Chemo-enzymatic Baeyer–Villiger oxidation facilitated with lipases immobilized in the supported ionic liquid phase. *Materials* **2021**, *14*, 3443. [CrossRef]
80. Costantini, A.; Califano, V. Lipase immobilization in mesoporous silica nanoparticles for biofuel production. *Catalysts* **2021**, *11*, 629. [CrossRef]
81. Zou, B.; Hu, Y.; Yu, D.; Xia, J.; Tang, S.; Liu, W.; Huang, H. Immobilization of porcine pancreatic lipase onto ionic liquid modified mesoporous silica SBA-15. *Biochem. Eng. J.* **2010**, *53*, 150–153. [CrossRef]
82. Zou, B.; Hu, Y.; Yu, D.; Jiang, L.; Liu, W.; Song, P. Functionalized ionic liquid modified mesoporous silica SBA-15: A novel, designable and efficient carrier for porcine pancreas lipase. *Colloid Surf. B* **2011**, *88*, 93–99. [CrossRef] [PubMed]
83. Hu, Y.; Tang, S.; Jiang, L.; Zou, B.; Yang, J.; Huang, H. Immobilization of Burkholderia cepacia lipase on functionalized ionic liquids modified mesoporous silica SBA-15. *Process Biochem.* **2012**, *47*, 2291–2299. [CrossRef]
84. Yang, J.; Hu, Y.; Jiang, L.; Zou, B.; Jia, R.; Huang, H. Enhancing the catalytic properties of porcine pancreatic lipase by immobilization on SBA-15 modified by functionalized ionic liquid. *Biochem. Eng. J.* **2013**, *70*, 46–54. [CrossRef]
85. Zou, B.; Hu, Y.; Jiang, L.; Jia, R.; Huang, H. Mesoporous material SBA-15 modified by amino acid ionic liquid to immobilize lipase via ionic bonding and cross-linking method. *Ind. Eng. Chem. Res.* **2013**, *52*, 2844–2851. [CrossRef]
86. Zou, B.; Hu, Y.; Cui, F.; Jiang, L.; Yu, D.; Huang, H. Effect of surface modification of low cost mesoporous SiO_2 carriers on the properties of immobilized lipase. *J. Colloid Interface Sci.* **2014**, *417*, 210–216. [CrossRef] [PubMed]
87. Zou, B.; Song, C.; Xu, X.; Xia, J.; Huo, S.; Cui, F. Enhancing stabilities of lipase by enzyme aggregate coating immobilized onto ionic liquid modified mesoporous materials. *Appl. Surf. Sci.* **2014**, *311*, 62–67. [CrossRef]
88. Zou, B.; Chu, Y.; Xia, J.; Chen, X.; Huo, S. Immobilization of lipase by ionic liquid-modified mesoporous SiO_2 adsorption and calcium alginate-embedding method. *Appl. Biochem. Biotechnol.* **2018**, *185*, 606–618. [CrossRef] [PubMed]
89. Bian, W.; Yan, B.; Shi, N.; Qiu, F.; Lou, L.-L.; Qi, B.; Liu, S. Room temperature ionic liquid (RTIL)-decorated mesoporous silica SBA-15 for papain immobilization: RTIL increased the amount and activity of immobilized enzyme. *Mater. Sci. Eng. C* **2012**, *32*, 364–368. [CrossRef]
90. Khademy, M.; Karimi, B.; Zareian, S. Ionic liquid-based periodic mesoporous organosilica: An innovative matrix for enzyme immobilization. *Chem. Sel.* **2017**, *2*, 9953–9957. [CrossRef]
91. Zhong, N.; Li, Y.; Cai, C.; Gao, Y.; Liu, N.; Liu, G.; Tan, W.; Zeng, Y. Enhancing the catalytic performance of Candida antarctica lipase B by immobilization onto the ionic liquids modified SBA-15. *Eur. J. Lipid. Sci. Tech.* **2018**, *120*, 1700357. [CrossRef]
92. Barbosa, A.S.; Lisboa, J.A.; Silva, M.A.O.; Carvalho, N.B.; Pereira, M.M.; Fricks, A.T.; Mattedi, S.; Lima, A.S.; Franceschi, E.; Soares, C.M.F. The novel mesoporous silica aerogel modified with protic ionic liquid for lipase immobilization. *Quim. Nova.* **2016**, *39*, 415–422. [CrossRef]
93. Lisboa, M.C.; Rodrigues, C.A.; Barbosa, A.S.; Mattedi, S.; Freitas, L.S.; Mendes, A.A.; Dariva, C.; Franceschi, E.; Lima, A.S.; Soares, C.M.F. New perspectives on the modification of silica aerogel particles with ionic liquid applied in lipase immobilization with platform in ethyl esters production. *Process Biochem.* **2018**, *75*, 157–165. [CrossRef]
94. Barbosa, M.; Santos, A.; Carvalho, N.B.; Figueiredo, R.; Pereira, M.M.; Lima, Á.S.; Freire, M.G.; Cabrera-Padilla, R.Y.; Soares, C.M.F. Enhanced activity of immobilized lipase by phosphonium-based ionic liquids used in the supports preparation and immobilization process. *ACS Sustain. Chem. Eng.* **2019**, *7*, 15648–15659. [CrossRef]
95. Philippot, K.; Serp, P. Concepts in Nanocatalysis. In *Nanomaterials in Catalysis*; Wiley-VCH Verlag GmbH & Co. KGaA: Berlin, Germany, 2012; pp. 1–54. [CrossRef]
96. Gupta, M.N.; Kaloti, M.; Kapoor, M.; Solanki, K. Nanomaterials as matrices for enzyme immobilization. *Artif. Cells Blood Substit. Immobil. Biotechnol.* **2010**, *39*, 98–109. [CrossRef]

Current Organic Chemistry, 2023, *27*, 1119-1122

COMMENTARY

Supported Ionic Liquid Phase for Biocatalysis: The Current Applications, Synthesis and Prospects

Anna Wolny[1] and Anna Chrobok[1,*]

[1]*Department of Chemical Organic Technology and Petrochemistry, Faculty of Chemistry, Silesian University of Technology, Krzywoustego 4, Gliwice 44-100, Poland*

ARTICLE HISTORY

Received: June 30, 2023
Revised: August 06, 2023
Accepted: August 23, 2023

DOI:
10.2174/0113852728269911231003072822

Abstract: In this work, the potential of supported ionic liquids-based biocatalysts was presented. Efforts are underway to identify suitable carrier matrices for biocatalytic reactions, considering the crucial role of surface morphology. Factors such as mechanical and thermal properties, surface area, pore volume, density, and functionalization potential are being carefully considered during selection. The correlation between carrier, enzyme, and il structures highlights the importance of constructing biocatalysts with exceptional catalytic activity. Enzymes immobilized on silp/sillp carriers generally exhibit enhanced activity compared to the native protein. Silp-type carriers improve process efficiency, enable easy separation and recycling of biocatalysts, and prolong the protein's lifespan.

Keywords: Biocatalysis, SILP/SILLP, implementation of ionic liquids (ILs), CALB, morphology, catalylic activity.

1. INTRODUCTION

The progress of organic biotransformations plays a crucial role in advancing chemical technologies. The incorporation of enzymatic processes contributes to improving environmental factors, resulting in more sustainable technology aligned with the goals outlined in the 2030 Agenda for Sustainable Development [1, 2]. Biocatalysts offer notable benefits, such as enhanced process enantioselectivity, conversion, yield, and the capability to function under mild reaction conditions despite their poor stability [3]. However, considerable progress has been made in the development of protein stabilization techniques, with immobilization emerging as a particularly notable method. Immobilization of enzymes involves embedding them on a solid support through physical forces (*e.g.,* hydrogen bonds, ionic interactions) or chemical bonds. Native protein immobilization usually improves both activity and thermal and mechanical stability. Additionally, heterogenization of the biocatalyst enables effortless separation and recycling [4]. In addition to immobilization methods, an interesting and efficient approach is the implementation of ionic liquids (ILs) to increase enzyme stability. The presence of ILs significantly enhances the activity of enzymes by effectively stabilizing the protein's folded 3-D structure and maintaining its active conformation [5]. The application of ILs offers a noteworthy advantage in terms of structural design flexibility, allowing for the customization of desired properties [6]. The most popular species forming ILs used as enzyme stabilizers are quaternary nitrogen cations, such as alkylammonium or dialkylimidazolium, and anions, such as dialkylphosphate or bis(trifluoromethanesulfonyl)imide (triflimide) [7, 8]. The integration of both stabilization techniques, using a solid matrix and ILs, into a single material is known as the supported ionic liquid phase (SILP) and is highlighted as a sustainable method [9]. In 2002, Lozano *et al.* initiated research on biocatalytic systems utilizing the SILP technique. They immobilized 1-alkyl-3-methylimidazolium triflimide on a solid adsorbent (Celite) and successfully applied it in the continuous synthesis of butyl butyrate and the kinetic resolution of 1-phenylethanol under supercritical CO_2 conditions. The results showed high enantioselectivity (99.9%) [10]. In recent years, Garcia-Verdugo *et al.* have examined the impact of ILs in SILP/SILLP matrices on enzyme activity in organic transformations [9]. Furthermore, their subsequent publication focused on the applications of SILP/SILLP biocatalysts in continuous flow processes [11]. Next, Lozano *et al.* provided a comprehensive overview of enzymatic continuous flow processes involving ILs and supercritical fluids [12]. In a separate review, Wolny *et al.* explored the materials and nanomaterials utilized in the SILP/SILLP technique for enzyme immobilization and their applications in organic synthesis [8]. The main objective of this work is to offer a concise summary of past accomplishments while also emphasizing the future prospects in this area of research.

2. SUPPORTED IONIC LIQUID PHASE

The immobilization of IL leads to the creation of a thin IL layer on the surface of the matrix. The main advantages of applying SILP techniques for biocatalysis include the reduction of the amount of IL employed in the process, the generation of fewer waste products, the ease of IL recycling, and the enhancement of mass transfer efficiency. The covalent bonding of IL into the support is known as the supported ionic liquid-like phase (SILLP) and prevents its leaching from the surface during the process. Silica, carbon materials, and polymers are the most extensively utilized carriers for IL immobilization [8, 9].

Another approach involves the physical immobilization of ILs, which is commonly favored due to its straightforward implementation and cost-effectiveness. A range of materials, such as silica [13], multiwalled carbon nanotubes [14], and monolithic cellulose-2.5-acetate/polyurethane hybrid [15], have been employed for the ad-

*Address correspondence to this author at the Department of Chemical Organic Technology and Petrochemistry, Faculty of Chemistry, Silesian University of Technology, Krzywoustego 4, Gliwice 44-100, Poland;
E-mail: anna.chrobok@polsl.pl

1875-5348/23

sorption of various ILs, resulting in the formation of SILP materials. However, a limitation lies in the potential for relatively easy leaching of IL from the solid surface. An innovative approach involves the implementation of low-toxic and readily biodegradable ILs based on trialkylammonium cations modified with D-glucose in the SILP technique. The exceptional ability of sugar ILs to form strong hydrogen bonds plays a crucial role in effectively stabilizing the active conformation of enzymes [14].

In chemical immobilization, IL moieties can be directly attached to the solid matrix or partially built up on the surface by modifying the functional groups already present in the matrix. As an illustration, the direct bonding of 1-methyl-3-(triethoxysilylpropyl)imidazolium-based IL to hydroxyl groups on the silica surface leads to the formation of SILLP carriers (Fig. **1A**) [16]. An additional example demonstrates that the hydroxyl groups present on the surface of carbon nanotubes can undergo oxidation to form carboxyl groups, which can subsequently react with 1-(3-aminopropyl)imidazole, resulting in the formation of an amide bond. The subsequent quaternization of the amine using alkyl chlorides enables the direct formation of ILs on the surface of carbon nanotubes (Fig. **1B**) [17]. It is also feasible to synthesize polymeric structures incorporating alkyl chloride groups, which can then be quaternized with imidazolium species to obtain SILLP materials (Fig. **1C**) [18]. The exemplary structures of SILLP materials are presented in Fig. (**1**).

Once a suitable SILP carrier is prepared, the enzyme can be immobilized on its surface, either supported by physical forces such as van der Waals, ionic interactions, and hydrogen bonds or through covalent bonds. Within the SILP biocatalyst, the immobilized enzyme functions as the active phase [8, 9]. The SILP biocatalysts offer the combined benefits of both homogeneous and heterogeneous catalysis and can greatly enhance the stability of enzymes.

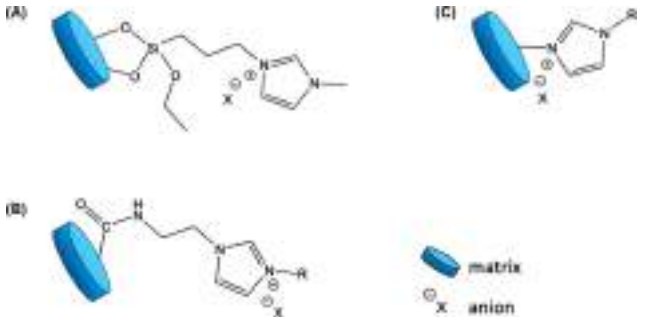

Fig. (1). Visualization of exemplary structures of SILLP materials (chemical immobilization *via*: (**A**) triethoxysilyl groups, (**B**) formation of amide bonds, (**C**) direct quaternisation of the amine).

3. SUPPORTED IONIC LIQUID PHASE BIOCATALYSTS IN ORGANIC SYNTHESIS

The development of novel SILP biocatalytic systems for the synthesis of fine chemicals aligns with the principles of green chemistry. SILP provides a diverse range of options for biocatalyst engineering, enabling the optimization of surface chemistry. This facilitates the incorporation of different properties, *e.g.,* enhancing hydrophobicity by elongating the alkyl chain in the cation of IL and influencing the surface morphology of the matrix. Below, several examples of enhanced performance of SILP biocatalysts are presented.

The activity of a silica-based SILP biocatalyst, consisting of a phosphonium-based IL and *Burkholderia cepacia* lipase, was investigated in olive oil hydrolysis. The SILP carrier allowed for an increase in relative activity of up to 231% and enabled efficient recycling for over 26 cycles [13]. In subsequent studies, a SILP comprising a biodegradable IL based on D-glucose was adsorbed onto multiwalled carbon nanotubes to achieve improved activity, selectivity, and stability of *Candida antarctica* lipase B (CALB). The catalytic performance of this biocatalyst was evaluated in the esterification reaction between acrylic acid and n-butanol. Impressively, the enzyme maintained its activity throughout five cycles, resulting in a product yield of over 90% [14].

Moreover, the application of multi-walled carbon nanotubes as a carrier for SILLP biocatalysts has been extensively studied. Specifically, CALB-SILLP showed exceptional performance in the Baeyer-Villiger oxidation of 2-adamantanone. Despite the harsh conditions involving 35% H_2O_2, the biocatalyst demonstrated a remarkable conversion rate of 92% over at least four reaction cycles [17]. Another study concentrated on the application of alkylimidazolium IL-functionalized silica for the immobilization of CALB. The biocatalyst's catalytic activity was tested in the glycerolysis of corn oil to produce diacylglycerols. The SILLP carrier enhanced the activity of the lipase (from 855 to 5044 U/g) and improved the selectivity from 3.72 to 11.99 (diacylglycerols/monoacylglycerols ratio). Furthermore, the biocatalyst exhibited excellent stability, as no loss of activity was observed over five reaction cycles at 50°C [19]. The incorporation of magnetic species (Fe_3O_4) into the silica SILLP biocatalyst was studied for the synthesis of trans-free plastic fats in enzymatic interesterifications of solid palm stearin and liquid rice bran oil. The enzyme maintained its activity for at least 4 cycles. The magnetic properties of the SILLP carrier facilitated the effortless separation of the biocatalyst using an external magnetic field [20].

The significant contribution of SILP/SILLP biocatalysts was observed in enantiomeric resolutions, exemplified by the esterification reaction between racemic 1-phenylethanol and vinylpropionate using CALB. The SILLP support was prepared by modifying styrene-divinylbenzene copolymers with dodecylimidazolium-based IL. Microwave assistance was employed in this study, and the enzyme exhibited high enantioselectivity (99.9%) towards the (R)-enantiomer. Additionally, the lipase maintained its activity over 12 reaction cycles, demonstrating high biocatalyst stability [21]. In other studies, 1-methyl-3-(triethoxysilylpropyl) imidazolium triflimide IL was attached to the surface of a hybrid material consisting of silica oxide and magnesium oxide. Subsequently, the lipase from Aspergillus oryzae was immobilized to create a SILLP biocatalyst dedicated to the kinetic resolution of ibuprofen racemate through enzymatic esterification. Promising outcomes were achieved, demonstrating a 35.23% conversion of ibuprofen and a high enantioselectivity of 95% for the (S)-ibuprofen ester [16]. Another research showed dynamic kinetic resolution of secondary alcohols (1-phenylethanol and 1-(1-naphthyl)ethanol) *via* enantioselective acylation in the presence of physically immobilized Ru complex and Novozyme 435 on 1-butyl-3-methylimidazolium triflimide adsorbed on multiwalled carbon nanotubes. The obtained catalytic system led to >96% yield and 99% of enantiomeric excess (6 h). Moreover, the proposed catalyst exhibited 4 times higher activity compared to that reported earlier in the literature [22].

The utilization of SILP/SILLP biocatalysis in continuous flow synthesis has a substantial impact, leading to a notable improvement in process efficiency. The continuous flow idea was presented in Fig. (**2**). A SILLP biocatalyst created by incorporating alkylimidazolium IL moieties into a polystyrene-divinylbenzene copolymer

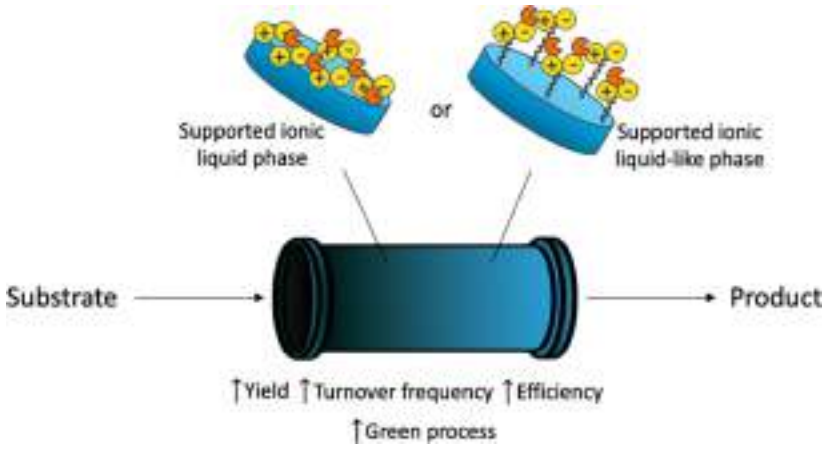

Fig. (2). Scheme of SILP/SILLP continuous flow system. *(A higher resolution / colour version of this figure is available in the electronic copy of the article).*

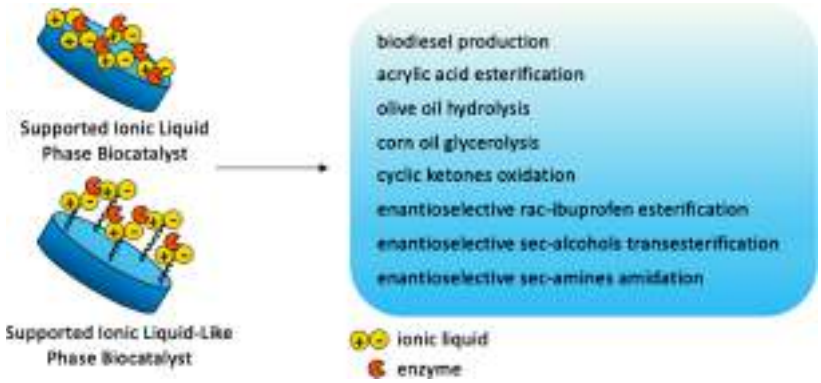

Fig. (3). SILP and SILLP biocatalyst in organic transformations. *(A higher resolution / colour version of this figure is available in the electronic copy of the article).*

matrix, serving as a support for CALB, was employed in the continuous flow synthesis of biodiesel under supercritical CO_2 conditions. The lipase exhibited exceptional catalytic activity, resulting in a remarkable 95% yield of methyl oleate. Moreover, it demonstrated long-term stability by maintaining its performance throughout 45 cycles of reuse. Crucially, no detectable leaching of the IL occurred during the process, ensuring its effective and reliable performance [18]. A polymeric hybrid cellulose-2.5-acetate/polyurethane material coated with alkylimidazolium IL was utilized as a SILP carrier for CALB and Candida rugosa lipase as well. The developed biocatalysts were evaluated in various reactions conducted under continuous flow conditions, including the enantioselective transesterification of racemic (R,S)-1-phenylethanol with vinyl butyrate and vinyl acetate, the esterification of (+/-)-2-isopropyl-5-methylcyclohexanol with propionic anhydride, and the amidation of (R,S)-1-phenylethylamine with ethyl methoxyacetate. Excellent enantioselectivities exceeding 80% and high conversion rates were observed in the aforementioned processes. Additionally, the SILP biocatalysts remained active for a minimum of 7 days, significantly enhancing the production efficiency of pure products [23]. The utilization of enzyme immobilized on the SILP carrier was also found in the continuous gas-phase system. The catalytic activity of CALB adsorbed on 1-octyl-3-methylimidazolium tetrafluoroborate embedded on a hybrid monolith was tested in the transesterification of vinyl propionate and 2-propanol. Conversion exceeding 30% and a short contact time of 24 s were retained for 700 h at 65°C. It showed high biocatalyst stability in the proposed reaction system [24].

SILP and SILLP biocatalysts were successfully applied in many organic transformations, including esterification, hydrolysis, and stereoselective reactions, in both batch and continuous flow conditions. Fig. (**3**) summarizes all of the described processes performed in the presence of SILP/SILLP biocatalysts.

CONCLUSION

The surface morphology of the carrier plays a significant role in biocatalytic reactions. Efforts are being made to investigate and identify appropriate matrices for biocatalytic reactions, considering the significant role played by the surface morphology of the carrier. Various factors, including mechanical and thermal properties, specific surface area, pore volume, density, and the potential for functionalization, are being carefully considered in the selection process. The correlations between the carrier, enzyme, and IL structures emphasize the significance of constructing biocatalysts with exceptional catalytic activity. The activities of enzymes immobilized on SILP/SILLP carriers are mostly enhanced compared to the native protein. It should be highlighted that the implementation of SILP-type carriers for enzymes improves process efficiency, provides effortless biocatalyst separation and recycling, and prolongs the protein's lifespan. Despite the presence of a few reports on the utilization of SILP/SILLP biocatalysts in continuous flow synthesis and enantioselective transformations, the quantity of such studies remains limited. The significant impact of flow catalysis was highlighted by Haumann *et al.* in their work dedicated to continuous gas-phase processes conducted in the presence of SILP/SILLP [25]. This underscores the importance of conducting additional research

in these significant domains to explore their potential further. Another crucial aspect concerning SILP/SILLP biocatalytic systems is their sustainability evaluation. Life cycle assessment, exergy analysis, and energy analysis are valuable tools for assessing the environmental impact of the developed technology [26]. Given the diverse range of reaction systems, detailed studies are required for each SILP/SILLP biocatalyst.

LIST OF ABBREVIATIONS

CALB = Lipase B from *Candida antarctica*

ILs = Ionic Liquids

SILP = Supported Ionic Liquid Phase

SILLP = Supported Ionic Liquid-like Phase

Triflimide = bis(trifluoromethanesulfonyl)imide

CONSENT FOR PUBLICATION

Not applicable.

FUNDING

This work was financially supported by the Silesian University of Technology (Poland), Grant no. 04/050/BKM23/0173.

CONFLICT OF INTEREST

The authors declare no conflict of interest, financial or otherwise.

ACKNOWLEDGEMENTS

Declared none.

REFERENCES

[1] Thore, S.; Tarverdyan, R. *Measuring Sustainable Development Goals Performance*; Elsevier: Amsterdam, The Netherlands, **2021**.

[2] Sheldon, R.A.; Arends, I.; Hanefeld, U. *Green Chemistry and Catalysis*; Wiley-VCH Verlag GmbH: Berlin, Germany, **2020**.

[3] Sheldon, R.A.; Woodley, J.M. Role of biocatalysis in sustainable chemistry. *Chem. Rev.,* **2018**, *118*(2), 801-838. htttp://dx.doi.org/10.1021/acs.chemrev.7b00203 PMID: 28876904

[4] Fernandez-Lafuente, R. Enzyme immobilization and its applications. *Molecules,* **2019**, *24*(24), 4619. htttp://dx.doi.org/10.3390/molecules24244619 PMID: 31861120

[5] Domínguez de María, P. *Ionic Liquids in Biotransformations and Organocatalysis: Solvents and Beyond*; John Wiley & Sons, Inc.: Hoboken, NJ, USA, **2012**. htttp://dx.doi.org/10.1002/9781118158753

[6] Vekariya, R.L. A review of ionic liquids: Applications towards catalytic organic transformations. *J. Mol. Liq.,* **2017**, *227*, 44-60. htttp://dx.doi.org/10.1016/j.molliq.2016.11.123

[7] Potdar, M.; Kelso, G.; Schwarz, L.; Zhang, C.; Hearn, M. Recent developments in chemical synthesis with biocatalysts in ionic liquids. *Molecules,* **2015**, *20*(9), 16788-16816. htttp://dx.doi.org/10.3390/molecules200916788 PMID: 26389873

[8] Wolny, A.; Chrobok, A. Ionic liquids for development of heterogeneous catalysts based on nanomaterials for biocatalysis. *Nanomaterials,* **2021**, *11*(8), 2030. htttp://dx.doi.org/10.3390/nano11082030 PMID: 34443861

[9] Fehrmann, R.; Riisager, A.; Haumann, M. *Supported Ionic Liquids: Fundamental and Applications,* 1st; Wiley-VCH Verlag GmbH: Berlin, Germany, **2014**. htttp://dx.doi.org/10.1002/9783527654789

[10] Lozano, P.; Diego, T.; Carrié, D.; Vaultier, M.; Iborra, J.L. Continuous green biocatalytic processes using ionic liquids and supercritical carbon dioxide. *Chem. Commun.,* **2002**, *7*(7), 692-693. htttp://dx.doi.org/10.1039/b200055e PMID: 12119678

[11] García-Verdugo, E.; Altava, B.; Burguete, M.I.; Lozano, P.; Luis, S.V. Ionic liquids and continuous flow processes: A good marriage to design sustainable processes. *Green Chem.,* **2015**, *17*(5), 2693-2713. htttp://dx.doi.org/10.1039/C4GC02388A

[12] Lozano, P.; Nieto, S.; Serrano, J.; Perez, J.; Sanchez-Gomez, G.; García-Verdugo, E.; Luis, S. Flow biocatalytic processes in ionic liquids and supercritical fluids. *Mini Rev. Org. Chem.,* **2017**, *14*(1), 65-74. htttp://dx.doi.org/10.2174/1570193X13666161103145723

[13] Barbosa, M.S.; Santos, A.J.; Carvalho, N.B.; Figueiredo, R.T.; Pereira, M.M.; Lima, Á.S.; Freire, M.G.; Cabrera-Padilla, R.Y.; Soares, C.M.F. Enhanced activity of immobilized lipase by phosphonium-based ionic liquids used in the supports preparation and immobilization process. *ACS Sustain. Chem. Eng.,* **2019**, *7*(18), 15648-15659. htttp://dx.doi.org/10.1021/acssuschemeng.9b03741

[14] Szelwicka, A.; Erfurt, K.; Jurczyk, S.; Boncel, S.; Chrobok, A. Outperformance in acrylation: Supported D-glucose-based ionic liquid phase on MWCNTs for immobilized lipase B from *Candida antarctica* as catalytic system. *Materials,* **2021**, *14*(11), 3090. htttp://dx.doi.org/10.3390/ma14113090 PMID: 34200059

[15] Sandig, B.; Michalek, L.; Vlahovic, S.; Antonovici, M.; Hauer, B.; Buchmeiser, M.R. A Monolithic hybrid cellulose-2.5- Acetate/polymer bioreactor for biocatalysis under continuous liquid-liquid conditions using a supported ionic liquid phase. *Chemistry,* **2015**, *21*(44), 15835-15842. htttp://dx.doi.org/10.1002/chem.201501618 PMID: 26493884

[16] Wolny, A.; Siewniak, A.; Zdarta, J.; Ciesielczyk, F.; Latos, P.; Jurczyk, S.; Nghiem, L.D.; Jesionowski, T.; Chrobok, A. Supported ionic liquid phase facilitated catalysis with lipase from *Aspergillus oryzae* for enhance enantiomeric resolution of racemic ibuprofen. *Environ. Technol. Innov.,* **2022**, *28*, 102936-102947. htttp://dx.doi.org/10.1016/j.eti.2022.102936

[17] Szelwicka, A.; Wolny, A.; Grymel, M.; Jurczyk, S.; Boncel, S.; Chrobok, A. Chemo-enzymatic Baeyer–Villiger oxidation facilitated with lipases immobilized in the supported ionic liquid phase. *Materials,* **2021**, *14*(13), 3443. htttp://dx.doi.org/10.3390/ma14133443 PMID: 34206178

[18] Lozano, P.; García-Verdugo, E.; Bernal, J.M.; Izquierdo, D.F.; Burguete, M.I.; Sánchez-Gómez, G.; Luis, S.V. Immobilised lipase on structured supports containing covalently attached ionic liquids for the continuous synthesis of biodiesel in $scCO_2$. *ChemSusChem,* **2012**, *5*(4), 790-798. htttp://dx.doi.org/10.1002/cssc.201100692 PMID: 22383391

[19] Zhong, N.; Li, Y.; Cai, C.; Gao, Y.; Liu, N.; Liu, G.; Tan, W.; Zeng, Y. Enhancing the catalytic performance of *Candida antarctica* lipase B by immobilization onto the ionic liquids modified SBA-15. *Eur. J. Lipid Sci. Technol.,* **2018**, *120*(4), 1700357. htttp://dx.doi.org/10.1002/ejlt.201700357

[20] Xie, W.; Zang, X. Lipase immobilized on ionic liquid-functionalized magnetic silica composites as a magnetic biocatalyst for production of trans -free plastic fats. *Food Chem.,* **2018**, *257*, 15-22. htttp://dx.doi.org/10.1016/j.foodchem.2018.03.010 PMID: 29622191

[21] Izquierdo, D.F.; Bernal, J.M.; Burguete, M.I.; García-Verdugo, E.; Lozano, P.; Luis, S.V. An efficient microwave-assisted enzymatic resolution of alcohols using a lipase immobilised on supported ionic liquid-like phases (SILLPs). *RSC Adv.,* **2013**, *3*(32), 13123. htttp://dx.doi.org/10.1039/c3ra42467g

[22] Heba, M.; Wolny, A.; Kastelik-Hryniewiecka, A.; Stradomska, D.; Jurczyk, S.; Chrobok, A.; Kuźnik, N. Green dynamic kinetic resolution—stereoselective acylation of secondary alcohols by enzyme-assisted ruthenium complexes. *Catalysts,* **2022**, *12*(11), 1395. htttp://dx.doi.org/10.3390/catal12111395

[23] Sandig, B.; Buchmeiser, M.R. Highly productive and enantioselective enzyme catalysis under continuous supported liquid-liquid conditions using a hybrid monolithic bioreactor. *ChemSusChem,* **2016**, *9*(20), 2917-2921. htttp://dx.doi.org/10.1002/cssc.201600994 PMID: 27650312

[24] Lee, C.; Sandig, B.; Buchmeiser, M.R.; Haumann, M. Supported ionic liquid phase (SILP) facilitated gas-phase enzyme catalysis – CALB catalyzed transesterification of vinyl propionate. *Catal. Sci. Technol.,* **2018**, *8*(9), 2460-2466. htttp://dx.doi.org/10.1039/C8CY00089A

[25] Marinkovic, J.M.; Riisager, A.; Franke, R.; Wasserscheid, P.; Haumann, M. Fifteen years of supported ionic liquid phase-catalyzed hydroformylation: Material and process developments. *Ind. Eng. Chem. Res.,* **2019**, *58*(7), 2409-2420. htttp://dx.doi.org/10.1021/acs.iecr.8b04010

[26] Gheewala, S.H. Life cycle assessment for sustainability assessment of biofuels and bioproducts. *Biof. Res. J.,* **2023**, *10*(1), 1810-1815. htttp://dx.doi.org/10.18331/BRJ2023.10.1.5

Applied Catalysis A, General 676 (2024) 119676

Contents lists available at ScienceDirect

Applied Catalysis A, General

journal homepage: www.elsevier.com/locate/apcata

Construction of trifloaluminate ionic liquid catalyst on the silica surface dedicated for continuous flow Diels-Alder synthesis

Anna Wolny [a], Piotr Latos [a], Katarzyna Szymańska [b], Sebastian Jurczyk [c], Agata Jakóbik-Kolon [d], Anna Chrobok [a,*]

[a] Department of Chemical Organic Technology and Petrochemistry, Faculty of Chemistry, Silesian University of Technology, Krzywoustego 4, Gliwice PL-44100, Poland
[b] Department of Chemical Engineering and Process Design, Faculty of Chemistry, Silesian University of Technology, Strzody 7, Gliwice PL-44100, Poland
[c] Institute for Engineering of Polymer Materials and Dyes, Lukasiewicz Research Network, Sklodowskiej-Curie 55, Torun PL-87100, Poland
[d] Department of Inorganic Chemistry, Analytical Chemistry and Electrochemistry, Faculty of Chemistry, Silesian University of Technology, Bolesława Krzywoustego 6, Gliwice 44-100, Poland

ARTICLE INFO

Keywords:
Ionic liquids
Supported ionic liquid phase
Immobilization
Diels-alder
Flow chemistry

ABSTRACT

Supported ionic liquid phases (SILP) are efficiently use for the construction of highly active, heterogeneous and recyclable catalysts. In this study, three strategies towards chemical immobilization of trifloaluminate ionic liquid catalyst into microporous/mesoporous silica support were investigated. The order of silica surface modification with trifloaluminate ILs components had crucial influence on the catalytic activity and stability which was tested in the model Diels-Alder reaction between isoprene and maleic anhydride in acetonitrile at room temperature. The best catalytic performance (maleic anhydride conversion > 97% in ten reaction cycles) was achieved for catalyst created through the synthesis of trifloaluminate ionic liquid in the first step with further bounding to the silica surface using 25 wt% of ionic liquid loading. The effective transformation of the Diels-Alder reaction to continuous flow synthesis led to 97% maleic anhydride conversion over 432 h with a TOF of 104.3 h^{-1} and significantly improved process sustainability.

1. Introduction

Heterogeneous catalysts play an important role in chemical industry due to their robustness and easy separation resulting in lower operational cost. The proper design of heterogeneous catalysts is crucial affecting not only their activity but also selectivity and stability. The careful choice of the carrier and the active phase effects final characteristics of the catalyst. Recently, supported ionic liquid phase (SILP) became a powerful tool for the designing of heterogeneous catalysts meeting global green chemistry assumptions [1–3]. Diversity in the ionic liquids (IL) structures and properties makes them widely use as catalysts in organic synthesis, particularly as acidic catalysts [4].

SILP catalysts can be synthesized by chemical anchoring or physical adsorption of IL moieties on the surface of a carrier. Integration of IL with a solid matrix by covalent bonding prevents leaching of catalytic phase from the surface and provides catalyst durability in the process [5,6]. Two methods of chemical immobilization of ILs, *via* cation or anion, can be used [7,8]. Immobilization of the IL *via* cation involves the modification of IL structure with siliceous precursors, *e.g.* 3-(chloropropyl)triethoxysilane, or 3-mercaptopropyl-trimethoxysilane. The resulted IL modified with ethoxysilane groups can be directly attached to the hydroxyl groups of silica. The fixation of the IL through the anion was primarily observed for chlorometallate ILs, especially in the wet impregnation method, leading to the formation of -Si-O-M bonds [7]. Brønsted or Lewis acidity can be introduced to SILP catalyst to the structure of the cation through functional groups, like $-SO_3H$, $-B(OH)_2$ or *via* anion, *e.g.* $[HSO_4]^-$, $[AlCl_4]^-$ of IL [8–10]. An alternative option involves the modification of the surface of carrier with neutral IL followed by subsequent immobilization of metal complexes or enzymes [10–22].

Incorporation of metal chlorides as Lewis acids in IL structure and formation of chlorometallates ILs prevents its leaching in organic synthesis and provides high product purity which is of particular importance for pharmaceutical applications. The heterogenization of chlorometallates ILs *via* chemical bound into the solid carrier was already described in several reports [7,17–22]. The low hydrolytic stability of these systems is the major drawback which influences the possibility of recycling of SILP catalysts. Chlorogallate(III) and chloroaluminate(III) ILs were bounded into mesoporous silica support and

* Corresponding author.
E-mail address: anna.chrobok@polsl.pl (A. Chrobok).

https://doi.org/10.1016/j.apcata.2024.119676
Received 3 December 2023; Received in revised form 4 February 2024; Accepted 9 March 2024
Available online 12 March 2024

used as catalysis in Diels-Alder cycloaddition under solventless conditions. Chlorogallate(III) SILP catalysts were the most active causing the full conversion of substrates and high *endo/exo* selectivities for various adducts. The stability of SILP catalysts in at least five reaction cycles was achieved [17]. Chloroaluminate(III) silica based SILP catalysts were also used in Friedel–Crafts alkylation of benzene with olefins, production of alkylated gasoline and trimerization of isobutene with improved yield, selectivity, and catalyst recyclability compared to homogenous version [7,18,19]. Other more hydrolytically stable metals species, as chloroferrate(III) and chloroindate(III) ILs chemically anchored on silica were used in the synthesis of diphenylmethane and its derivatives as well. Exceptional selectivity up to 100%, complete conversion of substrate and stability of SILP catalyst for 10 cycles were observed [20,21]. It was also reported that $SnCl_4$ was integrated with quaternary ammonium chloride IL immobilized on various silicas. SILP catalyst enhanced selectivity (94%) and conversion (76%) in condensation of isobutene and formaldehyde [22].

Another possibility of introducing metal moieties into ILs structure is the formation of water tolerant triflometallates ILs, *e.g.* trifloaluminate ILs in contrary to hydrolytically unstable chlorometallates ILs. Trifloaluminate IL are based on trifluoromethanesulfonate (triflate) anion derived from, *e.g.* 1-ethyl-3-methylimidazolium triflate [C_2mim][OTf] or 1-methyl-3-octylimidazolium triflate [C_8mim][OTf] complexed with $Al(OTf)_3$ in substoichiometric quantities $\chi_{Al(OTf)3} = 0.15$ and 0.25 (χ - molar fraction) forming homogenous liquids. During the synthesis of trifloaluminate ILs with increasing loading of $Al(OTf)_3$ higher than 0.25, the suspended solid was visible in the product even in 85 °C. Lewis acidity of was measured using Gutmann acceptor number (AN) approach positioning trifloaluminate ILs as medium-strength Lewis acids (AN = ca. 65). Our previous studies showed that trifloaluminate systems consist of hexacoordinate aluminum in multiply charged, oligonuclear anionic complexes, exhibiting diverse triflate bridging modes [23]. Trifloaluminate ILs were embedded *via* adsorption on multi-walled carbon nanotubes and used for the synthesis of chromanes in several cycles. High conversions (94–99%) and selectivities (80–89%) were achieved under SILP conditions [23]. The same catalytic system was tested for levulinic acid esters synthesis from α-angelica lactone. High performance of trifloaluminate SILP catalyst remained constant for 5 reaction cycles achieving full conversion and 100% selectivity of the butyl levulinate [24]. Trifloaluminate IL was also chemically grafted to silica and hybrid silica materials (CaO-SiO_2, MgO-SiO_2), and use in the batch and continuous flow aminolysis of epoxides. High conversion 81.1% and selectivity 95.9% through 72 h under flow conditions were reached in the presence of SILP based on MgO-SiO_2 [25].

It was confirmed that the order in which the silica surface is modified in the fabrication process of chloroaluminate SILP catalysts is crucial. Immobilization of ILs *via* triethoxysilyl groups located in the dialkylimidazolium cation, and subsequent complexation reaction of anion with $AlCl_3$, leads to the deposition of free aluminum chloride species on/in the silica material [7]. To mitigate this adverse occurrence in our previous work the following sequence was applied for the fabrication of chlorometallates SILP catalysts: synthesis of 1-methyl-3-(triethoxysilylpropyl)imidazolium chloride, the addition of gallium chloride and formation of chlorogallate ILs, and then its chemical immobilization on the silica surface [17]. However, this phenomenon for trifloaluminate SILP catalysts remains poorly understood.

Summing up, immobilization of ILs on the solid support can offer high stability of the SILP materials allowing their application in the continuous flow synthesis. However, the application of SILP catalytic systems have received more interest for the processes carried out in the gas phase [26–30]. On the other hand, due to the low stability of chlorometallate ILs they were not applied for the flow synthesis and water tolerant trifloaluminate systems can overcome this drawback.

In this work, seeking for the best recycling strategy, taking advantage of water stable triflometallate ILs the influence of the order of silica surface modification with trifloaluminate ILs components on the catalytic activity was determined following a multi-technique speciation study. The curtail sequence of the immobilization of reagents was proposed. Next, the trifloaluminate SILP catalyst was used for the model Diels-Alder reaction in batch process. After optimisation of the reaction conditions an efficient upgrade from batch to flow was demonstrated.

2. Experimental

2.1. Materials

1-methylimidazole (≥99.0%), (3-chloropropyl)triethoxysilane (≥95.0%), aluminum trifluoromethanesulfonate (99.9%), lithium trifluoromethanesulfonate (96.0%), silver trifluoromethanesulfonate (≥99.0%), polyethylene glycol (35.000 $gmol^{-1}$), hexadecyltrimethylammonium bromide (≥98,0%), tetraethyl orthosilicate (98.0%), maleic anhydride, isoprene (99.0%), dicyclopentadiene, myrcene (≥90%.0), ocimene (≥90%), methyl acrylate (99.0%), ethyl acrylate (99.0%), diethyl maleate (97.0%) were purchased from Sigma Aldrich, Merck Group, Poland. Multimodal porous SiO_2 [31], 1-methyl-3(triethoxysilylpropyl)imidazolium chloride ([tespmim]Cl) [7], 1-methyl-3(triethoxysilylpropyl)imidazolium triflate ([tespmim][OTf]) [25], 1-methyl-3(triethoxysilylpropyl)imidazolium triflate – aluminium triflate ([tespmim][OTf-Al$(OTf)_3$], $\chi_{Al(OTf)3} = 0.15$) [25] were prepared according to the literature (Supplementary Materials).

2.2. Catalyst preparation

SILP SiO_2-[tespmim][OTf-Al$(OTf)_3$], $\chi_{Al(OTf)3} = 0.15$ catalysts preparation:

SILP (1): [tespmim][OTf-Al$(OTf)_3$], $\chi_{Al(OTf)3} = 0.15$ (0.75 mmol) was added to the 25 mL round-bottomed flask and dissolved in toluene (10 mL) at 90°C, next SiO_2 (0.50 g) was added. Reaction mixture was stirred for 24 h. After that, material was filtered off, washed using Soxhlet extraction for 24 h at 120°C, filtered off under vacuum, and dried on the Schlenk line (rt, 24 h) yielded 0.52 g of SILP (1) with [tespmim][OTf-Al$(OTf)_3$], $\chi_{Al(OTf)3} = 0.15$ loading 25.3 wt% (determined by TGA).

SILP (2): [tespmim][OTf] (0.75 mmol) was added to the 25 mL round-bottomed flask and dissolved in toluene (10 mL) at 90°C, next SiO_2 (0.50 g) was added. Reaction mixture was stirred for 24 h. After that, material was filtered off, washed using Soxhlet extraction for 24 h at 120°C, filtered off under vacuum, and dried on the Schlenk line (rt, 24 h) yielded 0.51 g of product. EDX analysis was perform to confirm [tespmim][OTf] presence (Supplementary Materials, Fig.S11). Then, the obtained material (0.51 g) and the aluminium triflate (0.0217 g, molar ratio $\chi_{Al(OTf)3} = 0.15$) dissolved in acetonitrile (10 mL) were placed in 25 mL round-bottomed flask, and stirred for 24 h at 95°C. Next, material was filtered off, washed with acetonitrile (3 × 20 mL), and dried on the Schlenk line (rt, 24 h) yielded 0.5 g of SILP (2) with [tespmim][OTf-Al$(OTf)_3$], $\chi_{Al(OTf)3} = 0.15$ loading 19.2 wt% (determined by TGA).

SILP (3): [tespmim]Cl (0.75 mmol) was added to the 25 mL round-bottomed flask and dissolved in toluene (10 mL) at 90°C, next SiO_2 (0.50 g) was added. Reaction mixture was stirred for 24 h. After that, material was filtered off, washed using Soxhlet extraction for 24 h at 120°C, filtered off under vacuum, and dried on the Schlenk line (rt, 24 h) yielded 0.5 g of product. Next, the obtained material (0.5 g) and lithium triflate (0.15 g, 30 mol% per [tespmim]Cl loaded on material) dissolved in ethyl acetate (10 mL) were placed in 25 mL round-bottomed flask, and stirred for 24 h at room temperature. Next, material was filtered off, washed with ethyl acetate (3 × 20 mL), and dried on the Schlenk line (rt, 24 h) yielded 0.5 g of product. The filtrate underwent testing to detect the presence of Cl^- through treatment with $AgNO_3$. No formation of precipitated AgCl was observed. Furthermore, SEM-EDX analyses were conducted to confirm the complete Cl^- exchange for $[OTf]^-$ (Supplementary Materials, Fig.S13–14). Then, the obtained material (0.5 g) and the aluminium triflate (0.0218 g, molar ratio $\chi_{Al(OTf)3} = 0.15$) dissolved

in acetonitrile (10 mL) were placed in 25 mL round-bottomed flask, and stirred for 24 h at 95°C. Next, material was filtered off, washed with acetonitrile (3 × 20 mL), and dried on the Schlenk line (rt, 24 h) yielded 0.5 g of SILP (3) with [tespmim][OTf-Al(OTf)$_3$], $\chi_{Al(OTf)3} = 0.15$ loading 19.7 wt% (determined by TGA).

***SiO$_2$-Al(OTf)$_3$*:** Aluminium triflate (0.75 mmol) was added to the 25 mL round-bottomed flask and dissolved in acetonitrile (10 mL) at 90°C, and next SiO_2 (0.50 g) was added. Reaction mixture was stirred for 24 h. After that, material was filtered off, washed using Soxhlet extraction for 24 h at 120°C, filtered off under vacuum, and dried on the Schlenk line (rt, 24 h) yielded 0.5 g of SiO_2-Al(OTf)$_3$. SiO_2-Al(OTf)$_3$ loading was 36.5 wt% (determined by TGA).

2.3. General procedure of Diels-Alder reaction in batch system

The maleic anhydride (4 mmol) dissolved in acetonitrile (0.5 mL), *n*-decane (GC inert standard, 0.02 g), SILP(1−3) containing 0.1 mol% of Al(OTf)$_3$ (35 mg – 46 mg) (recalculated for maleic anhydride) were placed in a round-bottomed flask, and then the diene (6 mmol) was added dropwise. The reaction was stirred (100 rpm) at room temperature for 1–180 min, and monitored by gas chromatography (GC). After the reaction, the catalyst was filtered off, the solvent was removed using rotary evaporator, and the product was purified applying crystallization or column chromatography using chloroform as eluent (yield 95%) and characterised by ^{1}H and ^{13}C NMR spectroscopy.

Cycloadduct (c) ^{1}H NMR (400 MHz, cdcl3) δ 5.63 (s, 1 H), 3.43 – 3.28 (m, 2 H), 2.54 (m, J = 17.6, 15.7, 4.2 Hz, 2 H), 2.26 (m, J = 15.8, 10.3, 4.5 Hz, 2 H), 1.77 (s, 3 H) (Supplementary Materials, Fig.S20a). ^{13}C NMR (101 MHz, cdcl3) δ 174.49, 174.34, 136.7, 120.29, 40.23, 39.59, 28.55, 24.22, 23.62. (Supplementary Materials, Fig.S20b).

Cycloadduct (e) ^{1}H NMR (600 MHz, cdcl3) δ 6.32 (t, J = 2.1 Hz, 2 H), 3.59 – 3.57 (m, 2 H), 3.51 (dt, J = 3.2, 1.6 Hz, 2 H), 1.79 (d, J = 9.1 Hz, 1 H), 1.57 (d, J = 8.8 Hz, 1 H). (Supplementary Materials, Fig. S21a). ^{13}C NMR (151 MHz, cdcl3) δ 171.37, 135.69, 52.90, 47.22, 46.28. (Supplementary Materials, Fig.S21b).

Cycloadduct (g) ^{1}H NMR (400 MHz, dmso) δ 5.36 – 5.31 (m, 1 H), 5.18 (t, J = 7.8 Hz, 1 H), 3.11 – 3.05 (m, 1 H), 2.72 – 2.64 (m, 1 H), 2.45 – 1.96 (m, 6 H), 1.67 (s, 3 H), 1.55 (s, 3 H). (Supplementary Materials, Fig.S22a). ^{13}C NMR (101 MHz, dmso) δ 174.63, 172.71, 133.70, 131.88, 123.19, 121.04, 43.14, 41.62 (d, J = 6.8 Hz), 27.78. (Supplementary Materials, Fig.S22b).

Cycloadduct (j) ^{1}H NMR (400 MHz, dmso) δ 5.33 (s, 1 H), 5.18 (s, 1 H), 3.10 – 3.07 (m, 1 H), 2.71 – 2.65 (m, 1 H), 2.45 – 1.96 (m, 7 H), 1.67 (s, 3 H), 1.65 (s, 3 H), 1.56 (s, 3 H). (Supplementary Materials, Fig. S23a). ^{13}C NMR (101 MHz, dmso) δ 174.63, 172.71, 133.69, 131.87, 123.19, 121.04, 43.14, 41.65, 41.58, 27.78, 25.72, 24.64, 21.31, 17.67. (Supplementary Materials, Fig.S23b).

Cycloadduct (k) ^{1}H NMR (600 MHz, cdcl3) δ 6.10 (dq, J = 1.9, 1.0 Hz, 1 H), 5.55 (p, J = 1.6 Hz, 1 H), 5.29 (s, 3 H), 3.75 (s, 3 H), 1.94 (dd, J = 1.6, 0.9 Hz, 4 H). (Supplementary Materials, Fig.S25a). ^{13}C NMR (151 MHz, cdcl3) δ 211.65, 168.11, 136.34, 125.66, 125.58, 53.55, 52.00, 51.93, 18.45. (Supplementary Materials, Fig.S25b).

Cycloadduct (l) ^{1}H NMR (600 MHz, cdcl3) δ 6.18 (s, 1 H), 5.93 (s, 1 H), 3.62 (s, 3 H), 3.20 (s, 1 H), 2.98 – 2.92 (m, 1 H), 2.92 – 2.87 (m, 1 H), 1.45 – 1.40 (m, 2 H), 1.31 – 1.22 (m, 2 H). (Supplementary Materials, Fig.S24a). ^{13}C NMR (151 MHz, cdcl3) δ 137.90, 132.53, 51.63, 49.77, 45.82, 43.33, 42.67, 29.42. (Supplementary Materials, Fig.S24b).

Cycloadduct (n) ^{1}H NMR (600 MHz, cdcl3) δ 6.18 (dd, J = 5.7, 3.1 Hz, 1 H), 5.92 (dd, J = 5.7, 2.9 Hz, 1 H), 4.11 – 4.02 (m, 2 H), 3.21 – 3.17 (m, 1 H), 2.94 – 2.91 (m, 1 H), 2.90 – 2.87 (m, 1 H), 1.43 – 1.40 (m, 2 H), 1.26 (t, J = 7.2 Hz, 2 H), 1.22 (t, J = 7.1 Hz, 3 H). (Supplementary Materials, Fig.S26a). (Supplementary Materials, Fig.S26b).

Cycloadduct (p). ^{1}H NMR (600 MHz, cdcl3) δ 6.29 – 6.23 (m, 2 H), 4.06 (tddd, J = 17.9, 10.8, 7.2, 4.0 Hz, 4 H), 3.30 – 3.25 (m, 2 H), 3.20 – 3.11 (m, 2 H), 1.46 (dt, J = 8.4, 1.8 Hz, 1 H), 1.36 – 1.28 (m, 1 H), 1.22 (td, J = 7.1, 2.7 Hz, 6 H). (Supplementary Materials, Fig.S27a). ^{13}C NMR (151 MHz, cdcl3) δ 172.53, 134.96, 60.37, 48.79, 48.42, 46.45, 14.28. (Supplementary Materials, Fig.S27b).

2.4. SILP catalyst recycling

After the reaction, the SILP (1−3) were filtered off, washed with 30 mL of acetonitrile, dried under the vacuum on the Schlenk line (6 h, 20 °C) and reused. Catalysts recycling experiments were upscale 4-fold to 160 mg of the SILP (1−3).

2.5. General procedure of Diels-Alder reaction in flow system

The continuous-flow Diels-Alder reaction was performed in a fully automated Syrris Asia flow reactor with two pumps and four syringes. Pump A pumped maleic anhydride (2.0 M) in acetonitrile with flow 0.023 mLmin^{-1}, and pump B pumped isoprene with flow 0.007 mLmin^{-1}. The combined steams were flowed through the column reactor filled with 0.3 g of SILP(1) catalyst for 48 h at room temperature. Reaction progress was monitored by gas chromatography after 6, 24 and 48 h.

2.6. Materials characterisation and analysis

Gas chromatography (GC) analyses were performed on a SHIMADZU GC-2010 Plus equipped with a Zebron ZB-5MSi column (30 m×0.32 mm; 0.25 μm). Thermogravimetric analyses (TGA) of all materials were carried out on a thermobalance (Mettler Toledo STAR851). Samples (10 mg) were heated with temperature ramp between 25 and 800 °C at 20 °C min^{-1} and nitrogen flow of 100 mLmin^{-1}). BET surface area (S_{BET}), average pore size (d_p) and average pore volume (V_p) of all materials were measured on ASAP 2020 Plus Version 2.00 using low-temperature nitrogen adsorption-desorption (–196 °C), applying BET method and BJH model. SEM-EDX images of all materials were obtained on a Phenom Pro Desktop SEM instrument equipped with an EDS detector (15 kV) (Thermo Fischer Scientific). ICP (Inductively coupled plasma) analyses were performed on a Varian 710-ES spectrometer equipped with a sea-spray nebulizer and twister glass spray chamber was utilized (detailed description in Supplementary Materials). ^{29}Si MAS NMR of trifloaluminate SILP (1) material was recorded at 59.517 MHz using a Bruker HP-WB high-speed MAS probe. ^{1}H NMR and ^{13}C NMR spectra were obtained on a Varian system (400 MHz and 101 MHz, respectively).

3. Results and discussion

3.1. Trifloaluminate SILP catalysts synthesis

Lewis acidic type triflometallate ILs became alternative for poorly stable and highly corrosive chlorometallate ILs [8,10]. Superior moisture stability of ILs derived from triflate anions prolongs its catalytic performance and facilitate synthesis procedures. In this work, major studies are focused on trifloaluminate ILs due to a relatively low price of aluminium species. Until now, the application of trifloaluminate ILs as homogenous catalysts was described [23,24] and recent findings have demonstrated their efficiency when chemically grafted to silica hybrid materials, as MgO-SiO_2 and CaO-SiO_2 as well [25]. During the immobilization of chloroaluminate ILs *via* triethoxysilyl groups situated in the cation, and subsequent addition of aluminium chloride for anion complexation, the creation of bonds between the aluminium and oxygen located on the silica surface and inside the pores can occurred as a side process which lower the activity of the final catalyst [7,8]. Given this circumstance, the primary objective of this study was to determine the accurate sequence of steps employed in the synthesis of SILP systems utilizing triflometallate ILs.

A porous silica material with a hierarchical pore structure comprising micro-, meso-, and macropores was selected as a matrix for

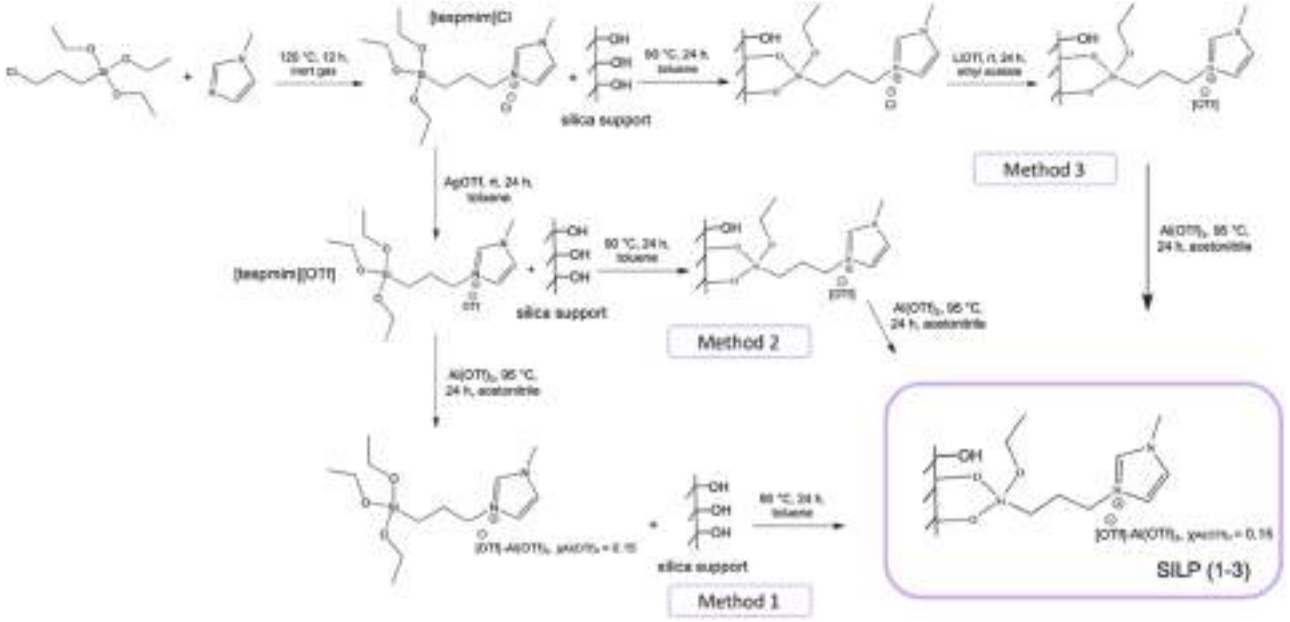

Scheme 1. Synthesis of SILP (1−3) *via three different methods.*

Table 1
Characterisation and catalytic activity of multimodal silica and catalysts based on $Al(OTf)_3$.

Material	S_{BET}, m^2g^{-1}	V_p, cm^3g^{-1}	d_p, nm	IL loading, wt % ±0.3[a]	MA conversion, % ±2.0
SiO_2	284.2	1.12	36	-	-
SILP (1)	92.9	0.55	28	25.3	97.45
SILP (2)	113.7	0.59	28	19.2	97.31
SILP (3)	109.7	0.61	28	19.7	97.45

[b]measured after 240 min
Reaction conditions: isoprene 3 mmol, maleic anhydride 2 mmol, acetonitrile 0.5 mL, SILP (1−3) or SiO_2-$Al(OTf)_3$ catalyst contains 0.1 mol% $Al(OTf)_3$ per maleic anhydride, 20°C, 180 min. MA conversion was determined using GC.
[a] determined by TGA; the standard deviation of 3 replicate experiments,

trifloaluminate SILP chemical immobilization. Such silica structure facilitates improved mass transport of organic reagents to and from active sites due to their unique design. The interconnected macropores serve as main transport pathways to smaller micro/mesopores, what play a crucial role in the activity of catalysts based on the matrix and selectivity of chemical reactions [17,31,32].

A silica porous material was created following a previously outlined method [17,31,32]. This involved employing porogens of varying sizes (such as polyethylene glycol and cetyltrimethylammonium bromide), along with inducing and freezing the transitional structures resulting from the phase separation process. The composition led to the formation of a porous, interconnected, open network with macropores of micrometer size (see Supplementary Materials Fig. S9-S15). In addition to the macropores, the material also exhibited textural mesopores with an average diameter of approximately 36 nm, a BET surface area of 284.2 m^2/g, and a total pore volume of 1.12 cm^3/g, (determined through low temperature nitrogen adsorption-desorption). Adsorption-desorption isotherms were added to Supplementary Materials (Figure S30). Further modification of the surface structure with ionic liquid may improve their properties and application prospects.

To explore the influence of the sequence of silica surface modification with trifloaluminate IL, the three different approaches of the immobilization were studied. All applied methods started from the synthesis of [tespmim]Cl to provide triethoxysilyl functionality in to ILs structure as a linker with hydroxyl groups on silica surface [7,17] as shown on Scheme 1. For all methods $\chi_{Al(OTf)3} = 0.15$ (molar fraction of $Al(OTf)_3$ used for complexation of $[OTf]^-$ anion) was chosen to design catalyst with medium-strength Lewis acidity.

Method 1 for the synthesis of SILP (1) is based on synthesis of trifloaluminate IL ([tespmim][OTf-$Al(OTf)_3$], $\chi_{Al(OTf)3} = 0.15$) in the first step, *via* anion exchange of [tespmim]Cl with silver triflate (1:1, n/n) [25], complexation reaction with aluminium triflate ($\chi_{Al(OTf)3} = 0.15$) at 95°C [20], and subsequent chemical immobilization on silica surface at 90°C in toluene [7] (loading of IL 25.3 wt%; Supplementary Materials Fig.S2). Next approach (Method 2 for the synthesis of SILP (2)) implies the synthesis of [tespmim][OTf], then chemical grafting to silica matrix (loading of IL 19.2 wt%; Supplementary Materials Fig.S3), and further addition of aluminium triflate ($\chi_{Al(OTf)3} = 0.15$) at 95°C in acetonitrile (loading of IL 19.2 wt%; Supplementary Materials Fig.S4). Method 3 for the synthesis of SILP (3) assumed direct bonding of [tespmim]Cl to the silica surface (loading of IL 19.7 wt%; Supplementary Materials Fig.S5), then anion exchange to aluminium triflate with LiOTf in ethyl acetate (loading of IL = 19.7 wt%; Supplementary Materials Fig.S6), ending with complexation with aluminium triflate ($\chi_{Al(OTf)3} = 0.15$) at 95°C in acetonitrile (loading of IL 19.7 wt%; Supplementary Materials Fig.S7). All three approaches are leading to SILP materials with catalytic properties. For comparison reasons SiO_2-$Al(OTf)_3$ was also fabricated using for the synthesis the same silica material and aluminium triflate dissolved in acetonitrile and stirred at 90°C (loading of $Al(OTf)_3$ 36.5 wt%; Supplementary Materials Fig.S8).

To ensure the complete exchange of all Cl^- anions with $[OTf]^-$ in each step of the synthesis of SILP(1−3), two methods were employed. The presence of Cl^- ions in liquid filtrates was examined through their reaction with AgNO3. The absence of AgCl confirmed the absence of unexchanged chlorides. In the case of solid SILP intermediates and final products, the EDX method was utilized (Supplementary Materials, Figure S13-14).

TGA, ICP, BET, SEM-EDX and ^{29}Si MAS NMR analyses were performed to characterise the obtained SILP materials and determine the choice of the most preferable immobilization procedure. The loading of [tespmim][OTf-$Al(OTf)_3$], $\chi Al(OTf)_3 = 0.15$ on silica matrix for SILP (1−3) materials was measured by TGA (Table 1). The highest IL loading was achieved for SILP (1) 25.3 wt% (Supplementary Materials Fig.S2), while for the SILP(2) and SILP(3) reached 19.7 wt% and 19.2 wt% (Supplementary Materials Fig.S4,S7), respectively. In order to

Table 2
Amount of $Al(OTf)_3$ in SILP (1−3) determined by ICP method.

Catalyst	Al concentration (measured)[a] mgL^{-1}	Al concentration (theoretical) mgL^{-1}	$\chi Al(OTf)_3$ (measured)[a]	$\chi Al(OTf)_3$ (theoretical)
[tespmim][OTf-Al$(OTf)_3$], $\chi_{Al(OTf)3} = 0.15$	5.87	5.76	0.1538	0.1509
SILP(1)	1.14	1.18	0.1461	0.1511
SILP(2)	1.70	1.79	0.1420	0.1500
SILP(3)	1.74	1.83	0.1424	0.1510

[a] standard deviation 2%.

determine the final content of $Al(OTf)_3$ in SILP(1−3) ICP analyses were performed (Supplementary Materials). Both concentration of the sample used for the analysis as well as the molar fraction theoretical and determined were added to the Table 2. First, [tespmim][OTf-Al$(OTf)_3$], $\chi Al(OTf)_3 = 0.15$ was analysed to confirm its precise alignment with the theoretical amount of $Al(OTf)_3$ employed in the synthesis. This analysis demonstrated the high accuracy of the method. ICP analyses of SILP (1−3) have revealed that the incorporation of $Al(OTf)_3$ into the catalyst structure remained consistent, irrespective of the synthetic method employed. The marginal differences between theoretical and measured values fall within the standard error.

The decreasing of specific surface area (BET) after IL immobilization on the silica surface was observed for all the SILP materials, what confirms the presence of IL on the surface of the carrier (Table 1). The modification of silica led to a decrease in pore size and volume, as indicated by BJH analysis. The silica exhibits small mesopores (4 nm), larger mesopores (36 nm) according to the pore size distribution diagram (Supplementary Materials, Fig.S31), and macropores (Supplementary Materials, Fig.S9). In case of SILP (1−3) materials, larger mesopores are visible (Supplementary Materials, Fig.S31) along with macropores (Supplementary Materials, Fig. S10, S12, S15). The adsorption-desorption isotherms of SiO2 and SILP(1−3) exhibit a similar type IV characteristic, typical for mesoporous materials (Supplementary Materials, Fig.S30). This similarity provides evidence of consistent pore shapes in the studied materials. Furthermore, the functionalization resulted in a reduction in specific surface area, pore sizes, and the blocking of small mesopores (Supplementary Materials, Fig.S31). The lower loading of ILs in the case of SILP (2−3) (with Cl^- and $[OTf]^-$ anions) may suggest a lower affinity of specific ILs to the silica surface making their immobilization more challenging. Determined high amounts of IL loading on the silica mainly arises from well-defined hierarchical pore structure and availability of evenly distributed numerous hydroxyl groups that facilitate the effective binding of a substantial amount of IL.

The developed porosity of SILP (1−3) is also clearly visible at SEM images supplied with EDX analyses demonstrating presence of new elements, such as Al, C, N, S on the silica matrix (Supplementary Materials Fig.S9-S15). The chemical attachment of [tespmim][OTf-Al$(OTf)_3$], $\chi Al(OTf)_3 = 0.15$ to the silica surface was proven by ^{29}Si MAS NMR (Supplementary Materials Fig.S16). The MAS NMR spectra indicate the vanishing of signals related to $(SiO)_2Si(OH)_2$ and $(SiO)_3Si$-OH groups, alongside the emergence of a new signal at −66 ppm. This clearly demonstrates the IL was chemically grafted to the siliceous surface. The reference material SiO_2-$Al(OTf)_3$ was characterized 36.5 wt% of Al$(OTf)_3$ loading on the surface (Supplementary Materials Fig.S8).

3.2. Catalytic activity of trifloaluminate SILP catalysts in Diels-Alder reaction

Heterogeneous trifloaluminate SILP (1−3) materials were tested as catalysts in a model Diels-Alder reaction between maleic anhydride (MA) and isoprene (Scheme 2). The cycloadducts formed during the Diels-Alder reaction are mostly used as intermediates in the production of pharmaceuticals, agrochemicals, flavours, fragrances, surfactants, or bio-based polymers. [33,34]. The Diels-Alder cycloaddition reaction is commonly conducted using harmful organic solvents, and often requires extended reaction times, occasionally even under elevated pressure. As an illustration, cycloaddition between maleic anhydride and isoprene was reported in hexane/nitrobenzene mixture for over 24 h [35]. Other studies presented benzene/CO_2 system at 33°C, 7.5 MPa in the presence of $AlCl_3$ catalyst for the same reaction [36]. Higher temperatures for this model reaction 65–75°C and reaction time up to 8 h for the reaction in cyclohexane were also applied [37]. Afresh report showed chlorogallate (III) SILP catalyst, that shorten the reaction time to 180 minutes under room temperature [17]. To overcome all drawbacks related to the presented literature reports concerning Diels-Alder cycloaddition, we offer water-tolerant trifloaluminate SILP catalyst as more ecologically friendly alternative to produce cycloadducts in more efficient way.

The results of maleic anhydride and isoprene cycloaddition in the presence of SILP(1−3) catalysts containing 0.1 mol% of $Al(OTf)_3$ per maleic anhydride at 20 °C are presented in Table 1 using 1.5 molar ratio of reactants and acetonitrile as solvent. Solvent was necessary to dissolve solid maleic anhydride. The reaction in solventless conditions was not effective. The conversion of maleic anhydride was determined using GC and no other by products were detected (selectivity 100%) (exemplary GC chromatogram was added to Supplementary Materials, Figure S28). SILP (1−3) exhibited high catalytic activity in this process enabling approximately 97.5% conversion of maleic anhydride. The application of a higher temperature (40°C) led to the almost full conversion (97.8%) of maleic anhydride after 120 min. Unfortunately, the development of a dark colour in reaction mixture, likely resulting from the partial polymerization of isoprene was observed. Other solvents were tested in the model reaction as well. The same results were obtained using dichloromethane, although the conversion was slightly lower after 180 minutes when ethyl acetate was employed (89.4%) (Supplementary Materials, Figure S29). Maleic anhydride is not dissolved in toluene, hexane, cyclohexane, isopropanol and diethyl ether. Due to the necessity of elimination of chlorinated solvents for further studies, acetonitrile was used. Next, a comparison in catalytic

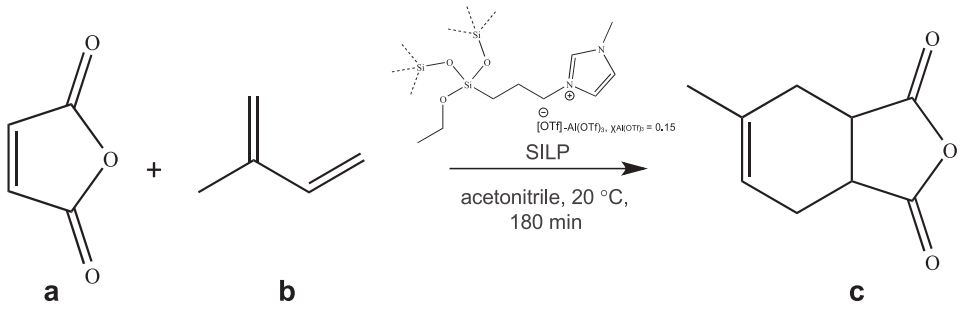

Scheme 2. Diels-Alder cycloaddition between maleic anhydride and isoprene in the presence of SILP catalyst.

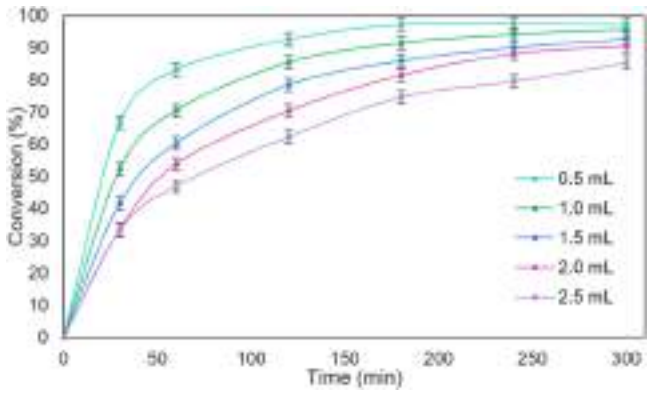

Fig. 1. The influence of acetonitrile amount on MA conversion. Reaction conditions: isoprene 3 mmol, maleic anhydride 2 mmol, acetonitrile 0.5–2.5 mL, SILP(1) catalyst with 0.1 mol% of $Al(OTf)_3$ per maleic anhydride, 20°C. MA conversion was determined using GC.

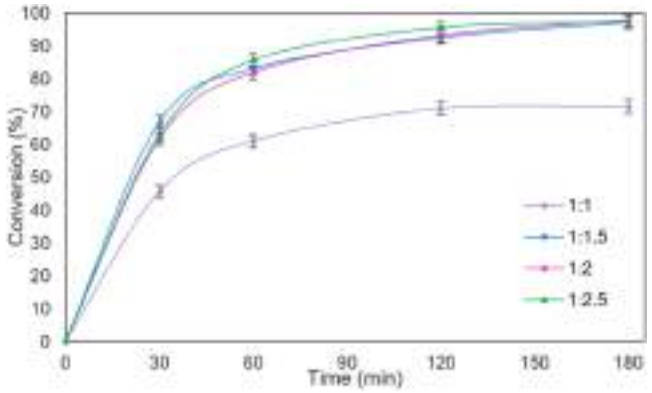

Fig. 2. The influence of maleic anhydride: isoprene molar ratio on MA conversion. Reaction conditions: isoprene 2–5 mmol, maleic anhydride 2 mmol, acetonitrile 0.5 mL, SILP(1) catalyst with 0.1 mol% of $Al(OTf)_3$ per maleic anhydride, 20°C. MA conversion was determined using GC.

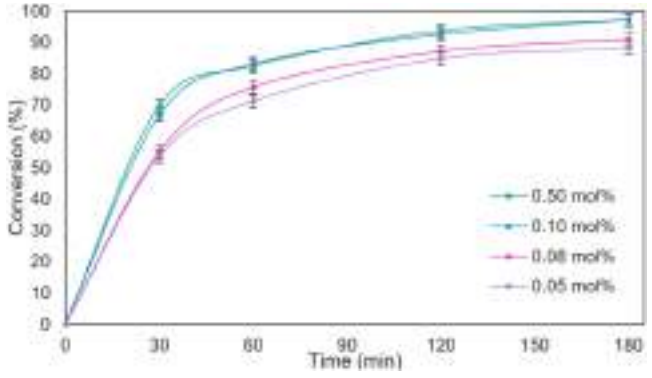

Fig. 3. The influence of catalyst loading on MA conversion. Reaction conditions: isoprene 3 mmol, maleic anhydride 2 mmol, acetonitrile 0.5 mL, SILP (1) catalyst with 0.05–0.5 mol% of $Al(OTf)_3$ per maleic anhydride, 20°C. MA conversion was determined using GC.

performance was undertaken between developed SILP catalysts and aluminium triflate chemically attached to the silica (SiO_2-$Al(OTf)_3$), and the results were shown in Table 1. Significantly higher loading of Al $(OTf)_3$ on the silica surface (36.5 wt%, Supplementary Materials Fig.S8) led to deterioration of free reagents flow through the material, and in consequence decline its catalytic performance.

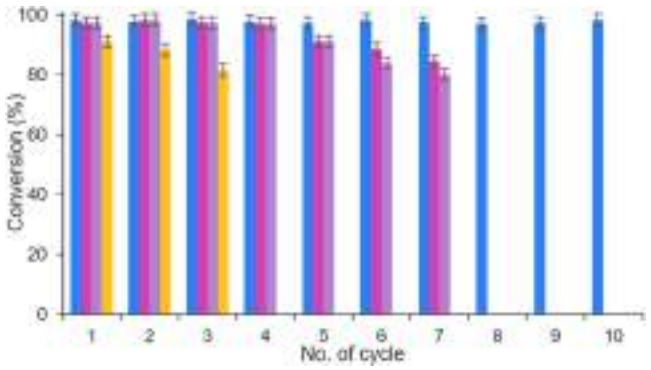

Fig. 4. The influence of IL immobilisation method on SILP (1−3) catalysts recycling; SILP (1) bue; SILP (2) purple; SILP (3) light purple; SiO_2-$Al(OTf)_3$ yellow. Reaction conditions: isoprene 3 mmol, maleic anhydride 2 mmol, acetonitrile 0.5 mL, SILP (1−3) catalysts with 0.1 mol% of $Al(OTf)_3$ per maleic anhydride, 20°C. MA conversion was determined using GC, reaction time 180 min.

Table 3
The influence of the structure of $Al(OTf)_3$-based catalysts on catalytic activity.

Catalyst	Time, min	MA conversion, %
SILP (1)	180	97.45
SiO_2-$Al(OTf)_3$	240	91.17
[tespmim][OTf-$Al(OTf)_3$)]	180	95.57
$Al(OTf)_3$	240	84.01

Reaction conditions: isoprene 3 mmol, maleic anhydride 2 mmol, 0.5 mL acetonitrile, catalyst with 0.1 mol% of $Al(OTf)_3$ per maleic anhydride, 20°C. MA conversion was determined using GC.

At this stage of research, given the lack of differences in catalytic activity among the acquired SILP (1−3) materials, SILP(1) was selected for subsequent optimization of reaction conditions in the model process. The studies on the influence of a solvent amount on maleic anhydride conversion showed that 0.5 mL of acetonitrile is the optimum volume per 2 mmol of maleic anhydride (4 mmol/cm^3) (Fig. 1). Lower amounts hindered the effective mixing of reagents due to the high volume of catalyst. Next, the influence of maleic anhydride: isoprene molar ratio on maleic anhydride conversion was determined (Fig. 2). The most beneficial result was obtained for 1:1.5 MA: isoprene molar ratio. A subsequent increase in the quantity of isoprene did not influence the enhancement of maleic anhydride conversion rates. Finally, the influence of catalyst loading on maleic anhydride conversion was examined and presented in Fig. 3. The results showed that the 0.1 mol% of Al $(OTf)_3$ per MA is enough for efficient catalysis. Lower amounts were not sufficient to obtained full conversion of substrate.

The next challenge was to demonstrate the stability of obtained SILP catalysts in consequent cycles of the reaction. And this time the differences in catalytic activity was clear revealing the importance of the sequence of silica surface modification steps.

Recycling of the SILP (1−3) and SiO_2-$Al(OTf)_3$ catalysts was studied over 10 reaction cycles under optimised conditions (Fig. 4). The recycling experiments were conducted using four times the initial amount of catalyst (160 mg). Following each recovery of the catalyst through filtration, washing with acetonitrile, and drying, the catalyst was weighed, and the reagent quantities for the next cycle were adjusted accordingly based on the recovered mass of the catalyst. After 10 cycles of SILP (1) 63% of catalyst was recovered. All catalysts were used in the same amounts, calculating for active phase. The highest stability was determined for SILP (1) material with no decline in catalytic stability in all studied cycles. SILP (2) and SILP (3) started loss their activities in fifth reaction cycle, conversion of MA after 180 min dropped to 91% and 90% respectively). It is worth to underline that both materials were

Table 4
Diels-Alder synthesis of maleic anhydride adducts in the presence of SILP (1) as a catalyst under evaluated batch conditions.

Dienophile	Diene	Product	Time, min	MA conversion, %
a	b	c	180	97.5
a	d	e	1	99.9
a	f	g	60	98.7
a	h	i	60	98.2
j	b	k	300	87.6 (3:1)[1,3]
j	b	l	120	88.0 (4:1)[2,4]
m	d	n	300	97.1 (4:1)[2,4]
o	d	p	180	80.2 (3:1)[2,4]

Reaction conditions: diene 3 mmol, dienophile 2 mmol, acetonitrile 0.5 mL, SILP (1) catalyst with 0.1 mol% for $Al(OTf)_3$ per dienophile, 20°C. MA conversion was determined using GC. [1]ratio of 1,3-/1,4-substituted isomers; [2]ratio of *endo:exo* isomers; [3]solventless conditions, SILP (1) catalyst with 5 mol% of $Al(OTf)_3$ per dienophile; [4]solventless conditions, SILP (1) catalyst with 1 mol% of $Al(OTf)_3$ per dienophile

prepared with the addition of aluminium triflate after the immobilization of IL ([tespmim][OTf] for SILP (2) or [tespmim]Cl for SILP (3)) on the surface of silica.

It can indicate that some aluminium triflate species embedded straight to the silica surface and partially the complexation reaction did not occur or some moieties of [tespmim][OTf]-$Al(OTf)_3$, $\chi Al(OTf)_3$ = 0.15 leached from silica matrix (loading of IL 10.8 wt% SILP (2), 9.2 wt % SILP (3) after fourth cycle, Supplementary Materials Fig.S17,S18). According to TGA analysis (Supplementary Materials Fig.S19) it can be observed that SILP (1) catalyst remained almost the same quantity of ILs (25.1 wt%) as before the recycling runs (25.3 wt%). Generally, the incorporation of aluminium triflate into the ionic liquid structure

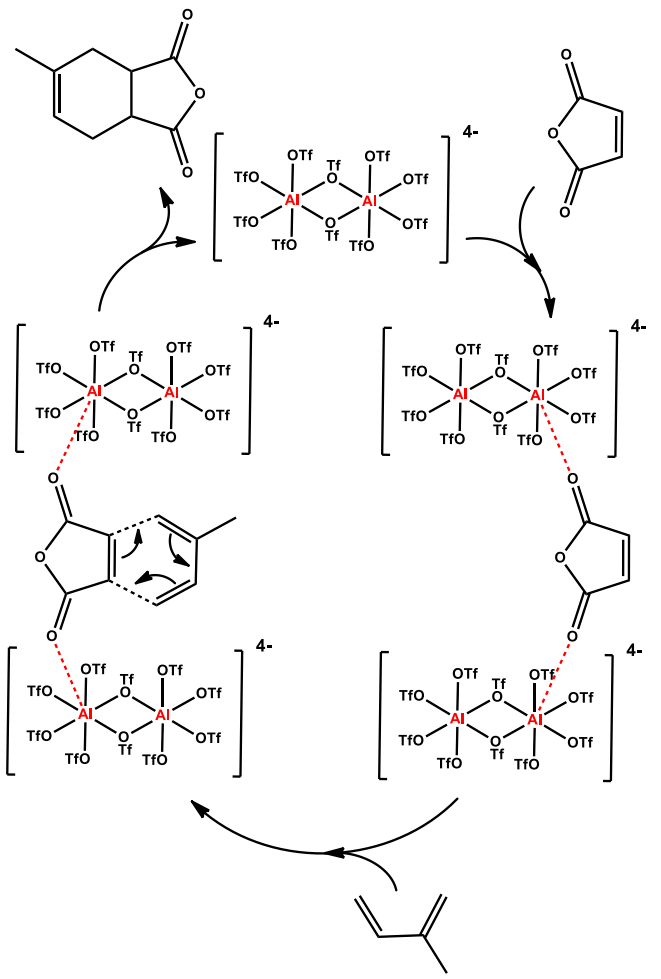

Scheme 3. The plausible mechanism of Diles-Alder reaction in the presence of SILP catalyst.

ensures stability and prevents the leaching of the active phase from the material. This was confirmed by experiments involving the recycling of SiO_2-Al(OTf)$_3$ where the Al(OTf)$_3$ is directly bounded to the surface what causing the lower activity expressed by only 82% conversion of MA after 180 minutes in third cycle.

Summing up SILP (1) catalyst ensures great catalytic performance in cycloaddition of maleic anhydride and isoprene in comparison with SiO_2-Al(OTf)$_3$, and Al(OTf)$_3$ (Table 3). Nearly full conversion of maleic anhydride after 180 min in the presence of SILP (1) with only of 0.1 mol % of Al(OTf)$_3$ was gained. Major advantage above homogeneous form of catalyst [tespmim][OTf-Al(OTf)$_3$)] is effortless and low-cost SILP(1) catalyst recycling and its extremely high stability under evaluated reaction conditions. Developed heterogeneous SILP catalytic system provides sustainability for studied process.

To prove the versatility of developed method for producing maleic anhydride cycloadducts in the presence of SILP (1) catalyst dienes, such as isoprene, cyclopentadiene, myrcene and ocimene, and also other dienophiles as methyl acrylate, ethyl acrylate, diethyl maleate were tested (Table 4). The reactions were tailored to achieve the highest possible conversion, beyond which no further conversion was detected. It was examined that the SILP (1) catalyst was active for all chosen dienes, and almost full conversions of dienophile were achieved in short reaction times.

According to our previous work [23], the structure of trifloaluminate systems, characterised by multinuclear NMR spectroscopy and FT-IR spectroscopy, revealed the existence of hexacoordinate aluminium in multiply-charged, oligonuclear anionic complexes, with multiple bridging triflate modes, e.g. $[Al_2(OTf)_{10}]^{4-}$ and $[Al_3(OTf)_{14}]^{5-}$. The plausible mechanism of Diels-Alder reaction with SILP (1) as Lewis acidic catalyst, with the example of dominant anionic species ($[Al_2(OTf)_{10}]^{4-}$ presents in the anion structure is proposed on Scheme 3. Trifloaluminate anion in SILP (1) acts as an electron pair acceptor to increase the reactivity of a substrate. Next the classical mechanism of Diels-Alder reaction occurs [38].

In summary, SILP (1) with the highest ILs loading (25.3 wt% versus 19.2 and 19.7 wt% for SILP (2−3)) emerges as the most efficient catalyst, demonstrating superior stability. It can be suspected that IL is bounded to the surface exclusively *via* the specially designed triethoxysilyl groups making the catalytically active anion of the catalyst accessible as a Lewis acid. Początek formularza

Regarding SILP (2−3), it cannot be discounted that Al(OTf)$_3$ is directly bounded to the silica surface. This is supported by the lower stability of the catalysts, potentially attributed to the leaching of some Al(OTf)$_3$ bound to the silica surface. Additionally, the specific surface area (S_{BET}) of SILP(1) is lower (92.9 m^2g^{-1} versus 113.7 and 109.7 m^2g^{-1} for SILP(2−3)), indicating a higher amount of immobilized ILs on the surface.

3.3. Trifloaluminate SILP catalysts in continuous flow Diels-Alder reaction

Based on the promising results obtained in the batch system, we decided to test the developed trifloaluminate SILP (1) catalyst for the continuous-flow synthesis. The catalytic activity experiments were performed in a fully automated Syrris Asia column flow reactor equipped with two pumps. Pump A was pumping a solution of maleic anhydride in acetonitrile, while pump B was utilized for isoprene. The steams were merged in a standard T-mixer, and then flowed to the column reactor filled with 0.3 g of SILP (1) material.

Experiments were carried out in various molar ratios of maleic anhydride to isoprene ranging from 1:1–1:2.5 and variable total flow rates ranging from 0.03 to 0.06 $mLmin^{-1}$, the obtained results were collected in Table 5. To maintain the stable reagents flow through the whole system, the backpressure regulator was introduced after the reactor and set to 2 bar (Fig. 5).

The influence of the molar ratio of substrates on the maleic anhydride conversion was examined for 0.06 $mLmin^{-1}$ of total reagents flow. The results obtained in continuous-flow system are quite compatible to those derived in batch. The conversion of maleic anhydride increased along with increasing molar ratio until it reached the 1:1.5 maleic anhydride to isoprene molar ratio. Further increasing the molar ratio of substrates did not lead to higher maleic anhydride conversion.

The influence of the residence time on the maleic anhydride conversion was determined for 1:1.5 maleic anhydride: isoprene molar ratio in total flow from 0.03 to 0.06 $mLmin^{-1}$. As shown in Table 5, increasing the residence time from 18.3 to 36.7 minutes resulted in higher catalyst performance, with substrate conversion improving from approximately 78–97%. A direct comparison of the residence times for batch and continuous systems indicated better efficiency for flow synthesis. The same maleic anhydride conversion value 97% was achieved in 36.7 min in flow and 180 min in batch system. Through all conducted experiments stable catalytic activity for 48 h duration of each attempt could be observed.

Exceptional stability of trifloaluminate SILP (1) material in batch and continuous-flow tests prompted the studies on catalyst long-term stability. The experiment was carried out under optimised conditions, 1:1.5 maleic anhydride: isoprene molar ratio in total flow of 0.06 $mLmin^{-1}$ at 20°C (Fig. 5).

The developed SILP (1) catalyst exhibited extremely stable activity, achieving a 97% maleic anhydride conversion over 432 h with a TOF of 104.3 h^{-1}. Superactivity of trifloaluminate SILP (1) catalyst under flow conditions can be explain by the use of multimodal porous silica used as a support for IL. Advanced porous nature of silica intensified reagents

Table 5
Catalytic activity of SILP (1) in Diels-Alder cycloaddition between maleic anhydride and isoprene under continuous flow conditions.

Flow, pump A, mLmin^{-1}	Flow, pump B, mLmin^{-1}	A:B ratio *(n:n)*	Catalyst loading, g	Residence time, min	Time, h	Conv., %	TOF, h^{-1}
0.0500	0.0100	1:1	0.3	18.3	6	57.7	134.7
					24	58.5	136.6
					48	58.1	135.6
0.0490	0.0110	1:1.12	0.3	18.3	6	67.8	155.1
					24	68.5	156.7
					48	67.7	154.9
0.0480	0.0120	1:1.25	0.3	18.3	6	71.2	159.6
					24	71.6	160.5
					48	71.3	159.8
					6	79.4	170.5
0.0460	0.0140	1:1.5	0.3	18.3	24	78.6	168.8
					48	78.9	169.5
0.0450	0.0150	1:1.67	0.3	18.3	6	77.7	163.3
					24	77.8	163.5
					48	76.9	161.6
		1:2.5	0.3		6	78.6	146.8
0.0400	0.0200			18.3	24	77.6	144.9
					48	78.1	145.9
					6	82.9	148.3
0.0383	0.0113	1:1.5	0.3	22.0	24	83.0	148.4
					48	82.8	148.1
					6	88.6	127.0
0.0307	0.0093	1:1.5	0.3	27.5	24	89.0	127.6
					48	88.8	127.3
					6	96.8	103.6
0.0230	0.0070	1:1.5	0.3	36.7	24	97.2	104.4
					48	97.3	104.5

Reaction conditions: pump A: maleic anhydride (2 M in acetonitrile), pump B: isoprene, 20°C. MA conversion was determined using GC. TOF definition was added to the Supplementary Materials.

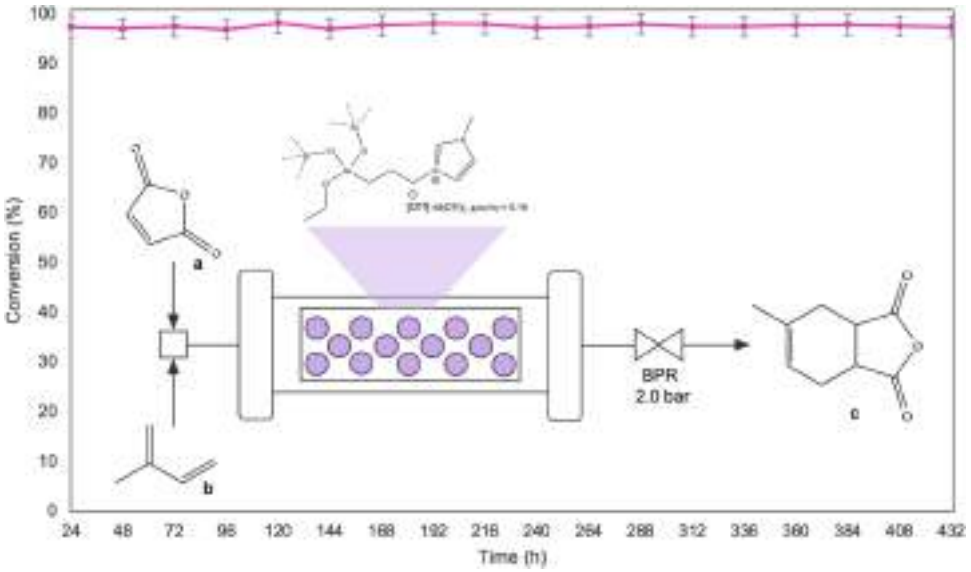

Fig. 5. Catalytic stability of SILP (1) in a flow Diels-Alder cycloaddition between maleic anhydride and isoprene. Reaction conditions: isoprene 0.007 mL/min, maleic anhydride 0.023 mL/min (2 M in acetonitrile), 0.3 g SILP (1) catalyst, 20°C. MA conversion was determined using GC.

mixing and flow through the material improving catalytic properties. The proposed continuous-flow system, utilizing trifloaluminate SILP (1) material, ensured efficient performance in the Diels-Alder reaction, resulting in high maleic anhydride conversion without the need for catalyst separation from the post-reaction mixture. The transformation of Diels-Alder synthesis to continuous-flow process significantly improved its sustainability.

4. Conclusions

In this study, the effective catalysis of in Diels-Alder reaction was reached after carful optimization of the catalyst preparation. Three approaches were explored for the chemical immobilization of trifloaluminate ionic liquid catalyst onto a microporous/mesoporous silica support. The most superior catalytic performance, attaining maleic anhydride conversion of over 97% in ten reaction cycles, was achieved by initially synthesizing the trifloaluminate ionic liquid. Subsequently, this was bound to the silica surface using a 25 wt% loading of the ionic liquid. This successful transformation of the Diels-Alder reaction into continuous flow synthesis resulted in a 97% conversion of maleic anhydride over 432 h (TOF 104.3 h^{-1}).

In the literature, limited reports are available concerning the use of continuous flow technic for the synthesis of Diels-Alder cycloadducts (Table 6). Stevens et al. performed cycloaddition between

Table 6
The comparison of reaction conditions for continuous synthesis of Diels-Alder adducts.

Catalyst	Diels-Alder model reaction	Reaction conditions	Parameters[a]	Lit.
Zeolite H-Beta	Cyclopentadiene and methyl acrylate	0.2 $mLmin^{-1}$, τ=1.8 min, dichloromethane, 100°C	α=95%, 89:11 (*endo/exo*), (7 h)	[39]
Zeolite H-Beta	Isoprene and maleic anhydride	0.1 $mLmin^{-1}$, τ=40.6 min, acetonitrile, 80°C	y= 76%, (72 h)	[40]
MacMillan catalyst attached to silica	Cyclopentadiene and *trans*-cinnamaldehyde	5 $\mu Lmin^{-1}$, τ=10 h, rt	y=95%, 83% (*endo*), (150 h)	[41,42]
MacMillan catalyst copolymerized with divinylbenzene	Cyclopentadiene and *trans*-cinnamaldehyde	5 $\mu Lmin^{-1}$, τ=5 h, acetonitrile:water (95:5; v/v), rt	y=61%, 90% (*endo*)	[43]
MnO_2	Cyclopentadiene and *tert*-butyl N-hydroxycarbamate	0.03 $mLmin^{-1}$, τ=30 min, dichloromethane, rt	y=99%	[44]
SILP(1)	Isoprene and maleic anhydride	0.03 $mLmin^{-1}$, τ=36.7 min, acetonitrile, rt	α=97%, (432 h)	This work

[a] a- conversion; y – yield; in the bracket time in which the catalyst produced product with stable yield.

cyclopentadiene and methyl acrylate in continuous system in the presence of various zeolites as Y, Ultrastable Y, ZSM-5, Beta and Mordenite. High conversion (>95%) and endo-selectivity (89:11) were obtained for this process. What is more, it was reported that flow synthesis achieved 14 times higher production in comparison to batch [39]. Kobayashi et al. used zeolite Beta in continuous cycloaddition of isoprene and acrolein. The catalyst was recyclable for 4 times and showed stability over 72 h [40]. Puglisi et al. investigated chiral MacMillan organocatalyst immobilized on silica for continuous cycloaddition between cyclopentadiene and unsaturated aldehydes. Catalyst assured high yields and satisfying selectivities for 150 h [41,42]. The same group presented chiral MacMillan catalyst grafted into polymer monolith in continuous flow Diels-Alder reaction. Again, high enantioselectivities (90%) and productivities at ambient temperature were reached [43]. Yamamoto et al. showed two catalytic systems for Diels-Alder continuous process. First was based on homogeneous CuCl/pyridine and the second one on heterogeneous MnO_2 catalyst. During this studies, high yields (>99%) and methods versatility were reported [44].

In summary, zeolite H-Beta, McMillan catalyst attached to the silica copolymerized with divinylbenzene or simple MnO2 were used as solid catalysts dedicated for flow synthesis of Diels-Alder cycloadducts. All catalysts were highly active and suitable for flow process, however the advantage of the method described in this work is found for several examples. The reaction of isoprene and maleic anhydride carried out at room temperature with residence time 36.7 min yielded product (conversion 97%) through 432 h (Table 6, entry 6) compering to the method presented in the literature for Zeolite H-Beta (Table 6, entry 1) (temp. 80°C, residence time 40.06 min, yield 76% through 72 h). As shown in the Table 6 employing elevated temperatures (80–100°C) led to reduced reaction times (residence times). The SILP (1) stands out as the first example showcasing an exceptional stability lasting 423 h demonstrated for Diels-Alder reaction. In this work due to the consistent design of trifloaluminate SILP catalysts *via* various synthesis pathways the high catalytic performance was reached, with special emphasis on catalyst stability.

CRediT authorship contribution statement

Agata Jakobik-Kolon: Formal analysis. **Anna Chrobok:** Conceptualization. **Sebastian Jurczyk:** Formal analysis. **Katarzyna Szymańska:** Investigation. **Piotr Latos:** Formal analysis. **Anna Wolny:** Investigation.

Declaration of Competing Interest

The authors declare that they have no known competing financial interests or personal relationships that could have appeared to influence the work reported in this paper.

Data availability

Data will be made available on request.

Acknowledgements

This work was funded by the National Science Centre, Poland. Grant no. UMO-2020/39/B/ST8/00693 and the part concerning catalysis in Diels-Alder reaction by the Silesian University of Technology (Poland), Grant no. 04/050/BKM23/0173.

Appendix A. Supporting information

Supplementary data associated with this article can be found in the online version at doi:10.1016/j.apcata.2024.119676.

References

[1] R.A. Scheldon, Green. Chem. 19 (2017) 18–43, https://doi.org/10.1039/C6GC02157C.
[2] A.P. De los Ríos, A. Irabien, F. Hollmann, F.J.H. Fernández, J. Chem. 2013 (2013) 402172, https://doi.org/10.1155/2013/402172.
[3] R. Ratti, SN Appl. Sci. 2 (2020) 263, https://doi.org/10.1007/s42452-020-2019-6.
[4] A.S. Amarasekara, Chem. Rev. 116 (2016) 6133–6183, https://doi.org/10.1021/acs.chemrev.5b00763.
[5] F. Giacalone, M. Gruttadauria, ChemCatChem 8 (2016) 664–684, https://doi.org/10.1002/cctc.201501086.
[6] W. Schwieger, T. Selvam, M. Klumpp, M. Hartmann, Supported Ionic Liquids: Fundamental and Applications, Wiley-VCH Verlag GmbH, Berlin, Germany, 2014, pp. 37–74.
[7] M.H. Valkenberg, C. deCastro, W.F. Hölderich, Green. Chem. 4 (2001) 88–93, https://doi.org/10.1039/B107946H.
[8] R. Skoda-Földes, Molecules 19 (2014) 8840–8884, https://doi.org/10.3390/molecules19078840 (doi.org/).
[9] M. Vafaeezadeh, H. Alinezhad, J. Mol. Liq. 218 (2016) 95–105, https://doi.org/10.1016/j.molliq.2016.02.017.
[10] A. Wolny, A. Chrobok, Molecules 27 (2022) 5900, https://doi.org/10.3390/molecules27185900.
[11] Y. Gu, G. Li, Adv. Synth. Catal. 351 (2009) 817–847, https://doi.org/10.1002/adsc.200900043.
[12] A. Wolny, A. Chrobok, Nanomaterials 11 (2021) 2030, https://doi.org/10.3390/nano11082030.
[13] E. Garcia-Verdugo, P. Lozano, S.V. Luis, Supported Ionic Liquids: Fundamental and Applications, Wiley-VCH Verlag GmbH, Berlin, Germany, 2014, pp. 351–368.
[14] R. Athavale, S. Gardi, F. Choudhary, D. Patil, N. Chandan, P. More, Appl. Catal. A Gen. 669 (2024) 119505, https://doi.org/10.1016/j.apcata.2023.119505.
[15] P. Patil, S. Kadam, D. Patil, P. More, Catal. Commun. 170 (2022) 106500, https://doi.org/10.1016/j.catcom.2022.106500.
[16] P. Patil, S. Kadam, D. Patil, P. More, J. Mol. Liq. 345 (2022) 117867, https://doi.org/10.1016/j.molliq.2021.117867.
[17] K. Matuszek, A. Chrobok, P. Latos, M. Markiton, K. Szymańska, A. Jarzębski, M. Swadźba-Kwaśny, Catal. Sci. Technol. 6 (2016) 8129–8137, https://doi.org/10.1039/C6CY01771A.
[18] P. Kumar, W. Vermeiren, J.-P. Dath, W.F. Hoelderich, Appl. Catal. A Gen. 304 (2006) 131–141, https://doi.org/10.1016/j.apcata.2006.02.030.
[19] S. Liu, J. Shang, S. Zhang, B. Yang, Y. Deng, Catal. Today 200 (2013) 41–48, https://doi.org/10.1016/j.cattod.2012.06.023.
[20] G. Wang, N. Yu, L. Peng, R. Tan, H. Zhao, D. Yin, D. Yin, Catal. Lett. 123 (2008) 252–258, https://doi.org/10.1007/s10562-008-9415-7.

[21] H. Zhao, N. Yu, J. Wang, D. Zhuang, Y. Ding, R. Tan, D. Yin, Microporous Mesoporous Mater. 122 (2009) 240–246, https://doi.org/10.1016/j.micromeso.2009.03.006.
[22] T.M. Jyothi, M.L. Kaliya, M. Herskowitz, M.V. Landau, Chem. Commun. 11 (2001) 992–993, https://doi.org/10.1039/B101843O.
[23] P. Latos, A. Culkin, N. Barteczko, S. Boncel, S. Jurczyk, L.C. Brown, P. Nockemann, A. Chrobok, M. Swadźba-Kwaśny, Front. Chem. 6 (2018), https://doi.org/10.3389/fchem.2018.00535.
[24] P. Latos, A. Szelwicka, S. Boncel, S. Jurczyk, M. Swadzba-Kwasny, A. Chrobok, ACS Sustain. Chem. Eng. 7 (2019) 5184–5191, https://doi.org/10.1021/acssuschemeng.8b06066.
[25] P. Latos, A. Wolny, J. Zdarta, F. Ciesielczyk, S. Jurczyk, T. Jesionowski, A. Chrobok, Environ. Technol. Innov. 31 (2023) 103164, https://doi.org/10.1016/j.eti.2023.103164.
[26] P. Latos, A. Wolny, A. Chrobok, Materials 16 (2023) 2106, https://doi.org/10.3390/ma16052106.
[27] M. Haumann, Commercial Applications of Ionic Liquids, Springer, Cham, Switzerland, 2020, pp. 49–67.
[28] M.I. Burguete, E. García-Verdugo, N. Karbass, S.V. Luis, V. Sans, M. Sokolova, Pure Appl. Chem. 81 (2009) 1991–2000, https://doi.org/10.1351/PAC-CON-08-11-02.
[29] J.M. Marinkovic, A. Riisager, R. Franke, P. Wasserscheid, M. Haumann, Ind. Eng. Chem. Res. 58 (2019) 2409–2420, https://doi.org/10.1021/acs.iecr.8b04010.
[30] P. Lozano, S.N. Cerón, J. Serrano, J. Pérez, G. Sánchez, E. Garcia-Verdugo, S. V. Luis, Mini-Rev. Org. Chem. 14 (2017) 65–74, https://doi.org/10.2174/1570193×13666161103145723.
[31] A. Drożdż, A. Chrobok, S. Baj, K. Szymańska, J. Mrowiec-Białoń, A. Jarzębski, Appl. Catal. A 467 (2013) 163, https://doi.org/10.1016/j.apcata.2013.07.009.
[32] A. Chrobok, S. Baj, W. Pudło, Jarzębski, Appl. Catal. A 366 (2009) 22, https://doi.org/10.1016/j.apcata.2009.06.040.
[33] J.A. Funel, S. Abele, Angew. Chem. 52 (2013) 3822–3863, https://doi.org/10.1002/anie.201201636.
[34] B. Briou, B. Améduri, B. Boutevin, Chem. Soc. Rev. 50 (2021) 11055–11097, https://doi.org/10.1039/D0CS01382J.
[35] X.-C. Lv, Z.-C. Tan, Q. Shi, H.-T. Zhang, L.-X. Sun, T. Zhang, J. Chem. Eng. Data 36 (2005) 932–935, https://doi.org/10.1016/j.jct.2004.05.008.
[36] N. Tomotaka, I. Yusuke, S. Masaki, I. Yoshio, A. Yasuhiko, AIChE J. 44 (1998) 1706–1708, https://doi.org/10.1002/aic.690440723.
[37] Y. Ikushima, N. Saito, M. Arat, Bull. Chem. Soc. Jpn. 64 (1990) 282–284, https://doi.org/10.1246/bcsj.64.282.
[38] R. Kalepu, S. Mishra, Rapid Commun. 132 (2020) 48, https://doi.org/10.1007/s12039-020-1749-8.
[39] S. Seghers, L. Protasova, S. Mullens, J.W. Thybaut, C.V. Stevens, Green. Chem. 19 (2017) 237–248, https://doi.org/10.1039/C6GC02334G.
[40] K. Masuda, S.G. Agalave, W. Chen, S.-y Onozawa, S. Shimada, K. Sato, S. Kobayashi, Asian J. Org. Chem. 12 (2023) e202200557, https://doi.org/10.1002/ajoc.202200557.
[41] R. Porta, M. Benaglia, V. Chiroli, F. Coccia, A. Puglisi, Isr. J. Chem. 54 (2014) 381–394, https://doi.org/10.1002/chin.201440033.
[42] V. Chiroli, M. Benaglia, F. Cozzi, A. Puglisi, R. Annunziata, G. Celentano, Org. Lett. 15 (2013) 3590–3593, https://doi.org/10.1021/ol401390z.
[43] V. Chiroli, M. Benaglia, A. Puglisi, R. Porta, R.P. Jumde, A. Mandoli, Green. Chem. 16 (2014) 2798, https://doi.org/10.1039/C4GC00031E.
[44] E. Nakashima, H. Yamamoto, Chem. Commun. 51 (2015) 12309–12312, https://doi.org/10.1039/C5CC03458B.

Supporting Materials

Construction of trifloaluminate ionic liquid catalyst on the silica surface dedicated for continuous flow Diels-Alder synthesis

Anna Wolny[a], Piotr Latos[a], Katarzyna Szymańska[b], Sebastian Jurczyk[c], Agata Jakóbik-Kolon[d], Anna Chrobok[a,]*

[a] Department of Chemical Organic Technology and Petrochemistry, Faculty of Chemistry, Silesian University of Technology, Krzywoustego 4, PL-44100 Gliwice, Poland, *anna.chrobok@polsl.pl

[b] Department of Chemical Engineering and Process Design, Faculty of Chemistry, Silesian University of Technology, Krzywoustego 4, PL-44100 Gliwice, Poland

[c] Institute for Engineering of Polymer Materials and Dyes, Lukasiewicz Research Network, Sklodowskiej-Curie 55, PL-87100 Torun, Poland

[d] Department of Inorganic Chemistry, Analytical Chemistry and Electrochemistry, Faculty of Chemistry, Silesian University of Technology, Bolesława Krzywoustego 6, 44-100 Gliwice, Poland

* Corresponding author: anna.chrobok@polsl.pl, Krzywoustego 4 Street, 44-100 Gliwice, Poland.

Materials and methods

[tespmim]Cl synthesis [7,14]: (3-chloropropyl)triethoxysilane (0.1 mol) and 1-methylimidazole (0.1 mol, freshly distilled) were placed into 100 mL round-bottomed flask at 80°C for 24 h (Ar atmosphere). The crude product was washed with diethyl ether (3 × 5 mL) and dried on the Schlenk line (24 h) yielded 96% of product.

^{1}H NMR (400 MHz, dmso) δ 9.26 (s, 1H), 7.80 (s, 1H), 7.74 (s, 1H), 4.14 (t, J = 7.1 Hz, 2H), 3.86 (s, 3H), 3.74 (q, J = 7.0 Hz, 6H), 1.85 – 1.77 (m, 2H), 1.14 (t, J = 7.0 Hz, 9H), 0.55 – 0.48 (m, 2H).

^{13}C NMR (151 MHz, dmso) δ 136.53 (s), 123.60 (s), 122.16 (s), 57.81 (s), 51.02 (s), 39.87 (d, J = 20.7 Hz), 39.74 – 39.72 (m), 39.72 – 39.08 (m), 35.71 (s), 23.58 (s), 18.12 (s), 6.65 (s).

[tespmim]OTf synthesis [17]: [tespmim]Cl (0.1 mol), silver triflate (0.12 mol) and ethyl acetate (50 mL) were introduced to the 100 mL dark roud-bottomed flask and mixed at room temperature for 24 h. Then, silver chloride was filtered off, washed with ethyl acetate, and the organic layer was checked for the chloride presence with $AgNO_3$ test and dried on the Schlenk line (24 h) yielded 99% of product.

^{1}H NMR (600 MHz, dmso) δ 9.07 (s, 1H), 7.75 (s, 1H), 7.69 (s, 1H), 4.12 (s, 2H), 3.84 (s, 3H), 3.75 (q, J = 7.0 Hz, 6H), 1.83 – 1.80 (m, 2H), 1.14 (t, J = 7.0 Hz, 9H), 0.52 (m, J = 7.6, 4.2 Hz, 2H).

^{13}C NMR (151 MHz, dmso) δ 158.30 (s), 136.53 (s), 123.60 (s), 122.16 (s), 57.81 (s), 51.02 (s), 39.87 (d, J = 20.7 Hz), 39.74 – 39.72 (m), 39.72 – 39.08 (m), 35.71 (s), 23.58 (s), 18.12 (s), 6.65 (s).

[tespmim][OTf-Al(OTf)$_3$], $\chi_{Al(OTf)3}$ = 0.15 synthesis [17]: [tespmim][OTf] and the appropriate mass of aluminium triflate (molar ratio $\chi_{Al(OTf)3}$ = 0.15) were put to the 50 mL flask and stirred at 120 °C until homogeneous yielded 99% (3 g) of product without purification.
^{1}H NMR (600 MHz, dmso) δ 9.13 (s, 1H), 7.83 (s, 1H), 7.72 (s, 1H), 4.19 (s, 2H), 3.88 (s, 3H), 3.79 (q, J = 7.0 Hz, 6H), 1.85 – 1.81 (m, 2H), 1.21 (t, J = 7.0 Hz, 9H), 0.61 (m, J = 7.6, 4.2 Hz, 2H).
^{13}C NMR (151 MHz, dmso) δ 159.43 (s), 142.71 (s), 129.12 (s), 127.96 (s), 60.11 (s), 54.80 (s), 42.88 (d, J = 20.7 Hz), 40.12 – 39.99 (m), 39.87 – 39.08 (m), 36.33 (s), 24.91 (s), 19.02 (s), 6.90 (s).

Multimodal porous silica [14, 28, 29]:
Polyethylene glycol 35 000 (8.67 g) was dissolved in 1 M HNO_3 (100 mL) and then tetraethoxysilane (82.8 mL) was added dropwise under stirring (500 rpm) in an ice bath. Cetyltrimethylammonium bromide (3.8 g) was added next and after mixing the solution was transferred into forms and left to gel at 40 ◦C and aged for 7 days. The received alcogels were impregnated with 1 M ammonia water solution for 9 h at 90 ◦C, rinsed with water, dried, and calcinated at 550 ◦C for 10 h (ramp of 1 ◦C min^{-1}). After calcination, the monoliths were crushed.

ICP method
The content of aluminum in catalyst as well as sole ionic liquid samples was determined using inductively coupled plasma atomic emission spectrometry (ICP-AES). Varian 710-ES spectrometer (Varian, Palo Alto, CA, USA) equipped with a sea-spray nebulizer and twister glass spray chamber was utilized. The following parameters were applied: RF power 1.0 kW, plasma flow (argon) 15 L/min, auxiliary flow (argon) 1.5 L/min, nebulizer pressure (argon) 210 kPa, pump rate 15 rpm, emission lines of Al: λ= 237.312, 236.705 and 396.152 nm.
The samples: [tespmim][OTf-Al(OTf)$_3$], χAl(OTf)$_3$ = 0.15 (0.0125 g), SILP(1) (0.0101 g), SILP(2) (0.0204 g), SILP(3) (0.0203 g) were dissolved by heating in concentrated nitric acid for 2 h and then diluted with deionized water to 20 mL (18 MΩ·cm, Simplicity Water Purification Systems, Millipore SAS). Analysis was conducted from diluted samples filtered through a 0.22 µm syringe filter. Blank sample was also prepared. The result given is the average of results obtained for three aluminum analytical lines used with error not exceeding 2%. The calibration curve method was used to determine the concentration of aluminum. Standards were prepared by diluting 1000 mg/L of Al standard solution (Certipur, Merck). The concentration of Al in the calibration solutions ranged from: 0.1 - 10 mg/L. A linear model of the calibration curve was assumed, with a minimum correlation coefficient of 0.999.

TOF calculation

$$TOF = \frac{n_{product}}{n_{SILP\ active\ site}\, t}\ h^{-1}$$

Analyses

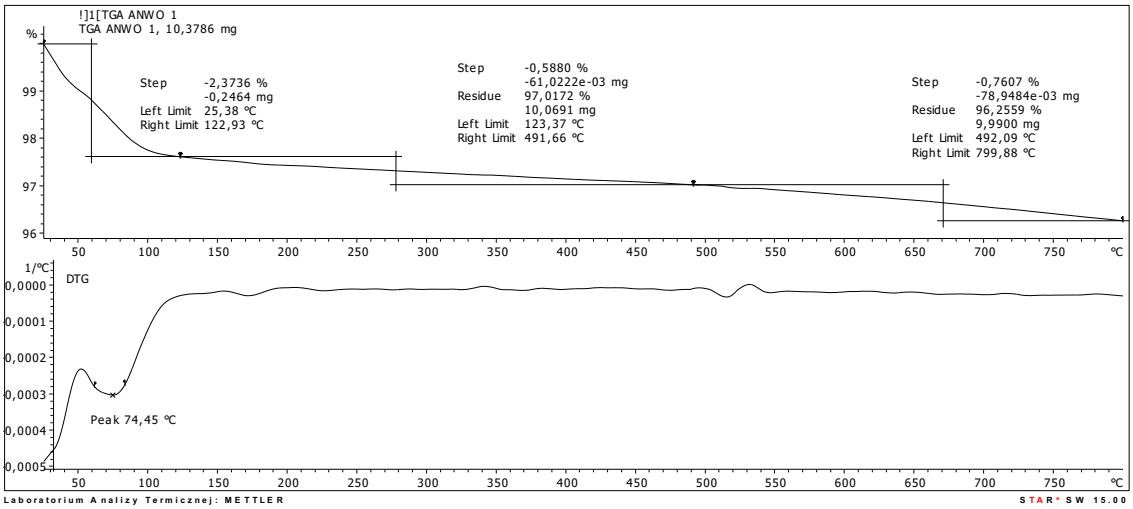

Figure S1. Thermogravimetric analysis of SiO_2.

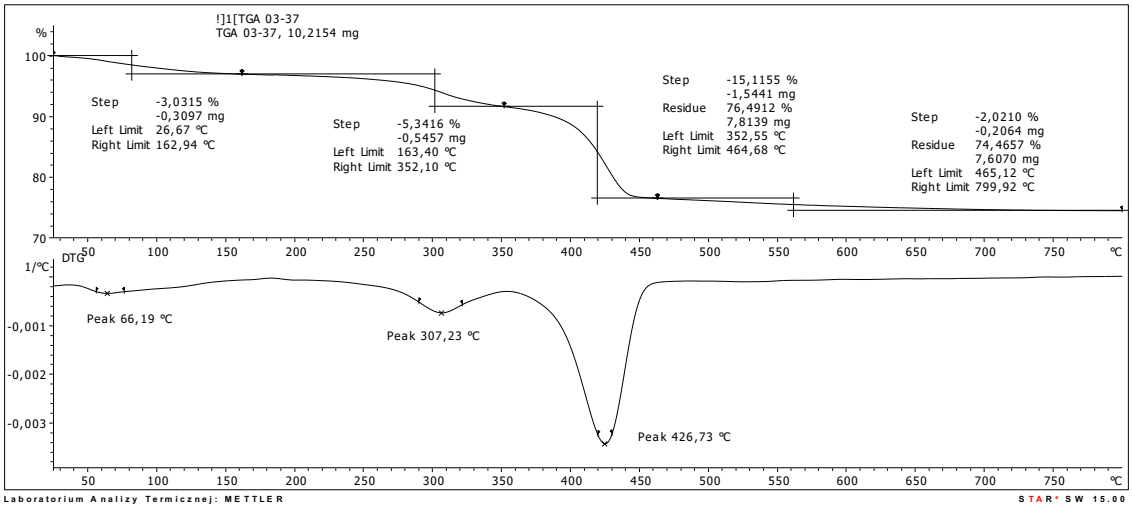

Figure S2. Thermogravimetric analysis of SiO_2-[tespmim][OTf]-$Al(OTf)_3$, $\chi_{Al(OTf)_3}$ = 0.15 SILP (1).

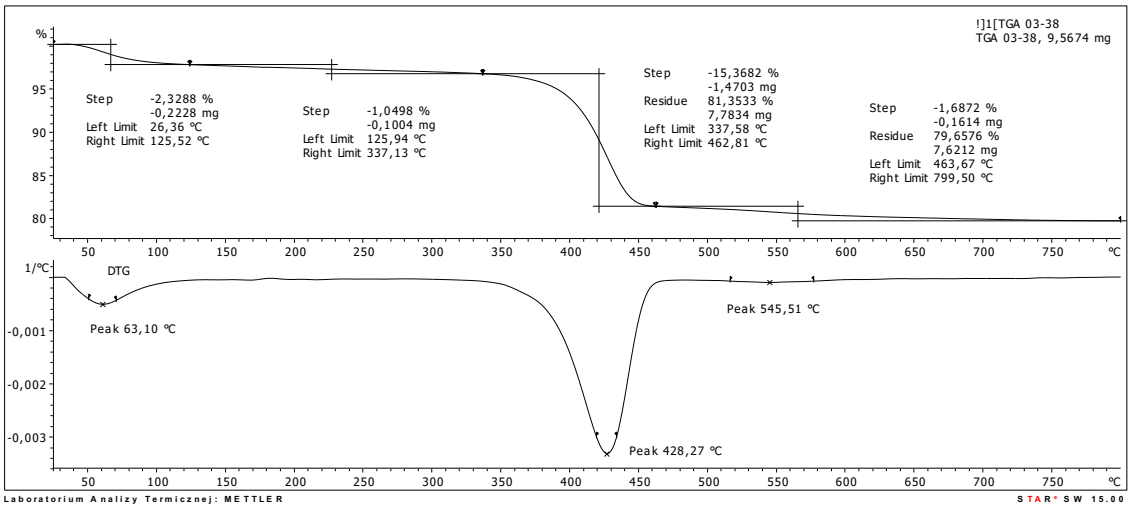

Figure S3. Thermogravimetric analysis of SiO_2-[tespmim]OTf (Method 2).

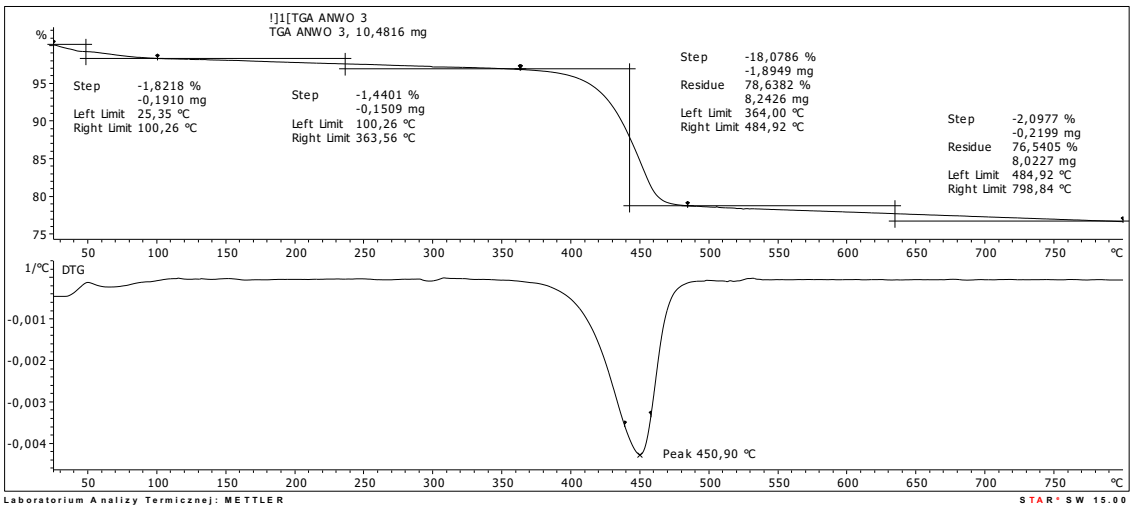

Figure S4. Thermogravimetric analysis of SiO_2-[tespmim][OTf]-$Al(OTf)_3$, $\chi_{Al(OTf)_3}$ = 0.15 SILP (2).

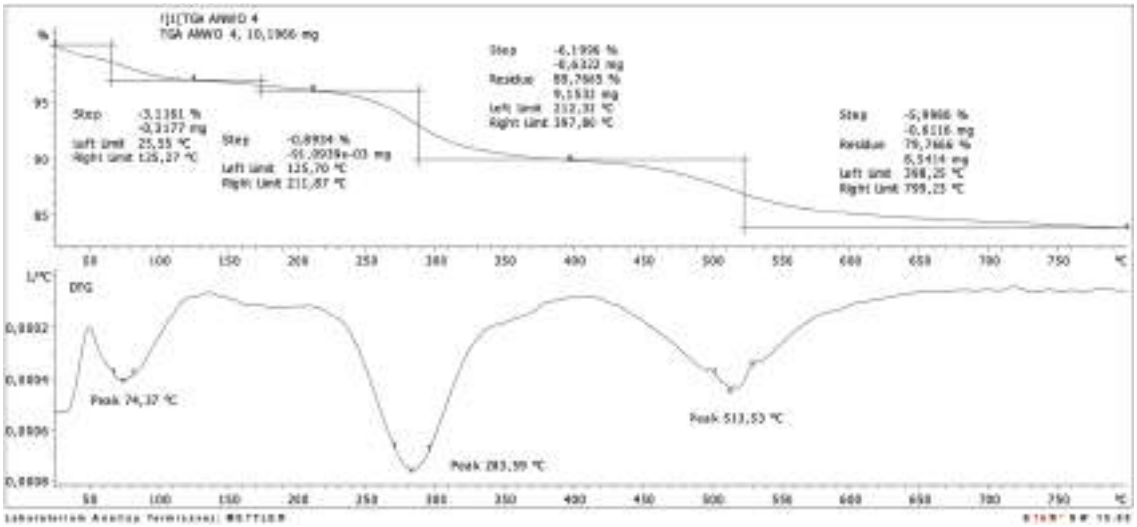

Figure S5. Thermogravimetric analysis of SiO_2-[tespmim]Cl (Method 3).

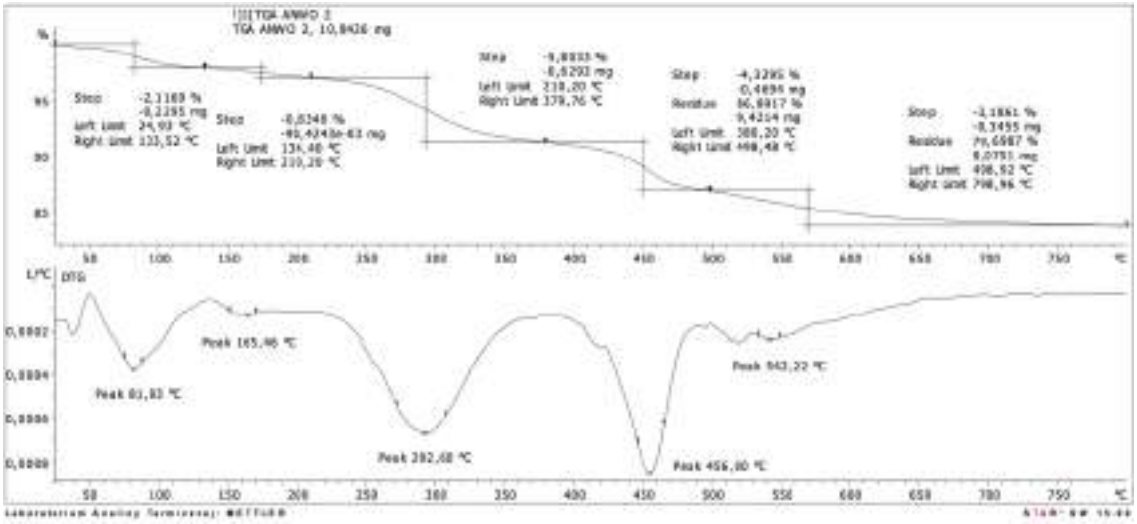

Figure S6. Thermogravimetric analysis of SiO_2-[tespmim]OTf (Method 3).

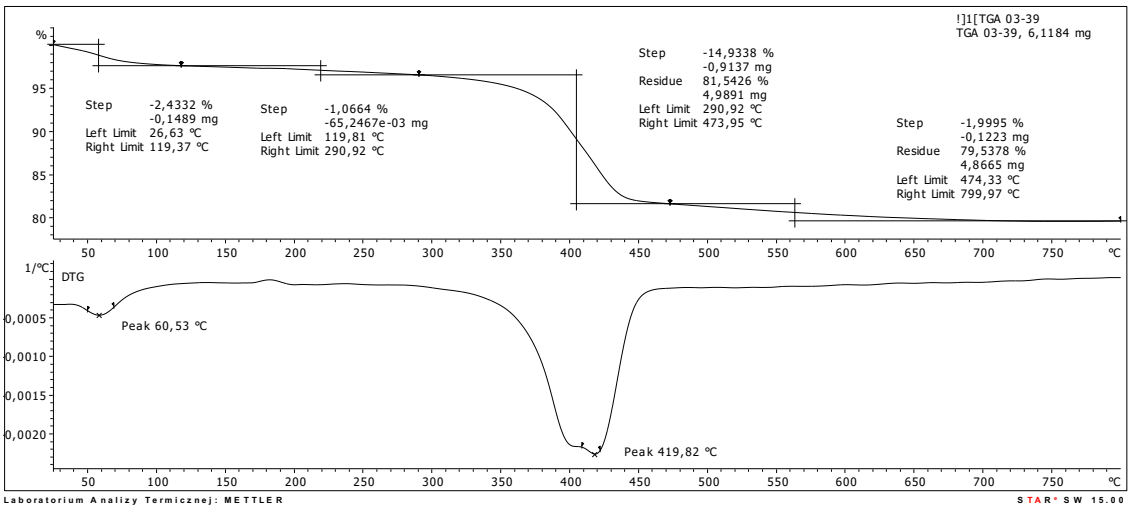

Figure S7. Thermogravimetric analysis of SiO_2-[tespmim][OTf]-Al(OTf)$_3$, $\chi_{Al(OTf)_3}$ = 0.15 SILP (3).

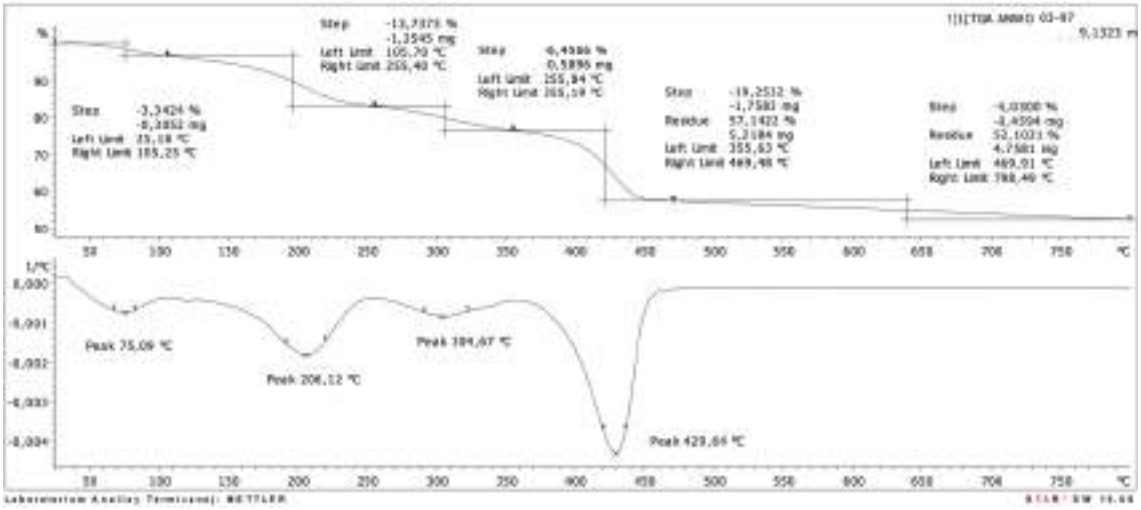

Figure S8. Thermogravimetric analysis of SiO_2-Al(OTf)$_3$.

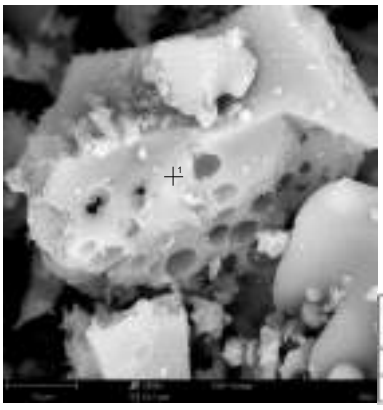

Element Symbol	Element Name	Atomic Conc.	Weight Conc.
O	Oxygen	72.04	59.47
Si	Silicon	27.96	40.53

Figure S9. The SEM-EDX analysis of SiO_2.

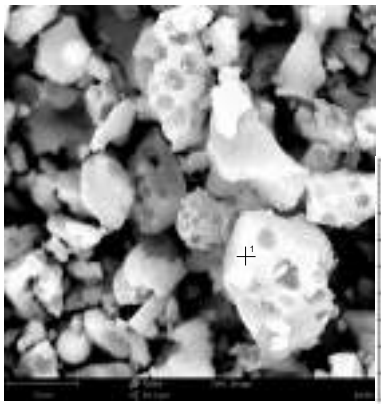

Element Symbol	Element Name	Atomic Conc.	Weight Conc.
O	Oxygen	59.18	52.38
Si	Silicon	18.86	29.30
C	Carbon	10.50	6.98
F	Fluorine	5.52	5.80
N	Nitrogen	4.93	3.82
S	Sulfur	0.75	1.32
Al	Aluminium	0.27	0.40

Figure S10. The SEM-EDX analysis of SiO_2-[tespmim][OTf]-$Al(OTf)_3$, $\chi_{Al(OTf)_3}$ = 0.15 SILP (1).

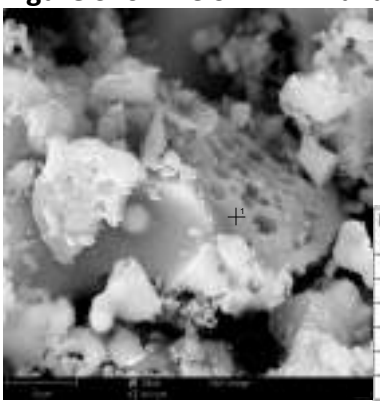

Element Symbol	Element Name	Atomic Conc.	Weight Conc.
O	Oxygen	60.51	54.93
Si	Silicon	16.55	26.37
C	Carbon	15.43	10.51
F	Fluorine	3.93	4.24
N	Nitrogen	2.44	2.12
S	Sulfur	1.15	1.83

Figure S11. The SEM-EDX analysis of SiO_2-[tespmim][OTf] (2).

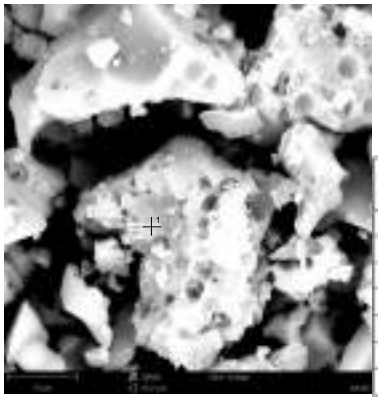

Element Symbol	Element Name	Atomic Conc.	Weight Conc.
O	Oxygen	52.17	51.21
C	Carbon	27.94	20.59
Si	Silicon	11.23	19.35
N	Nitrogen	5.33	4.58
F	Fluorine	2.81	3.28
S	Sulfur	0.44	0.86
Al	Aluminium	0.08	0.13

Figure S12. The SEM-EDX analysis of SiO_2-[tespmim][OTf]-$Al(OTf)_3$, $\chi_{Al(OTf)_3}$ = 0.15 SILP (2).

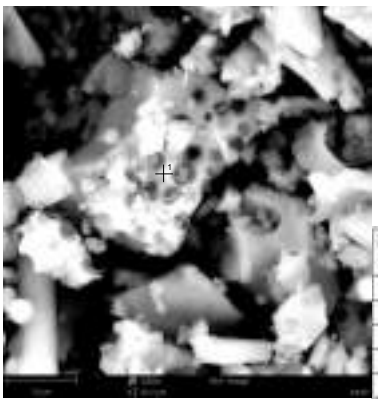

Element Symbol	Element Name	Atomic Conc.	Weight Conc.
O	Oxygen	61.39	55.22
Si	Silicon	18.85	29.77
C	Carbon	12.42	8.38
N	Nitrogen	6.64	5.23
Cl	Chlorine	0.70	1.40

Figure S13. The SEM-EDX analysis of SiO_2-[tespmim]Cl (3)

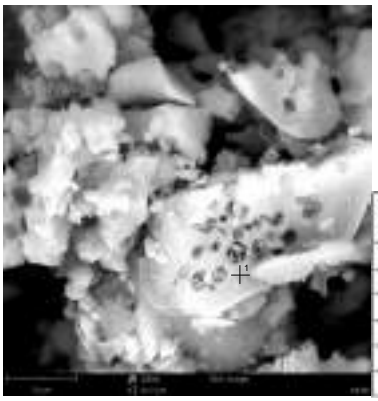

Element Symbol	Element Name	Atomic Conc.	Weight Conc.
O	Oxygen	58.16	51.79
Si	Silicon	19.91	31.12
C	Carbon	15.20	10.16
F	Fluorine	2.72	2.87
N	Nitrogen	3.08	2.40
S	Sulfur	0.93	1.66

Figure S14. The SEM-EDX analysis of SiO_2-[tespmim][OTf] (3).

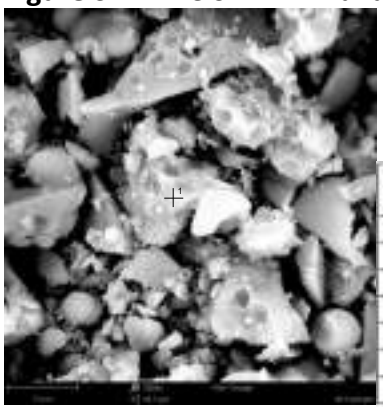

Element Symbol	Element Name	Atomic Conc.	Weight Conc.
O	Oxygen	51.73	47.24
Si	Silicon	14.94	23.95
C	Carbon	19.85	13.61
F	Fluorine	7.59	8.23
S	Sulfur	1.95	3.58
N	Nitrogen	3.61	2.88
Al	Aluminium	0.34	0.52

Figure S15. The SEM-EDX analysis of SiO_2-[tespmim][OTf]-$Al(OTf)_3$, $\chi_{Al(OTf)_3}$ = 0.15 SILP (3).

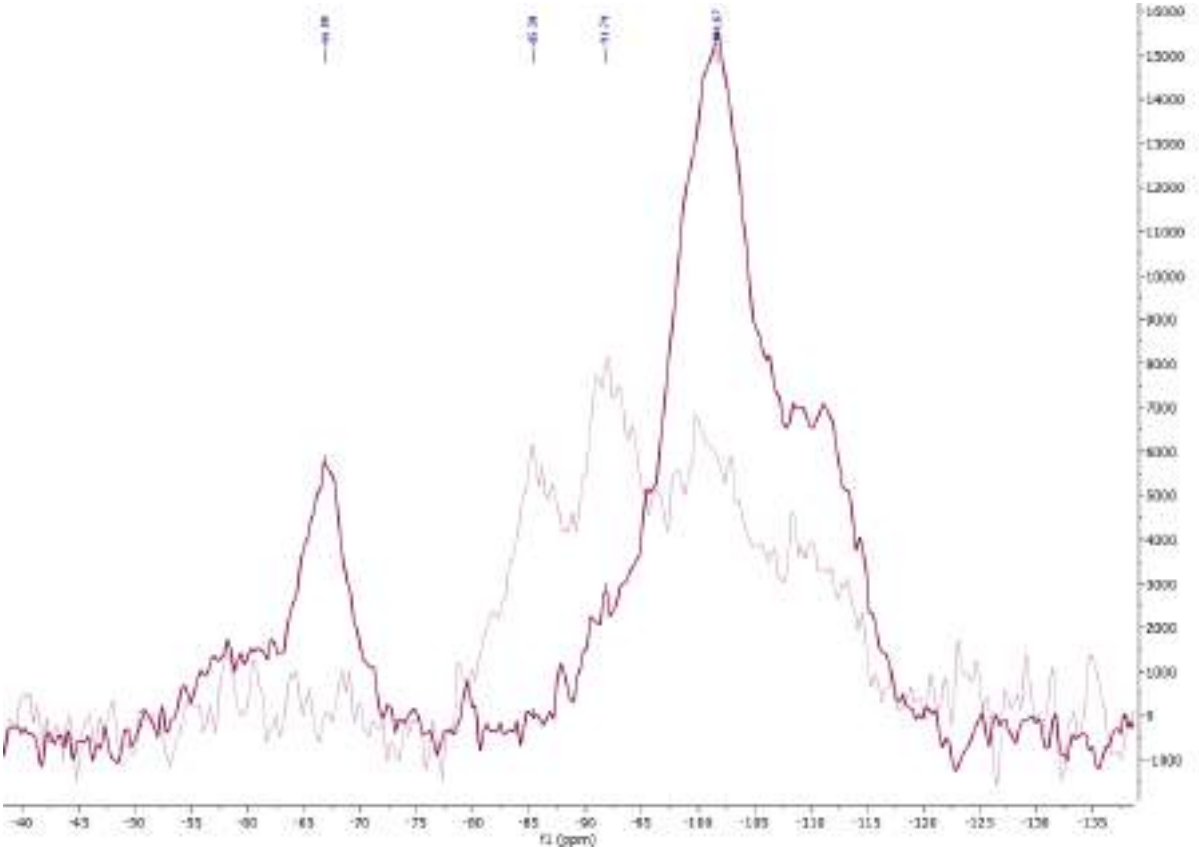

Figure S16. ^{29}Si MAS NMR spectra of SiO_2-[tespmim][OTf]-$Al(OTf)_3$, $\chi_{Al(OTf)_3}$ = 0.15.

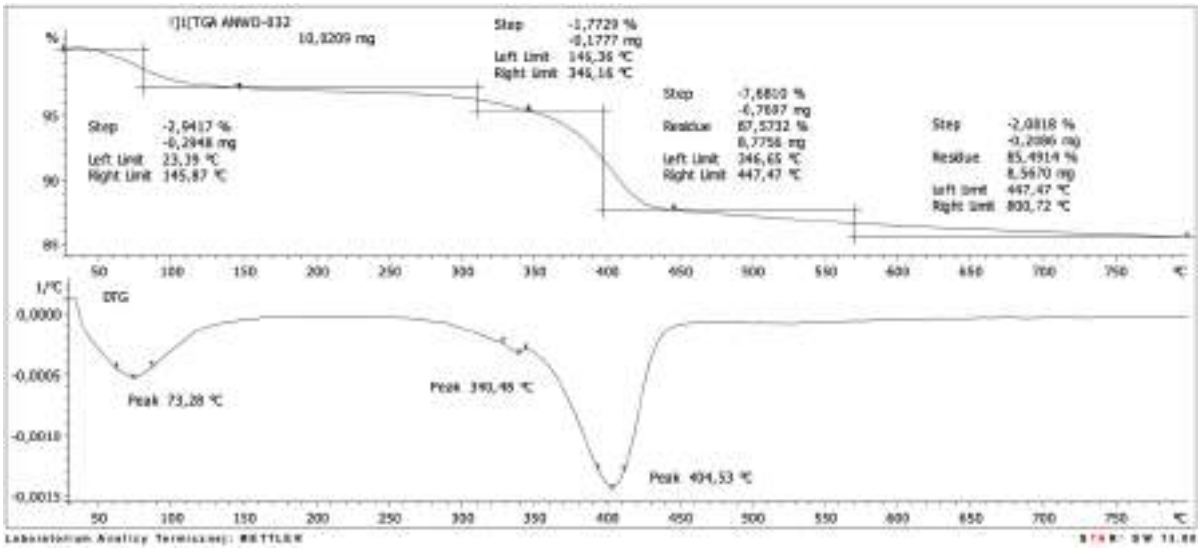

Figure S17. Thermogravimetric analysis of SiO_2-[tespmim][OTf]-$Al(OTf)_3$, $\chi_{Al(OTf)_3}$ = 0.15 SILP (2) after fourth cycle.

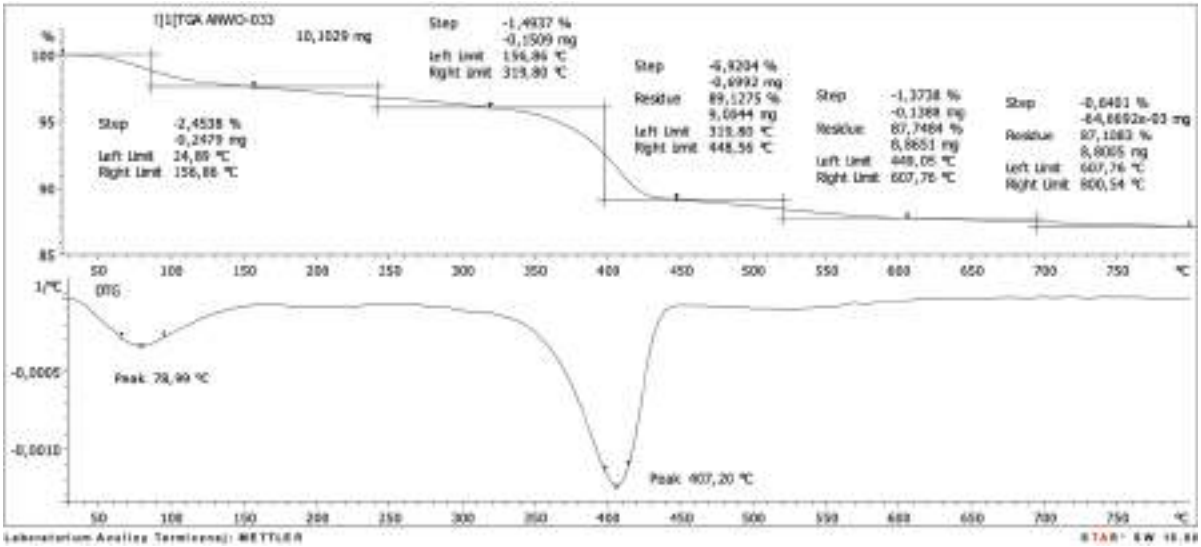

Figure S18. Thermogravimetric analysis of SiO_2-[tespmim][OTf]-$Al(OTf)_3$, $\chi_{Al(OTf)_3}$ = 0.15 SILP (3) after fourth cycle.

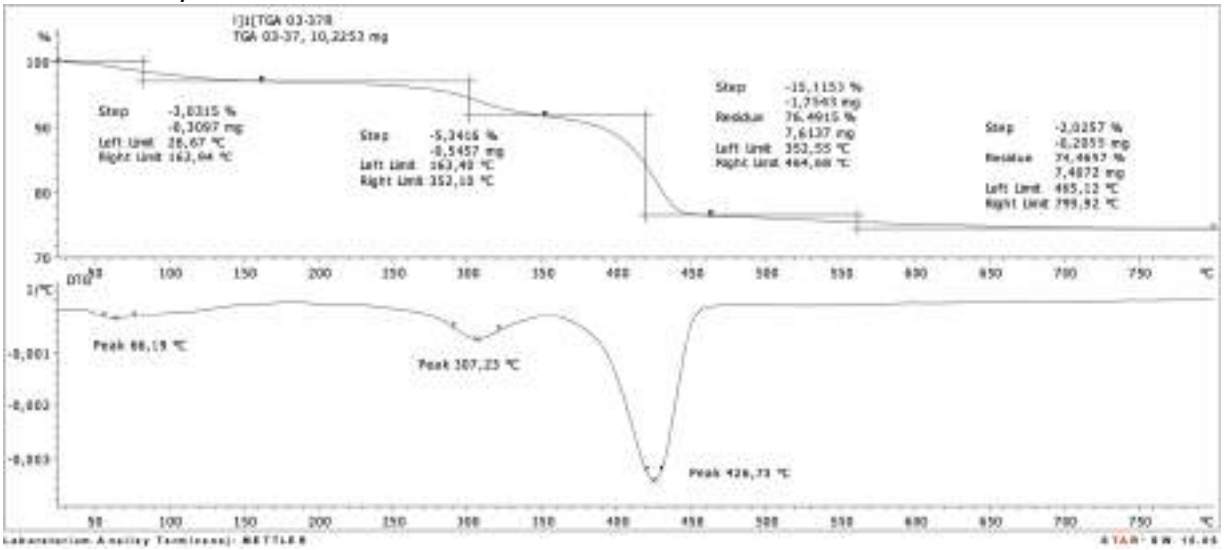

Figure S19. Thermogravimetric analysis of SiO_2-[tespmim][OTf]-$Al(OTf)_3$, $\chi_{Al(OTf)_3}$ = 0.15 SILP (1) after recycling.

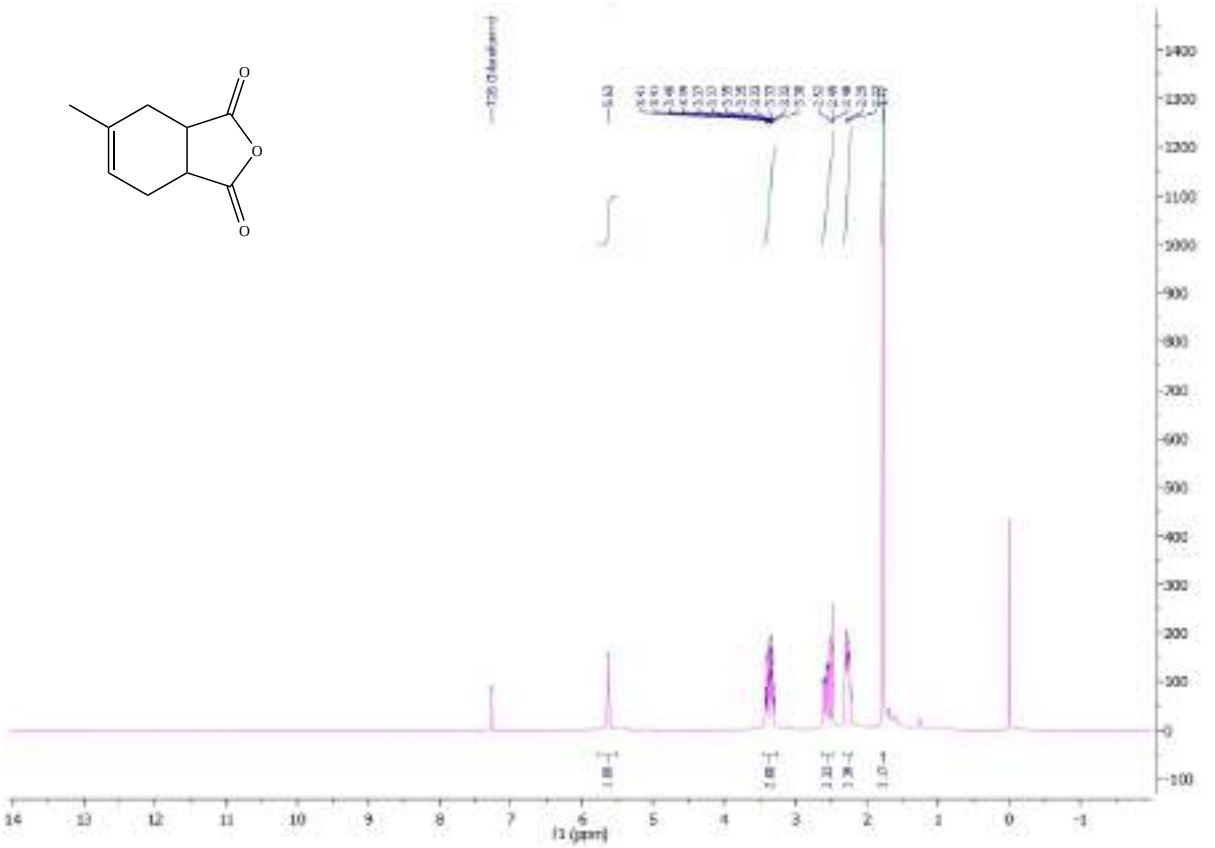

Figure S20a. ^{1}H NMR analysis of cycloadduct (c).

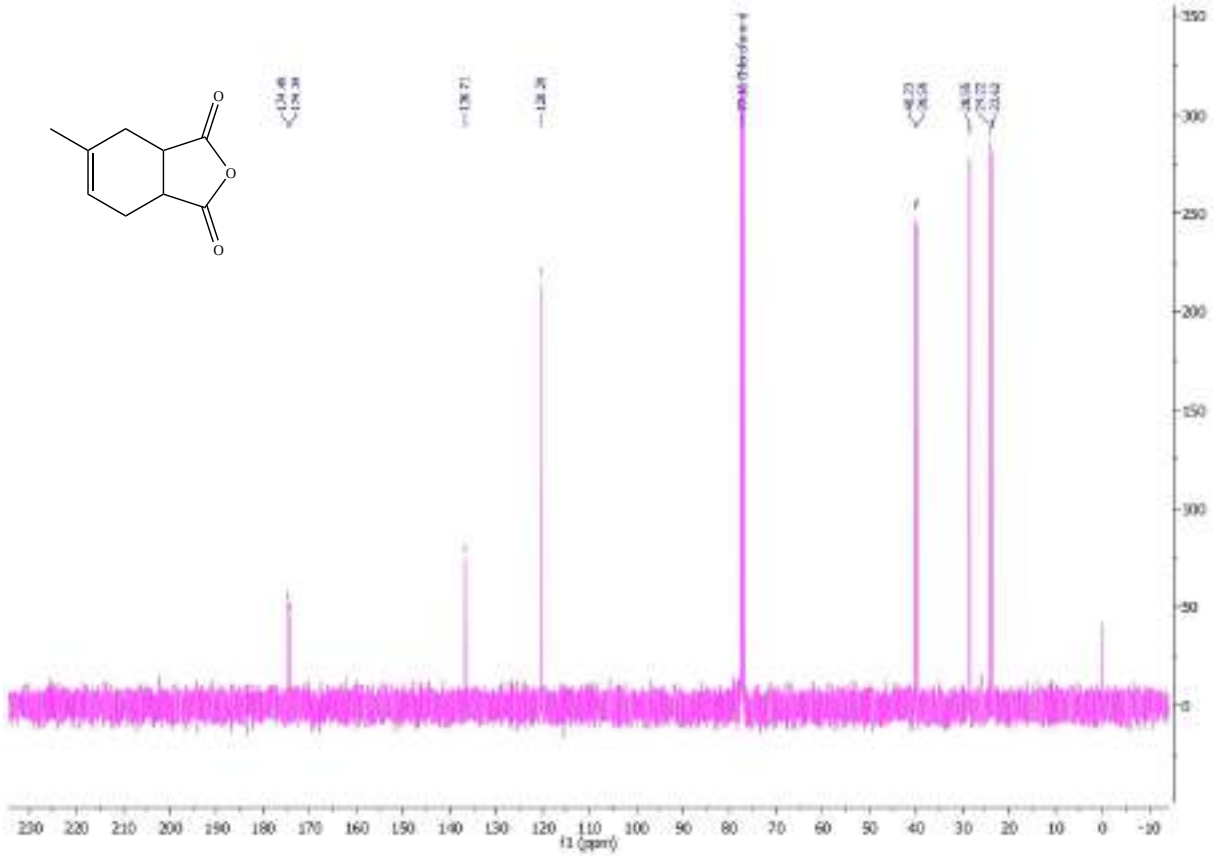

Figure S20b. ^{13}C NMR analysis of cycloadduct (c).

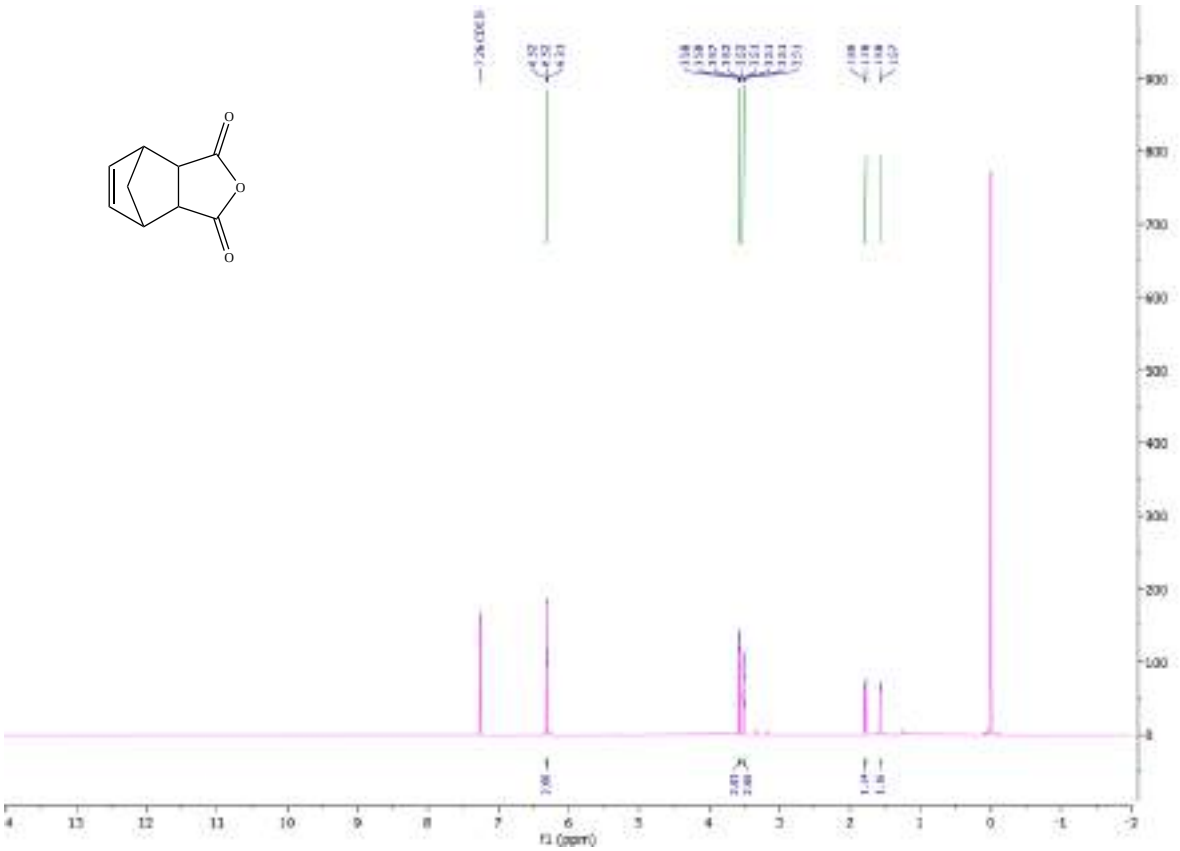

Figure S21a. ^{1}H NMR analysis of cycloadduct (e).

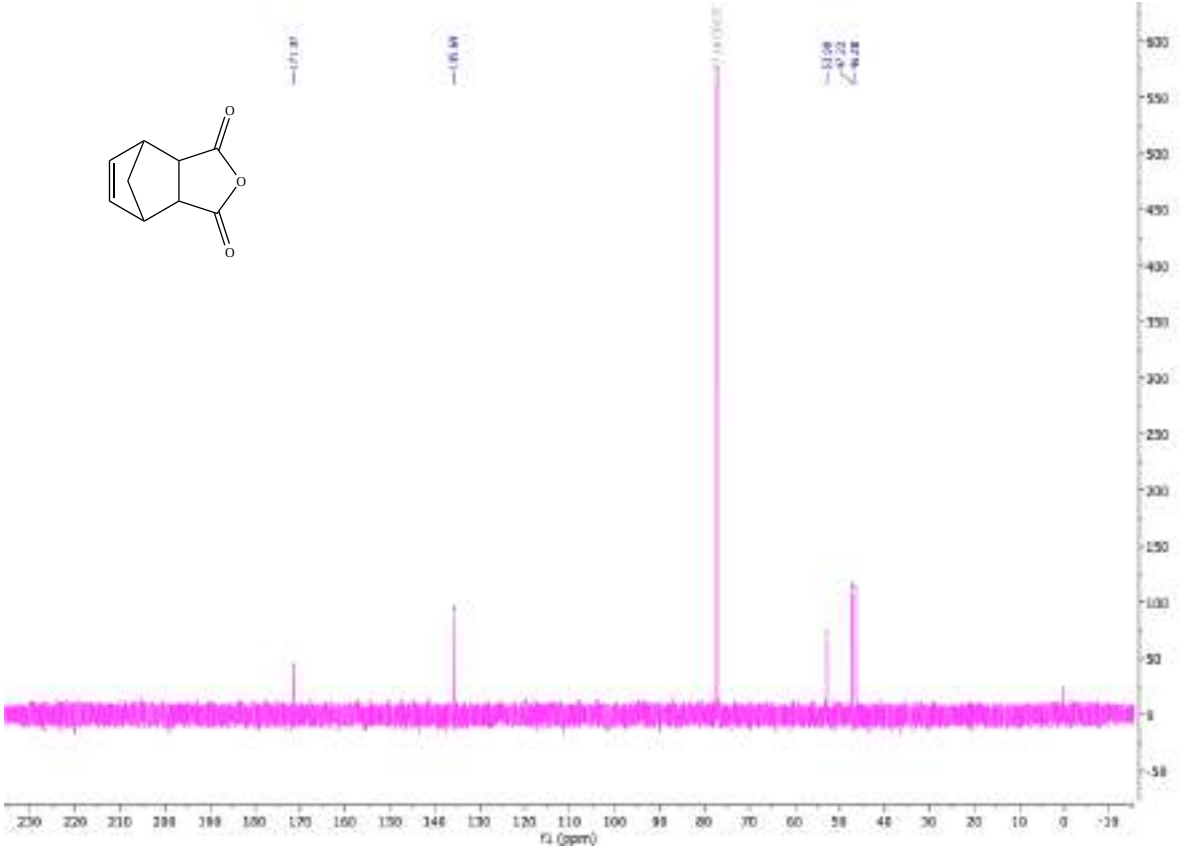

Figure S21b. ^{13}C NMR analysis of cycloadduct (e).

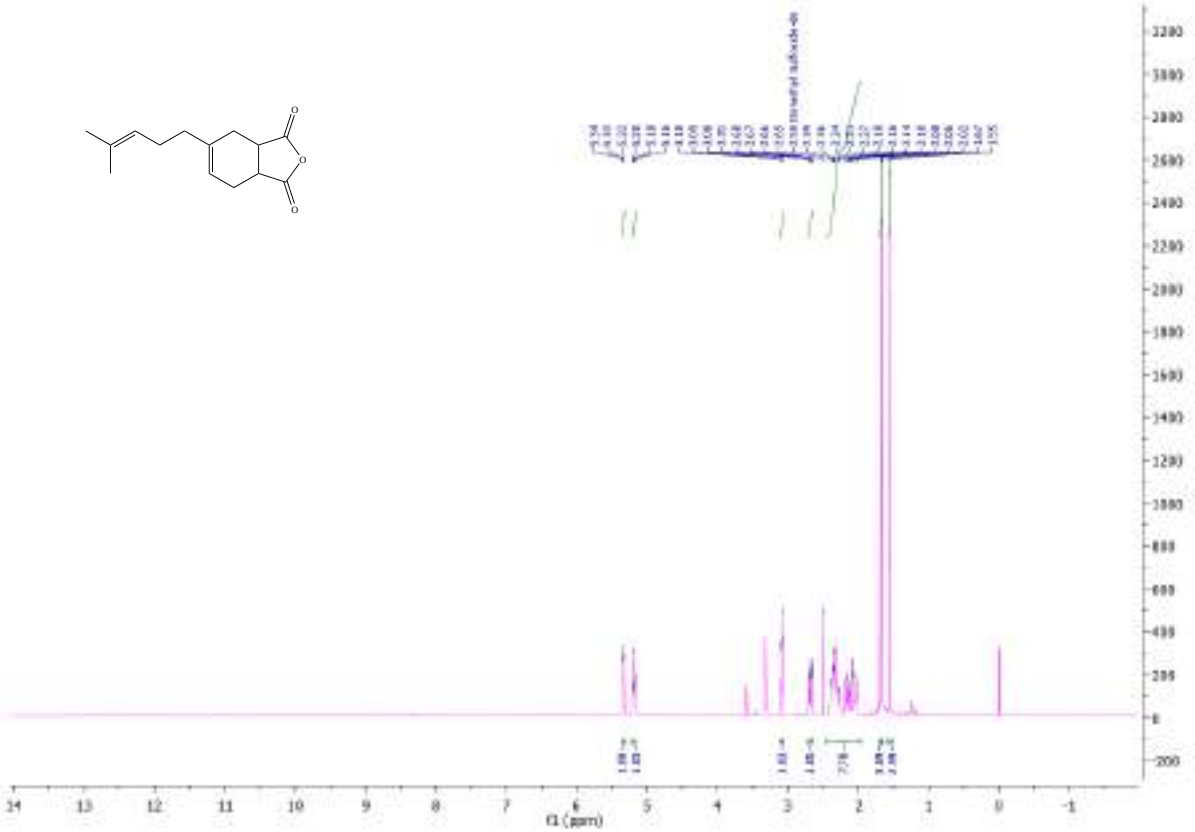

Figure S22a. ^{1}H NMR analysis of cycloadduct (g).

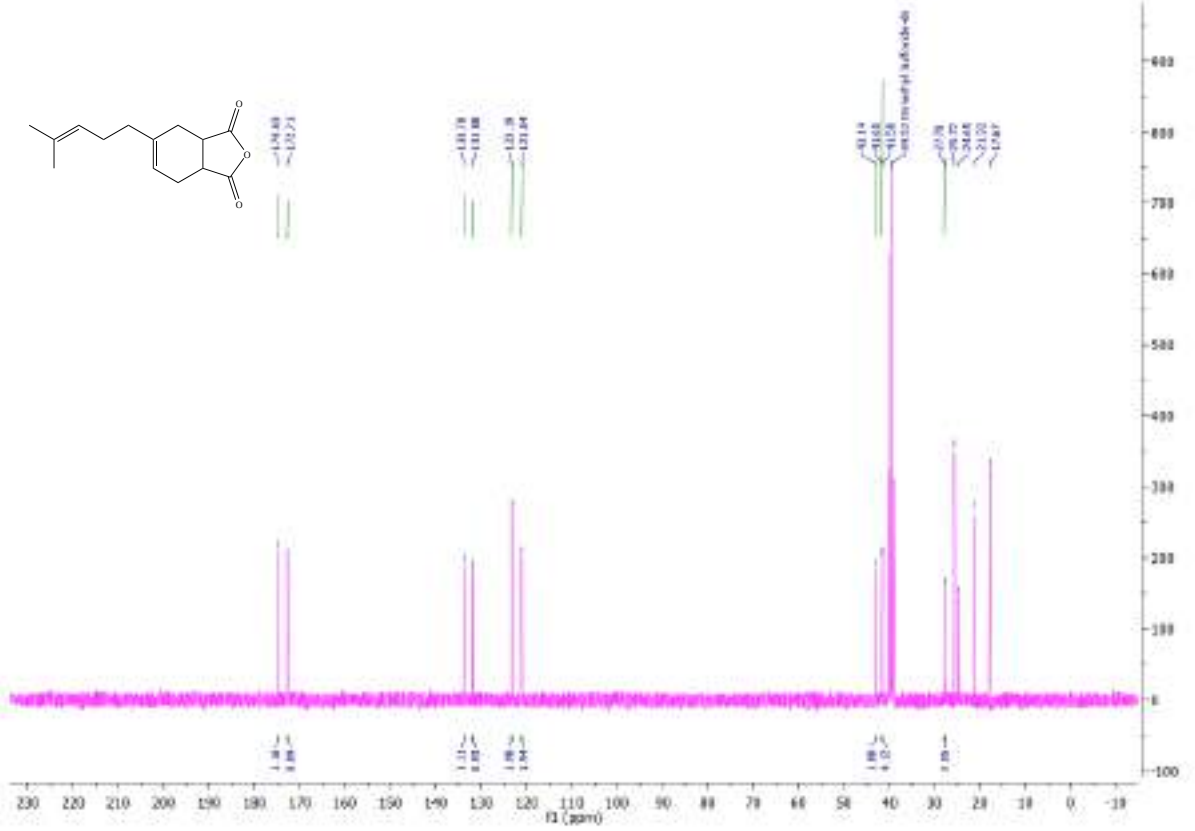

Figure S22b. ^{13}C NMR analysis of cycloadduct (g).

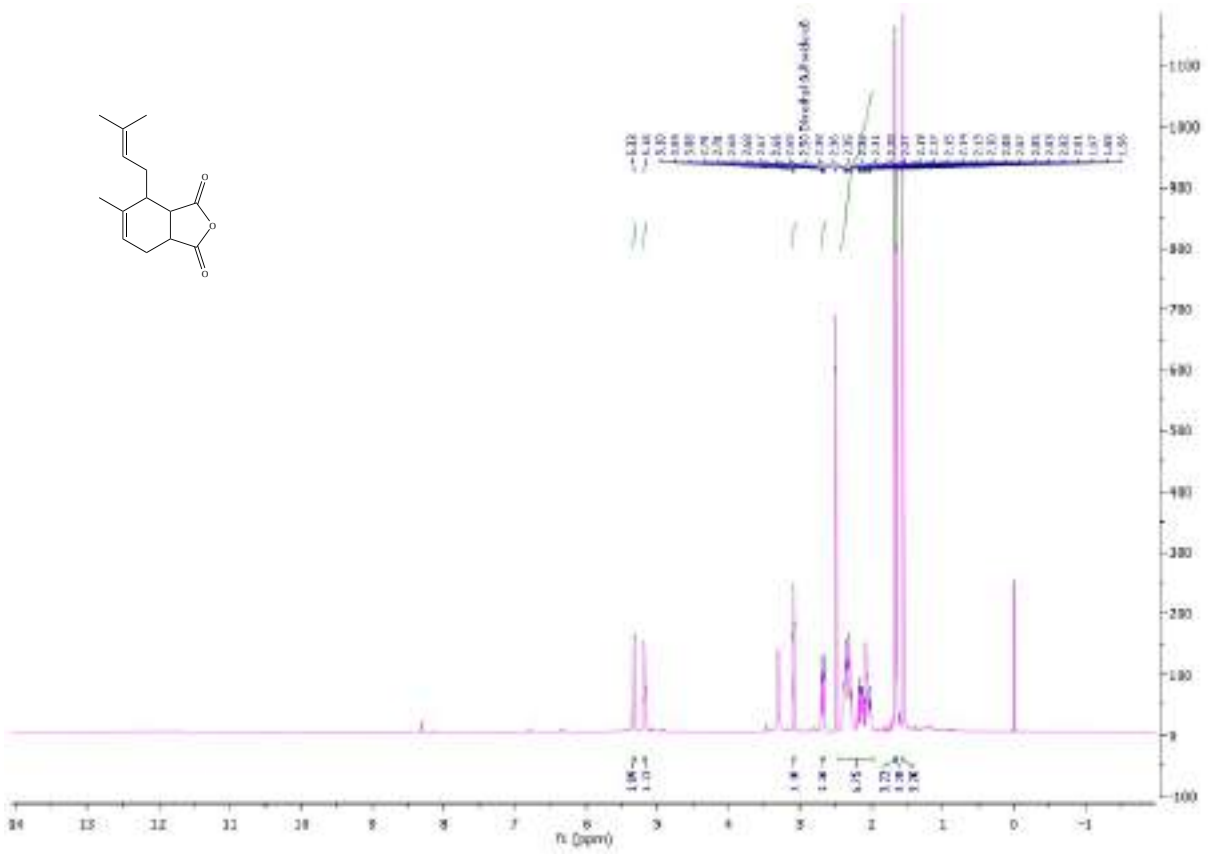

Figure S23a. ^{1}H NMR analysis of cycloadduct (i).

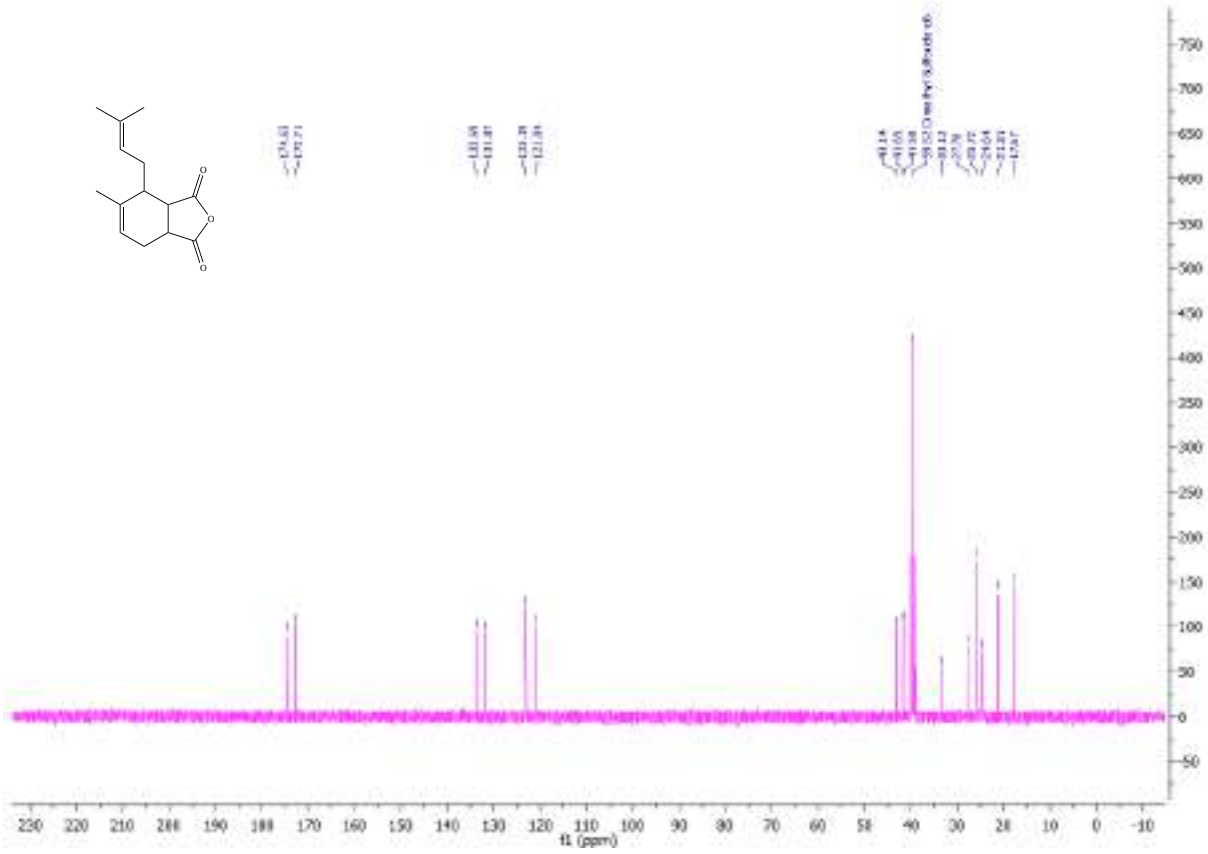

Figure S23b. ^{13}C NMR analysis of cycloadduct (i).

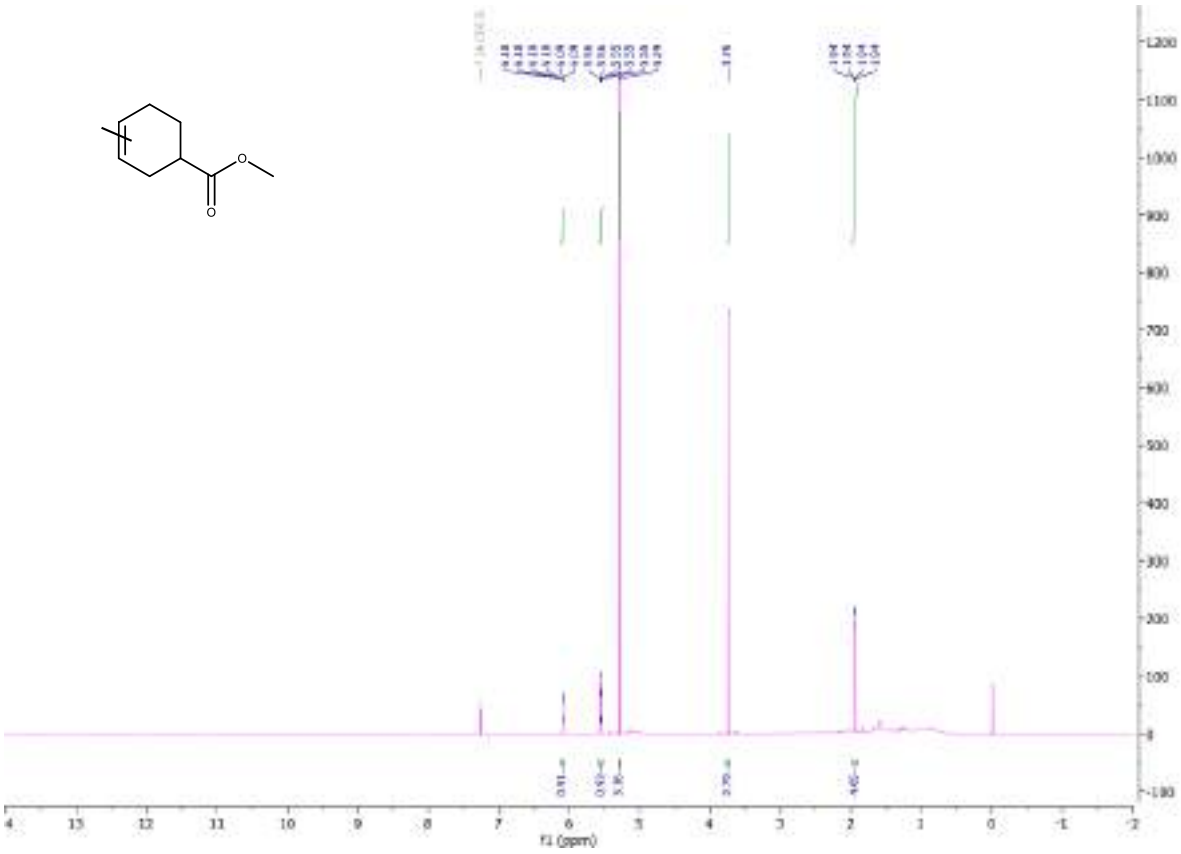

Figure S24a. ^{1}H NMR analysis of cycloadduct (k).

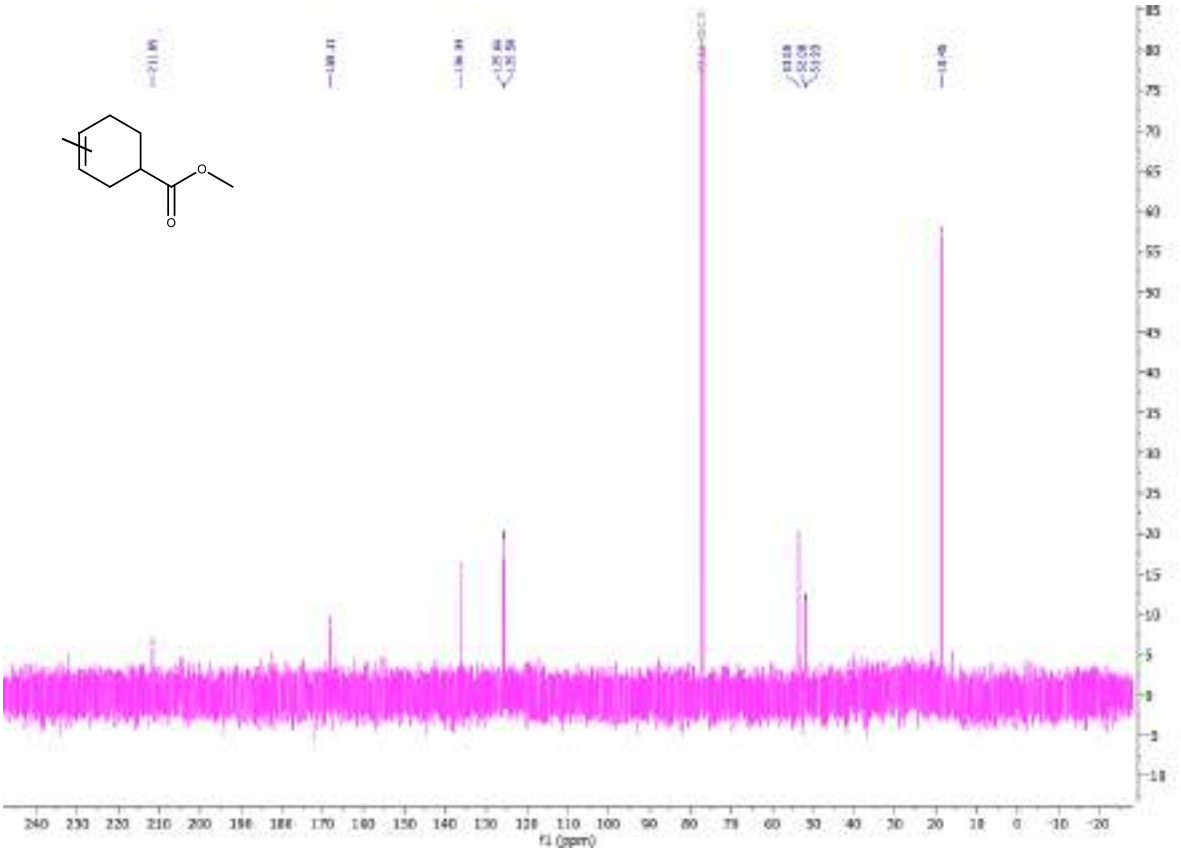

Figure S24b. ^{13}C NMR analysis of cycloadduct (k).

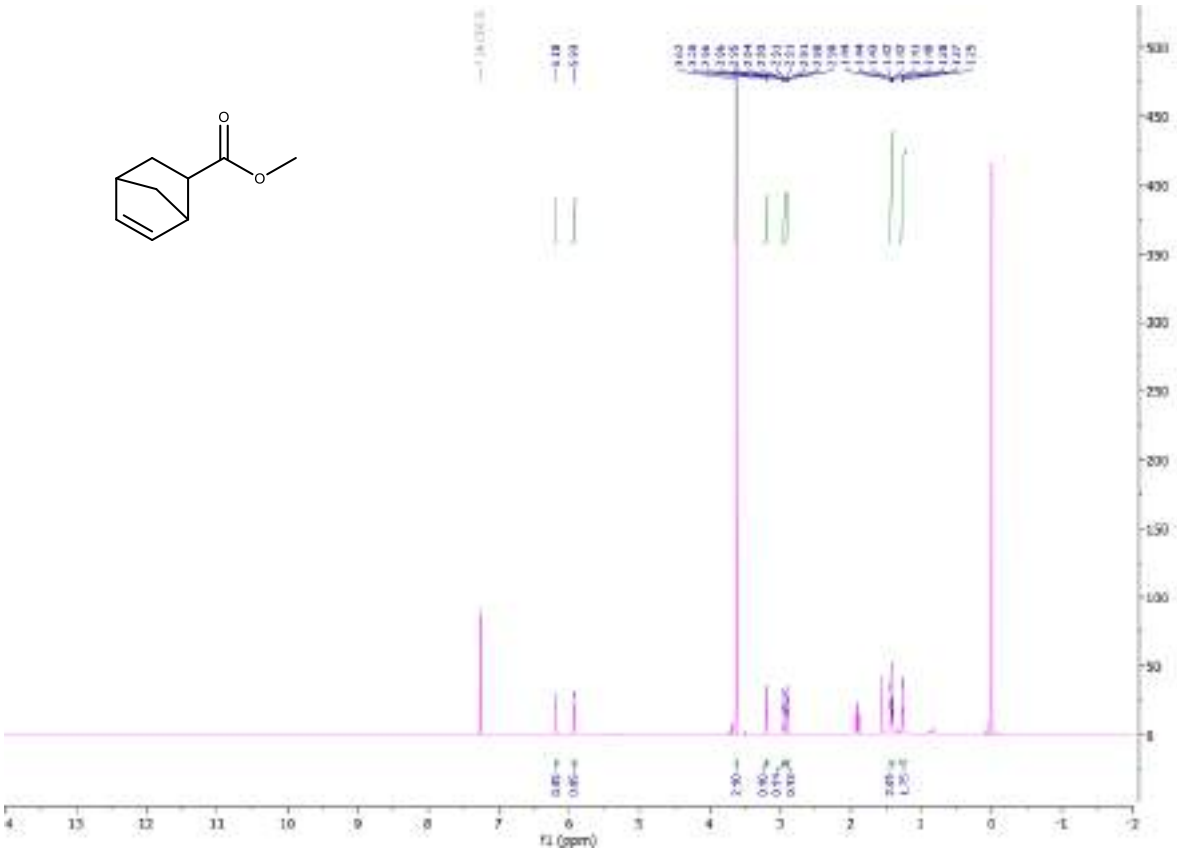

Figure S25a. ^{1}H NMR analysis of cycloadduct (I).

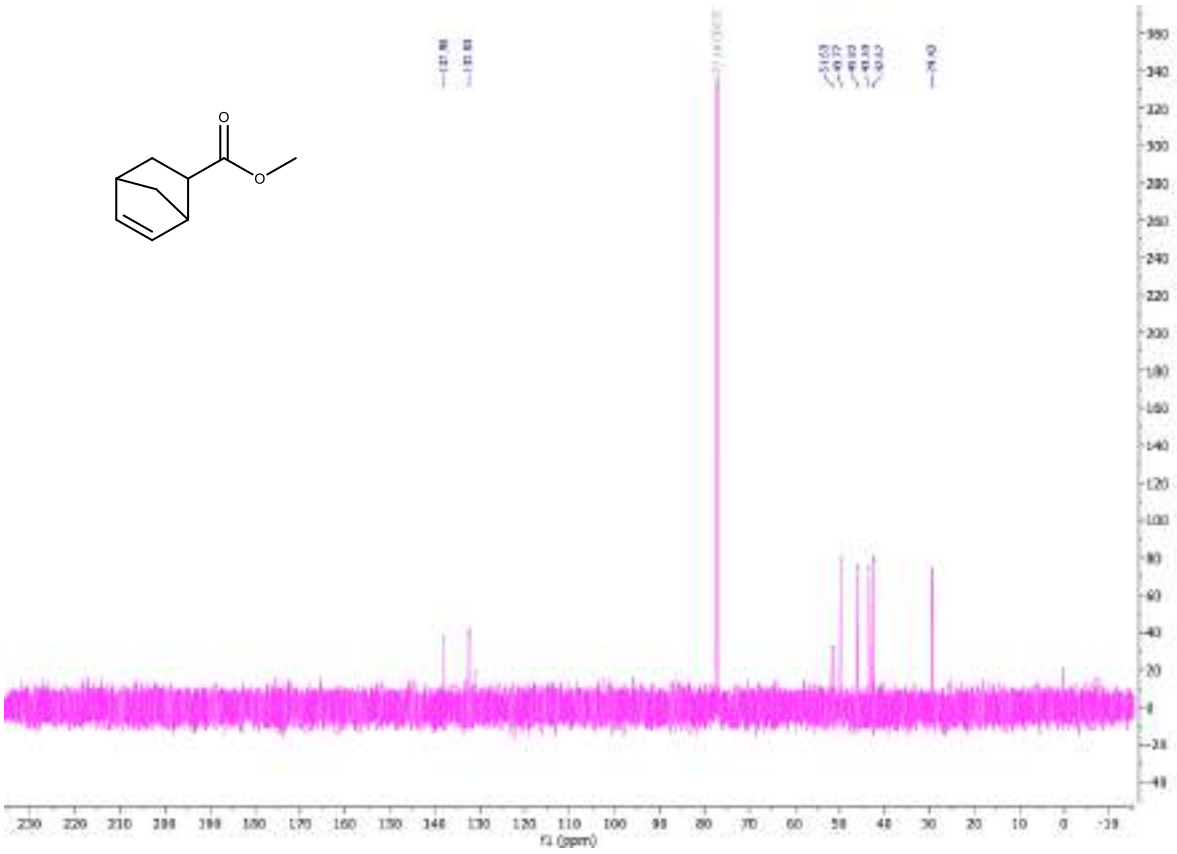

Figure S25b. ^{13}C NMR analysis of cycloadduct (I).

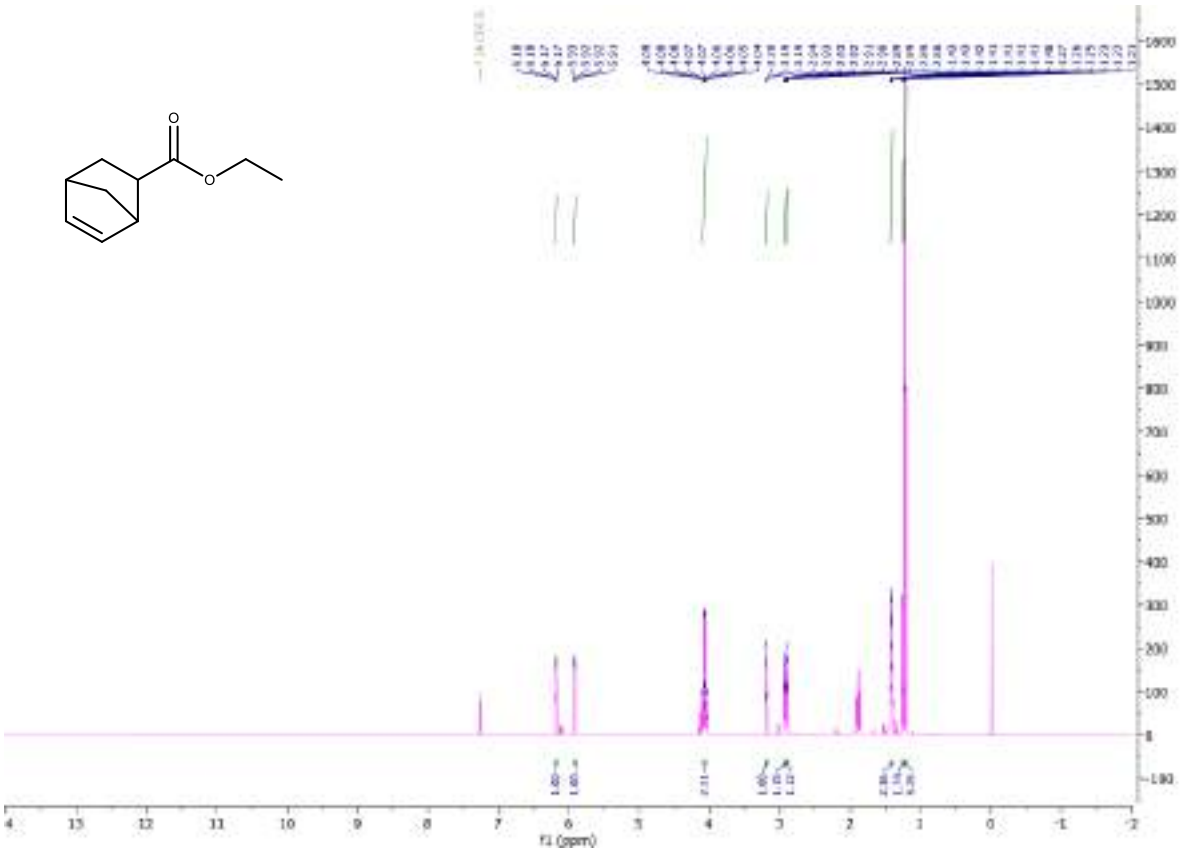

Figure S26a. ^{1}H NMR analysis of cycloadduct (n).

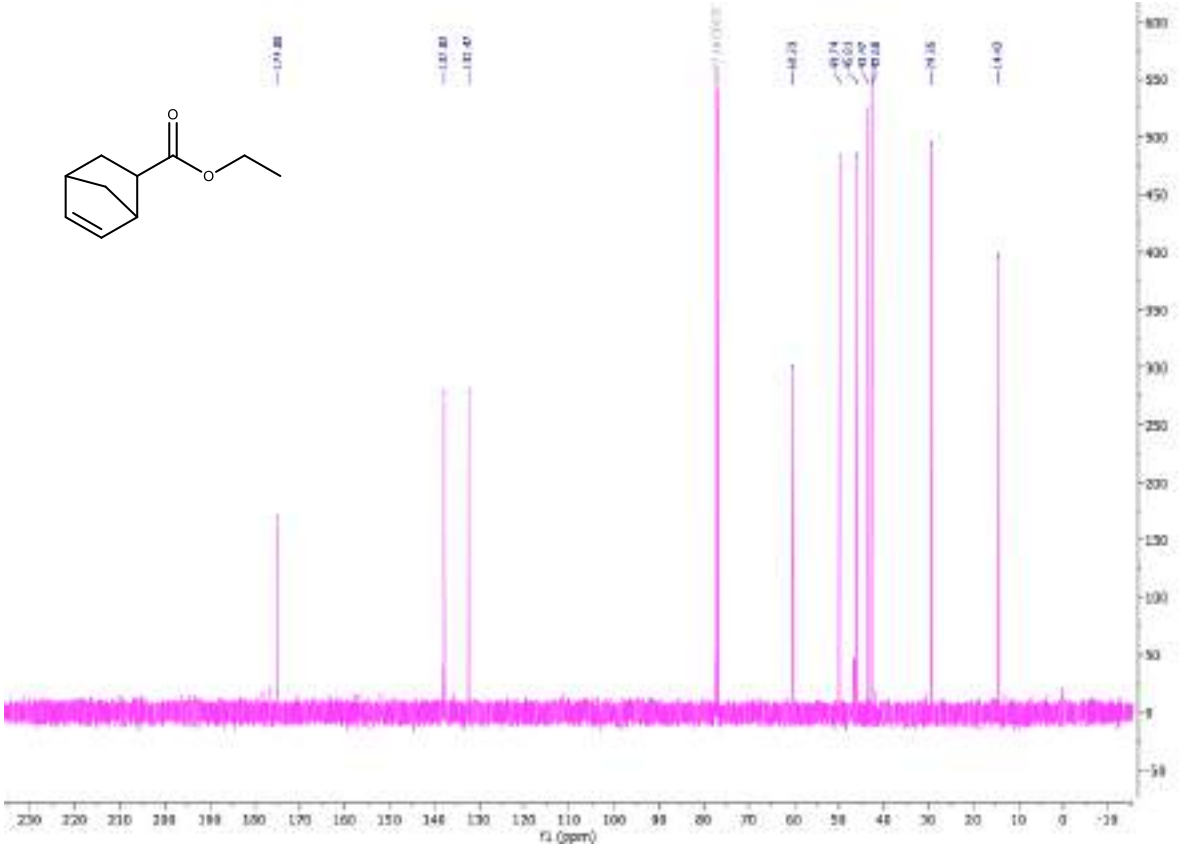

Figure S26b. ^{13}C NMR analysis of cycloadduct (n).

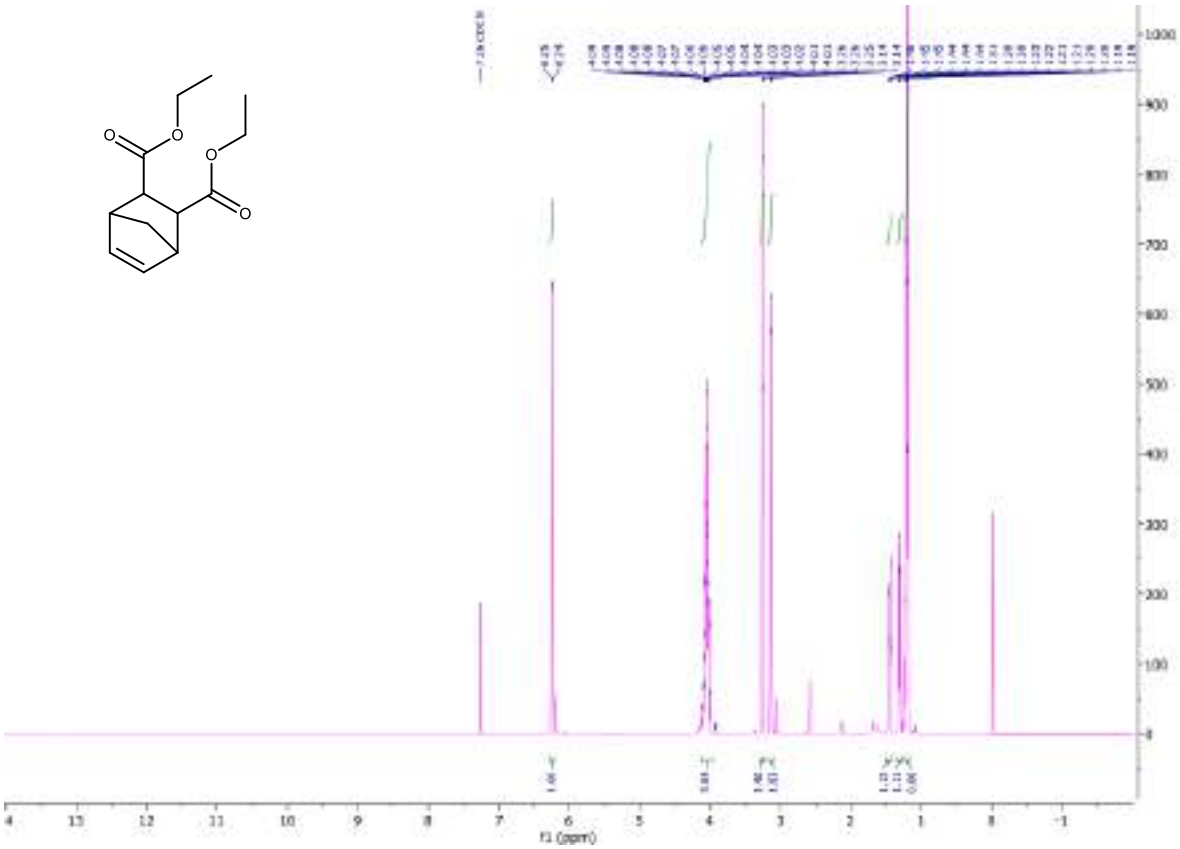

Figure S27a. ^{1}H NMR analysis of cycloadduct (p).

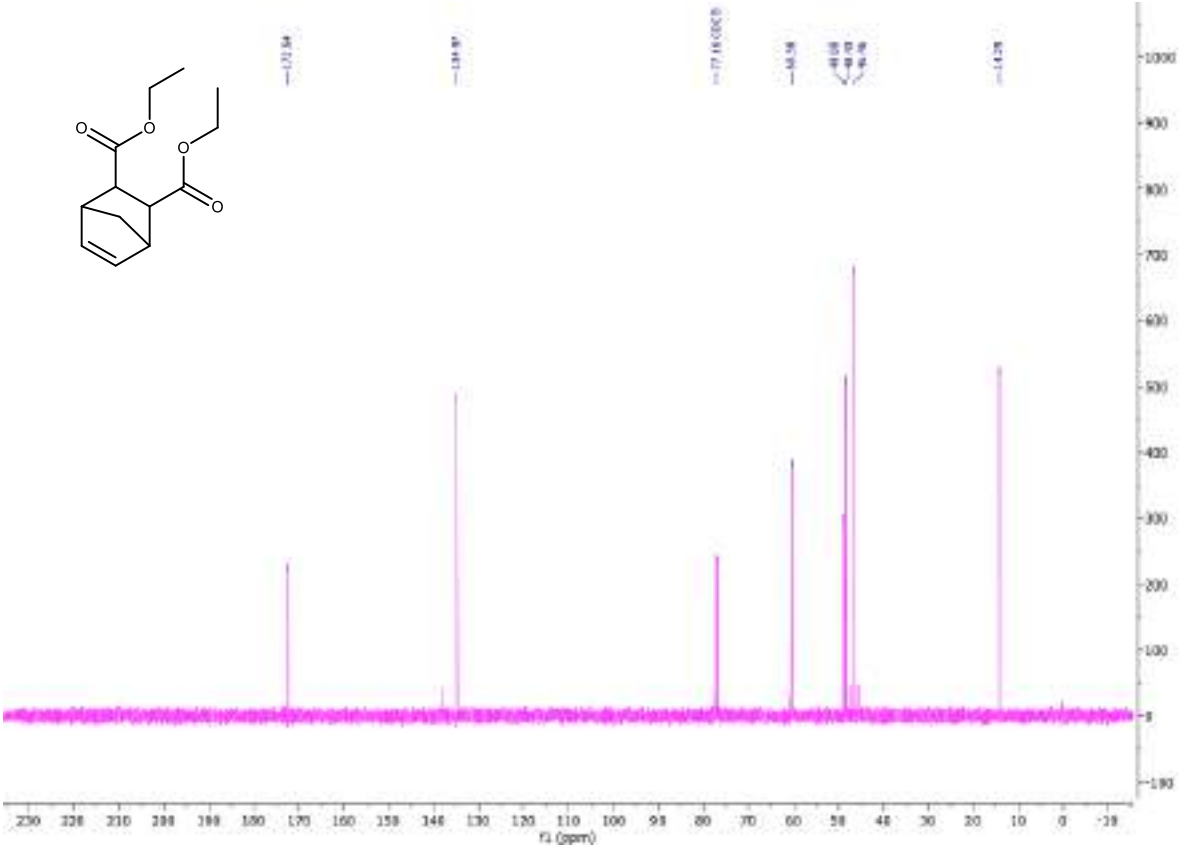

Figure S27b. ^{13}C NMR analysis of cycloadduct (p).

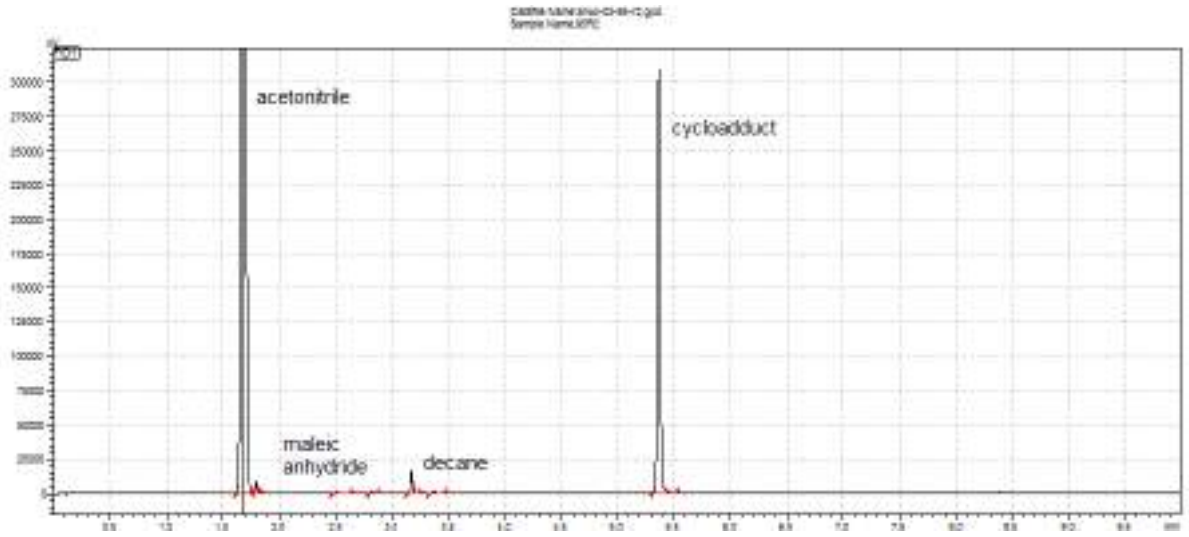

Figure S28. Exemplary GC graph of reaction between maleic anhydride and isoprene.

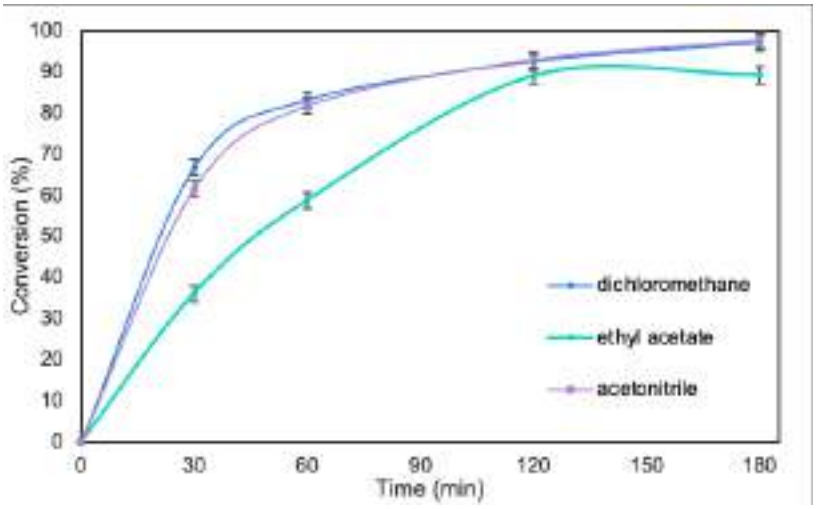

Figure S29. The influence of solvent on MA conversion.

Reaction conditions: isoprene 3 mmol, maleic anhydride 2 mmol, solvent 0.5 mL, SILP(1) catalyst with 0.1 mol% of $Al(OTf)_3$ per maleic anhydride, 20°C. MA conversion was determined using GC.

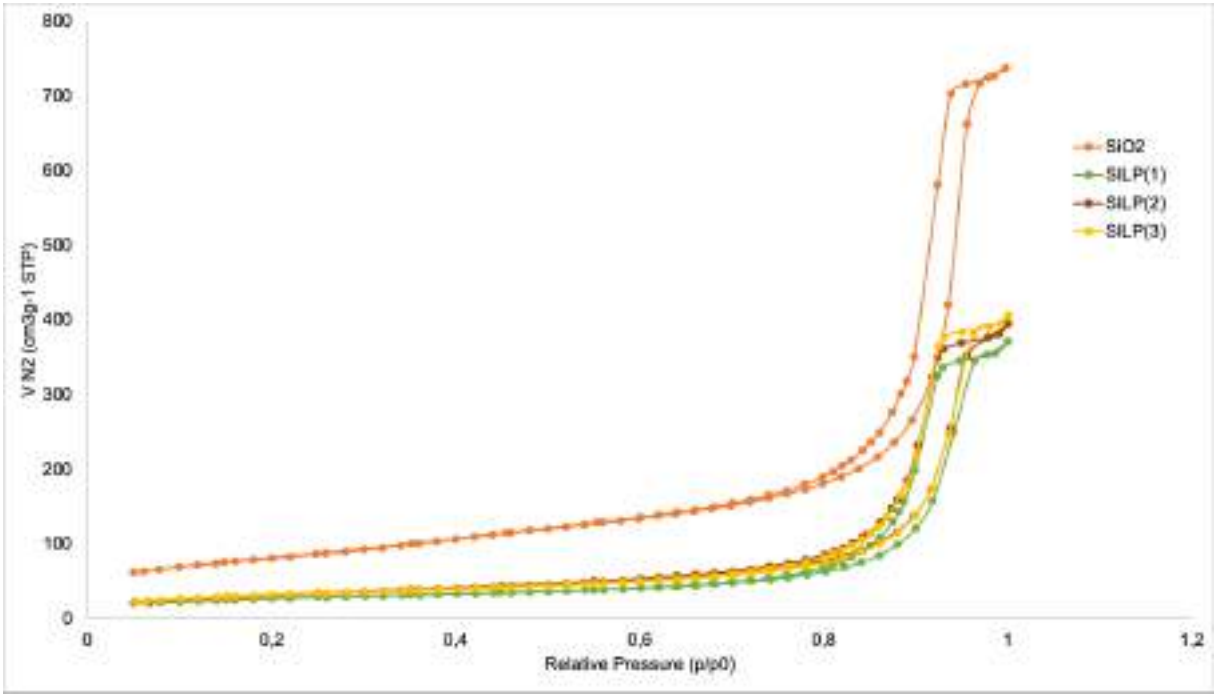

Figure S30. Adsorption-desorption isotherms.

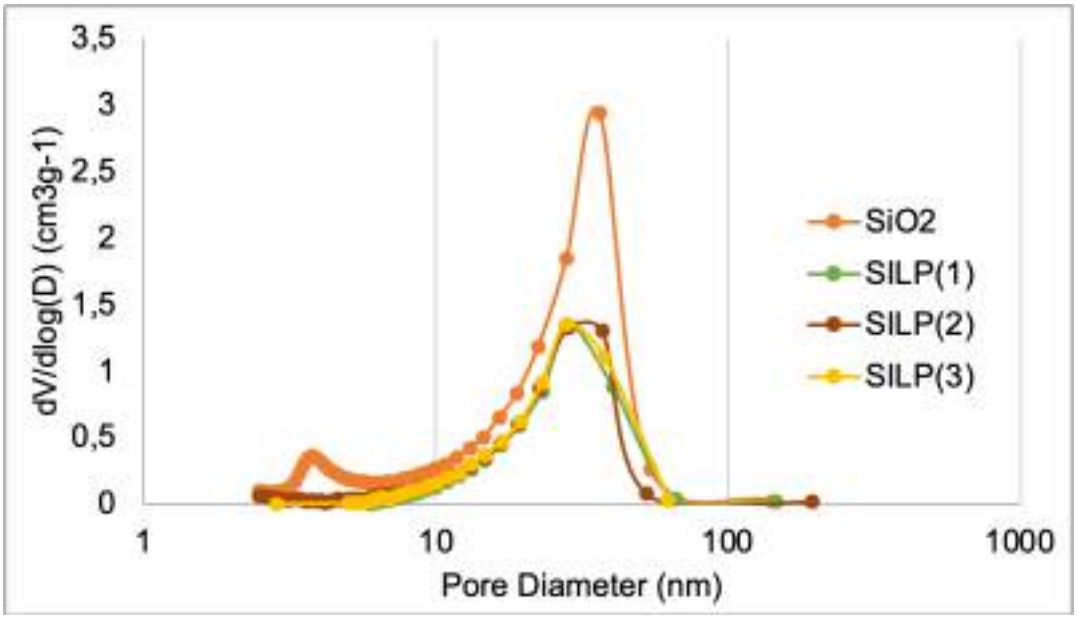

Figure S31. Pore size distribution.

Environmental Technology & Innovation 28 (2022) 102936

Contents lists available at ScienceDirect

Environmental Technology & Innovation

journal homepage: www.elsevier.com/locate/eti

Supported ionic liquid phase facilitated catalysis with lipase from *Aspergillus oryzae* for enhance enantiomeric resolution of racemic ibuprofen

Anna Wolny [a], Agnieszka Siewniak [a], Jakub Zdarta [b], Filip Ciesielczyk [b], Piotr Latos [a], Sebastian Jurczyk [c], Long D. Nghiem [d], Teofil Jesionowski [b], Anna Chrobok [a,*]

[a] *Department of Chemical Organic Technology and Petrochemistry, Faculty of Chemistry, Silesian University of Technology, Krzywoustego 4, PL-44100 Gliwice, Poland*
[b] *Institute of Chemical Technology and Engineering, Faculty of Chemical Technology, Poznan University of Technology, Berdychowo 4, PL-60965 Poznan, Poland*
[c] *Institute for Engineering of Polymer Materials and Dyes, Lukasiewicz Research Network, Sklodowskiej-Curie 55, PL-87100 Torun, Poland*
[d] *Centre for Technology in Water and Wastewater, University of Technology Sydney, Ultimo NSW 2007, Australia*

ARTICLE INFO

Article history:
Received 8 August 2022
Received in revised form 29 September 2022
Accepted 11 October 2022
Available online 21 October 2022

Keywords:
Ionic liquids
Supported ionic liquid phase
Lipase from *Aspergillus oryzae*
Immobilization
Racemic resolution
Ibuprofen

ABSTRACT

Supported ionic liquid phase (SILP) was used as a carrier for lipase from *Aspergillus oryzae* (LAO) and used as a biocatalyst for enantiomeric resolution of racemic ibuprofen *via* esterification leading to *(S)*-(+)-ibuprofen ester. Using native form of lipase, outstanding results were achieved, obtaining *(S)*-(+)-ibuprofen propyl ester with enantiomeric excess (*ee*) of 99.9% and high conversion of racemic ibuprofen after 24 h ($\alpha = 34.8\%$) and respectively $ee = 99.9\%$ with $\alpha = 45.2\%$ after 48 h. Several hybrid materials composited with silica and metal-based oxides including magnesium, calcium, and zirconia were evaluated as supports for LAO with various surface characteristics. The selected ionic liquid 1-methyl-3-(triethoxysilylpropyl)imidazolium bis(trifluoromethylsulfonyl)imide was immobilized *via* the covalent bound onto the surface of solid material and in the second step LAO was anchored. Optimized results in enantiomeric resolution of racemic ibuprofen (35.23% conversion of *rac*-ibuprofen after 7 days with 95% *ee* of ester) were obtained for SILP biocatalyst based on MgO· SiO_2 (1:1) (ionic liquid loading 6.79%, enzyme loading 3.96%). This is proposed as a generic approach to tailoring supported ionic liquids phase biocatalysts for industrially-relevant reactions, to generate both environmentally and economically sustainable processes.

1. Introduction

Many pharmaceuticals are chiral. They exist as a pair of stereoisomers (or enantiomers) with identical chemical formula, however, geometrically these stereoisomers of the same compound cannot superimpose onto each other after any conformational changes (Nguyen et al., 2022). Industrial production of pharmaceuticals often results initially in a racemate, or a racemic mixture of equal amount of both enantiomers. In most cases, two enantiomers of the same

* Corresponding author.
E-mail addresses: teofil.jesionowski@put.poznan.pl (T. Jesionowski), anna.chrobok@polsl.pl (A. Chrobok).

https://doi.org/10.1016/j.eti.2022.102936

compound differ markedly from each other in terms of their therapeutic effects and toxicology. Enantiomeric conversion of chiral pharmaceuticals is, therefore, of significant scientific, industrial, and environmental interest (Wsól et al., 2004; Nguyen et al., 2021; Raczyńska et al., 2021).

As a commonly used over-the-counter medicine to treat pain and fever, ibuprofen is one of the most significant chiral pharmaceuticals. The two enantiomers of ibuprofen *(R)*-(-)-ibuprofen and *(S)*-(+)-ibuprofen exhibits vastly different pharmacological properties and metabolic profiles. *(S)*-(+)-enantiomer has the desired pharmacological activity and is capable of inhibiting cyclooxygenase (COX), while *(R)*-(-)-ibuprofen is not a COX inhibitor and is responsible for the intensification of the inflammatory process. *(S)*-(+)-enantiomer of ibuprofen is 160 times more therapeutically active than *(R)*-(-)-ibuprofen (Adams et al., 1976). More importantly, the *(R)*-(-)-ibuprofen can cause potential side effects (Evans, 2001). Recent studies have focused on the isolation of pure *(S)*-(+)-ibuprofen for faster and more precise therapeutic outcome and lowering the risk of side effects.

Racemic resolution of ibuprofen enantiomers can be achieved *via* kinetic resolution with enzymatic esterification or hydrolysis, high performance liquid chromatography, and diastereoisomeric crystallization (José et al., 2015). In enantiomeric esterification, lipases of fungal sources, such as *Candida rugosa*, *Rhizomucor miehei,* can preferentially catalyze the conversion of *(S)*-(+)-ibuprofen. On the other hand, the lipase B from *Candida antarctica* preferentially converts the *(R)*-(-)-ibuprofen to ester. Other fungal lipases from *Candida* sp, *Aspergillus niger*, *Pseudomona* sp, *Aspergillus terreus*, *Fusarium oxysporum*, *Mucor javanicus*, *Penicillium solitum*, *Rhizopus javanicus, Rhizomucor miehei*, *Rhodothermus marinus* and esterase from *Aeropyrum pernyx* as well as porcine pancreas (José et al., 2015; Wei et al., 2016; Zappaterra et al., 2021; Bachosz et al., 2022; Verri et al., 2016) have been also studied as biocatalysts in enantiomeric esterification but with less success, perhaps with the exception of esterase from *Thermotoga maritima* (Wei et al., 2016).

To increase or even promote the stability, selectivity, specificity and, in certain cases, activity of lipases, these enzymes can be immobilized onto a solid substrate what is important also from the industrial application viewpoint (Zdarta et al., 2022a,b; Bilal et al., 2019; Boudrant et al., 2020; Szelwicka et al., 2020; Markiton et al., 2017; Szelwicka et al., 2019a,b; Mateo et al., 2007a,b). Enzyme immobilization may be coupled to enzyme purification (Dos Santos et al., 2015; Barbosa et al., 2015). The biomolecules immobilization provides also higher resistance against adverse effects of the reaction conditions (Rodrigues et al., 2013). Particularly, a controlled immobilization using porous supports reduces diffusional limitations and partitions as well as enzyme aggregation and its inhibition and prevents against internal conformational changes in enzyme structure (Mateo et al., 2007a,b). Furthermore, multipoint enzyme immobilization reduces leaching of the enzyme from the support and provides additional enzyme rigidization (Garcia-Galan et al., 2011). It should be highlighted that various solid supports were used for enzyme binding including silica, biochar, metal oxides, polymer fibers, and protein-coated microcrystals (Hong et al., 2014; Huang et al., 2015; Jesionowski et al., 2014; Zdarta et al., 2022c; Jiang et al., 2022; Svetozarević et al., 2022). Finally, heterogenization of enzymes enables the easy separation and recycle or use of the flow system (Szelwicka et al., 2019a,b; Baumann et al., 2020).

The current industry challenge in enantiomeric esterification is to obtain the more therapeutically enantiomer at the highest chiral purity possible, defined as enantiomeric excess (*ee*). Formula to calculate *ee*, which is a measurement of purity of a chiral substance is available in the Supplementary Materials. The *ee* for pure ibuprofen ester noted in many works was far below 50% while other previous works only presented medium *ee,* up to 90%. Truly beneficial results of racemic resolution for *ee* higher than 90% are rather rare (José et al., 2015). Very often the full conversion of substrate is not reached due to the detrimental influence of reaction time on *ee*. Reaction times necessary to reach the final results are from several to several dozen hours and were depended on the reactivity of alcohol used for esterification. Very few studies have described near complete conversion of *(S)*-(+)-ibuprofen with high enantioselectivity to *(S)*-(+)-enantiomer of ibuprofen ester using lipase from *Candida rugosa* as a catalyst (Huang et al., 2015; Siódmiak et al., 2012; Mohammadi et al., 2016; Ghofrani et al., 2021). Some important achievements to date are discussed below.

Lipase from *Candida rugosa* was used for the enantioselective esterification reaction of racemic ibuprofen with 1-propanol in cyclohexane as a reaction medium at 30 °C. The highest conversion (44.2% after 140 h), with enantiomeric excess of product equal 68.3% was achieved (Siódmiak et al., 2012). Protein-coated microcrystals prepared from lipase form *Candida rugosa* applied in esterification of racemic ibuprofen with isooctanol in isooctane was extremely active biocatalyst causing the 97.3% *ee* of *(S)*-(+)-ibuprofen ester and total conversion of substrate 49.8% after 8 h. Moreover, studied biocatalyst exhibits good operational stability, retained active in 15 successive batches (Huang et al., 2015). Another example of active system is lipase from *Rhizomucor miehei* immobilized on epoxy-functionalized silica and used for esterification of ibuprofen with 1-propanol in anhydrous isooctane at 0 °C. The obtained conversion was low (around 23.7% after 24 h), but the *ee* was high 92% (Mohammadi et al., 2016). In the recent work lipase from *Candida rugosa* immobilized on silica nanoparticles showed 45% conversion of substrate with 1-propanol and 96% enantioselectivity to *(S)*-(+)-ibuprofen ester at 37 °C after 50 min. Unfortunately, authors did not mention the amount of enzyme immobilized on the surface of silica (Mohammadi et al., 2016). On the other hand, in the only one work describing the enantioselective transport of *(S)*-(+)-ibuprofen through a supported liquid membrane based on ionic liquids, lipase from *Aspergillus oryzae* (Novo) as one of several other enzymes with low activity was tested for comparison reasons. The best result (*ee* 75% for *(S)*-(+)-ibuprofen ester) was obtained for the combination of lipase from *Candida rugosa* and 1-butyl-3-methylimidazolium bis(trifluoromethylsulfonyl)imide [bmim][NTf_2] (Miyako et al., 2003).

Ionic liquids (ILs) with unique properties (negligible vapor pressure with polar and non-polar regions in the organized 'nanostructures' with hydrogen-bonded polymeric supramolecules) can maintain enzymes in their active conformation

(Itoh, 2017; Zhao, 2015). ILs were used in many biotransformations (Lozano et al., 2017; Drożdż et al., 2015), including several applications in enantiomeric esterification of ibuprofen (Wei et al., 2016; Miyako et al., 2003; Naik et al., 2007). Advantageous results were obtained for thermostable esterase (EST10) from *Thermotoga maritima* with ionic liquid based on $[BF_4]^-$ anion. *(S)*-(+)-ibuprofen ethyl ester was obtained after 10 h of the reaction at 75 °C with high conversion of substrate (47.4%) and high *ee* 96.6% (Wei et al., 2016).

ILs can be integrated with a solid phase carrier to form a supported ionic liquid phase (SILP) system for enzymes in biocatalysis. In the SILP system, ILs form a thin layer on the solid carrier, thus, reducing the amount of IL used in the process. The enzyme can be immobilized within the ILs layer *via* adsorption. These heterogeneous SILP biocatalysts are efficient and have good recyclability (Garcia-Verdugo et al., 2014; Szelwicka et al., 2021a,b; Fernandez-Lafuente et al., 1998; Lee et al., 2018). However, they have not been yet applied for racemic resolution of ibuprofen enantiomers.

In this work, recent advances in enantiomeric esterification of ibuprofen were utilized to develop a robust biocatalytic system based on the lipase from *Aspergillus oryzae* (LAO). Seeking for the best synthetic strategy, biocatalytic reactions were conducted in both homogeneous and heterogeneous conditions, with enzyme adsorbed on IL attached to the surface of various silica-based hybrid materials with covalent bound as SILP, used for the first time in this transformation. The combination of affordable biocatalyst and process advantages leads to a greener alternative, competitive with existent applications.

2. Materials and methods

2.1. Materials

Ibuprofen racemate (≥98.0 wt. %) was purchase from Chemat (Poland). Native lipase B from *Candida antarctica* (CALB) in aqueous-glycerol solution (activity 5000 U L kg^{-1}), native lipase from *Aspergillus oryzae* (LAO) in aqueous-glycerol solution (activity 100,000 U g^{-1}) was purchase from Sigma-Aldrich (Merck Group, Poland) (description of materials can be found in the Supplementary Materials).

2.2. Analysis of materials

Chiral high-performance liquid chromatography (HPLC) was performed on a liquid chromatograph (Alliance, Waters 2690 system) with Waters PDA detector and Chiralcel OD Daicel (250 × 4,6 mm; 10 μm) column. TGA analysis of all obtained materials and biocatalysts were conducted on a thermobalance (Mettler Toledo TGA851e). SEM-EDS images of synthesized supports and biocatalyst were performed applying a Phenom Pro Desktop SEM instrument equipped with an EDS detector (15 kV) (Thermo Fischer Scientific). BET surface area (S_{BET}), average pore size (d_p) and average pore volume (V_p) of obtained materials were determined by means of the BET method and the BJH model, applying low-temperature (−196 °C) nitrogen sorption (ASAP 2020, Micromeritic Instruments Co.) ^{29}Si MAS NMR spectra of SILP materials were recorded at 59.517 MHz using a Bruker HP-WB high-speed MAS probe. ^{1}H NMR and ^{13}C NMR spectra were obtained on a Varian system (400 MHz and 101 MHz, respectively).

2.3. Synthesis of materials

Sol–gel SiO_2 (Stöber et al., 1968; Klapiszewski et al., 2014), ZrO_2·SiO_2 (Degórska et al., 2021; Jankowska et al., 2019), MgO·SiO_2 (Ciesielczyk et al., 2014; Kołodziejczak-Radzimska et al., 2018) materials and 1-methyl-3-(triethoxysilylpropyl) imidazolium chloride ([tespmim][Cl]) (Matuszek et al., 2016) were prepared according to the literature described elsewhere.

2.3.1. Synthesis of heterogeneous biocatalysts

Synthesis of SILP silica-based materials (Kołodziejczak-Radzimska et al., 2018; Valkenberg et al., 2002; Wolny and Chrobok, 2021, 2022): MgO–SiO_2, ZrO_2-SiO_2, SiO_2 or sol–gel SiO_2 (0.3 g) was suspended in a methanol/water system (5 mL; 4:1, *v/v*) in a 25 mL round-bottom flask and then [tespmim][Cl] ionic liquid (0.3 mmol) was added. The reaction mixture was stirred at 90 °C for 24 h. Obtained material was filtered off, washed with 100 mL of methanol and dried under the vacuum on the Schlenk line (6 h, 70 °C).

Anion exchange in SILP-[tespmim][Cl] materials (Fernandez-Lafuente et al., 1998): In a 25 mL round-bottom flask, SILP-[tespmim][Cl] (0.3 g) was suspended in a dichloromethane (3 mL) and then lithium Li[NTf_2] (30% mol. excess *via* [tespmim][Cl] content) dissolved in a 3 mL of deionized water was added dropwise. The reaction mixture was stirred at room temperature for 24 h. The resulted SILP-IL material was filtered off, washed with 100 mL of deionized water (until the absence of chloride — test with $AgNO_3$) and dried under the vacuum on the Schlenk line (6 h, 70 °C).

Lipase immobilization (Szelwicka et al., 2021b; Fernandez-Lafuente et al., 1998): SILP-IL material (0.3 g) and native LAO in aqueous-glycerol solution (2.25 g) were placed in a 25 mL round-bottom flask and then 4 mL of deionized water was introduced. Obtained mixture was stirred in a thermostatic shaker (250 rpm) at 20 °C for 3 h. Then, the biocatalyst was filtered off, washed with deionized water (100 mL) and dried under vacuum on the Schlenk line (24 h, 20 °C).

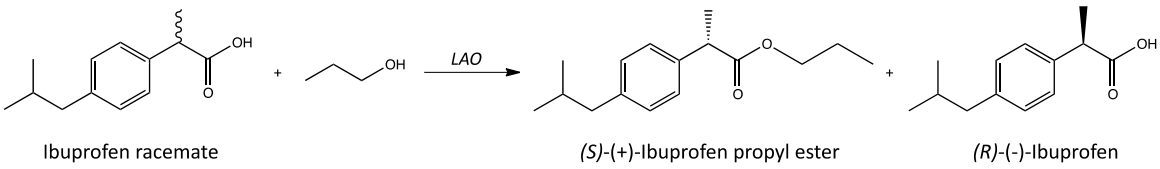

Fig. 1. Enantioselective esterification of racemic ibuprofen with 1-propanol in isooctane.

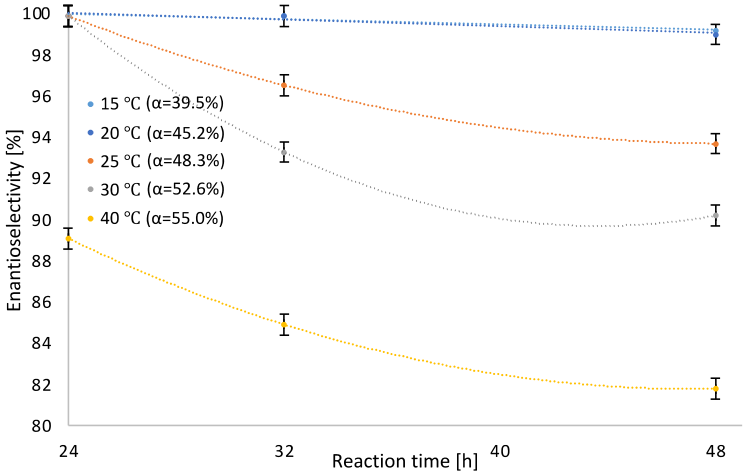

Fig. 2. The influence of temperature on *ee* of *(S)*-(+)-ibuprofen ester. *Reaction conditions: rac*-ibuprofen 1 mmol, 1-propanol 2 mmol, isooctane 2 mL, LAO 1.5 mL, 250 rpm.

2.3.2. Enantiomeric resolution of racemic ibuprofen

General procedure of homogeneous ibuprofen racemate esterification: In a 10 mL vial, ibuprofen racemate (1 mmol) was dissolved in isooctane (2 mL), then 1-propanol (2 mmol) and LAO (1.5 mL) were added. The reaction was performed at 20 °C and stirred in a thermostatic shaker (250 rpm) for 48 h.

General procedure of heterogeneous ibuprofen racemate esterification: In a 3 mL vial, ibuprofen racemate (0.1 mmol) was dissolved in isooctane (0.4 mL), then 1-propanol (0.2 mmol) and 90 mg of SiO_2/Mg(1:1)/[tespmim][NTf_2]/LAO were added. The reaction was performed at 20 °C and stirred in a thermostatic shaker (250 rpm) for 7 days.

Recycle of the heterogeneous biocatalyst: After the reaction, the biocatalyst was filtered off, washed with 25 mL of isooctane, dried under the vacuum on the Schlenk line (6 h, 20 °C) and reused.

3. Results and discussion

3.1. Catalytic activity of native enzyme

In the preliminary studies the optimization of the reaction condition for esterification of *rac*-ibuprofen with two-fold molar excess of 1-propanol as a model alcohol, using isooctane as a solvent in the presence of commercially available, aqueous-glycerol solution of LAO was performed (Fig. 1). The conversion of racemic ibuprofen and enantioselectivity of the process were determined using chiral HPLC (Supplementary Materials Fig.S1).

First, the amount of LAO necessary to convert the *rac*-ibuprofen to ester with high conversion and selectivity was studied (Supplementary Materials Fig.S2). The increasing of the amount of LAO from 0.50 to 1.0 mL causing the increase of reaction rate, but the conversion of (S)-(+)-ibuprofen was not full. Using 1.5 mL of LAO outstanding results were obtained. LAO can convert *rac*-ibuprofen (conversion $\alpha = 34.8\%$, $ee = 99.9\%$) after 24 h and respectively 45.2% and 99.9% after 48 h, $E > 200$, (Supplementary Materials Fig.S2) with high conversion and selectivity. Further increasing of the amount of LAO to 2.0 mL did not affect the yield and selectivity. For comparison the reaction was carried out using the same reaction conditions in the presence of lipase B from *Candida antarctica* using 1.5 mL of enzyme. As the result only 11% of substrate conversion after 48 h was observed (with 26.1% *ee* to *(R)*-(-)-ibuprofen ester).

In order to accelerate the reaction, the temperature was increased from 15 °C to 40 °C. Only slight increase in the reaction rate was observed and the conversion reached almost 50% at 40 °C but the ee_p dropped suddenly up to 82% due to progressive inactivation of the enzyme in higher temperature (Fig. 2 and Supplementary Materials Fig.S3). The reaction carried out at 15 °C slowed down but the *ee* remained as at 20 °C. The most advantageous temperature is 20 °C.

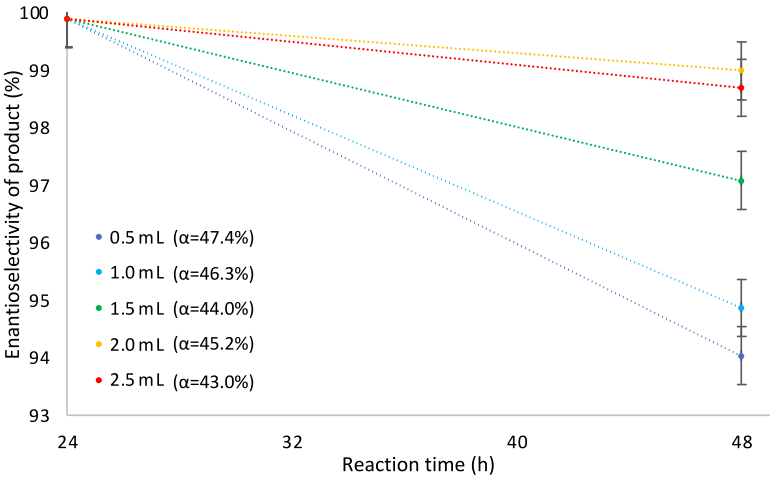

Fig. 3. The influence of the amount of solvent on *ee* of *(S)*-(+)-ibuprofen ester. *Reaction conditions: rac*-ibuprofen 1 mmol, 1-propanol 2 mmol, isooctane, LAO 1.5 mL, 20 °C 250 rpm.

Next, the influence of solvent on the reaction rate was searched. The most commonly used solvents for enantiomeric esterification of ibuprofen were tested (Supplementary Materials Tab.S1). Satisfactory conversion and *ee* (around 90%) were obtained in solvents, like hexane, cyclohexane and heptane. Dichloroethane, acetonitrile and propylene carbonate had an adverse effect on the course of the reaction. The representative of hydrophilic IL [emim][$EtSO_4$] (1-ethyl-3-methylimidazolium ethylsulfate), which dissolve ibuprofen as well as hydrophobic [bmim][NTf_2] not miscible with ibuprofen were also tested. Lack of substrate conversion was observed with the use of [emim][$EtSO_4$] as solvent. The necessity of adding co-solvent (isooctane) to the reaction carried out with [bmim][NTf_2] in order to dissolve substrate influenced the reaction course and the results were promising (conversion 46.9% and 90.4% *ee* after 48 h). Summing up, the best results were obtained in isooctane (conversion 45.2% and 99.9% *ee* after 48 h) where the reaction system was biphasic. The upper phase was composed of solvent and reagents along with LAO created the second phase. Additionally, test concerning the amount of isooctane used for the reaction revealed that the more concentrated reaction mixture is the lower the enantioselectivity is reached (Fig. 3 and Supplementary Materials Fig.S4).

A suitable selection of alcohol moiety (C1–C4) has a significant influence on the conversion and on the enantioselectivity of esterification reaction. The results show that 1-propanol and 1-butanol are excellent substrates for the esterification of ibuprofen, due to the high conversion and enantioselectivity (Fig. 4 and Supplementary Materials Fig.S5). Application of methanol or ethanol for esterification entails the drastic lowering of product purity (*ee* below 88% for methanol). Based on the results, it is essential to apply the C3–C4 alcohols to achieve a high conversion and excellent enantioselectivity when using the LAO as catalyst in enantioselective esterification. Longer alcohol chain and thus increased hydrophobicity of the substrate improve the activity of lipase. This beneficial effect of hydrophobic environment or hydrophobic support's surface on maintaining active conformation of lipase is known as "interfacial activation" (Arana-Peña et al., 2020).

Finally, the influence of molar ratio of ibuprofen:1-propanol was examined in order to evaluate its influence on the reaction parameters (Fig. 5 and Supplementary Materials Fig.S6). The dilution of reaction mixture with alcohol (molar ratio 1:4) caused the slowing down of the reaction, on the other hand the concentration (molar ratio 1:0.5) resulted in lowering of *ee*.

Concluding this part of studies, high-performance of biphasic reaction system: organic reactants/LAO in the process of racemic resolution of ibuprofen was demonstrated. As already mentioned, the focus on LAO was dictated by the drive to find both active and economically attractive system. Next, in this work we set to explore whether the SILP catalysis pathway with LAO may offer an enhancement of catalytic activity of enzyme.

3.2. Catalytic activity of immobilized LAO/SILP system

Superactive biocatalysts play a crucial role in the development of sustainable synthetic processes, while their heterogenization is an important goal for clean technology. The heterogeneous biocatalyst offers many advantages, either used in a fixed bed configuration or simply filtered off or centrifuged from a stirred tank reactor and then reactivated for reuse. Encouraged by the past results (Drożdż et al., 2015; Szelwicka et al., 2021a,b) we decided to develop a SILP dedicated for LAO. By supporting ILs, the required amount of ionic phase can be significantly reduced.

To this aim various silicas and silica-based materials were selected as supports with various surface characteristics (Table 1). Commercially available silica-based supports as well as those fabricated in laboratory, under specific process condition offers unique structural properties including well developed surface area as well surface activity. In order to

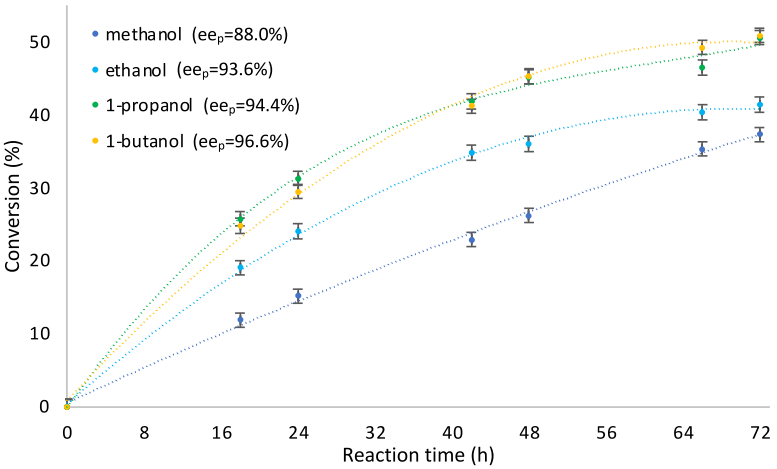

Fig. 4. The influence of the alcohol used for esterification of *rac*-ibuprofen. *Reaction conditions: rac*-ibuprofen 1 mmol, alcohol 2 mmol, isooctane, LAO 1.5 mL, 20 °C 250 rpm.

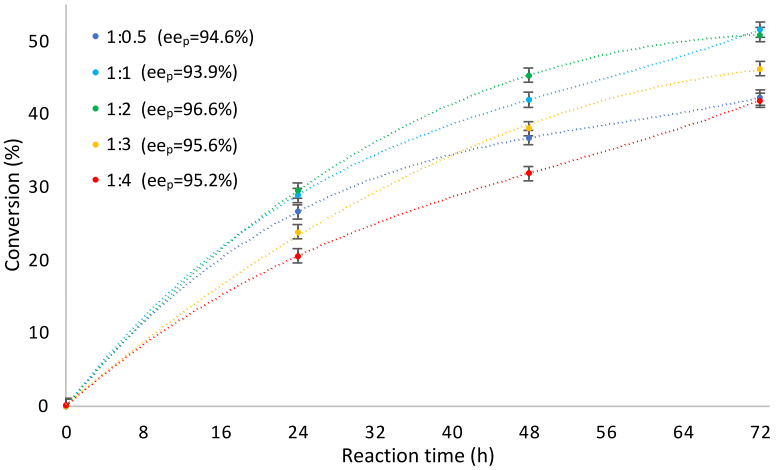

Fig. 5. The influence of the ibuprofen: alcohol molar ratio used for esterification of *rac*-ibuprofen. *Reaction conditions: rac*-ibuprofen 1 mmol, 1-propanol, isooctane, LAO 1.5 mL, 20 °C 250 rpm.

Table 1
Characterization of silica-based supports and biocatalysts.

Matrix	S_{BET} (m^2 g^{-1})	V_p (cm^3 g^{-1})	d_p (nm)	IL, (wt% ± 0.3)[c]	LAO, (wt% ± 0.3)[c]
$MgO{\cdot}SiO_2$ (1:1)	469	0.07	2.1	6.79	3.96
$MgO{\cdot}SiO_2$ (1:5)	289	0.12	2.8	5.05	5.12
$MgO{\cdot}SiO_2$ (5:1)	72	0.05	1.3	7.53	2.64
$CaO{\cdot}SiO_2$ (1:1)	24.9	0.01	1.2	4.29	4.98
$ZrO_2{\cdot}SiO_2$ (1:1)	394	0.10	2.3	–	–
SiO_2[a]	118	0.33	11.1	–	–
SiO_2[b]	200	0.59	11.8	9.4	19.38

[a]Silica used for this study prepared using sol-gel method.
[b]Commercially available silica.
[c]Determined using TGA; the standard deviation of 3 replicate experiments.

enhance structural properties of silicas and highlight other interesting features, they are often combined with metal-based oxides, including among others magnesium oxide, calcium oxide or zirconia. Preparation of such hybrid materials enable to form attractive supports with improved textural and structural properties which predispose them for application in adsorption processes or in immobilization of organic or bioorganic species onto their surface (Degórska et al., 2021). The functionality of as prepared or commercially available silica-based materials results in most cases from the nature of

surface silanol (≡Si-OH), magnesil (-Mg-OH) or others (-Ca-OH, ≡Zr-OH) groups which exhibit relative high affinity, *e.g.* for enzymes and at the same time improve their activity and enantioselectivity, *e.g.* of lipase from *Candida rugosa*, through electrostatic interactions and changes in conformation of enzyme (Salgin and Takac, 2007; Kołodziejczak-Radzimska et al., 2018). Pure commercially available silicas, without modification, and obtained oxide materials were used for comparison reason.

In the next step the ionic liquid was immobilized on the prepared in advance silica-based materials. According to the literature, the efficient way for the anchoring of IL to the surface of silica includes binding cation *via* triethoxysilyl functionality located in the alkyl chain of imidazolium ring (Skoda-Földes, 2014; Valkenberg et al., 2002; Wolny and Chrobok, 2021, 2022). This synthetic route was used in this work (Fig. 7). In the first step, (3-chloropropyl)triethoxysilane was treated with 1-methylimidazole to yield 1-methyl-3-(triethoxysilylpropyl) imidazolium chloride, [tespmim]Cl. Then, the IL was covalently tethered to the silica. The exchange of Cl^- anion for $[NTf_2]^-$ resulted in the final support formation, *e.g.* SiO_2/Mg(1:1)/[tespmim][NTf_2] (Fig. 7). The optimum loading of IL was achieved for experiments with 0.3 mmol of IL for 0.3 g of silica, *e.g.* for MgO·SiO2 (1:1) 6.79 wt%. Increasing the IL amount in immobilization process (from 0.3 mmol to 0.5 mmol) did not increase the IL loading on the matrix remaining it unchanged. However, the decreasing of the IL amount upon the immobilization (from 0.2 mmol to 0.3 mmol) resulted in lowering of its loading (IL loading 4.09 wt%).

TGA, SEM, ^{29}Si NMR and BET analysis were performed to characterize performed process and produced materials. Attachment of the ionic liquid to silica materials was proven by ^{29}Si MAS NMR analysis. MAS-NMR spectra shows the disappearance of the signals assigned to $(SiO)_2Si$-$(OH)_2$ and $(SiO)_3$Si-OH groups, as well as the appearance of the new signal at −66 ppm, what definitely indicates the grafting of the IL to the siliceous surface (Supplementary Materials Fig.S9) (Skoda-Földes, 2014; Valkenberg et al., 2002; Wolny and Chrobok, 2021). Additionally, SEM images of the materials before and after ILs deposition confirmed the presence of irregular shaped particles with slightly bigger tendency to form agglomerate structured in case of ILs coated samples (Supplementary Materials Fig.S15–S17). The MgO·SiO_2 1:1 material is characterized by the highest value of BET surface area of 469 m^2 g^{-1} among tested materials followed by pore volume of 0.07 cm^3 g^{-1} and pore size of 2.1 nm. Changes in the initial precursors ratio resulted in significant drop of all parameters of the porous structure. Surprisingly, the IL loading onto MgO·SiO_2 material determined by TGA did not follow the same trend and varied from 5.05 wt% for MgO·SiO_2 1:5 to 7.53 wt% for MgO·SiO_2 5:1 suggesting that textural properties and structure of the support as well as nature of surface functional groups also affect IL loading. Preparation of hybrid combinations that besides silica, contain also other metal oxides, on the one hand, resulted in improved parameters of the porous structure and on the other hand offers additional functional groups related, *e.g.* with magnesium, which can easily interact with analyzed biomolecules. When immobilization adsorption is considered the amount of active sites onto support surface is of key importance. That is why by selecting support type, the method of its synthesis as well as percentage contribution of specific components, the efficiency of IL loading can be controlled as confirmed, *e.g.* in case of MgO–SiO_2 materials — the more MgO in the material structure the higher amount of IL was bounded. The proposition of the role of magnesium in bounding process was demonstrated on Fig. 7. Silica combination with CaO resulted in 4.29 wt% of IL loading. The highest amount of IL was immobilized on the commercially available silica mainly due to the well-defined porous structure, the presence of a numerous of surface hydroxyl groups and their uniform distribution that reduces steric hindrances and promote efficient binding of significant amount of IL.

The final step in the preparation of biocatalyst included the immobilization of aqueous-glycerol solution of LAO on the surface of support *via* physical adsorption. Native lipase from *Aspergillus oryzae* (LAO) was commercially available product (Sigma-Aldrich) in the form of aqueous-glycerol solution (activity 100,000 U g^{-1}). Additionally, the Lowry protein assay was performed to determine the amount of protein in commercial product that was found to be 43.7 mg/mL. Physical immobilization of LAO was performed in water with a 7-fold mass excess of LAO solution over the SILP carrier and resulted *e.g.* in 3.96 wt% loading of enzyme for SiO_2/Mg(1:1)/[tespmim][NTf_2]/LAO. Increasing the LAO amount during immobilization step (from 7-fold to 10-fold) did not increase the LAO loading, but decreasing the LAO amount to 3-fold resulted in decreasing of its loading (2.09%).

The created biocatalysts, *e.g.* SiO_2/Mg(1:1)/[tespmim][NTf_2]/LAO were analyzed using TGA and SEM analysis (Supplementary Materials Fig.S18), which results confirm effective enzyme deposition. Loading of LAO on supports modified with IL was determined with TGA. The highest amount 19.38 wt% of LAO was tethered on the surface of commercially available silica confirming that this material is the most prone to functionalization by IL that directly facilitate high enzyme loading. Other materials included 2.64–5.12 wt% of LAO. It can be seen that the lowest amount of IL (5.05 wt%) was attached to the MgO–SiO_2 1:5 material and also on this system, the highest amount of enzyme was deposited. This confirms that even low amount of IL provides a sufficient amount of functional groups capable for enzyme binding. These data are also in agreement with hypothesis that the presence of silica in the structure of oxide material facilitates homogeneous distribution of surface functional moieties. For the material SiO_2·Mg(1:1) after anchoring of [tespmim][NTf_2] (SiO_2/Mg(1:1)-IL; S_{BET} 117 m^2 g^{-1}, V_p 0.07 cm^3 g^{-1}, d_p 2.2 nm) and next after immobilization of enzyme (SiO_2/Mg(1:1)-IL-LAO; S_{BET} 83.2 m^2 g^{-1}, V_p 0.04 cm^3 g^{-1}, d_p 2.2 nm) surface characteristics were also determined.

Heterogeneous biocatalysts were tested for racemic ibuprofen resolution using selected above reaction conditions (Fig. 6 and Supplementary Materials Fig.S7). Mass of each biocatalyst was recalculated to obtained biocatalyst with the same content of LAO (3.56 mg/1 mmol of *rac*-ibuprofen). To this aim 0.082 mL of native LAO (aqueous-glycerol solution) was used which contains 3.56 mg of protein. The most active was biocatalyst SiO_2/Mg(1:1)/[tespmim][NTf_2]/LAO causing the 35% conversion of *rac*-ibuprofen after 7 days with 95% *ee* of ester (E = 83, Supplementary Materials Fig.S7).

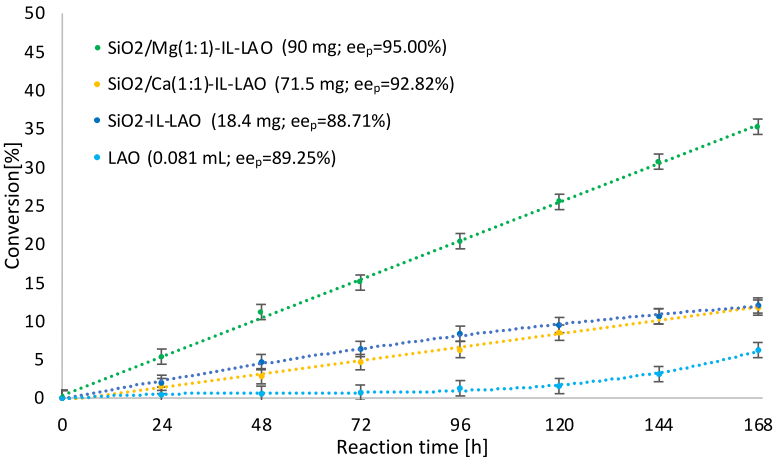

Fig. 6. The influence of the SILP support used for esterification of *rac*-ibuprofen. *Reaction conditions: rac*-ibuprofen 0.1 mmol, 1-butanol 0.2 mmol, isooctane 0.4 mL, 3.56 mg of LAO in native or immobilized form, 20 °C, 250 rpm.

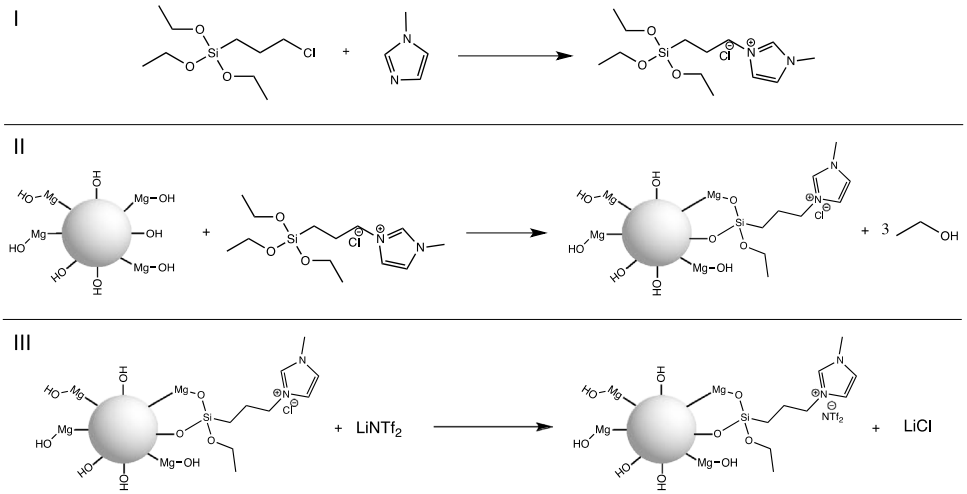

Fig. 7. Immobilization of [tespmim][NTf_2] onto silica surface.

Surprisingly, enrichment (SiO_2·Mg(1:5)) or lowering (SiO_2·Mg(5:1)) of the content of MgO in the support caused the complete deactivation of the final biocatalyst. Probably the amount of MgO in the support (SiO_2·Mg(1:1)) according to the proposed mechanism of the IL immobilization *via* chemical bounding (Fig. 7) was on the proper level, causing the effective immobilization of IL and activating LAO. Although prolongation of process duration did not result in improvement of process yield and its *ee*, it should be highlighted that lower amount of enzyme immobilized on the surface generates higher activity of heterogeneous catalyst (Fig. 6) as well as immobilization improves enzyme stabilization and facilitates its recycle potential. Unfortunately, SiO_2/Ca(1:1)/[tespmim][NTf_2]/LAO was not active enough giving the low conversion. The same phenomenon was observed for the biocatalyst with very high loading of lipase immobilized on the pure surface of silica SiO_2/[tespmim][NTf_2]/LAO. The catalyst did not affect too much the conversion probably due to lipase overloading onto silica surface (agglomeration) that leads to blocking of enzyme active sites and formation of diffusional limitations. Finally, the native LAO used in the same amount (3.56 mg) as was loaded on other heterogeneous biocatalysts was poorly active. It is the proof of the activation of LAO on the surface of Mg-doped silica. The immobilization of lipase on the unmodified MgO–SiO_2 matrix failed (using TGA the protein was not detected). Additionally, bared SILP, without enzyme on the surface was not catalytically active. Only after modification of the surface with IL lipase was able to embed on the support and catalyze the ibuprofen resolution.

The attempts to accelerate the reaction by adding more biocatalysts (40–90 mg) were limited (Fig. 8 and Supplementary Materials Fig.S8). Higher amount of biocatalyst (150 mg) required the increasing of solvent, what was caused with difficulties with stirring of the reaction mixture which was extremity dense. The addition of extra amount of solvent resulted in diluting the reaction mixture and slowing down the reaction rate and lowering the conversion to 19%.

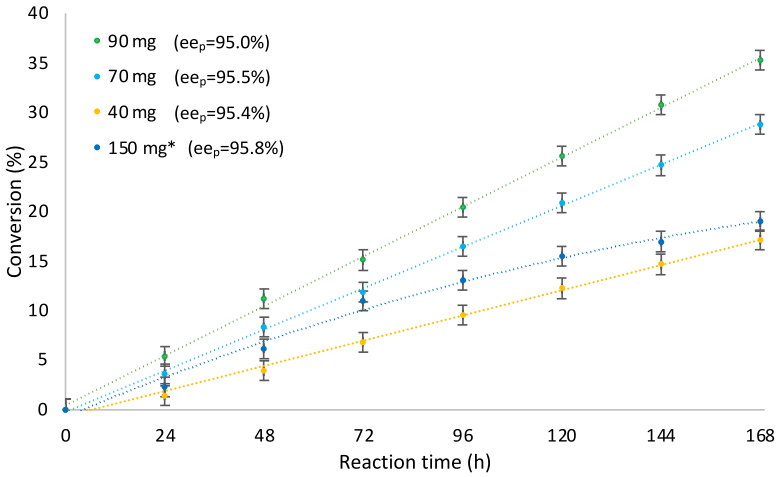

Fig. 8. The influence of the amount of SiO_2/Mg(1:1)/[tespmim][NTf_2]/LAO used for esterification of *rac*-ibuprofen. *Reaction conditions: rac*-ibuprofen 0.1 mmol, 1-butanol 0.2 mmol, isooctane 0.4 mL, SiO_2/Mg(1:1)/[tespmim][NTf_2]/LAO with 3.56 mg of immobilized protein, 20 °C, 250 rpm; * isooctane 1 mL.

Table 2
The comparison of the most important results for enantiomeric resolution of racemic ibuprofen *via* esterification.

Biocatalyst	Reaction conditions	Reaction indicator	Reference
Lipase from *Candida rugosa*	1-propanol, cyclohexane, 30 °C, 140 h	Conversion 44.2%, *ee* 68.3%	Siódmiak et al. (2012)
Protein-coated microcrystals prepared from lipase form *Candida rugosa*	Isooctanol, isooctane 50 °C, 8 h	Conversion 49.83%, *ee* 97.34%	Huang et al. (2015)
Lipase from *Rhizomucor miehei* immobilized on epoxy-functionalized silica	1-propanol, isooctane, 0 °C, 24 h	Conversion 23.7%, *ee* 92%	Mohammadi et al. (2016)
Candida rugosa immobilized on silica nanoparticles	1-propanol, isooctane, 37 °C, 50 min	Conversion 45%, *ee* 96%	Ghofrani et al. (2021)
Lipase from *Aspergillus oryzae*	1-propanol, isooctane, 20 °C, 48 h	Conversion 35%, *ee* 99.9%	This work
Lipase from *Aspergillus oryzae* immobilized on SILP	1-propanol, isooctane, 20 °C, 7 days	Conversion 35%, *ee* 95%	This work

The recyclability of SiO_2/Mg(1:1)/[tespmim][NTf_2]/LAO is demonstrated in Fig. 9. In the first case, the decrease in selectivity in the second cycle of the reaction was from *ee* 96.7% to 88% after 5 days of reaction and from *ee* 95.5% to 85.5% after 7 days of reaction. Although a dilution of the reaction system up to 1 mL caused the decreasing in the reaction rate, it allowed to maintain the same high enantioselectivity (1st cycle *ee* 96.3%, 2^{ed} cycle *ee* 95.4% after 5 days and 1st cycle *ee* 95.8%, 2^{ed} 94.2% cycle after 7 days). The long stability of biocatalyst is due to the stabilization effect of the SILP which is known from their exceptional properties, inter alia, maintenance of the active conformations of the enzymes. Moreover, used IL provides suitable microenvironment for immobilization of lipase that facilitate repeated use of the biocatalysts. The TGA analysis of the biocatalyst after second cycle (experiment with 90 mg of biocatalyst) revealed that the amount of enzyme on the modified surface of silica (SiO2/Mg(1:1)/[tespmim][NTf_2]/LAO) stayed intact (4.04 wt %, Supplementary Materials Fig.S33). Additionally, the experiments with fast catalyst filtration demonstrated no further ibuprofen conversion in the filtrate after catalyst's removal (Supplementary Materials Fig.S34). These are the proofs that the reason of the lower activity is the enzyme inhibition in this long term process (186 h). Even if the excess of catalyst was used (150 mg) the slow inhibition was visible.

Summing up, the developed catalyst is highly active in the resolution of racemic ibuprofen *via* esterification and can compete with catalysts described in the literature what was demonstrated in Table 2.

4. Conclusions

In this work two novel approaches for kinetic resolution of ibuprofen *via* enantiomeric esterification were applied. Lipase from *Aspergillus oryzae* was a very effective enzyme for this purpose. A SILP system was used for designing heterogeneous biocatalyst based on silica-based hybrid carriers. The SILP biocatalytic system showed improved enzyme stability and reusability. Results in this study show *(S)*-(+)-ibuprofen ester *ee* 99.9% with $\alpha = 34.8\%$, after 24 h and respectively *ee* = 99.9% with $\alpha = 45.2\%$ after 48 h using native LAO is competitive with other literature results.

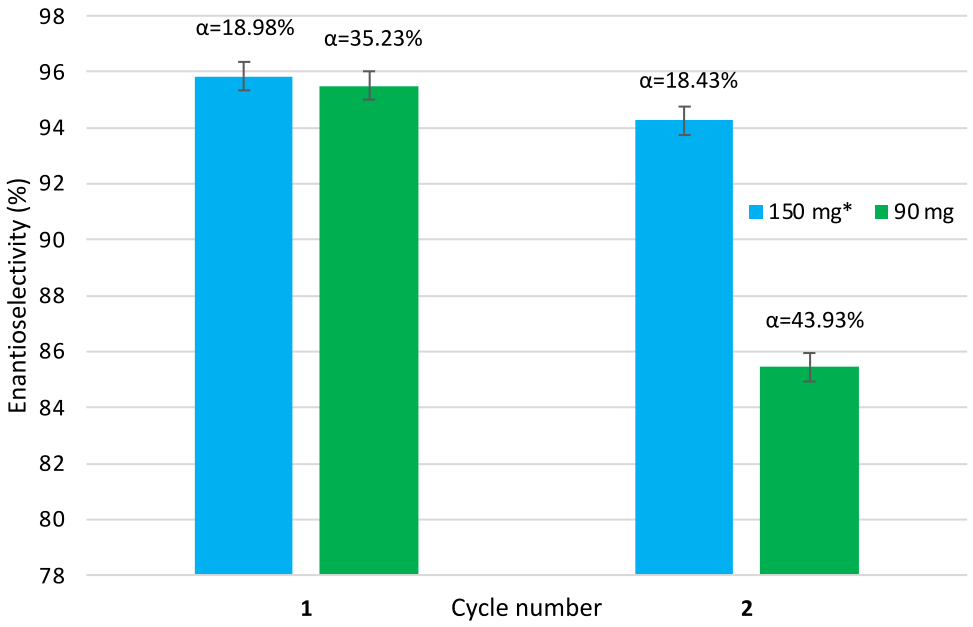

Fig. 9. The recycling of SiO_2/Mg(1:1)/[tespmim][NTf_2]/LAO used for esterification of *rac*-ibuprofen; 168 h; where α means conversion; error bars show the standard deviation of 3 replicate experiments. *Reaction conditions: rac*-ibuprofen 0.1 mmol, 1-butanol 0.2 mmol, isooctane 0.4 mL, MgO·SiO_2-[tespmim][NTf_2]-LAO biocatalyst; * isooctane 1 mL.

Using heterogeneous biocatalyst SiO_2/Mg(1:1)/[tespmim][NTf_2]/LAO (ionic liquid loading 6.79%, enzyme loading 3.96%) the conversion of *rac*-ibuprofen reached 35% after 7 days with 95% *ee* of ester. Although a dilution of the reaction system caused the decreasing in the reaction rate, it allowed to maintain the high enantioselectivity of *(S)*-(+)-enantiomer of ibuprofen in the second cycle. Overall, this work represents a novel alternative for an effective stabilization of LAO in the organic environments.

CRediT authorship contribution statement

Anna Wolny: Conceptualization, Methodology, Investigation, Formal analysis, Visualization, Writing – original draft. **Agnieszka Siewniak:** Methodology, Investigation, Formal analysis. **Jakub Zdarta:** Conceptualization, Writing – review and editing. **Filip Ciesielczyk:** Methodology, Investigation. **Piotr Latos:** Methodology, Investigation, Formal analysis. **Sebastian Jurczyk:** Methodology, Investigation. **Long D. Nghiem:** Conceptualization, Writing – review and editing. **Teofil Jesionowski:** Conceptualization, Writing – review and editing, Supervision, Project administration, Funding acquisition. **Anna Chrobok:** Conceptualization, Writing – review and editing, Supervision, Project administration, Funding acquisition.

Declaration of competing interest

The authors declare that they have no known competing financial interests or personal relationships that could have appeared to influence the work reported in this paper.

Funding

This work was supported by the National Science Centre, Poland (grant no. UMO-2020/39/B/ST8/00693).

Appendix A. Supplementary data

Supplementary material related to this article can be found online at https://doi.org/10.1016/j.eti.2022.102936. ^{1}H, ^{13}C spectra of ionic liquid and (S)-(+)-ibuprofen, ^{29}Si NMR solid state, TGA, SEM-EDS analysis of synthesized SILPs and biocatalysts (PDF).

References

Adams, S.S., Bresloff, P., Mason, C.G., 1976. Pharmacological differences between the optical isomers of ibuprofen: Evidence for metabolic inversion of the (−)-Isomer. J. Pharm. Pharmacol. 28, 256–257.

Arana-Peña, S., Rios, N.S., Carballares, D., Gonçalves, L.R.B., Fernandez-Lafuente, R., 2020. Immobilization of lipases via interfacial activation on hydrophobic supports: Production of biocatalysts libraries by altering the immobilization conditions. Catal. Today 362, 130–140.

Bachosz, L., Vu, M.T., Nghiem, L.D., Zdarta, J., Nguyen, L.N., Jesionowski, T., 2022. Enzyme-based control of membrane biofouling for water and wastewater purification: A comprehensive review. Environ. Technol. Innov. 25, 102106.

Barbosa, O., Ortiz, A., Torres, R., Rodrigues, R.C., Fernandez-Lafuente, R., 2015. Strategies for the one-step immobilization-purification of enzymes as industrial biocatalysts. Biotechnol. Adv. 33, 435.

Baumann, M., Moody, T.S., Smyth, M., Wharry, S.A., 2020. Perspective on continuous flow chemistry in the pharmaceutical industry. Org. Process. Res. Dev. 24, 1802.

Bilal, M., Zhao, Y., Noreen, S., Shah, S.Z.H., Bharagava, R.N., Iqbal, H.M.N., 2019. Modifying bio-catalytic properties of enzymes for efficient biocatalysis: a review from immobilization strategies viewpoint. Biocatal. Biotransform. 37, 159.

Boudrant, J., Woodley, J.M., Fernandez-Lafuente, R., 2020. Parameters necessary to define an immobilized enzyme preparation. Process. Biochem. 90, 66.

Ciesielczyk, F., Przybysz, M., Zdarta, J., Piasecki, A., Paukszta, D., Jesionowski, T., 2014. The sol–gel approach as a method of synthesis of xmgo·ySiO_2 powder with defined physicochemical properties including crystalline structure. J. Sol-Gel Sci. Technol. 71, 501–513.

Degórska, O., Zdarta, J., Synoradzki, K., Zgoła-Grześkowiak, A., Ciesielczyk, F., Jesionowski, T., 2021. From core-shell like structured zirconia/magnetite hybrid towards novel biocatalytic systems for tetracycline removal: Synthesis, enzyme immobilization, degradation and toxicity study. J. Environ. Chem. Eng. 9, 105701.

Dos Santos, J.C.S., Barbosa, O., Ortiz, C., Berenguer-Murcia, A., Rodrigues, R.C., Fernandez-Lafuente, R., 2015. Importance of the support properties for immobilization or purification of enzymes. ChemCatChem 7, 2413.

Drożdż, A., Erfurt, K., Bielas, R., Chrobok, A., 2015. Chemo-enzymatic Baeyer–Villiger oxidation in the presence of *Candida antarctica* lipase B and ionic liquids. New J. Chem. 39, 1315–1321.

Evans, A.M., 2001. Comparative pharmacology of s(+)-ibuprofen and (RS)-ibuprofen. Clin. Rheumatol. 20, 9–14.

Fernandez-Lafuente, R., Armisén, P., Sabuquillo, P., Fernández-Lorente, G., M. Guisán, J., 1998. Immobilization of lipases by selective adsorption on hydrophobic supports. Chem. Phys. Lipids 93, 185–197.

Garcia-Galan, C., Berenguer-Murcia, A., Fernandez-Lafuente, R., Rodrigues, R.C., 2011. Potential of different enzyme immobilization strategies to improve enzyme performance. Adv. Synth. Catal. 353, 2880–2904.

Garcia-Verdugo, E., Lozano, P., Lui, S.V., 2014. Biocatalytic processes based on supported ionic liquids. In: Fehrmann, R., Riisager, A., Haumann, M. (Eds.), Supported Ionic Liquids: Fundamentals and Applications. Wiley-VCH, Weinheim, pp. 351–368.

Ghofrani, S., Allameh, A., Yaghmaei, P., Norouzian, D., 2021. Immobilization of *Candida rugosa* Lipase for resolution of racemic ibuprofen. J. Pharm. Sci. 29, 117–123.

Hong, S.G., Kim, H.S., Kim, J., 2014. Highly stabilized lipase in polyaniline nanofibers for surfactant-mediated esterification of ibuprofen. Langmuir 30, 911–915.

Huang, S., Li, X., Xu, L., Ke, C., Zhang, R., Yan, Y., 2015. Protein-coated microcrystals from *Candida rugosa* Lipase: Its immobilization, characterization, and application in resolution of racemic Ibuprofen. Appl. Biochem. Biotechnol. 177, 36–47.

Itoh, T., 2017. Ionic liquids as tool to improve enzymatic organic synthesis. Chem. Rev. 117, 10567–10607.

Jankowska, K., Ciesielczyk, F., Bachosz, K., Zdarta, J., Kaczorek, E., Jesionowski, T., 2019. Laccase immobilized onto Zirconia–Silica hybrid doped with cu^{2+} as an effective biocatalytic system for decolorization of dyes. Materials 12, 1252.

Jesionowski, T., Zdarta, J., Krajewska, B., 2014. Enzyme immobilization by adsorption: A review. Adsorption 20, 801–821.

Jiang, Q., Fang, R., Gul, I., Aer, L., Zhao, Y., Guo, J., Tang, L., 2022. Halohydrin dehalogenase immobilization in magnetic biochar for sustainable halocarbon biodegradation and biotransformation. Environ. Technol. Innov. 27, 102759.

José, C., Toledo, M.V., Briand, L.E., 2015. Enzymatic kinetic resolution of racemic ibuprofen: Past, present and future. Crit. Rev. Biotechnol. 36, 891–903.

Klapiszewski, Ł., Królak, M., Jesionowski, T., 2014. Silica synthesis by the sol-gel method and its use in the preparation of multifunctional biocomposites. Cent. Eur. J. Chem. 12, 173–184.

Kołodziejczak-Radzimska, A., Zdarta, J., Ciesielczyk, F., Jesionowski, T., 2018. An organofunctionalized MgO ·SiO_2 hybrid support and its performance in the immobilization of lipase from *Candida rugosa*. Korean J. Chem. Eng. 35, 2220–2231.

Lee, C., Sandig, B., Buchmeiser, M.R., Haumann, M., 2018. Supported ionic liquid phase (SILP) facilitated gas-phase enzyme catalysis – CALB catalyzed transesterification of vinyl propionate. Catal. Sci. Technol. 8, 2460–2466.

Lozano, P., Alvarez, E., Bernal, J.M., Nieto, S., Gomez, C., Sanchez-Gomez, G., 2017. Ionic liquids for clean biocatalytic processes. Curr. Green Chem. 4, 116–129.

Markiton, M., Boncel, S., Janas, D., Chrobok, A., 2017. Highly active nanobiocatalyst from lipase noncovalently immobilized on multiwalled carbon nanotubes for baeyer–Villiger synthesis of lactones. ACS Sustain. Chem. Eng. 5, 1685.

Mateo, C., Palomo, J.M., Fernandez-Lorente, G., Guisan, J.M., Fernandez-Lafuente, R., 2007a. Improvement of enzyme activity, stability and selectivity via immobilization techniques. Enzyme Microb. Technol. 40, 1451.

Mateo, C., Palomo, J.M., Fernandez-Lorente, G., Guisan, J.M., Fernandez-Lafuente, R., 2007b. Improvement of enzyme activity, stability and selectivity via immobilization techniques. Enzyme Microb. Technol. 40, 1451–1461.

Matuszek, K., Chrobok, A., Latos, P., Markiton, M., Szymańska, K., Jarzębski, A., Swadźba-Kwaśny, M., 2016. Silica-supported chlorometallate(III) ionic liquids as recyclable catalysts for diels–alder reaction under solventless conditions. Catal. Sci. Technol. 6, 8129–8137.

Miyako, E., Maruyama, T., Kamiya, N., Goto, M., 2003. Enzyme-facilitated enantioselective transport of (S)-ibuprofen through a supported liquid membrane based on ionic liquids. Chem. Commun. 23, 2926–2927.

Mohammadi, M., Gandomkar, S., Habibi, Z., Yousefi, M., 2016. One pot three-component reaction for covalent immobilization of enzymes: Application of immobilized lipases for kinetic resolution of Rac-ibuprofen. RSC Adv. 6, 52838–52849.

Naik, P.U., Nara, S.J., Harjani, J.R., Salunkhe, M.M., 2007. Ionic liquid anchored substrate for enzyme catalysed kinetic resolution. J. Mol. Catal. B Enzyme 44, 93–98.

Nguyen, A.Q., Nguyen, L.N., McDonald, J.A., Nghiem, L.D., Leusch, F.D.L., Neale, P.A., Khan, S.J., 2021. Chiral inversion of 2-arylpropionoic acid (2-APA) enantiomers during simulated biological wastewater treatment. Water Res. 209, 117871.

Nguyen, Q.A., Vu, H.P., McDonald, J.A., Nguyen, L.N., Leusch, F.D.L., Neale, P.A., Khan, S.J., Nghiem, L.D., 2022. Chiral inversion of 2-arylpropionic acid enantiomers under anaerobic conditions. Environ. Sci. Technol. 56, 8197–8208.

Raczyńska, A., Jadczyk, J., Brzezińska-Rodak, M., 2021. Altering the stereoselectivity of whole-cell Biotransformations via the physicochemical parameters impacting the processes. Catalysts 11, 781.

Rodrigues, R.C., Ortiz, C., Berenguer-Murcia, A., Torres, R., Fernandez-Lafuente, R., 2013. Modifying enzyme activity and selectivity by immobilization. Chem. Soc. Rev. 42, 6290–6307.
Salgin, S., Takac, S., 2007. Additives on the activity and enantioselectivity of *Candida rugosa* Lipase in a biphasic medium. Chem. Eng. Technol. 30, 1739–1743.
Siódmiak, T., Rumiński, J.K., Marszałł, M.P., 2012. Application of lipases from *Candida Rugosa* in the enantioselective esterification of (R, S)-ibuprofen. Curr. Org. Chem. 16, 972–977.
Skoda-Földes, R., 2014. The use of supported acidic ionic liquids in organic synthesis. Molecules 19, 8840.
Stöber, W., Fink, A., Bohn, E., 1968. Controlled growth of monodisperse silica spheres in the micron size range. J. Colloid Interface Sci. 26, 62–69.
Svetozarević, M., Šekuljica, N., Onjia, A., Barać, B., Mihajlović, M., Knežević-Jugović, Z., Mijind, D., 2022. Biodegradation of synthetic dyes by free and cross-linked peroxidase in microfluidic reactor. Environ. Technol. Innov. 26, 102373.
Szelwicka, A., Boncel, S., Jurczyk, S., Chrobok, A., 2019a. Exceptionally active and reusable nanobiocatalyst comprising lipase noncovalently immobilized on multi-wall carbon nanotubes for the synthesis of diester plasticizers. Appl. Catal. A: Gen 574, 41.
Szelwicka, A., Erfurt, K., Jurczyk, S., Boncel, S., Chrobok, A., 2021a. Outperformance in acrylation: Supported D-glucose-based ionic liquid phase on MWCNTs for immobilized lipase b from *Candida antarctica* as catalytic system. Materials 14, 3090.
Szelwicka, A., Kolanowska, A., Latos, P., Jurczyk, S., Boncel, S., Chrobok, A., 2020. Carbon nanotube/PTFE as a hybrid platform for Lipase B from *Candida Antarctica* in transformation of α-angelica lactone into alkyl levulinates. Catal. Sci. Technol. 10, 3255.
Szelwicka, A., Wolny, A., Grymel, M., Jurczyk, S., Boncel, S., Chrobok, A., 2021b. Chemo-enzymatic baeyer–Villiger oxidation facilitated with lipases immobilized in the supported ionic liquid phase. Materials 14, 3443.
Szelwicka, A., Zawadzki, P., Sitko, M., Boncel, S., Czardybon, W., Chrobok, A., 2019b. Continuous flow chemo-enzymatic baeyer–Villiger oxidation with superactive and extra-stable enzyme/carbon nanotube catalyst: an efficient upgrade from batch to flow. Org. Process. Res. Dev. 23, 1386.
Valkenberg, M.H., deCastro, C., Hölderich, W.F., 2002. Immobilisation of ionic liquids on solid supports. Green Chem. 4, 88.
Verri, F., Diaz, U., Macario, A., Corma, A., Giordano, G., 2016. Optimized hybrid nanospheres immobilizing *Rhizomucor miehei* Lipase for chiral Biotransformation. Process. Biochem. 51, 240–248.
Wei, T., Yang, K., Bai, B., Zang, J., Yu, X., Mao, D., 2016. Enzymatic hydrolytic resolution of racemic ibuprofen ethyl ester using an ionic liquid as cosolvent. Molecules 21, 905.
Wolny, A., Chrobok, A., 2021. Ionic liquids for development of heterogeneous catalysts based on nanomaterials for biocatalysis. Nanomaterials 11, 2030.
Wolny, A., Chrobok, A., 2022. Silica-based supported ionic liquid-like phases as heterogeneous catalysts. Molecules 27, 5900.
Wsól, V., Skálová, L., Szotáková, B., 2004. Chiral inversion of drugs: Coincidence or principle?. Curr. Drug. Metab. 5, 517–533.
Zappaterra, F., Rodriguez, M.E.M., Summa, D., Semeraro, B., Costa, S., Tamburini, E., 2021. Biocatalytic approach for direct esterification of ibuprofen with sorbitol in biphasic media. Int. J. Mol. Sci. 22, 3066.
Zdarta, J., Jankowska, K., Bachosz, K., Degórska, O., Kaźmierczak, K., Nguyen, L.N., Nghiem, L.D., Jesionowski, T., 2022c. Enhanced wastewater treatment by immobilized enzymes. Curr. Pol. Rep. 7, 167–179.
Zdarta, J., Jesionowski, T., Pinelo, M., Meyer, A.S., Iqbal, H.M.N., Bilal, M., Nguyen, L.N., Nghiem, L.D., 2022b. Free and immobilized biocatalysts for removing micropollutants from water and wastewater: Recent progress and challenges. Bioresour. Technol. 344, 126201.
Zdarta, J., Nguyen, L.N., Jankowska, K., Jesionowski, T., Nghiem, L.D., 2022a. A contemporary review of enzymatic applications in the remediation of emerging estrogenic compounds. Crit. Rev. Environ. Sci. Technol. 52, 2661–2690.
Zhao, H., 2015. Protein stabilization and enzyme activation in ionic liquids: Specific ion effects. J. Chem. Technol. Biotechnol. 91, 25–50.

Supported ionic liquid phase facilitated catalysis with lipase from *Aspergillus oryzae* for enhance enantiomeric resolution of racemic ibuprofen

SUPPLEMENTARY MATERIALS

Anna Wolny,[a] Agnieszka Siewniak,[a] Jakub Zdarta,[b] Filip Ciesielczyk,[b] Piotr Latos,[a] Sebastian Jurczyk,[c] Long D. Nghiem,[d] Teofil Jesionowski,[b] Anna Chrobok[a*]*

[a] Department of Chemical Organic Technology and Petrochemistry, Faculty of Chemistry, Silesian University of Technology, Krzywoustego 4, PL-44100 Gliwice, Poland, anna.chrobok@polsl.pl

[b] Institute of Chemical Technology and Engineering, Faculty of Chemical Technology, Poznan University of Technology, Berdychowo 4, PL-60965 Poznan, Poland, teofil.jesionowski@put.poznan.pl

[c] Institute for Engineering of Polymer Materials and Dyes, Lukasiewicz Research Network, Sklodowskiej-Curie 55, PL-87100 Torun, Poland

[d] Centre for Technology in Water and Wastewater, University of Technology Sydney, Ultimo NSW 2007, Australia

Materials

Ibuprofen racemate (≥98.0 wt. %) was purchase from Chemat (Poland). Native lipase B from *Candida antarctica* (CALB) in aqueous-glycerol solution (activity 5000 $U \cdot L \cdot kg^{-1}$), native lipase from *Aspergillus oryzae* (LAO) in aqueous-glycerol solution (activity 100,000 $U \cdot g^{-1}$), isooctane (≥99.0 wt. %), lithium bis(trifluoromethanesulfonyl)imide (≥99.0 wt. %), propylene carbonate (≥99.0 wt. %), acetic acid (glacial) 100% (≥99.8 wt. %), 1-methylimidazole (≥99.0 wt. %), (3-chloropropyl)triethoxysilane (≥95.0 wt. %), magnesium ethoxide (MET) (≥98.0 wt. %), tetraethyl orthosilicate (TEOS) (≥95.0 wt. %), zirconium(IV) isopropoxide (TZIP) (≥ 99.0 wt. %), calcium silicate (≥87 wt. % SiO_2 basis, 12-22 wt. % Ca as CaO basis; 7.0-10.0 μm) and silica (≥99.8 wt. %; 0.011 μm, 175-225 m^2/g) were purchased from Sigma-Aldrich (Merck Group, Poland). Methanol, ethanol, toluene and acetonitrile were purchase from STANLAB (Poland). 1-propanol, 1-butanol, cyclohexane and dichloroethane were purchase from CHEMPUR (Poland). Hexane (≥95.0 wt. %), heptane (≥99.2 wt. %) and 2-propanol (≥99.8 wt. %) were purchased from WITKO (Poland). 2-propanol (≥99.7 wt. %) and ammonia solution (≥25.0 wt. %) were purchase from Avantor Performance Materials (Poland). 1-ethyl-3-methylimidazolium dibutylphosphate (≥98.0 wt. %), 1-butyl-3-methylimidazolium acetate (≥98.0 wt. %), 1-butyl-3-methylimidazolium bis(trifluoromethylsulfonyl)imide (≥99.0 wt. %), 1-ethyl-3-methylimidazolium ethylsulfate (≥98.0 wt. %) were purchased from IoLiTech Ionic Liquids Technologies GmbH (Germany).

Analytical methods

HPLC was performed on a liquid chromatograph (Alliance, Waters 2690 system) with Waters PDA detector and Chiralcel OD Daicel (250×4,6 mm; 10 μm) column. The solvent system included hexane/2-propanol/acetic acid (100:0.1:0.15; *v/v/v*) and the flow rate was 0.5 mL/min (0-15 min); 1 mL/min (15-50 min); 0.5 mL/min (50-55 min). During the reaction 20 μL of the samples diluted in 1 mL of hexane were collected to verify enantioselectivity and the reaction progress via

standard curves of ibuprofen enantiomers. TGA analysis of all obtained materials and biocatalysts were conducted on a thermobalance (Mettler Toledo TGA851e). 15 mg of sample was heated in a range of 25-800 °C and the rate was set at 10 °C/min under a dynamic nitrogen flow 60 mL/min. The analysis were performed in a reference to standard – 70 µL Al_2O_3 crucibles. The thermograms allowed to calculate the amount of ionic liquids bonded to the materials and the amount of lipase immobilized on the supports surface. SEM-EDS images of synthesized supports and biocatalyst were performed applying a Phenom Pro Desktop SEM instrument equipped with an EDS detector (15 kV) (Thermo Fischer Scientific). BET surface area (A_{BET}), average pore size (S_p) and average pore volume (V_p) of obtained materials were determined by means of the BET method and the BJH model, applying low-temperature (–196 °C) nitrogen sorption (ASAP 2020, Micromeritic Instruments Co.) The measurement was conducted at a variety of defined partial pressures at which adsorption of N_2 took place. Prior to the analysis, samples were degassed at 120 °C within 4 hours. The results were obtained in the form of adsorption/desorption isotherms (amount of N_2 adsorbed vs. relative pressure), which allowed for calculations of mentioned parameters of the porous structure. ^{29}Si MAS NMR spectra of *supported ionic liquid phase* materials were recorded at 59.517 MHz using a Bruker HP-WB high-speed MAS probe equipped with a 4 mm zirconia rotor to record the NMR spectra at a spinning speed of 8 kHz. ^{1}H NMR and ^{13}C NMR spectra were obtained on a Varian system (400 MHz and 101 MHz, respectively). Lowry test was performed to determine the concentration of the protein in the *Aspergillus oryzae* commercial solution. The standard curve was prepared using bovine serum albumin. Prepared Lowry solution (0.5 mL) was mixed with diluted sample (0.5 mL) and after 20 min Folin solution (0.25 mL) was added. After 30 min of incubation the absorbance was measured using a spectrophotometer.

Calculation methods

Enantiomeric excess (ee)

$$ee_p = \frac{A_{SE} - A_{RE}}{A_{SE} + A_{RE}}$$

$$ee_s = \frac{A_{RI} - A_{SI}}{A_{RI} + A_{SI}}$$

ee_p – enantiomeric excess of the product

ee_s – enantiomeric excess of the substrate

A_{SE} – surface area of (S)-(+)-ibuprofen ester

A_{RE} – surface area of (R)-(-)-ibuprofen ester

A_{SI} – surface area of (S)-(+)-ibuprofen

A_{RI} – surface area of (R)-(-)-ibuprofen*

*determined by HPLC

Enantiomeric ratio (E)

$$E = \frac{\ln\left[\frac{1 - ee_s}{1 + \frac{ee_s}{ee_p}}\right]}{\ln\left[\frac{1 + ee_s}{1 + \frac{ee_s}{ee_p}}\right]}$$

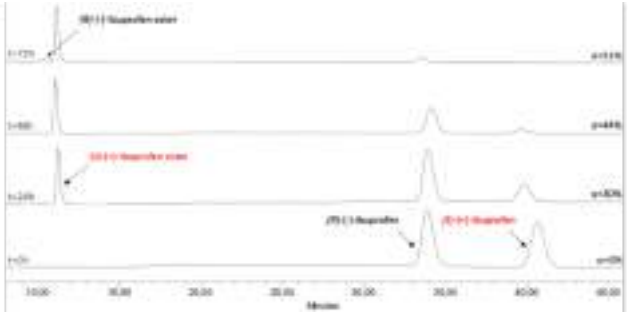

Figure S1. The exemplary chromatogram of the changes in concentration of reagents in the reaction mixture during the reaction time. HPLC with chiral Column: Chiralcel OD Daicel.

Table S1. Solvent effect.

Solvent	Reaction time (h)	ee_s (%)	ee_p (%)	α (%)
isooctane	24	53.6	99.9	34.8
isooctane	48	82.5	99.0	45.2

cyclohexane	24	34.2	99.9	25.5
cyclohexane	48	67.3	99.0	40.2
hexane	24	38.2	99.9	27.6
hexane	48	74.2	96.0	43.7
heptane	24	47.8	96.0	34.2
heptane	48	81.4	93.2	45.2
toluene	24	22.4	99.0	18.5
toluene	48	63.0	95.6	39.7
propylene carbonate	24	7.0	99.0	6.4
propylene carbonate	48	11.0	99.0	10.1
acetonitrile	24	5.9	99.0	5.6
acetonitrile	48	7.4	93.7	7.4
dichloroethane	24	3.6	99.0	3.4
dichloroethane	48	15.1	90.4	14.3
[emim][$EtSO_4$]	24	1.7	99.9	1.6
[emim][$EtSO_4$]	48	2.9	99.9	2.8
[bmim][NTf_2]/ isooctane[1]	24	66.1	83.6	44.2
[bmim][NTf_2]/ isooctane[1]	48	79.8	90.4	46.9

[1][bmim][NTf_2]/isooctane (1:1;*v:v*); ee_s – enantioselectivity of substrate, ee_p – enantioselectivity of product, α – conversion of ibuprofen.

Reaction conditions: *rac*-ibuprofen 1 mmol, 1-propanol 2 mmol, solvent 2 mL, LAO 1.5 mL, 20 °C, 250 rpm.

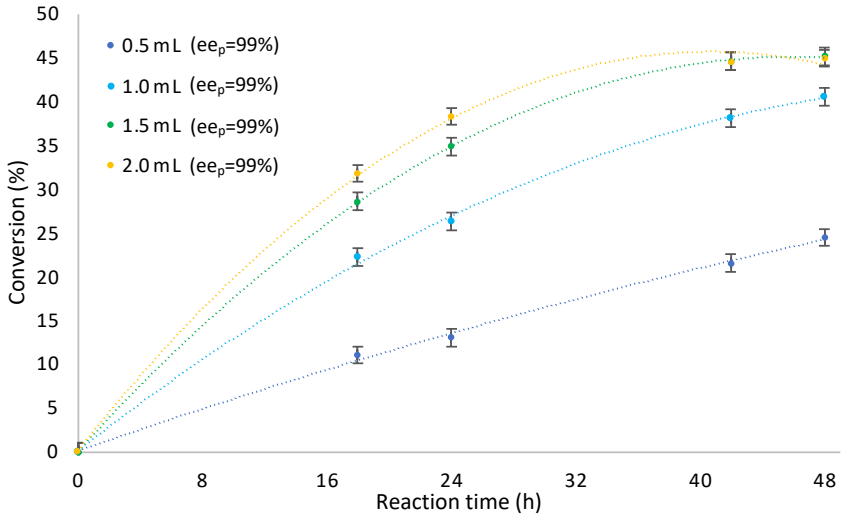

Figure S2. The influence of the amount of LAO on esterification of *rac*-ibuprofen.

Reaction conditions: *rac*-ibuprofen 1 mmol, 1-propanol 2 mmol, isooctane 2 mL, LAO, 20 °C 250 rpm; ee_p-enantioselectivity of product.

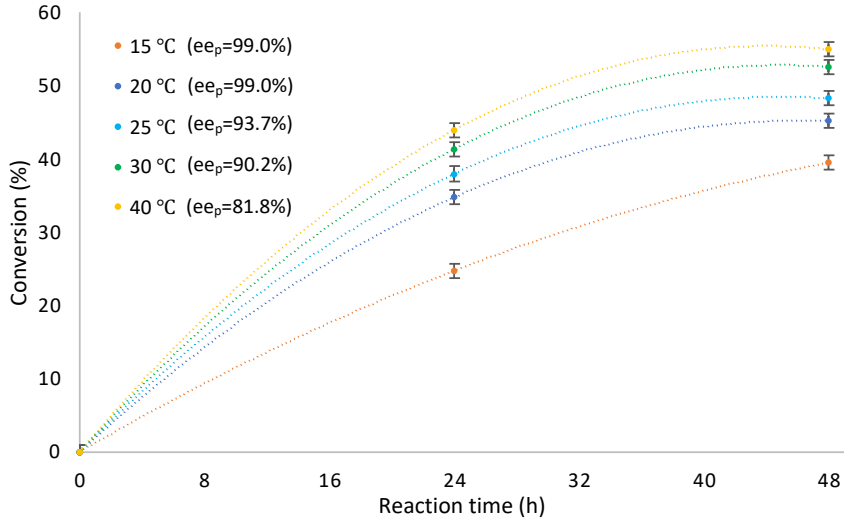

Figure S3. The influence of temperature on esterification of *rac*-ibuprofen.

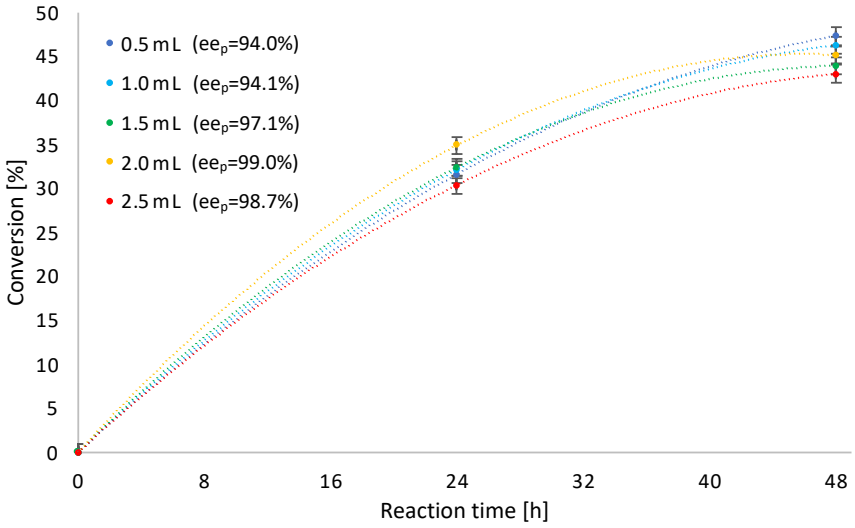

Figure S4. The influence of the amount of solvent on esterification of *rac*-ibuprofen.

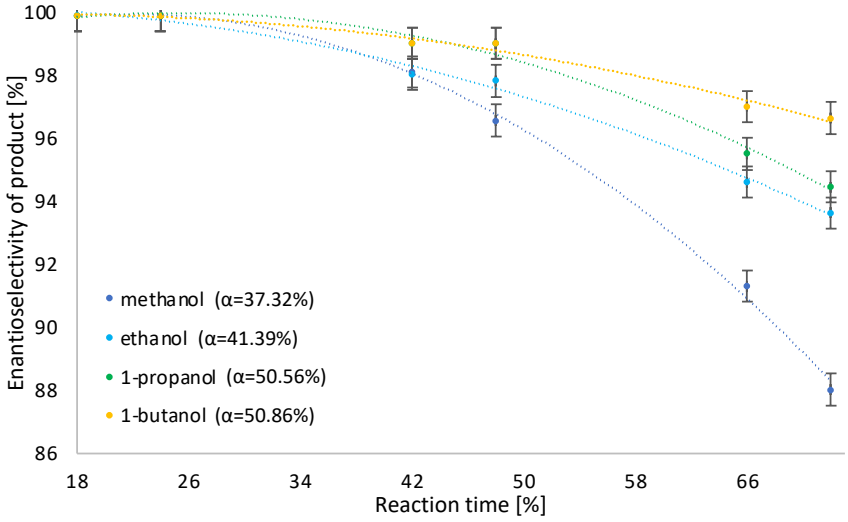

Figure S5. The influence of the alcohol on *ee* of (S)-(+)-ibuprofen ester.

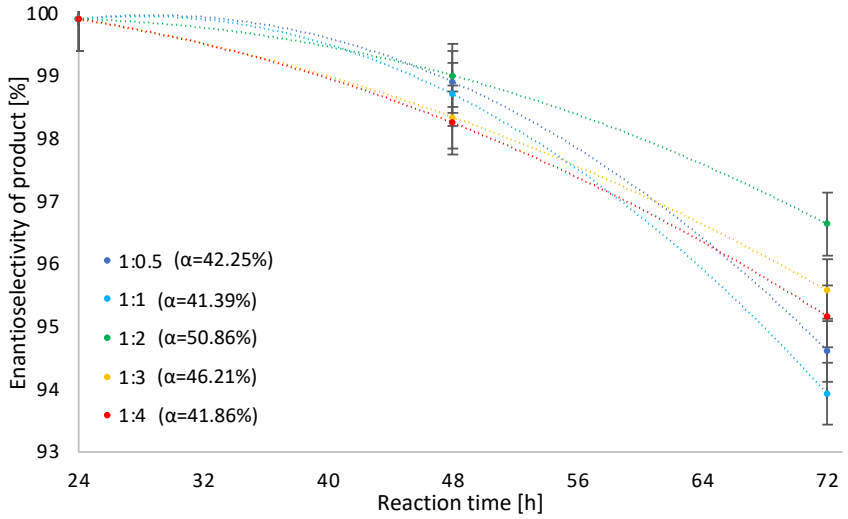

Figure S6. The influence of the ibuprofen: alcohol molar ratio on *ee* of (S)-(+)-ibuprofen ester.

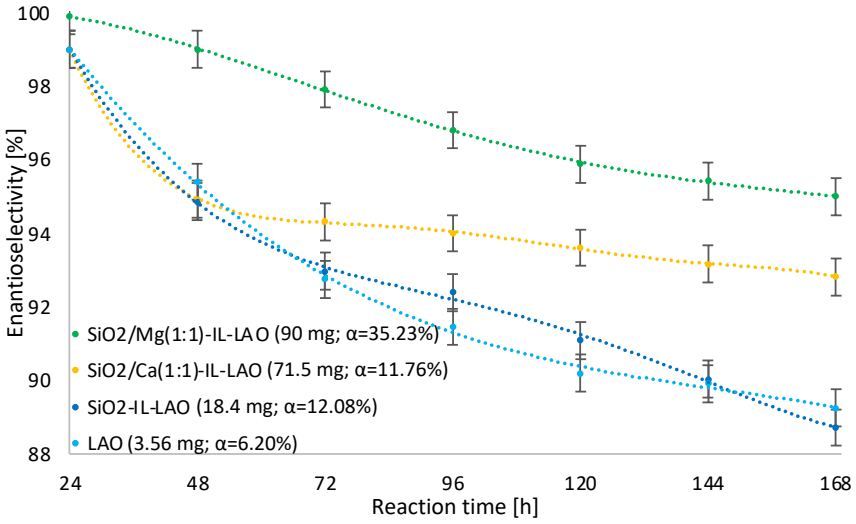

Figure S7. The influence of the SILP support on *ee* of (S)-(+)-ibuprofen ester.

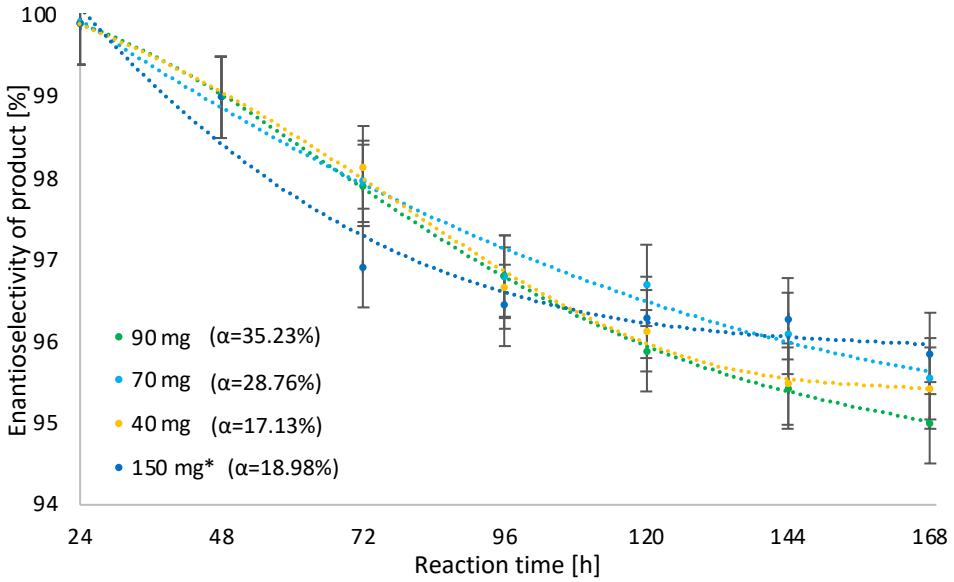

Figure S8. The influence of the amount of SiO_2/Mg(1:1)/[tespmim][NTf2]/LAO on *ee* of (S)-(+)-ibuprofen ester.

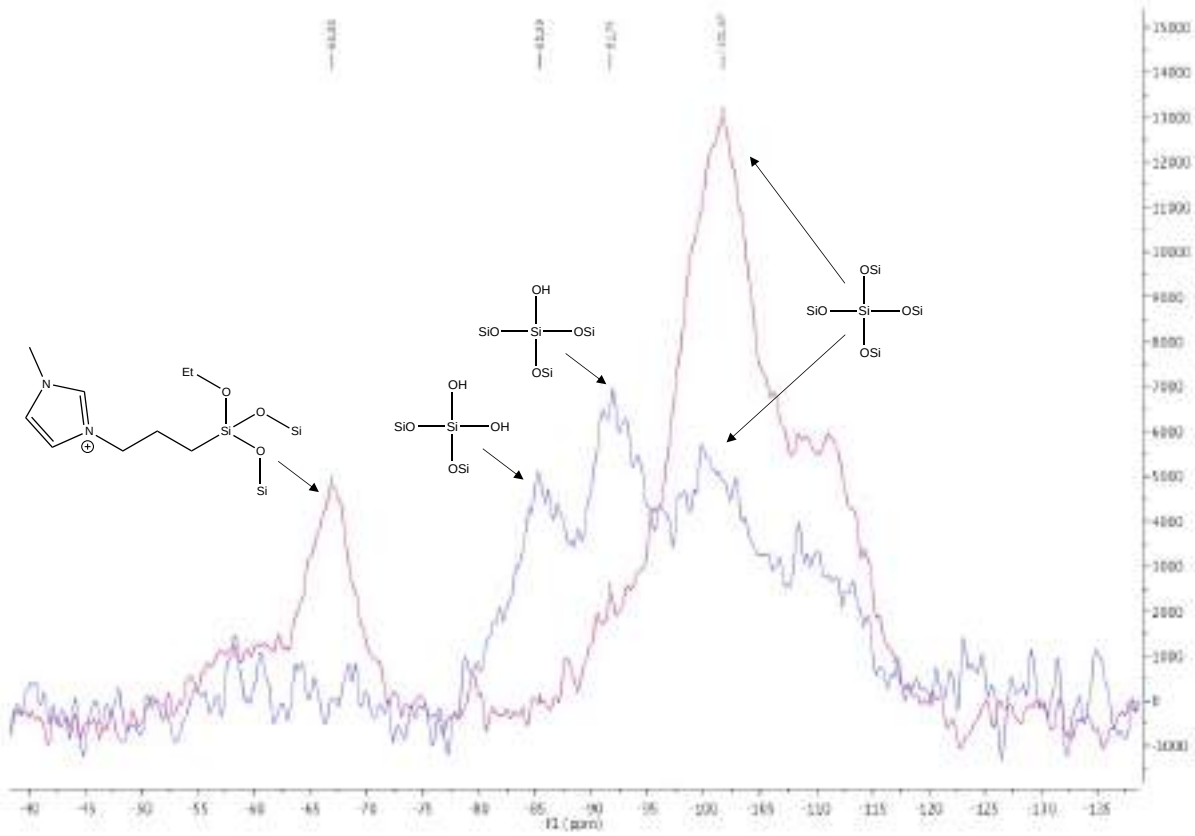

Figure S9. ^{29}Si MAS NMR spectra of SiO_2/Mg(1:1) (blue) and SiO_2/Mg(1:1)/[tesmpim] [NTf_2] (pink).

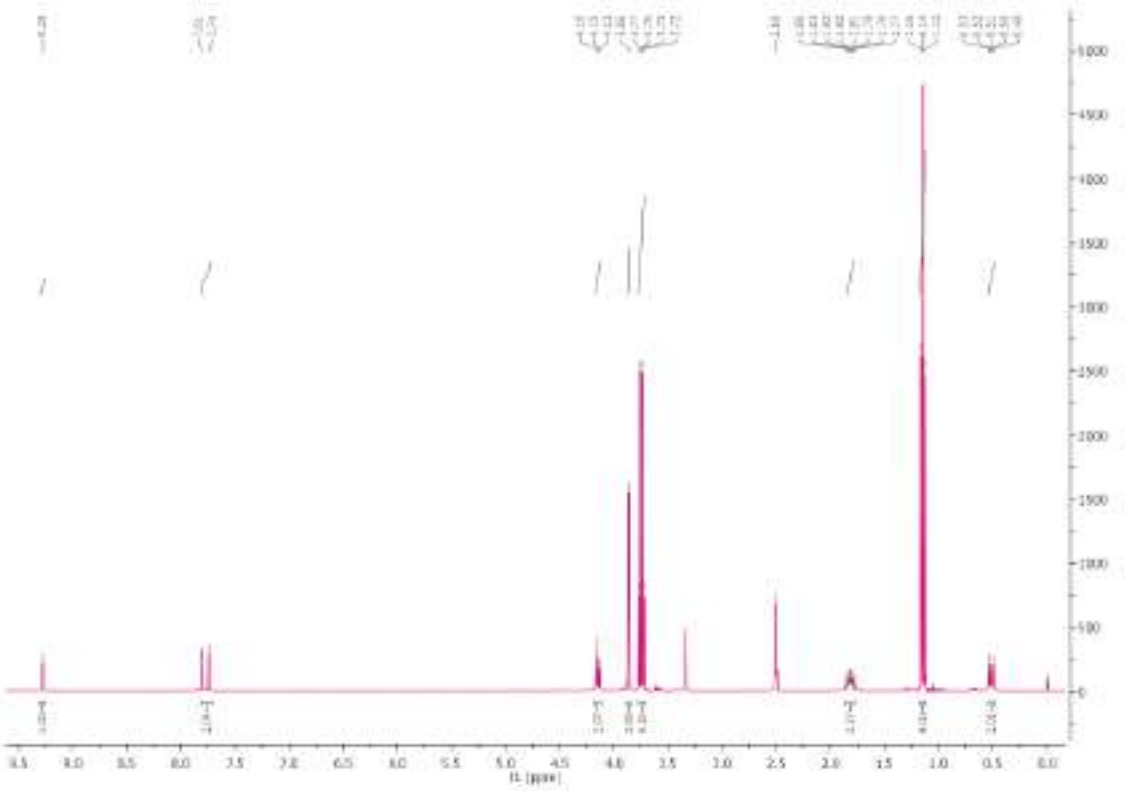

Figure S10. ^{1}H NMR spectra of [tesmpim]Cl.

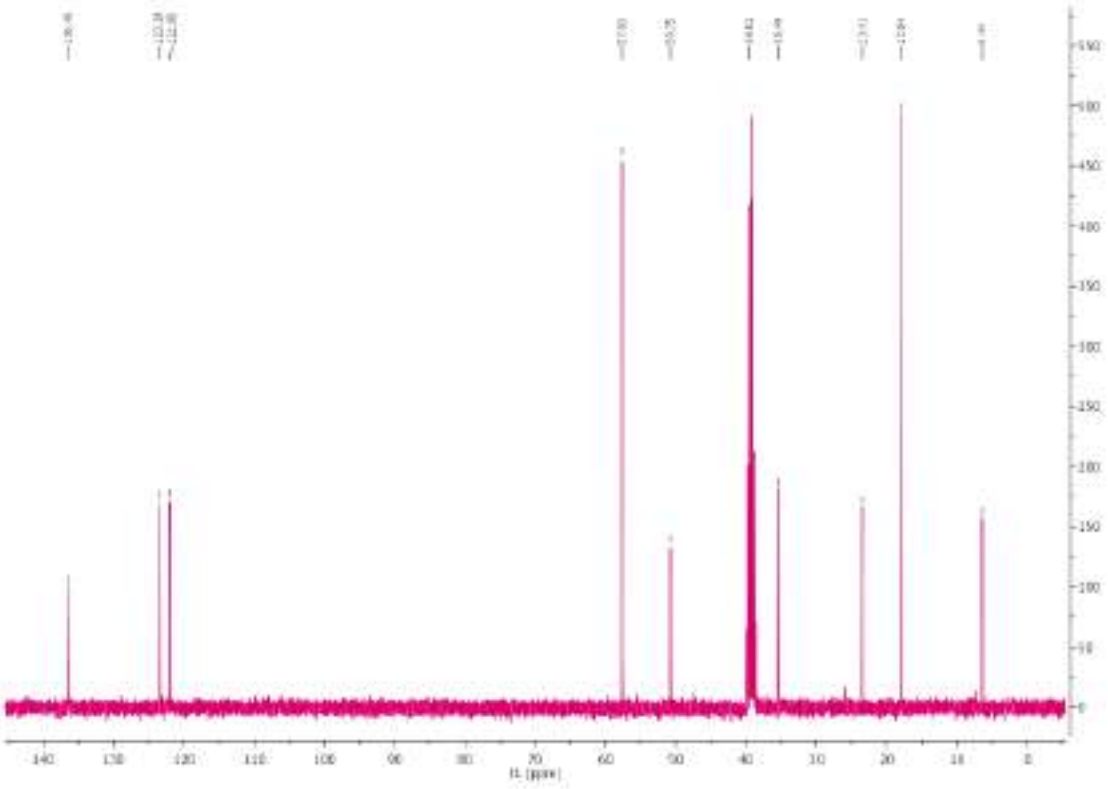

Figure S11. ^{13}C NMR spectra of [tesmpim]Cl.

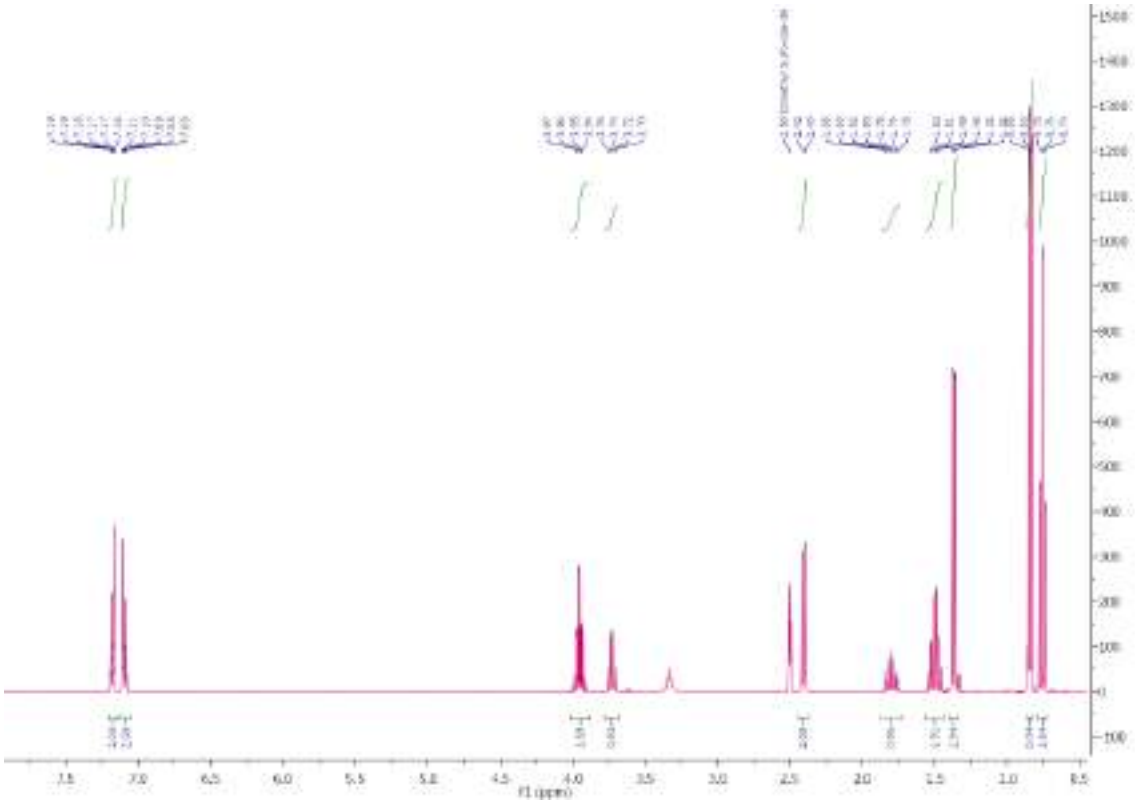

Figure S12. ^{1}H NMR spectra of (S)-(+)-ibuprofen propyl ester.

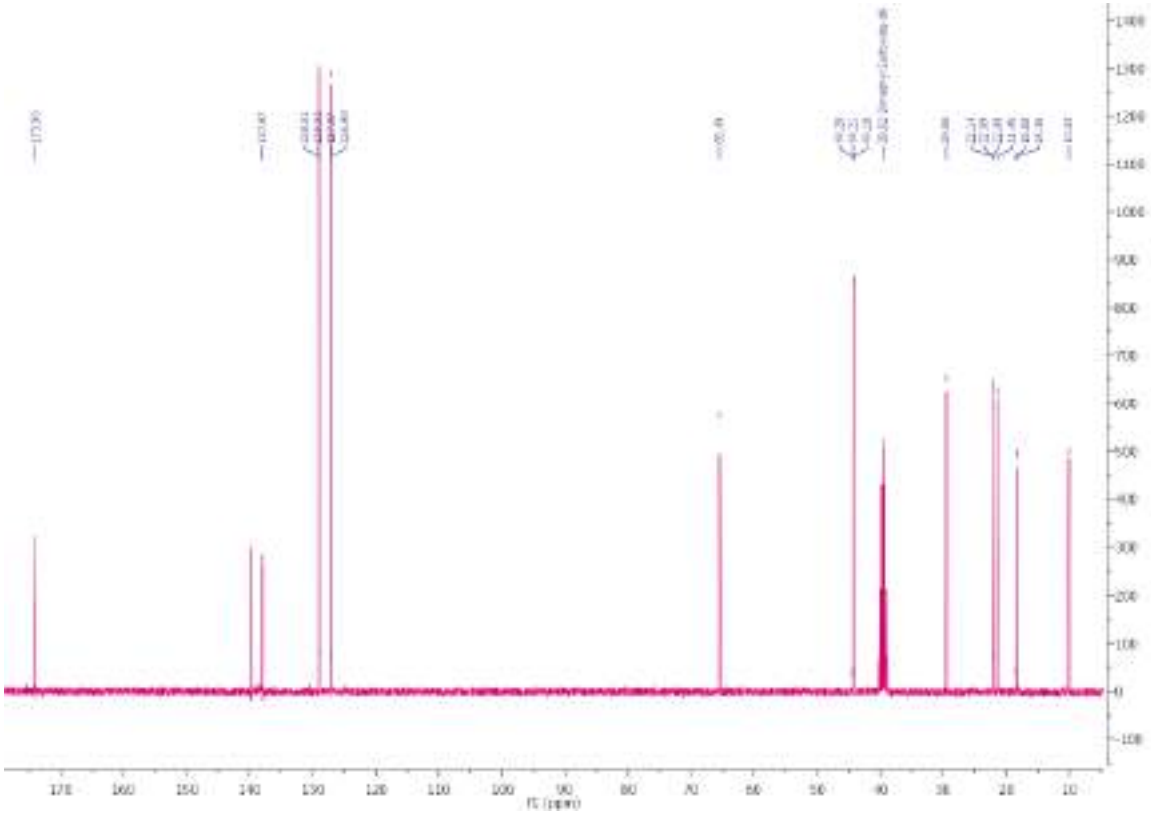

Figure S13. ^{13}C NMR spectra of (S)-(+)-ibuprofen propyl ester.

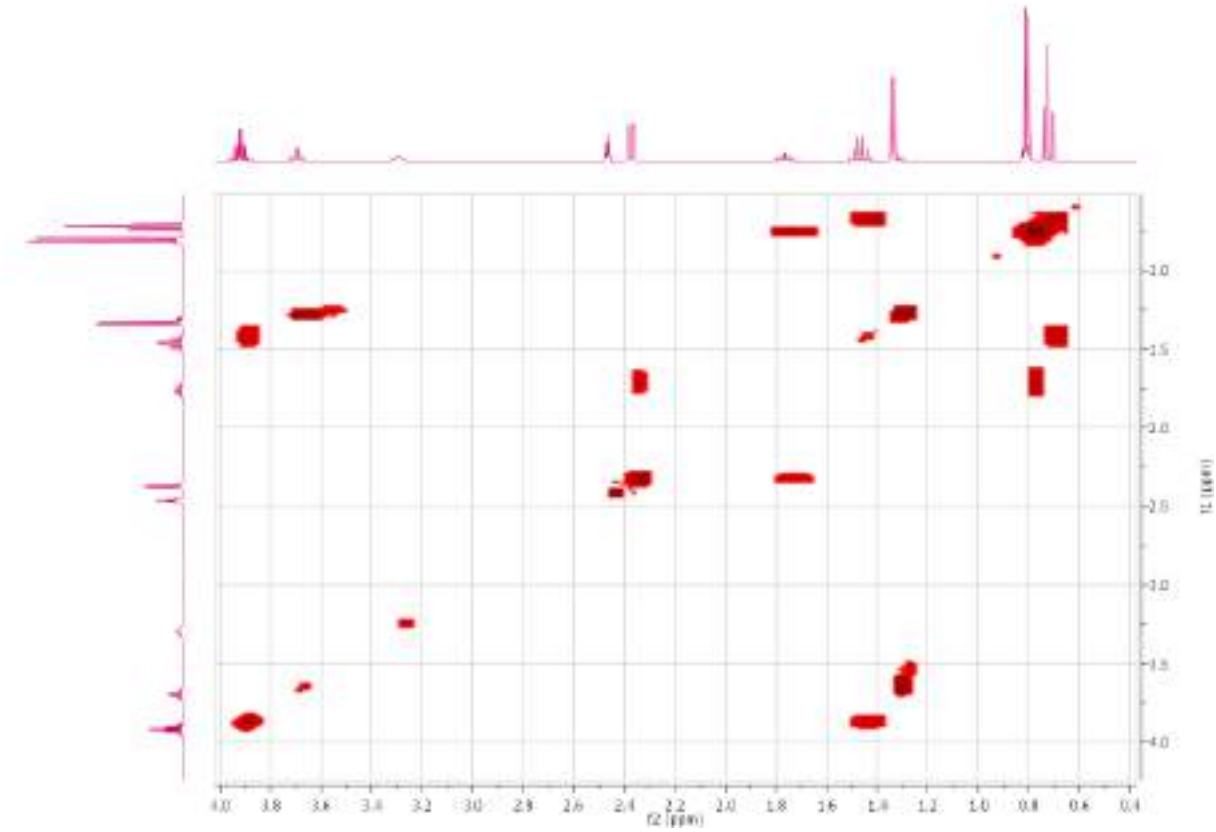

Figure S14. COSY NMR spectra of (S)-(+)-ibuprofen propyl ester.

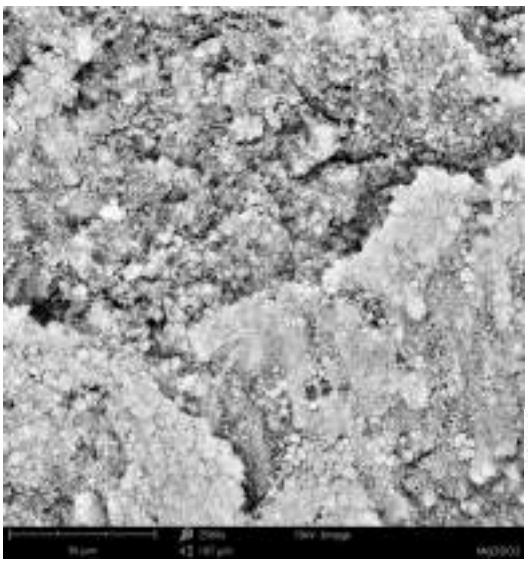

Element Number	Element Symbol	Element Name	Atomic Conc.	Weight Conc.
8	O	Oxygen	73.80	62.40
14	Si	Silicon	19.69	29.23
12	Mg	Magnesium	6.51	8.36

Figure S15. The SEM-EDS analysis of SiO_2/Mg(1:1) support.

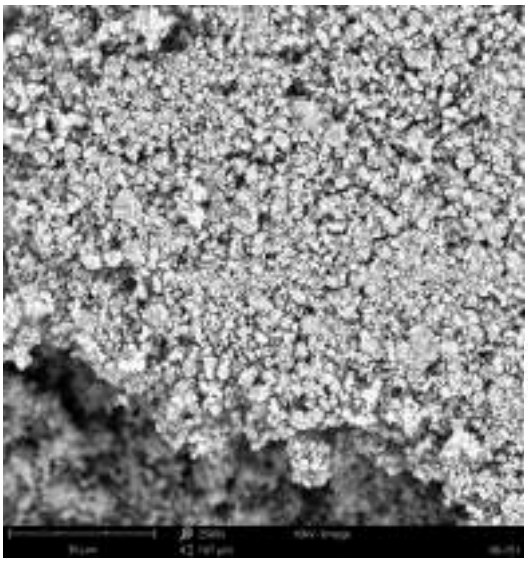

Element Number	Element Symbol	Element Name	Atomic Conc.	Weight Conc.
8	O	Oxygen	54.83	49.31
14	Si	Silicon	17.00	26.84
6	C	Carbon	15.77	10.65
7	N	Nitrogen	7.36	5.79
12	Mg	Magnesium	4.18	5.70
17	Cl	Chlorine	0.86	1.70

Figure S16. The SEM-EDS analysis of SiO_2/Mg(1:1)/[tesmpim]Cl support.

Element Number	Element Symbol	Element Name	Atomic Conc.	Weight Conc.
6	C	Carbon	50.93	42.05
8	O	Oxygen	42.32	46.54
14	Si	Silicon	3.65	7.05
12	Mg	Magnesium	1.38	2.31
9	F	Fluorine	1.13	1.47
7	N	Nitrogen	0.58	0.56
16	S	Sulfur	0.01	0.02

Figure S17. The SEM-EDS analysis of SiO_2/Mg(1:1)/[tesmpim][NTf_2] support.

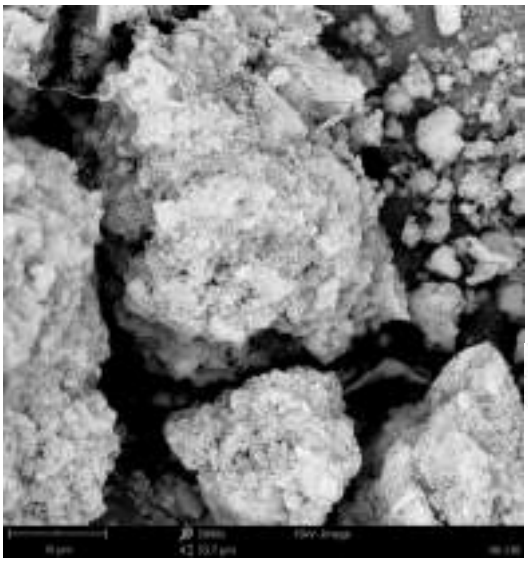

Element Number	Element Symbol	Element Name	Atomic Conc.	Weight Conc.
8	O	Oxygen	51.99	50.62
6	C	Carbon	23.28	17.02
14	Si	Silicon	8.74	14.93
7	N	Nitrogen	6.87	5.86
9	F	Fluorine	5.96	6.89
12	Mg	Magnesium	3.16	4.68

Figure S18. The SEM-EDS analysis of SiO_2/Mg(1:1)/[tesmpim][NTf_2]/LAO biocatalyst.

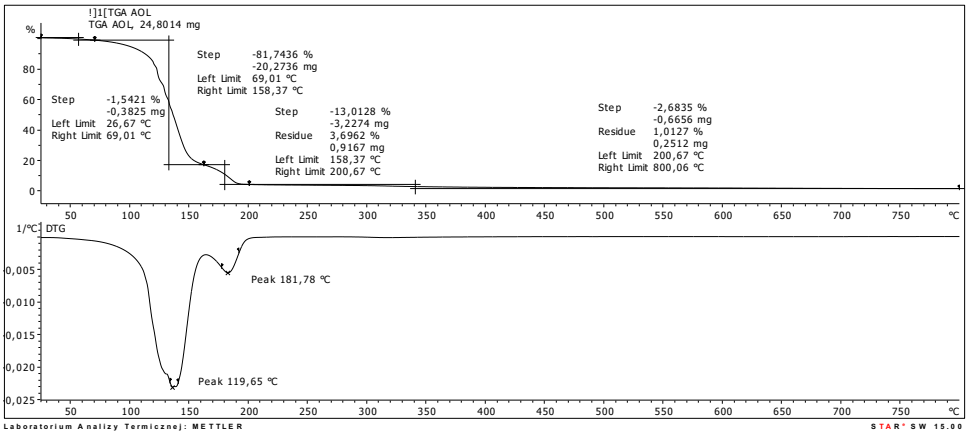

Figure S19. Thermogravimetric analysis of LAO.

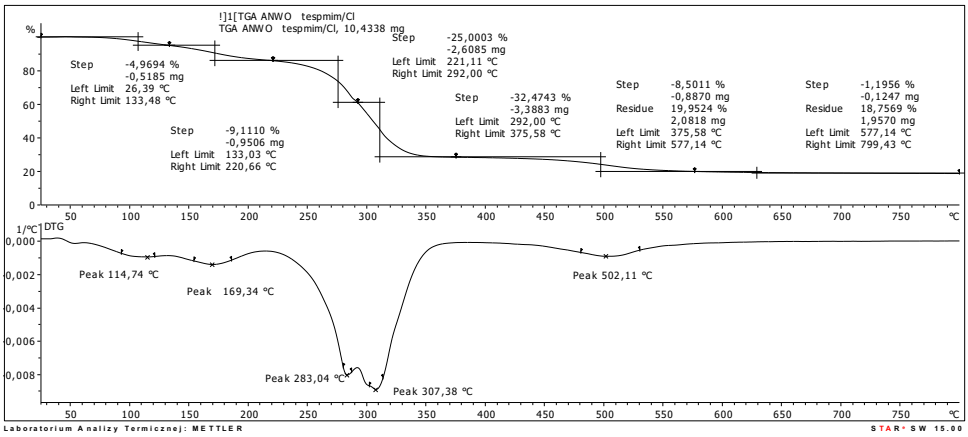

Figure S20. Thermogravimetric analysis of [tesmpim]Cl.

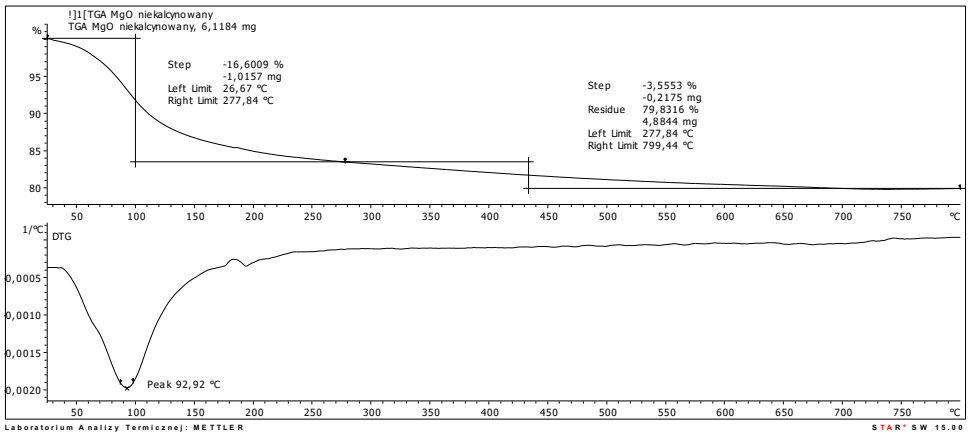

Figure S21. Thermogravimetric analysis of SiO_2/Mg(1:1) support.

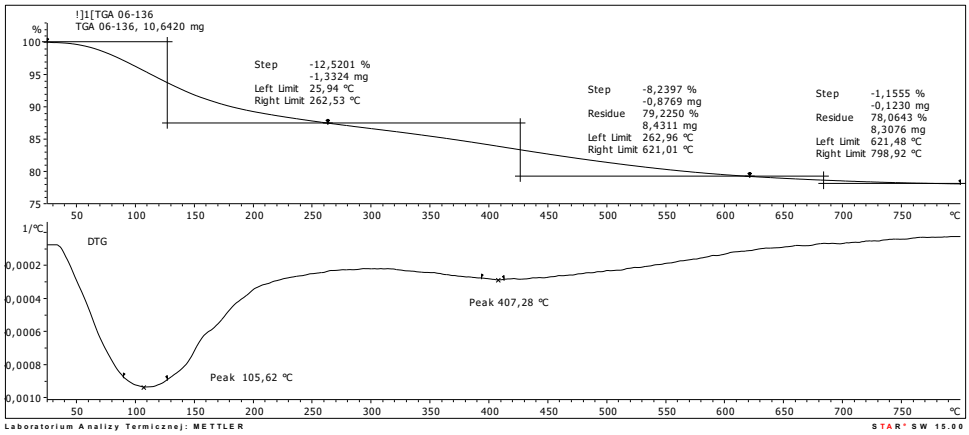

Figure S22. Thermogravimetric analysis of SiO_2/Mg(1:1)/[tesmpim]Cl support.

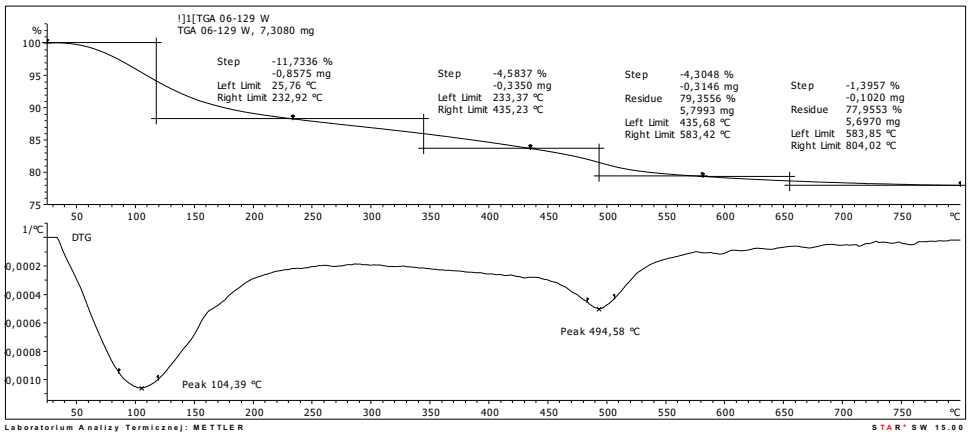

Figure S23. Thermogravimetric analysis of SiO_2/Mg(1:1)/[tesmpim][NTf_2] support.

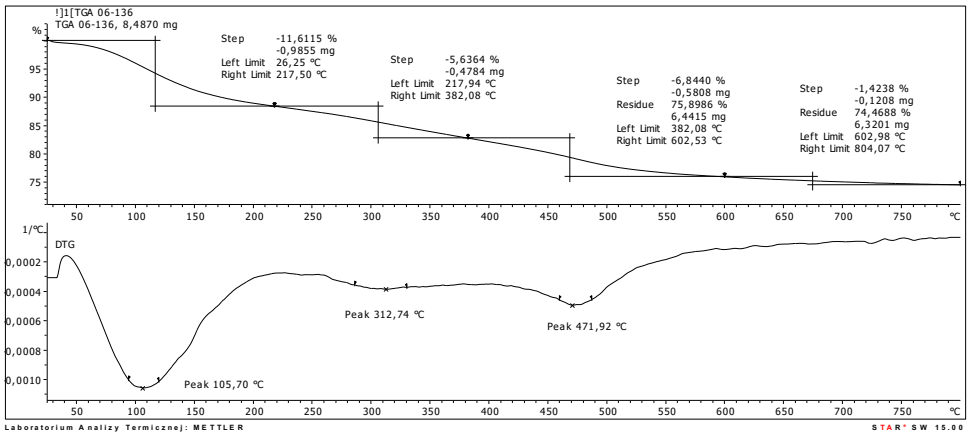

Figure S24. Thermogravimetric analysis of SiO_2/Mg(1:1)/[tesmpim][NTf_2]/LAO biocatalyst.

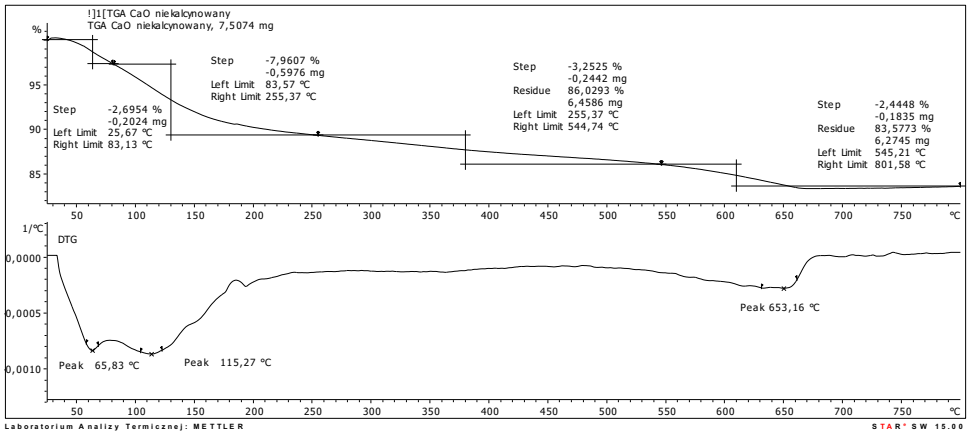

Figure S25. Thermogravimetric analysis of SiO_2/Ca(1:1) support.

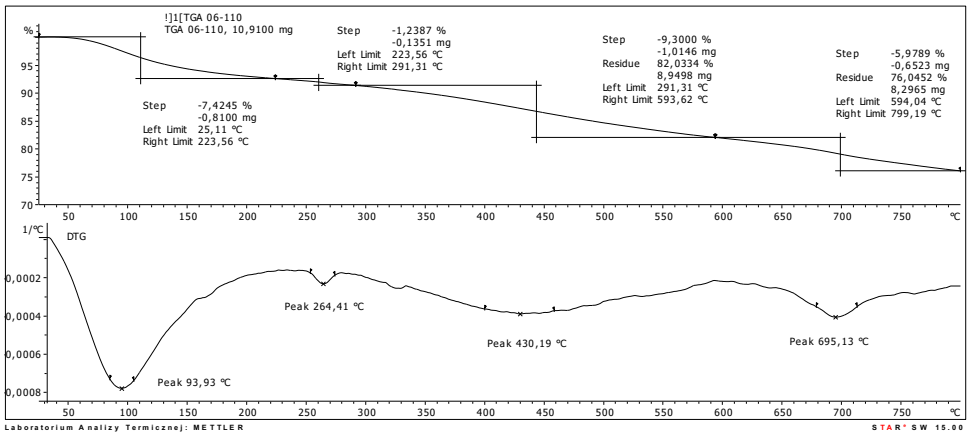

Figure S26. Thermogravimetric analysis of SiO_2/Ca(1:1)/[tesmpim]Cl support.

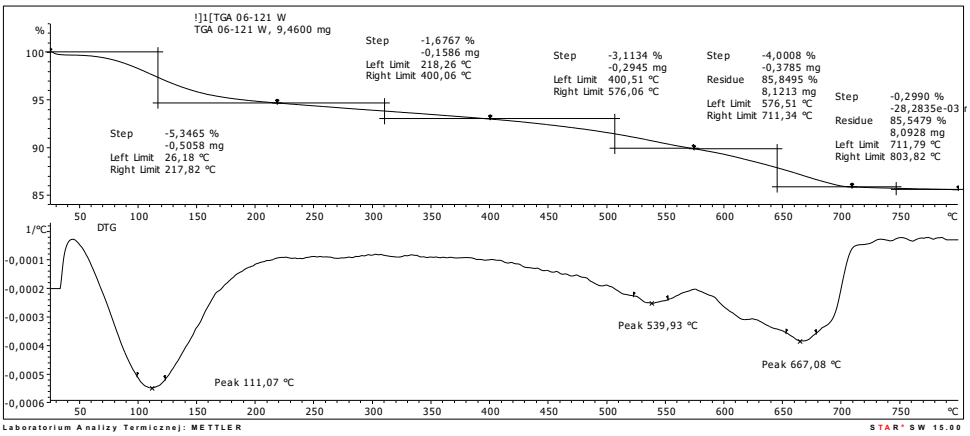

Figure S27. Thermogravimetric analysis of SiO_2/Ca(1:1)/[tesmpim][NTf_2] support.

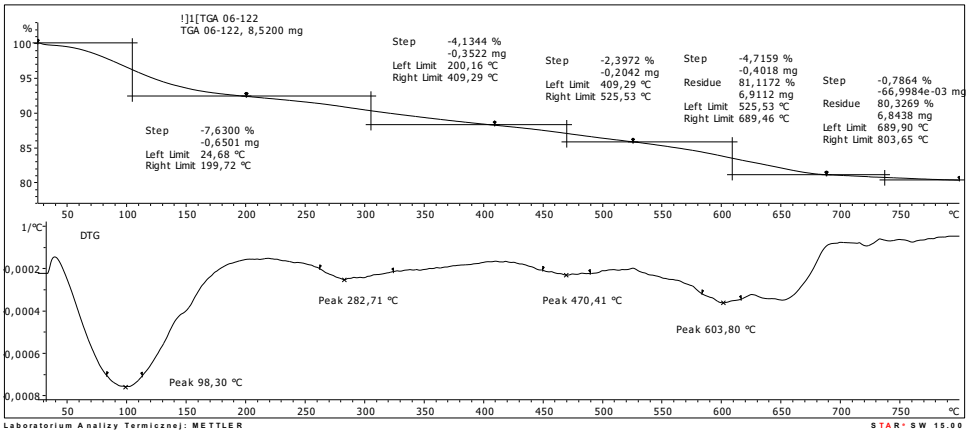

Figure S28. Thermogravimetric analysis of SiO_2/Ca(1:1)/[tesmpim][NTf_2]/LAO biocatalyst.

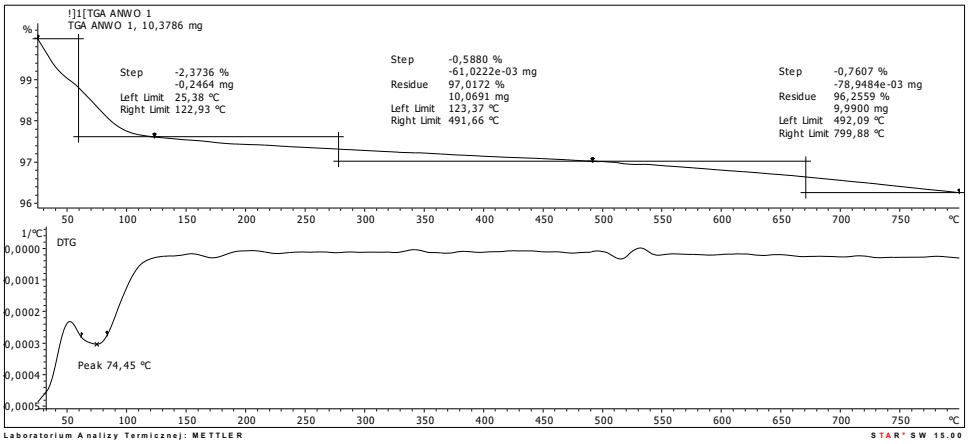

Figure S29. Thermogravimetric analysis of SiO_2^b support.

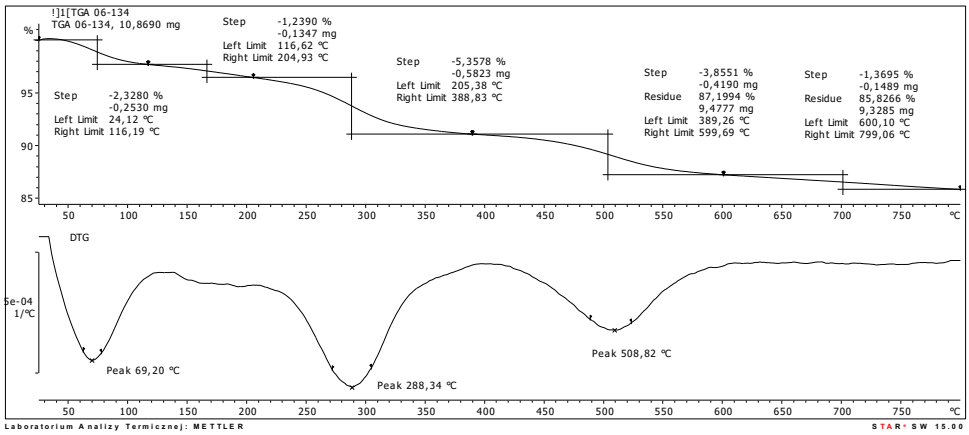

Figure S30. Thermogravimetric analysis of SiO_2[b]/[tespmim]Cl support.

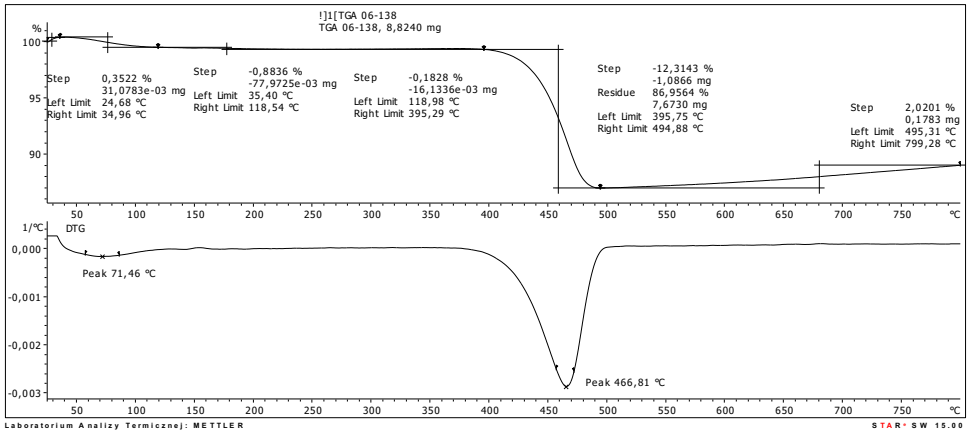

Figure S31. Thermogravimetric analysis of SiO_2[b]/[tespmim]/[NTf_2] support.

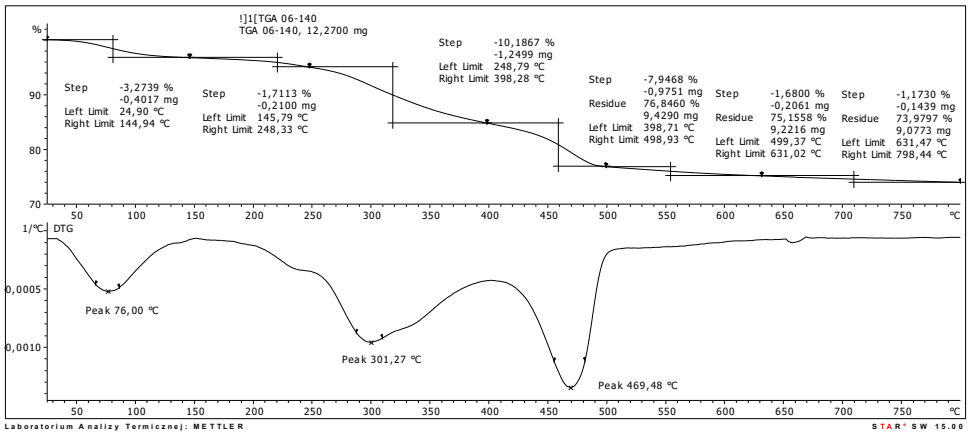

Figure S32. Thermogravimetric analysis of SiO_2[b]/[tespmim][NTf_2]/LAO biocatalyst.

[b] commercially available silica

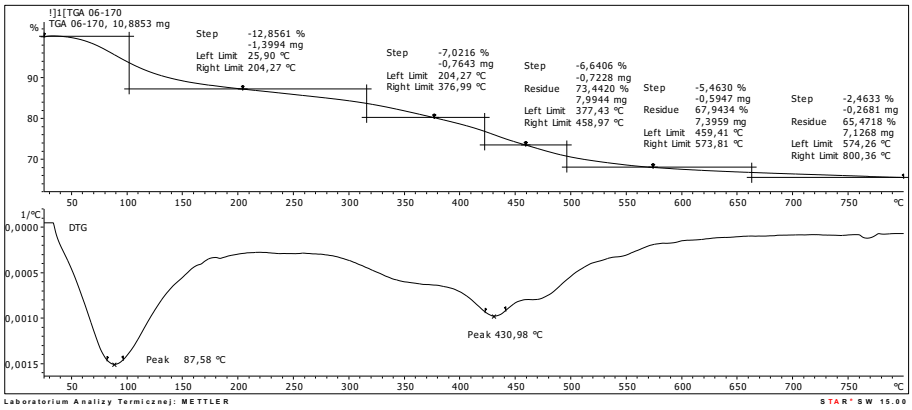

Figure S33. Thermogravimetric analysis of SiO_2/Mg(1:1)/[tesmpim][NTf_2]/LAO biocatalyst after recycling.

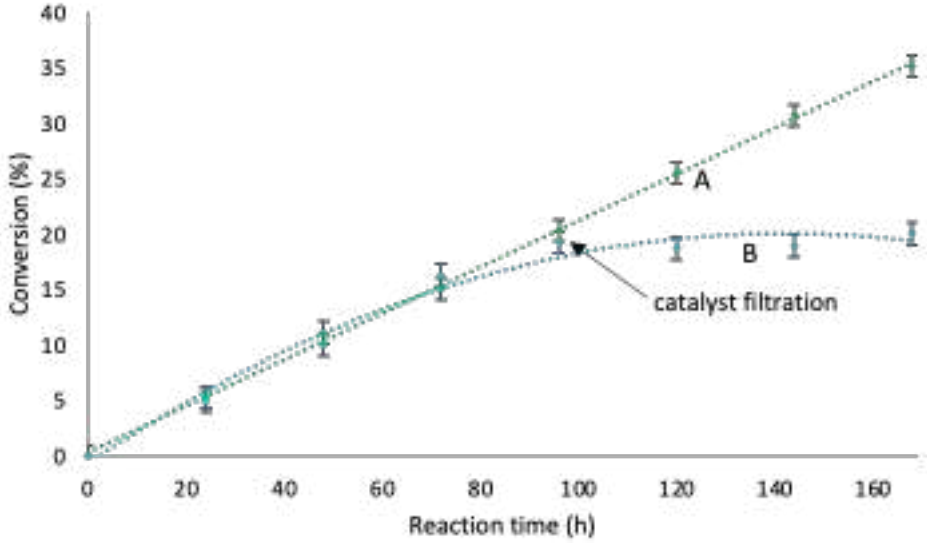

Figure S34. A) 90 mg SiO_2/Mg(1:1)/[tesmpim][NTf_2]/LAO biocatalyst, *rac*-ibuprofen 0.1 mmol, butanol 0.2 mmol, isooctane 0.4 mL; B) The experiment with fast biocatalyst filtration.

Green Chemistry

PAPER

View Article Online
View Journal

Cite this: DOI: 10.1039/d4gc03821e

Robust biocatalyst for the green continuous flow synthesis of esters from biomass-derived furfuryl alcohol and C8–C18 carboxylic acids†

Anna Wolny,[a] Dagmara Więcławik,[a] Jakub Zdarta,[b] Sebastian Jurczyk,[c] Teofil Jesionowski[b] and Anna Chrobok*[a]

A sustainable method suitable for industrial-scale continuous flow synthesis of esters from biomass-derived furfuryl alcohol (FA) and C_8–C_{18} carboxylic acids was developed. Under optimized reaction conditions, lipase from *Aspergillus oryzae* immobilized on an octyl-silane $MgO{\cdot}SiO_2$ material demonstrated high activity. A conversion of 88.7–90.2% for FA with 100% selectivity to esters using a FA : fatty acid molar ratio of 1 : 3 and cyclohexane as the solvent at 25 °C in 45 min was achieved in a batch system. The biocatalyst retained its high activity for at least 10 consecutive reaction cycles. Successful upgradation from a batch to continuous flow reactor led to an increased FA conversion of up to 96.8%, with a reagent flow rate of 0.070 mL min^{-1} and a residence time of 10.5 minutes. The biocatalyst maintained excellent performance for 30 h. The developed method, considered within the framework of green chemistry metrics, ensures a balance between the high activity, stability, recyclability, and biodegradability of the catalyst. This work proposes as a generic approach to green chemistry dedicated to support the biocatalytic continuous flow synthesis of value-added chemicals.

Received 2nd August 2024,
Accepted 19th August 2024

DOI: 10.1039/d4gc03821e

rsc.li/greenchem

Introduction

Abundant, inexpensive, and renewable lignocellulosic biomass is suitable for the production of value-added biobased chemicals, guiding chemical industry towards sustainable development and circular economy.[1] To achieve carbon neutrality, the demand for selective catalysts and technologies for biomass valorization will increase in addition to the requirements for clean production. Biocatalysis fits well into these goals.[2] Generally, enzymes serve as renewable catalysts with low toxicity that operate effectively under mild and safe conditions, demonstrating energy efficiency while considerably minimizing waste formation. Despite their excellent catalytic properties, enzymes typically require enhancement before being implemented on an industrial scale, where multiple cycles of high yield processes are desired. One of the properties typically improved through immobilization is enzyme stability. Other critical enzyme properties that should be enhanced for prolonged use in industrial reactors include activity, resistance to inhibition by reaction products, and ease of regeneration. However, the methods for increasing the recyclability or stability of enzymes for continuous flow synthesis remain challenging.[3,4]

Hemicellulose, a component of lignocellulose, undergoes hydrolysis to produce D-xylose, which is subsequently dehydrated to furfural.[5] Furfural is next converted into furfuryl alcohol, a multifunctional chemical compound based on furan.[6] The majority of furfuryl alcohol is used in the production of furan resins, tetrahydrofurfuryl alcohol and esters and carboxylic acids.[7] Esters of long-chain acids and furfuryl alcohol are used mostly as biolubricants, especially esters of oleic acid. A broad range of furfuryl alcohol fatty acid esters are used as surfactants, solvents, plasticizers, biofuel additives, emulsifiers, food additives, and flavors.[8–11] Achieving high selectivity in the esterification of furfuryl alcohol presents a significant issue.[12,13] Furfuryl alcohol readily undergoes polymerization in the presence of minerals or strong organic acids, resulting in the formation of thermostable polymers or difurfuryl ethers.[14–17]

Biocatalysis employing enzymes, such as lipases, for the production of furfuryl alcohol esters may bring significant benefits compared to the use of traditional acids. Using alternative biocatalytic approaches employing commercially available Novozym 435 for the esterification of furfuryl alcohol

[a]Department of Chemical Organic Technology and Petrochemistry, Faculty of Chemistry, Silesian University of Technology, Krzywoustego 4, PL-44100 Gliwice, Poland. E-mail: anna.chrobok@polsl.pl
[b]Institute of Chemical Technology and Engineering, Faculty of Chemical Technology, Poznan University of Technology, Berdychowo 4, PL-60965 Poznan, Poland
[c]Institute for Engineering of Polymer Materials and Dyes, Lukasiewicz Research Network, Sklodowskiej-Curie 55, PL-87100 Torun, Poland

†Electronic supplementary information (ESI) available: FTIR, TGA/DTG, SEM-EDS, NMR, graphs, appendix 2 (green metrics analysis). See DOI: https://doi.org/10.1039/d4gc03821e

with oleic acid, octanoic acid, or castor oil at temperatures ranging from 55 to 60 °C resulted in nearly complete conversion of oleic acid (99%)[18] and castor oil (89%),[9] whereas only 77% of octanoic acid underwent esterification after 24 h.[19] Novozym 435 is an active lipase derived from *Candida antarctica* lipase B (CALB) immobilized on macroporous acrylic resin. However, the reuse of Novozym 435 is difficult due to the tendency of the resin to swallow in organic solvents, hindering isolation and recycling efforts, leading to the conclusion that further study is required to meet the challenges of flow processes.[20,21]

Immobilization is the primary technique for enhancing the activity and stability of lipases. Various types of supports with differing mechanical, thermal, and structural properties, such as porosity, surface activity, and hydrophobicity/hydrophilicity, have frequently been used as carriers for lipases. Inorganic materials, carbon materials, polymers (or biopolymers) and composite materials served as matrixes for adsorption or covalent bonding of lipases, as previously reviewed.[22–24] Lipases demonstrated their highest catalytic activity on hydrophobic surfaces, attributed to the protein immobilization in its monomeric, open form, a phenomenon known as interfacial activation.[25–28] In the case of hydrophilic supports, such as silica, modification of the surface with hydrophobic groups is necessary to achieve the highest lipase efficiency. Modification of silica surface with alkyl groups (*e.g.* methyl, octyl, hexadecyl) and used as a support for CALB was tested in Bayer–Villiger oxidation of cyclic ketones to lactones with hydrogen peroxide. High activity of the biocatalyst was reached despite harsh reaction conditions.[29] In other studies, a hydrophobic ionic liquid (triethoxysilylpropyl)imidazolium bis (trifluoromethylsulfonyl) imide was attached to the silica-magnesium oxide support to enhance the activity of lipase from *Aspergillus oryzae* (LAO) and enable its immobilization on the surface. The biocatalyst demonstrated high activity, enantioselectivity and stability in the kinetic resolution of ibuprofen racemate *via* enantiomeric esterification to (*S*)-ibuprofen ester (35.2% conversion, 95% enantioselectivity).[30]

The main aim of this work was to design a sustainable method for the esterification of biomass-derived furfuryl alcohol with C8–C18 carboxylic acids. To face the existing problems in this contribution, we combine our expertise in the design and study of activity of biocatalysts with the potential offered by the possibility of tailoring the surface chemistry of the supports to report the catalytic applications of enzymatic continuous flow synthesis. The novel aspect of this study is represented mainly by the efficient approach to produce heterogeneous catalysts characterized by the stability (thermal, chemical, and mechanical) supported by the ease of enzyme isolation and recycling for flow synthesis that is omitted in the available literature. The goal has been achieved *via* the implementation of an innovative, novel heterogeneous biocatalyst, which enabled the application of a flow reactor. Therefore, both high activity and, not least, the stability of the biocatalyst are of high importance. Inspired by the activation of two lipases from *Candida rugosa* and *Aspergillus oryzae* in the presence of metal cations the tailoring of the silica matrix *via* the incorporation of Mg^{2+} was performed. Subsequent introduction of hydrophobic alkyl organosilanes on the surface of silica was used as a strategy to enhance enzyme loading and help to avoid leaching. The sustainability of the presented method was measured using green metrics.

Results and discussion

Biocatalyst preparation

In our quest for a robust biocatalyst dedicated for the esterification of furfuryl alcohol and synthesis of biomass derived biofuel additives, we propose the tailoring of the support surface for lipase immobilization. The expected improvement of the stability of enzyme can facilitate continuous use. This approach is supported by structural studies, which can underpin the rational design and development of biocatalysts and in turn lead to a more sustainable and cost-effective process. Enhanced enzyme performance is reflected in higher biocatalyst productivity, which determines the enzyme cost in the particular process.

The selection of the *Aspergillus oryzae* lipase (LAO) was driven by its superior catalytic efficiency in esterification reactions. The advantage of immobilized lipases is that they operate in nonaqueous media, but they require a certain amount of water. A layer of water, or a water shell, bound to the protein by hydrogen bonds, is crucial for maintaining the three-dimensional structure and activity.[25–28] Additionally, LAO is relatively stable in organic solvents and under high substrate concentrations. Notably, LAO was acknowledged as a GRAS (generally regarded as safe) enzyme by the FDA.[31] Straightforward adsorption of LAO on the tailor-made solid surface was chosen to simplify the protocol for enzyme immobilization. The hybrid material of MgO with silica ($MgO{\cdot}SiO_2$) was selected as the carrier for LAO. MgO provides changes in textural and structural properties of the material by introducing besides silanol (≡Si–OH) magnesil (–Mg–OH) groups.[29,31,32] Additionally, the improvement of the activity of lipase from *Candida rugosa* in solution in the presence of chloride Li^+, Na^+, K^+, Mg^{2+} and Zn^{2+} salts was detected.[32] Next, to enhance the enzyme-surface affinity the hydrophobicity of the carrier was increased. The hydrophobicity of the silica surface can be introduced by simple modification *via* physical or chemical bonding of *e.g.* alkyl organosilanes,[29] hydrophobic ionic liquids[28,30] or performing reaction in hydrophobic solvents, such as ionic liquids.[34,35] In this work chemical modification with triethoxy(octyl)silane or triethoxy(hexadecyl)silane was performed (Scheme 1).

In the first step of the synthesis of the biocatalyst, a siliceous support $MgO{\cdot}SiO_2$ (1 : 1, n : n) was synthesized through the sol–gel method according to the method described in the literature.[36] The synthesized oxide material was chemically modified with the alkyl organosilanes, like triethoxy(octyl) silane (C_8) or triethoxy(hexadecyl)silane (C_{16}), by stirring the reagents in the isopropanol/water mixture at 85 °C for 24 h.

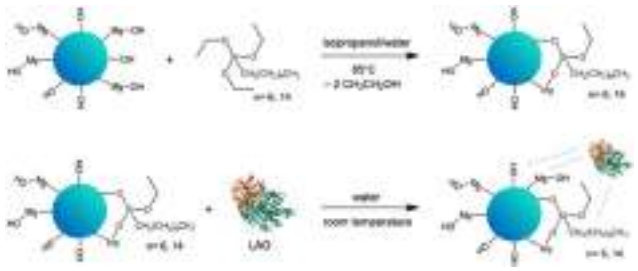

Scheme 1 Preparation of MgO·SiO_2-C_8-LAO; blue dashed lines indicate adsorption interactions.

The pristine SiO_2 (used as delivered) and MgO·SiO_2 materials were applied as references, whereas the calcination process performed at 800 °C was applied to examine how changes in porous structure will affect the properties of the materials towards modification and LAO immobilization.

The chemical grafting of alkyl groups to the siliceous materials (MgO·SiO_2-C_8, MgO·SiO_2-C_{16}, MgO·SiO_2-$C_{8(calc.)}$, and SiO_2-C_8) was proven by FT-IR (ESI, Fig. S1†). From the presented graphs, due to the presence of characteristic bands of methyl and methylene groups from modifier molecules in the range of 2850 to 3000 cm^{-1}, it is clear that the functionalizing agent was deposited efficiently.

The presence and also loading of alkyl groups on MgO·SiO_2 was determined by TG/DTG analyses (ESI, Fig. S2–S9†) and is presented in Table 1. Obtained analyses revealed that the longer alkyl chain is the lower amount of alkyl groups was grafted to the material, respectively 8.03 wt% of C_8 and 5.86 wt% of C_{16}. Furthermore, the calcination of the MgO·SiO_2 support led to a reduction in the chemical immobilization of C_8 groups (1.21 wt%), which is likely related to the decreased number of available surface hydroxyl groups capable of binding the modifier. The same effect was observed for the modification of pristine SiO_2 which resulted in the introduction of only 5.87 wt% of C_8 groups. It is speculated that the presence of magnesium oxide provided additional hydroxyl groups on the surface of the hybrid material, enabling more efficient grafting of the octyl groups.

Additionally, SEM images before and after modification with alkyl groups showed the affinity of support material particles towards agglomeration and formation of irregular structures that is characteristic of silica-based materials after modification (ESI, Fig. S10–S16†). Moreover, the elemental composition of the surface of SiO_2, MgO·SiO_2, and MgO·$SiO_{2(calc.)}$ materials and their modified forms with alkyl groups was studied with an EDS detector (ESI, Fig. S10–S16†). EDS analyses proved the presence of carbon atoms uniformly distributed on the surface coming from grafted alkyl groups on the surface of modified materials, hence confirming effective incorporation of hydrophobic groups onto the surface of the oxide system.

Finally, in order to prepare the biocatalyst, the aqueous solution of LAO was mixed with siliceous materials MgO·SiO_2-C_8, MgO·SiO_2-C_{16}, MgO·SiO_2-$C_{8(calc.)}$, SiO_2-C_8 and MgO·SiO_2 at room temperature for 3 h to perform physical immobilization of lipase on the surface. According to the TG/DTG analyses (ESI, Fig. S17 and S18†) it was observed that longer alkyl chains led to the decrease of the amount of immobilized lipase from 4.24 wt% for MgO·SiO_2-C_8-LAO to 1.54 wt% for MgO·SiO_2-C_{16}-LAO, probably due to the appeared higher steric hindrance in the case of longer alkyl chains. The lower amount of surface functional groups introduced during the modification step (1.21 wt%) resulted in a reduced adsorption of LAO (2.16 wt%) on the calcined material (ESI, Fig. S19†). In comparison with SiO_2-C_8 (9.25 wt% of LAO, ESI, Fig. S20†), MgO·SiO_2-C_8 showed a lower sorption capacity due to the higher amount of grafted octyl groups on the MgO·SiO_2 surface, which caused steric hindrances in the adsorption of LAO moieties. Lack of LAO on the surface of non-modified MgO·SiO_2 according to the TG/DTG thermograms proved that the presence of alkyl groups is crucial (ESI, Fig. S21†). The affinity of the pristine surface of MgO·SiO_2 to LAO is too low to enable efficient adsorption.

Modifying the silica surface with MgO increased both the affinity of the enzyme for the matrix and adsorption capacity of the support material. The increased surface porosity, attributed to additional –Mg–OH groups, has also been observed in previous studies.[30,32,33] Similarly, modifying silica with alkyl organosilanes had a beneficial impact. Lipases demonstrate higher catalytic performance in hydrophobic environments due to their reduced affinity for essential water molecules. This characteristic is crucial for the interfacial activation.[25–27]

After the immobilization of lipase, SEM images revealed even higher agglomeration of the particles of the matrix, which is growing shifting from pristine SiO_2 and MgO·SiO_2 *via* alkyl modified materials to final biocatalysts (ESI, Fig. S22–S26†). The highest particle agglomeration is observed for the SiO_2-C_8-LAO biocatalyst, where the highest amount of lipase was immobilized (9.25 wt%), clearly showing that immobilization increased the support particles to form aggregates. EDS analyses confirmed the presence of nitrogen atoms coming from the protein structure for all biocatalysts.

It can be expected that the highest loading of lipase may not necessarily result in elevated catalytic activity. This could be attributed to the generally reduced accessibility of the substrate and/or variations in enzyme conformations, including inactive ones, for this particular substrate. Additionally, the presence of crowded lipase agglomerations could contribute to

Table 1 Alkyl groups and LAO loadings in biocatalysts

Material	Alkyl groups loading[a] (wt% ± 0.3)	LAO loading[a] (wt% ± 0.3)
MgO·SiO_2-C_8-LAO	8.03	4.24
MgO·SiO_2-$C_{8(calc.)}$-LAO	1.21	2.16
MgO·SiO_2-C_{16}-LAO	5.86	1.54
SiO_2-C_8-LAO	5.87	9.25
MgO·SiO_2-LAO	—	Not detected

[a] Determined using TG/DTG; the standard deviation of 3 replicate experiments.

the decline in activity. Hence, conducting further catalytic tests is essential to determine the optimal lipase loading on the surface of the catalyst.[37]

In the catalytic studies presented below, the most active catalyst was found to be MgO·SiO_2-C_8-LAO (4.24 wt% of LAO), which was subsequently subjected to adsorption–desorption analysis using the BET method and BJH model for characterization (Table 2). Adsorption–desorption isotherms (ESI, Fig. S27†), the pore size distribution diagram (ESI, Fig. S28†) and S_{BET} micropores examined the high microporosity of the supports and biocatalyst. The characteristics of the MgO·SiO_2 material (S_{BET} 421 m^2 g^{-1}, V_p 0.06 cm^3 g^{-1}, d_p 2.1 nm), after chemical modification with alkyl groups C_8 (S_{BET} 325 m^2 g^{-1}, V_p 0.05 cm^3 g^{-1}, d_p 2.1 nm), and biocatalyst MgO·SiO_2-C_8-LAO (S_{BET} 236 m^2 g^{-1}, V_p 0.02 cm^3 g^{-1}, d_p 2.1 nm) were determined. This data clearly shows that the introduction of alkyl groups, as well as lipase adsorption, caused a reduction in the specific surface area and partial blocking of micropores, which results from the successively decreasing specific surface area of the micropores. The decrease in surface area and pore volume is typical for materials upon enzyme immobilization; however, the unchanged pore diameters indicate that the enzyme is primarily deposited on the surface of the support or deep within the pores of the material, leading to a reduction in pore volume after immobilization.

Catalytic activity of MgO·SiO_2-C_8-LAO in esterification of furfuryl alcohol and C8–C18 carboxylic acids in a batch system

The catalytic activity of MgO·SiO_2-C_8-LAO was studied in an industrially relevant process of esterification of furfuryl alcohol with fatty acids (C_8–C_{18}). In the preliminary studies, the activity of the developed biocatalysts was tested in a model esterification of furfuryl alcohol and caprylic acid (Scheme 2) in a batch system. The reaction was carried out at room temperature with hexane as a solvent and with triple molar excess of caprylic acid to furfuryl alcohol. Samples were collected during the reaction, and the conversion of furfuryl alcohol and selectivity to ester were determined using gas chromatography (GC). In every case, 100% selectivity was observed, making the conversion equal to the yield. The mass of the biocatalyst used for the comparative reactions presented in Table 3 was recalculated in order to contain fixed, the same amount of enzyme in the system (6.36 mg of LAO), *e.g.* in 150 mg of MgO·SiO_2-C_8-LAO and other heterogenous biocatalysts.

As shown in Table 3 and Fig. S30 and S31 (ESI†), the heterogenization of native LAO resulted in significantly higher catalytic performance of lipase compared to the native form

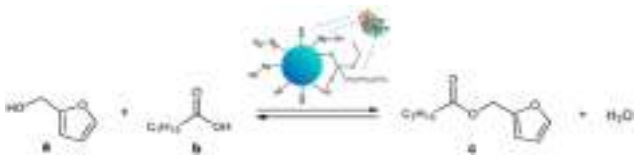

Scheme 2 Esterification of furfuryl alcohol and caprylic acid in the presence of the developed catalysts.

(87.1–90.2% conversion *versus* 83.5%), reaching 277% activity recovery and 90.2% conversion of furfuryl alcohol in 45 min for the reaction with MgO·SiO_2-C_8-LAO. Definitely it is a fundamental achievement for the isolation and recycling of enzyme. The commercially available native form of CALB used in the same amount as LAO is slightly less active (74.7%).

The unique interfacial activation of LAO on the hydrophobic support MgO·SiO_2-C_8 resulted in an improved activity of the immobilized lipase. Lipases exhibit two distinct conformations which are in equilibrium: an inactive closed form where the active site is shielded from the reaction medium by a polypeptide chain called a lid, and an open form where the lid is displaced, fully exposing the active site to the reaction medium.[25–28] The protein strongly adsorbed on the surface after immobilization, affecting the equilibrium and fixing the open form of the lipase.

Additionally, the porous form of the matrix permits an "operational stabilization" of the enzyme, stabilizing the enzyme against interaction with other molecules, *e.g.* from the enzymatic extract and limiting the contact with any external hydrophobic interface or the effects of vigorous stirring.

As expected, the highest activity was observed for the benchmark Novozym 435 (92.4% conversion of furfuryl alcohol after 30 min). The recycling test of Novozym 435 revealed issues with filtering off the biocatalyst after the reaction due to the swelling of the resin. As previously mentioned, the objective of this work was to find an alternative to Novozym 435 due to technical issues related to its use, such as filtration, operation as a fixed bed in a flow reactor, and regeneration difficulties.

The crucial parameter of the developed heterogeneous biocatalysts is the structure and hydrophilicity of the surface of the carrier. An additional calcination of the MgO·SiO_2 matrix did not affect the stabilization of active conformation of LAO as suspected (89.4% conversion in 45 min).

Changes in crystalline structure influenced the amount of grafted C_8 groups (for MgO·SiO_2-C_8: 8.03 wt% of C_8, for MgO·$SiO_{2(calc.)}$-C_8: 1.21 wt% of C_8) and adsorbed LAO on the

Table 2 Structural characteristics of the MgO·SiO_2-C_8-LAO biocatalyst

Material	S_{BET} (m^2 g^{-1})	S_{BET} micropores (m^2 g^{-1})	V_p (cm^3 g^{-1})	d_p (nm)	C_8 loading[a] (wt% ± 0.3)	LAO loading[a] (wt% ± 0.3)
MgO·SiO_2	421	314	0.06	2.1	—	—
MgO·SiO_2-C_8	325	243	0.05	2.1	8.03	—
MgO·SiO_2-C_8-LAO	236	169	0.02	2.1	8.03	4.24

[a] Determined using TGA; the standard deviation of 3 replicate experiments.

Table 3 The influence of siliceous support modification on biocatalyst performance in the esterification of furfuryl alcohol

Biocatalyst	Time (min)	Furfuryl alcohol conversion[a] (%)	Activity (μmol min^{-1})	Specific activity (μmol mg^{-1} min^{-1})	Activity recovery[b] (%)
LAO	120	83.5	7.3	1.1	—
CALB	120	74.7	6.1	1.0	—
Novozym 435	30	92.4	30.1	4.7	493
$MgO{\cdot}SiO_2$-LAO[c]	120	6.1	—	—	—
SiO_2-C_8-LAO	90	87.1	10.0	1.6	137
$MgO{\cdot}SiO_2$-C_8-LAO	45	90.2	20.2	3.2	277
$MgO{\cdot}SiO_{2(calc.)}$-C_8-LAO	45	89.4	20.3	3.2	277
$MgO{\cdot}SiO_2$-C_{16}-LAO	45	87.3	20.4	3.2	277

Reaction conditions: furfuryl alcohol 1.0 mmol, caprylic acid 3.0 mmol, cyclohexane 0.5 mL, biocatalyst containing 6.36 mg of LAO (146 μL of LAO solution (43.7 mg mL^{-1}); 530 μL of CALB solution (12 mg mL^{-1}); 118 mg of Novozym 435; 300 mg of $MgO{\cdot}SiO_2$-LAO; 69 mg of SiO_2-C_8-LAO; 150 mg of $MgO{\cdot}SiO_2$-C_8-LAO; 294 mg of $MgO{\cdot}SiO_{2(calc.)}$-C_8-LAO; 413 mg of $MgO{\cdot}SiO_2$-C_{16}-LAO), 25 °C, 250 rpm. [a] Determined using GC. [b] Activity recovery = (activity of immobilized enzyme/activity of native enzyme)·100%. [c] 300 mg of biocatalyst (maximum possible loading).

surface (for $MgO{\cdot}SiO_2$-C_8-LAO: 4.24 wt% of LAO, for $MgO{\cdot}SiO_{2(calc.)}$-C_8-LAO: 2.16 wt% of LAO), that is lower as in the case of uncalcined materials. It is worth underlining that lower enzyme loading resulted in high activity recovery and conversion of the substrate probably due to uniform enzyme deposition and escaped the trap of enzyme overloading. Hence, to avoid an additional high energy-consuming step in catalyst preparation that does not improve lipase performance, matrix calcination is not recommended.

Introducing a longer alkyl group C_{16} instead of C_8 to oxide materials influenced the immobilization step ($MgO{\cdot}SiO_2$-C_{16} 1.54 wt% *versus* 4.24 wt% on $MgO{\cdot}SiO_2$-C_8-LAO) and slightly decreased the activity of the enzyme (87.3% conversion in 45 min) and longer alkyl chains caused larger steric hindrances, decreasing the capacity of protein to adsorb on the surface. Additionally, the presence of alkyl hydrophobic groups on the $MgO{\cdot}SiO_2$ surface is crucial to maintain LAO immobilization and high activity, which was proven by TG/DTG analyses (ESI, Fig. S21†). Only 6.1% conversion of furfuryl alcohol after 120 minutes of reaction in the presence of $MgO{\cdot}SiO_2$-LAO was detected, even with the maximum possible loading of biocatalyst (300 mg). A higher amount of biocatalyst prevented effective stirring.

The important aspect of improving the LAO activity was to introduce Mg species to silica and create $MgO{\cdot}SiO_2$ oxide material. The presence of Mg particles in the siliceous material likely improved the activation and stabilization of the active conformation of the enzyme through electrostatic interactions between Mg^{2+} ions and LAO amino acids by providing additional spatial rearrangements in the α-helix and β-sheet orientation.[38] This effect led to higher performance of the immobilized biomolecules. A slightly different approach based on Mg^{2+} doped-*Candida rugosa* lipase (CRL) which was encapsulated into a zeolitic imidazolate framework (ZIF) structure was reported.[38] The presence of Mg^{2+} changed the conformation of CRL, confirmed by circular dichroism and fluorescence spectroscopy. This effect improved the structural stability of the enzyme and an increase in catalytic performance, up to two-fold higher, was observed compared to materials lacking metal ions. Additionally, as mentioned above, Mg^{2+} also provided more efficient grafting of the octyl groups. The increase in reaction rate (90.2% conversion of alcohol for $MgO{\cdot}SiO_2$-C_8-LAO in 45 min, *versus* 87.1% for SiO_2-C_8-LAO in 90 min) and 2 times higher enzyme specific activity (3.2 μmol mg^{-1} min^{-1} for $MgO{\cdot}SiO_2$-C_8-LAO and 1.6 μmol mg^{-1} min^{-1} for SiO_2-C_8-LAO, respectively) confirmed the significant influence of MgO on enzyme activity. Additionally, the presence of advanced microporous channel systems enhances the flow of the reaction mixture through the biocatalyst, once again resulting in excellent lipase catalytic performance.

Key reaction parameters

Optimization of the reaction parameters for a model reaction in the presence of the $MgO{\cdot}SiO_2$-C_8-LAO biocatalyst was studied. First, the influence of the type of solvent (cyclohexane, toluene, hexane, and isooctane) used for the reaction was tested (Fig. 1). The choice of a proper solvent in biocatalysis is necessary to avoid the fast deactivation of the enzyme. The biocatalyst demonstrated superior catalytic performance in cyclo-

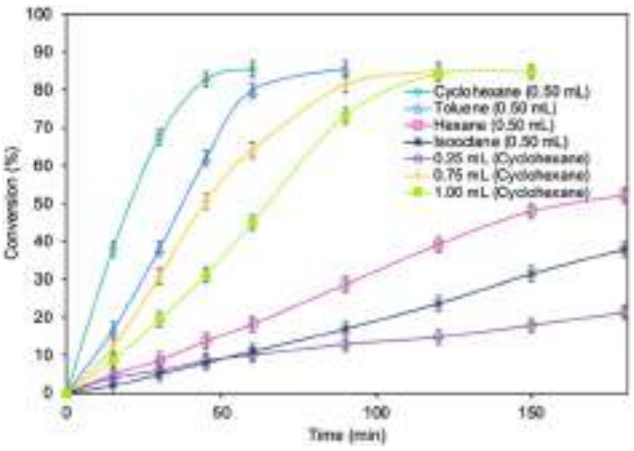

Fig. 1 The influence of type of solvent and its amount on furfuryl alcohol conversion. Reaction conditions: furfuryl alcohol 1.0 mmol, caprylic acid 3.0 mmol, solvent, $MgO{\cdot}SiO_2$-C_8-LAO 100 mg, 25 °C, 250 rpm; conversion was determined using GC.

hexane (86.2% conversion in 60 min), and next in toluene (85.7% conversion in 90 min), achieving 100% selectivity in both cases (see ESI, Fig. S29†). Using hexane and isooctane, furfuryl alcohol conversions reached 52.6% and 37.4%, respectively, in 180 min. Acetonitrile, being a more hydrophilic solvent, was also tested and showed no conversion of furfuryl alcohol. This can be attributed to the strong affinity of acetonitrile to the essential water required by the lipase. Solvents such as methanol, ethanol or alkyl carbonates as greener alternatives were not suitable due to their reactivity with caprylic acid. Additionally, hydrophilic solvents tend to attract the essential water in lipase, leading to its deactivation.[25,39] Unfortunately, using less than 0.50 mL of cyclohexane per 1 mmol of furfuryl alcohol for the synthesis resulted in lower biocatalyst activity due to problems with mixing of the reagents in the presence of heterogeneous $MgO{\cdot}SiO_2$-C_8-LAO, making the solventless process impossible. Higher amounts of cyclohexanone, such as 0.75 and 1.0 mL, resulted in slower reaction rates due to the lower concentration of reagents.

Subsequently, the influence of the amount of $MgO{\cdot}SiO_2$-C_8-LAO biocatalyst was studied (Fig. 2). Using 150 mg of the biocatalyst per 1 mmol of furfuryl alcohol resulted in an even higher furfuryl alcohol conversion (90.2%) within a shorter reaction time of 45 min. Increasing the amount of biocatalyst to 175 mg did not lead to a higher conversion or reaction rate (90.4% in 45 min). As observed, using only 25 mg of biocatalyst still enabled a high conversion of furfuryl alcohol (84.8%), similar to the reaction with 150 mg, but in longer time, after 180 min. This indicates lower robustness of the system due to the reduced amount of immobilized LAO. This observation confirms the exceptionally high activity of the developed $MgO{\cdot}SiO_2$-C_8-LAO biocatalyst. For further studies 150 mg of $MgO{\cdot}SiO_2$-C_8-LAO was used.

The influence of molar ratio of the furfuryl alcohol to caprylic acid on the catalytic performance of the biocatalyst in furfuryl alcohol esterification was also examined (Fig. 3). The best outcome was obtained for 3-fold molar excess of caprylic acid, achieving 90.2% conversion of furfuryl alcohol in 45 min. Increasing the molar excess of acid further did not affect the conversion. The studies concerning the influence of temperature (Fig. 4) revealed the similar catalytic performance of $MgO{\cdot}SiO_2$-C_8-LAO at 25 °C, 30 °C and 35 °C. As expected, lower temperature (20 °C) caused a slight decrease in reaction rate, designating 25 °C as the most favourable temperature. Higher temperature (40 °C) resulted in retardation of the reaction, probably due to partial deactivation of the lipase-based biocatalyst. According to the literature, LAO maintains its optimum activity at around 30 °C and pH 7, with a significant drop in activity observed at 40 °C, which is consistent with the obtained results.[40]

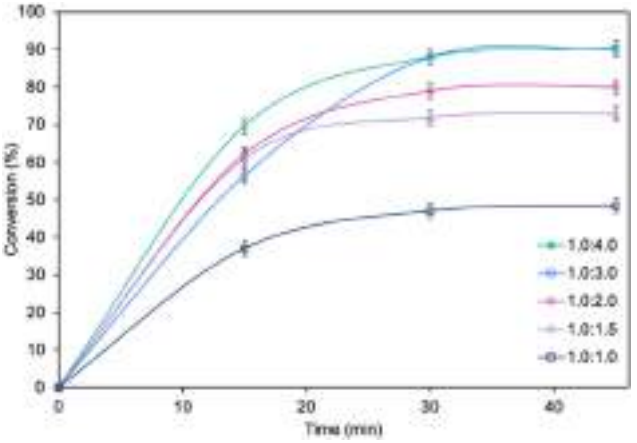

Fig. 3 The influence of the furfuryl alcohol to caprylic acid molar ratio on furfuryl alcohol conversion. Reaction conditions: furfuryl alcohol 1.0 mmol, caprylic acid, cyclohexane 0.5 mL, $MgO{\cdot}SiO_2$-C_8-LAO 150 mg, 25 °C, and 250 rpm; conversion was determined using GC.

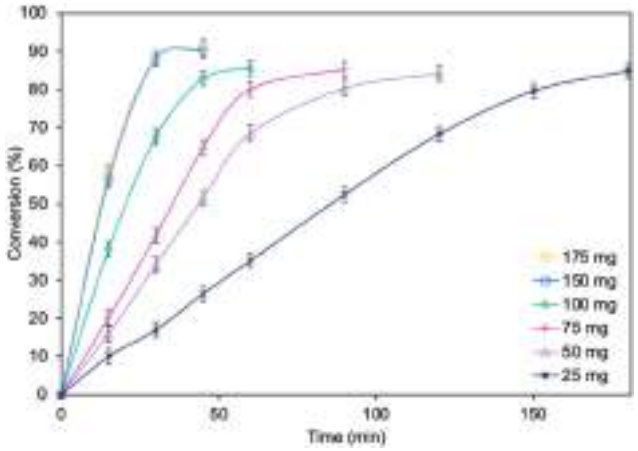

Fig. 2 The influence of $MgO{\cdot}SiO_2$-C8-LAO content on furfuryl alcohol conversion. Reaction conditions: furfuryl alcohol 1.0 mmol, caprylic acid 3.0 mmol, cyclohexane 0.5 mL, $MgO{\cdot}SiO_2$-C_8-LAO, 25 °C, and 250 rpm; conversion was determined using GC.

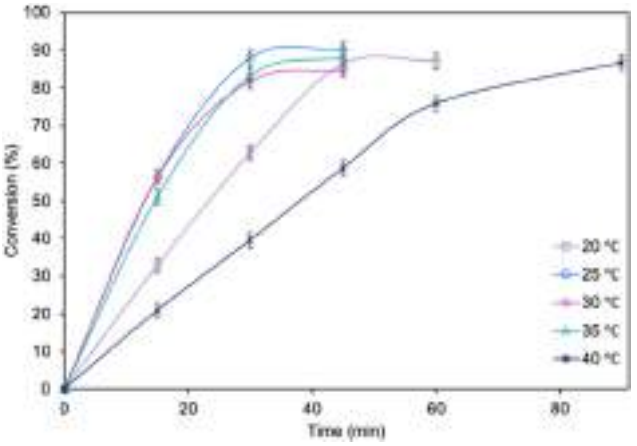

Fig. 4 The influence of temperature on furfuryl alcohol conversion. Reaction conditions: furfuryl alcohol 1.0 mmol, caprylic acid 3.0 mmol, cyclohexane 0.5 mL, $MgO{\cdot}SiO_2$-C_8-LAO 150 mg, 250 rpm; conversion was determined using GC.

Finally, the potential for easy and safe biocatalyst reuse is essential for the advancement of environmentally friendly and effective catalytic systems. The recycling ability of $MgO{\cdot}SiO_2$-C8-LAO was studied in the esterification of furfuryl alcohol by upscaling the process twofold to 2 mmol of furfuryl alcohol, which consequently required 300 mg of biocatalyst in batch mode. As presented in Fig. 5, the developed $MgO{\cdot}SiO_2$-C_8-LAO retained its catalytic performance for 10 consecutive runs in furfuryl alcohol esterification but a progressive drop was observed. A reduction in conversion to 84.6% was observed after the 10^{th} cycle. TG/DTG analyses of the reused biocatalyst showed no changes in LAO loading, which indicates the slow deactivation of LAO (ESI, Fig. S33†).

Additionally, the 'reaction stop' experiment, which involved the rapid removal of the biocatalyst from the reaction mixture, demonstrated no further conversion of furfuryl alcohol in the filtrate (ESI, Fig. S33†), which confirms that there was no leaching of LAO into the reaction system. Hence, the observed drop in biocatalytic properties is mainly related to enzyme inhibition by the substrate or products, or due to enzyme inactivation by denaturation.

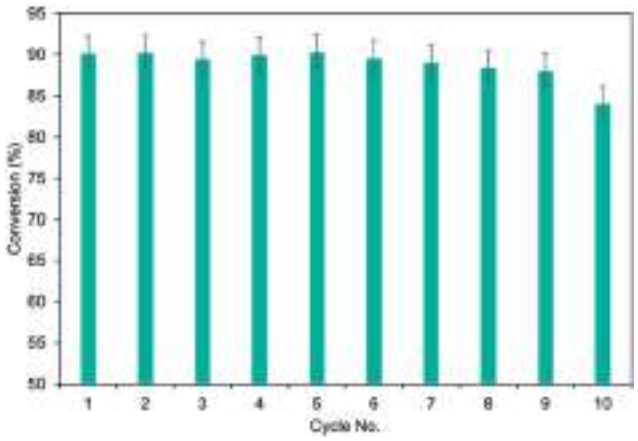

Fig. 5 The recycling study of $MgO{\cdot}SiO_2$-C_8-LAO in furfuryl alcohol esterification. Reaction conditions: furfuryl alcohol 2.0 mmol, caprylic acid 6.0 mmol, cyclohexane 1 mL, $MgO{\cdot}SiO_2$-C_8-LAO 300 mg, 25 °C, 250 rpm, and 45 min; conversion was determined using GC.

Further, to use the developed biocatalytic system for the synthesis of other fatty esters of furfuryl alcohol, the following acids were used: caprylic acid, pelargonic acid, capric acid, lauric acid and oleic acid (Table 4). In all cases high conversion of alcohol (88.7–90.2%) was achieved. As expected, the longer alkyl chain of fatty acid caused steric hindrance and prolonged reaction times (from 45 min for C_7 to 90 min for C_{17}). Nevertheless, in all cases esters were isolated with high yields, confirming that the biocatalyst is universal for the synthesis of esters from biomass-derived furfuryl alcohol and C_8–C_{18} carboxylic acids. The selectivity of the esterification reached 100% for each ester.

Catalytic activity of $MgO{\cdot}SiO_2$-C_8-LAO in esterification of furfuryl alcohol and C8–C18 carboxylic acids in a flow system

Continuous flow synthesis of fine chemicals and pharmaceuticals is expected to improve the selectivity, safety, and sustainability of chemical production while also reducing costs. Encouraged by the high activity and stability of the designed biocatalysts, the upgrade of the batch esterification to a flow process was studied. Experiments were carried out in a fully automated Syrris Asia column packed-bed type flow microreactor filled with 300 mg of $MgO{\cdot}SiO_2$-C_8-LAO biocatalyst. Before all experiments a fresh mixture of furfuryl alcohol (6.2 g), octanoic acid (27.4 g) and cyclohexane (31.7 mL) was prepared and then pumped to the column reactor filled with the biocatalyst. To keep the stable reagent flow through the column reactor, the system was equipped with a backpressure regulator and set

Table 4 Synthesis of esters of C8–C18 carboxylic acids and furfuryl alcohol

Fatty acid	Furfuryl ester	Time (min)	Furfuryl alcohol conversion[a] (%)	Isolated yield of ester (%)
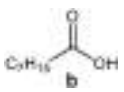 b	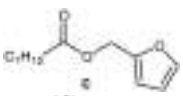 c	45	90.2	88
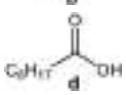 d	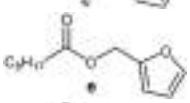 e	60	89.8	86
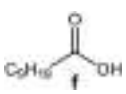 f	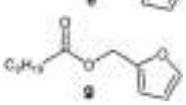 g	60	89.4	88
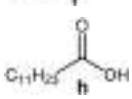 h	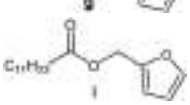 i	60	88.7	85
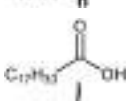 j	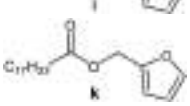 k	90	89.9	87

Reaction conditions: furfuryl alcohol 1.0 mmol, fatty acid 3.0 mmol, cyclohexane 0.5 mL, $MgO{\cdot}SiO_2$-C_8-LAO 150 mg, 25 °C, 250 rpm. [a] Conversion was determined using GC.

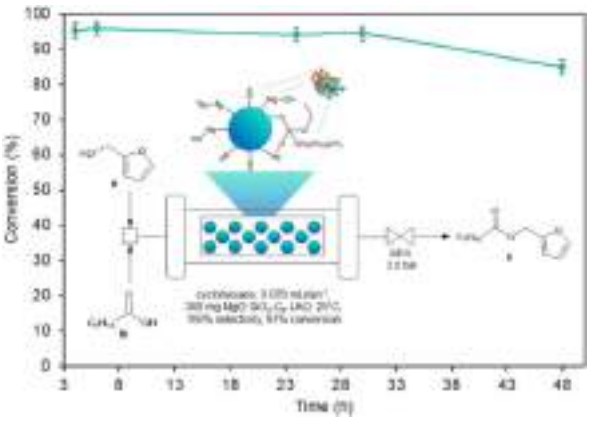

Fig. 6 Conversion of furfuryl alcohol under continuous flow conditions catalysed by MgO·SiO_2-C_8-LAO over time. Reaction conditions: furfuryl alcohol in cyclohexane (2.0 M), caprylic acid (1 : 3, n : n, furfuryl alcohol : caprylic acid), MgO·SiO_2-C_8-LAO 300 mg, and 25 °C. Conversion of furfuryl alcohol was determined using GC.

to 2 bar (Fig. 6). Experiments were carried out under the conditions optimised in the batch system. Total reagent flow rates ranging from 0.04 to 0.20 mL min^{-1} were tested (Table 5).

The use of reagent residence times in the catalytic zone, ranging from 10.5 to 18.4 minutes, associated with reagent flow rates of 0.04 mL min^{-1}, 0.06 mL min^{-1}, and 0.07 mL min^{-1} (τ = 18.4 min, 12.3 min, and 10.5 min) resulted in a high conversion of furfuryl alcohol, reaching 96.8% and remaining stable for at least 3 h, while the reduction of residence time below 10.5 min led to a reduction in the conversion of furfuryl alcohol. For 0.08 mL min^{-1}, 0.1 mL min^{-1}, and 0.2 mL min^{-1} reagent flow a significant deterioration of alcohol conversion to 92.3%, 85.2%, and 79.1% respectively was noticed. The optimal flow reaction conditions, considering the highest conversion of furfuryl alcohol (96.8%) achieved using 0.07 mL min^{-1} (τ = 10.5 min) with the space–time–yield SPY of 6651 (g h^{-1} L^{-1}), were determined and used for stability tests of MgO·SiO_2-C_8-LAO over the long-term experiment. The biocatalyst exhibited excellent stability over 30 h, with furfuryl alcohol conversion reaching 96.8%. A slight drop to 85.7% was observed after 48 h of conducting the process.

Table 5 Results of esterification of furfuryl alcohol with caprylic acid under continuous flow conditions catalysed by the MgO·SiO_2-C_8-LAO system

Reagents flow (mL min^{-1})	Residence time[a] (min)	Furfuryl alcohol conversion (%)	SP[b] (g h^{-1} mg^{-1})	STY[c] (g h^{-1} L^{-1})
0.04	18.4	1 h, 96.7 2 h, 96.7 3 h, 96.6	0.13	2173
0.06	12.3	1 h, 96.5 2 h, 96.2 3 h, 96.6	0.28	4867
0.07	10.5	1 h, 96.5 2 h, 96.8 3 h, 96.6	0.38	6651
0.08	9.2	1 h, 91.7 2 h, 92.3 3 h, 91.8	0.96	8244
0.10	7.4	1 h, 85.2 2 h, 84.5 3 h, 84.8	0.69	11 904
0.20	3.7	1 h, 78.4 2 h, 79.1 3 h, 78.3	2.53	43 814

Reaction conditions: furfuryl alcohol in cyclohexane (2.0 M), caprylic acid (1 : 3, n : n, furfuryl alcohol : caprylic acid), MgO·SiO_2-C_8-LAO 300 mg (volume 0.735 mL), 25 °C. Furfuryl alcohol conversion was determined using GC. [a] $\tau = V_{biocatalyst}/F_{reagents}$ (mL min^{-1}). [b] Specific productivity SP = $m_{product}/\tau m_{protein}$ (g h^{-1} mg^{-1}). [c] Space–time–yield STY = $m_{product}/\tau V_{biocatalyst}$ (g h^{-1} L^{-1}).

The productivity of this process of 0.376 g h^{-1} (1.67 mmol h^{-1}) is quite efficient, especially considering the reactor size (bed volume 0.735 mL) with a space–time–yield SPY of 6651 (g h^{-1} L^{-1}). Additionally, the stability of the catalyst bed up to 30 h can ensure the production of 11.28 g of product. The esterification of furfuryl alcohol represented in this work can be considered as a relatively slow reaction that requires a residence time of 10.5 min; however, rapid mixing and heat transfer bring safety and quality advantages. Moreover, 21 times higher productivity compering to batch process was reached (6651 *versus* 320 (g h^{-1} L^{-1})) recalculating for the volume of used biocatalyst.

The STY is a reasonable and important quantity for the comparability of continuously operated flow processes. Chemical reactions can generally be categorized by reaction time into three groups: rapid reactions that are completed within seconds, intermediate reactions that take between 1 second and 10 minutes, and slow reactions that require more than 10 minutes to complete. According to examples in the literature, a residence time of approximately 10 minutes in continuous flow biocatalysis is deemed favourable.[41] In some cases, enzyme-catalysed flow reactions can last up to 20 minutes or even more for micro and macroreactors with the flow rates ranging from 0.05 to 1.45 mL min^{-1} with the most often used rates being around 0.1–0.2 mL min^{-1}. Reactor volumes generally range from 0.3 to 12 mL, with an average volume of around 1 mL. For example, hydroxynitrile lyases covalently immobilized in a siliceous monolithic microreactor were applied for the fast production of chiral cyanohydrins in 4 min at 0.1 mL min^{-1} in a 0.96 mL rector with STY 1229 [g L^{-1} h^{-1}].[42] Other examples described much lower parameters of STY, around 10–60 [g L^{-1} h^{-1}]. For example, the formylglycine generating enzyme from *Thermomonospora curvata* immobilized on epoxy-activated Sepharose beads (1.0 mL packed-bed reactor, residence time 20 min, flow 0.5 mL min^{-1}) used for aldehyde tag conversion showed 10 times higher productivity (STY = 21.6) compared to the batch process.[43]

For the upscaling of the process described in this work for large-scale production of esters scaling up to a packed-bed macroreactor with higher reactor volume should be tested first. Next, probably the numbering up increasing the number of channels in the macroreactors what is a common strategy in the scale-up of flow chemistry enabling the retention of the

transfer properties, such as mixing, heat transfer associated with the micro-environment.[44]

Summing up, under flow conditions, a higher conversion of furfuryl alcohol 96.8% was achieved, compared to the 90.2% in a batch reactor, along with a shortened reaction residence time to 10.5 min *versus* 45 min in the batch process. These outstanding results for the continuous flow process might be explained by effective enzyme adsorption and the provision of a suitable hydrophobic microenvironment, which resulted in high enzyme activity over a prolonged period.

Green chemistry metrics

To emphasize the sustainability of the developed method for the synthesis of furfuryl esters, a green metrics analysis of all literature data was conducted in accordance with green chemistry principles using J. Clark's Green Chemistry Metrics toolkit (Appendix 2, ESI†).[46]

The MgO·SiO_2-C_8-LAO biocatalyst used in the batch and flow synthesis of furfuryl caprylate was compared to metal-based catalysts (Y_2O_3-ZrO_2 and Fe-DTP-ZIF-8), commercial biocatalyst (Novozym 435), and coupling reagent (EDC) described in the literature for the synthesis of furfuryl acetate, furfuryl oleate, furfuryl caprylate, furfuryl ricinoleate, and furfuryl 2-furoate (Table 6). No by-products were observed in almost all cases, reaching 100% selectivity of the process, except the lower esterification selectivity of 86.3% obtained in the presence of the Fe-DTP-ZIF-8 catalyst (iron-exchanged heteropolyacid encapsulated inside ZIF-8). A yield of ester higher than 90% was achieved only in two instances: with the biocatalysts described in this work and with Novozym 435 (entries 3, 7 and 8), highlighting the significance of our research. Once again, it is worth underlining that the lack of or difficulties with recycling of Novozym 435 could be a significant obstacle for its application in the flow process.

Biocatalysts are considered as biodegradable and environmentally friendly alternatives to metal-based and traditional acidic catalysts, which enhances the green factor of the developed methods (entries 3, 4, 5, 7, and 8). The possibility of catalyst recycling and its stability are among the most important aspects when considering the environmental impact and applicability of the developed method. Recyclability of designed catalytic systems was proved only for Fe-DTP-ZIF-8 for at least 5 cycles (entry 2) *versus* at least 10 cycles obtained for MgO·SiO_2-C_8-LAO in a batch system and high STY = 6651 (g h^{-1} L^{-1}) for a

Table 6 Green chemistry metrics evaluated for furfuryl ester synthesis

Catalyst/reagent	Y_2O_3-ZrO_2 [a]	Fe-DTP-ZIF-8 [b]	Novozym 435 [c]	Novozym 435 [d]	Novozym 435 [e]	EDC [f]	MgO·SiO_2-C_8-LAO batch [g]	MgO·SiO_2-C_8-LAO flow [h]
Entry	1	2	3	4	5	6	7	8
Acid	Acetic acid	Acetic acid	Oleic acid	Caprylic acid	Ricinoleic acid	Furoic acid	Caprylic acid	Caprylic acid
Yield of product (%)	88	75.7	99.9	73	88.6	70.8	90.2	96.8
Selectivity of the esterification (%)	100	86.3	100	100	100	100	100	100
Atom economy (%)	88.6	88.6	95.3	92.6	95.5	91.4	92.6	92.6
RME (%)	31	47.9	95.1	68.7	56.1	31.3	38.1	40.9
Solvent choice		—[i]	—[i]	—[i]	—[i]			
Catalyst or reagent								
Recoverable catalyst			No data	No data	No data			
Critical elements								
Energy								
Reaction run below solvent boiling point								
Batch/flow								
Work-up		—[i]	—[i]	—[i]	—[i]			
Health and safety								
Ref.	13	12	18	19	9	45	This work	This work

[a] Reaction conditions: furfuryl alcohol 10 mmol, acetic acid 50 mmol, Y_2O_3-ZrO_2 0.2 g, 110 °C, 7 h. [b] Reaction conditions: furfuryl alcohol 46 mmol, acetic acid 28 mmol, Fe-DTP-ZIF-8 0.006 g, 100 °C, 6 h. [c] Reaction conditions: furfuryl alcohol 71 mmol, oleic acid 71 mmol, Novozym 435 1 g, 60 °C, 533.29 Pa, 6 h. [d] Reaction conditions: furfuryl alcohol 1 mmol, caprylic acid 1 mmol, Novozym 435 (0.01 g), 55 °C, 24 h. [e] Reaction conditions: furfuryl alcohol 3 mmol, caprylic acid 1 mmol, Novozym 435 0.06 g, 60 °C, 28 mmHg vacuum, 5 h. [f] Reaction conditions: furfuryl alcohol 2 mmol, 2-furoic acid 6 mmol, 1-ethyl-3-(3-dimethylaminopropyl)carbodiimide – EDC 0.06 g, dichloromethane 3 mL, 90 °C, microwave 200 W, 30 min. [g] Reaction conditions: furfuryl alcohol 1 mmol, caprylic acid 3 mmol, cyclohexane 0.50 mL, MgO·SiO_2-C_8-LAO 0.15 g, 25 °C, 45 min. [h] Reaction conditions: furfuryl alcohol 19 mmol, caprylic acid 57 mmol, cyclohexane 95 mL, MgO·SiO_2-C_8-LAO 0.30 g, 0.070 mL min^{-1} reagent flow, 25 °C, 10.5 min (residence time), 48 h (to consume all furfuryl alcohol). [i] Solventless conditions, no data concerning work-up; flag system: the green flag denotes preferred, amber is acceptable, and red is undesirable. Appendix 2, ESI.†

flow system (entries 7 and 8, respectively, this work). The possibility of recycling of Y_2O_3–ZrO_2 (entry 1) and Novozym 435 (entry 4) was only postulated. Atom economy for esterification reactions is lower than 100% due to the formation of water molecules during the synthesis. On the other hand, water can be beneficial during work-up through extraction and can also enhance the catalytic performance of lipase.[25,39]

Reaction mass efficiency (RME) for furfuryl ester synthesis typically ranges from 31% to 69%, except for entry 3 (95.1%). This efficiency is largely dependent on the yield and the excess of reagents used in each method. The synthesis of furfuryl esters can be performed under solventless conditions, but at high temperature, under pressure and long reaction time (110 °C, 7 h, entry 1; 100 °C, 6 h, entry 2; 60 °C, 533.29 Pa, 6 h, entry 3; 55 °C, 24 h, entry 4; 60 °C, 28 mmHg vacuum, entry 5) or with solvents like dichloromethane (90 °C, microwave 200 W, 30 min, entry 6) and cyclohexane (25 °C, 45 min, entry 7; 25 °C, 10.5 min residence time, entry 8). It is noteworthy that the majority of existing examples of the synthesis of furfuryl esters were performed in batch systems (entries 1–7). However, continuous flow synthesis demonstrated in this work not only enhances production efficiency but also improves the environmental sustainability of the developed method.

The work-up procedure was described only for entries 1,[13] 6,[45] and 7, 8.[This work] Furfuryl esters can be isolated *via* distillation under reduced pressure or high temperature, or extraction with organic solvents, such as heptane,[This work] dichloromethane,[13,45] and column chromatography.[13,45] The red flags in the Health and safety row for our study resulted from the need for the use of hydrophobic organic solvents to extract the furfuryl ester from the post-reaction mixture. The developed method of continuous flow synthesis of furfuryl esters in the presence of the $MgO{\cdot}SiO_2$-C_8-LAO biocatalyst considered under green chemistry metrics in this work strikes a balance between a highly active, stable, recyclable, and biodegradable catalyst, and an environmentally friendly and sustainable approach to chemical production. Future research should focus on developing more eco-friendly isolation methods to enhance the environmental sustainability of the process.

The sustainable character of the developed method of production of furfuryl octanoate in continuous flow in the presence of the $MgO{\cdot}SiO_2$-C_8-LAO biocatalyst has been already assessed using the Green Chemistry Metrics Analysis. Next, another approach was considered by evaluating not only the ester synthesis method but also the preceding life cycle stages.

To evaluate the method in terms of life cycle thinking,[47] a synthesis tree was drawn (Fig. 7).

All necessary substrates to produce ester, furfuryl alcohol, and octanoic acid can be obtained from natural sources, such

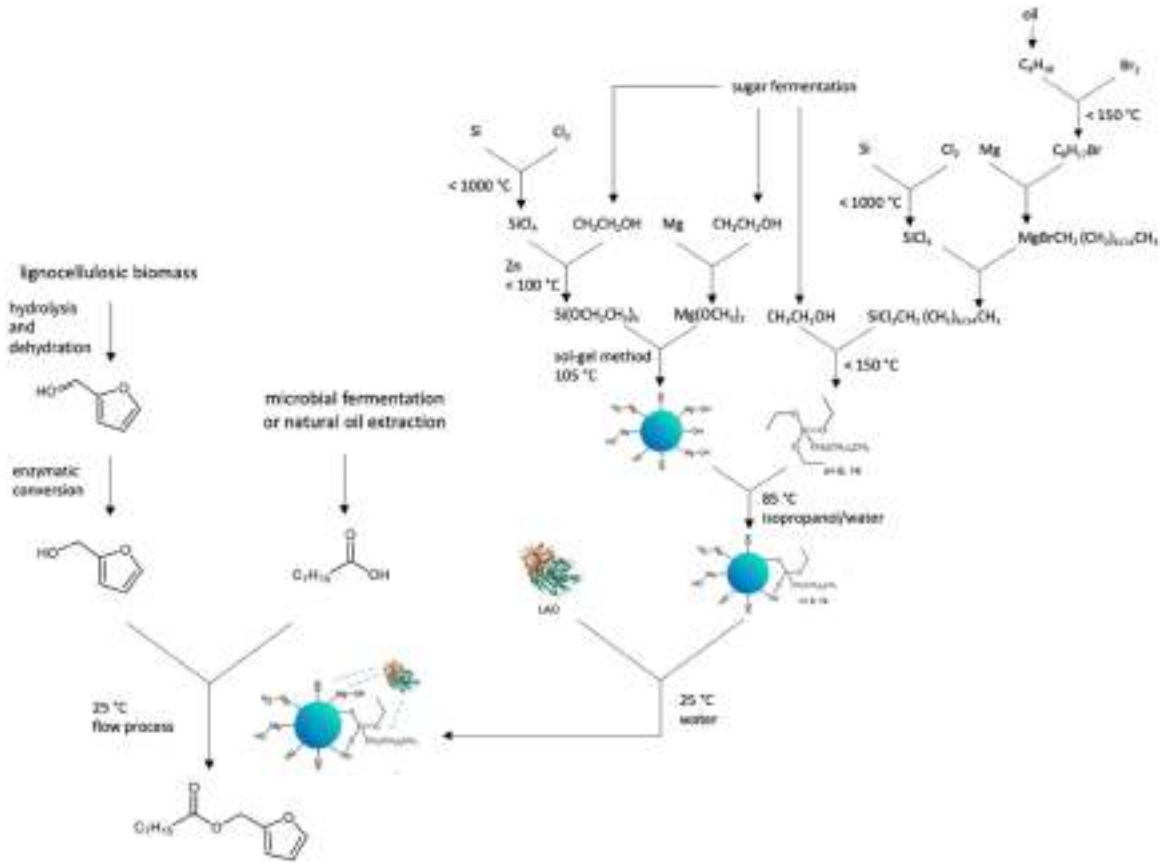

Fig. 7 Synthesis tree for furfuryl octanoate under continuous flow conditions catalysed by $MgO{\cdot}SiO_2$-C_8-LAO.

as lignocellulosic biomass,[48–50] coconut and palm kernel oil[51] or microbial production from renewable carbon sources.[52] In the context of waste management and closed-loop economy principles, it is especially important to use waste as a resource for producing other substances. Various strategies of furfuryl alcohol and octanoic acid have been employed including continuous flow production, the use of deep eutectic solvents, ionic liquids, and enzymes, all aimed at achieving the most environmentally sustainable technologies.[48–52] The production of the $MgO{\cdot}SiO_2$-C_8-LAO biocatalyst includes the use of LAO, which is considered generally safe, whereas several critical factors can be observed in the process of the synthesis of the $MgO{\cdot}SiO_2$-C_8 support. The primary issue arises from the inclusion of volatile fluorohydrocarbons in the synthesis of silicon compounds, which poses environmental risks such as acid rain, ozone layer depletion, and global warming. However, some alternative methods for preparing valuable organosilicon molecules using enzymes have already been reported.[53]

Experimental

Materials and methods

All reagents and lipases were supplied by Sigma-Aldrich (Merck Group, Poland). $MgO{\cdot}SiO_2$ was synthesized according to the literature (Ciesielczyk *et al.*, 2014; Kołodziejczak-Radzimska *et al.*, 2018).[33,36] GC was performed on a SHIMADZU GC-2010 Plus equipped with a Zebron ZB-5MSi column (30 m × 0.32 mm; 0.25 μm). TG/DTG analyses of all materials were performed using a TGA/SDTA 851 Mettler-Toledo thermogravimeter in the temperature range 25 °C–800 °C at a heating rate of 10 °C min^{-1} in a stream of nitrogen (60 mL min^{-1}). BET surface area (S_{BET}), average pore size (d_p) and average pore volume (V_p) of the $MgO{\cdot}SiO_2$ based materials were determined on an ASAP 2020 Plus Version 2.00 using low-temperature nitrogen adsorption–desorption (−196 °C) according to the BET method and BJH model. SEM-EDX images of all materials were recorded on a Phenom Pro Desktop SEM coupled with an EDS detector (15 kV) (Thermo Fischer Scientific). FTIR analyses of modified materials were performed on a Vertex 70 apparatus over 4000–420 cm^{-1} (at a resolution of 0.5 cm^{-1}) (Bruker, Germany) by mixing 2.0 mg of the material and 200 mg of anhydrous KBr. ^{1}H NMR and ^{13}C NMR spectra of furfuryl esters were recorded on a Varian system (400 MHz and 101 MHz, respectively). The Lowry test was utilized to determine the protein concentration in the commercial solutions of *Aspergillus oryzae* and CALB. A standard curve was generated employing bovine serum albumin. A mixture comprising 0.5 mL of prepared Lowry solution and 0.5 mL of diluted sample was created (20 min incubation), followed by the addition of 0.25 mL of Folin solution (30 min incubation), and the absorbance measurement using a spectrophotometer.

Modification of silica-based materials with alkyl organosilanes.[29] SiO_2, $MgO{\cdot}SiO_2$ or $MgO{\cdot}SiO_{2(calc.)}$ (200 mg) was suspended in an isopropanol : water mixture (4 mL; 4 : 1, v : v) in a 25 mL round-bottom flask, then triethoxy(octyl)silane or triethoxy(hexadecyl)silane (0.2 mmol) was added, and the reaction mixture was stirred at 85 °C for 24 h. After that, the material was filtered off, washed with isopropanol (3 × 20 mL) and dried under vacuum on a Schlenk line (rt, 4 h).

Lipase immobilization.[25,30] Siliceous material (200 mg), native LAO (1.4 g) and 3 mL of deionized water were stirred in a 25 mL round-bottom flask in a thermostatic shaker (250 rpm) at 20 °C for 3 h. After that, the biocatalyst was filtered off, washed with deionized water (3 × 20 mL) and dried under vacuum on a Schlenk line (rt, 24 h).

General procedure of furfuryl alcohol esterification in a batch system. In a 5 mL vial, furfuryl alcohol (0.1 mmol), cyclohexane (0.5 mL), and fatty acid (0.3 mmol) were mixed, and then 150 mg of $MgO{\cdot}SiO_2$-C_8-LAO were added. The reaction was performed at 25 °C and stirred in a thermostatic shaker (250 rpm) for 45 min. Reaction progress was monitored by GC. After the reaction, the biocatalyst was filtered off, and the product was separated by 1 M solution of K_2CO_3 (20 mL)/heptane (3 × 10 mL) extraction system, washed with brine and water (3 × 10 mL), dried with anhydrous sodium sulphate, filtrate, then the solvent was evaporated, and the obtained ester was analysed *via* ^{1}H and ^{13}C NMR (ESI, Fig. S34–S43†). Furfuryl caprylate (c), yield 88%: ^{1}H NMR (400 MHz, DMSO-d6) δ 7.65 (dd, 1H), 6.47 (ddd, 2H), 5.04 (s, 2H), 2.29 (t, 2H), 1.51 (m, 2H), 1.28–1.19 (m, 10H), 0.85 (t, J = 6.9 Hz, 3H). ^{13}C NMR (101 MHz, DMSO-d6) δ 172.45, 149.42, 143.60, 143.54, 110.56, 57.27, 33.29, 31.07, 28.30, 28.28, 24.40, 21.98, 13.84. Furfuryl nonanoate (e), yield 86%: ^{1}H NMR (400 MHz, DMSO-d6) δ 7.66 (dd, 1H), 6.36 (ddd, 2H), 5.06 (s, 2H), 2.33 (t, 2H), 1.61 (m, 2H), 1.29–1.25 (m, 8H), 0.85 (t, 3H). ^{13}C NMR (101 MHz, DMSO-d6) δ 172.43, 149.43, 143.61, 143.55, 110.56, 57.26, 40.15, 33.30, 31.07, 28.51, 28.28, 24.40, 21.98, 13.84. Furfuryl decanoate (g), yield 88%: ^{1}H NMR (400 MHz, $CDCl_3$) δ 7.41 (dd, 1H), 6.49 (ddd, 2H), 5.06 (s, 2H), 2.31 (t, 2H), 1.53 (m, 2H), 1.29–1.18 (m, 12H), 0.84 (t, 3H). ^{13}C NMR (101 MHz, $CDCl_3$) δ 173.61, 149.81, 143.30, 110.66, 110.58, 57.99, 34.30, 31.92, 29.33, 29.30, 29.24, 29.22, 25.02, 22.77, 14.22. Furfuryl laurate (i), yield 85%: ^{1}H NMR (400 MHz, $CDCl_3$) δ 7.42 (dd, 1H), 6.37 (ddd, 2H), 5.31 (t, 2H), 5.06 (s, 2H), 2.29 (t, 2H), 1.99 (m, 4H), 1.50 (m, 2H), 1.32–1.22 (m, 16H), 0.85 (t, 3H). ^{13}C NMR (101 MHz, $CDCl_3$) δ 173.61, 149.81, 143.30, 110.66, 110.58, 57.99, 34.30, 31.92, 29.36, 29.33, 29.30, 29.26, 29.24, 29.22, 25.02, 22.77, 14.22. Furfuryl oleate (k), yield 87%: ^{1}H NMR (400 MHz, DMSO-d6) δ 7.65 (dd, 1H), 6.45 (ddd, 2H), 5.06 (s, 2H), 2.31 (t, 2H), 1.53 (m, 2H), 1.29–1.18 (m, 12H), 0.84 (t, 3H). ^{13}C NMR (101 MHz, DMSO-d6) δ 172.40, 149.40, 143.55, 129.67, 127.69, 110.61, 57.27, 33.65, 33.28, 31.29, 30.89, 29.09, 29.02, 28.83, 28.68, 28.59, 28.49, 28.43, 28.34, 26.55, 24.37, 22.07, 13.86.

Recycling of the heterogeneous biocatalyst. After the reaction, $MgO{\cdot}SiO_2$-C_8-LAO was filtered off, washed with cyclohexane (3 × 20 mL), dried under vacuum on a Schlenk line (2 h, 20 °C) and reused.

General procedure of furfuryl alcohol esterification in a flow system. The continuous flow furfuryl alcohol esterification was

performed in a fully automated Syrris Asia flow reactor. The mixture of furfuryl alcohol in cyclohexane (2.0 M) and caprylic acid (1 : 3, n : n) was pumped with a flow of 0.070 mL min^{-1} through the column reactor filled with 300 mg of $MgO{\cdot}SiO_2$-C_8-LAO biocatalyst at 25 °C for 48 h. Reaction progress was monitored by GC.

Conclusions

Green chemistry is essential for achieving Sustainable Development Goals. Innovative chemical methodologies must focus on consolidating high-yield reactions into a minimal number of unit operations, by using green solvents and integrating advanced starting materials. At every early stage of research, assessing developing technologies using green metrics is necessary. Despite their excellent catalytic properties, enzymes typically require enhancement before being implemented on an industrial scale, where multiple cycles of high yield processes are desired. One of the properties typically improved through immobilization is enzyme stability. Other critical enzyme properties that should be enhanced for prolonged use in industrial reactors include activity, resistance to inhibition by reaction products, and ease of regeneration. The strategy to improve enzyme properties during the performance *via* a tailor-made enzyme immobilization protocol is the goal of this work.

The novelty of this work lies in the innovative approach to a catalyst matrix ($MgO{\cdot}SiO_2$) and modifying its surface with alkyl groups for LAO immobilization, which brings a high enhancement in the efficiency of the enzyme during 30 h of performance in the synthesis of esters from biomass-derived furfuryl alcohol and C_8–C_{18} carboxylic acids in a flow system while maintaining low environmental hazard.

The sustainability of the developed method was assessed through green metrics and life cycle thinking, which are effective tools for designing environmentally friendly chemical processes.

Author contributions

Anna Wolny: writing – original draft, conceptualization, methodology, validation, data curation, investigation, formal analysis, project administration, funding acquisition. Dagmara Więcławik: investigation. Jakub Zdarta: writing – review & editing, resources. Sebastian Jurczyk: formal analysis. Teofil Jesionowski: conceptualization, writing – review & editing. Anna Chrobok: conceptualization, methodology, data curation, writing – review & editing.

Data availability

The data supporting this article have been included as part of the ESI.†

Conflicts of interest

There are no conflicts to declare.

Acknowledgements

This work was funded by the National Science Centre, Poland. Grant no. UMO-2023/49/N/ST8/01633 (PRELUDIUM-22).

References

1 A. Saravanan, P. R. Yaashikaa, P. S. Kumar, P. Thamarai, V. C. Deivayanai and G. Rangasamy, *Ind. Crops Prod.*, 2023, **200**, 116822, DOI: 10.1016/j.indcrop.2023.116822.
2 R. A. Sheldon and J. M. Woodley, *Chem. Rev.*, 2018, **118**, 801–838, DOI: 10.1021/acs.chemrev.7b00203.
3 J. M. Bolivar, J. M. Woodley and R. Fernandez-Lafuente, *Chem. Soc. Rev.*, 2022, **51**, 6251–6290, DOI: 10.1039/D2CS00083K.
4 P. Lozano and E. García-Verdugo, *Green Chem.*, 2023, **25**, 7041–7057, DOI: 10.1039/D3GC01878D.
5 A. Racha, C. Samanta, S. Sreekantan and B. Marimuthu, *Energy Fuels*, 2023, **37**, 11475–11496, DOI: 10.1021/acs.energyfuels.3c01174.
6 N. Li and M. H. Zong, *ACS Catal.*, 2022, **12**, 10080–10114, DOI: 10.1021/acscatal.2c02912.
7 Q. Li, C. Ma, J. Di, J. Ni and Y. C. He, *Bioresour. Technol.*, 2022, **34**, 126376, DOI: 10.1016/j.biortech.2021.126376.
8 V. Antón, J. Muñoz-Embid, I. Gascón, M. Artal and C. Lafuente, *Energy Fuels*, 2017, **31**, 4143–4154, DOI: 10.1021/acs.energyfuels.7b00304.
9 S. Mukherjee and M. Ghosh, *Carbohydr. Polym.*, 2017, **157**, 1076–1084, DOI: 10.1016/j.carbpol.2016.10.075.
10 M. E. Fortunato, F. Taddeo, R. Vitiello, R. Turco, R. Tesser, V. Russo and M. Di Serio, *ACS Sustainable Chem. Eng.*, 2023, **11**, 12406–12413, DOI: 10.1021/acssuschemeng.3c02882.
11 A. L. Raley, J. P. Beldin and R. J. Franks, *J. Chem. Biochem.*, 2019, **7**, DOI: 10.15640/jcb.v7n1a3.
12 R. S. Malkar, H. Daly, C. Hardacre and G. D. Yadav, *React. Chem. Eng.*, 2019, **4**, 1790–1802, DOI: 10.1039/C9RE00167K.
13 P. Kumar, R. K. Pandey, M. S. Bodas, S. P. Dagade, M. K. Dongare and A. V. Ramaswamy, *J. Mol. Catal. A: Chem.*, 2002, **181**, 207–213, DOI: 10.1016/S1381-1169(01)00365-X.
14 T. T. Mokoena, W. A. A. Ddamba and B. M. Keikotlhaile, *S. Afr. J. Chem.*, 1999, **52**, 73–78.
15 E. M. Wewerka, *J. Appl. Polym. Sci.*, 1968, **12**, 1671–1681, DOI: 10.1002/app.1968.070120716.
16 R. González, R. Martínez and P. Ortiz, *Makromol. Chem.*, 1992, **193**, 1–9, DOI: 10.1002/macp.1992.021930101.
17 H. E. Hoydonckx, D. E. De Vos, S. A. Chavan and P. A. Jacobs, *Top. Catal.*, 2004, **27**, 83–96, DOI: 10.1023/B:TOCA.0000013543.96438.1a.
18 A. Sengupta, T. Dey, M. Ghosh, J. Ghosh and S. Ghosh, *J. Inst. Eng. (India): Ser. E*, 2012, **93**, 31–36, DOI: 10.1007/s40034-013-0008-7.

19 Y. Satyawali, V. Akemeier, W. Dejonghe, H. De Wever and W. Van Hecke, *Waste Biomass Valorization*, 2019, **10**, 311–317, DOI: **10.1007/s12649-017-0060-5**.
20 M. Markiton, S. Boncel, D. Janas and A. Chrobok, *ACS Sustainable Chem. Eng.*, 2017, **5**, 1685–1691, DOI: **10.1021/acssuschemeng.6b02433**.
21 A. Szelwicka, S. Boncel, S. Jurczyk and A. Chrobok, *Appl. Catal., A*, 2019, **574**, 41–47, DOI: **10.1016/j.apcata.2019.01.030**.
22 C. Mateo, J. M. Palomo, G. Fernandez-Lorente, J. M. Guisan and R. Fernandez-Lafuente, *Enzyme Microb. Technol.*, 2017, **40**, 1451–1463, DOI: **10.1016/j.enzmictec.2007.01.018**.
23 C. Garcia-Galan, Á. Berenguer-Murcia, R. Fernandez-Lafuente and R. C. Rodrigues, *Adv. Synth. Catal.*, 2011, **353**, 2885–2904, DOI: **10.1002/adsc.201100534**.
24 E. P. Cipolatti, A. Valério, R. O. Henriques, D. E. Moritz, J. L. Ninow, D. M. G. Freire, E. A. Manoel, R. Fernandez-Lafuente and D. De Oliveira, *RSC Adv.*, 2016, **6**, 104675–104692, DOI: **10.1039/C6RA22047A**.
25 R. Fernandez-Lafuente, P. Armisén, P. Sabuquillo, G. Fernández-Lorente and J. M. Guisán, *Chem. Phys. Lipids*, 1998, **93**, 185–197, DOI: **10.1016/S0009-3084(98)00042-5**.
26 G. Fernandez-Lorente, J. Rocha-Martín and J. M. Guisan, *Methods Mol. Biol.*, 2020, **2100**, 143–158, DOI: **10.1007/978-1-0716-0215-7_9**.
27 S. Arana-Peña, N. S. Rios, D. Carballares, L. R. B. Gonçalves and R. Fernandez-Lafuente, *Catal. Today*, 2021, **362**, 130–140, DOI: **10.1016/j.cattod.2020.03.059**.
28 A. Wolny and A. Chrobok, *Nanomaterials*, 2021, **11**, 2030, DOI: **10.3390/nano11082030**.
29 A. Drozdz, A. Chrobok, S. Baj, K. Szymańska, J. Mrowiec-Białoń and A. B. JarzÈ©bski, *Appl. Catal., A*, 2013, **467**, 163–170, DOI: **10.1016/j.apcata.2013.07.009**.
30 A. Wolny, A. Siewniak, J. Zdarta, F. Ciesielczyk, P. Latos, S. Jurczyk, L. D. Nghiem, T. Jesionowski and A. Chrobok, *Environ. Technol. Innovation*, 2022, **28**, 102936, DOI: **10.1016/j.eti.2022.102936**.
31 J. J. Shangguan, Y. Q. Liu, F. J. Wang, J. Zhao, L. Q. Fan, S. X. Li and J. H. Xu, *Appl. Biochem. Biotechnol.*, 2011, **165**, 949–962, DOI: **10.1007/s12010-011-9311-2**.
32 S. Salgin and S. Takac, *Chem. Eng. Technol.*, 2007, **30**, 1739–1743, DOI: **10.1002/ceat.200700285**.
33 A. Kołodziejczak-Radzimska, J. Zdarta, F. Ciesielczyk and T. Jesionowski, *Korean J. Chem. Eng.*, 2018, **35**, 2220–2231, DOI: **10.1007/s11814-018-0146-1**.
34 R. A. Sheldon, *Green Chem.*, 2021, **23**, 8406–8427, DOI: **10.1039/D1GC03145G**.
35 P. Lozano, E. Alvarez, J. M. Bernal, S. Nieto, C. Gomez and G. Sanchez-Gomez, *Curr. Green Chem.*, 2017, **4**, 116–129, DOI: **10.2174/2213346104666171115160413**.
36 F. Ciesielczyk, M. Przybysz, J. Zdarta, A. Piasecki, D. Paukszta and T. Jesionowski, *J. Sol-Gel Sci. Technol.*, 2014, **71**, 501–513, DOI: **10.1007/s10971-014-3398-1**.
37 R. M. Blanco, P. Terreros, M. Fernández-Pérez, C. Otero and G. Diaz-Gonzalez, *J. Mol. Catal. B: Enzym.*, 2004, **30**, 83–93, DOI: **10.1016/j.molcatb.2004.03.012**.
38 J. Lin, Y. Cheng, O. M. Lai, C. P. Tan, W. Panpipat, C. Shen and L. Z. Cheong, *ChemistrySelect*, 2022, **7**, e202202721, DOI: **10.1002/slct.202202721**.
39 A. Kumar, K. Dhar and S. S. Kanwar, *Biol. Proced. Online*, 2016, **18**, DOI: **10.1186/s12575-016-0033-2**.
40 J. Toida, K. Kondoh, M. Fukuzawa, K. Ohnishi and J. Sekiguchi, *Biosci., Biotechnol., Biochem.*, 1995, **59**, 1199–1203, DOI: **10.1271/bbb.59.1199**.
41 P. De Santntis, L. E. Meyer and S. Kara, *React. Chem. Eng.*, 2020, **5**, 2155–2184, DOI: **10.1039/D0RE00335B**.
42 J. Coloma, Y. Guiavarc'h, P. L. Hagedoorn and U. Hanefeld, *Catal. Sci. Technol.*, 2020, **10**, 3613–3621, DOI: **10.1039/D0CY00604A**.
43 Q. Peng, B. Zang, W. Zhao, D. Li, J. Ren, F. Ji and L. Jia, *Catal. Sci. Technol.*, 2020, **10**, 484–492, DOI: **10.1039/C9CY01856E**.
44 L. Capaldo, Z. Wen and T. Noël, *Chem. Sci.*, 2023, **14**, 4230–4247, DOI: **10.1039/D3SC00992K**.
45 Ł. Janczewski, D. Zieliński and B. Kolesińska, *Open Chem.*, 2021, **19**, 265–280, DOI: **10.1515/chem-2021-0034**.
46 C. R. McElroy, A. Constantinou, L. C. Jones, L. Summerton and J. H. Clark, *Green Chem.*, 2015, **17**, 3111–3121, DOI: **10.1039/C5GC00340G**.
47 P. Jessop, *Green Chem.*, 2020, **22**, 13–15, DOI: **10.1039/C9GC90119A**.
48 V. K. Vaidyanathan, K. Saikia, P. S. Kumar, A. K. Rathankumar, G. Rangasamy and G. D. Saratale, *Bioresour. Technol.*, 2023, **378**, 128975, DOI: **10.1016/j.biortech.2023.128975**.
49 Y. Bao, Z. Du, X. Liu, H. Liu, J. Tang, C. Qin, C. Liang, C. Huang and S. Yao, *Green Chem.*, 2024, **26**, 6318–6338, DOI: **10.1039/D4GC00883A**.
50 K. J. Yong, T. Y. Wu, C. B. T. Loong Lee, Z. J. Lee, Q. Liu, J. Md Jahim, Q. Zhou and L. Zhang, *Biomass Bioenergy*, 2022, **161**, 106458, DOI: **10.1016/j.biombioe.2022.106458**.
51 Y. Chen, Y. She, J. Lei, D. Wang, S. Wu and K. Men, *IOP Conf. Ser.: Earth Environ. Sci.*, 2021, **705**, 012013, DOI: **10.1088/1755-1315/705/1/012013**.
52 J. H. Ahn, K. H. Jung, E. S. Lim, S. M. Kim, S. O. Han and Y. Um, *Bioresour. Technol.*, 2023, **381**, 129147, DOI: **10.1016/j.biortech.2023.129147**.
53 N. S. Sarai, B. J. Levin, J. M. Roberts, D. E. Katsoulis and F. H. Arnold, *ACS Cent. Sci.*, 2021, **7**, 944–953, DOI: **10.1021/acscentsci.1c00182**.

Electronic Supplementary Information (ESI)

Robust biocatalyst for the green continuous flow synthesis of esters from biomass-derived furfuryl alcohol and C_8-C_{18} carboxylic acids

Anna Wolny,[a] Dagmara Więcławik,[a] Jakub Zdarta,[b], Sebastian Jurczyk[c], Teofil Jesionowski,[b] Anna Chrobok[a]*

[a] Department of Chemical Organic Technology and Petrochemistry, Faculty of Chemistry, Silesian University of Technology, Krzywoustego 4, PL-44100 Gliwice, Poland, anna.chrobok@polsl.pl

[b] Institute of Chemical Technology and Engineering, Faculty of Chemical Technology, Poznan University of Technology, Berdychowo 4, PL-60965 Poznan, Poland, teofil.jesionowski@put.poznan.pl

[c] Institute for Engineering of Polymer Materials and Dyes, Lukasiewicz Research Network, Sklodowskiej-Curie 55, PL-87100 Torun, Poland

Space-time-yield (STY) for batch process

$STY = m_{product}/t_{reaction\ time}V_{biocatalyst}$ $(gh^{-1}L^{-1})$
$STY = 0.0884g / 0.75h \cdot 0.000368L = 320.7\ (gh^{-1}L^{-1})$

Specific productivity (SP) for batch process

$SP = m_{product}/t_{reaction\ time}m_{protein}$ $(gh^{-1}mg^{-1})$
$SP = 0.0884g / 0.75h \cdot 6.36mg = 0.019\ (gh^{-1}mg^{-1})$

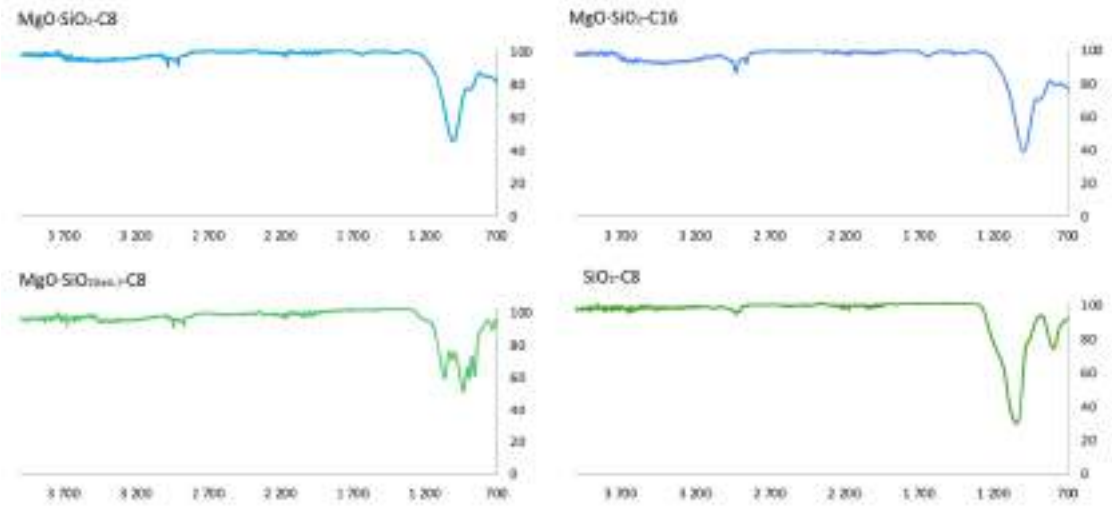

Fig. S1. FT-IR analysis of $MgO{\cdot}SiO_2$-C_8, $MgO{\cdot}SiO_2$-C_{16}, $MgO{\cdot}SiO_2$-$C_{8(calc.)}$, SiO_2-C_8.

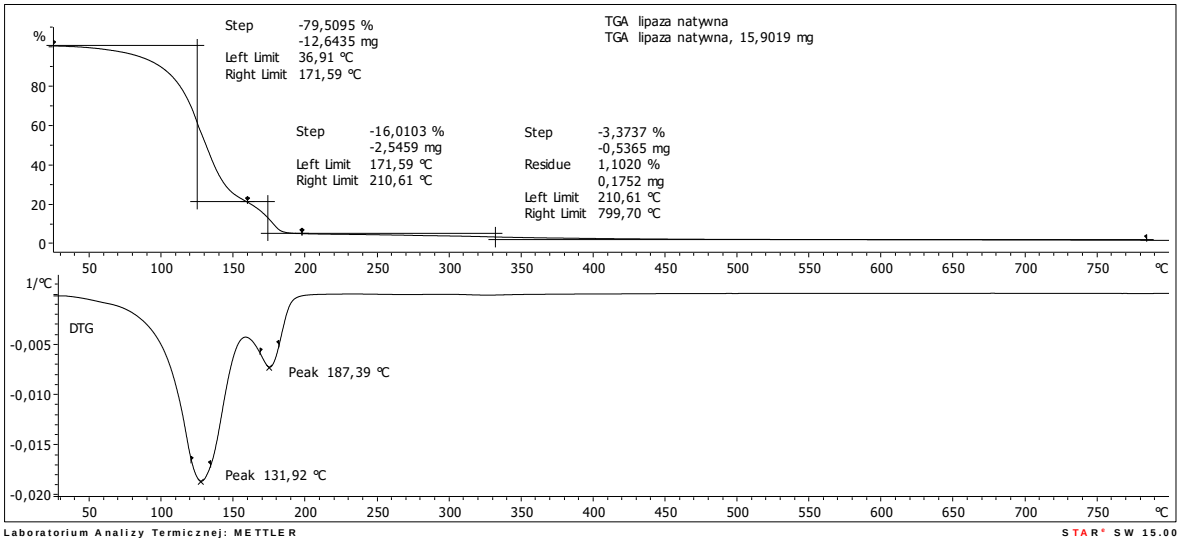

Fig. S2. TG/DTG analysis of LAO.

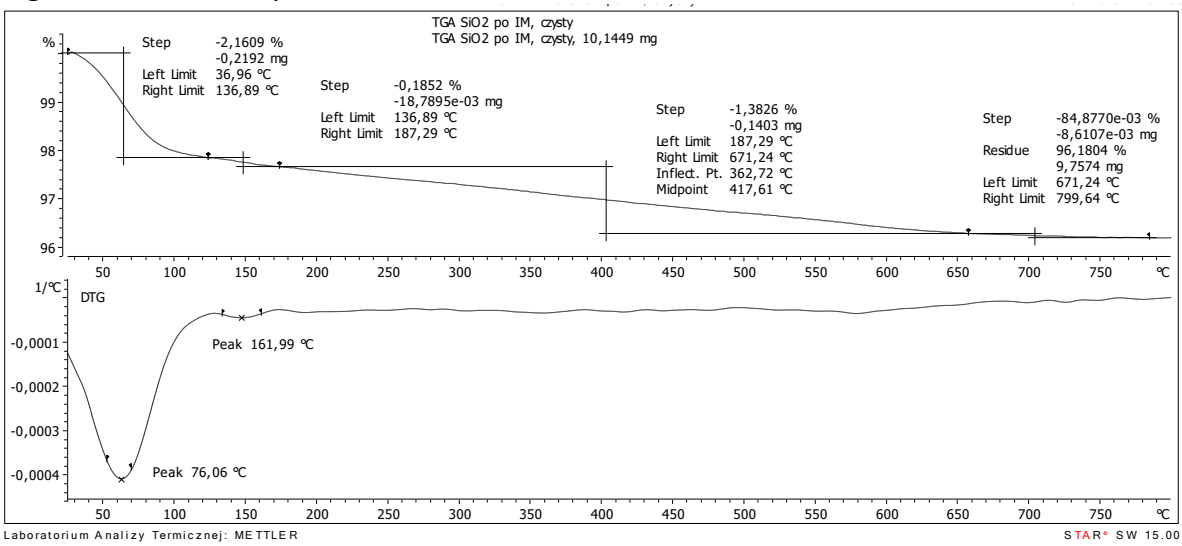

Fig. S3. TG/DTG analysis of SiO_2.

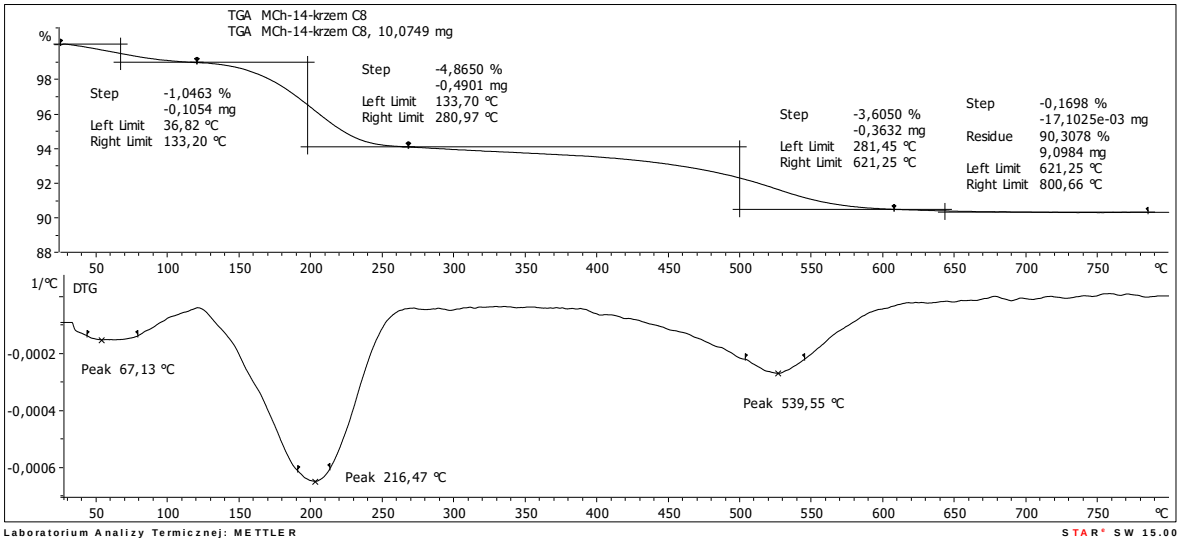

Fig. S4. TG/DTG analysis of SiO_2-C_8.

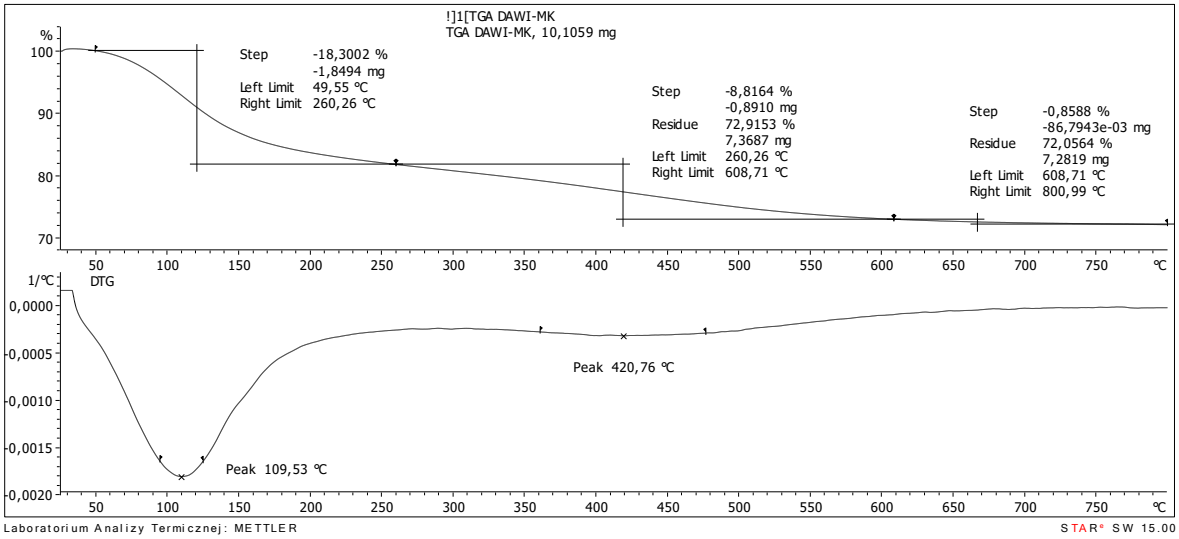

Fig. S5. TG/DTG analysis of $MgO \cdot SiO_2$.

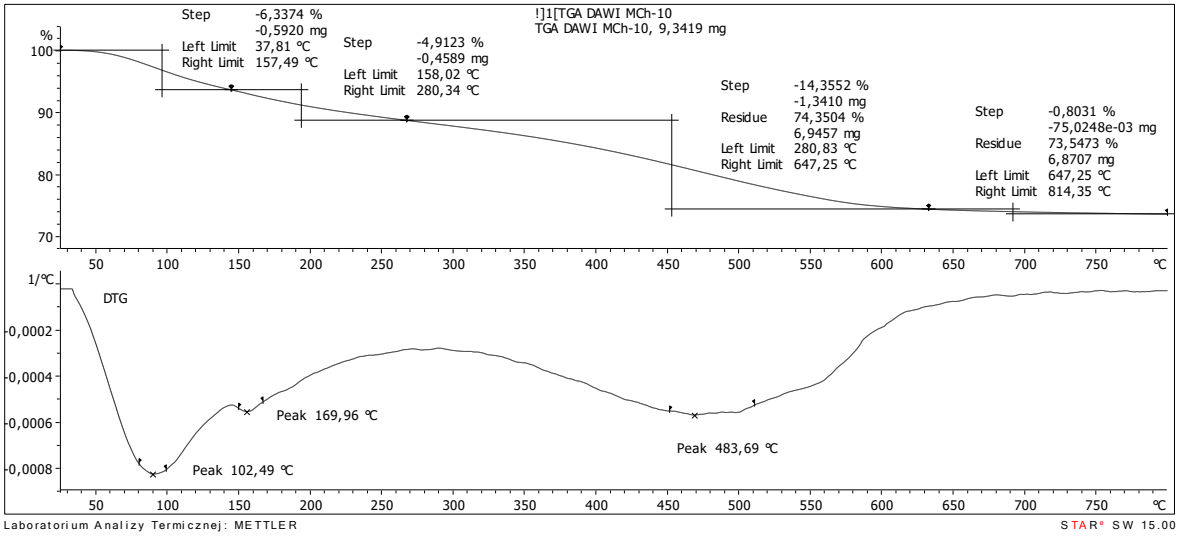

Fig. S6. TG/DTG analysis of $MgO \cdot SiO_2$-C_8.

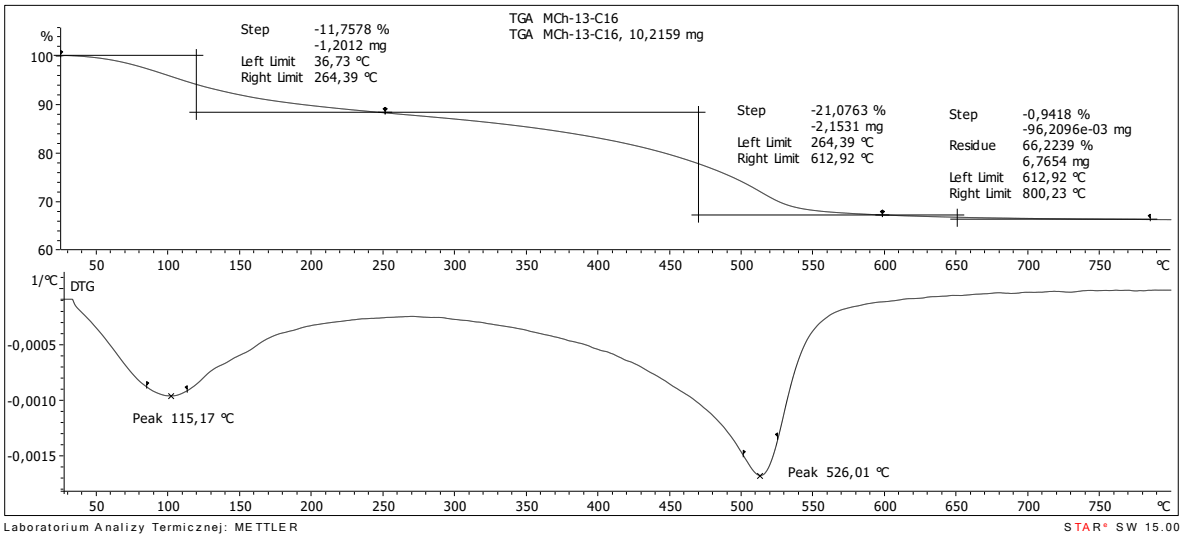

Fig. S7. TG/DTG analysis of $MgO \cdot SiO_2$-C_{16}.

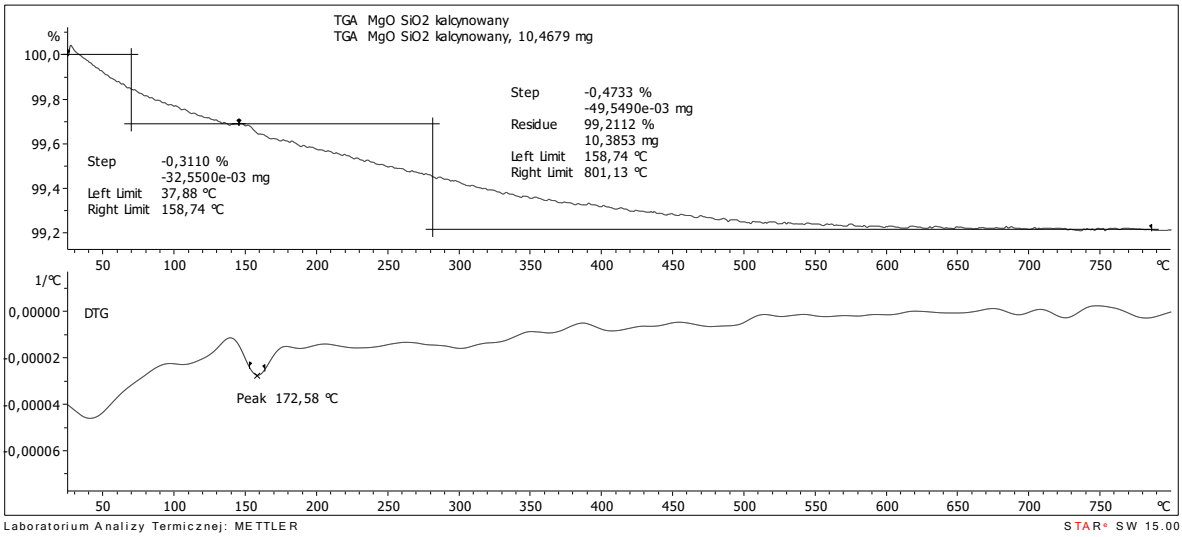

Fig. S8. TG/DTG analysis of $MgO \cdot SiO_{2(calc.)}$.

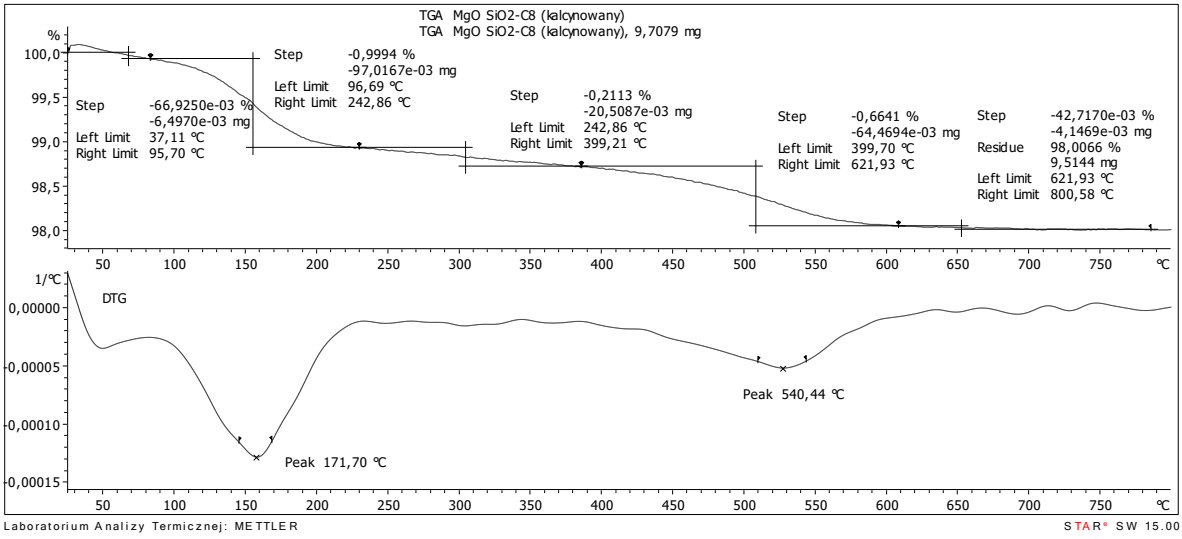

Fig. S9. TG/DTG analysis of $MgO \cdot SiO_{2(calc.)}$-C_8.

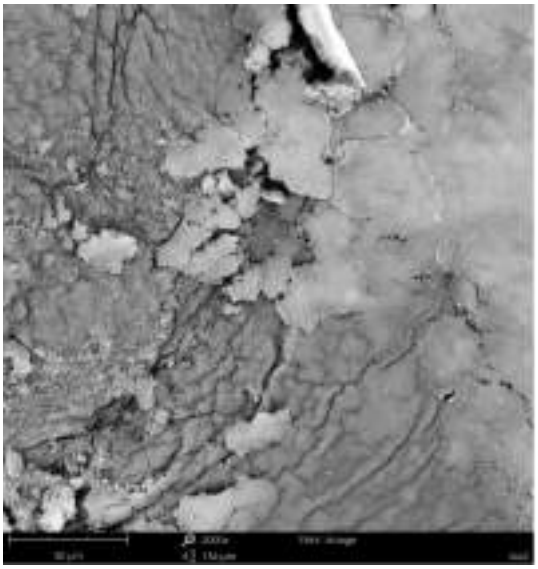

Element Number	Element Symbol	Element Name	Atomic Conc.	Weight Conc.
8	O	Oxygen	72.04	59.47
14	Si	Silicon	27.96	40.53

Fig. S10. SEM-EDS analysis SiO_2.

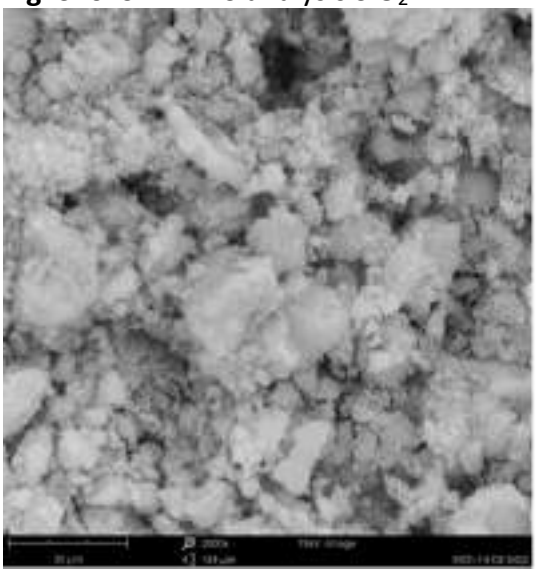

Element Number	Element Symbol	Element Name	Atomic Conc.	Weight Conc.
8	O	Oxygen	68.75	56.68
14	Si	Silicon	29.50	43.21
6	C	Carbon	1.75	0.11

Fig. S11. SEM-EDS analysis SiO_2-C_8.

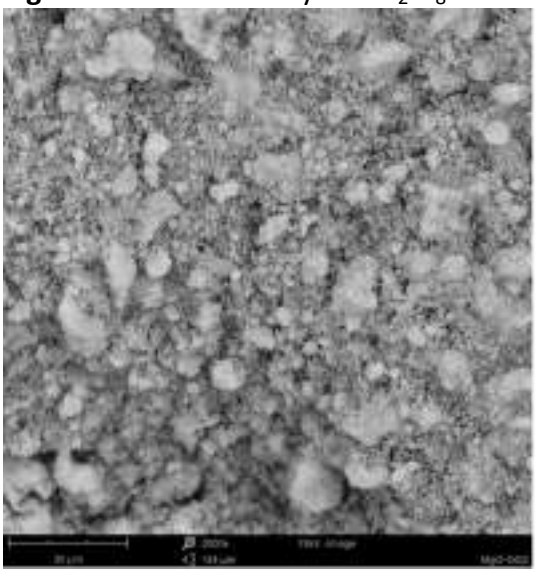

Element Number	Element Symbol	Element Name	Atomic Conc.	Weight Conc.
8	O	Oxygen	68.42	56.74
14	Si	Silicon	17.80	25.90
12	Mg	Magnesium	13.78	17.36

Fig. S12. SEM-EDS analysis $MgO{\cdot}SiO_2$.

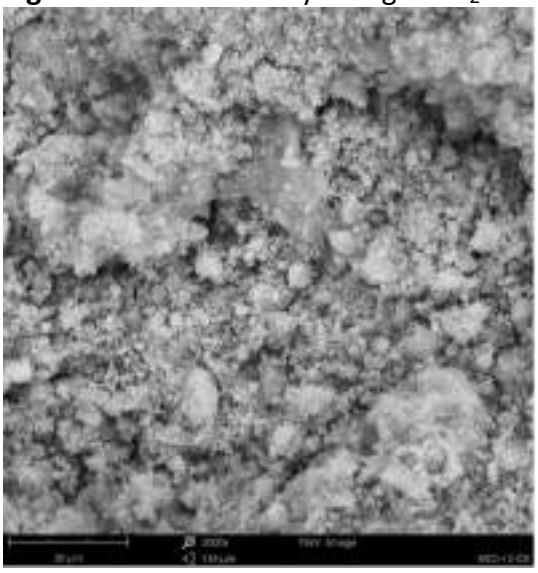

Element Number	Element Symbol	Element Name	Atomic Conc.	Weight Conc.
8	O	Oxygen	62.92	53.67
14	Si	Silicon	16.98	25.42
12	Mg	Magnesium	12.27	15.90
6	C	Carbon	7.83	5.01

Fig. S13. SEM-EDS analysis $MgO{\cdot}SiO_2$-C_8.

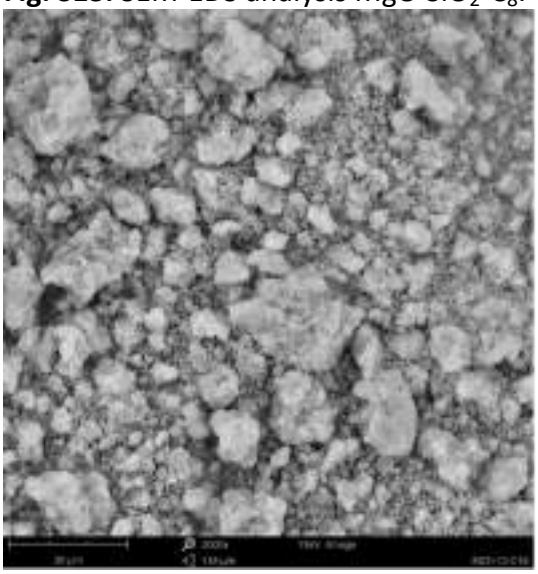

Element Number	Element Symbol	Element Name	Atomic Conc.	Weight Conc.
8	O	Oxygen	67.57	59.21
14	Si	Silicon	14.07	21.64
12	Mg	Magnesium	10.52	14.00
6	C	Carbon	7.84	5.16

Fig. S14. SEM-EDS analysis MgO·SiO_2-C_{16}.

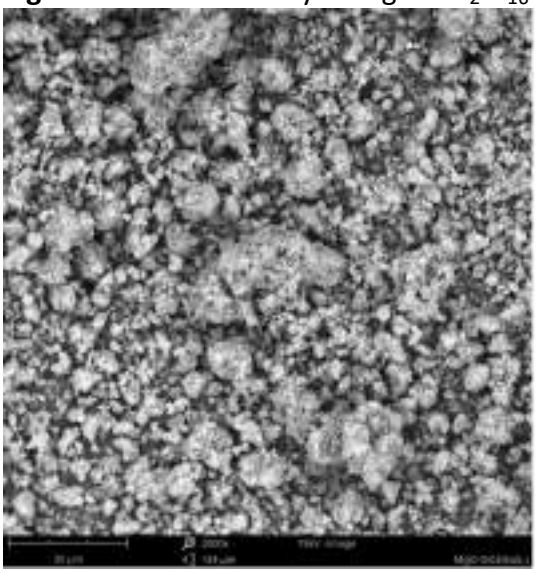

Element Number	Element Symbol	Element Name	Atomic Conc.	Weight Conc.
8	O	Oxygen	54.63	41.83
14	Si	Silicon	27.34	36.88
12	Mg	Magnesium	18.24	21.29

Fig. S15. SEM-EDS analysis MgO·$SiO_{2(calc.)}$.

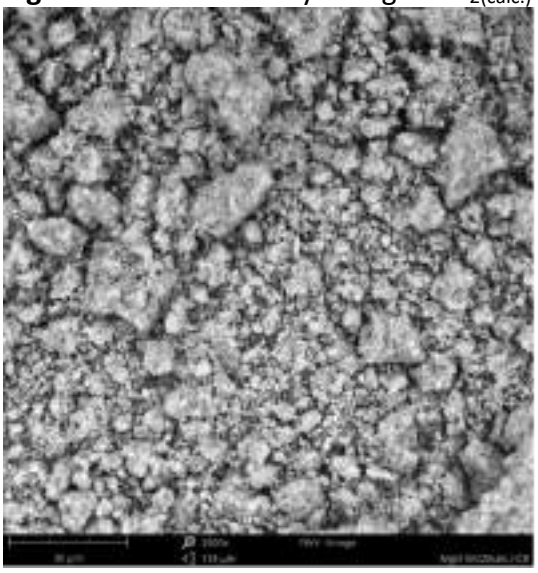

Element Number	Element Symbol	Element Name	Atomic Conc.	Weight Conc.
8	O	Oxygen	65.28	56.13
14	Si	Silicon	15.10	22.80
12	Mg	Magnesium	12.72	16.61
6	C	Carbon	6.90	4.46

Fig. S16. SEM-EDS analysis MgO·$SiO_{2(calc.)}$-C_8.

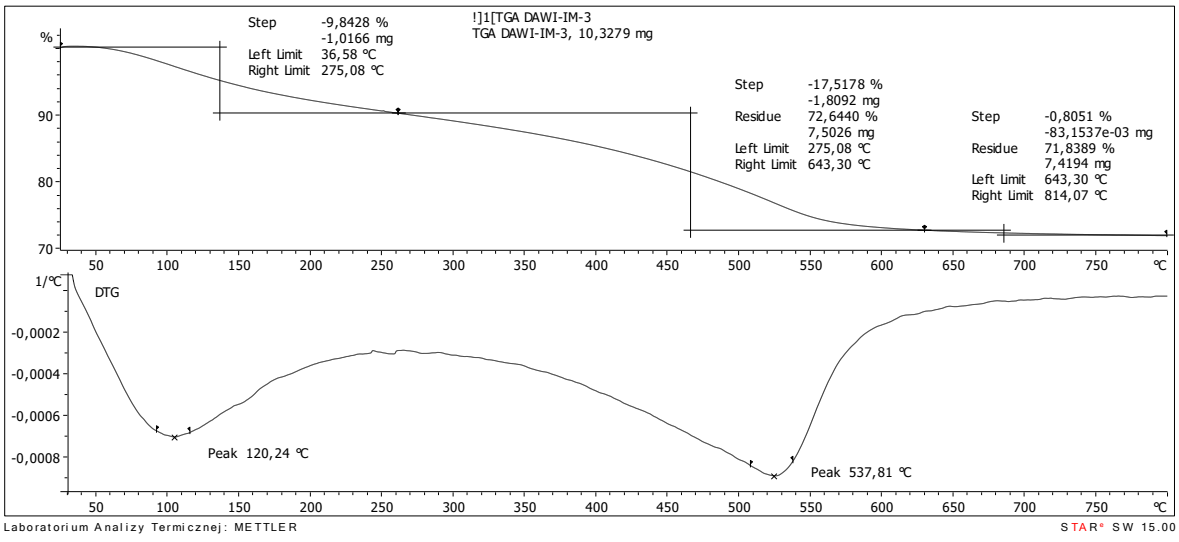

Fig. S17. TG/DTG analysis of MgO·SiO_2-C_8-LAO.

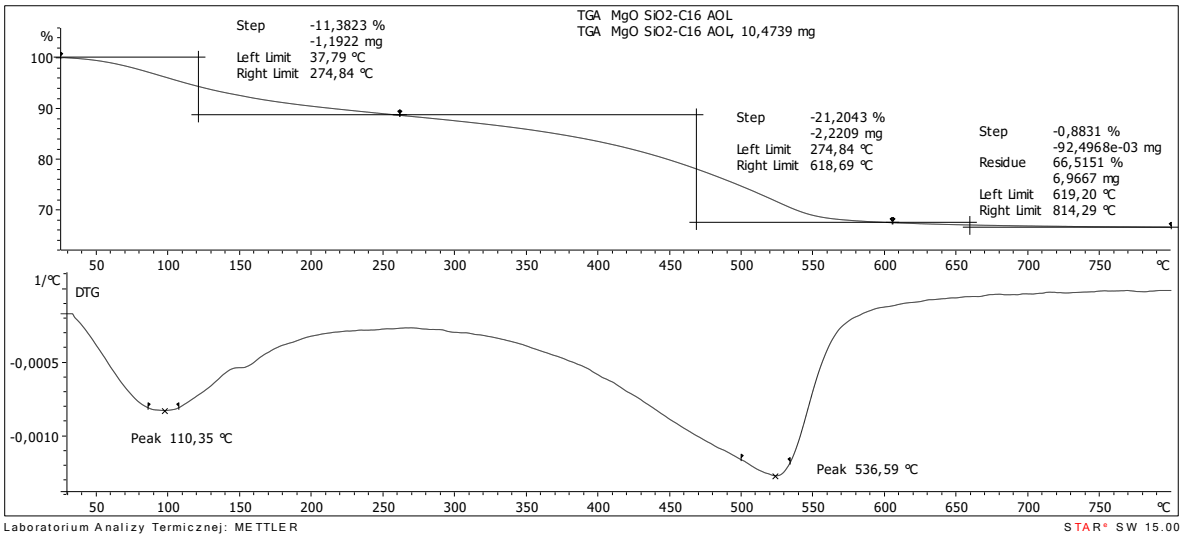

Fig. S18. TG/DTG analysis of $MgO \cdot SiO_2$-C_{16}-LAO.

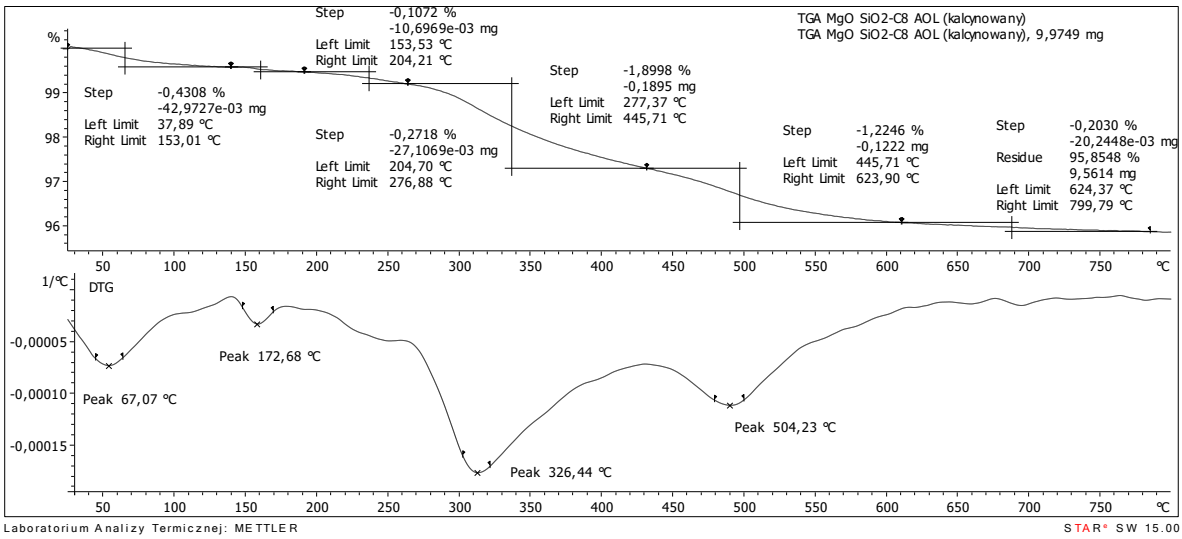

Fig. S19. TG/DTG analysis of $MgO \cdot SiO_{2(calc.)}$-C_8-LAO.

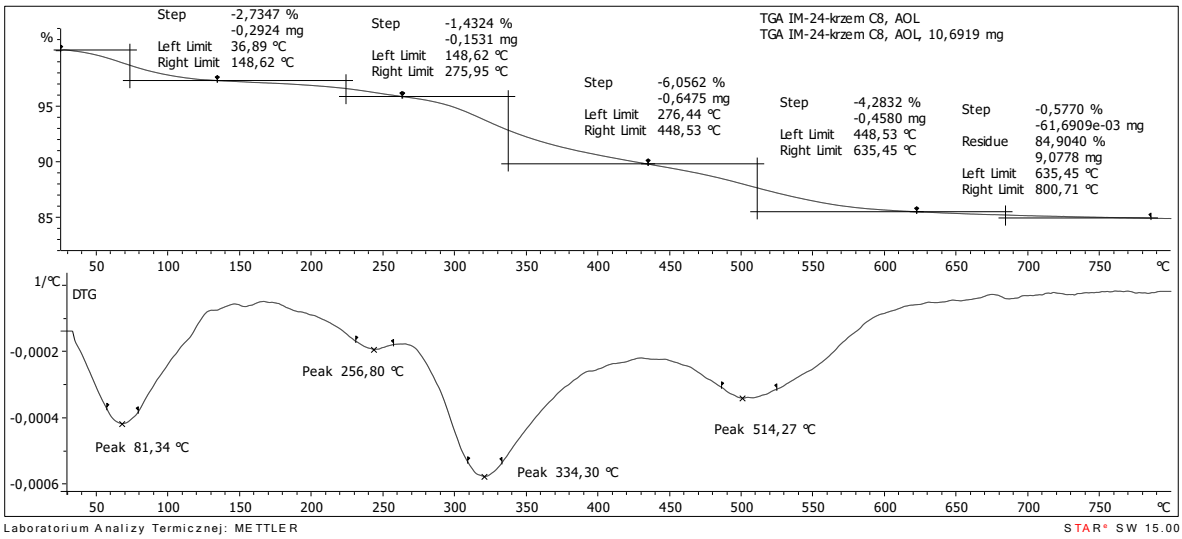

Fig. S20. TG/DTG analysis of SiO_2-C_8-LAO.

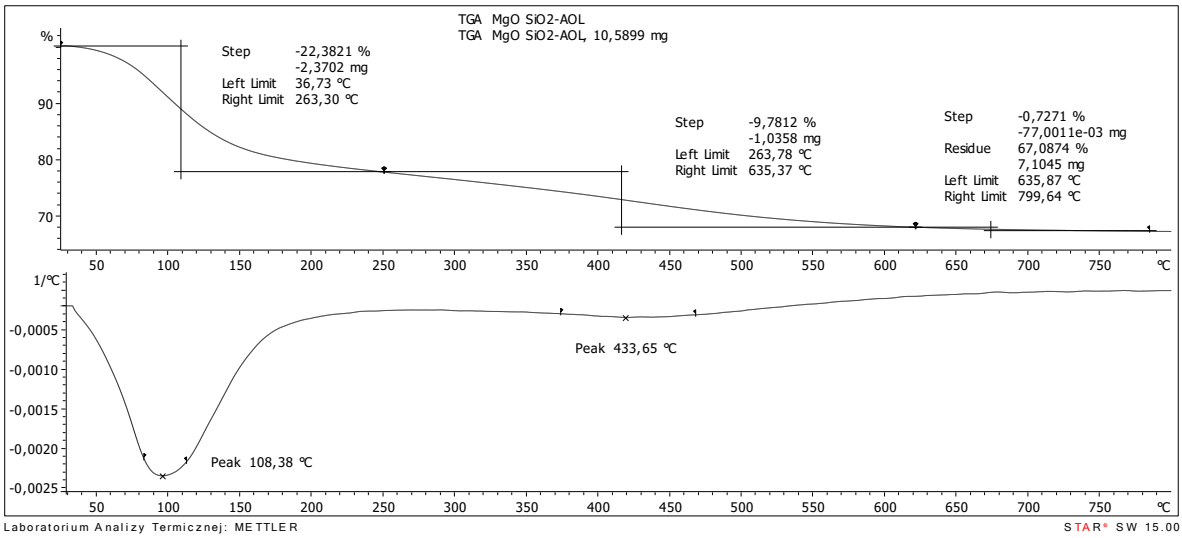

Fig. S21. TG/DTG analysis of MgO·SiO_2-LAO.

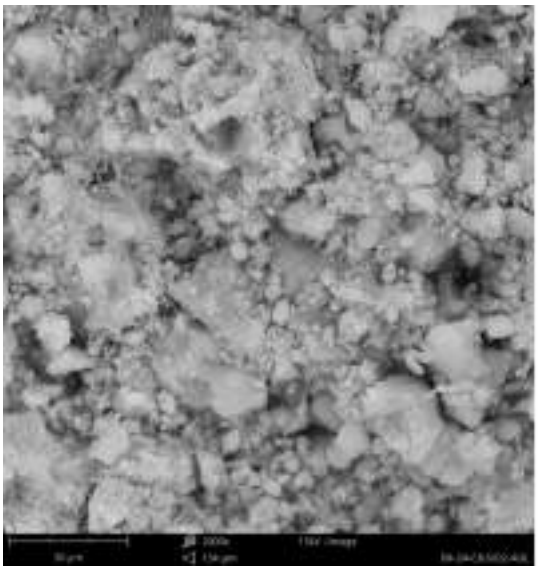

Element Number	Element Symbol	Element Name	Atomic Conc.	Weight Conc.
8	O	Oxygen	66.04	58.09
14	Si	Silicon	21.39	33.03
6	C	Carbon	8.53	5.63
7	N	Nitrogen	3.61	2.78
9	F	Fluorine	0.41	0.43
16	S	Sulfur	0.02	0.04

Fig. S22. SEM-EDS analysis of SiO_2-LAO.

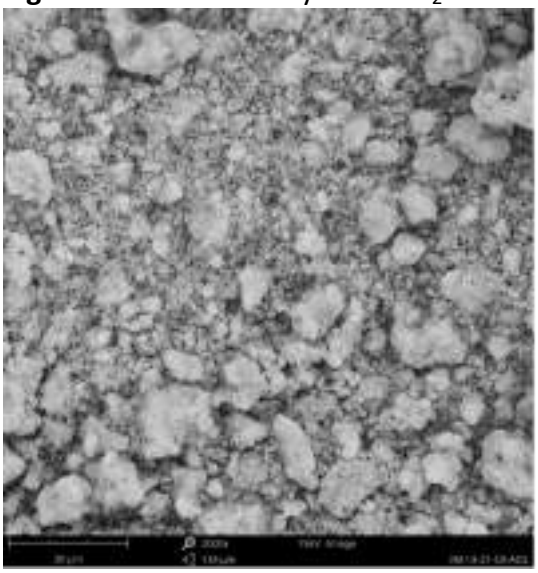

Element Number	Element Symbol	Element Name	Atomic Conc.	Weight Conc.
8	O	Oxygen	69.29	60.30
14	Si	Silicon	13.34	20.38
12	Mg	Magnesium	11.34	14.99
6	C	Carbon	3.85	2.52
7	N	Nitrogen	1.81	1.38
9	F	Fluorine	0.29	0.30
15	P	Phosphorus	0.06	0.10
16	S	Sulfur	0.02	0.04

Fig. S23. SEM-EDS analysis of MgO·SiO_2-C_8-LAO.

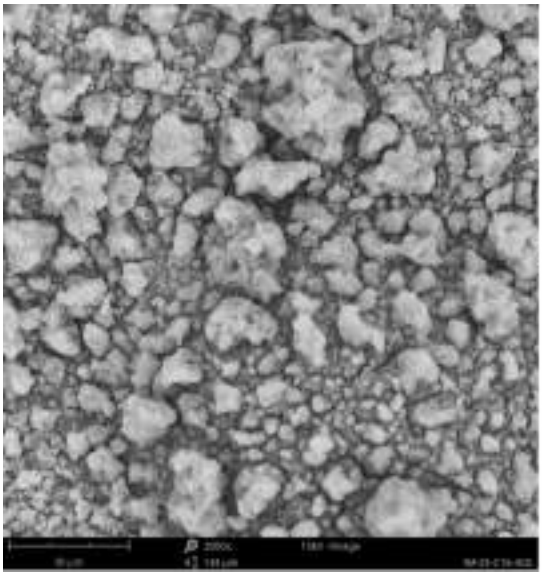

Element Number	Element Symbol	Element Name	Atomic Conc.	Weight Conc.
8	O	Oxygen	65.74	58.63
14	Si	Silicon	12.23	19.15
12	Mg	Magnesium	10.33	14.00
6	C	Carbon	9.52	6.38
7	N	Nitrogen	1.79	1.39
9	F	Fluorine	0.32	0.33
15	P	Phosphorus	0.04	0.06
16	S	Sulfur	0.03	0.05

Fig. S24. SEM-EDS analysis of $MgO{\cdot}SiO_2$-C_{16}-LAO.

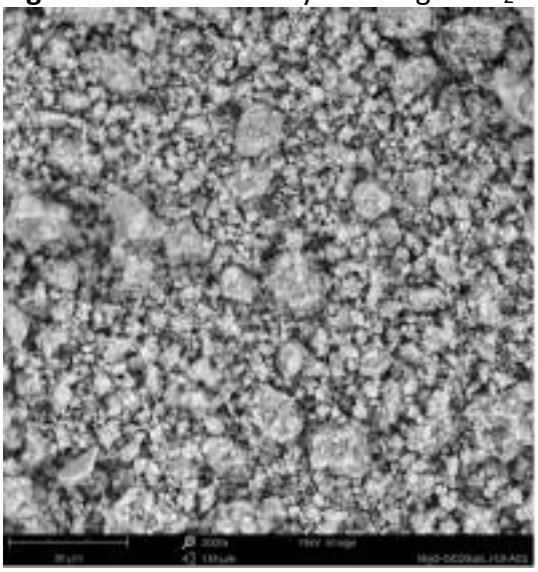

Element Number	Element Symbol	Element Name	Atomic Conc.	Weight Conc.
8	O	Oxygen	60.27	53.24
14	Si	Silicon	12.79	21.38
12	Mg	Magnesium	11.33	15.21
6	C	Carbon	10.12	6.71
7	N	Nitrogen	4.49	3.47

Fig. S25. SEM-EDS analysis of $MgO{\cdot}SiO_{2(calc.)}$-C_8-LAO.

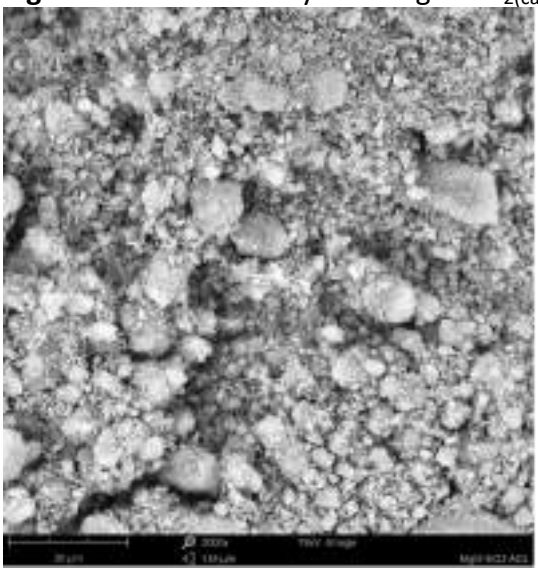

Element Number	Element Symbol	Element Name	Atomic Conc.	Weight Conc.
8	O	Oxygen	56.58	48.77
14	Si	Silicon	17.52	26.51
12	Mg	Magnesium	11.12	14.56
6	C	Carbon	9.19	5.94
7	N	Nitrogen	5.59	4.22

Fig. S26. SEM-EDS analysis of $MgO{\cdot}SiO_2$-LAO.

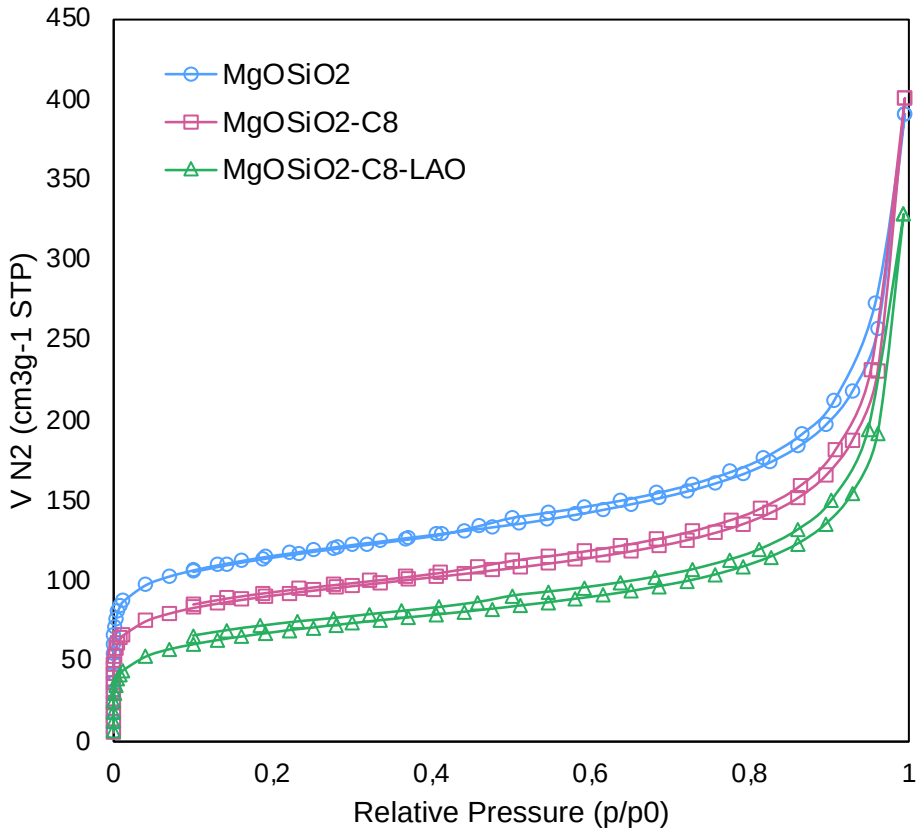

Fig. S27. Adsorption-desorption isotherms of MgO·SiO_2, MgO·SiO_2-C_8, MgO·SiO_2-C_8-LAO.

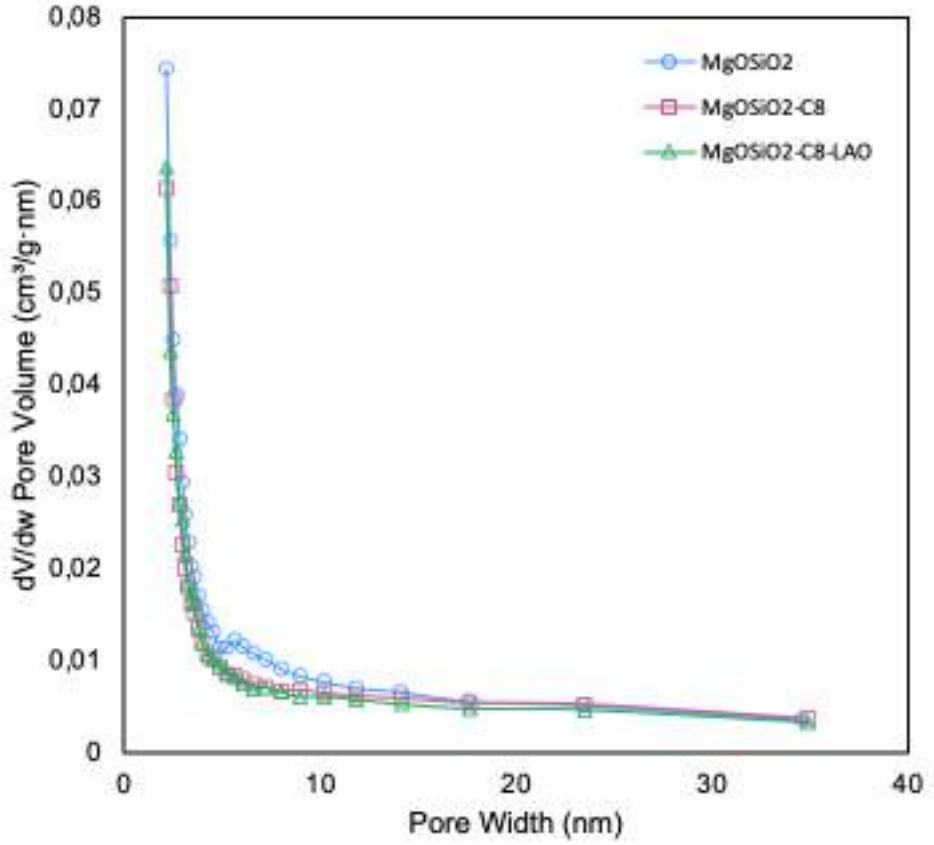

Fig. S28. Pore size distributions of MgO·SiO_2, MgO·SiO_2-C_8, MgO·SiO_2-C_8-LAO.

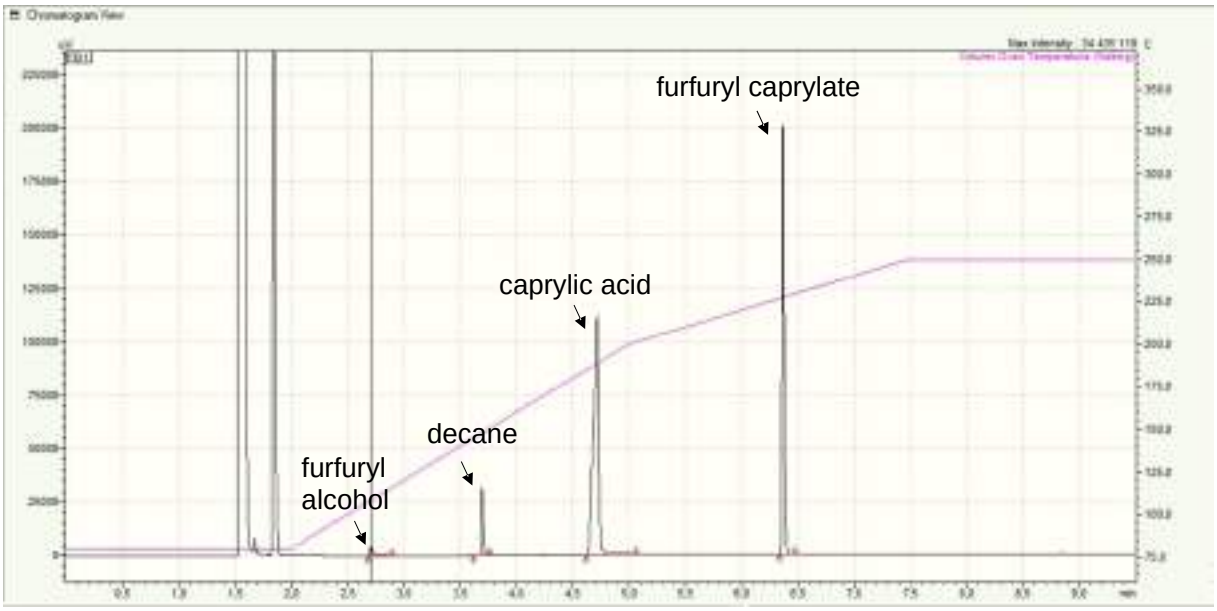

Fig. S29. Chromatogram GC analysis of esterification of furfuryl alcohol and caprylic acid.

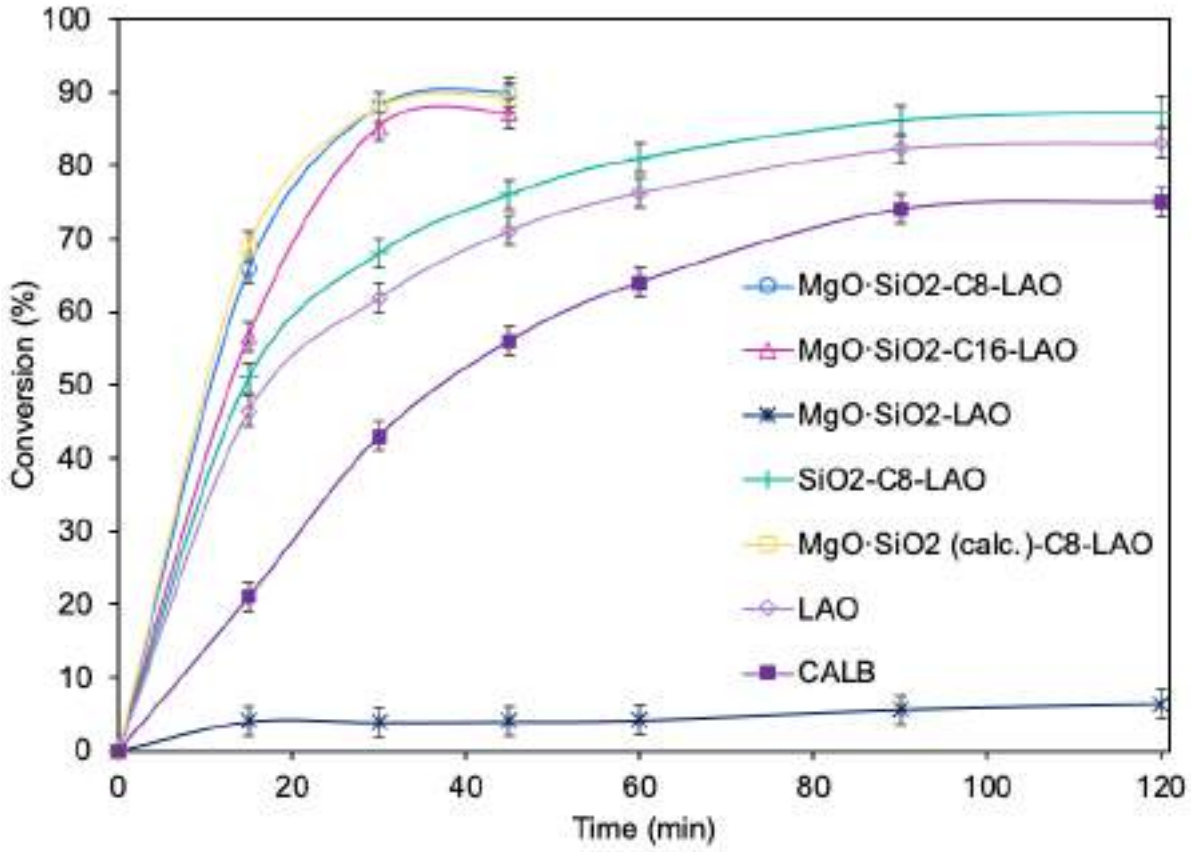

Fig. S30. The influence of siliceous support modification on biocatalyst performance on furfuryl alcohol esterification.

Reaction conditions: furfuryl alcohol 1.0 mmol, caprylic acid 3.0 mmol, cyclohexane 0.5 mL, biocatalyst containing 6.36 mg of LAO, (146 µL of LAO solution (43.7 $mgmL^{-1}$); 530 µL of CALB solution (12 $mgmL^{-1}$); 300 mg of $MgO{\cdot}SiO_2$-LAO; 69 mg of SiO_2-C_8-LAO; 150 mg of $MgO{\cdot}SiO_2$-C_8-LAO; 294 mg of $MgO{\cdot}SiO_{2(calc)}$-C_8-LAO; 413 mg of $MgO{\cdot}SiO_2$-C_{16}-LAO;), 25℃, 250 rpm; determined using GC).

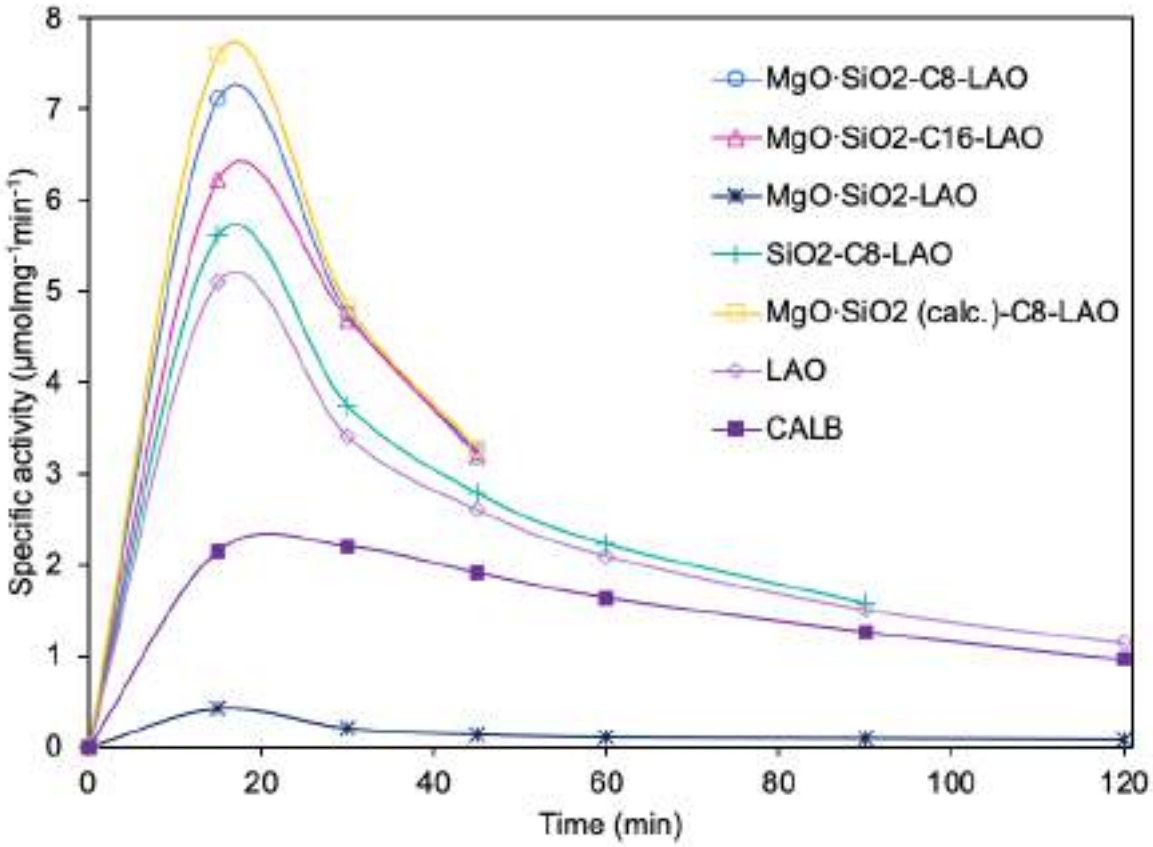

Fig. S31. The influence of siliceous support modification on biocatalyst performance on furfuryl alcohol esterification.

Reaction conditions: furfuryl alcohol 1.0 mmol, caprylic acid 3.0 mmol, cyclohexane 0.5 mL, biocatalyst containing 6.36 mg of LAO, (146 μL of LAO solution (43.7 $mgmL^{-1}$); 530 μL of CALB solution (12 $mgmL^{-1}$); 300 mg of MgO·SiO_2-LAO; 69 mg of SiO_2-C_8-LAO; 150 mg of MgO·SiO_2-C_8-LAO; 294 mg of MgO·$SiO_{2(calc)}$-C_8-LAO; 413 mg of MgO·SiO_2-C_{16}-LAO;), 25℃, 250 rpm; determined using GC).

Fig. S32. TG/DTG analysis of MgO·SiO_2-C_8-LAO after recycling.

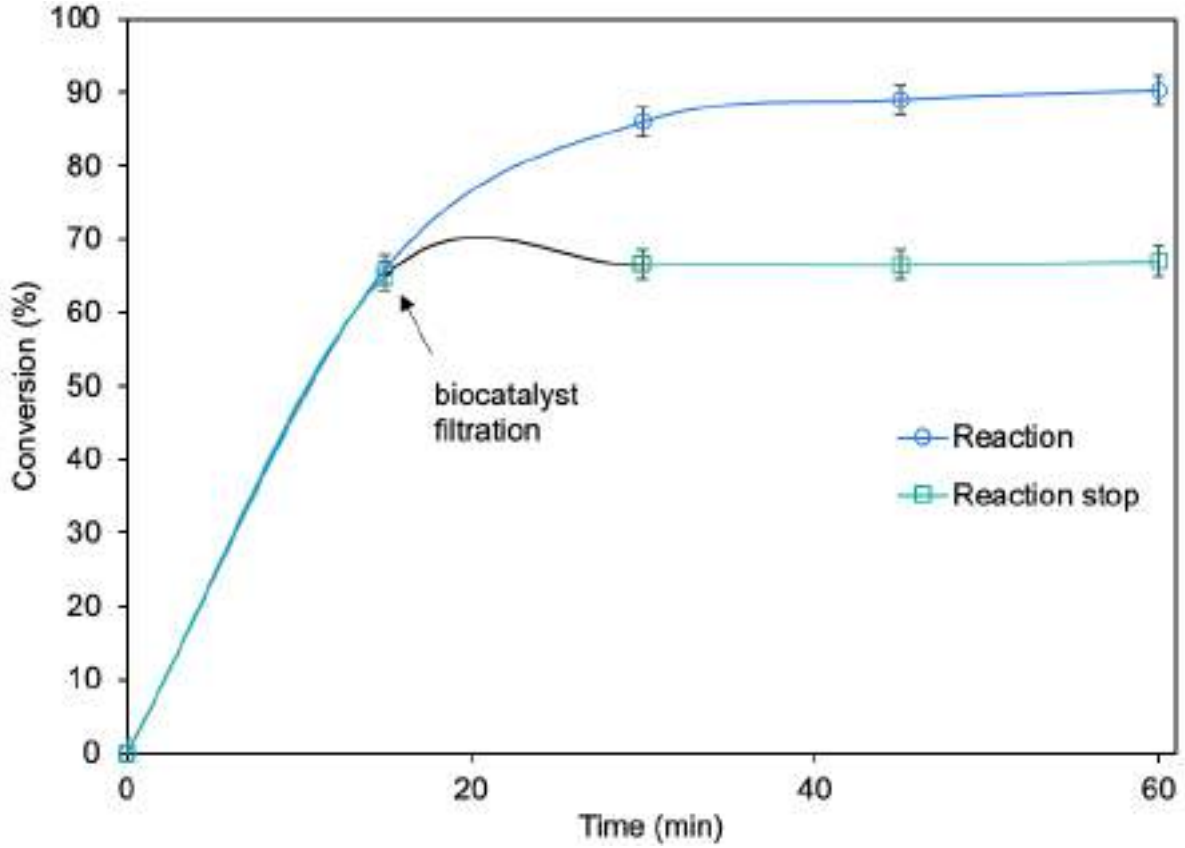

Fig. S33. Fast biocatalyst filtration from reaction mixture. “Reaction stop” experiment.

Reaction conditions: furfuryl alcohol 1.0 mmol, caprylic acid 3.0 mmol, cyclohexane 0.5 mL, biocatalyst (6.36 mg of lipase, *e.g.* 150 mg of MgO·SiO_2-C_8-LAO), 25℃, 250 rpm.

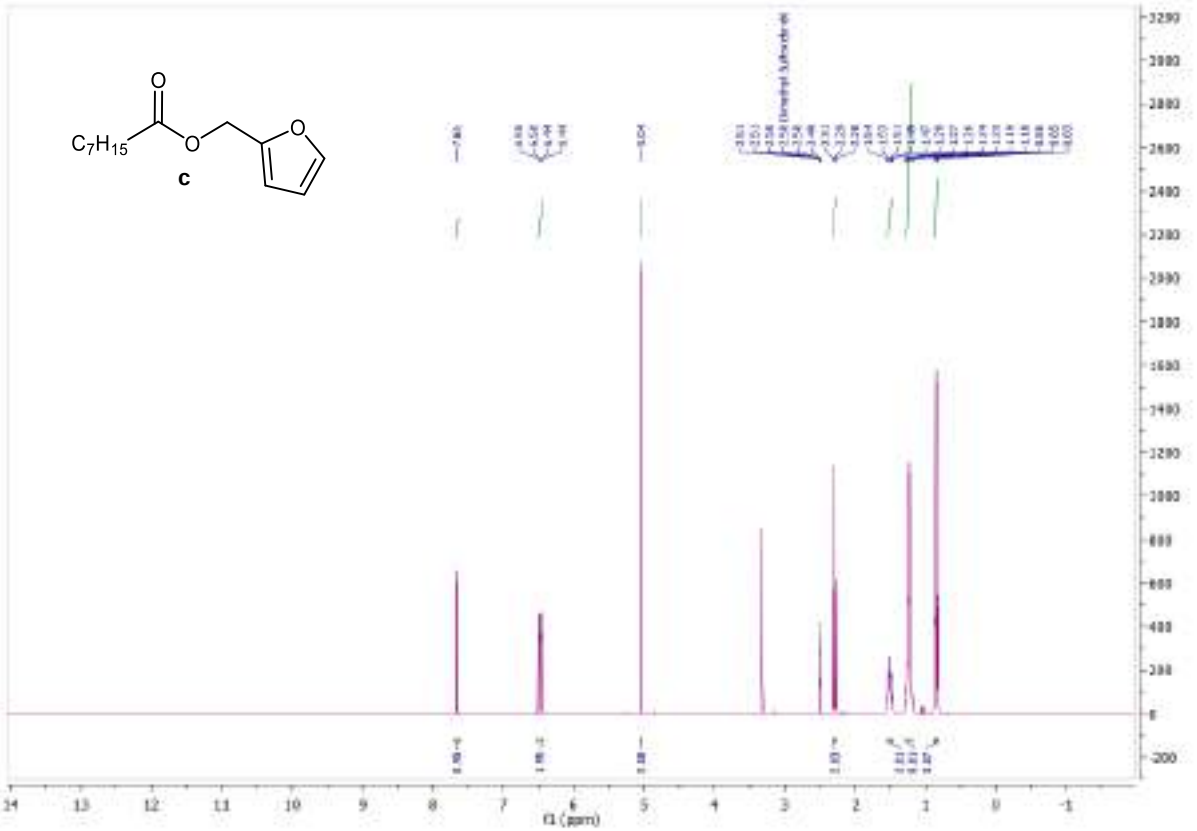

Fig. S34. ^{1}H NMR spectra of furfuryl caprylate (c).

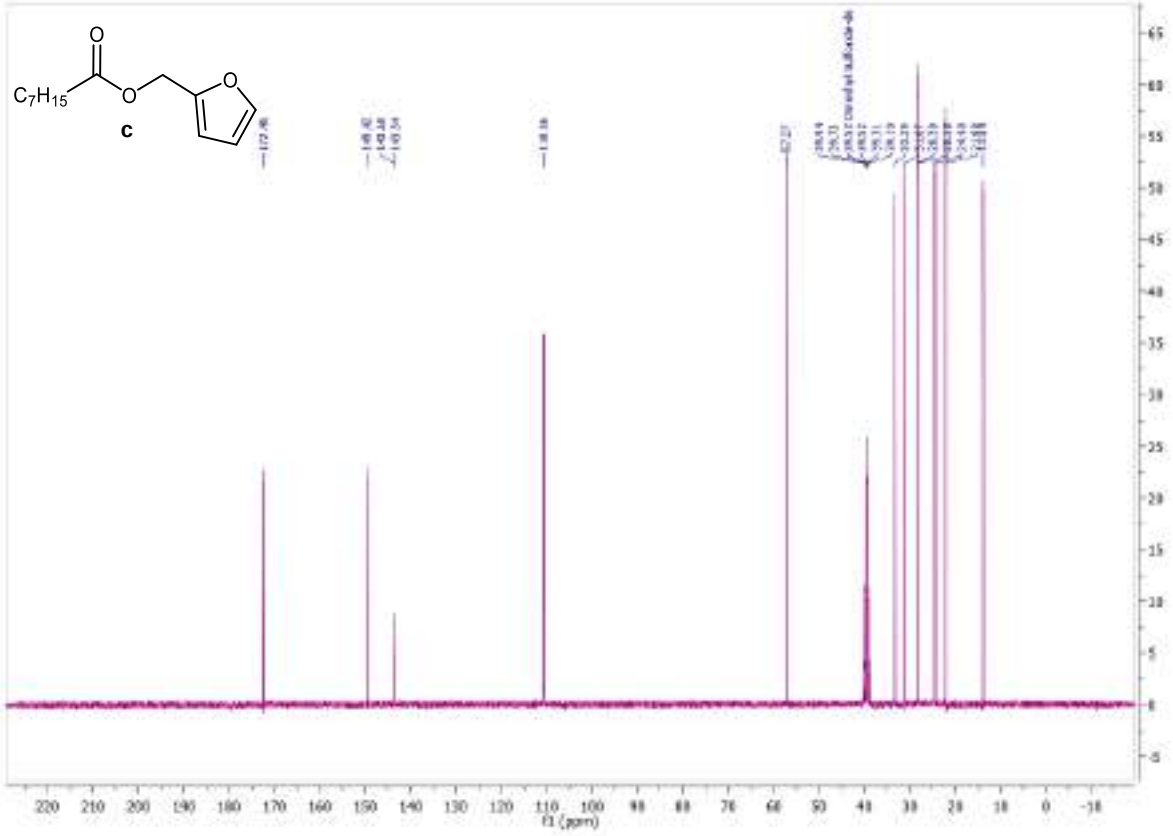

Fig. S35. ^{13}C NMR spectra of furfuryl caprylate (c).

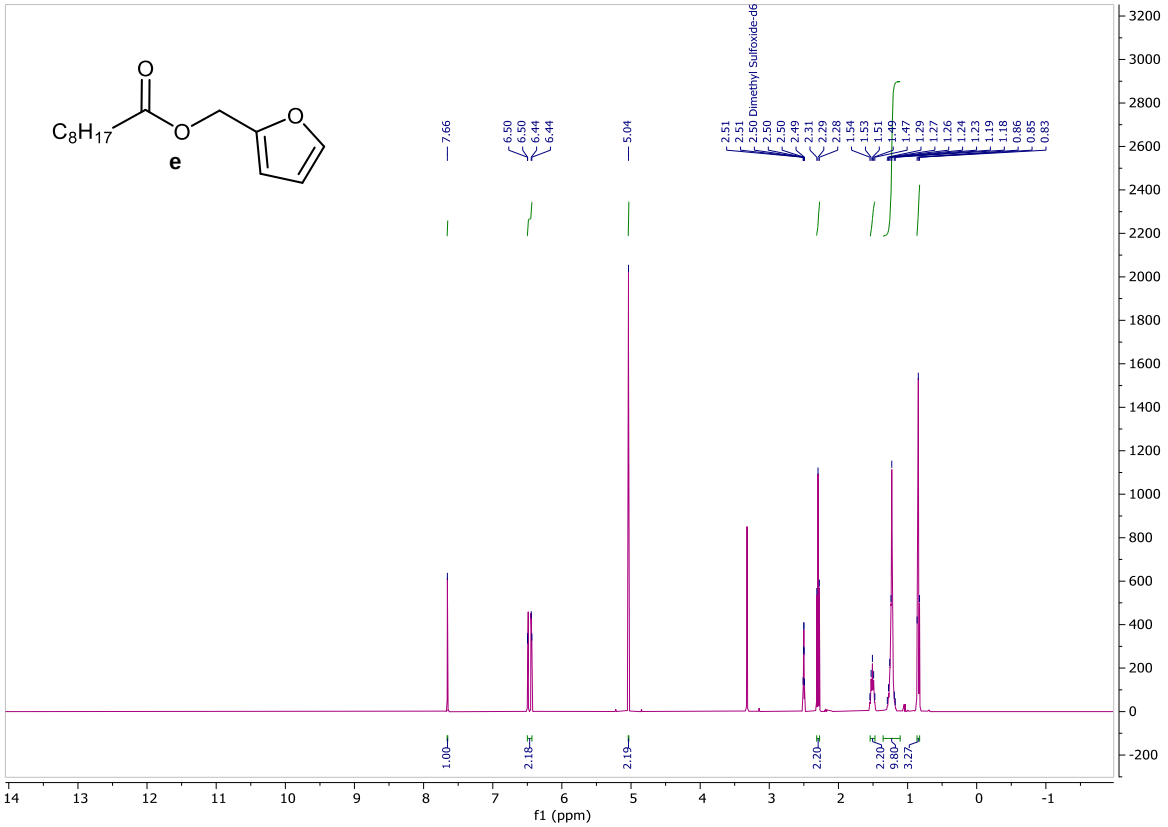

Fig. S36. ^{1}H NMR spectra of furfuryl nonanoate (e).

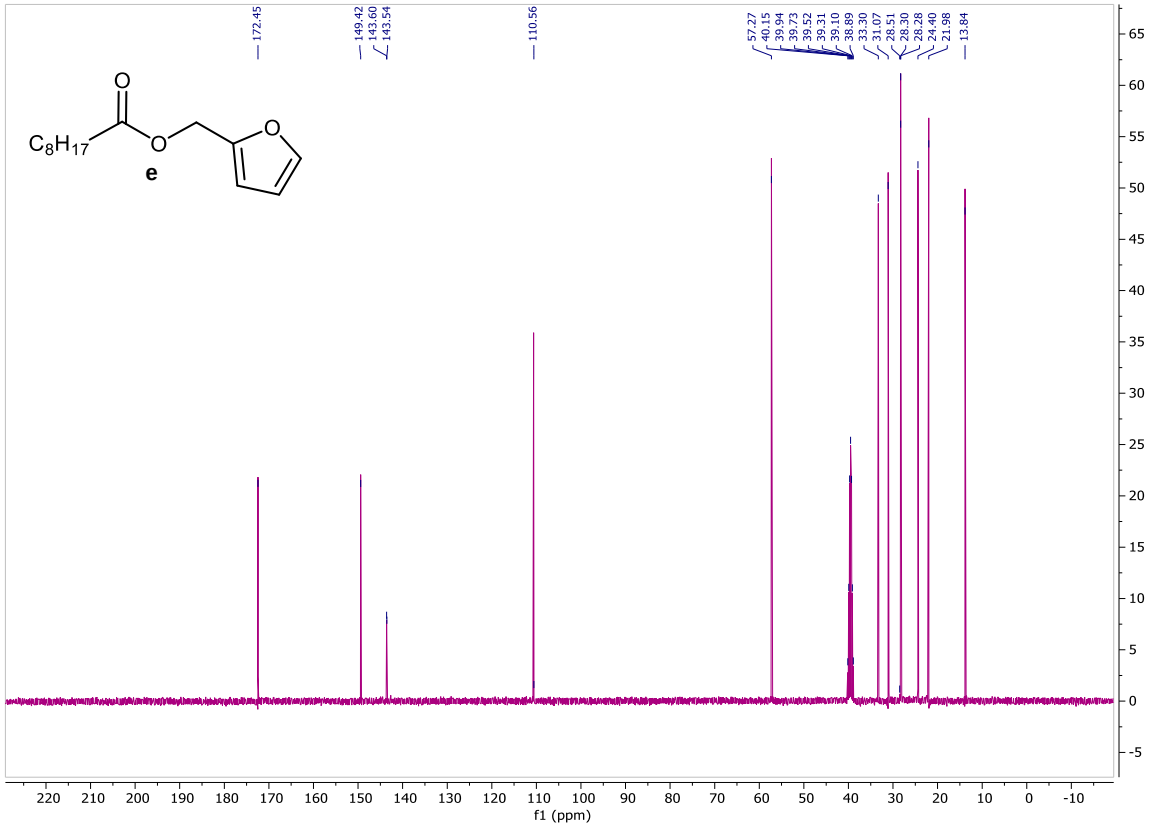

Fig. S37. ^{13}C NMR spectra of furfuryl nonanoate (e).

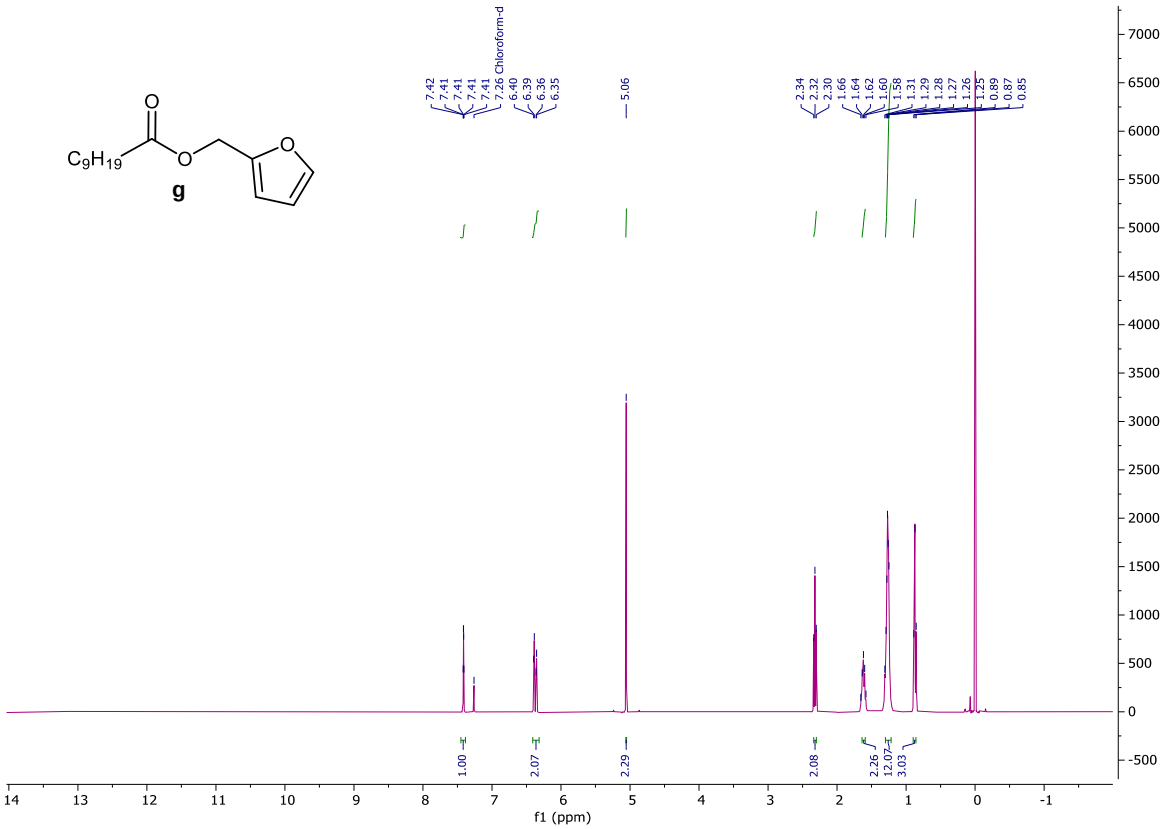

Fig. S38. ^{1}H NMR spectra of furfuryl decanoate (g).

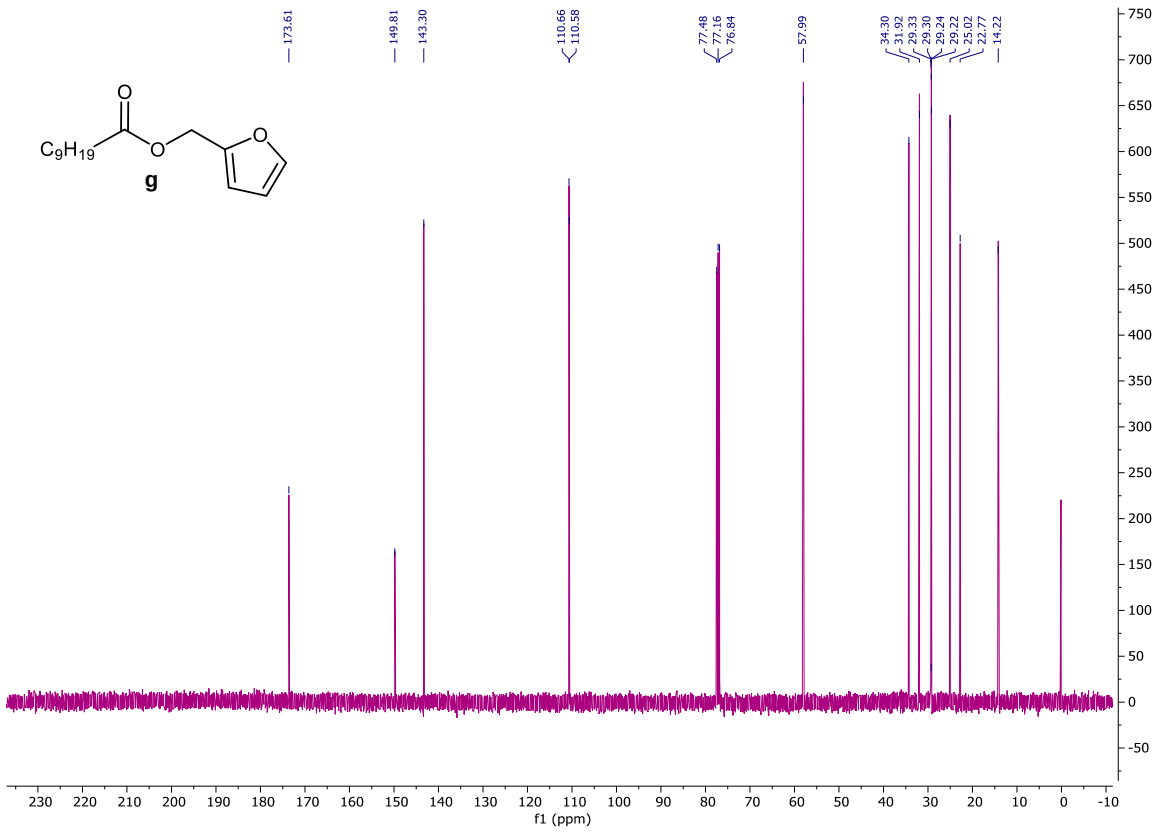

Fig. S39. ^{13}C NMR spectra of furfuryl decanoate (g).

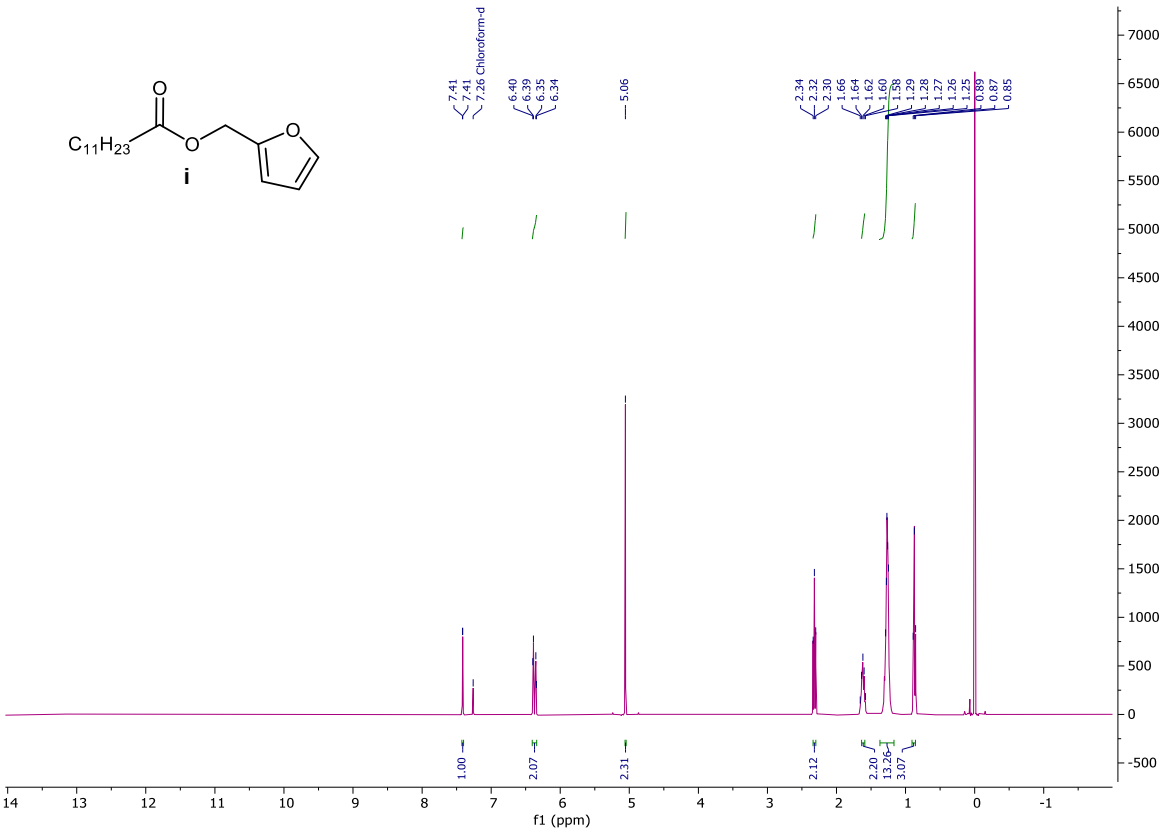

Fig. S40. ^{1}H NMR spectra of furfuryl laurate (i).

Fig. S41. ^{13}C NMR spectra of furfuryl laurate (i).

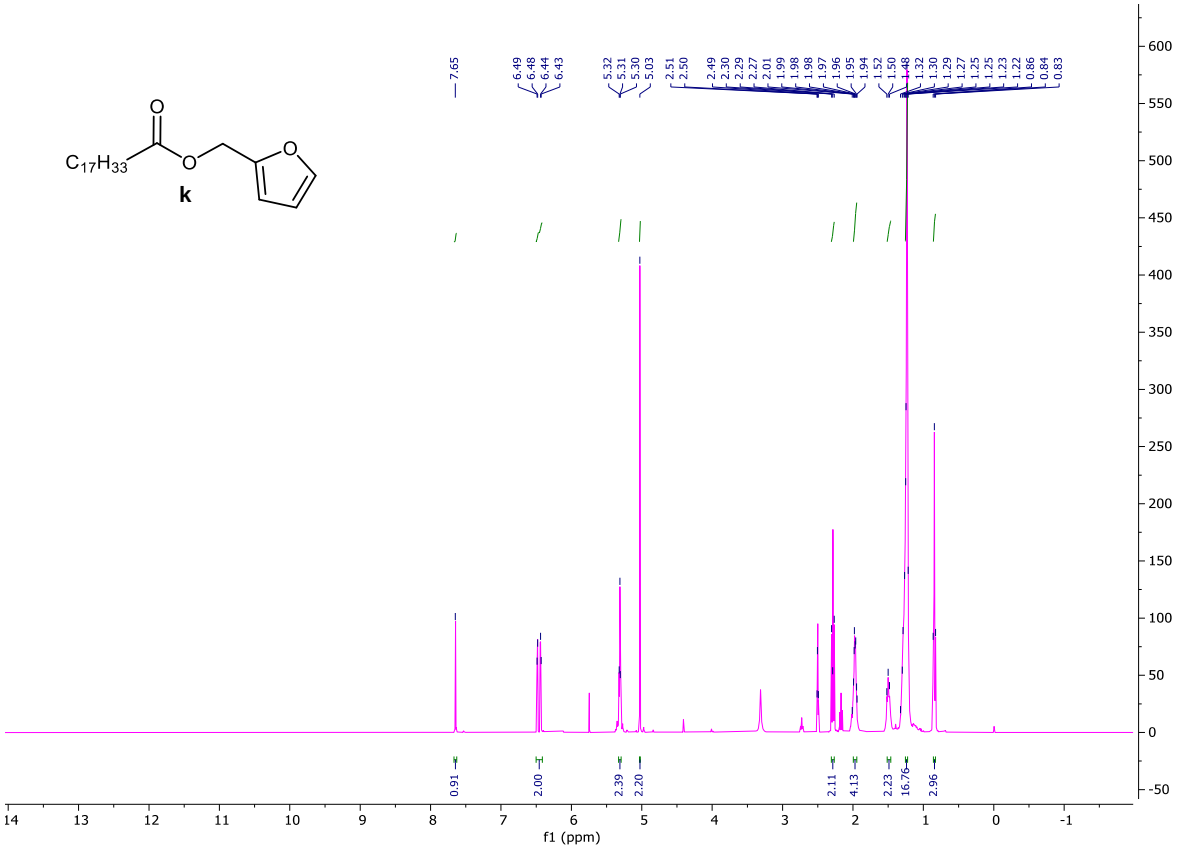

Fig. S42. ^{1}H NMR spectra of furfuryl oleate (k).

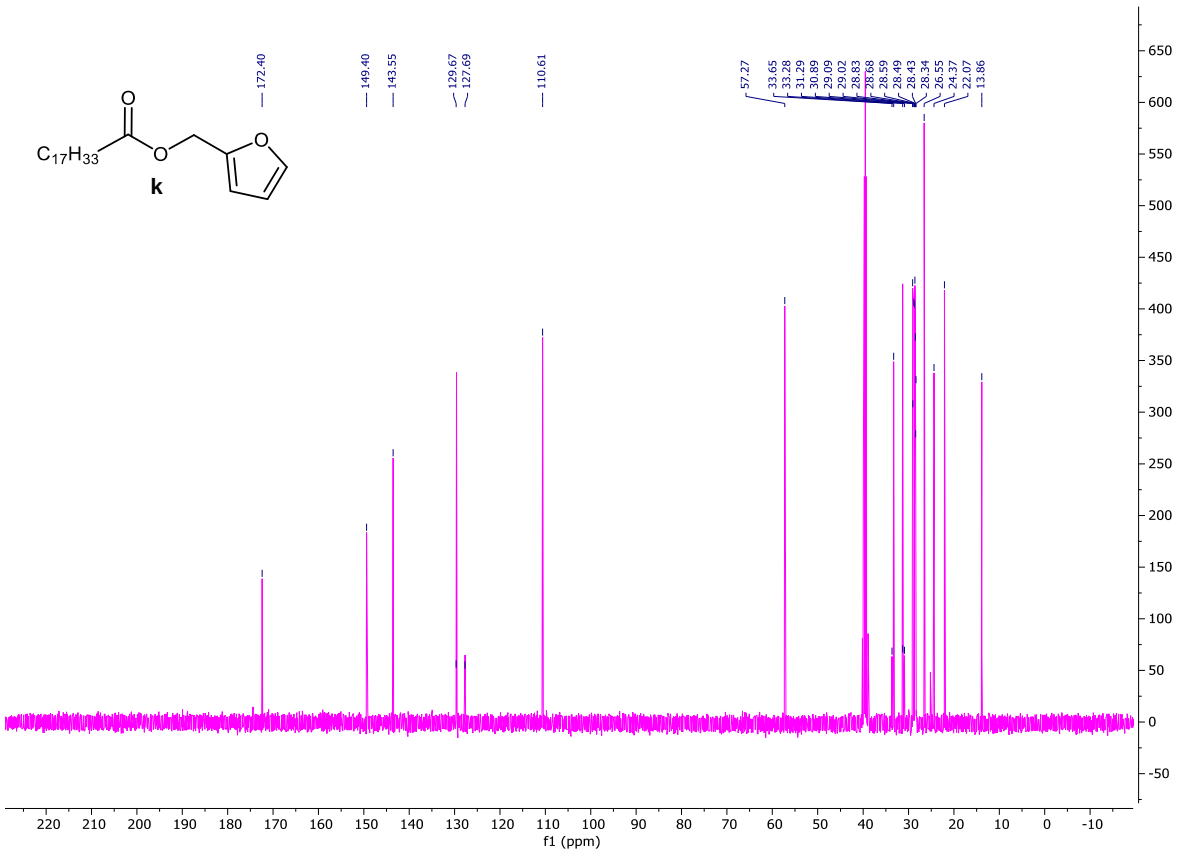

Fig. S43. ^{13}C NMR spectra of furfuryl oleate (k).

Supplementary Information: Appendix 2 **Summary of First Pass Metrics Toolkit**

Yield, AE, RME, MI/PMI and OE

Reactant (Limiting Reactant First)	Mass (g)	MW	Mol	Catalyst	Mass (g)	Reagent	Mass (g)	Reaction solvent	Volume (cm^3)	Density ($g\,ml^{-1}$)	Mass (g)	Work up chemical	Mass (g)	Workup solvent	Volume (cm3)	Density ($g\,ml^{-1}$)	Mass (g)
furfuryl alcohol	0,10	98,00	0,001	MgO-SiO2-C8-LAO	0,15			cyclohexane	0,50	0,78	0,39	K2CO3	1,38	water	10,00	1,00	10,00
octanoic acid	0,43	144,00	0,003									Na2SO4	0,20	heptane	30,00	0,68	20,52
Total	0,53	242,00			0,15		0,00				0,39		1,58				30,52

$$RME = \frac{mass\ of\ isolated\ product}{total\ mass\ of\ reactants} \times 100$$

$$AE = \frac{molecular\ weight\ of\ product}{total\ molecuair\ weight\ of\ reactants} \times 100$$

$$mass\ intensity = \frac{total\ mass\ in\ a\ process\ or\ process\ step}{mass\ of\ product}$$

$$OE = \frac{RME}{AE} \times 100$$

		Flag	
Yield	90,2		90,2
Conversion	90,2		90,2
Selectivity	100,0		100,0
AE	92,6		
RME	38,1	OE	41,2
PMI total	164,2		
PMI Reaction	5,3		
PMI reactants, reagents, catlyst	3,4		
PMI reaction solvents	1,9		
PMI Workup	158,9		
PMI Workup chemical	7,8		
PMI workup solvents	151,1		

	Mass	MW	Mol
Product	0,202	224,000	0,0009
	mass		
Unreacted limiting reactant	0,0096		

Experimental (general): In a 5 mL vial, furfuryl alcohol (0.1 mmol), cyclohexane (0.5 mL), fatty acid (0.3 mmol) were mixed, and then 150 mg of MgO-SiO2-C8-LAO were added. The reaction was performed at 25 °C and stirred in a thermostatic shaker (250 rpm) for 45 min. Reaction progress was monitored by GC. After the reaction, the biocatalyst was filtered off, and the product was separated by 1M solution of K2CO3 (10 mL)/heptane (3x10 mL) extraction system, brine, and dried with anhydrous sodium sulphate, filtrate, then solvent was evaporated, and obtained ester was analyzed via 1H and 13C NMR.

Instructions for use: Enter your data into the tables above to automatically calculate yield, AE, RME, MI/PMI and OE.
Use the blank boxes in the tables to enter experimental data and note the flags for each Key Parameter.
Printing tips: This spreadsheet is designed to be printed with 'landscape', 'narrow margin' and 'fit all columns on one page' settings

Solvents (First Pass)

		List solvents below
Preferred solvents	**water,** EtOH, nBuOH, AcOipr, AcOnBu, PhOMe, MeOH, tBuOH, BnOH, ethyleneglycol, acetone, MEK, MIBK, AcOEt, sulfolane	water
Problematic solvents: (acceptable only if substitution does not offer advantages)	DMSO, cyclohexanone, DMPU, AcOH, Ac2O, Acetonitrile, AcOMe, THF, **heptane**, Me-cyclohexane, toluene, xylene, MTBE, **cyclohexane**, chlorobenzene, formic acid, pyridine, Me-THF	cyclohexane, heptane
Hazardous solvents: These solvents have significant health and/or safety concerns.	dioxane, pentane, TEA, diisopropyl ether, DME, DCM, DMF, DMA, NMP, methoxyethanol, hexane	
Highly hazardous solvents: The solvents which are agreed not to be used, even in screening	Et_2O, Benzene, CCl_4, chloroform, DCE, nitromethane, CS_2, HMPA	

Catalyst/enzyme (First Pass)

		Tick
Catalyst or enzyme used, **or** reaction takes place without	Green Flag	+
Use of stoichiometric quantities of reagents	Amber Flag	
Use of reagents in excess	Red Flag	

		Tick
Facile recovery of catalyst/enzyme	Green Flag	
catalyst/enzyme not recovered	Amber Flag	+

Critical elements

Supply remaining	Flag colour	Note element
5-50 years	Red Flag	
50-500 years	Amber Flag	+
+500 years	Green Flag	

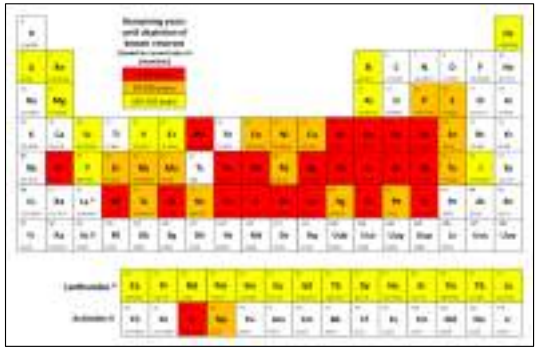

Energy (First Pass)		Tick
Reaction run between 0 to 70°C	Green Flag	+
Reaction run between -20 to 0 or 70 to 140°C	Amber Flag	
Reaction run below -20 or above 140°C	Red Flag	

		Tick
Reaction run at reflux	Red Flag	
Reaction run 5°C or more below the solvent boiling point	Green Flag	+

Batch/flow		Tick
Flow	Green Flag	
Batch	Amber Flag	+

Work Up		List
quenching filtration centrifugation crystallisation	Green Flag	filtration of biocatalyst
solvent exchange, quenching into aqueous solvent	Amber Flag	extraction with 1M potassium carbonate aqueous solution and heptane
chromatography/ion exchange high temperature distillation/evaporations/sublimation (> 140°C at atmospheric multiple recrystallisation	Red Flag	

Health & safety	Red Flag	Amber Flag	Green Flag	List substances and H-codes	List substances and H-codes	List substances and H-codes
				cyclohexane (H225, H304, H315, H336, H400, H410)	furfuryl alcohol (H302, H331, H319, H351, H335, H373)	water
Highly explosive	H200, H201, H202, H203	H205, H220, H224	If no red or amber flagged H codes present then green flag	heptane (H225, H304, H315, H336, H400, H410)	caprylic acid (H314, H318, H412)	K2CO3 (H315, H319, H335)
Explosive thermal runaway	H230, H240, H250	H241				Na2SO4
Toxic	H300, H310, H330	H301, H311, H331,				brine
Long Term toxicity	H340, H350, H360, H370, H372	H341, H351, H361, H371, H373				
Environmental implications	H400, H410, H411, H420	H401, H412				

Use of chemicals of environmental concern		List substances of very high concern
Chemical identified as Substances of Very High Concern by ChemSec which are utilised	Red Flag	not applicable

Supplementary Information: Appendix 2 **Summary of First Pass Metrics Toolkit**

Yield, AE, RME, MI/PMI and OE

Reactant (Limiting Reactant First)	Mass (g)	MW	Mol	Catalyst	Mass (g)	Reagent	Mass (g)	Reaction solvent	Volume (cm^3)	Density ($g\,ml^{-1}$)	Mass (g)	Work up chemical	Mass (g)	Workup solvent	Volume (cm3)	Density ($g\,ml^{-1}$)	Mass (g)
furfuryl alcohol	18,63	98,00	0,190	MgO-SiO2-C8-LAO	0,30			cyclohexane	95,00	0,78	74,01	K2CO3	1,38	water	10,00	1,00	10,00
octanoic acid	82,11	144,00	0,570									Na2SO4	0,20	heptane	30,00	0,68	20,52
Total	100,74	242,00			0,30		0,00				74,01		1,58				30,52

$$RME = \frac{mass\ of\ isolated\ product}{total\ mass\ of\ reactants} \times 100$$

$$AE = \frac{molecular\ weight\ of\ product}{total\ molecuair\ weight\ of\ reactants} \times 100$$

$$mass\ intensity = \frac{total\ mass\ in\ a\ process\ or\ process\ step}{mass\ of\ product}$$

$$OE = \frac{RME}{AE} \times 100$$

		Flag
Yield	96,8	96,8
Conversion	96,8	96,8
Selectivity	100,0	100,0
AE	92,6	
RME	40,9	OE 44,2
PMI total	5,0	
PMI Reaction	4,2	
PMI reactants, reagents, catlyst	2,5	
PMI reaction solvents	1,8	
PMI Workup	0,8	
PMI Workup chemical	0,0	
PMI workup solvents	0,7	

	Mass	MW	Mol
Product	41,220	224,000	0,1840
	mass		
Unreacted limiting reactant	0,5960		

Experimental (general): The continuous-flow furfuryl alcohol esterification was performed in a fully automated Syrris Asia flow reactor. The mixture of furfuryl alcohol in cyclohexane (2.0 M) and caprylic acid (1:3, n:n) was pumped with a flow 0.070 mLmin-1 through the column reactor filled with 300 mg of MgO-SiO2-C8-LAO biocatalyst at 25°C for 48 h. Reaction progress was monitored by GC. After the reaction product (from 5 mL sample of reaction mixture) was separated by 1M solution of K2CO3 (20 mL)/heptane (3x10 mL) extraction system, brine, and dried with anhydrous sodium sulphate, filtrate, then solvent was evaporated, and obtained ester was analyzed via 1H and 13C NMR.

Instructions for use: Enter your data into the tables above to automatically calculate yield, AE, RME, MI/PMI and OE.
Use the blank boxes in the tables to enter experimental data and note the flags for each Key Parameter.
Printing tips: This spreadsheet is designed to be printed with 'landscape', 'narrow margin' and 'fit all columns on one page' settings

Solvents (First Pass)

		List solvents below
Preferred solvents	**water,** EtOH, nBuOH, AcOipr, AcOnBu, PhOMe, MeOH, tBuOH, BnOH, ethyleneglycol, acetone, MEK, MIBK, AcOEt, sulfolane	water
Problematic solvents: (acceptable only if substitution does not offer advantages)	DMSO, cyclohexanone, DMPU, AcOH, Ac2O, Acetonitrile, AcOMe, THF, **heptane**, Me-cyclohexane, toluene, xylene, MTBE, **cyclohexane**, chlorobenzene, formic acid, pyridine, Me-THF	cyclohexane, heptane
Hazardous solvents: These solvents have significant health and/or safety concerns.	dioxane, pentane, TEA, diisopropyl ether, DME, DCM, DMF, DMA, NMP, methoxyethanol, hexane	
Highly hazardous solvents: The solvents which are agreed not to be used, even in screening	Et_2O, Benzene, CCl_4, chloroform, DCE, nitromethane, CS_2, HMPA	

Catalyst/enzyme (First Pass)

		Tick
Catalyst or enzyme used, **or** reaction takes place without	Green Flag	+
Use of stoichiometric quantities of reagents	Amber Flag	
Use of reagents in excess	Red Flag	

		Tick
Facile recovery of catalyst/enzyme	Green Flag	
catalyst/enzyme not recovered	Amber Flag	+

Critical elements

Supply remaining	Flag colour	Note element
5-50 years	Red Flag	
50-500 years	Amber Flag	+
+500 years	Green Flag	

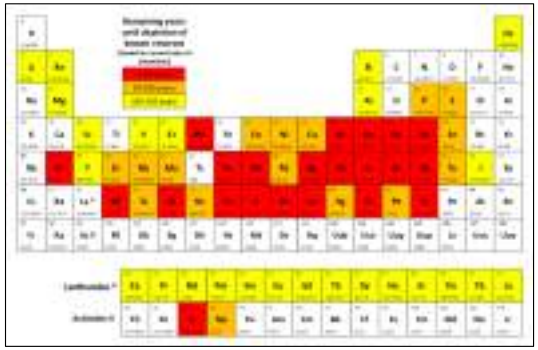

Energy (First Pass)		Tick
Reaction run between 0 to 70°C	Green Flag	+
Reaction run between -20 to 0 or 70 to 140°C	Amber Flag	
Reaction run below -20 or above 140°C	Red Flag	

		Tick
Reaction run at reflux	Red Flag	
Reaction run 5°C or more below the solvent boiling point	Green Flag	+

Batch/flow		Tick
Flow	Green Flag	+
Batch	Amber Flag	

Work Up		List
quenching filtration centrifugation crystallisation	Green Flag	
solvent exchange, quenching into aqueous solvent	Amber Flag	extraction with 1M potassium carbonate aqueous solution and heptane
chromatography/ion exchange high temperature distillation/evaporations/sublimation (> 140°C at atmospheric multiple recrystallisation	Red Flag	

Health & safety	Red Flag	Amber Flag	Green Flag	List substances and H-codes	List substances and H-codes	List substances and H-codes
				cyclohexane (H225, H304, H315, H336, H400, H410)	furfuryl alcohol (H302, H331, H319, H351, H335, H373)	water
Highly explosive	H200, H201, H202, H203	H205, H220, H224	If no red or amber flagged H codes present then green flag	heptane (H225, H304, H315, H336, H400, H410)	caprylic acid (H314, H318, H412)	K2CO3 (H315, H319, H335)
Explosive thermal runaway	H230, H240, H250	H241				Na2SO4
Toxic	H300, H310, H330	H301, H311, H331,				brine
Long Term toxicity	H340, H350, H360, H370, H372	H341, H351, H361, H371, H373				
Environmental implications	H400, H410, H411, H420	H401, H412				

Use of chemicals of environmental concern		List substances of very high concern
Chemical identified as Substances of Very High Concern by ChemSec which are utilised	Red Flag	not applicable

Supplementary Information: Appendix 2 **Summary of First Pass Metrics Toolkit**

Yield, AE, RME, MI/PMI and OE

Reactant (Limiting Reactant First)	Mass (g)	MW	Mol	Catalyst	Mass (g)	Reagent	Mass (g)	Reaction solvent	Volume (cm^3)	Density ($g\,ml^{-1}$)	Mass (g)	Work up chemical	Mass (g)	Workup solvent	Volume (cm3)	Density ($g\,ml^{-1}$)	Mass (g)	
furfuryl alcohol	0,98	98,00	0,010	Y2O3-ZrO2	0,20							NaHCO3	no data	water	15,00	1,00	15,00	
acetic acid	3,00	60,00	0,050									Na2SO4	no data	dichloromethane	40,00	1,33	53,20	
												NaCl	no data	ethyl acetate				no data
														petroleum ether				no data
Total	3,98	158,00			0,20		0,00				0,00		0,00				68,20	

FA 10 mmol 98 0,98
C2 50 mmol 60 3
FA_C8 8,8 mmol 140

$$RME = \frac{mass\ of\ isolated\ product}{total\ mass\ of\ reactants} \times 100$$

$$AE = \frac{molecular\ weight\ of\ product}{total\ molecular\ weight\ of\ reactants} \times 100$$

$$mass\ intensity = \frac{total\ mass\ in\ a\ process\ or\ process\ step}{mass\ of\ product}$$

$$OE = \frac{RME}{AE} \times 100$$

		Flag
Yield	88,0	88,0
Conversion	88,0	88,0
Selectivity	100,0	100,0
AE	88,6	
RME	31,0	OE 34,9
PMI total	58,7	
PMI Reaction	3,4	
PMI reactants, reagents, catlyst	3,4	
PMI reaction solvents	0,0	
PMI Workup	55,4	
PMI Workup chemical	0,0	
PMI workup solvents	55,4	

	Mass	MW	Mol
Product	1,232	140,000	0,0088
	mass		
Unreacted limiting reactant	0,1176		

Experimental (general): Alcohol (10 mmol) was added to acid (50 mmol) containing (20%, w/w with respect to substrate) and mixture was heated to 110 °C for 7 h. The reaction was monitored by TLC. After completion of reaction, the catalyst was filtered; filtrate was concentrated, diluted with water (15 ml) and extracted with CH2Cl2 (2 x 20 ml).The organic layer was separated, washed with 10% aqueous NaHCO3, brine, water and dried over Na2SO4. The solvent was removed and the crude product was chromatographed on silica gel column (3% EtOAc in light petroleum ether) to afford the product in high yield. The structure was confirmed by 1H NMR, mass spectroscopy and also by comparison with authentic sample. After the reaction, the catalyst is recovered with retention of its catalytic activity. It can be further reactivated for reuse by heating it at 500 °C in the presence of air.

Instructions for use: Enter your data into the tables above to automatically calculate yield, AE, RME, MI/PMI and OE.
Use the blank boxes in the tables to enter experimental data and note the flags for each Key Parameter.
Printing tips: This spreadsheet is designed to be printed with 'landscape', 'narrow margin' and 'fit all columns on one page' settings

Solvents (First Pass)

		List solvents below
Preferred solvents	water, EtOH, nBuOH, AcOipr, AcOnBu, PhOMe, MeOH, tBuOH, BnOH, ethylene glycol, acetone, MEK, MIBK, AcOEt, sulfolane	water, AcOEt
Problematic solvents: (acceptable only if substitution does not offer advantages)	DMSO, cyclohexanone, DMPU, AcOH, Ac2O, Acetonitrile, AcOMe, THF, heptane, Me-cyclohexane, toluene, xylene, MTBE, cyclohexane, chlorobenzene, formic acid, pyridine, Me-THF	petroleum ether
Hazardous solvents: These solvents have significant health and/or safety concerns.	dioxane, pentane, TEA, diisopropyl ether, DME, DCM, DMF, DMA, NMP, methoxyethanol, hexane	DCM
Highly hazardous solvents: The solvents which are agreed not to be used, even in screening	Et_2O, Benzene, CCl_4, chloroform, DCE, nitromethane, CS_2, HMPA	

Catalyst/ enzyme (First Pass)

		Tick
Catalyst or enzyme used, **or** reaction takes place without	Green Flag	+
Use of stoichiometric quantities of reagents	Amber Flag	
Use of reagents in excess	Red Flag	

		Tick	
Facile recovery of catalyst/enzyme	Green Flag	+	in high temperature (500 °C)
catalyst/enzyme not recovered	Amber Flag		

Critical elements

Supply remaining	Flag colour	Note element
5-50 years	Red Flag	
50-500 years	Amber Flag	+
+500 years	Green Flag	

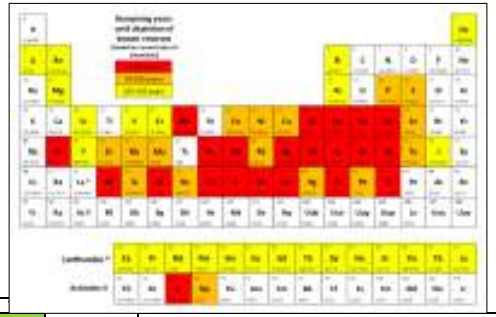

Energy (First Pass)

Reaction run between 0 to 70°C	Green Flag	
Reaction run between -20 to 0 or 70 to 140°C	Amber Flag	+
Reaction run below -20 or above 140°C	Red Flag	

		Tick
Reaction run at reflux	Red Flag	
Reaction run 5°C or more below the solvent boiling point	Green Flag	+

Batch/flow		Tick
Flow	Green Flag	
Batch	Amber Flag	+

Work Up		List
quenching filtration centrifugation crystallisation	Green Flag	filtration of catalyst
solvent exchange, quenching into aqueous solvent	Amber Flag	diluted with water, extracted with CH2Cl2, washed with 10% aqueous NaHCO3, brine, water and dried over Na2SO4
chromatography/ion exchange high temperature distillation/evaporations/sublimation (> 140 °C at atmospheric multiple recrystallisation	Red Flag	column chromatography: 3% EtOAc in light petroleum ether

Health & safety				List substances and H-codes	List substances and H-codes	List substances and H-codes
	Red Flag	Amber Flag	Green Flag	petroleum ether (H225 H304 H315 H336 H411)	furfuryl alcohol (H302, H331, H319, H351, H335, H373)	water
Highly explosive	H200, H201, H202, H203	H205, H220, H224	If no red or amber flagged H codes present then green flag			NaHCO3
Explosive thermal runaway	H230, H240, H250	H241				Na2SO4
Toxic	H300, H310, H330	H301, H311, H331,				acetic acid (H226, H314)
Long Term toxicity	H340, H350, H360, H370, H372	H341, H351, H361, H371, H373				ethyl acetate (H225 H319 H336)
Environmental implications	H400, H410, H411, H420	H401, H412				

Use of chemicals of environmental concern		List substances of very high concern
Chemical identified as Substances of Very High Concern by ChemSec which are utilised	Red Flag	not applicable

Supplementary Information: Appendix 2

Summary of First Pass Metrics Toolkit

Yield, AE, RME, MI/PMI and OE

Reactant (Limiting Reactant First)	Mass (g)	MW	Mol	Catalyst	Mass (g)	Reagent	Mass (g)	Reaction solvent	Volume (cm^3)	Density ($g ml^{-1}$)	Mass (g)	Workup chemical	Mass (g)	Workup solvent	Volume (cm3)	Density ($g ml^{-1}$)	Mass (g)
acetic acid	1,68	60,00	0,028	Fe-DTP-ZIF-8	0,01												
furfuryl alcohol	4,51	98,00	0,046														
Total	6,19	158,00			0,01		0,00				0,00		0,00				0,00

$$RME = \frac{mass\ of\ isolated\ product}{total\ mass\ of\ reactants} \times 100$$

$$AE = \frac{molecular\ weight\ of\ product}{total\ molecualr\ weight\ of\ reactants} \times 100$$

$$mass\ intensity = \frac{total\ mass\ in\ a\ process\ or\ process\ step}{mass\ of\ product}$$

$$OE = \frac{RME}{AE} \times 100$$

		Flag
Yield	75,7	75,7
Conversion	87,7	87,7
Selectivity	86,3	86,3
AE	88,6	
RME	47,9	OE 54,1
PMI total	2,1	
PMI Reaction	2,1	
PMI reactants, reagents, catlyst	2,1	
PMI reaction solvents	0,0	
PMI Workup	0,0	
PMI Workup chemical	0,0	
PMI workup solvents	0,0	

	Mass	MW	Mol
Product	2,967	140,000	0,0212
	mass		
Unreacted limiting reactant	0,2070		

Experimental (general): Known amounts of furfuryl alcohol (0.046 mol) and acetic acid (0.28 mol) were added into the glass reactor and the total volume of the reaction mixture was 21 mL. 0.006 g of Fe-DTP@ZIF-8 was added to the above reaction mixture and the temperature raised to 100 °C. Thereafter, the mixture was maintained under isothermal conditions until the reaction was completed, typically within 6 h. The reaction mass was agitated at 800 rpm with the stirrer speed optimized to ensure removal of external mass transfer limitations. Periodically, samples were withdrawn and analysed by a GC.

Instructions for use: Enter your data into the tables above to automatically calculate yield, AE, RME, MI/PMI and OE.
Use the blank boxes in the tables to enter experimental data and note the flags for each Key Parameter.
Printing tips: This spreadsheet is designed to be printed with 'landscape', 'narrow margin' and 'fit all columns on one page' settings

Solvents (First Pass)

		List solvents below
Preferred solvents	water, EtOH, nBuOH, AcOipr, AcOnBu, PhOMe, MeOH, tBuOH, BnOH, ethylene glycol, acetone, MEK, MIBK, AcOEt, sulfolane	
Problematic solvents: (acceptable only if substitution does not offer advantages)	DMSO, cyclohexanone, DMPU, AcOH, Ac2O, Acetonitrile, AcOMe, THF, heptane, Me-cyclohexane, toluene, xylene, MTBE, cyclohexane, chlorobenzene, formic acid, pyridine, Me-THF	no data
Hazardous solvents: These solvents have significant health and/or safety concerns.	dioxane, pentane, TEA, diisopropyl ether, DME, DCM, DMF, DMA, NMP, methoxyethanol, hexane	
Highly hazardous solvents: The solvents which are agreed not to be used, even in screening	Et_2O, Benzene, CCl_4, chloroform, DCE, nitromethane, CS_2, HMPA	

Catalyst/enzyme (First Pass)

		Tick
Catalyst or enzyme used, or reaction takes place without	Green Flag	+
Use of stoichiometric quantities of reagents	Amber Flag	
Use of reagents in excess	Red Flag	

		Tick
Facile recovery of catalyst/enzyme	Green Flag	
catalyst/enzyme not recovered	Amber Flag	+

Critical elements

Supply remaining	Flag colour	Note element
5-50 years	Red Flag	+
50-500 years	Amber Flag	
+500 years	Green Flag	

Energy (First Pass)

					Tick
Reaction run between 0 to 70°C	Green Flag		Reaction run at reflux	Red Flag	
Reaction run between -20 to 0 or 70 to 140°C	Amber Flag	+	Reaction run 5°C or more below the solvent boiling point	Green Flag	+
Reaction run below -20 or above 140°C	Red Flag				

Batch/flow		Tick
Flow	Green Flag	
Batch	Amber Flag	+

Work Up		List
quenching filtration centrifugation crystallisation	Green Flag	
solvent exchange, quenching into aqueous solvent	Amber Flag	
chromatography/ion exchange high temperature distillation/evaporations/sublimation (>140 °C at atmospheric multiple recrystallisation	Red Flag	

no data

Health & safety	Red Flag	Amber Flag	Green Flag	List substances and H-codes	List substances and H-codes	List substances and H-codes
					furfuryl alcohol (H302, H331, H319, H351, H335, H373)	acetic acid (H226, H314)
Highly explosive	H200, H201, H202, H203	H205, H220, H224	If no red or amber flagged H codes present then green flag			
Explosive thermal runaway	H230, H240, H250	H241				
Toxic	H300, H310, H330	H301, H311, H331,				
Long Term toxicity	H340, H350, H360, H370, H372	H341, H351, H361, H371, H373				
Environmental implications	H400, H410, H411, H420	H401, H412				

Use of chemicals of environmental concern		List substances of very high concern
Chemical identified as Substances of Very High Concern by ChemSec which are utilised	Red Flag	not applicable

Supplementary Information: Appendix 2 **Summary of First Pass Metrics Toolkit**

Yield, AE, RME, MI/PMI and OE

Reactant (Limiting Reactant First)	Mass (g)	MW	Mol	Catalyst	Mass (g)	Reagent	Mass (g)	Reaction solvent	Volume (cm^3)	Density ($g\,ml^{-1}$)	Mass (g)	Work up chemical	Mass (g)	Workup solvent	Volume (cm3)	Density ($g\,ml^{-1}$)	Mass (g)
oleic acid	20,00	282,50	0,071	Novozyme 435	1,00									no data			
furfuryl alcohol	6,96	98,00	0,071														
Total	26,96	380,50			1,00		0,00				0,00		0,00				0,00

$$RME = \frac{mass\ of\ isolated\ product}{total\ mass\ of\ reactants} \times 100$$

$$AE = \frac{molecular\ weight\ of\ product}{total\ molecuair\ weight\ of\ reactants} \times 100$$

$$mass\ intensity = \frac{total\ mass\ in\ a\ process\ or\ process\ step}{mass\ of\ product}$$

$$OE = \frac{RME}{AE} \times 100$$

		Flag
Yield	99,9	99,9
Conversion	99,9	99,9
Selectivity	100,0	100,0
AE	95,3	
RME	95,1	OE 99,8
PMI total	1,1	
PMI Reaction	1,1	
PMI reactants, reagents, catlyst	1,1	
PMI reaction solvents	0,0	
PMI Workup	0,0	
PMI Workup chemical	0,0	
PMI workup solvents	0,0	

	Mass	MW	Mol
Product	25,638	362,500	0,0707
	mass		
Unreacted limiting reactant	0,0268		

Experimental (general): Oleic acid (20 g) and furfuryl alcohol at 1:1 mole ratio were taken in 100 mL round bottom flask with continuous stirring by a magnetic stirrer bar at 60 °C, in the presence of Candida antartica lipase B at 5 % level (w/w) on the weight of total acid and alcohol and the reactions were carried out at reduced pressure of 533.29 Pa absolute. The reaction course was followed by determining the acid value of the product as a function of time.

Instructions for use: Enter your data into the tables above to automatically calculate yield, AE, RME, MI/PMI and OE.
Use the blank boxes in the tables to enter experimental data and note the flags for each Key Parameter.
Printing tips: This spreadsheet is designed to be printed with 'landscape', 'narrow margin' and 'fit all columns on one page' settings

Solvents (First Pass)

		List solvents below
Preferred solvents	water, EtOH, nBuOH, AcOipr, AcOnBu, PhOMe, MeOH, tBuOH, BnOH, ethylene glycol, acetone, MEK, MIBK, AcOEt, sulfolane	
Problematic solvents: (acceptable only if substitution does not offer advantages)	DMSO, cyclohexanone, DMPU, AcOH, Ac2O, Acetonitrile, AcOMe, THF, heptane, Me-cyclohexane, toluene, xylene, MTBE, cyclohexane, chlorobenzene, formic acid, pyridine, Me-THF	no data
Hazardous solvents: These solvents have significant health and/or safety concerns.	dioxane, pentane, TEA, diisopropyl ether, DME, DCM, DMF, DMA, NMP, methoxyethanol, hexane	
Highly hazardous solvents: The solvents which are agreed not to be used, even in screening	Et_2O, Benzene, CCl_4, chloroform, DCE, nitromethane, CS_2, HMPA	

Catalyst/enzyme (First Pass)

		Tick
Catalyst or enzyme used, **or** reaction takes place without	Green Flag	+
Use of stoichiometric quantities of reagents	Amber Flag	
Use of reagents in excess	Red Flag	

		Tick
Facile recovery of catalyst/enzyme	Green Flag	
catalyst/enzyme not recovered	Amber Flag	no data

Critical elements

Supply remaining	Flag colour	Note element
5-50 years	Red Flag	
50-500 years	Amber Flag	
+500 years	Green Flag	+

Energy (First Pass)		Tick
Reaction run between 0 to 70°C	Green Flag	+
Reaction run between -20 to 0 or 70 to 140°C	Amber Flag	
Reaction run below -20 or above 140°C	Red Flag	
Reaction run at reflux	Red Flag	
Reaction run 5°C or more below the solvent boiling point	Green Flag	+

Batch/flow		Tick
Flow	Green Flag	
Batch	Amber Flag	+

Work Up		List
quenching filtration centrifugation crystallisation	Green Flag	
solvent exchange, quenching into aqueous solvent	Amber Flag	
chromatography/ion exchange high temperature distillation/evaporations/sublimation (> 140°C at atmospheric multiple recrystallisation	Red Flag	

no data

Health & safety	Red Flag	Amber Flag	Green Flag	List substances and H-codes	List substances and H-codes	List substances and H-codes
					furfuryl alcohol (H302, H331, H319, H351, H335, H373)	oleic acid
Highly explosive	H200, H201, H202, H203	H205, H220, H224	If no red or amber flagged H codes present then green flag			
Explosive thermal runaway	H230, H240, H250	H241				
Toxic	H300, H310, H330	H301, H311, H331,				
Long Term toxicity	H340, H350, H360, H370, H372	H341, H351, H361, H371, H373				
Environmental implications	H400, H410, H411, H420	H401, H412				

Use of chemicals of environmental concern		List substances of very high concern
Chemical identified as Substances of Very High Concern by ChemSec which are utilised	Red Flag	not applicable

Supplementary Information: Appendix 2 **Summary of First Pass Metrics Toolkit**

Yield, AE, RME, MI/PMI and OE

Reactant (Limiting Reactant First)	Mass (g)	MW	Mol	Catalyst	Mass (g)	Reagent	Mass (g)	Reaction solvent	Volume (cm^3)	Density ($g\,ml^{-1}$)	Mass (g)	Work up chemical	Mass (g)	Workup solvent	Volume (cm3)	Density ($g\,ml^{-1}$)	Mass (g)
furfuryl alcohol	0,10	98,00	0,001	Novozyme 435	0,01												
octanoic acid	0,14	144,00	0,001														
Total	0,24	242,00			0,01		0,00				0,00		0,00				0,00

$$RME = \frac{mass\ of\ isolated\ product}{total\ mass\ of\ reactants} \times 100$$

$$AE = \frac{molecular\ weight\ of\ product}{total\ molecuair\ weight\ of\ reactants} \times 100$$

$$mass\ intensity = \frac{total\ mass\ in\ a\ process\ or\ process\ step}{mass\ of\ product}$$

$$OE = \frac{RME}{AE} \times 100$$

		Flag	
Yield	73,0		73,0
Conversion	73,0		73,0
Selectivity	100,0		100,0
AE	92,6		
RME	68,7	OE	74,2
PMI total	1,5		
PMI Reaction	1,5		
PMI reactants, reagents, catlyst	1,5		
PMI reaction solvents	0,0		
PMI Workup	0,0		
PMI Workup chemical	0,0		
PMI workup solvents	0,0		

	Mass	MW	Mol
Product	0,164	224,000	0,0007
	mass		
Unreacted limiting reactant	0,0265		

Experimental (general): Equimolar amounts of the C3–C18 acids and furfuryl alcohol (FA) were mixed. Before adding 0.2 wt% of catalyst to the mixture, the stirrer was set to 250 rpm and the temperature was set to 55 °C. The reaction mixture was stirred for 24 h at the corresponding temperature.

Authors did not decribed scale of experiments, so we calculated it for 1 mmol of FA amount.

Instructions for use: Enter your data into the tables above to automatically calculate yield, AE, RME, MI/PMI and OE.
Use the blank boxes in the tables to enter experimental data and note the flags for each Key Parameter.
Printing tips: This spreadsheet is designed to be printed with 'landscape', 'narrow margin' and 'fit all columns on one page' settings

Solvents (First Pass)

		List solvents below
Preferred solvents	water, EtOH, nBuOH, AcOipr, AcOnBu, PhOMe, MeOH, tBuOH, BnOH, ethylene glycol, acetone, MEK, MIBK, AcOEt, sulfolane	
Problematic solvents: (acceptable only if substitution does not offer advantages)	DMSO, cyclohexanone, DMPU, AcOH, Ac2O, Acetonitrile, AcOMe, THF, heptane, Me-cyclohexane, toluene, xylene, MTBE, cyclohexane, chlorobenzene, formic acid, pyridine, Me-THF	
Hazardous solvents: These solvents have significant health and/or safety concerns.	dioxane, pentane, TEA, diisopropyl ether, DME, DCM, DMF, DMA, NMP, methoxyethanol, hexane	
Highly hazardous solvents: The solvents which are agreed not to be used, even in screening	Et_2O, Benzene, CCl_4, chloroform, DCE, nitromethane, CS_2, HMPA	

no data

Catalyst/enzyme (First Pass)

		Tick
Catalyst or enzyme used, **or** reaction takes place without	Green Flag	+
Use of stoichiometric quantities of reagents	Amber Flag	
Use of reagents in excess	Red Flag	

		Tick
Facile recovery of catalyst/enzyme	Green Flag	
catalyst/enzyme not recovered	Amber Flag	

no data

Critical elements

Supply remaining	Flag colour	Note element
5-50 years	Red Flag	
50-500 years	Amber Flag	
+500 years	Green Flag	+

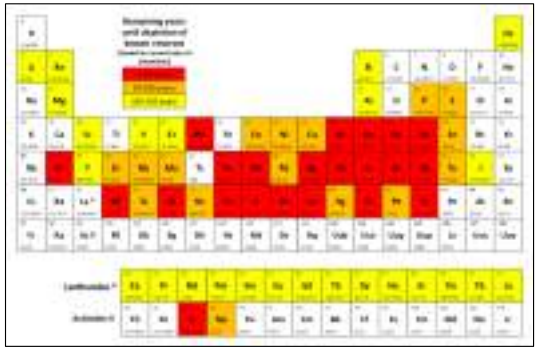

Energy (First Pass)		Tick
Reaction run between 0 to 70°C	Green Flag	+
Reaction run between -20 to 0 or 70 to 140°C	Amber Flag	
Reaction run below -20 or above 140°C	Red Flag	

		Tick
Reaction run at reflux	Red Flag	
Reaction run 5°C or more below the solvent boiling point	Green Flag	+

Batch/flow		Tick
Flow	Green Flag	
Batch	Amber Flag	+

Work Up		List
quenching filtration centrifugation crystallisation	Green Flag	
solvent exchange, quenching into aqueous solvent	Amber Flag	
chromatography/ion exchange high temperature distillation/evaporations/sublimation (> 140°C at atmospheric multiple recrystallisation	Red Flag	

no data

Health & safety	Red Flag	Amber Flag	Green Flag	List substances and H-codes	List substances and H-codes	List substances and H-codes
					furfuryl alcohol (H302, H331, H319, H351, H335, H373)	
Highly explosive	H200, H201, H202, H203	H205, H220, H224	If no red or amber flagged H codes present then green flag		caprylic acid (H314, H318, H412)	
Explosive thermal runaway	H230, H240, H250	H241				
Toxic	H300, H310, H330	H301, H311, H331,				
Long Term toxicity	H340, H350, H360, H370, H372	H341, H351, H361, H371, H373				
Environmental implications	H400, H410, H411, H420	H401, H412				

Use of chemicals of environmental concern		List substances of very high concern
Chemical identified as Substances of Very High Concern by ChemSec which are utilised	Red Flag	not applicable

Supplementary Information: Appendix 2 **Summary of First Pass Metrics Toolkit**

Yield, AE, RME, MI/PMI and OE

Reactant (Limiting Reactant First)	Mass (g)	MW	Mol	Catalyst	Mass (g)	Reagent	Mass (g)	Reaction solvent	Volume (cm^3)	Density ($g\,ml^{-1}$)	Mass (g)	Work up chemical	Mass (g)	Workup solvent	Volume (cm3)	Density ($g\,ml^{-1}$)	Mass (g)
ricinoleic acid	0,30	298,50	0,001	Novozyme 435	0,06												
furfuryl alcohol	0,30	98,00	0,003														
Total	0,60	396,50			0,06		0,00				0,00		0,00				0,00

$$RME = \frac{mass\ of\ isolated\ product}{total\ mass\ of\ reactants} \times 100$$

$$AE = \frac{molecular\ weight\ of\ product}{total\ molecuair\ weight\ of\ reactants} \times 100$$

$$mass\ intensity = \frac{total\ mass\ in\ a\ process\ or\ process\ step}{mass\ of\ product}$$

$$OE = \frac{RME}{AE} \times 100$$

		Flag
Yield	88,6	88,6
Conversion	88,6	88,6
Selectivity	100,0	100,0
AE	95,5	
RME	56,1	OE 58,8
PMI total	2,0	
PMI Reaction	2,0	
PMI reactants, reagents, catlyst	2,0	
PMI reaction solvents	0,0	
PMI Workup	0,0	
PMI Workup chemical	0,0	
PMI workup solvents	0,0	

	Mass	MW	Mol
Product	0,337	378,500	0,0009
	mass		
Unreacted limiting reactant	0,0343		

Experimental (general): The esterification reaction was conducted at 3:1 molar ratio of FA: COFA in a flat bottom flask and stirred at 200 rpm at 60°C temperature for different course of time with 10% (w/w, on total weight of substrate) of immobilized lipase. The reaction was performed in a complete solvent free environment and under vacuum 28 mmHg for 5 h. The reverse molar ratio si.e. excess amount of COFA were not tried as the removal of excess fatty acid will be difficult from the ester of FA and COFA.

Authors did not decribed scale of experiments, so we calculated it for 1 mmol of ricinoleic acid amount.

Instructions for use: Enter your data into the tables above to automatically calculate yield, AE, RME, MI/PMI and OE.
Use the blank boxes in the tables to enter experimental data and note the flags for each Key Parameter.
Printing tips: This spreadsheet is designed to be printed with 'landscape', 'narrow margin' and 'fit all columns on one page' settings

Solvents (First Pass)

		List solvents below
Preferred solvents	water, EtOH, nBuOH, AcOipr, AcOnBu, PhOMe, MeOH, tBuOH, BnOH, ethylene glycol, acetone, MEK, MIBK, AcOEt, sulfolane	
Problematic solvents: (acceptable only if substitution does not offer advantages)	DMSO, cyclohexanone, DMPU, AcOH, Ac2O, Acetonitrile, AcOMe, THF, heptane, Me-cyclohexane, toluene, xylene, MTBE, cyclohexane, chlorobenzene, formic acid, pyridine, Me-THF	
Hazardous solvents: These solvents have significant health and/or safety concerns.	dioxane, pentane, TEA, diisopropyl ether, DME, DCM, DMF, DMA, NMP, methoxyethanol, hexane	
Highly hazardous solvents: The solvents which are agreed not to be used, even in screening	Et_2O, Benzene, CCl_4, chloroform, DCE, nitromethane, CS_2, HMPA	

no data

Catalyst/enzyme (First Pass)

		Tick
Catalyst or enzyme used, **or** reaction takes place without	Green Flag	+
Use of stoichiometric quantities of reagents	Amber Flag	
Use of reagents in excess	Red Flag	

		Tick
Facile recovery of catalyst/enzyme	Green Flag	
catalyst/enzyme not recovered	Amber Flag	

no data

Critical elements

Supply remaining	Flag colour	Note element
5-50 years	Red Flag	
50-500 years	Amber Flag	
+500 years	Green Flag	+

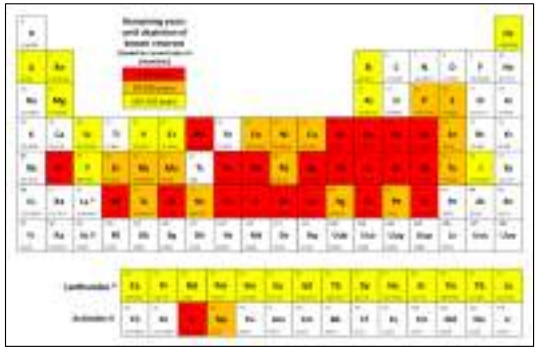

Energy (First Pass)		Tick
Reaction run between 0 to 70°C	Green Flag	+
Reaction run between -20 to 0 or 70 to 140°C	Amber Flag	
Reaction run below -20 or above 140°C	Red Flag	

		Tick
Reaction run at reflux	Red Flag	
Reaction run 5°C or more below the solvent boiling point	Green Flag	+

Batch/flow		Tick
Flow	Green Flag	
Batch	Amber Flag	+

Work Up		List
quenching filtration centrifugation crystallisation	Green Flag	
solvent exchange, quenching into aqueous solvent	Amber Flag	
chromatography/ion exchange high temperature distillation/evaporations/sublimation (> 140°C at atmospheric multiple recrystallisation	Red Flag	

no data

Health & safety	Red Flag	Amber Flag	Green Flag	List substances and H-codes	List substances and H-codes	List substances and H-codes
					furfuryl alcohol (H302, H331, H319, H351, H335, H373)	ricinoleic acid
Highly explosive	H200, H201, H202, H203	H205, H220, H224	If no red or amber flagged H codes present then green flag			
Explosive thermal runaway	H230, H240, H250	H241				
Toxic	H300, H310, H330	H301, H311, H331,				
Long Term toxicity	H340, H350, H360, H370, H372	H341, H351, H361, H371, H373				
Environmental implications	H400, H410, H411, H420	H401, H412				

Use of chemicals of environmental concern		List substances of very high concern
Chemical identified as Substances of Very High Concern by ChemSec which are utilised	Red Flag	not applicable

Supplementary Information: Appendix 2 **Summary of First Pass Metrics Toolkit**

Yield, AE, RME, MI/PMI and OE

Reactant (Limiting Reactant First)	Mass (g)	MW	Mol	Catalyst	Mass (g)	Reagent	Mass (g)	Reaction solvent	Volume (cm^3)	Density ($g ml^{-1}$)	Mass (g)	Work up chemical	Mass (g)	Workup solvent	Volume (cm3)	Density ($g ml^{-1}$)	Mass (g)	
furfuryl alcohol	0,20	98,00	0,002			EDC	0,94	dichloromethane	3,00	1,33	3,99	NaOH	0,40	water	15,00	1,00	15,00	
2-furoic acid	0,67	112,00	0,006									MgSO4		dichloromethane	50,00	1,33	66,50	
												HCl	0,37	hexane				no data
														ethyl acetate				no data
Total	0,87	210,00			0,00		0,94				3,99		0,77				81,50	

$$RME = \frac{mass\ of\ isolated\ product}{total\ mass\ of\ reactants} \times 100$$

$$AE = \frac{molecular\ weight\ of\ product}{total\ molecular\ weight\ of\ reactants} \times 100$$

$$mass\ intensity = \frac{total\ mass\ in\ a\ process\ or\ process\ step}{mass\ of\ product}$$

$$OE = \frac{RME}{AE} \times 100$$

		Flag	
Yield	70,8		70,8
Conversion	70,8		70,8
Selectivity	100,0		100,0
AE	91,4		
RME	31,3	OE	34,3
PMI total	323,8		
PMI Reaction	21,3		
PMI reactants, reagents, catlyst	6,6		
PMI reaction solvents	14,7		
PMI Workup	302,4		
PMI Workup chemical	2,8		
PMI workup solvents	299,6		

	Mass	MW	Mol
Product	0,272	192,000	0,0014
	mass		
Unreacted limiting reactant	0,0572		

Experimental (general): 2-Furoic acid (0.672 g, 6 mmol, 3 equiv.) and EDC (1.06 mL, 6 mmol, 3 equiv.) were dissolved in DCM (3 mL) using a 10-mL pressure vial. Next, furfuryl alcohol (0.17 mL, 2 mmol, 1 equiv.) was added, and the reaction was carried out under MW conditions (standard mode, 30 min, 90 °C). The reaction mixture was then diluted with DCM (50 mL), washed successively using H_2O (5mL), 1N HCl (2x5mL), H_2O (5mL), 1M NaOH (2x5 mL), and H_2O (5 mL), and dried under anhydrous $MgSO_4$. Product was purified by flash chromatography (hexane/ethyl acetate 10:1) and obtained as yellow oil with 71% yield (0.272 g).
1-ethyl-3-(3-dimethylaminopropyl)carbodiimide (EDC)

Instructions for use : Enter your data into the tables above to automatically calculate yield, AE, RME, MI/PMI and OE.
Use the blank boxes in the tables to enter experimental data and note the flags for each Key Parameter.
Printing tips: This spreadsheet is designed to be printed with 'landscape', 'narrow margin' and 'fit all columns on one page' settings

Solvents (First Pass)

		List solvents below
Preferred solvents	water, EtOH, nBuOH, AcOipr, AcOnBu, PhOMe, MeOH, tBuOH, BnOH, ethylene glycol, acetone, MEK, MIBK, AcOEt, sulfolane	water, AcOEt
Problematic solvents: (acceptable only if substitution does not offer advantages)	DMSO, cyclohexanone, DMPU, AcOH, Ac2O, Acetonitrile, AcOMe, THF, heptane, Me-cyclohexane, toluene, xylene, MTBE, cyclohexane, chlorobenzene, formic acid, pyridine, Me-THF	
Hazardous solvents: These solvents have significant health and/or safety concerns.	dioxane, pentane, TEA, diisopropyl ether, DME, DCM, DMF, DMA, NMP, methoxyethanol, hexane	DCM, hexane
Highly hazardous solvents: The solvents which are agreed not to be used, even in screening	Et_2O, Benzene, CCl_4, chloroform, DCE, nitromethane, CS_2, HMPA	

Catalyst/ enzyme (First Pass)

		Tick
Catalyst or enzyme used, or reaction takes place without	Green Flag	
Use of stoichiometric quantities of reagents	Amber Flag	
Use of reagents in excess	Red Flag	+

		Tick
Facile recovery of catalyst/enzyme	Green Flag	
catalyst/enzyme not recovered	Amber Flag	

Critical elements

Supply remaining	Flag colour	Note element
5-50 years	Red Flag	
50-500 years	Amber Flag	
+500 years	Green Flag	+

Energy (First Pass)

Reaction run between 0 to 70°C	Green Flag	
Reaction run between -20 to 0 or 70 to 140°C	Amber Flag	+
Reaction run below -20 or above 140°C	Red Flag	

		Tick
Reaction run at reflux	Red Flag	+
Reaction run 5°C or more below the solvent boiling point	Green Flag	

Batch/flow		Tick
Flow	Green Flag	
Batch	Amber Flag	+

Work Up		List
quenching filtration centrifugation crystallisation	Green Flag	
solvent exchange, quenching into aqueous solvent	Amber Flag	extraction: DCM (50 mL), washed with H2O (5 mL), 1 N HCl (2x5mL), H2O (5mL), 1 M NaOH (2x5mL), and H2O (5mL), dried under anhydrous MgSO4.
chromatography/ion exchange high temperature distillation/evaporations/sublimation (>140 °C at atmospheric pressure) multiple recrystallisation	Red Flag	Product was purified by flash chromatography (hexane/ethyl acetate 10:1)

Health & safety				List substances and H-codes	List substances and H-codes	List substances and H-codes
	Red Flag	Amber Flag	Green Flag		furfuryl alcohol (H302, H331, H319, H351, H335, H373)	water
Highly explosive	H200, H201, H202, H203	H205, H220, H224	If no red or amber flagged H codes present then green flag	EDC (H302 H311 H315 H317 H319 H373 H410)	dichloromethane (H315 H319 H336 H351 H373)	NaOH (H290, H314)
Explosive thermal runaway	H230, H240, H250	H241				MgSO4
Toxic	H300, H310, H330	H301, H311, H331,				ethyl acetate (H225 H319 H336)
Long Term toxicity	H340, H350, H360, H370, H372	H341, H351, H361, H371, H373				2-furoic acid (H315, H319, H335)
Environmental implications	H400, H410, H411, H420	H401, H412				HCl (37%) (H290, H314, H335)

Use of chemicals of environmental concern		List substances of very high concern
Chemical identified as Substances of Very High Concern by ChemSec which are utilised	Red Flag	not applicable